REPORT DOCUMENTATION PAGE

Form Approved OMB NO. 0704-0188

1. REPORT DATE (DD-MM-YYYY)	2. REPORT TYPE	3. DATES COVERED (From - To)
02-06-2009	Final Report	1-Apr-2003 - 30-Sep-2008

4. TITLE AND SUBTITLE

Reaction Mechanisms of Energetic Materials in the Condensed Phase: Long-term Aging, Munition Safety and Condensed-Phase Processes in Propellants and Explosives

5a. CONTRACT NUMBER

5b. GRANT NUMBER

ARO MI-PR--

5c. PROGRAM ELEMENT NUMBER

611102

6. AUTHORS

Richard Behrens

5d. PROJECT NUMBER

5e. TASK NUMBER

5f. WORK UNIT NUMBER

7. PERFORMING ORGANIZATION NAMES AND ADDRESSES

Sandia National Laboratories - Livermore 31.00
PO Box 969

Livermore, CA 94550 -

8. PERFORMING ORGANIZATION REPORT NUMBER

9. SPONSORING/MONITORING AGENCY NAME(S) AND ADDRESS(ES)

U.S. Army Research Office
P.O. Box 12211
Research Triangle Park, NC 27709-2211

10. SPONSOR/MONITOR'S ACRONYM(S)

ARO

11. SPONSOR/MONITOR'S REPORT NUMBER(S)

43381-CH.4

12. DISTRIBUTION AVAILIBILITY STATEMENT

Approved for public release; federal purpose rights

13. SUPPLEMENTARY NOTES

The views, opinions and/or findings contained in this report are those of the author(s) and should not contrued as an official Department of the Army position, policy or decision, unless so designated by other documentation.

14. ABSTRACT

The achievements of this five-year project are summarized. The primary achievement is the development of a new paradigm to investigate the complex reaction processes that control the behavior of heterogeneous energetic materials in munitions throughout their life cycle. It is known as Concepts Methods and Protocols for Reaction Hierarchy and Network Development (CoMPReHND). Results from the decomposition of a high-nitrogen compound, triaminoguanidinium-(5,5')azobitetrazolate (TAGzT) and its interaction with RDX illustrate its use and

15. SUBJECT TERMS

propellants, explosives, reaction mechanisms, kinetics, safety, aging, IM, complex reaction processes, HMX, RDX, TAGzT, high nitrogen compounds, BDNPA/F, PBX9501, thermal decomposition

16. SECURITY CLASSIFICATION OF:			17. LIMITATION OF ABSTRACT	15. NUMBER OF PAGES	19a. NAME OF RESPONSIBLE PERSON
a. REPORT	b. ABSTRACT	c. THIS PAGE			Richard Behrens
UU	UU	UU	UU		19b. TELEPHONE NUMBER: 925-294-2170

Report Title

Reaction Mechanisms of Energetic Materials in the Condensed Phase: Long-term Aging, Munition Safety and Condensed-Phase Processes in Propellants and Explosives

ABSTRACT

The achievements of this five-year project are summarized. The primary achievement is the development of a new paradigm to investigate the complex reaction processes that control the behavior of heterogeneous energetic materials in munitions throughout their life cycle. It is known as Concepts Methods and Protocols for Reaction Hierarchy and Network Development (CoMPReHND). Results from the decomposition of a high-nitrogen compound, triaminoguanidinium-(5,5')azobitetrazolate (TAGzT) and its interaction with RDX illustrate its use and provide an explanation for the increased burn rates of propellants with TAGzT.

The report summarizes work on the decomposition of BDNPA/F and several HMX-based explosive formulations: PBX9501, LX-04, LX-10, LX-14 and EDC-37. The results on the HMX-based explosives suggest that Estane binder used in the PBX9501 and the LX-14 formulations may increase the rate of decomposition of HMX in these formulations compared to HMX by itself or in the other formulations.

The report describes the development of the reaction modeling and kinetics (REMKIN) compiler and analysis tool, which provides a means to develop mathematical models of complex reaction processes. Finally, a report the JANNAF workshop on "R&D Required to Implement New Ingredients in Munitions" and the development of a new paradigm to develop EM is described.

List of papers submitted or published that acknowledge ARO support during this reporting period. List the papers, including journal references, in the following categories:

(a) Papers published in peer-reviewed journals (N/A for none)

Maharrey, S., et al., High mass resolutions SIMS. Applied Surface Science, 2004. 231-232: p. 972-975.

Maharrey, S. and R. Behrens, Thermal Decomposition of Energetic Materials 5. Reaction Processes of 1,3,5-Trinitrohexahydro-s-triazine (RDX) Below Its Melting Point. Journal of Physical Chemistry, 2005. 109: p. 11236-11249.

Behrens, R., Thermal Decomposition Processes of Energetic Materials in the Condensed Phase at Low and Moderate Temperatures, in Overviews of Recent Research on Energetic Materials, R.W. Shaw, T.B. Brill, and D.L. Thompson, Editors. 2005, World Scientific Publishing Co.: Singapore. p. 29 - 74.

Rauch, R. and R. Behrens, Vapor Pressures and Thermal Decomposition Processes of Bis(2,2-dinitropropyl) acetal (BDNPA) and Bis(2,2-dinitropropyl) formal (BDNPA). Propellants Explosives Pyrotechnics, 2007. 32(2): p. 97-116.

Number of Papers published in peer-reviewed journals: 4.00

(b) Papers published in non-peer-reviewed journals or in conference proceedings (N/A for none)

Number of Papers published in non peer-reviewed journals: 0.00

(c) Presentations

Number of Presentations: 0.00

Non Peer-Reviewed Conference Proceeding publications (other than abstracts):

Behrens, R. and S. Maharrey, Reaction Kinetics of RDX in the Condensed Phase, in Proceedings of the 39th JANNAF Combustion Subcommittee Mtg. 2003, CPIA: Colorado Springs, CO.

Behrens, R. Thermal Decomposition Processes in Energetic Materials in the Condensed Phase at Low and Moderate Temperatures. in AIChE Engineered Particle Systems: Synthesis, Processes and Applications Topical Conference. 2003. San Francisco, CA: AIChE.

Behrens, R. and D. Wiese-Smith, Reaction Kinetics of RDX in the Condensed Phase, in 40th JANNAF Combustion Meeting. 2005, CPIA Publication: Charleston, South Carolina. p. June 2005.

Behrens, R. Understanding the Effects of Age on the Reaction Processes that Underlie Insensitive Munitions. in Insenstive Munitions -- The Effect of Ageing Upon Lifecycle Workshop. 2005. Helsinki, Finland: NATO MSIAC.

Behrens, R., et al. Interim Report: Workshop on R&D Required to Implement New Energetic Ingredients in Munitions. in 41st JANNAF Combustion Subcommitte Meeting. 2006. San Diego, California: CPIA.

Behrens, R., D. Wiese-Smith, and H. Hayden. Reaction Processes that Control the Thermal Decomposition of Mixtures of TAGzT and RDX. in 41st JANNAF Combustion Subcommitte Meeting. 2006. San Diego, California: CPIA.

Hayden, H., et al. Thermal Decomposition of High Nitrogen Compounds: TAGzT. in 41st JANNAF Combustion Subcommittee Meeting. 2006. San Diego, California: CPIAC.

Behrens, R. and R.L. Swanson. A New Paradigm for R&D to Implement New Energetic Materials in Munitions. in 2007 Insensitive Munitions and Energetic Materials Technology Symposium. 2007. Miami, Florida: National Defense Industrial Association.

Behrens, R. and R. Swanson, A New Paradigm for R&D to Implement New Energetic Materials in Munitions, in PARARI 8th Australian Explosive Ordnance Symposium. 2007: Melbourne, Australia.

Behrens, R., et al., Workshop on Research and Development Required to Implement New Energetic Ingredients in Munitions. 2007, Chemical Propulsion Information Agency: Aberdeen, MD. p. 1-765.

Behrens, J., Richard , D. Wiese-Smith, and H. Hayden, Reactions of TAG-based Energetic Materials, in 42nd JANNAF Combustion Subcommittee Meeting. 2008, CPIAC: Boston, MA.

Number of Non Peer-Reviewed Conference Proceeding publications (other than abstracts): 11

Peer-Reviewed Conference Proceeding publications (other than abstracts):

Number of Peer-Reviewed Conference Proceeding publications (other than abstracts): 0

(d) Manuscripts

Number of Manuscripts: 0.00

Patents Submitted

METHOD FOR CONTROLLING THE BURNING RATE OF A NITRAMINE PROPELLANT AND FOR DESIGNING COMPOSITIONS THEREFOR

Patents Awarded

Graduate Students

NAME	PERCENT_SUPPORTED
Heather Hayden PhD@ George Wash	0.00
FTE Equivalent:	**0.00**
Total Number:	**1**

Names of Post Doctorates

NAME	PERCENT_SUPPORTED
Rory Rauch, Intern Defense Nuclear F	0.00
FTE Equivalent:	**0.00**
Total Number:	**1**

Names of Faculty Supported

NAME	PERCENT_SUPPORTED
FTE Equivalent:	
Total Number:	

Names of Under Graduate students supported

NAME	PERCENT_SUPPORTED
FTE Equivalent:	
Total Number:	

Student Metrics

This section only applies to graduating undergraduates supported by this agreement in this reporting period

The number of undergraduates funded by this agreement who graduated during this period:	0.00
The number of undergraduates funded by this agreement who graduated during this period with a degree in science, mathematics, engineering, or technology fields:.....	0.00
The number of undergraduates funded by your agreement who graduated during this period and will continue to pursue a graduate or Ph.D. degree in science, mathematics, engineering, or technology fields:.....	0.00
Number of graduating undergraduates who achieved a 3.5 GPA to 4.0 (4.0 max scale):	0.00
Number of graduating undergraduates funded by a DoD funded Center of Excellence grant for Education, Research and Engineering:	0.00
The number of undergraduates funded by your agreement who graduated during this period and intend to work for the Department of Defense	0.00
The number of undergraduates funded by your agreement who graduated during this period and will receive scholarships or fellowships for further studies in science, mathematics, engineering or technology fields:	0.00

Names of Personnel receiving masters degrees

NAME
Total Number:

Names of personnel receiving PHDs

NAME
Heather Hayden PhD@ George Washingt
Total Number: **1**

Names of other research staff

NAME	PERCENT_SUPPORTED	
Sean Maharrey, PhD	0.10	No
Deneille Wiese-Smith	0.10	No
Richard Behrens, PhD	0.10	No
FTE Equivalent:	**0.30**	
Total Number:	**3**	

Sub Contractors (DD882)

Inventions (DD882)

5 **METHOD FOR CONTROLLING THE BURNING RATE**

Patent Filed in US? (5d-1) Y

Patent Filed in Foreign Countries? (5d-2) N

Was the assignment forwarded to the contracting officer? (5e) N

Foreign Countries of application (5g-2):

5a: Richard Behrens

5f-1a: Sandia National Laboratories

5f-c: 7011 East Avenue

Livermore CA 94550

5a: Christine Michienzi

5f-1a: U.S. Navy/Indian Head

5f-c: 3817 Strauss Avenue

Indian Head MD 20640

5a: Heather Hayden

5f-1a: U.S. Navy/Indian Head

5f-c: 3817 Strauss Avenue

Indian Head MD 20640

Reaction Mechanisms of Energetic Materials in the Condensed Phase: Long-term Aging, Munition Safety and Condensed-Phase Processes in Propellants and Explosives

Richard Behrens
Sandia National Laboratories
Combustion Research Facility
Livermore, CA 94551-0969
Project No: 43381CH
Final Report, March 31, 2009

Abstract

The main achievements of this five-year project, spanning FY03 through FY08, are summarized. The primary achievement was the development of a new paradigm to investigate the complex reaction processes that control the behavior of heterogeneous energetic materials in munitions throughout their life cycle. It is known as Concepts Methods and Protocols for Reaction Hierarchy and Network Development (CoMPReHND). Results from the decomposition of a high-nitrogen compound, triaminoguanidinium-(5,5')azobitetrazolate (TAGzT) and its interaction with RDX illustrate its use. It was found that hydrazine is a major product formed in the decomposition of TAGzT and it interacts more rapidly with RDX than RDX can decompose on its own. This interaction is a likely explanation for the increased burn rates of RDX-based gun propellants that contain TAGzT.

The report also summarizes work that was done on the decomposition of several HMX-based explosive formulations: PBX9501, LX-04, LX-10, LX-14 and EDC-37. Results on the decomposition of the BDNPA/F plasticizer used in PBX9501 are summarized. The results on the HMX-based explosives suggest that the Estane binder used in the PBX9501 and the LX-14 formulations may increase the rate of decomposition of HMX in these formulations compared to HMX by itself or in the other formulations. The results also show that the complex nucleation and growth of microscopic bubbles due to the decomposition of HMX in local reaction environments within the solid HMX is still observed in the HMX in all formulations that were investigated.

The function of the newly developed reaction modeling and kinetics (REMKIN) compiler and analysis tool is described. It provides the means to create mathematical models of the reaction networks that characterize the complex reaction processes that characterize the decomposition of organic compounds in the condensed phase (OCiCP).

Finally, the concepts for the development of a new paradigm for R&D required to implement new energetic ingredients in munitions is described. These concepts are an outgrowth of a JANNAF workshop on "R&D Required to Implement New Ingredients in Munitions" that was organized in conjunction with staff at ARL and ARO and supported by the Army, Navy, Air Force and Sandia. Some of the underlying concepts for this

paradigm were created, developed and demonstrated in our research conducted for this project.

Contents

Abstract....1
Contents....2
Introduction....3
History and Project Overview....5
Army and DoD Collaborations....8
The CoMPReHND Paradigm....9
Illustration of the Use of CoMPReHND: TAGzT + RDX....15
Summary of Other Topics Addressed in This Project....26
Development of Chemical Imaging Precision Mass Spectrometry Apparatus (ChIPMA)....26
Development of Reaction Modeling and Kinetics (REMKIN) compiler and analysis tool....27
RDX & HMX Reaction processes....28
HiN compounds....28
A New Paradigm for the development of Energetic Materials....29
List of Publications....34
Conclusions....35
References....36
Appendices....39
Chemical Imaging Precision Mass Analyzer (ChIPMA) report....39
ARO interim reports summarizing HMX decomposition & REMKIN....39
Chapter from Overview of Recent Research on Energetic Materials....39
Reports on RDX, BDNPA/F, TAGzT and TAGzT interactions with RDX....39
Reports on "R&D Required to Implement New Energetic Ingredients in Munitions"....39

Introduction

Army Objectives: An ongoing area of active interest for the Army is the development of new munitions that achieve higher performance objectives, while meeting new insensitive munition (IM) requirements and reduced life-cycle costs. Historically, these objectives have been met using an 'Edisonian' synthesize, formulate and test approach. To transition to a more scientific basis for munition development requires predicting the response of weapons to fire, shock, impact, electrostatic discharge, and long-term aging. This demands a deep understanding of the physical and chemical processes that occur in energetic materials. Acquiring this knowledge requires a suite of experimental investigations, ranging from characterizing shock and impact effects to elucidating chemical reaction mechanisms operating in situations from slow heating to detonation.

The goal of our project is to develop the means to determine physical and chemical reaction pathways that control the thermal decomposition of energetic materials at lower temperatures and heating rates, which are associated with safety, long-term aging and the first stages of combustion. For example, external heating of armaments causes decomposition of their energetic materials, potentially resulting in deflagration or detonation and damage to surrounding material and personnel. Although thermal decomposition mechanisms are known for some energetic materials, these data have yet to be linked to events occurring in an externally heated munition. Linking chemical reaction mechanisms determined from laboratory scale experiments to the behavior of actual explosive devices provides three significant advantages. First, the response of existing munitions to adverse stimuli may be accurately predicted. Second, knowledge of how chemical mechanisms control sensitivity and performance of energetic materials used in munitions will allow development of new materials and formulations with improved properties. Finally, insight into decomposition mechanisms will allow degradation of performance and safety to be predicted when munitions are stored at elevated temperatures (e.g., operations in the Middle East). It will also allow improved interpretation of accelerated aging measurements used to evaluate the long-term stability of munitions.

Scientific Issues: Understanding the thermal decomposition of energetic materials is difficult due to the complex nature of the reaction processes. The first difficulty arises from the predominance of simultaneous parallel chemical reaction pathways that are coupled and where the decomposition may occur simultaneously in the gaseous, liquid and solid phases. The second difficulty arises from ***inherent*** heterogeneity that characterizes formulations of propellants and explosives and ***emergent*** heterogeneity that arises in these materials as they decompose.

While extensive work has been done over the past two decades to understand and characterize complex reaction mechanisms in chemical, biological and genetic systems,[2] careful consideration of the processes that control reactions in energetic materials reveals that their reactions are more complex and they require additional concepts to address their reaction processes than in previous work on complex reaction mechanisms in chemical systems. New concepts must be developed to address the gap in understanding that occurs between the fields of chemistry and material science.

Chemistry typically deals with reactions that involve individual molecules. For example, these reactions may involve unimolecular decomposition or the transfer of atoms in bimolecular collisions. The important point is that these are isolated events, which are primarily controlled by the electronic structure of the molecules participating in the reaction.

Material science, on the other hand, deals with aggregates of atoms or molecules that play a role in determining properties and reaction processes at larger spatial scales. For example, electrical properties of solid-state electronics are determined by how elemental additives influence the band structure of crystalline silicon, or how the grain structure of metal alloys determine their constitutive properties or corrosion resistance. The important point is that the "building blocks" of materials that are well understood and characterized are usually either atomic elements or simple molecules. The building blocks are typically stable and undergo limited changes.

Reactions of energetic materials involve processes that do not entirely fall within the paradigms that underlie either chemistry or material science. The reactions typically occur in the condensed phase and involve mixtures of intrinsically reactive organic molecules and polymers. From the material science point of view, the building blocks are unstable and may be transformed in different ways, which depend upon the reaction conditions. Thus, not only the movement of the building blocks, but also their decomposition will lead to changes in the properties of the material. From the chemistry point of view, the reactions are not isolated from each other or their surroundings. Hence, the fundamental criteria that underlie the basis of elementary reaction kinetics are not met.

To understand and investigate the reactions of energetic materials has required the development of a new paradigm, which draws from the fields of chemistry and material science, to address the specific issues associated with the reaction of organic compounds and organic materials in the condensed phase (OCiCP and OMiCP). This involves developing the means to investigate and understand reaction processes in materials in which *inherent* and *emergent* heterogeneity play a major role in the establishment and operation of the reaction network that controls the behavior of an energetic material over a range of conditions. This new paradigm incorporates concepts that were conceived and developed, in part, by the tasks undertaken in this project.

The new paradigm is called "Concepts, Methods and Protocols for Reaction Hierarchy and Network Development" (CoMPReHND). It was conceived based on the work done in this project and developed in the closing months of the final year of this project. While the concepts and structure of the paradigm have been developed, the creation of five publications to define its structure and illustrate its use is currently underway, but funds are no longer available from this project to support this effort.

This report summarizes the work undertaken in this project and highlights its major accomplishment, which is the development of the CoMPReHND paradigm. We first present a history and overview of the work done in project. Next, we present of brief description of the CoMPReHND paradigm. This is followed by a section with a brief summary of the accomplishments of each task with reference to interim reports and

selected papers that are included in the appendices. Finally, we conclude with suggestions for future work.

History and Project Overview.

The original goals outlined in our proposal for this project were:

1. Expand on our previous studies to increase our understanding of the reaction mechanisms and kinetics controlling the decomposition of cyclic nitramines (RDX and HMX).
2. Explore cyclic nitramine decomposition in a binder matrix to assess changes in decomposition processes when nitramines are incorporated into propellant or explosive formulations. These changes may arise from reactions with other ingredients in the formulation or by the confinement of gaseous decomposition products due to encapsulation of nitramine particles in polymeric binders, such as HTPB or Viton.
3. Understand how chemical functionality, molecular structure, and physical properties influence processes controlling thermal decomposition of energetic materials.
4. Develop mathematical models of the physical and chemical processes controlling energetic material decomposition. These models will enable large scale, multidimensional, time-dependent codes to use the detailed thermal decomposition data from our experiments.

As in many scientific research endeavors, our efforts to address each of these goals uncovered new insights and realizations that altered our thinking and lead to new approaches to address the underlying goal of understanding and characterizing the reaction processes that control the behavior of energetic materials over a range of environments encountered in a munitions life cycle. During the course of this project, we addressed the following six tasks:

1. Development of Chemical Imaging Precision Mass Spectrometry Apparatus (ChIPMA) to perform microscopic chemical imaging.
2. Development of Reaction Modeling and Kinetics (REMKIN) compiler and analysis tool to automate the process of developing and parameterizing reaction networks.
3. Investigation and modeling of reaction networks that control the thermal decomposition of RDX & HMX by themselves and in formulations.
4. Investigation of high-nitrogen (HiN) compounds and formulations that are under development by the Army and Navy for Advanced Gun Propellants.
5. Organization of a national workshop to assess R&D required to implement new energetic ingredients in future munitions. This lead to a concept for a new R&D paradigm to develop energetic materials needed to meet future munition requirements.
6. Conception and development of CoMPReHND.

Work on the first five tasks lead to a careful consideration of many aspects that control the reaction of energetic materials in the condensed phase. For example, in our early work examining the reactions of RDX and HMX,[3-6] it was recognized that the reaction process controlling their decomposition was complex. However, at the time we used the chemist's paradigm to construct a reaction mechanism that consisted of four parallel and coupled chemical reactions to interpret our results. In the ensuing years, we examined an array of different types of energetic compounds and materials. From these studies, it became apparent that geometrical features associated with the initial or emerging morphology of the material lead to a heterogeneous environment that played a significant, and often dominant, role in controlling the their reaction processes. For example, this lead to our further studies on RDX in this project that showed the role of gas-phase reactions and the emergence or a new local reaction environment on the surface of RDX particles.[7]

In a long-standing effort to develop mathematical models to predict the performance or safety aspects of explosives or propellants, the modeling community has been forced to rely on simple global reaction models of condensed phase processes, which are essentially empirical fits of small-scale engineering tests. The complexity of our early experimental results clearly showed that simple global reaction models were insufficient to characterize reaction behavior of energetic materials over the range of conditions encounter during a normal life cycle.

To address this issue, we embarked on developing mathematical models to characterize the complex reaction mechanisms that were observed in our experiments with a range of energetic materials. Our first effort was to build a mathematical model to represent the thermal decomposition of 2,4-dinitroimidazole (24DNI).[8] This was followed shortly thereafter by the creation of mathematical models characterizing the thermal decomposition of trinitroazetidine (TNAZ)[9] and HMX.[10] The models of 24DNI and TNAZ took almost a year to develop and the model of HMX encountered numerical analysis issues that prevented the optimization of the model parameters. While this work was successful in developing the first models of these complex processes, it also pointed to the need for a more efficient means to postulate, evaluate and parameterize mathematical models to characterize the decomposition processes.

To address this need, an effort was devoted to develop a new numerical algorithm that can be used to simulate the complex reaction processes that are probed in our experiments. The algorithm is known as the reaction modeling and kinetics (REMKIN) compiler and analysis tool. It was developed with partial funding from this project.[11, 12] Using REMKIN, reaction models can now be created in several days, rather than many months.

With regard to heterogeneity, we recognized that this was an important factor to investigate in our original proposal. Our original plan was to continue to investigate the reaction processes of HMX that had already shown the importance of emergent heterogeneity and to start new investigations of the reaction of HMX in formulations, such as PBX9501, LX04 and LX10, to assess the role of inherent heterogeneity. While we collected a significant amount of data on the thermal decomposition of HMX-based formulations, an opportunity arose during the course of this project to examine a new class of energetic materials being developed for advanced gun propellants (AGP). A

project to investigate the burn rates of AGPs[13, 14] that tested an array of new high-nitrogen (HiN) compounds showed a range of effects on the burn rate of the propellant. Some compounds had little effect on the burn rate, while others had a substantial effect. This discovery provided an opportunity to understand how different HiN compounds affect the burn rate of the RDX-based AGPs. Hence, we curtailed further work on the HMX formulation and started an investigation of the HiN compounds and APGs.

With regard to developing new ingredients for munitions, this is an example of a major achievement of developing a more scientific approach to understand the behavior that controls the reactions of energetic materials. In our efforts to probe the reaction of HiN compounds, we discovered that one of the major products formed from the decomposition of bis(triaminoguanidinium) 5,5'-azobitetrazolate (TAGzT) is hydrazine, N_2H_4. Furthermore, we found that when TAGzT is mixed with RDX the N_2H_4 reacts more rapidly with RDX than RDX can decompose by itself. Thus, via the formation of N_2H_4, adding TAGzT to an RDX-based propellant increases its burn rate. While this was encouraging, we also discovered that the dissociation of TAGzT to triaminoguanidine (TAG) and azobitetrazole (ABT) commences at ~110°C. This onset temperature for decomposition of TAGzT may make its use in formulations that require higher temperature processing problematic. To circumvent this issue we are currently working with synthetic chemists to create new TAG-based salts that will decompose to form hydrazine, but are more stable than TAGzT.

In recognition of requirements for new energetic materials needed to design future munitions that meet new performance, IM and life cycle requirements, Bill Anderson (ARL), Brad Forch (ARL), Bob Shaw (ARO) and I organized a workshop on "R&D Required to Implement New Energetic Ingredients in Munitions". It was held at the Battelle Conference Center, Aberdeen, MD on 29-31 August 2006, sponsored by CPIAC and supported by ARO, ONR, AFOSR, ARL, and DOE. The participants discussed: (1) conventional methods for evaluating ingredients, (2) system requirements for new energetic materials, (3) what technically limits the implementation of new ingredients in munitions, (4) new experimental concepts for evaluating performance and deleterious features of new ingredients, and (5) new modeling/simulation methods for evaluating and predicting performance and deleterious features of new compounds and materials. From these discussions, it became apparent that the perceived risk for investing in the development of new energetic materials was high due to limited success over the past fifty years in implementing new ingredients in munitions. To reduce this perceived risk, it is important to have (1) programmatic efforts focused in the areas of controlled chemical propulsion, interaction at targets, and meeting IM requirements and (2) new experimental and theoretical methods that provide more insight into the reactive processes and can provide meaningful data 100 times faster and use 100 times less energetic material. Several teams were formed to develop detailed research plans in the areas of synthesis and scaleup, formulations, super-small scale testing, modeling/simulation, new diagnostics, data mining, health and environmental compliance issues, and material design parameters. From these efforts, a new R&D paradigm is being developed to meet future munition requirements.

Work on the first five tasks sparked considerable thought on how to understand the reaction processes in energetic materials that are used in munitions. The overwhelming

and obvious conclusions from the observations are that the reaction processes are complex and take place in the condensed phase. The fact that the reaction processes are complex is not by itself that unusual. Many processes that are characterized by complex mechanism have been successfully investigated and understood over the years.[2] Examples range from biochemical reaction networks that characterize metabolism to gas-phase reaction networks that characterize combustion. In each of these cases, understanding of the process is developed by first conducting experiments and analyzing the results to elucidate the reaction hierarchy. The reaction hierarchy is then refined to form a reaction network that characterizes the reaction process. For chemical systems, this approach has been successful in situations where the chemical reactions occur in isolated environments. For example, chemical reactions in dilute solution or gas-phase reactions at low density.

For energetic materials, many reactions of concern occur in the condensed phase. Thus, the conditions that have enabled the analysis of complex reaction mechanisms in many systems are not met for the case of energetic materials. Hence, new concepts and methods are required to probe complex processes of energetic materials (or organic materials in general) in the condensed phase. In considering these issues, it was recognized that we had developed many of the instruments and methods needed to probe reaction processes of organic compounds in the condensed phase (OCiCP) over the past several decades. What remained to be developed was the concepts and language needed to describe, characterize and understand reactions of OCiCP. This led to the development of the new CoMPReHND paradigm.

While progress on the publication of the papers describing the CoMPReHND paradigm are currently limited by time and funding constraints, a brief summary is useful for illustrating the culmination of the work carried out in this, and previous ARO supported, projects.

Army and DoD Collaborations

Army collaborations. (1) We are directly working with Bill Anderson (ARL) to develop models for reactions of RDX and the HiN compounds. (2) We have collaborated with Barry Fishburn (ARDEC) on the investigation of materials for the IM program. (3) We are currently work with Phil Samuels (ARDEC) to investigate new formulations being developed to meet IM requirements. We are specifically looking at new formulations to help resolve compatibility and safety issues.

DoD collaborations. (1) We are working with Chris Michienzi (Navy/IH) and Heather Hayden (Navy/IH) on the reactions of HiN compounds for AGPs. (2) Thesis advisor for Heather Hayden's thesis work at George Washingtion University. (3) Chair, Kinetics Panel for JANNAF Combustion Subcommittee. (4) Organized JANNAF workshop on "R&D Required to Implement New Energetic Ingredients in Munitions" with Bill Anderson.

The CoMPReHND Paradigm

The reactions in a mixture of TAGzT and RDX provides an illustration of the issues that must be addressed to develop and parameterize a reaction network for ingredients that are being considered for use in advanced gun propellants. The reaction process is illustrated with pictures selected from a time-lapse movie of the reaction between RDX and TAGzT at 150°C taken with a hot-stage microscope.

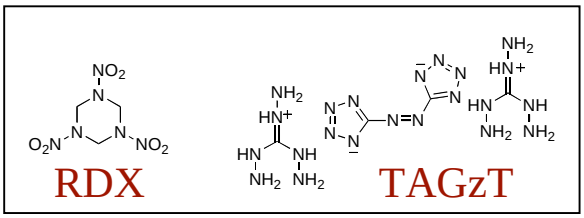

A picture of the starting mixture of TAGzT and RDX contained in a glass tube is shown in Figure 1. The mixture consists of translucent yellow rods of TAGzT and clear particles of RDX. The RDX particles range in size between 50 and 100μm. The TAGzT rods are rectangular solids with widths of tens of microns and lengths of hundreds of microns.

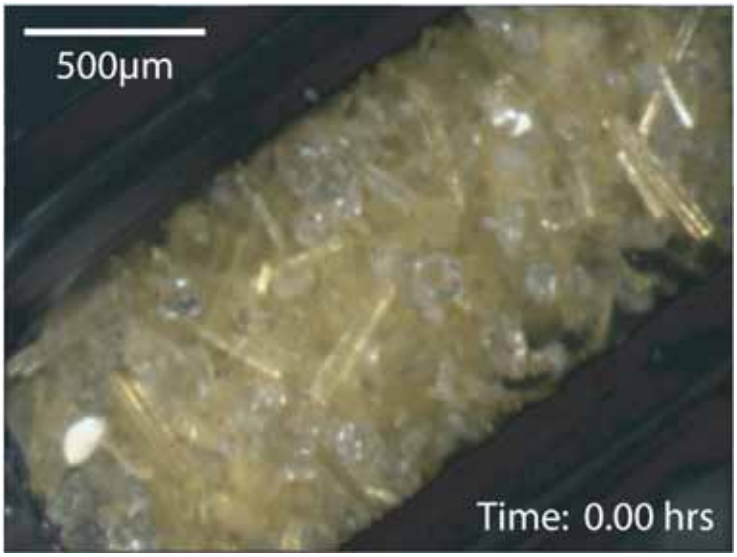

Figure 1. Mixture of RDX (clear particles) and TAGzT (yellow rods) taken prior to decomposition at 150°C.

A sequence of pictures that illustrate the different morphological features of the sample that are observed in a time-lapse movie of its decomposition is shown in Fig. 2. At ~0.2 hours the color of the TAGzT has become a deeper yellow and the number of smaller TAGzT particles has diminished. At ~0.8 hours, the TAGzT particles have become an opaque yellow and a shiny clear film is starting to form on their surfaces. The RDX particles remain clear, but their diameter is decreasing. From 0.8 to 1.4 hours, the general morphological structures of the TAGzT and RDX particles do not change significantly, but their dimensions are decreasing. At ~1.7 hours, the color of the sample is changing from yellow to red and the RDX particles are now changing as they start to interact with the reddish residue being formed. From ~1.7 to ~1.9 hours, the residue from the TAGzT decomposition interacts with the remaining RDX to form a reddish residue. This residue reacts vigorously producing a bubbling mass, which decomposes completely in the following ~0.1 hour.

These time-lapse pictures show the complex nature of the decomposition processes that occur in energetic materials and illustrate how different regions of the sample are more or

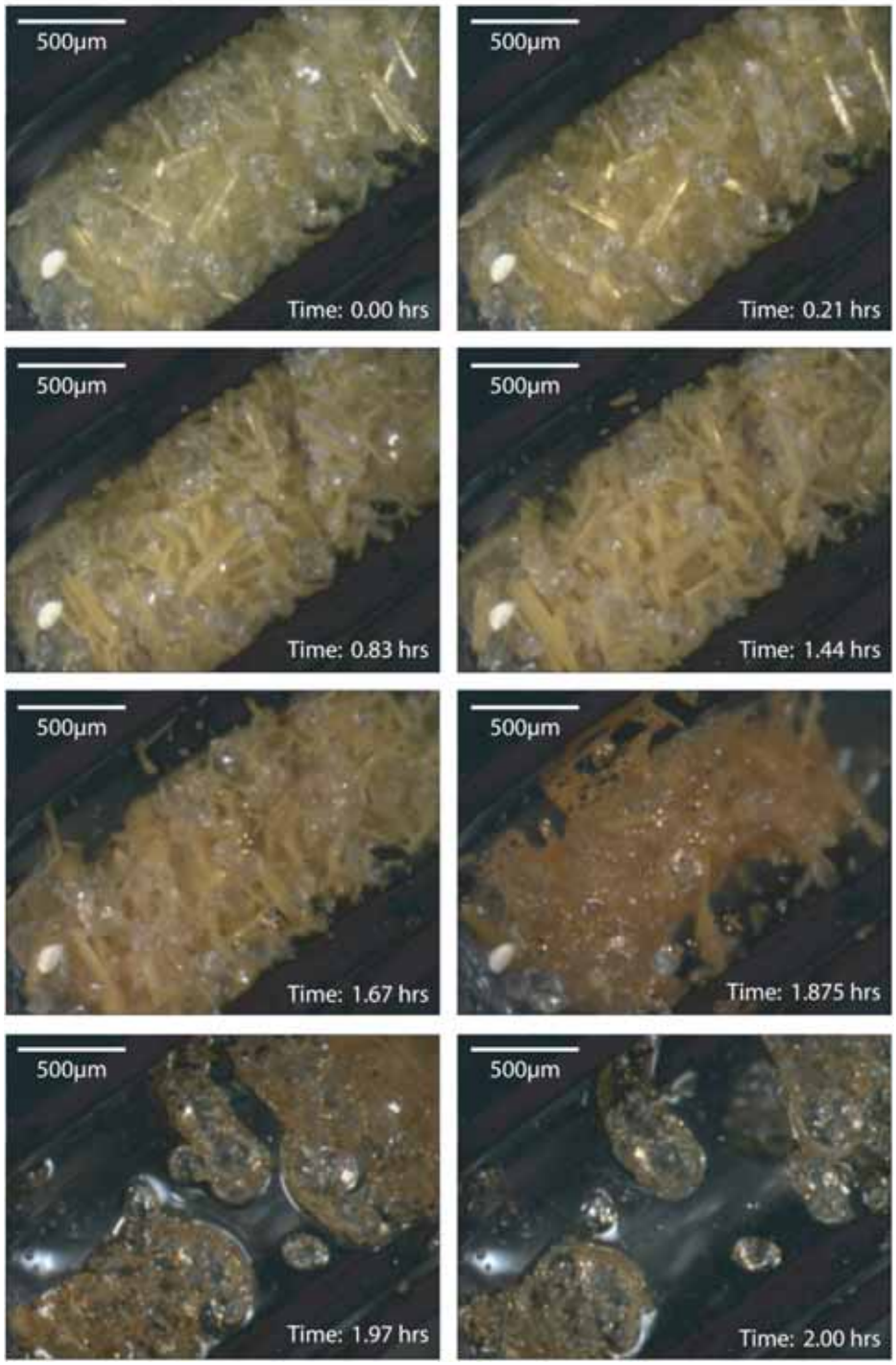

Figure 2. Sequence of pictures from a time-lapse movie of the decomposition of a mixture of RDX and TAGzT at 150°C. The time from the start of the experiment is shown in the lower right of each picture.

less reactive during different stages of the decomposition process. It also illustrates the

role that heterogeneity plays in controlling the overall decomposition process.

To accurately characterize these types of reaction processes, one must address the following set of primary questions: (1) What controls the reaction process? (2) How fast does it happen? (3) How are the reaction processes related across spatial scales whose dimensions range from those of molecules to those of particles or aggregates of particles? To answer these questions requires: (1) knowing the structure of the reaction network that controls the process, and (2) knowledge of the parameters that control different regions of the network. Having this knowledge provides a means to assess the relative contributions of different regions of the network under the various conditions encountered during a munitions life cycle.

To answer these primary questions and determine a reaction network that characterizes these types of processes, the chemist or material scientist must first ask himself or herself what we know about reactions of mixtures of organic compounds in the condensed phase. A basic set of questions that may be posed is:

1. Which ingredients are involved?
2. How do they react?
3. Where do the reactions occur?
    a. Are they localized?
    b. If they are localized, where are they localized?
    c. What determines where they are localized?
4. How are processes that occur at different spatial scales related?
5. How do the ingredients react with each other?
    a. What are their products? Are they solids, liquids, or gases?
    b. Which products are reactive?
    c. Do reactive products create new regions in the reaction network?
    d. What is the extent of coupling between different regions of the network? How are they coupled?
    e. How do the dominant reactions change as a function of temperature and pressure in the system?

These questions all lead to the central question of how do we determine the reaction network and construct mathematical models to describe it.

The general elements of our approach to answer this central question are illustrated in Figure 3. The task can be divided into two major endeavors: (1) network construction, and (2) network parameterization. These two endeavors are common for creating a network to describe any process. What makes the endeavor unique for a particular type of process are the elements that comprise the network. For example, in gas-phase combustion the elements that comprise the structure of the network are elementary reactions and the information that allow its parameterization are the rate constants of the elementary reactions and transport properties of the gases.

For reactions of organic compounds in the condensed phase, it is necessary to define the elements that will be used to construct the reaction networks. After considering the types of processes that are observed in reactions such as those illustrated with TAGzT+ RDX, we introduced the concept of *local reaction environments (LRE)* to account for the elements that comprise the reaction network. An LRE is comprised of an elementary

reaction manifold that describes the chemical activity that takes place within an LRE. Ultimately, one would like to know all of the elements that comprise the elementary

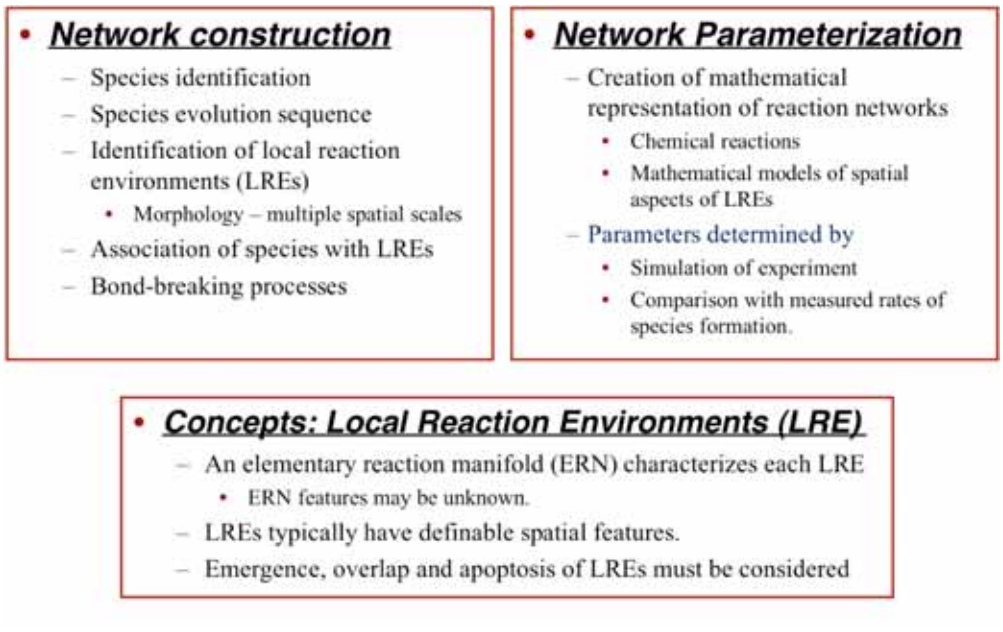

Figure 3. Essential features of reaction networks that characterize the reactions of organic compounds in the condensed phase.

reaction manifold (ERN) of an LRE. However, many of the underlying features of an ERN may be unknown. The important point is that an LRE has been identified as part of a reaction network and its behavior will be characteristic of the reaction processes wherever it occurs in a sample. Aspects of emergence, overlap and apoptosis of LREs must be considered in constructing the reaction network.

Using the concept of LREs, network construction focuses on identifying the LREs and determining the features of their ERMs to the extent possible. This process is based on first identifying the species formed in the reaction process and then determining their evolution sequence. This information provides insight into the reaction pathways that will ultimately comprise the reaction network. In addition to the identities of the species and the sequence of their evolution, it is necessary to determine the spatial aspects of the reaction process.

While several of the spatial aspects may be gleaned from data such as the time-lapse movies of the decomposition of the TAGzT/RDX sample, the features that we typically consider in our experiments are illustrated in Figure 4. The left side of the illustration shows a cross section of the reaction cell that we typically use in our simultaneous thermogravimetric modulated beam mass spectrometry (STMBMS) experiments. The right side shows the types of LREs that may contribute to the reaction network characterizing an OCiCP. Note that the LREs can originate from the experimental configuration (e.g., material present in the solid and gas phase at the start of an experiment) to LREs that emerge during the course of an experiment (e.g., the nucleation

and growth of bubbles within a solid compound). It is also worthwhile to note that the number of LREs that contribute to a network that comprise an experiment may range from very few (e.g., an experiment to measure the vapor pressure and heat of vaporization of a compound will have only two) to many (e.g., the decomposition of the mixture of TAGzT and RDX in the reaction cell).

In addition to illustrating the range of LREs that may be present in an experiment, Figure 4 also illustrates the essence of how we collect the data to construct and a parameterize the reaction network. The STMBMS experiments allow the species within the reaction cell to be identified and their number density determined as a function of time during an experiment. The identities of the species and their sequence of evolution are used in conjunction with postmortem examination of the sample and hot-stage microscopy to determine the reaction hierarchy and construct the reaction network. Once the network is developed, the associated set of differential equations representing the time-dependent behavior of each species may be constructed, solved and compared to the data measured in an STMBMS experiment. This provides the means simulate the reaction network, test its viability by comparing it to the STMBMS data, and refine the network elements and their associated parameters.

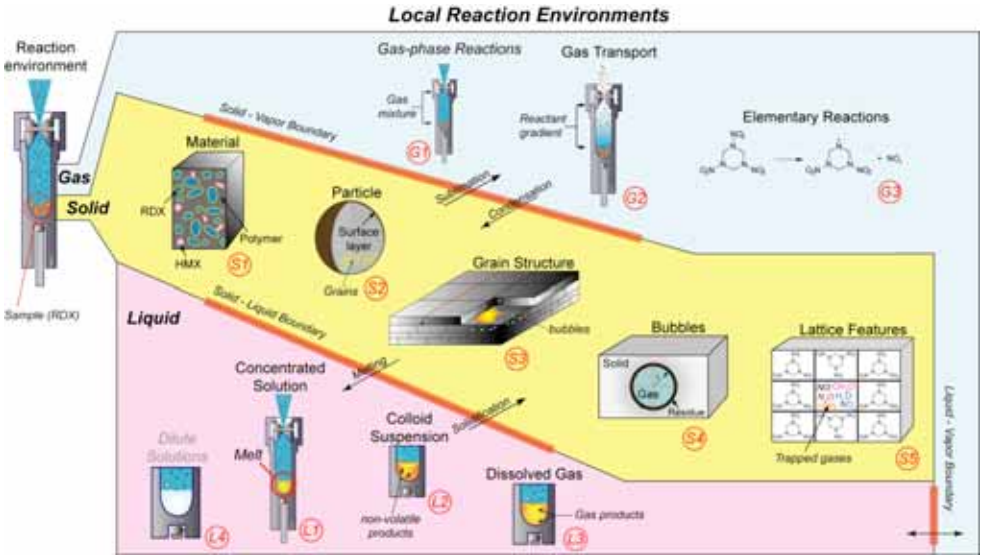

Figure 4. Illustration of the types of different local reaction environments (LRE) that may be present in an experiment.

While this approach to studying complex reaction processes of OCiCP may seem simple, its implementation has involved the design and construction of unique instruments, the creation of numerical algorithms to analyze the data and to construct and simulate the reaction networks, and the development of methods and protocols to control experimental conditions and enable experiments to probe different regions of the reaction network. An illustration taken from a figure in a paper being prepared to describe and illustrate the CoMPReHND paradigm is shown in Figure 5.

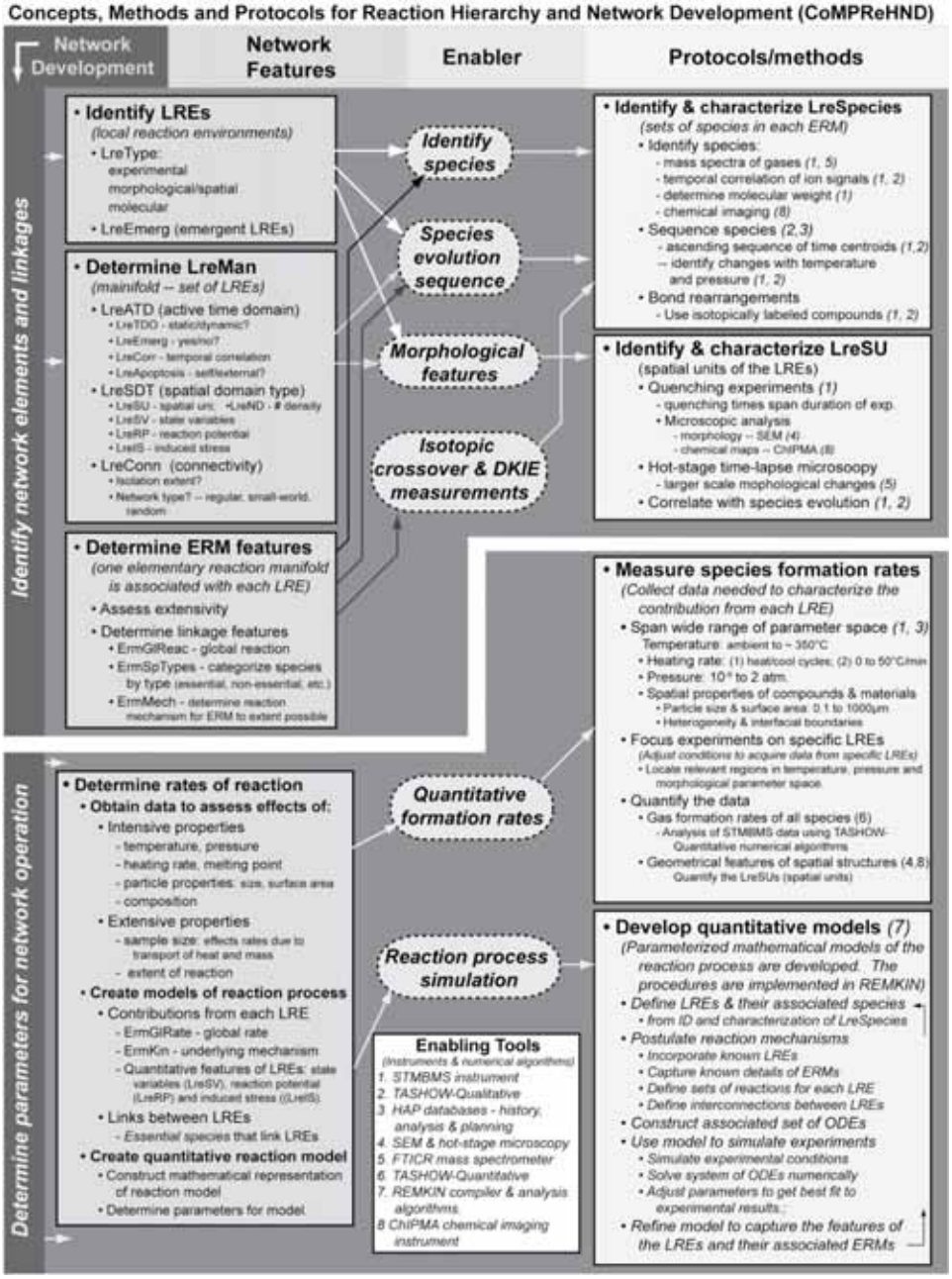

Figure 5. Diagram taken from paper being prepared to describe and illustrate the CoMPReHND paradigm. It outlines the concepts that we have developed to construct and parameterize reaction networks to characterize the decomposition processes of OCiCP. It links these concepts to the associated methods and protocols that we use to probe these processes through the enablers. The enabling tools used to implement these methods and protocols are listed.

As illustrated in Fig. 5, *network development* is divided into two sections. One section covers identification of network elements and linkages. The other section covers determination of the parameters for network operation. Each section contains: (1)

elements describing the relevant *network features*, (2) the general concepts that *enable* the development of network features, and (3) the *methods and protocols* used to acquire and analyze the data and simulate the reaction processes. The tools used to implement the various methods and protocols are listed in the box near the bottom of the illustration.

The network features listed in the section for identification of network elements and linkages outlines many of the concepts being developed to describe reactions of OCiCP. It includes concepts used to characterize LREs, LRE manifolds and the elementary reaction manifolds (ERMs) that characterize each LRE. The details of these concepts are contained in the paper we are preparing for publication.

The network features listed in the section on network parameterization focus on determining the rates of reaction within the network. This effort focuses on three general areas: (1) obtaining data to assess the effects of intensive and extensive properties; (2) creating qualitative models of the reaction process; and (3) creating quantitative mathematical models of the reaction network.

In each of the sections, the concepts that characterize the network features are connected to the methods and protocols used to collect and analyze the data and simulate the reaction process via the *enablers* listed in the center of the diagram. For example, the network features needed to identify the elements and determine their linkages are connected to the methods and protocols by four enablers: (1) species identification, (2) species evolution sequence, (3) morphological features, and (4) isotopic crossover and deuterium kinetic isotope effect measurements. Each of these enablers are linked to the methods and protocols used to collect or analyze the relevant data. For each of individual methods or protocols a set of numbers are listed which indicate the tools that are used to implement the method or protocol. For example to identify the species, the STMBMS instrument (1) and the FTICR mass spectrometer (5) are used. Similarly, each of the methods or protocols is implemented with a related to a set of tools.

Illustration of the Use of CoMPReHND: TAGzT + RDX

In this section the use of the CoMPReHND paradigm is illustrated with results from our investigation of the reaction of TAGzT and RDX.[15-17] The intent is to illustrate the major steps involved in collecting and analyzing the data needed to determine and parameterize a network that characterizes a reaction process.

The species formed in the decomposition of a mixture of TAGzT and RDX are first measured using the STMBMS instrument as illustrated in Fig. 6. Between 165 and 185°C TAGzT decomposes and interacts with the RDX. The RDX vapor is represented by the green line. The main RDX decomposition products first appear when the RDX melts at ~200°C. The orange curve represents the evolution of oxy-s-triazine from the decomposition of RDX. At this stage, the ion signals representing the species evolving from the reaction cell provide initial insight into the main features of the reaction process.

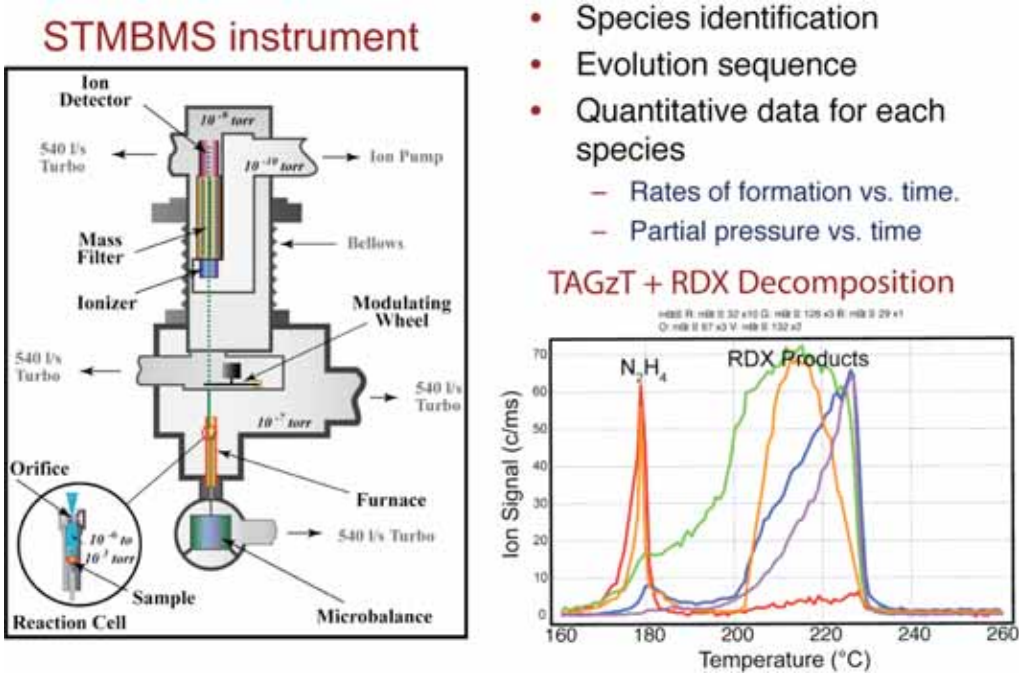

Figure 6. Schematic illustration of STMBMS instrument and data collected using STMBMS to investigate reaction of mixture of TAGzT and RDX.

Since a quadrupole mass spectrometer is used to collect the mass spectra with the STMBMS instrument, the m/z value associated with the ion signals are only measured to integer mass resolution. This data is usually insufficient to determine the formulas of the

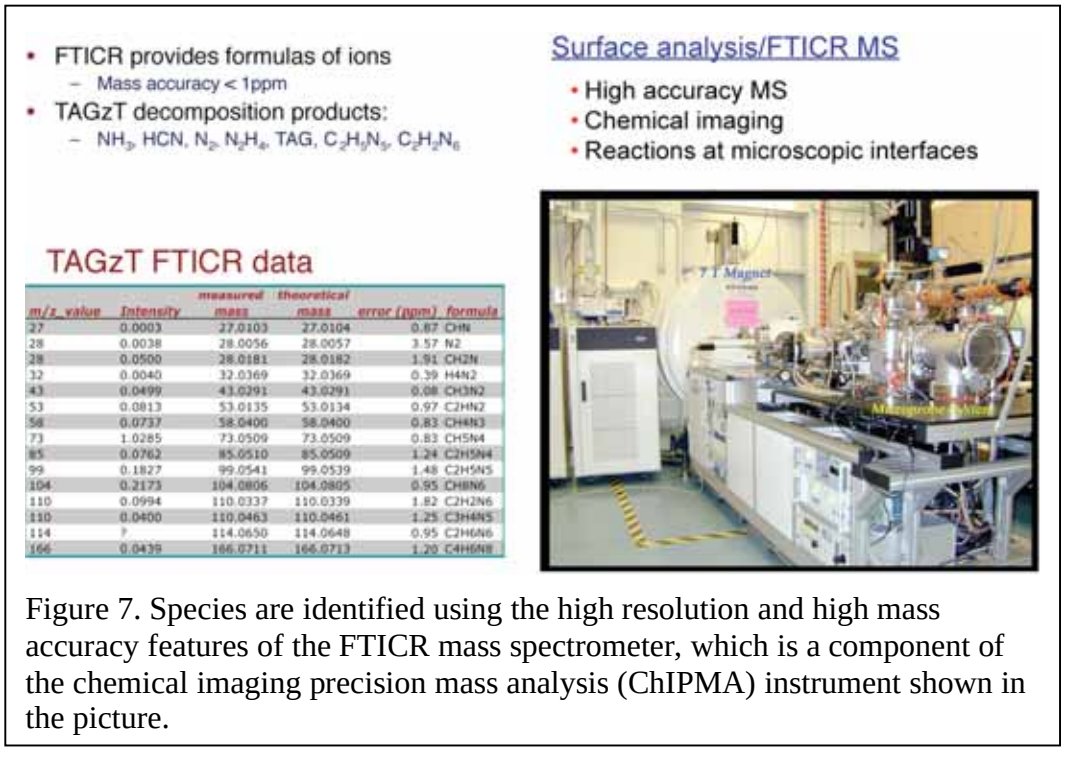

m/z value	Intensity	measured mass	theoretical mass	error (ppm)	formula
27	0.0003	27.0103	27.0104	0.87	CHN
28	0.0038	28.0056	28.0057	3.57	N2
28	0.0500	28.0181	28.0182	1.91	CH2N
32	0.0040	32.0369	32.0369	0.39	H4N2
43	0.0499	43.0291	43.0291	0.08	CH3N2
53	0.0813	53.0135	53.0134	0.97	C2HN2
56	0.0737	56.0400	56.0400	0.83	CH4N3
73	1.0285	73.0509	73.0509	0.83	CH5N4
85	0.0762	85.0510	85.0509	1.24	C2H5N4
99	0.1827	99.0541	99.0539	1.48	C2H5N5
104	0.2173	104.0806	104.0805	0.95	CH8N6
110	0.0994	110.0337	110.0339	1.82	C2H2N6
110	0.0400	110.0463	110.0461	1.25	C3H4N5
114	?	114.0650	114.0648	0.95	C2H6N6
166	0.0439	166.0711	166.0713	1.20	C4H6N8

Figure 7. Species are identified using the high resolution and high mass accuracy features of the FTICR mass spectrometer, which is a component of the chemical imaging precision mass analysis (ChIPMA) instrument shown in the picture.

ions of the more complex species that evolve during the reaction. To help identify the species, thermal decomposition data is also collected using our Fourier Transform ion cyclotron resonance (FTICR) mass spectrometer, which is part of our chemical imaging precision mass analysis (ChIPMA) instrument shown in Figure 7. In these experiments a small amount of sample is placed in a small glass microreactor that is heated with the direct insertion probe (DIP) of the FTICR mass spectrometer. The species evolve from the microreactor directly into the ionizer of the mass spectrometer. The formulas of the ions are determined from the high resolution and accurate mass measurements as illustrated in the table in Fig. 7. Once the formulas of the various ion signals are known, this information is used in conjunction with the time correlation analysis of the ion signal data collected in the STMBMS experiments. This allows the ion signals associated with each species emanating from the reaction cell to be identified, grouped and assigned a stoichiometric formula. This provides the information needed to identify the species.

Once the species are identified, the next step is to collect data from a series of

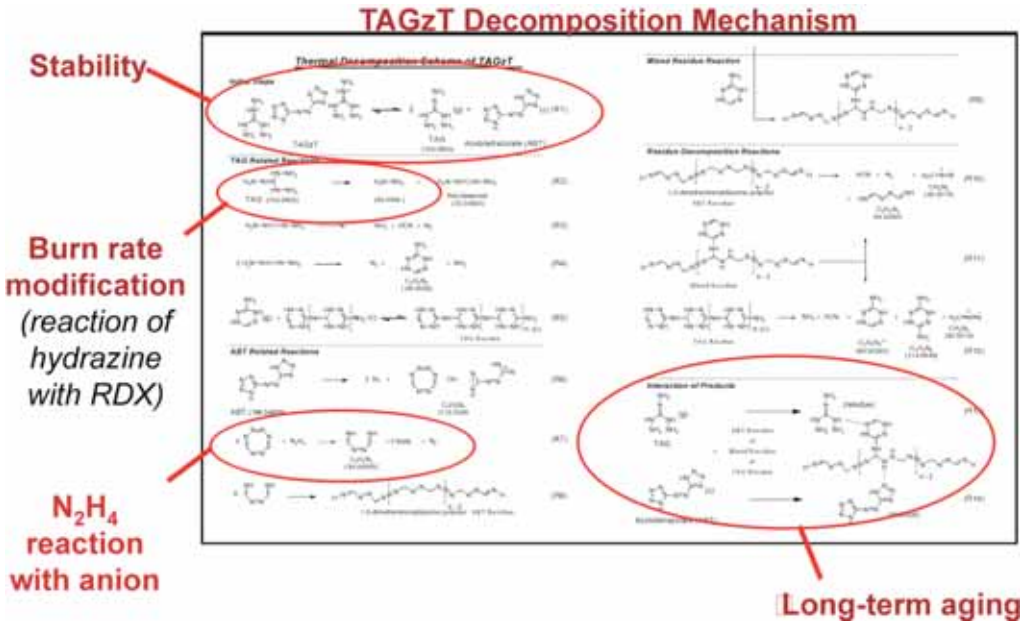

Figure 8. Reaction mechanism characterizing the decomposition of TAGzT.

experiments conducted under isothermal conditions. The temperature of the sample and the pressure of gases confined in the reaction cell are varied in a controlled manner to allow different regions of the parameter space of the reaction process to be probed. The sequence of evolution of the various species formed in the process under isothermal conditions provides the information needed to elucidate the reaction pathways. Combining visual inspection of the data with the postulation of possible reactions, a set of reaction pathways that characterize the process is constructed. The reaction mechanism that controls the decomposition of TAGzT was developed using this approach[15] and is shown in Figure 8.

The process that controls the decomposition of TAGzT is relatively complex. A few of the key reactions are highlighted in Fig. 8. The first reaction to occur is the dissociative

sublimation of TAGzT to triaminoguanidine (TAG) and the azobitetrazole (ABT) (R1). This is a reversible reaction, which first appears in our experiments at 110°C. Another important reaction is the decomposition of the TAG to form hydrazine (R2). In experiments with TAGzT and RDX it has been shown that the reaction between hydrazine and RDX is quite rapid and is a likely explanation for the increased burn rate of the AGPs that contain TAGzT.[16] Reactions between the species formed from the anion of the TAGzT salt, or from the anion of other TAG-based salts, will be important in assessing whether a TAG-based salt is likely to form hydrazine that can interact with other ingredients, such as RDX, in a propellant. Finally, the residue formed in the decomposition of TAGzT (R8, R9) may interact with other ingredients (R13, R14) in the final stages of the reaction process, as illustrated in the time-lapse movie sequence shown in Figure 2. If the residue is formed at lower temperatures, its interaction with the TAGzT may lead to an acceleration of the degradation rate of TAGzT, or other ingredients in a propellant, during normal life cycle conditions.

Once the elements and linkages of a reaction network are developed, the network may be used to (1) provide insight into how to modify ingredients in a formulation to eliminate potential problems in its life cycle or (2) develop a mathematical representation of the network that can be used in predictive simulations of munition behavior.

To develop mathematical models of the reaction network, the reaction processes that occur within the reaction cell are simulated and tested by comparison to the data as illustrated in Figure 9. This process is carried out using the reaction modeling and kinetics (REMKIN) compiler and analysis tool, which has been described in detail elsewhere.[1] The primary steps of the REMKIN compilation and analysis procedure are

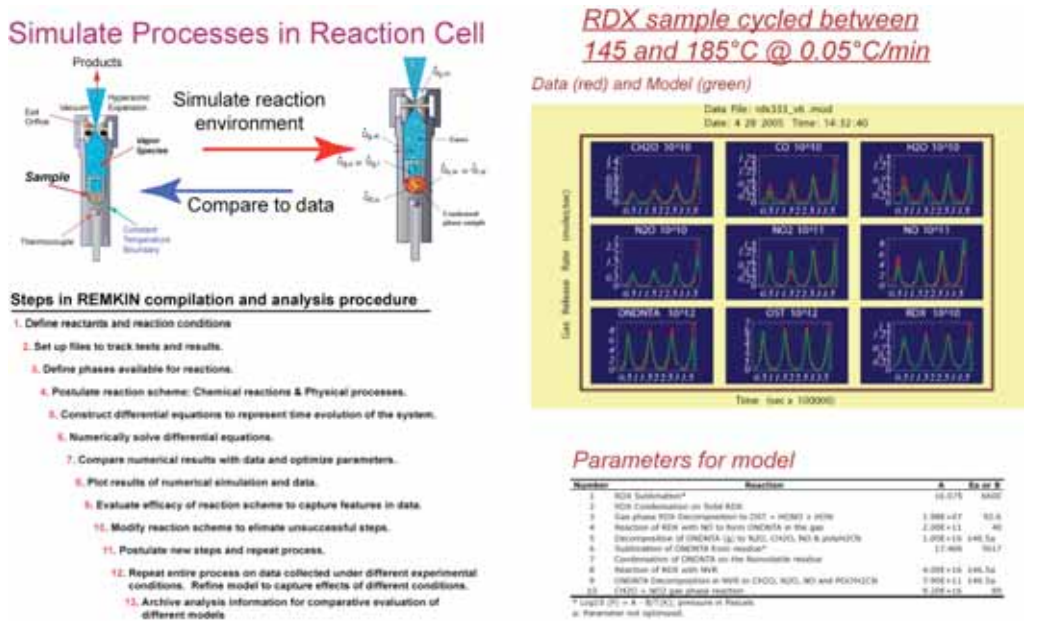

Figure 9. Illustration of process used to parameterize a reaction network using REMKIN.[1] The reaction model for the decomposition of RDX below its melting point is used for illustration. RDX is cycled between 145 and 185°C to obtain temperature dependent data needed to parameterize reaction network.

listed in Figure 9. It allows the user first to define the basis set of species, phases, LREs and reaction conditions. This provides the basis for postulating elements of the reaction network. Once a subset of the reaction network is postulated, REMKIN automatically constructs and solves the associated set of differential equations and the compares the results of the simulation to the measured data. This provides the user an assessment of the efficacy of the network elements used to characterize the reaction process and provides the means to optimize the parameters that characterize the individual reaction elements in the network.

This process is illustrated with the characterization of the relatively simple decomposition of RDX below its melting point as illustrated in Figure 9. A ten-step model is used to characterize the reaction process. It consists of (1) sublimation and condensation of RDX and the less volatile decomposition products, (2) the decomposition of RDX in the gas phase, and (3) the condensation of hexahydro-1-nitroso-3,5-dinitro-s-triazine (ONDNTA) on the surface of the RDX particles that leads to the emergence of a new LRE located on the surface of the RDX particles. The rate of reaction in this emergent LRE increases during the course of an experiment and eventually overtakes the rate of RDX reaction in the gas phase. The data from an experiment conducted below the melting point of RDX as it is cycled between 145 and 185°C is shown in red and the results from the parameterized model that simulates the reaction process is shown in green. Application of REMKIN in this manner allows us to develop reaction networks that characterize reaction processes of energetic materials that occur in the condensed phase that were heretofore not possible.

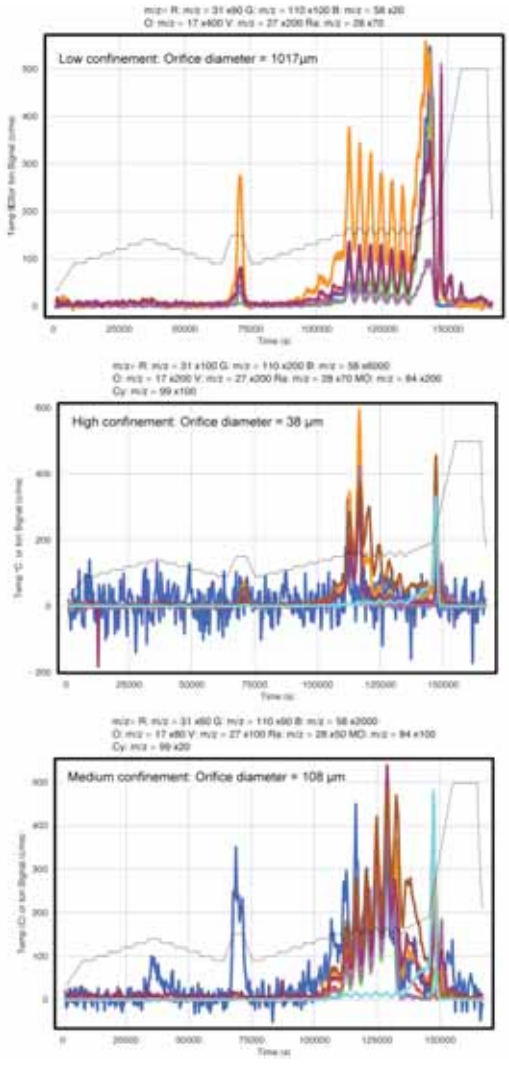

Figure 10. Ion signals representing species that evolve from TAGzT as it decomposes under three different gas confinement conditions. The black curve represents the temperature of the sample.

REMKIN is now being used to develop mathematical models to characterize the decomposition of TAGzT and eventually will be used to characterize the interaction between TAGzT and RDX, as well as mixtures of other ingredients.

To complete our illustration of the CoMPReHND paradigm, we exemplify the role of morphological features in the decomposition of TAGzT and then

provide a brief illustration of its reaction with RDX.

The morphological changes that occur during the decomposition of an OCiCP are often associated with the transformation of the reactant into a set of intermediate species during the course of the decomposition process. These morphological features are typically coupled with the rates of the underlying chemical reactions involving the various species and result in the net rate of their production during different stages of the reaction process. This behavior is illustrated in Figure 10, with the ion signals representing various species formed during the decomposition of TAGzT over a range of different gas confinement conditions.

The experiments are designed to investigate the various aspects of the decomposition process and gather the data that is necessary to create and parameterize the reaction network. The temperature of the sample (black curves in Fig. 10) is first varied in a set of isothermal steps between 90 and 140°C to look for the initial reactions in the decomposition process. The ion signal at m/z=58 represents the evolution of TAG, which occurs in the lower temperature region. This is followed by heating the sample to an isothermal temperature of 150°C, during which time some form of a nucleation and growth process occurs that creates conditions in the sample that promote the decomposition of TAGzT to N_2H_4, NH_3, HCN and N_2. Next, the sample is heated in another set of isothermal steps to gather more information on the decomposition process of TAGzT. This is followed by a series of heating and cooling cycles that span the decomposition of a major portion of the sample. This provides information on the temperature dependence of the underlying reaction processes as significant

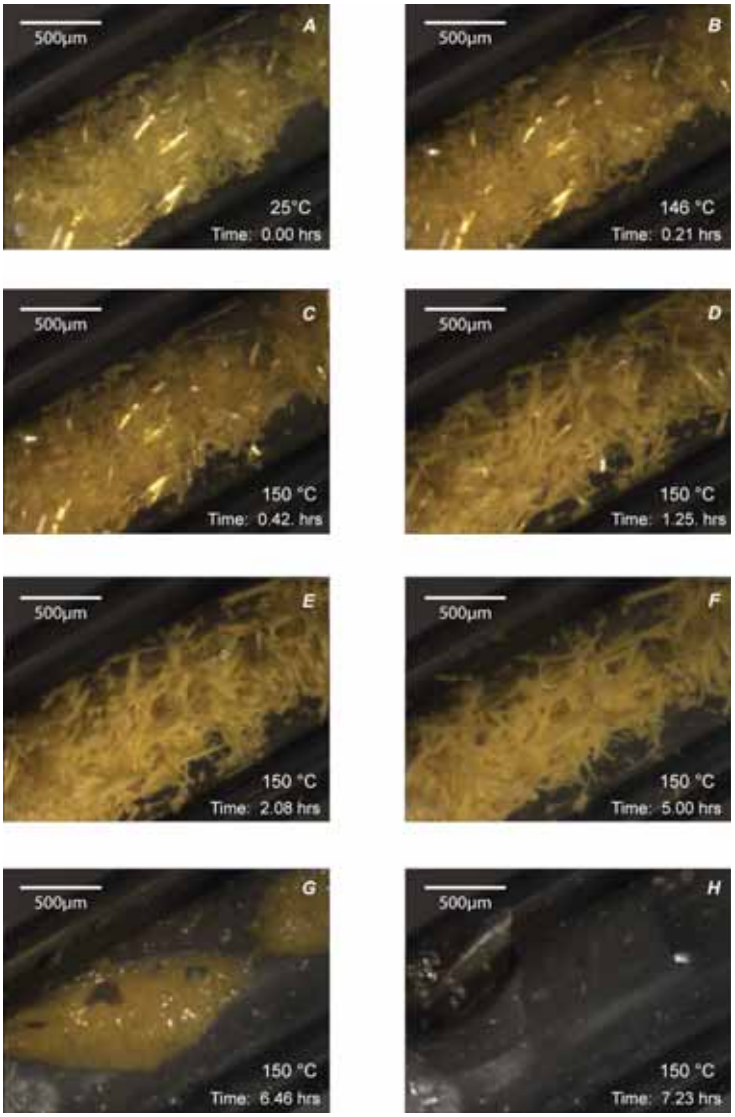

Figure 11. Pictures from a time-lapse movie of the decomposition of TAGzT at 150°C.

changes occur in the composition of the sample. The heating and cooling cycles are followed by another set of isothermal temperature steps that are aimed at determining the reaction process of the residue formed during the decomposition of TAGzT (note: it is intended that the TAGzT has completely decomposed by this point and only the less volatile decomposition products remain). Finally, this series of isothermal steps is followed by heating the sample to 500°C to examine the full decomposition of the remaining residue.

Closer examination of the results of the experiments conducted using three different gas confinement conditions shows significant differences in the various stages of the decomposition process. These may be correlated with the morphological changes observed in the decomposition of TAGzT using time-lapse microphotography using a hot-stage microscope (Fig. 11).

The first stage of the decomposition process involves the evolution of TAG(g) from the sample. While results from a series of experiments show that TAG(g) is in a "quasi-equilibrium" with TAGzT(s), the evolution of TAG from the solid TAGzT leaves behind a azobitetrazolate (ABT) product. The evolution of TAG from the surface of the particles implies that the ABT product remains behind on the surface of the TAGzT. Species derived from the ABT are likely to make up the clear liquid compound that appears to form on the surface of the TAGzT particles in the early stages of the time-lapse hot-stage microphotography measurements (panels E and F in Figure 11).

A comparison of the decomposition process under low and high confinement conditions shows a very dramatic difference in the rate of decomposition of TAGzT. Under low confinement conditions (top graph in Fig. 10), the identities of the products and their relative rates of formation during the course of the experiment do not change appreciably. In contrast, the decomposition of TAGzT under higher confinement (center graph) occurs much more rapidly under the same thermal conditions. In this case, the decomposition of

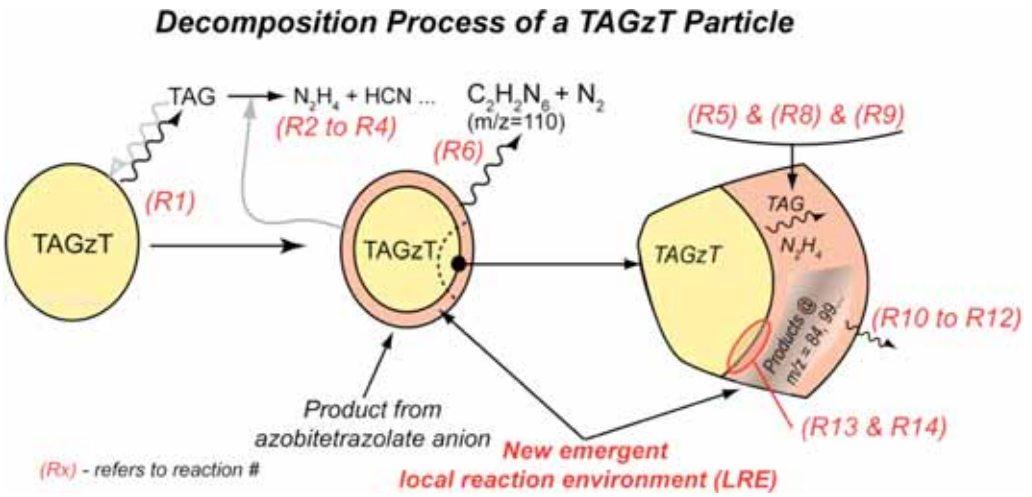

Figure 12. Illustration of the morphological structures of local reaction environments that are created during the decomposition of TAGzT. The elements of the reaction network that are associated with the LREs are indicated by their reaction number (see Fig. 8).

TAGzT is complete by the end of the second thermal cycle. In addition to difference in the rates of decomposition under low and high confinement, the amount and nature of the *low volatility residue* (LVR) formed in the decomposition of TAGzT differs as can be seen by the difference in the species that evolve from each LVR as it is heated to 500°C in the end of the experiment.

The complex nature of the decomposition process can be investigated more carefully by conducting an experiment in which the gas confinement is between the two extremes of the first two experiments. This is illustrated with the data in the third panel of Fig. 10, which was run using a 108 μm orifice. Notice that in this experiment the rate of reaction increases in each subsequent thermal cycle. Thus under these conditions the species that are being formed in the condensed phase that lead to a higher rate of reaction are being formed in a control manner that results in an increase the contribution from this region of the reaction network to the overall decomposition rate. The species formed in this part of the reaction network are probably the same ones that are operational in panels E and F in the time-lapse hot-stage decomposition of TAGzT at 150°C.

Using both the temporal behaviors of the ion signals that represent the species that evolve from TAGzT during its decomposition along with the microphotographs of the decomposition of TAGzT in the time-lapse hot-stage microscopy measurements, a diagram of the morphological features that play a role in the reaction network may be created as shown in Figure 12. The drawing illustrates four main morphological features of the decomposition process. First, the TAG evaporates from the surface of the TAGzT particles. This will be the dominant process during the first stage of the decomposition process. It is associated with Reaction R1 in the TAGzT reaction mechanism. Second, TAG can dissociate in the gas phase to N_2H_4, NH_3, HCN and N_2 (reactions R2 to R4). Third, a residue of intermediate species forms on the surface of the TAGzT particles. Initially, the species are associated with ABT, which decomposes to $C_2H_2N_6$ via reaction R6. Fourth, a new LRE is created at the boundary between the TAGzT remaining in a particle and the LVR on its surface. The movement of TAGzT decomposition products through the LVR on the surface of the particle will result in reactions such as those represented by R5, R8 and R9. This leads to a build up of the LVR on the surface of the particles. Once this LRE is established, then the LVR can continue to interact with the TAGzT via reactions such as R13 and R14. The LVR can also decompose via reactions such as R10, R11, or R12. As can be seen from the time-lapse photographs, eventually the TAGzT is consumed and the contribution from reactions such as R5, R8, R9, R13, R14 cease and the species that evolve for the remainder of the experiment evolve from the LVR via reactions such as R10 to R12.

It is useful to emphasize the importance of the concept of local reaction environments that we have introduced to describe the reaction processes of OCiCP. For our example of the decomposition of TAGzT, the following LREs are significant components that comprise the reaction network: (1) the gas-phase region above the sample; (2) the surface of the TAGzT; (3) the boundary between the surface of the TAGzT particles and the LVR that grows on its surface; and (4) the LVR that accumulates during the decomposition process. The reactions that occur in each of these LREs and the transport processes that influence their reaction rates will be different in each LRE. Changing the

reaction conditions will control the extent to which each LRE contributes to the overall reaction process as illustrated by the results shown in Figure 10.

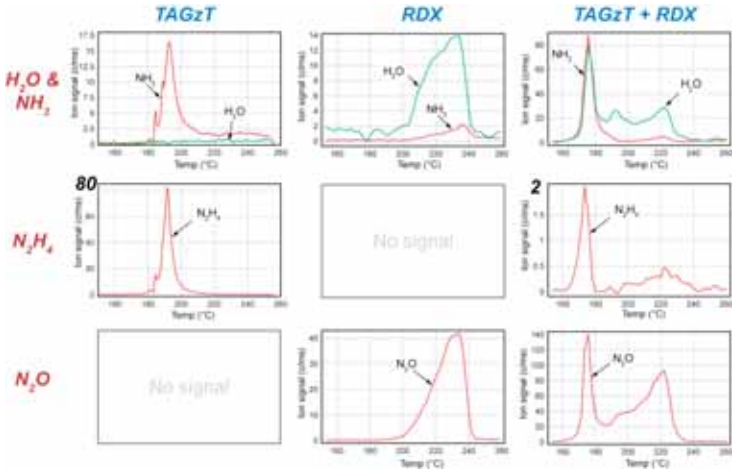

Figure 13. Illustration of how species, formed in the decomposition of RDX and TAGzT individually, interact when the two ingredients are mixed together. The decrease in the hydrazine signal and the rise in the H_2O and N_2O signals are indicative of a strong interaction between the two ingredients.

Reaction of TAGzT with RDX. We have used CoMPReHND to examine the interaction between TAGzT and RDX, which are being investigated for use in advanced gun propellants. It has been observed that the replacement of some RDX with TAGzT in an RDX-based gun propellant increases its burn rate significantly.[13, 14] The question of why this happens with a high-nitrogen compound such as TAGzT, but not with a similar compound such as GUzT was of interest to help guide the design of new energetic compounds.

While we have found that RDX and TAGzT interact with each other in a number of different ways, a key interaction that apparently leads to the increased burn rate of RDX-based propellants that contain TAGzT is the interaction of hydrazine with the RDX. The results showing ion signals that represent the key species in this interaction are presented in Figure 13 for decomposition experiments with TAGzT and RDX by themselves and a mixture of TAGzT and RDX. The results show that hydrazine reacts rapidly with RDX. This can be seen first by the significant decrease in the rate of evolution of hydrazine from the reaction cell when RDX is present (the maximum value drops from 80 to 2 counts/ms). Concurrently, with the generation of hydrazine from TAGzT there is an increase in the signals associated with water and N_2O. These are anticipated in a reaction between N_2H_4 and the NO_2 groups from RDX. Examining the change in the ion signals representing these species suggests that a simple reaction of N_2H_4 with the NO_2 groups to form H_2O, N_2O and N_2 may explain the interaction. However, experiments done with TAGzT and the ^2H, ^{15}N isotopomers of RDX show that the 44 signal is comprised not only of N_2O, but also as CH_2NO or H_2N_3 species. This, and other results from the isotopic crossover experiments, indicates that the hydrazine interacts with the RDX molecule and triggers its decomposition.

The effect on the burn rate can be explained by considering the morphological aspects of the reaction network and where and how hydrazine is likely to interact with RDX below its melting point. Figure 14 illustrates a number of LREs in which there can be a reaction between TAGzT, or TAGzT decomposition products, and RDX. The one that is most likely responsible for the increased burn rate is the reaction of RDX with hydrazine in the gas phase. In considering the various steps in the decomposition of RDX below its

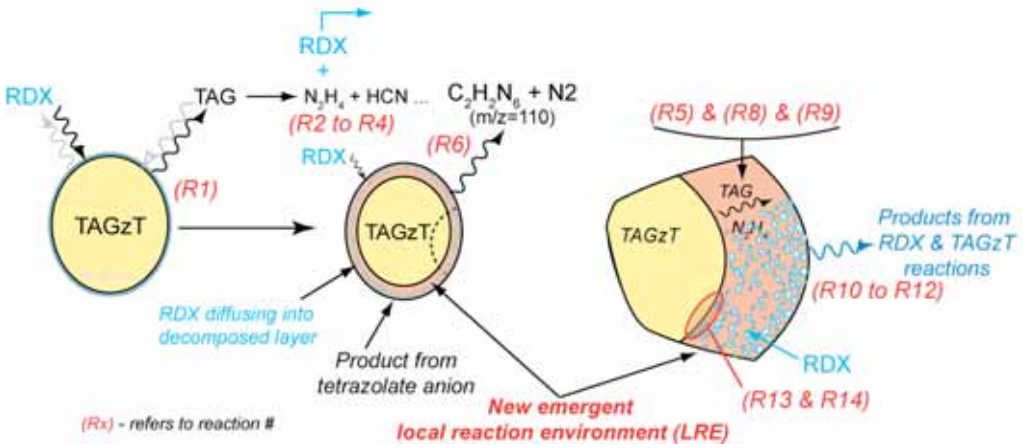

Figure 14. Illustration of the morphological structures of local reaction environments that are created during the decomposition of a mixture of RDX and TAGzT. The elements of the TAGzT reaction network that are associated with the LREs are indicated by their reaction number (see Fig. 8).

melting point (Fig. 9), one finds that the rates of sublimation and recondensation of RDX on the surface of the particles is approximately four orders of magnitude greater than the decomposition rate of RDX. This will tend to establish a "quasi-equilibrium" between RDX in the gas phase and RDX on the surface of the particle during the initial stages of heating in the combustion process. However, when a reactant, such as hydrazine, is introduced that reacts rapidly with the RDX, then the rate of reaction of RDX may increase by up to four orders of magnitude, if a sufficient amount of the new reactant can be introduced into the gas-phase environment surrounding the RDX particles.

Examination of the N_2O signal in Fig. 13 shows that the RDX reacts to form N_2O in two regions. One is when the TAGzT decomposes between 170 and 190°C. The other is between 200 and 240°C, which is attributable to the normal decomposition of RDX in the liquid phase. This is a good illustration that TAGzT accelerates the burn rate of the RDX-propellants by providing a new ingredient that interacts more rapidly with the RDX than RDX can decompose by itself. It clearly does not act as a catalyst, which would be expected to increase the reaction rate of many RDX molecules before it is removed from the system.

The results of our experiments with TAGzT and mixtures of TAGzT and RDX illustrate how the CoMPReHND paradigm has been used to identify the elements and linkages that comprise the reaction network of TAGzT and its interaction with RDX. We have recently quantified the data from these experiments and plan to work on developing the parameterized mathematical models of the reaction network, as has been done for RDX.

We have demonstrated that the CoMPReHND paradigm opens new opportunities to examine the reactions of complex heterogeneous organic materials in a manner that heretofore has not existed. While this work demonstrates a new approach for increasing our depth of understanding of complex reaction processes, it has also raised interesting

questions of how one creates numerical algorithms that presents data in a form that enables human perceptive capabilities to learn and and recognize patterns that lead to new discoveries and knowledge. Part of the further development of CoMPReHND will seriously consider how to systematize the presentation of the chemical, spatial and time-dependent information that enables rapid human learning that can be used for developing the pattern recognition required for new discovery.

Summary of Other Topics Addressed in This Project

The following sections are brief summaries of topics that were investigated with partial support from the ARO project. For each summary, there is a copy of either a corresponding paper or report presented in the Appendix.

Development of Chemical Imaging Precision Mass Spectrometry Apparatus (ChIPMA)

A new instrument has been designed and developed to investigate the reactions of organic compounds in local reaction environments (LREs). The new instrument is the first in the world to couple a focused ion beam and laser ablation surface analysis system to a high performance Fourier Transform ion cyclotron resonance (FTICR) mass spectrometer. The instrument is designed to collect mass spectra of ions, created by the interaction of focused liquid metal ion beams or lasers with a region of the sample surface, as a function of spatial location. The mass spectra are collected with either a reflectron time-of-flight (ToF) or an FTICR mass spectrometer. The mass spectral data is collected as a function of spatial location and are analyzed with numerical algorithms to provide the identification of chemical compounds as a function of spatial location within a sample. The unique operating characteristics of the FTICR mass spectrometer (i.e., high mass resolution, accuracy and range, and the ability to employ variety of MS/MS methods) allow complex materials to be examined. A copy of a report is included in the appendix that provides an overview of the design criteria, a description of the instrument and results from initial tests. The tests illustrate the operation of a number of features of the instrument.

The ChIPMA instrument has a broad range of applications that range from chemistry and material science to biotechnology and medicine. With respect to work related to this ARO project, it was envisioned that the instrument would provide the ability to examine LREs formed within partially decomposed energetic materials, such as HMX or HMX-based formulation. In our development of the instrument, it became apparent that success in examining energetic materials such as HMX would depend on our ability to prepare flat thin samples that could be coated, or place on specific types of substrates such as gold or silver. To prepare these samples, a Leica cryo-ultramicrotome was acquired and initial methods to prepare samples were started under another project. We did not have the resources to pursue the development of methods to prepare samples of energetic materials.

The ChIPMA instrument has been developed to a point in which the next steps needed to apply it to the investigation of reactions in energetic materials lies in the area of sample preparation and analysis.

Development of Reaction Modeling and Kinetics (REMKIN) compiler and analysis tool.

The Reaction Modeling and Kinetics (REMKIN) compiler and analysis tool is a set of numerical algorithms that are used to create mathematical models of reaction networks that characterize the chemical reaction processes of materials in the condensed phase. REMKIN was initially created to develop mathematical models of reactions of energetic materials, such as RDX and HMX, in the condensed phase.

REMKIN is now the primary set of numerical algorithms that are used in the implementation of the Concepts, Methods and Protocols for Reaction Hierarchy and Network Development (CoMPReHND) paradigm, which is used to investigate the reactions of heterogeneous materials in the condensed phase. It consists of two sets of numerical algorithms: REMKIN_Mechanism and REMKIN_Simulation.

REMKIN_Mechanism is used to identify the elements and determine the linkages in the reaction network that characterizes the reaction process of a material in the condensed phase. It allows the user to gather and assess the information collected in experiments using the STMBMS, FTICR mass spectrometer and time-lapse hot-stage microscopy. It enables the user to identify the species involved in the reaction process, determine their sequence of evolution, and identify and characterize local reaction environments that play a role in the reaction network. Its general purpose is to present data to a user in a format that allows the user to recognize patterns in the underlying data, which enables the discovery of the elements and linkages that comprise a reaction network. It is also anticipated that REMKIN_Mechanism will eventually assume the role of quantifying the data for our numerical simulations, which is now done with our TASHOW numerical algorithms.

REMKIN_Simulation is used simulate the behavior of a material's reaction network under the conditions found in a reaction cell used in an STMBMS experiment. This allows the user to determine the parameters that characterize the elements of the reaction network using an iterative method based on a cycle of simulation and comparison to experimental results. The code first prompts the user to enter the species, local reaction environments, and experimental conditions, which define the basis set that is used to construct a reaction network and determine its operating parameters. The user next defines a portion of the reaction network. The code automatically interprets this information and uses it to create and solve the associated set of differential equations, compares the solution with the results from the experiment and provides an assessment of the degree of agreement between the simulation and the data. This information is then returned to the user, who can refine the parameters for the portion of the reaction network being simulated or, if the results are satisfactory, add additional features to the reaction network until the full network has been parameterized.

In summary, the two main components of REMKIN implement of the two primary aspects of network development in CoMPReHND: (1) identification of network elements and linkages and (2) determination of parameters for network operation.

RDX & HMX Reaction processes

The reaction processes of RDX and HMX have been studied extensively in our work. The new work on these two compounds in this project has focused on the reaction of RDX below its melting point and the reaction of HMX in HMX-based formulations.

The results on the decomposition of RDX below its melting point have been published[7] and additional data has been collected that is being used to develop models for the decomposition of RDX in the gas phase (see interim ARO reports in Appendix). Since these experiments allow the contribution from reactions of RDX in the gas phase to be distinguished from reaction in on the surface of the particles, these results provide the first experimental information on the decomposition of RDX in the gas phase.

Our investigations on the decomposition of HMX have been expanded to include HMX manufactured in the United Kingdom, and HMX in LX-04, LX-10, LX-14, PBX9501 and EDC-37 formulations. We have also investigated the decomposition of the plasticizer, BDNPA/F, that is used in the PBX9501 formulation.[18] The results of these experiments have shown the following: (1) The decomposition of HMX below its melting point is still dominated by the nucleation and growth of local reaction environments within the HMX that results in the creation of micron size bubbles within the HMX. (2) Reaction occurs on the surface of HMX particles that is similar to that observed on the surface of RDX particles. (3) The reaction of HMX occurs more rapidly in PBX9501. At first, this was attributed to the presence of the BDNPA/F plasticizer increasing the reaction rate of HMX. However, in similar experiments with LX-14, which contains Estane, but no plasticizer, a similar increased rate of HMX decomposition was observed. Thus, these results suggest that Estane may introduce a new reaction pathway in the reaction network that results in the faster decomposition of HMX. The work on HMX is summarized in the interim ARO reports presented in Appendix.

The data on RDX and HMX are currently being incorporated into papers that we are writing on the development and use of the CoMPReHND paradigm.

HiN compounds

Two HiN compounds, TAGzT and GUzT, have been examined as part of this project. As described above we have discovered that hydrazine is one of the main decomposition products from TAGzT. We have also found in mixtures of TAGzT with RDX that the hydrazine formed from TAGzT reacts more rapidly with RDX than RDX can decompose by itself. The generation of hydrazine from TAGzT and its interaction with RDX most likely accounts for the increased burn rates observed in propellant containing TAGzT.

We have also found that the first step in the decomposition of TAGzT is the dissociative sublimation to form TAG and ABT. We first observed signals attributable to TAG (g) at ~110°C. This lower decomposition temperature may presents issues in formulating new propellants that require higher processing temperatures. We are currently working with synthesis chemists at LLNL (Phil Pagoria) and LANL (David Chavez) to develop new compounds that will generate hydrazine, but will be more stable than TAGzT.

A series of JANNAF papers summarizing our work on TAGzT has been published[15-17] and are included in the Appendix.

A New Paradigm for the development of Energetic Materials.

Historically, research into the chemical reaction processes of energetic materials has primarily focused on combustion issues. Since the nineteen sixties, the JANNAF Combustion Subcommittee has provided the focus for much of the work done in this community. In recent years, the number of practitioners in this area has been decreasing and funding to support this field of research has been dwindling. In 2005, members of this community assessed the current situation and decided that we should consider moving the focus of our work from creating detailed models of traditional energetic ingredients, such as AP, RDX and HMX, to investigations of new materials such as high-nitrogen compounds or ionic liquids.

To develop a plan to address this issues Bill Anderson (ARL), Brad Forch (ARL), Bob Shaw (AROP) and I organized and held a workshop on "R&D Required to Implement New Energetic Ingredients in Munitions". The workshop was held at the Battelle Conference Center, Aberdeen, MD on 29-31 August 2006 to assess the R&D required to implement new energetic ingredients in munitions. The participants discussed: (1) conventional methods for evaluating ingredients, (2) system requirements for new energetic materials, (3) what technically limits the implementation of new ingredients in munitions, (4) new experimental concepts for evaluating performance and deleterious features of new ingredients, and (5) new modeling/simulation methods for evaluating and predicting performance and deleterious features of new compounds and materials. From these discussions, it became apparent that the perceived risk for investing in the development of new energetic materials was high due to limited success over the past fifty years in implementing new ingredients in munitions. To reduce this perceived risk, it is important to have (1) programmatic efforts focused in the areas of controlled chemical propulsion, interaction at targets, and meeting IM requirements and (2) new experimental and theoretical methods that provide more insight into the reactive processes and can provide meaningful data 100 times faster and use 100 times less energetic material. Several teams have been formed to develop detailed research plans in the areas of synthesis and scaleup, formulations, super-small scale testing, modeling/simulation, new diagnostics, data mining, health and environmental compliance issues, and material design parameters. From these efforts, a new R&D paradigm is being developed to meet future munition requirements.

The findings of the workshop were summarized in an interim report presented at the 2006 JANNAF Combustion meeting[19] and a final report summarizing all presentations and outcomes from the workshop.[20] As a follow on from the workshop, Roger Swanson (NOSSA) and I summarized many of the ideas from the workshop and created an outline for a new paradigm for the development of energetic materials for future munitions. The new paradigm is described in a paper presented at NDIA and Eighth Australian Explosive Ordnance PARARI meetings.[21, 22] The general ideas have been summarized in a short article published in the MSICA Newsletter[23] and is reproduced here.

A NEW PARADIGM FOR R&D TO IMPLEMENT NEW ENERGETIC MATERIALS IN MUNITIONS

History of R&D and EM Developments

To maintain technologically viable munitions in the 21st century, strictly from the point of view of the energetic materials (EM) used for propellants and explosives in those munitions, we must answer the following questions: Will maintaining the status quo be sufficient?; Will the technology developed in the years following WWII be sufficient to provide energetic materials, propellants, and explosives required for future munitions and weapons to meet new threats and provide needed defenses?; and Will the existing synthesize and test paradigm used for the development of energetic materials be sufficient, or will a new paradigm be required?

Modern development of energetic materials for chemical propulsion and warheads can be traced back to the mid- and late-19th century and the beginning of the mid-20th century with the development of nitroglycerine, nitrocellulose, and other energetic organic nitrate/nitramine compounds, such as RDX, HMX, and TATB. Most sophisticated plastic bonded explosives and propellants were developed just before and during WWII. Most of the "new" solid rocket motor propellants were developed during the first two decades of the Cold War. This era preceded the development of today's computer enabled technologies. Hence, development utilized contemporary methods of the era, which used a cycle of synthesis and test to implement a trial and error approach. This is commonly known as the "Edisonian" method. This paradigm remains the basis for developing new ingredients for munitions.

Many munitions specialists and experts consider this paradigm for the development of new propellants and explosives as too slow (lacking time responsiveness), largely unsuccessful, or with only limited successes, and with high risk. Therefore, it is deemed unworthy of significant investment. In some circles, this paradigm is disparagingly referred to as "tweaking molecules". Historically, the design of new molecules focused on improving thermo-chemistry; i.e., more energy per unit volume. This equilibrium-based concept focused only on improving performance. That approach does not address the issues of reactivity that most often causes a new material to fail safety or aging requirements. Thus, the formulator is, in reality, tasked with creating a material with as much energy content as possible, but is so stable that the energy is not released until desired. The parameter space to design these materials is quite small and not likely to be found by trial and error.

To circumvent the limitations associated with the current "Edisonian" approach requires development of a new R&D paradigm that can facilitate rapid creation of new propellants and explosives, with orders of magnitude less material, and at the same time providing new data that can be used to guide the design of new compounds, composite materials, and applications. This new paradigm must also include development of new experimental methods and diagnostics tools to provide the material scientist and engineer with the experimental tools needed to design new formulations to meet the system requirements of the future.

The design of new materials to satisfy a small and restricted chemical parameter space is not unique to energetic materials. Similar challenges are encountered in the development of new drugs. The pharmaceutical industry must design or identify compounds with high efficacy to treat a specific disease, without detrimental side effects. This is analogous to EM development where efficacy is performance and satisfying safety and aging requirements are akin to avoiding detrimental side effects. Thus, using the pharmaceutical industries R&D paradigm for drug development to guide a new paradigm for EM development may hold promise.

New instruments, new experimental methods, and new computational capabilities will allow and facilitate the investigation of complex reactive systems that heretofore have not been available for use in investigating energetic materials. These tools have been applied to address complex issues in biological and biochemical systems and have revolutionized opportunities in these areas. These tools, however, have not been applied in our overall industry to address the complex reaction issues that underlie the behaviors of propellants and explosives. Our "Implementation Strategy" must be a new paradigm whereby we do not reject, but minimize, trial and error and maximize our current "technological opportunities" while continuing to develop new instruments, methods, and capabilities.

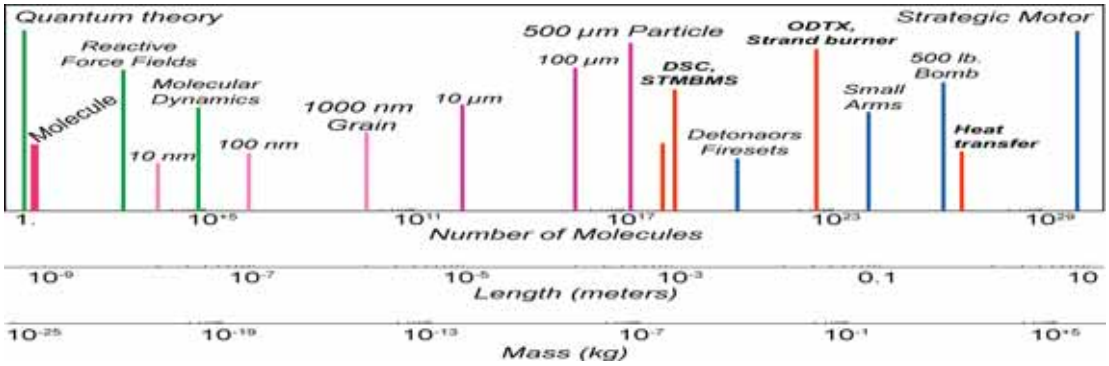

Figure 1. Illustration of spatial scales that may be characteristic of different reaction environments in energetic materials (magenta lines). Experimental methods (red), theory and modeling (green), energetic system articles (blue).

Figure 1. Scale of Issues

The ultimate goal of the scientific and engineering communities is to understand, measure, model, and predict the complex chemical processes that occur between the ingredients that comprise an EM formulation in response to thermal, mechanical and electrical energy. The heterogeneous nature of these materials makes it necessary to understand their chemical reactivity over a wide range of spatial scales. If these processes can be understood and modeled from the molecular/atomic to macroscopic spatial scales (see Figure 1), the future performance or behavior of macro-sized, orders of magnitude, infinitely more complex systems may be modeled with the advanced computational capabilities now available; and perhaps they may also be understood and their behavior predicted[1]. Table 1 projects the major payoffs that can be expected from

future investment in energetic material R&D, as additional focused research is accomplished.

A New Paradigm vs. a Shift of the Current Paradigm

Given the large number of requirements that must be satisfied to make a new propellant or explosive that meets very high performance goals while being as safe and as stable as possible, it is not surprising that the slow empirical "Edisonian" paradigm has not been successful for the development of new energetic materials. The pharmaceutical industry, for example, often encounters similar problems of having to satisfy many different types of requirements, ranging from efficacy to safety[2] and cost. It has overcome these obstacles by developing new scientific methods to probe the chemical, biological, and medical issues and requirements for new materials, including new methods to enhance screening and to develop a better understanding of diseases, in our terminology—requirements to guide the development of new drugs, vaccines, and treatment therapies.

Compared to the energetics product area, the pharmaceutical industry has somewhat clearer requirements statements, such as the development of drugs for well-described diseases. Their quest for product improvement in efficacy, safety and cost, however, can be seen as very similar to the need for the resolution of energetics products limitations that are well known and apparently acceptable status-quo (Table 1). Effective development of new energetic materials for munitions in the future must use a requirements-driven approach similar to that used by the pharmaceutical and biotechnology industries. This approach will require the development of a new paradigm that can develop new propellants and explosives much more rapidly, with orders of magnitude less material, and providing new data that can be used to guide the design of new compounds and composite materials.

Research Area	***Energetic System***	***Major Payoff Projected***
Propulsion		
	Rocket Motors	Enhanced energy in heavy lift systems.
		Energetic binders to increase I_{sp}.
	Guidance Systems	Tailorable burn rates to provide in flight control resulting in more precise target interdiction.
	Guns	Tailorable burn rates to permit reduced gun weight, erosion, corrosive products, and extended gun life.
Warheads	Micro-propulsion	Programmable on-board micro-propulsion devices to steer warheads for increased accuracy/lethality.
	Energetic Payload	Use of controlled payload output utilizing different types of energetic material to permit a desired type of

		reaction with a particular target.
High Energy IM Systems	Propulsives & Warheads	Enhanced energetics knowledge to optimize tradeoffs between insensitivity and system requirements
	Propulsives & Warheads	Enhanced IM knowledge to provide safer- high performance systems that are less costly to transport, store and maintain.
Surveillance (Aging)	Propulsives & Warheads	New evaluation methods that can provide a better means for understanding aging behavior to optimize the life expectancy, assure safe continued performance and overall lowest life cycle cost.

Table 1: R&D Expectations

Conclusions

There is a critical need to create a plan for R&D investment strategies that would enable the rapid implementation of new energetic ingredients, e.g., high nitrogen compounds, energetic binders, ionic liquids, and future materials, while meeting insensitive munitions (IM), aging, quality assessment and cost requirements. The disparity is growing between the availability of new energetic material technology and the need for increased functionality and preparedness in the future weapons arsenal. The transition from the current "paradigm" of the propellant and explosive material design and development process requires an ability to leap ahead of war-planners and weaponeers to provide futuristic possibilities that can both elevate performance levels and provide new warfare tactics and strategies.

That "leap ahead" can only be achieved with a new paradigm; one that embraces new sense, test, analyze, and design technology opportunities and developments and relies less and less on the "Edisonian" approach of the past. To achieve these ends we must develop near (2 year), mid (5 year) and long-term (10+ year) strategies that seek to accomplish the following:

(1) Establish an ongoing dialogue with war-planners to permit the early molding of weapons requirements based on reachable energetic material technology growth, contributing to the rapid deployment of emerging weapons.
(2) Develop initiatives to provide the material scientist/engineer with the experimental tools needed to design new formulations required to meet system requirements of the future.
(3) Develop strategies that produce the capability to design weapons for advanced land, air, and naval conflicts and space-based military encounters.

We should also explore the concept of a virtual laboratory enterprise or consortium to bring the scientific and engineering communities together to understand, measure, model, develop, and—most importantly—predict the actions and inter-relationships of complex energetic molecular formulations so that application developments can progress at a faster pace with greater assurances of safety, reliability, and performance.

Authors:

Richard Behrens Jr. Ph.D.; rbehren@sandia.gov

Sandia National Laboratories, Combustion Research Facility
P.O. Box 969, MS9052, Livermore, CA 94551-0969
Phone: (925) 294-2170, Fax: (925) 294-2276

Roger L. Swanson; Roger.Swanson@navy.mil
Naval Ordnance Safety and Security Activity, Farragut Hall (Bldg D-323)
3817 Strauss Avenue Suite 108, Indian Head MD 20640-5151
Phone: (301) 744-4447, Fax: (301) 744-6087

References

1. Swanson, R. L., Inter-Relationships between U.S. Navy Insensitive Munitions, Quality Evaluation (Aging), and Explosive Safety Programs. *Proceedings of the FINNEX 2002 Seminar*, 9-11 September 2002, Levi, Kittilä, Finland. p. 4.

2. Lackman, T, Screening of Potentially Explosive Substances. *Proceedings of the 13th Jan Hansson Symposium on Chemical Problems Connected with the Stability of Explosives*, Backaskog, Sweden, 6-10 June 2004 p1.

List of Publications

Peer Reviewed

Maharrey, S., et al., *High mass resolutions SIMS.* Applied Surface Science, 2004. **231-232**: p. 972-975.

Maharrey, S. and R. Behrens, *Thermal Decomposition of Energetic Materials 5. Reaction Processes of 1,3,5-Trinitrohexahydro-s-triazine (RDX) Below Its Melting Point.* Journal of Physical Chemistry, 2005. **109**: p. 11236-11249.

Behrens, R., *Thermal Decomposition Processes of Energetic Materials in the Condensed Phase at Low and Moderate Temperatures*, in *Overviews of Recent Research on Energetic Materials*, R.W. Shaw, T.B. Brill, and D.L. Thompson, Editors. 2005, World Scientific Publishing Co.: Singapore. p. 29 - 74.

Rauch, R. and R. Behrens, *Vapor Pressures and Thermal Decomposition Processes of Bis(2,2-dinitropropyl) acetal (BDNPA) and Bis(2,2-dinitropropyl) formal (BDNPA).* Propellants Explosives Pyrotechnics, 2007. **32**(2): p. 97-116.

Conference & JANNAF papers

Behrens, R. and S. Maharrey, *Reaction Kinetics of RDX in the Condensed Phase*, in *Proceedings of the 39th JANNAF Combustion Subcommittee Mtg.* 2003, CPIA: Colorado Springs, CO.

Behrens, R. *Thermal Decomposition Processes in Energetic Materials in the Condensed Phase at Low and Moderate Temperatures*. in *AIChE Engineered Particle Systems: Synthesis, Processes and Applications Topical Conference*. 2003. San Francisco, CA: AIChE.

Behrens, R. and D. Wiese-Smith, *Reaction Kinetics of RDX in the Condensed Phase*, in *40th JANNAF Combustion Meeting*. 2005, CPIA Publication: Charleston, South Carolina. p. June 2005.

Behrens, R. *Understanding the Effects of Age on the Reaction Processes that Underlie Insensitive Munitions*. in *Insenstive Munitions -- The Effect of Ageing Upon Lifecycle Workshop*. 2005. Helsinki, Finland: NATO MSIAC.

Behrens, R., et al. *Interim Report: Workshop on R&D Required to Implement New Energetic Ingredients in Munitions.* in *41st JANNAF Combustion Subcommitte Meeting*. 2006. San Diego, California: CPIA.

Behrens, R., D. Wiese-Smith, and H. Hayden. *Reaction Processes that Control the Thermal Decomposition of Mixtures of TAGzT and RDX*. in *41st JANNAF Combustion Subcommitte Meeting*. 2006. San Diego, California: CPIA.

Hayden, H., et al. *Thermal Decomposition of High Nitrogen Compounds: TAGzT*. in *41st JANNAF Combustion Subcommittee Meeting*. 2006. San Diego, California: CPIAC.

Behrens, R. and R.L. Swanson. *A New Paradigm for R&D to Implement New Energetic Materials in Munitions*. in *2007 Insensitive Munitions and Energetic Materials Technology Symposium*. 2007. Miami, Florida: National Defense Industrial Association.

Behrens, R. and R. Swanson, *A New Paradigm for R&D to Implement New Energetic Materials in Munitions*, in *PARARI 8th Australian Explosive Ordnance Symposium*. 2007: Melbourne, Australia.

Behrens, R., et al., *Workshop on Research and Development Required to Implement New Energetic Ingredients in Munitions.* 2007, Chemical Propulsion Information Agency: Aberdeen, MD. p. 1-765.

Behrens, J., Richard , D. Wiese-Smith, and H. Hayden, *Reactions of TAG-based Energetic Materials*, in *42nd JANNAF Combustion Subcommittee Meeting*. 2008, CPIAC: Boston, MA.

Conclusions

A new paradigm has been defined to address issues of reaction processes in OCiCP and OMiCP, which fall in a gap between chemistry and material science. The CoMPReHND paradigm is used to first identify the elements and linkages that comprise a reaction network that characterizes the reaction of OMiCP and then to create a mathematical model that characterizes the reaction network and determine its operating parameters through numerical simulation and comparison with experiment. The paradigm consists of: (1) new concepts developed to describe the type of processes that may be encountered in the reactions of OCiCP and OMiCP, (2) unique instruments to make the measurements needed to collect the data required to construct and parameterize the reaction network, (3) methods and protocols to design and conduct experiments that provide sufficient information to span a large portion of the parameter space for the network, and (40

numerical algorithms to analyze data and create and parameterize the reaction networks. It is important to note that there is a high degree of coupling between experiment and modeling/simulation.

To improve our ability to understand and accurately characterize the behavior of energetic materials, it is important to recognize the role the heterogeneity plays in controlling their reaction and develop new methods to assess and characterize it. We have introduced the concept of local reaction environments as a basis for characterizing reaction processes in these materials. It is important to also recognize that this heterogeneity may be either intrinsic or emergent. The results of our work with RDX, HMX and mixtures of high-nitrogen compounds with RDX illustrate various aspects of these issues.

The energetic materials community needs to develop a more scientific approach for the development of new energetic materials for future munitions. Support for research efforts that focus on developing the scientific tools needed to understand complex heterogeneous materials that fall in the gap between the paradigms used in the field of chemistry and materials science will be required.

References

1. Behrens, R., *Thermal Decomposition of HMX: Morphological and Chemical Changes Induced at Slow Decomposition Rates*, in *Proceedings of the 38th JANNAF Combustion Subcommittee Mtg.* 2002, CPIA: Destin, Florida. p. 397-408.
2. Ross, J., I. Schreiber, and M.O. Vlad, *Determination of Complex Reaction Mechanisms - Analysis of Chemical, Biological, and Genetic Networks*. 2006, Oxford University Press: New York City. p. 136.
3. Behrens, R., Jr., *Thermal Decomposition of Energetic Materials: Temporal Behaviors of the Rates of Formation of Gaseous Pyrolysis Products from Condensed-Phase Decomposition of Octahydro-1,3,5,7-tetranitro-1,3,5,7-tetrazocine.* Journal of Physical Chemistry, 1990. **94**: p. 6706-6718.
4. Behrens, R. and S. Bulusu, *Thermal-Decomposition Of Energetic Materials .2. Deuterium-Isotope Effects and Isotopic Scrambling In Condensed-Phase Decomposition Of Octahydro-1,3,5,7-Tetranitro-1,3,5,7-Tetrazocine.* Journal Of Physical Chemistry, 1991. **95**(#15): p. 5838-5845.
5. Behrens, R. and S. Bulusu, *Thermal-Decomposition Of Energetic Materials .4. Deuterium-Isotope Effects and Isotopic Scrambling (H/D; C-13/O-18; N-14/N-15) In Condensed-Phase Decomposition Of 1,3,5-Trinitrohexahydro-S-Triazine.* Journal Of Physical Chemistry, 1992. **96**(#22): p. 8891-8897.
6. Behrens, R. and S. Bulusu, *Thermal-Decomposition Of Energetic Materials .3. Temporal Behaviors Of the Rates Of Formation Of the Gaseous Pyrolysis Products From Condensed-Phase Decomposition Of 1,3,5-Trinitrohexahydro-S-Triazine.* Journal Of Physical Chemistry, 1992. **96**(#22): p. 8877-8891.

7. Maharrey, S. and R. Behrens, *Thermal Decomposition of Energetic Materials 5. Reaction Processes of 1,3,5-Trinitrohexahydro-s-triazine (RDX) Below Its Melting Point.* Journal of Physical Chemistry, 2005. **109**: p. 11236-11249.
8. Behrens, R., L. Minier, and S. Bulusu, *Coupling Experimental Data and a Prototype Model to Probe the Physical and Chemical Processes of 2,4-Dintiroimidazole Solid-Phase Thermal Decomposition*, in *34th JANNAF Combustion Subcommittee Meeting*, CPIA, Editor. 1997, CPIA Publication # 662: West Palm Beach, FL. p. 549-567.
9. Anderson, K., et al., *Modeling the Thermal Decomposition of TNAZ and NDNAZ.* 11th International Detonation Symposium, 1998. **1**: p. 239-245.
10. Behrens, R., S.B. Margolis, and M.L. Hobbs, *A Zero-Dimensional Model of Experimental thermal Decomposition of HMX*, in *11th International Detonation Symposium*. 1998, Office of Naval Research: Snowmass, CO. p. 533-543.
11. Behrens, R. and S. Maharrey, *Reaction Kinetics of RDX in the Condensed Phase*, in *Proceedings of the 39th JANNAF Combustion Subcommittee Mtg.* 2003, CPIA: Colorado Springs, CO.
12. Behrens, R. and D. Wiese-Smith, *Reaction Kinetics of RDX in the Condensed Phase*, in *40th JANNAF Combustion Meeting.* 2005, CPIA Publication: Charleston, South Carolina. p. June 2005.
13. Walsh, C. and C. Knott, *Gun Propellant Formulations with High Nitrogen Modifiers*, in *Propellant Development & Compatibility Subcommitte Meeting*. 2003, CPIA.
14. Knott, C., C. Walsh, and S. Prickett, *TPE Based Gun Propellants with High Nitrogen Modifiers*, in *Propellant Development and Compatibility Subcommittee Meeting.* 2004, CPIA.
15. Hayden, H., et al. *Thermal Decomposition of High Nitrogen Compounds: TAGzT*. in *41st JANNAF Combustion Subcommittee Meeting*. 2006. San Diego, California: CPIAC.
16. Behrens, R., D. Wiese-Smith, and H. Hayden. *Reaction Processes that Control the Thermal Decomposition of Mixtures of TAGzT and RDX*. in *41st JANNAF Combustion Subcommitte Meeting*. 2006. San Diego, California: CPIA.
17. Behrens, J., Richard , D. Wiese-Smith, and H. Hayden, *Reactions of TAG-based Energetic Materials*, in *42nd JANNAF Combustion Subcommittee Meeting*. 2008, CPIAC: Boston, MA.
18. Rauch, R. and R. Behrens, *Vapor Pressures and Thermal Decomposition Processes of Bis(2,2-dinitropropyl) acetal (BDNPA) and Bis(2,2-dinitropropyl) formal (BDNPA).* Propellants Explosives Pyrotechnics, 2007. **32**(2): p. 97-116.
19. Behrens, R., et al. *Interim Report: Workshop on R&D Required to Implement New Energetic Ingredients in Munitions.* in *41st JANNAF Combustion Subcommitte Meeting*. 2006. San Diego, California: CPIA.
20. Behrens, R., et al., *Workshop on Research and Development Required to Implement New Energetic Ingredients in Munitions.* 2007, Chemical Propulsion Information Agency: Aberdeen, MD. p. 1-765.

21. Behrens, R. and R. Swanson, *A New Paradigm for R&D to Implement New Energetic Materials in Munitions*, in *PARARI 8th Australian Explosive Ordnance Symposium*. 2007: Melbourne, Australia.

22. Behrens, R. and R.L. Swanson. *A New Paradigm for R&D to Implement New Energetic Materials in Munitions*. in *2007 Insensitive Munitions and Energetic Materials Technology Symposium*. 2007. Miami, Florida: National Defense Industrial Association.

23. Behrens, R. and R.L. Swanson, *A New Paradigm for R&D to Implement New Energetic Materials in Munitions*, in *Lettre MSIAC Newsletter*. 2007: Belgium. p. 3.

Appendices

Chemical Imaging Precision Mass Analyzer (ChIPMA) report

ARO interim reports summarizing HMX decomposition & REMKIN

Chapter from Overview of Recent Research on Energetic Materials

Reports on RDX, BDNPA/F, TAGzT and TAGzT interactions with RDX

Reports on "R&D Required to Implement New Energetic Ingredients in Munitions"

Development of a New Instrument to Investigate Reactions of Organic Compounds in Local Reaction Environments

Rich Behrens, Robert Bastasz, Sean Maharrey, Josh Whaley, Aaron Highley

Sandia National Laboratories, Livermore, CA

ABSTRACT.

A new instrument has been designed and developed to investigate the reactions of organic compounds in local reaction environments (LREs). The new instrument is the first in the world to couple a focused ion beam and laser ablation surface analysis system to a high performance Fourier Transform ion cyclotron resonance (FTICR) mass spectrometer. The instrument is designed to collect mass spectra of ions, created by the interaction of focused liquid metal ion beams or lasers with a region of the sample surface, as a function of spatial location. The mass spectra are collected with either a reflectron time-of-flight (ToF) or an FTICR mass spectrometer. The mass spectral data is collected as a function of spatial location and are analyzed with the AXSIA numerical algorithms to provide the identification of chemical compounds as a function of spatial location within a sample. The unique operating characteristics of the FTICR mass spectrometer (i.e., high mass resolution, accuracy and range, and the ability to employ variety of MS/MS methods) allow complex materials to be examined. This report presents an overview of the design criteria, a description of the instrument and results from initial tests. The tests illustrate the operation of a number of features of the instrument. Data is presented on the ToF secondary ion mass spectrometry (ToF-SIMS) analysis of a small part made using the LIGA process, and the use of the ToF and FTICR mass spectrometers to measure high mass species of CsI clusters, and polymers. A brief description of new methods to prepare and analyze polymeric samples using gold and silver metallization methods is presented along with initial data.

INTRODUCTION

Identifying and characterizing the reactions of organic compounds in local reaction environments (LRE) has broad applications in the fields of chemistry and material science. Degradation of materials can result in loss of performance, modification of safety response, and possibly failure of a materials used in many different applications. As the demand to reduce the cost weapon life cycle costs increases, the ability to predict failures will play a much more important role in maintaining an enduring stockpile.

In general, the failure modes will be related to change in the properties of materials used to construct various components, which in turn may lead to the failure of the component to meet its design specifications. For many manufactured systems (e.g., automobiles or computers), failure modes can be characterized by historical data gathered from the field. However, for military systems the number of units available for testing is often small and historical data is not sufficient for estimating life expectancy. Thus, other means to characterize failure modes must be developed, which are based on a more fundamental understanding of how the changing properties of materials may lead to failure.

To address these long-term aging issues of materials is challenging for two reasons. First, the reactive processes that control degradation are often complex and nonlinear. Thus, for many materials an understanding of the underlying processes that control degradation is not available. Second, the reactions occur at very slow rates in localized regions (i.e., interfacial boundaries), making it very difficult to detect and characterize these changes.

To address these issues, we embarked on the design of a new instrument to probe reaction processes on microscopic spatial scales in FY2000. Sandia has made a significant capital equipment investment to support this effort. In addition, funds from several different programs (DOE and DoD) have been used to design, develop, construct and test the new instrument.

To guide the design of the new instrument we selected an explosively driven isolator lens as a representative component that would illustrate the types of aging issues found in a wide range of components. A schematic cross section of the isolator lens along with the various types of materials and material interfaces found in the isolator lens are shown in Figure 1. The isolator lens is constructed from a polycarbonate housing, contains two different types of explosive formulations, PBX9407 (RDX based) and PBX9501 (HMX based), and a brass insert. During the manufacturing process, adhesive is applied at various material interfaces to assist in the assembly process. From a material degradation point of view, the isolator lens illustrates a number of the issues that are relevant to characterization of age-related degradation processes. First, since the explosives are composite materials, changes in the ingredients (i.e., the Estane binder, BDNPA/F plasticizer or HMX in the PBX9501) may lead to changes in the properties of the explosive that affect its performance. Second, there are a number of interfaces between different materials where reactions may occur that will affect the device performance. For example, there may be interactions between the copper or zinc in the brass and ingredients of the PBX9501. This may lead to a degradation of the explosive and result in a detonation wave that does not meet design specifications. Third, adhesive is used at the interface between the PBX9501 and the polycarbonate housing. There may be interactions at this interface that are detrimental to proper operation of the component.

Using the isolator lens as a guide, our objective was to design and construct an instrument that could identify and characterize subtle changes that may occur in the materials that comprise a component such as the isolator lens. This is a significant challenge for it requires the ability to identify and detect changes in *complex* materials that occur at *slow rates* in *microscopic* regions. The instrument must be able to identify a range of different types of materials, such as polymers, adhesives, explosives, ceramics or metals, on a microscopic spatial scale at very low concentrations. To achieve these objectives we embarked on the design and construction of an instrument that we refer to as the chemical microprobe/FTICR mass spectrometer. The instrument should be able to identify the

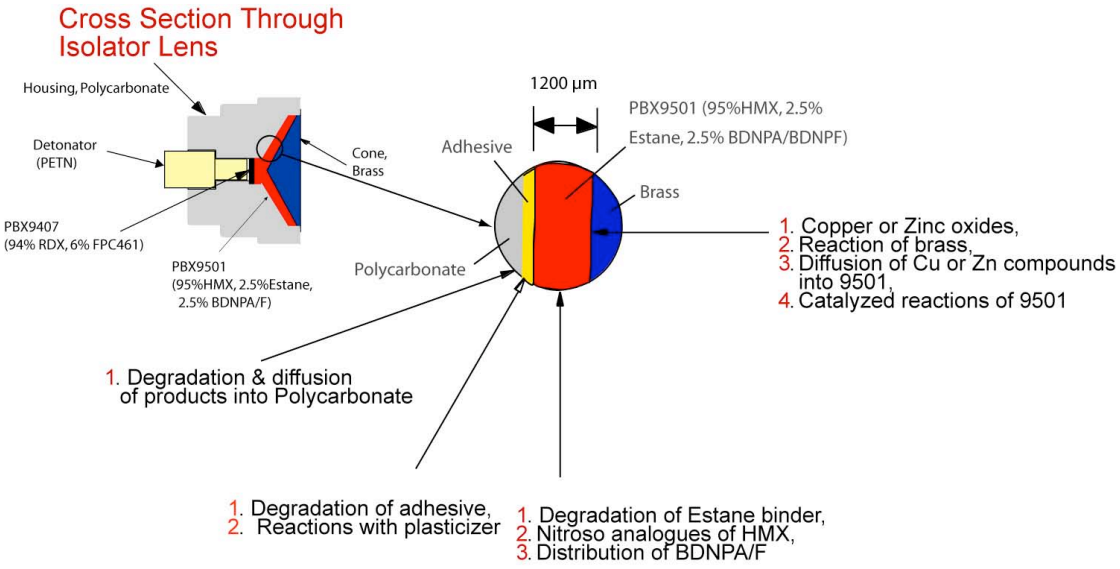

Figure 1. Cross-section through materials comprising an isolator lens. Items by red numbers list possible materials issues in various regions of the isolator lens.

chemicals and provide a map of their location in various regions within the component. This information will allow subtle changes in materials to be detected before they would have a detrimental effect on the performance or safety of the component. It would also provide new data on how various materials within a components change with time and provide a basis for developing age-aware models of the degradation processes.

Since the inception of this project we have designed and tested several different concepts in working toward our design goal. In the past year, we have finally succeeded in achieving our original design objectives. In this report we present an overview of the current design and illustrate the major features of the instrument with data collected over the past several months.

Now that the original design objectives for the instrument have been achieved, or exceeded, our next steps will focus on sample preparation of systems of interest and investigations of the physics and chemistry of the focused ion beam and laser sampling processes for polymers, organics, explosives and other types of materials.

APPROACH

To achieve our objectives required the design of a radically new instrument that utilized and coordinated recent advances in chemical physics (e.g., recent Nobel prize for matrix assisted laser desorption and ionization – MALDI, Koichi Tanaka, 2002), new mass spectrometry methods, computer-based experiment control and data collection, numerical algorithms to elucidate useful information from extremely large data sets, and the development of databases to track and retrieve the data. The following objectives were used to guide the design of the instrument:

1. Sufficient spatial resolution to probe material interfaces and mesoscale aspects of composite materials.
    a. Spatial resolution down to 100 nm.
    b. The ability to resolve morphological features of materials and correlate with chemical constituents.
2. Collect mass spectra of chemical compounds at each spatial location.
    a. Incorporate methods that provide high sensitivity, allowing smaller areas of a surface to be chemically resolved.
3. Mass spectra must be of sufficient quality to identify complex chemical compounds: polymers, explosives, propellants, alloys, electronics.
    a. Recognize that this is a tradeoff with sensitivity. For example, the number of different types of ions needed to identify an element is one, whereas the number of different types of ions needed to identify more complex molecules can range from tens to hundreds.
4. Detect the presence of minor chemical constituents in a background of other compounds.
    a. This is necessary to detect signatures of slow reaction processes associated with aging.
    b. Recognize that both sensitivity and degree of molecular complexity issues are also influential for this issue. This is the “looking for a needle in the haystack” problem. Recognize that this will require collecting large sets of data and using numerical algorithms to probe the data for minor constituents.

5. Provide microscopic imaging capability -- comparable to scale and resolution of SEM pictures.
    a. This must relate chemical constituents to morphological features of the sample.

To implement these objectives our design approach focused on the following areas:

1. The use of focused ion beams and lasers to remove microscopic samples of chemicals constituents from selected regions of a sample surface.
2. The use of state-of-the-art mass spectrometric capabilities to identify chemical species.
3. Use of new numerical algorithms to correlate spatial and mass spectral data and provide the identity and spatial location of chemical components.

A picture of the new instrument is shown in Figure 2. The instrument is comprised of two main sections: the surface analysis system, shown in the foreground and the Fourier Transform ion cyclotron resonance (FTICR) mass spectrometer shown in the background. The original design of the instrument was used to examine an aluminum/Ag-epoxy interface, used in high energy density capacitors, for evidence of silver segregation. The results from these measurements are shown in Figure 3 and illustrate the general aspects of our design goals. In these measurements a focused liquid metal Ga^+ ion beam was rastered across the surface of the sample, generating secondary ions that evolve from the surface of the sample and are detected with a mass spectrometer. In the image on the left, all of the ions are collected as the ion beam is rastered across the surface. The image shows the boundary between the aluminum on the left and the Ag-epoxy material on the right. To obtain the location of the aluminum and silver, the ion beam is divided into a series of short pulses as the beam is rastered across the sample surface. This allows the m/z values of the different ions to be separated by their time of arrival at the ion detector. By gating the detector with a specific time delay, ions at various m/z values will form the resulting image. The image on the right in Fig. 3 shows the result for gating aluminum and silver secondary ions.

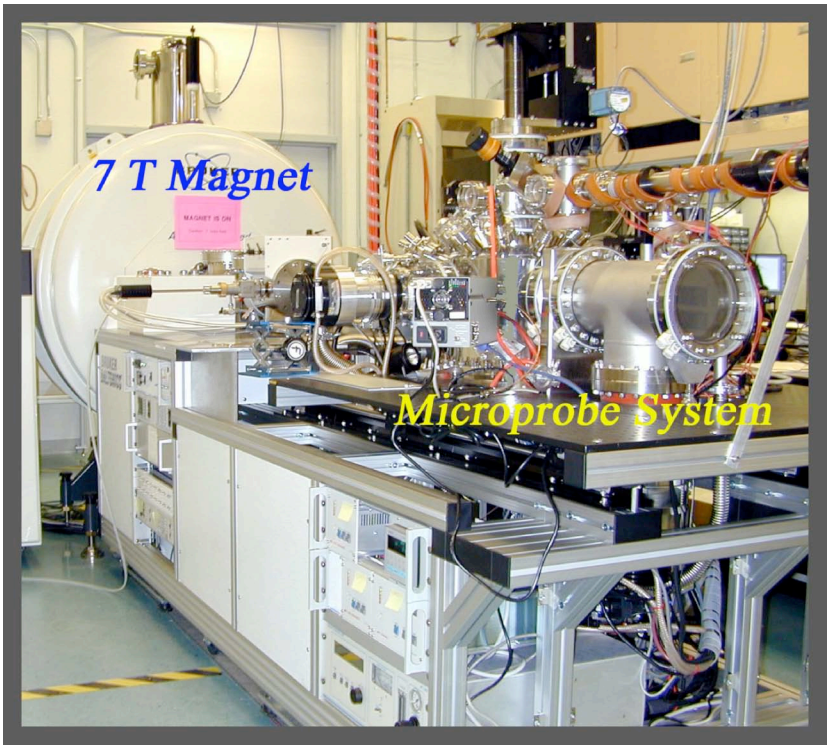

Figure 2. Picture of the chemical microprobe/FTICR mass spectrometry instrument, *circa* 2001.

The linear time-of-flight mass spectrometer, used in the original design, was not designed for high resolution (m/Δm ~ 50), since the high-resolution mass spectra were to be measured by the FTICR mass spectrometer. The ability to collect high-resolution mass spectra using the FTICR mass spectrometer was demonstrated with the Al/Ag-epoxy sample. The spectra collected are shown in Figure 4. The spectra show the presence of a number of different types of low mass ions that are comprised of Al, Ag, Ga, Na, and clusters of these atomic species.

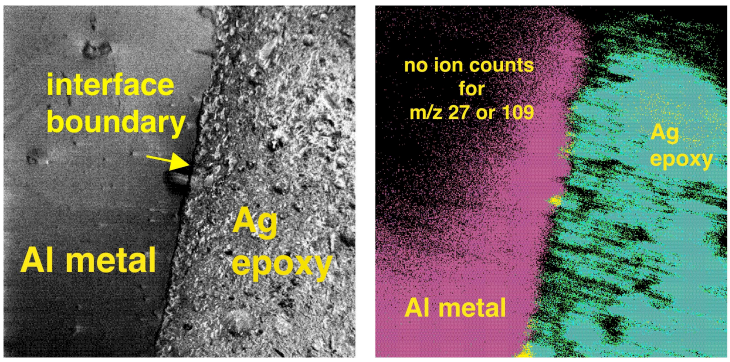

Figure 3. Images of high energy density capacitor aluminum/Ag-epoxy interface taken with the original design of CM/FTICR mass spec instrument. Images from Ga^+ ion beam induced secondary ion emission. Left image: total ion current. Right image: secondary ions of aluminum (magenta) and silver (green). Image size: 500 x 500 µm.

The data collected using the original instrument design illustrates the general features of our primary design goals. The chemical constituents through a section of material from an electrical component were mapped as a function of location and high-resolution mass spectra of the species from different regions of the sample were measured. Analysis of these results showed that there was not a significant amount of silver segregation to the Al/Ag-epoxy interface, which was thought may lead to failure of the component.

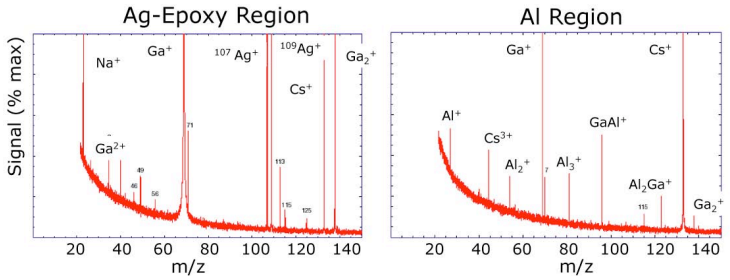

Figure 4. High resolution FTICR mass spectra of the Ag-epoxy and aluminum regions of the high energy density capacitor.

While the original design of the instrument met some of our design objectives, it fell short in several areas:

1. First, and foremost, it was difficult to transfer ions from the surface analysis system and trap them in the ICR cell of the FTICR mass spectrometer. Only ions at relatively low m/z values (m/z 20 to 500 Daltons) could be trapped. The types of ions that could be trapped were limited to metals or salts. Efforts to trap ions of organic or polymeric compounds that were generated in the surface analysis system were unsuccessful. Thus, our original design goal of examining complex polymeric or organic compounds could not be achieved. Creating ions in the surface analysis/microprobe system (Fig. 2) and transporting them into the ICR cell in the 7 Tesla magnet could not be achieved with the original simple design of the electrostatic ion optics. (Note: In developing our initial design concept for the instrument, we thought that an ion trap may be required to interface the surface analysis portion of the instrument to the FTICR mass spectrometer. However, cost and design time considerations eliminated the incorporation of an intermediary ion trap from the original design.)
2. Second, the resolution of the bent-axis linear ToF mass spectrometer was too low. The mass resolution of 50 made collecting mass spectra, even in the low mass region below 100 Da, of little use since individual masses could not be resolved. The bent axis linear ToF design was

selected to accommodate switching between collecting data with the ToF mass spectrometer and transporting the ions to the FTICR mass spectrometer for analysis. Linear ToF mass spectrometers are known to provide low mass resolution and bending the ion trajectories aggravates the problem. We were unaware of coaxial ToF designs{Kovtoun, 2002 #1101} at the time.

3. Third, it was not possible to collect high resolution, or moderate resolution, mass spectra as a function of spatial location. In our original operating mode, ions could be imaged only at individual m/z values. This would provide a spatial map of only the compound associated with the selected m/z value. In this mode of operation the operator would determine which ion to observe during each measurement and discard all of the ions being formed at other m/z values. This wastes information and is dependent on the operator's idea of which ions to measure. For the most part only the major ions will be monitored, as in our example on the Al/Ag-epoxy interface. To look for signs of aging it is necessary to detect and identify new constituents formed in the samples at very low concentrations. Thus, to achieve this objective it will be necessary to collect mass spectra at each spatial location in the image. By collecting an extensive amount of spatial and spectral information, the identities and locations of all species in the sample can be determined.
4. Fourth, new analysis methods to characterize the chemical composition of samples from large data sets of spatially resolved mass spectral data is required. To address this issue we incorporated data analysis code, AXSIA, developed by Paul Kotula and Mike Keenan (1800) to analyze spatially resolved X-ray data[3] and recently extended to analyze mass spectral data.
5. Fifth, it was cumbersome to switch between ToF and FTICR operating modes. In ToF mode the ions must be accelerated at high voltages to transport the ions through the drift region and provide enough energy to be detected by the microchannel plate ion detectors. To achieve these accelerating voltages the sample is floated at several thousand volts above ground potential. In contast, for FTICR mode the ions created at the surface must have low energies so that they can be trapped within the ICR cell for analysis.

These five limitations guided the redesign of the instrument and the development of the associated data acquisition and analysis software.

A schematic diagram of the current design of the instrument is shown in Figure 5. The surface microprobe, spatially resolved, high performance mass spectrometry instrument is divided into three main sections. One section consists of the surface analysis system, shown on the left-hand side of the diagram. The second section consists of a high-resolution mass spectrometer shown on a right-hand side of the diagram. The third system consists of the ion trap interface that allows ions to be transported from the surface analysis system, stored in the ion trap, and then passed on for analysis to the FTICR mass spectrometer.

The surface analysis portion of the system has been redesigned to address the limitations of the initial design. The surface analysis section can function as a stand-alone unit. It is comprised of the following five main sections: a high vacuum system, a micro positioning stage to manipulate the sample, a Gallium liquid metal Ion gun, UV and IR lasers, and a reflectron ToF mass spectrometer.[4]

The focused liquid metal ion gun and lasers are used to remove small portions of material from the surface of a sample. The liquid metal ion gun deposits energy from 25 keV gallium ions into small regions of the substrate, creating collision cascades, which results in the removal of representative chemical compounds from specific locations on the sample surface. The lasers deposit energy in specific regions of the sample surface in either the ultraviolet or infrared wavelength range, resulting in the removal of material from specific regions of the sample surface. Deposition of energy from

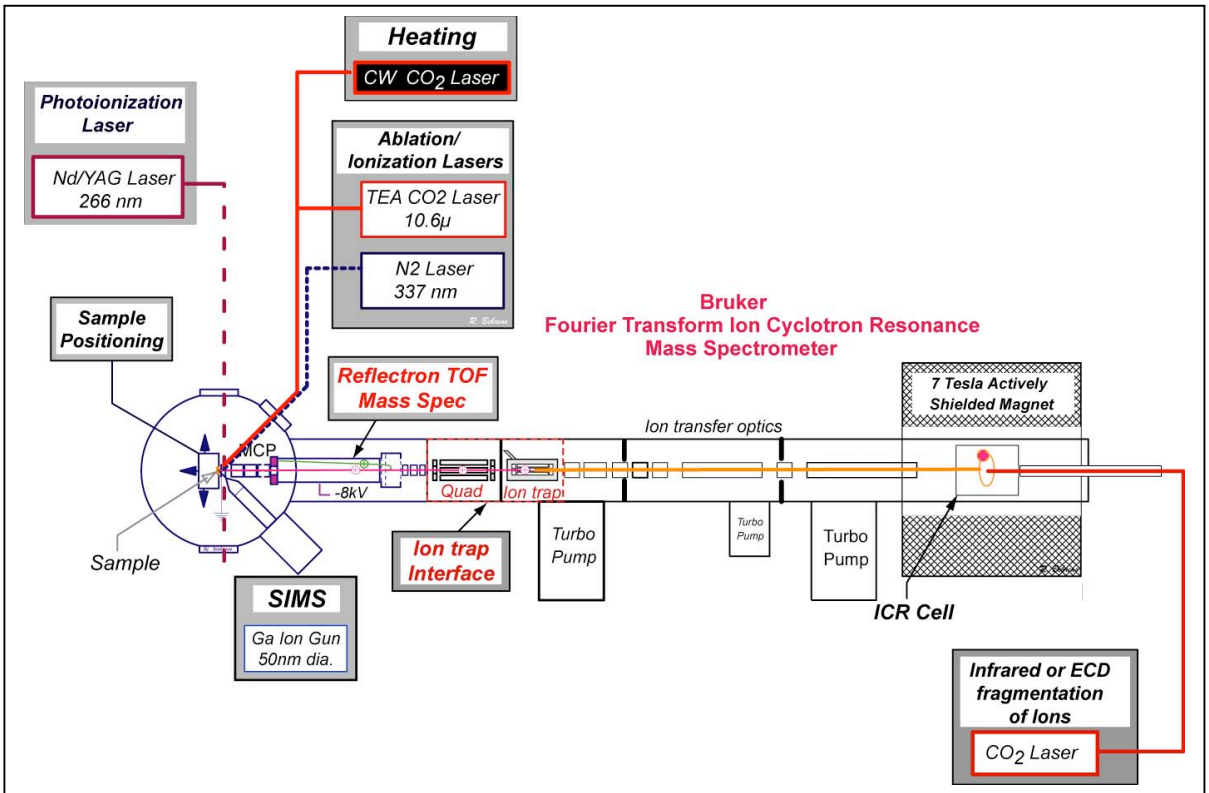

Figure 5. Schematic diagram of the surface microprobe, spatially resolved, high performance mass spectrometry instrument.

either the focused-ion beam or the lasers results in the ablation of material and the formation of ions from selected regions of the surface. Most of the material that is removed from a selected region of the sample surface is in the form of neutral atoms and molecules. A small portion of the particles leaving the surface is ionized. These ions are analyzed with the ToF mass spectrometer to determine their m/z values. The resulting mass spectra from a given point of the surface represent the chemical constituents at that location. To identify the characteristics of the chemical constituents, at the selected point on the surface, requires either understanding how the energy deposited by either the focused ion beam or the lasers interacts and modifies the chemical constituents as they are heated and expand into the vacuum, or running standards to calibrate the instrument for a particular type of measurement.

A new time-of-flight mass spectrometer has been designed and incorporated into the instrument.[5, 6] It is designed to maintain the sample near ground potential, and thus requires the mass spectrometer to float at a high potential (- 8 to -10 kV). A reflectron design was used to improve mass resolution. In typical reflectron designs, the axes of the incident and reflected ions from the electrostatic mirror are bent at an angle, allowing the ion detector to be outside of the pathway of the incident ions. However, our design required that the ion optics of the ToF mass spectrometer serve a dual purpose of both recording ToF spectra, when operating in ToF mode, and transmitting ions to the FTICR mass spectrometers, when operating in the FTICR mode. This required a coaxial design for the reflectron ToF mass spectrometer, in which the ions travel from the sample along an axis normal to the reflecting mirror and are reflected in an annular geometry back toward the microchannel plate detector along the same axis. This design requires that the incident ions must first pass through the center of the microchannel plate detector, before being reflected and detected.[6]

A new design to transport all ions from the surface of a sample to the FTICR mass spectrometer was also developed. In this design an ion trap assembly was incorporated into the system to serve as an interface between the surface analysis section and the FTICR mass spectrometer. In this design, ions generated at the sample surface are transported through the ion optics of the ToF mass spectrometer and stored in an ion trap. After a sufficient number of ions have accumulated in the ion trap, the ions are expelled from the trap and transported through another set of ion optics to the ICR cell in the FTICR mass spectrometer for analysis.

The ions from the surface analysis system pass into the ion trap interface, where they are guided by means of a quadrupole mass filter into an ion trap in which energy is removed from the incoming ions through collisions with inert gas in the ion trap. The ions are confined within the ion trap by means of a hexapole field and electrostatic end caps. In addition to storing ions, the ion trap interface can also be used for MS/MS analysis by varying the energy of the ions as they pass from the quadrupole into the ion trap. At lower energies the ions merely pass through the quadrupole and are stored in the ion trap, whereas at higher energies the collisions with atoms of inert gas in the ion trap lead to fragmentation of the ions and results in the formation of daughter ions. Identification of the daughter ions provides additional information that can be used to determine the structure of the original molecule.

As a result of these major modifications to the instrument, we have developed a two-part experimental methodology for generation of the experimental data that meets our design goals. First, fast acquisition ToF mass spectra of sample surfaces and material interfaces are imaged with high spatial resolution and analyzed for localized regions of chemical interest. This information may be used to probe for unusual mass spectral signatures, indications of known chemical degradation/decomposition of chemical constituents, or indicators of chemical migration/diffusion across interfaces. Second, the localized regions of chemical ambiguity can be further measured with the high mass resolution and accuracy of the FTICR instrument to obtain exact mass (empirical formula) and chemical structure information. These two techniques, coupled together, can provide unambiguous chemical mappings of sample interfaces at high spatial resolution.

Furthermore, our initial test results from FTICR-SIMS measurements of polymeric samples indicate that FTICR mass spectra can also be collected as a function of spatial location on the surface of a sample. This will enable the use of high resolution and high mass accuracy mass spectral data to be used for chemical analysis of samples using the AXSIA code. This capability will exceed our original design goals.

RESULTS

The design, construction, assembly and testing of the new instrument has been challenging. The most time consuming issues in the redesign of the instrument have involved operating the reflectron ToF mass spectrometer at high voltages (-8kV) within the vacuum chamber. This required special precautions to eliminate leakage currents between lens elements and the incorporation of new high-speed communication interfaces though fiber optic coupling to transfer the signals from the floating MCP detector (-10kV) to the data acquisition equipment.

The ion trap interface was designed by Bruker Daltonics and acquired though the Interfacial Bioscience Grand Challenge LDRD project (cost ~ $200k). It was designed as a front-end to interface electrospray ion sources (John Fenn – Nobel Prize 2002) to the FTICR mass spectrometer. Our initial results show that it works very well as an interface between the surface analysis system and the FTICR mass spectrometer.

In the remainder of this report we present data, acquired over the past several months, that illustrates the operation and capabilities of the new instrument. While the materials we examine are not from an isolator lens, they illustrate the major research and analytical capabilities of the instrument. We believe that this represents a major milestone in that we have created a new instrument that can examine materials in a manner not available anywhere else in the world. Its utilization will provide new means to bridge the gap between the atomistic and molecular world of the chemist and the macroscopic world of the materials scientists and engineers.

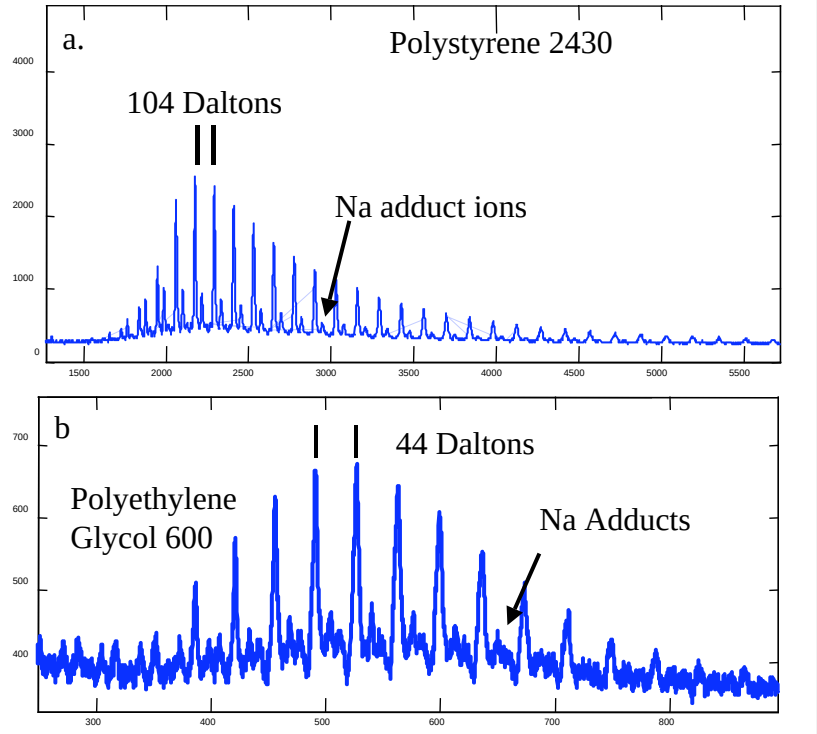

Figure 6. Reflectron ToF mass spectra of two polymer samples: a. Polystyrene 2430 oligomer distribution with the correct 104 Dalton separation; b. Polyethylene glycol 600 sample, monomer unit separation of 44 Daltons. The Na adduct distribution of each sample is also clearly indicated.

We present data on three types of materials to illustrate the main attributes of the instrument:

1. ToF mass spectra of polymer samples using SIMS.
2. The spatial and spectral analysis of a spring made using the LIGA process. The investigation probes the homogeneity of the Mn/Ni alloy created during the electrochemical deposition process.
3. The investigation of thin films of polystyrene (PS) using SIMS and the FTICR mass spectrometer. This investigation forms the basis for developing sample preparation methods to examine "real world" polymeric and composite materials.

ToF spectra of polymers. Figure 6 depicts two ToF-SIMS spectra of thin polymer films obtained with the new coaxial reflectron ToF mass spectrometer. These represent the first polymer samples to be successfully imaged with the ToF instrument. The upper image is the high mass region, extending to ca. 5000 Daltons, of a polystyrene 2430 thin film (M_w=2430), while the lower image is a polyethylene glycol 600 film (M_w=600). Both films were deposited on Ag substrates. What we can see in both images is that the oligomer distribution for each polymer is well resolved with the proper monomer unit separation, 104 Daltons for polystyrene and 44 Daltons for polyethylene glycol. The smaller Na^+ adduct distribution is also clearly indicated in each spectrum by the smaller peaks ca. 23 Daltons right of the large polymer peaks. These spectra were obtained under the same ionization and ion extraction/focusing conditions and demonstrate the mass range and broad mass band

transmittance capability of the new coaxial ToF mass spectrometer design. Further tests are ongoing on these same thin film samples to improve the ToF spectrum resolution and develop a reproducible sample preparation technique. Extension of the ToF spectrum and imaging techniques to thick polymer films and interfaces, characteristic of real component samples, is proceeding and is described below.

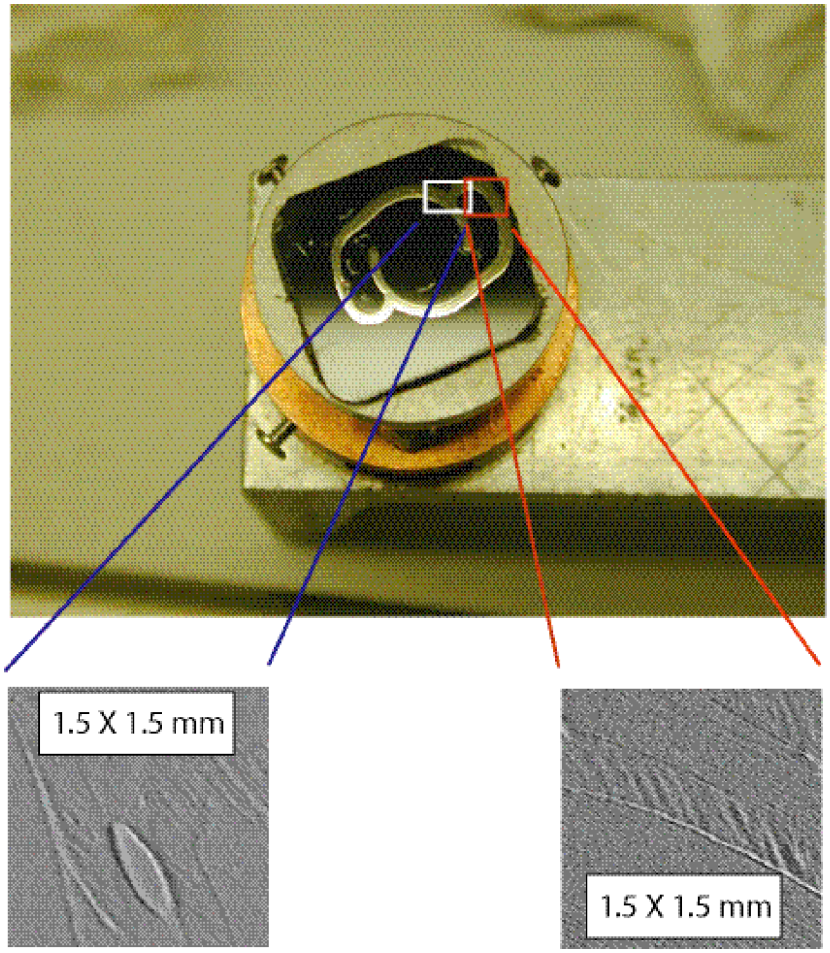

Figure 7. LIGA spring. Upper image is the optical picture of the complete spring, encapsulated in a polymer-potting matrix and mounted on a stainless steel sample mount. Lower images are Ga^+ ion beam induced secondary electron images of two regions of the spring taken with our instrument.

Spatially resolved SIMS images. To test the spatially resolved spectral imaging capabilities of the new instrument, we have examined a Ni:Mn spring actuator formed using the LIGA process. The degree of homogeneity of the Ni:Mn alloy formed during the electrochemical deposition of Ni and Mn during manufacture of the part is of interest, since this will determine the mechanical properties of the spring. The electrochemical deposition technique used to grow the spring should produce a uniform composition of Ni:Mn over its surface, but current methods of analysis do not have the spatial resolution to determine this effectively. We have conducted initial studies on this component in ToF-SIMS mode to determine if we can image the composition of the surface at higher spatial resolutions and determine if the composition varies.

A picture of the Ni:Mn spring actuator used for our analysis is shown in Figure 7. The spring is imbedded in a polymer-potting matrix, its surface is polished and then it is attached to a stainless steel sample mount. The focused liquid metal ion beam is used to generate secondary electrons from the sample surface and create images, similar to SEM pictures, of selected regions of the sample surface. Secondary electron images of two regions, which were examined for chemical constituents and composition, are shown in the lower pictures in Fig. 7. Region 1, indicated by white in the optical picture, shows the junction of the outer structure to the inner spring arm. This region contains a deposition defect, seen as the dimple in the middle of the image. Region 2, shown in red, is part of the outer spring structure.

To analyze the chemical constituents on the surface of the sample in this test case, SIMS spectra were recorded from 900 points in a 30x30 array positioned over the Regions 1 and 2 of the sample. The SIMS spectra were recorded by positioning the Ga^+ ion beam at the center of each pixel and summing 10,000 spectra at each of the 900 selected locations. Note that in these measurements the ion beam samples only a region in the center of each pixel and not the full area of each pixel. However, since this data was collected, new hardware was obtained and installed that allows the beam to be rastered, allowing the full area of each pixel to be sampled.

The SIMS data collected for each image was analyzed using the AXSIA code.[3] The AXSIA image analysis software calculates the best least-square mass spectrum basis set necessary to reproduce all of the mass spectra from each pixel in the spatial image array as simple linear combinations of the basis set.

The AXSIA analysis for a 30x30 ToF-SIMS study of the LIGA spring in Region 1 is shown in Figure

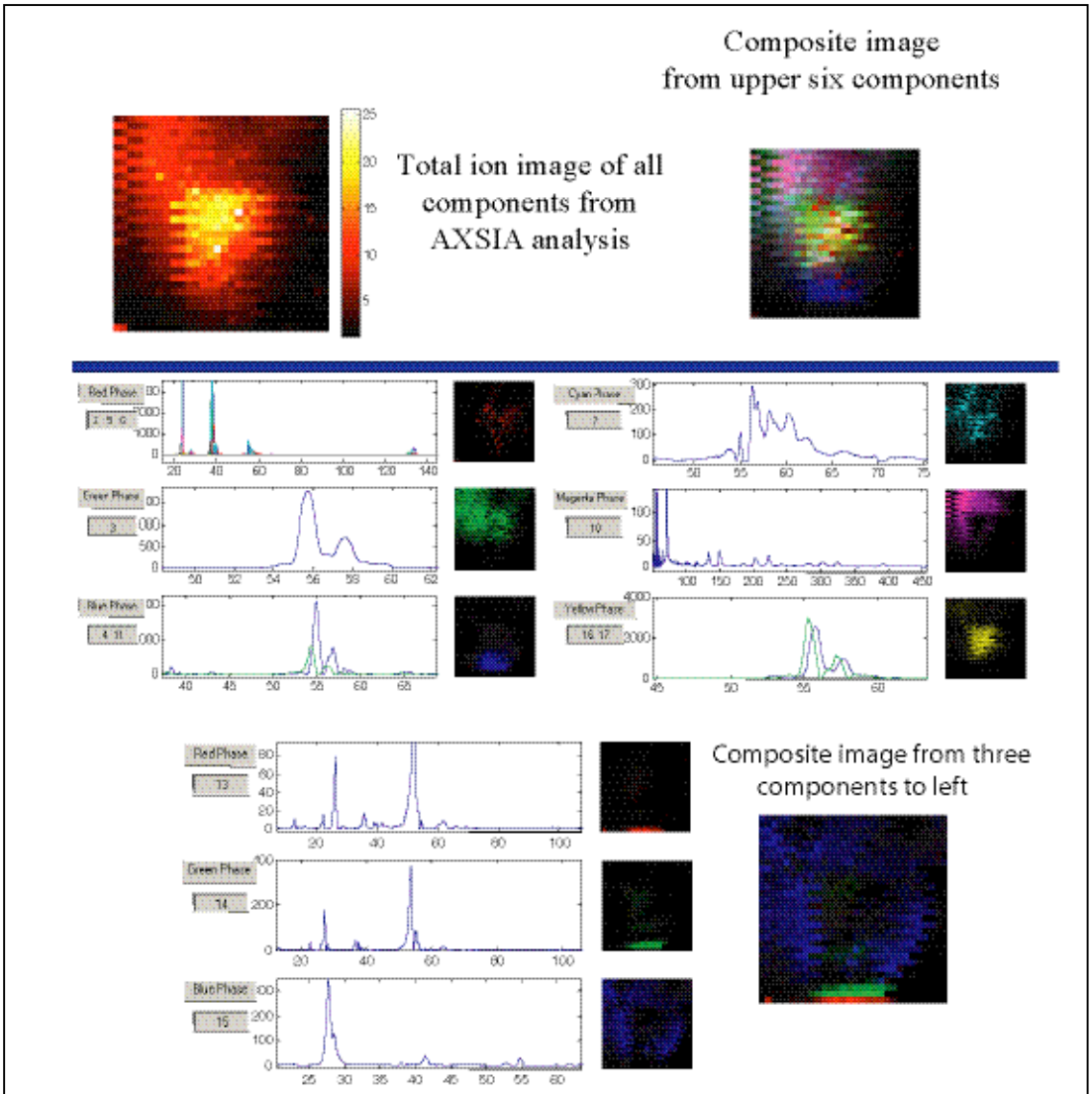

Figure 8. AXSIA spectral image analysis of Region 1 of the LIGA spring. Upper left spatial image depicts the total AXSIA 19-component spatial image. Upper right image depicts the composite image of the 6 components shown in the middle of the figure. Lower image depicts the composite image of the 3 components to the left of the image.

8. The analysis produced 19 pure components (elements in the basis set), representing the distinct chemical phases (mass spectra) in the 30x30 image. The upper left image shows the total 19-component spatial image, while the image to the right depicts the composite spatial image of the 6 components in the middle of the figure. The middle images show the 6 major components (mass spectra and corresponding spatial images) while the lower 3 components represent minor chemical phases, with their composite image shown to the right.

The total image and upper composite image indicates that the dimple feature shown in the Region 1 of Figure 7, images as a very strong feature, in relation to the surrounding spring material. This

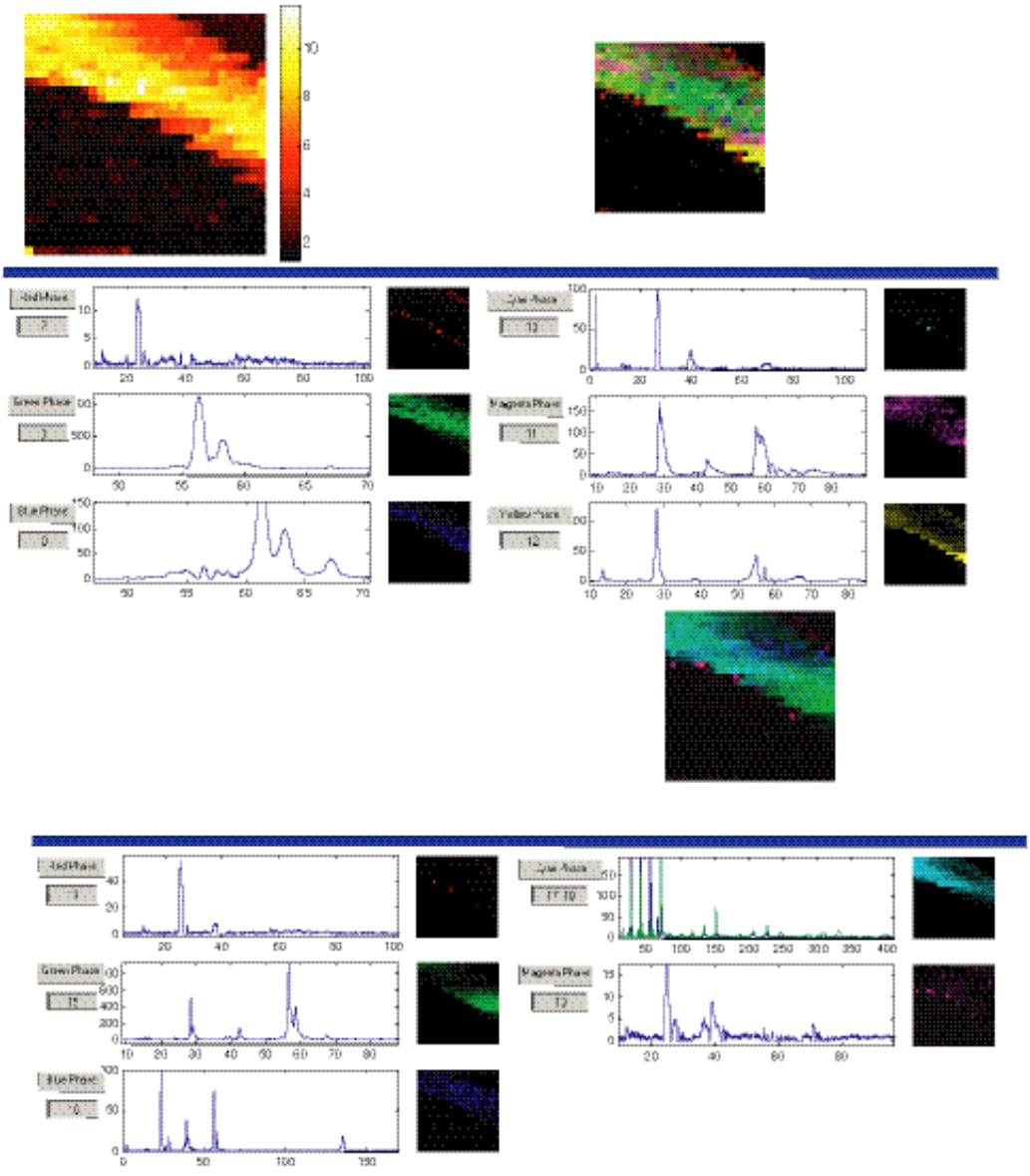

Figure 9. AXSIA analysis of LIGA spring region 2. Upper left spatial image represents the total 19-component image. Upper right image represents the composite image of the 6 components in the middle of the figure. The lower image is the composite of the 5 components at the bottom.

feature is best represented by the component image shown as the yellow spatial image in the middle set of components, the spectrum associated with this image indicates that this feature represents a strong Manganese signal (m/z 55). While the remaining spring is represented by the middle green component image and represents predominantly the Nickel component (m/z 56 and 58). The polymer-potting matrix is represented by the middle magenta image and the corresponding mass spectrum component indicates a high molecular weight polymer signature, while an unknown feature with the same nominal spatial profile as the polymer component is shown by the lower blue image component and represents a chemical phase of m/z 28. This feature is interesting in that there is a possibility of a minor silicon (m/z 27.977) contaminant in the LIGA process. However, the ToF instrument does not have the required mass accuracy or resolution to distinguish silicon from N_2 (m/z 28.006), so we cannot definitively determine this component. However, future measurements, using the FTICR mass spectrometer, should be able to identify these species.

The AXSIA analysis of Region 2 from the spring actuator is shown in Figure 9. The image in the upper left represents the total ion image from the analysis and the image in the upper right represents the composite image of the six components shown in the center of the figure. The principal nickel and manganese components are represented by the middle green and yellow spatial images, respectively. The Ni component is well distributed over the entire part, as it is the principal component in the LIGA spring, while the Mn is preferentially deposited near the edges of the part. The lower images, minor components, indicate that the Ni can be further separated into two components, the pure Ni, lower green component, and a Ni:Polymer component, lower blue image. This could possibly be do to the polishing of the part after potting, and would indicate that the LIGA surface was not uniformly polished before mounting.

FTICR-based SIMS spectra. One of the major achievements has been collecting SIMS spectra of

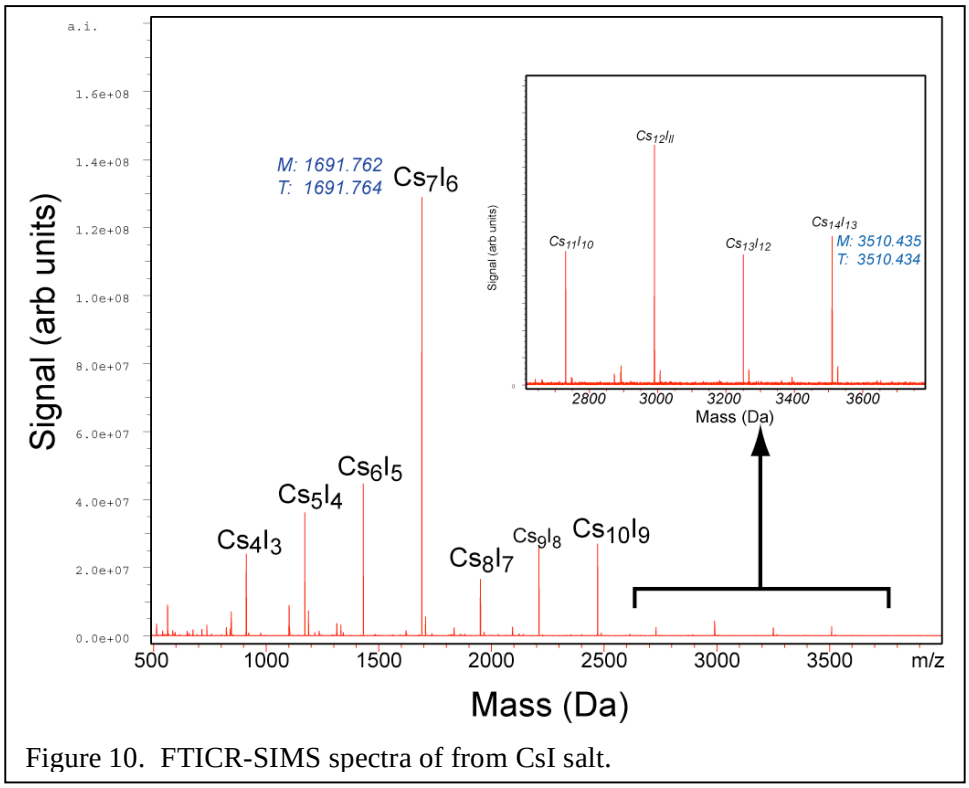

Figure 10. FTICR-SIMS spectra of from CsI salt.

samples from the surface analysis system with the FTICR mass spectrometer. This achievement has demonstrated that the new reflectron ToF transfer optics along with the new ion trap interface allows ions that are created in the surface analysis system to be transferred to the FTICR mass spectrometer for analysis.

The first sample used to test the system was cesium iodide (CsI), since this salt yields a large number of secondary ions of Cs and a range of different ions of Cs_xI_y clusters from the collision cascades induced by the incoming 25 keV Ga^+ ions. This allows the instrument to be tested and tuned over a broad mass range.

The measurements were made by first obtaining ToF-SIMS spectra to verify that the samples were producing adequate ion yield, and then switching the instrument to FTICR-SIMS mode. The switching from ToF to FTICR mode simply involves changing the polarity of the back element of the reflectron mirror from positive to negative polarity and setting a shallow voltage well to act as an initial ion deceleration stage before exiting the ToF side of the instrument and entering the FTICR ion trap interface.

An FTICR-SIMS spectrum of CsI clusters is shown in Figure 10. This spectrum shows the high mass range of the CsI clusters formed in the experiment. Clusters ranging from $Cs_4I_3^+$ up to $Cs_{14}I_{13}^+$ are observed. The accuracy of the mass measurements is shown for the Cs_7I_6 ion (measured mass = 1691.762; theoretical mass = 1691.764) and the $Cs_{14}I_{13}$ ion (measured mass = 3510.435; theoretical mass = 3510.434). This spectrum of CsI clusters illustrates the major improvement over the previous instrument design, in which only Cs^+, CsI^+ and Cs_2I^+ ions were observed.

The spectrum of polydimethylsiloxane (Fig. 11) is the first complex molecular species measured with the surface analysis/FTICR mass spectrometer. The spectrum shows groups of peaks representing oligomers of polydimethylsiloxane ranging from 18 to 29 monomer units. The inset graph shows the expanded spectrum of the n=20 oligomer. The high mass resolution capability of the FTICR mass spectrometer allows the individual m/z ions that form the isotopic distribution of the n=20 oligomer to be resolved and accurate measurements of each individual m/z ion to be determined. This allows the atomic composition of each oligomer to be accurately determined. The ability to measure mass spectra of polymers with this degree of mass accuracy and resolution will allow changes in the polymer at an atomistic level to be determined from the data.

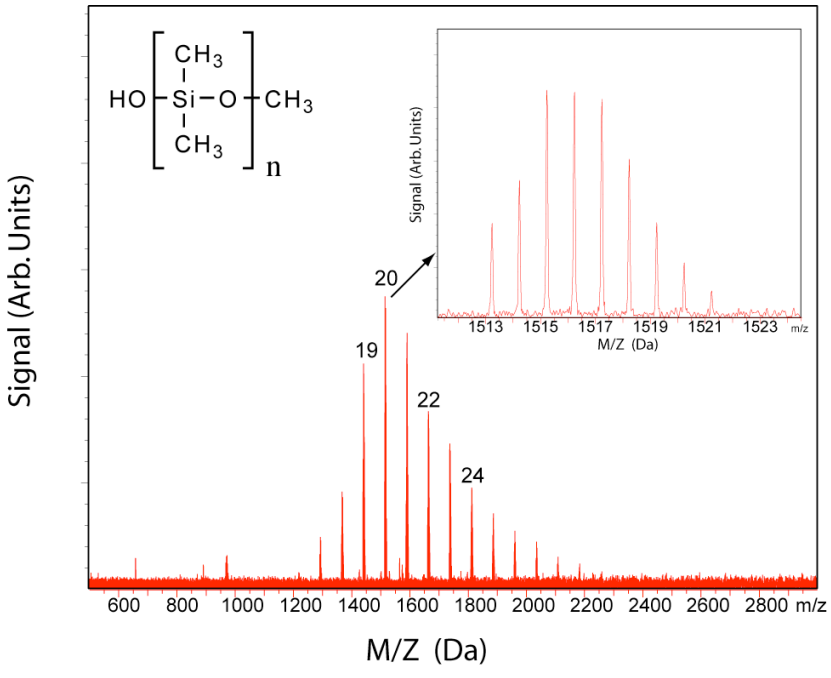

Figure 11. FTICR-SIMS spectra of polydimethylsiloxane deposited on silver foil.

The ability to collect these FTICR-SIMS spectra of CsI clusters and polydimethylsiloxane, in a relatively straightforward manner, demonstrates that we have achieved, and exceeded, our original design goals for the instrument.

Utilization of the laser ablation and ionization methods will be examined in the near future as we now move from the task of testing and debugging the mass spectrometry subsystems to developing methods to examine real world samples. We now move from the realm of the physics of ion optics, beam guidance, mass spectrometry, and instrument control systems to the realm of the physics of energy interactions with matter, molecular dynamics, fluid flow and the analysis of "real world" samples.

Analysis of "real world" samples. The next task is developing methods to probe chemical reactions in samples. Our first project in this area is an investigation of the degradation of hydroxy-terminated polybutadiene polymers, which are used in rocket motor propellants. This type of polymer is used in the B83 spin rocket motor propellant and may be used in the replacement spin rocket motors on the B61. It is also used extensively in NASA and DoD strategic rocket motor systems. Oxidation and degradation of the polybutadiene binder can lead to the creation of cracks within the propellant grain, which may lead to "crack burning" when the motor is fired and result in the failure of the motor.

Two general approaches can be used to examine the degradation of polymers in general, and polybutadiene in particular, using surface analysis probes such as SIMS or laser ablation and ionization. In the first approach, energetic ions or lasers are focused on the sample and a large amount of energy is deposited in a small volume of sample. This raises the temperature of the sample in this small volume and leads to the scissioning of many bonds and the formation of small molecular fragments from the polymer. Mass spectra of these low molecular weight fragments are measured and provide what is commonly referred to as the "fingerprint" region of the mass spectrum.

The finger print region of the mass spectrum may be used to examine the oxidation of a polymer. For example, the oxidation of polybutadiene leads to oxidation across the carbon-carbon double bond in the polybutadiene monomer unit.

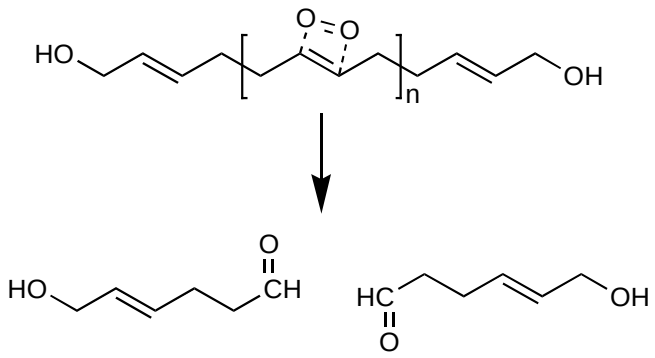

When a polybutadiene sample is examined with the surface probes before and after oxidation, the atomic composition of the ions in the finger print region will change. Prior to oxidation, ions will contain only carbon and hydrogen constituents and ions such as C_3H_4(40), C_3H_3(39), C_4H_5 (53) and C_4H_6 (54) will be observed. With an oxidized sample, additional ion fragments such as C_2H_3O (43), C_3H_4O (56), and C_3H_5O (57) will be observed. Thus, the extent of oxide containing species present in a sample as a function of location in the sample can be used to characterize the oxidation process of the polymer.

While measurements of oxygen containing species in the finger print region provide information about the oxidation process, they do not provide information about the extent of bond scissioning that occurs in the sample. To examine the change in the molecular weight distribution of the polymer due

to oxidation or other degradation mechanisms, the second general approach for examining polymers must be used: measuring the distribution of oligomers.

Sampling the oligomer distributions with ion beam and laser probes is a more challenging problem. The energy must be deposited in a manner that doesn't disrupt the polymer to such an extent that there are no longer any long chain polymer remaining that are representative of the oligomer distribution in the original sample. For the surface probe techniques, such as SIMS or direct laser ablation, that rely on not only ablating material but also forming ions, it is important that the energy deposited in the sample produce a sufficient quantity of ions for analysis. For the analysis of many carbon and hydrogen containing polymers, such as polybutadiene, the ion yield from direct irradiation of the sample is small. To circumvent this problem it has been found that by placing thin films of these polymers on either silver or gold surfaces, Ag^+ or Au^+ ion adducts of these polymers could be formed and analyzed in SIMS experiments or laser ablation experiments. A complex process determines the formation of ions of these polymers.

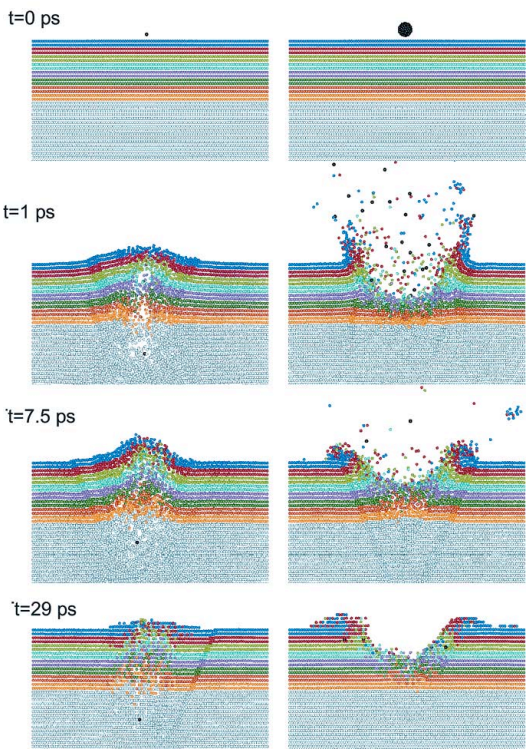

Figure 12. Molecular dynamics simulation of 15 keV Ga^+ and C_{60}^+ clusters impacting an Ag [111] surface. The layers of silver are color coded to track the motion of the Ag atoms. From Postowa et. al.[2]

Examining the processes that lead to the formation of ions of the polymers using the surface analysis probes provides insight into how to investigate real world samples. A number of molecular dynamics studies of these processes have been done over the past several years. Barbara Garrison and her group at Penn State University have examined both SIMS[1, 2, 7-10] and laser ablation.[11, 12] For example, using molecular dynamics simulations of the interaction of focused ion beams of Ga^+ and C_{60}^+, with a Ag [111] surface have been made[2] and the results are shown in Figure 12. The simulations show that the interaction of a 15 keV Ga^+ ion with the surface is quite different from the interaction of a 15 keV C_{60}^+ cluster with the surface. The Ga^+ ion penetrates quite deeply into the silver creating a collision cascade as it moves deeper into the sample, whereas the C_{60}^+ cluster deposits most of its energy in the upper layers of the sample. Thus, dividing the energy of the incoming projectile between 60 individual carbon atoms results in deposition of a larger portion of the energy near the surface of the sample.

The calculations show that the mode of deposition of energy in the surface of the sample has a large influence on the nature of the molecules and ions that are removed from the surface and upper layers of the sample. These types of calculations have been used to examine organic and polymeric compounds using SIMS and laser ablation probes. Two other molecular dynamics simulations illustrate the process of a liftoff of organic compounds from metal substrates. The interaction of an SF_5^+ projectile with biphenyl on the surface of a silicon substrate is illustrated in Figure 13. The incoming projectile strikes the Si surface, dissociates into atomic species and then deposits energy in the Si atoms, creating a collision cascade in the silicon. The motion of the Si atoms at the surface imparts energy to the biphenyl molecules on the surface and leads to liftoff of these molecules.

In another molecular dynamics simulation the liftoff of a polystyrene tetramer on a silver surface is illustrated in Figure 14. This calculation simulates the dynamics of a common class of methods used in SIMS experiments to characterize the polymer chains of lower molecular weight polymers (< 10,000 Da). In these methods thin films of polymers are deposited on either Ag and Au surfaces and examined with SIMS. It has been found that the large polymer chains form cations with Ag or Au as they lift off the surface. The signals associated with these large Ag or Au cations with polymer chains have been found to be several orders of magnitude larger than in experiments in which the projectiles from the focused ion beams interacted with either thin films of polymers on other substrates or with thick samples of the polymers.[13]

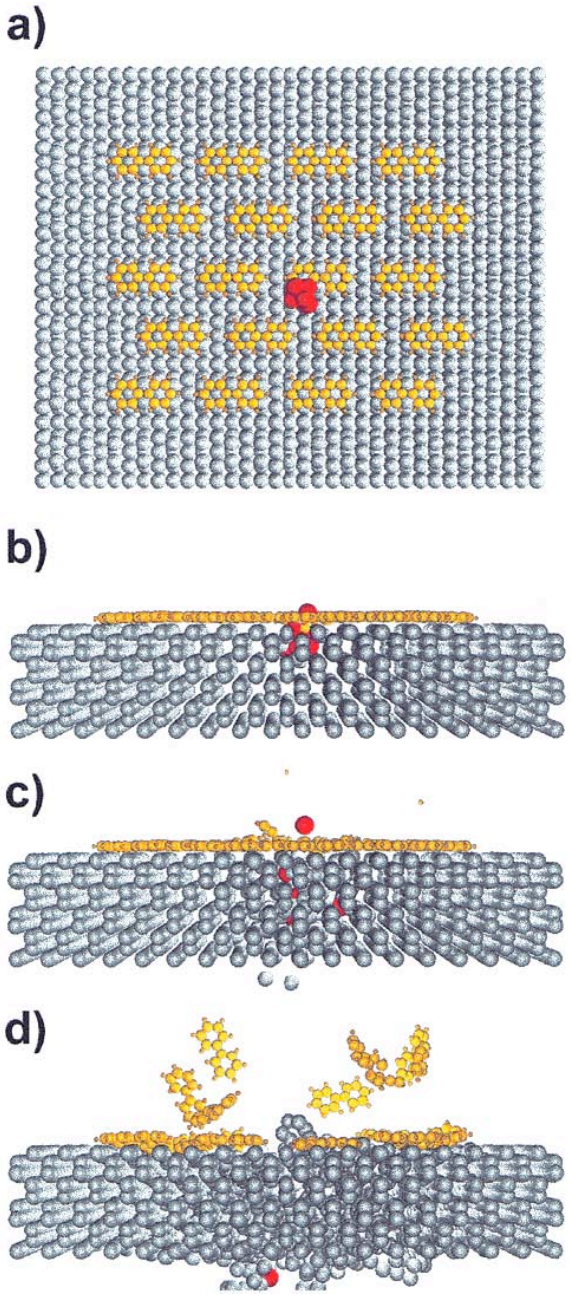

Figure 13. Collision cascade and ejection occurring for SF_5 bombardment of a layer of biphenyl molecules on Si [001]–(2x1). Si atom are represented by silver spheres, C and H atoms by gold spheres, and S and F atoms by red spheres. From Garrison et. al.[1]

From these types of experimental and molecular dynamics simulations of SIMS experiments with organic and polymeric compounds, several general features of the ion beam interactions with the sample substrate are important to consider in developing methods for analyzing polymeric compounds with SIMS (similar

features are also found in laser ablation methods). These features may be summarized as follows:

1. The incoming energetic particle should interact with a substrate, such as Si, Ag, or Au, allowing energy to be first transferred into atoms in the substrate and subsequently transferred from the excited substrate atoms to the polymer, leading to liftoff from the surface.
2. Distributing the energy of the incoming projectile amongst multiple atoms results in deposition of greater amounts of energy near the surface of the sample. This leads to increased ablation and ion yields. This effect is quite dramatic when comparing the ablation of a surface with Ga^+ and C_{60}^+ ions, but enhanced near surface material removal has also been observed with the use of gold clusters (Au^+ to Au_3^+).[14]
3. The type of element used for the substrate plays on important role in the yield of ions from the surface. Recent experimental work has shown that Ag and Au are good substrates for creating cationic complexes of Ag or Au with the polymer that can be detected in the SIMS measurements.
4. The flux of projectiles to the surface will also play a role in the types of species that are ablated and ionized as the energetic projectiles interact with the sample surface.

Using these general guidelines and recent work exploring the use of thin film gold coatings to enhance the analysis of real world polymer materials,[13, 15] we are undertaking a series of experiments aimed at developing this methodology to analyze materials from our weapon components with the new instrument.

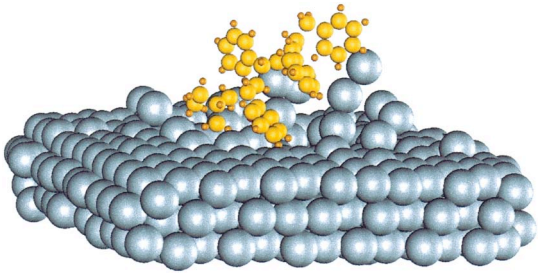

Figure 14. Cooperative uplifting mechanism for polystyrene on Ag. From Garrison et. al. [1]

In this set of experiments our near-term goal is to develop a method to examine the aging of hydroxy-terminated polybutadiene polymers used in rocket motor propellants. The fingerprint region of the mass spectrum will be used to measurement species that are formed by oxidation. The higher molecular weight region will be examined for evidence of smaller polymeric fragments from polymer scission. SIMS measurements of a polybutadiene sample can lead to charging of the sample, which can degrade the quality of the mass spectra and limit imaging capabilities. Using an electron flood gun for charge compensation usually circumvents this problem. However, we are investigating a more general approach, in which we coat the polymeric samples with a thin coating of gold. This coating will eliminate charging of the sample and may allow for a more controlled ionization of the underlying polymer by (1) providing a means for redistributing the energy of the incoming ion and (2) allowing metal cations of the polymer to be formed during liftoff from the surface.

To develop this method and perform initial tests with the new instrument, a series of samples have been prepared for investigation. A schematic diagram illustrating the three different types of samples is shown in Figure 15. Three types of samples are prepared. One sample has a monolayer of polymer on the surface (Fig. 15a). The second sample has the same substrate with a 10 monolayer thick film of polymer on the surface (15b). The final sample has a thick film of polymer on the substrate surface and is coated with a thin layer of gold (~ 20 nmoles/cm2) coated on top of the polymer film (15c). Samples a and b are prepared by depositing a 100 nm thick film of Ag or Au on a polished silicon substrate. For preparation of gold films, the silicon surface is first coated with a ~10nm thick titanium film to improve adhesion. The polymer films are spin-coated on the metal substrates.

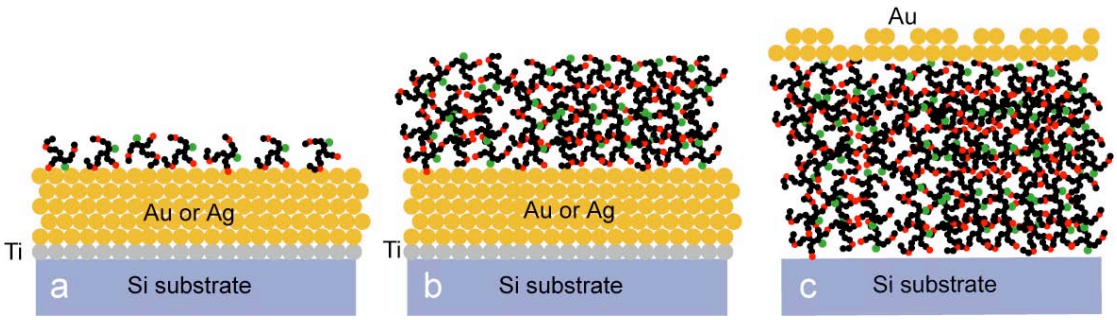

Figure 15. Schematic diagram of samples being used in experiments to develop methods to examine real world samples of polymer and component materials. A. One monolayer of polymer on Au or Ag substrate; B. 10 monolayers of polymer on Au or Ag substrate; C. Thick film of polymer with 2 nm film of Au coating.

Sample c is prepared by first spin-coating the polymer on the silicon substrate and then vapor depositing a 2 nm layer of gold on top of the polymer film.

A series of samples have been prepared with polystyrene (MWa = 2430) and polybutadiene. To date we have examined samples of polystyrene coated on Ag substrates. Samples with submonolayer, one monolayer and ten-monolayer coverage have been examined with FTICR-SIMS measurements. These initial measurements were primarily used to test and adjust the new surface analysis to FTICR mass spectrometer interface. A mass spectrum of the 10 monolayer thick film on the Ag substrate is shown in Figure 16 for the high mass region of the spectrum. The mass spectrum contains two regions with different types of ions. From approximately 1000 to 1400 Da there are a series of groups of peaks that are silver clusters. From approximately 1500 to 2500 Da are the oligomers of the polystyrene complexed with a silver cation. The integers from 12 to 20 represent the number of monomers in each oligomer. It is interesting to note that the groups of peaks representing the silver clusters are clearly identifiable as silver clusters, since the mass peaks are separated by 2 Da (^{107}Ag and ^{109}Ag). However, examination of the group of peaks associated with each type of cluster reveals that none of the groups contained only silver atoms. The one group that has been identified is the $Ag_{12}K^+$ cluster. It is interesting that only silver clusters that form a complex with another element are observed.

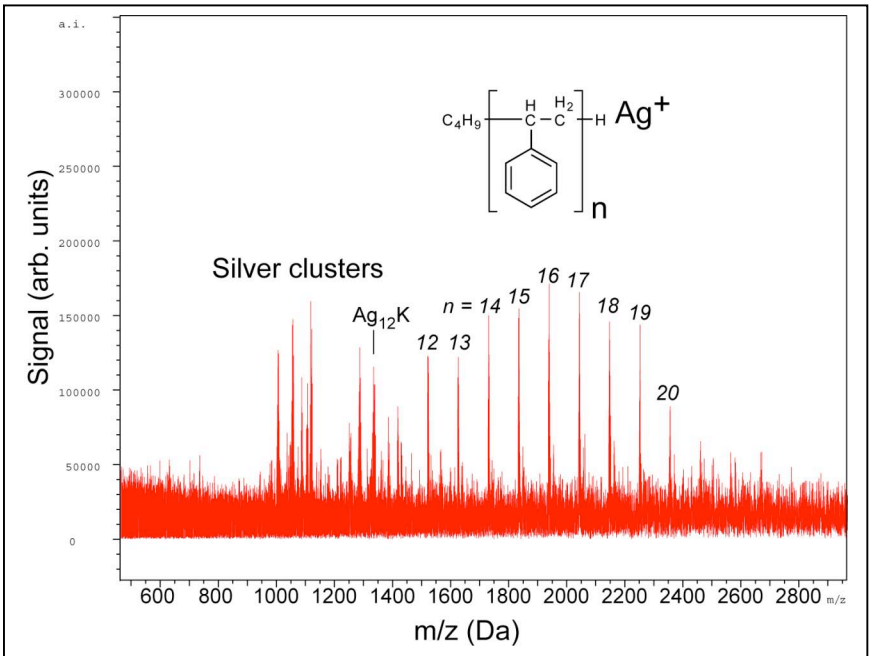

Figure. 16. FTICR-SIMS spectrum of a 10 monolayer thick sample of polystyrene coated on a Ag substrate.

To illustrate the unique capabilities of the instrument the expanded spectra of the n=16 and n=18 oligomers are shown in Figures 17. The high mass resolution provided by the FTICR mass spectrometer allows each peak in the isotope distribution for the selected ion to be

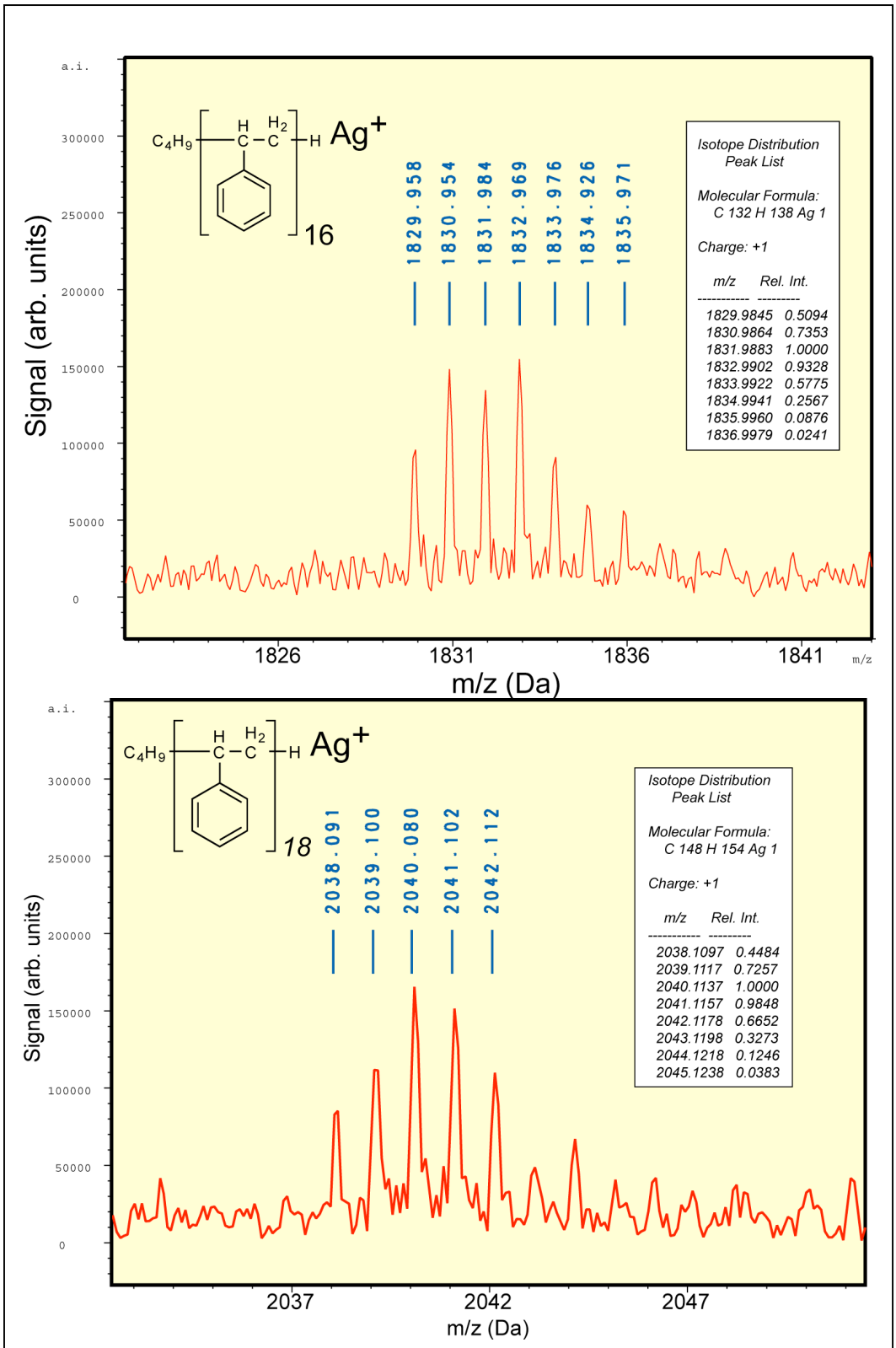

Figure 17. Expanded regions of the FTICR mass spectrum shown in Fig. 16 for the 16mer and 18mer of the Ag^+ cation of polystyrene. The isotope distribution list shows the theoretical mass and relative intensity of each peak in the isotope resolved. The high mass accuracy allows the exact mass of each peak to be determined and compared

to the theoretical mass of each m/z value listed in the isotope distribution list for a specific ion. Matching the peaks in the spectrum to the m/z values in the isotope distribution for the ion provides unambiguous assignment of the stoichiometry for each measured ion. The measured mass values shown for each peak in Fig. 17 is based on a mass calibration from a mass spectrum of CsI clusters measured in a separate experiment. The data shown in Fig. 17 specifically identifies a set of ion species that can be used to internally calibrate the mass spectrum shown in Fig. 16 and provide greater accuracy for assigning the other peaks in the mass spectrum.

Many spectra, similar to those shown in Figures 16 and 17, have been collected on the three polystyrene samples of different thicknesses using FTICR-SIMS. Spectra in the high mass region of the polystyrene mass spectrum have been recorded from sample areas ranging from 1500x1500μm down to 500x500μm on the 10 monolayer thick PS sample. High mass region spectra of PS were not observed in initial tests when smaller sample areas were measured (e.g.,, 300x300μm). This suggests that the Ga^+ beam flux on the surface may be rising to a level where many of the oligomers are fragmented by the incoming ion beam. For our initial mode of operation in the FTICR-SIMS experiments the ion beam was continually on as it was rastered across the sample surface. In this operating mode, the dose rate of ions to the sample ranged from $2x10^{12}$ to $2x10^{13}$ ions/(sec cm^2). This dose rate is higher than that used in *static* SIMS experiments, which have an upper limit of ~ 10^{11} ions/cm^2/sec. Thus, we anticipate that the fragmentation of species on the sample surface will be higher than observed in *static* SIMS experiments. The effect of dose rate can be seen in our initial experiments by comparing the polystyrene spectra collected using the pulsed ion beam operation for ToF-SIMS spectra, Figure 6, with the FTICR-SIMS spectra, Figure 16. The distribution of PS oligomers is clearly shifted to lower values in the FTICR-SIMS measurements.

The next steps in our efforts to develop methods to examine real world polymeric samples are as follows:

1. Examine the effect of beam dose rates on the spectra from thin film samples on Au surfaces to determine the optimum operating conditions.
2. Determine the best spatial resolution that can be obtained in the fingerprint and high mass ranges for polybutadiene using ToF-SIMS and FTICR-SIMS.
3. Determine the best methods for coating polymeric samples with metal films to enhance ion yields, reduce charging, and provide better spatial resolution.
4. Develop numerical codes to automate data analysis of FTICR mass spectrometry measurements and prepare the data for analysis by the AXSIA code.

CONCLUSIONS

Five years after embarking on the design and development of a new instrument to address fundamental issues related to aging of materials in nuclear weapon components, we have finally achieved, and exceeded, our original design objectives. The instrument utilizes both liquid metal focused ion beams and infrared and ultraviolet lasers to deposit energy in selected regions of a sample surface and remove and ionize representative compounds from the region. The ions are analyzed with two different types of mass spectrometers. The mass spectra can be collected as a function of position on the sample surface, providing chemical maps of the compounds that comprise the sample.

This is the first instrument anywhere in the world to integrate an ion and laser beam based surface analysis system with a high performance FTICR mass spectrometer. The FTICR mass spectrometer provides high mass resolution ($m/\Delta m$ = 50,000 to 1,000,000) and high mass accuracy (< 1ppm), which enables accurate identification of ions in the mass spectra of complex materials, such as

polymers and organic compounds. It also allows the use of MS/MS methods to fragment the constituent ions in the mass spectra and provide additional information that can be used to determine the structure of the compounds. Furthermore, since the ions created by the focused ion beam or lasers are first accumulated and stored in an ion trap prior to analysis in the ICR cell, measuring the mass spectra is independent of the sample ablation and ionization process. This is not the case for ToF-SIMS or ToF-Ablation measurements, where the ablation and ionization process is intimately tied to the measurement of the mass spectra.

To provide more rapid mass spectral analysis, to decrease the time to acquire images of chemicals on a sample surface, to improve sensitivity and to provide for operation independent of the FTICR mass spectrometer, a reflectron ToF mass spectrometer was incorporated into the instrument. Incorporating a reflectron ToF mass spectrometer into the instrument required a somewhat unique and unusual design. To facilitate switching between ToF and FTICR operation, the sample had to be maintained near ground potential and the reflectron ToF mass spectrometer also had to serve as the ion optics for transporting ions from the sample surface to the FTICR mass spectrometer. This required (1) a coaxial geometry for the incident and reflected ion pathways in the ToFMS and (2) that the ion optics and drift tube float at a high voltage. This required the use of an annular microchannel plate ion detector and high-speed, fiber optically coupled, transmitters/receivers to connect the signal from the ion detector to the data acquisition equipment.

To successfully transport ions from the surface analysis system to the FTICR mass spectrometer required incorporating a relatively complex ion trap interface between the two systems. The interface consists of a quadrupole mass filter leading to a hexapole ion trap. The ions from the surface analysis system are focused onto the entrance of the quadruple mass filter, which then guides the ions into the ion trap, where they are stored momentarily, and then ejected and transported into the ICR cell for analysis.

Data using both mass spectrometers has been collected on polymeric test samples as well as a LIGA part. To analyze the mass spectra as a function of spatial location, the AXSIA numerical code is used to determine the principal chemical components of the sample and their location. Testing the data acquisition capabilities of the instrument and the analysis features of AXSIA has revealed interesting features of the LIGA part. This provides a good example of the types of features that can be examined various nuclear weapon components.

Having demonstrated the successful operation of the new instrument, we have turned our focus to developing sample preparation and analysis methods that will provide detailed information into the chemical changes that occur in materials over time. Recent experimental investigations and molecular dynamics simulations of the interaction of focused ion beams and lasers with materials has revealed new understanding of the physics associated with ablation and ionization of compounds from the surface of samples. Based on this work we are investigating methods of preparing metalized polymeric samples to aid in the analysis of real world samples. Our initial work focuses on investigating the preparation and analysis of polystyrene and polybutadiene on Ag and Au substrates, and the coating of these polymers with Au films. Examination of polybutadiene will lay the foundation for examining the aging rocket motor propellants.

In conclusion, a new and unique instrument is now operational that can be used to address a wide range of chemical and material issues. For nuclear weapon surveillance, it would be wise to critically review the history of significant finding investigations (SFIs), assess the availability of assets returned from the stockpile for surveillance, and develop a prioritized plan for investigating the materials and components of highest concern. For the development of new materials or devices, the instrument can be used to obtain highly detailed information that will provide new insight into the details of new manufacturing processes. Our examination of the LIGA spring armature is an example of this type of investigation. However, one can envision providing new insight into other issues related to

microscale devices, such as the effect of dormancy on the operation of micromachines, or the detailed chemical nature of microfluidics devices. Finally, from the physical science research point of view there are a number of interesting issues related to understanding and controlling the interaction of energy with small volumes of matter. The issues range from the fluid dynamics of hot rapidly expanding mixtures of unusual combinations of elements and molecules (e.g., the formation of clusters of metals or salts along with fragments of polymers) to the creation of shock waves within polymers or biological samples by heating gold nanoparticles within the samples with picosecond laser pulses. The instrument now provides new capabilities to address many of these issues.

REFERENCES

1. Garrison, B.J., A. Delcorte, and K.D. Krantzman, *Molecule liftoff from surfaces.* Accounts of Chemical Research, 2000. 33(2): p. 69-77.
2. Postawa, Z., et al., *Enhancement of sputtering yields due to C-60 versus Ga bombardment of Ag{111} as explored by molecular dynamics simulations.* Analytical Chemistry, 2003. 75(17): p. 4402-4407.
3. Kotula, P.G., M.R. Keenan, and J.R. Michael, *Automated analysis of SEM X-ray spectral images: A powerful new microanalysis tool.* Microscopy And Microanalysis, 2003. 9: p. 1-17.
4. Mamyrin, B.A., et al., *The mass-reflectron, a new non-magnetic time-of-flight mass spectrometer with high resolution.* Zhurnal Eksperimental'noi i Teoreticheskoi Fiziki, 1973. 64(1): p. 82-9.
5. Kovtoun, S.V. and R.J. Cotter, *Mass-correlated pulsed extraction: Theoretical analysis and implementation with a linear matrix-assisted laser desorption/ionization time of flight mass spectrometer*. Journal of the American Society for Mass Spectrometry, 2000. 11(10): p. 841-853.
6. Kovtoun, S.V., R.D. English, and R.J. Cotter, *Mass correlated acceleration in a reflectron MALDI TOF mass spectrometer: An approach for enhanced resolution over a broad mass range.* Journal of the American Society for Mass Spectrometry, 2002. 13(2): p. 135-143.
7. Delcorte, A., P. Bertrand, and B.J. Garrison, *Collision cascade and sputtering process in a polymer*. Journal of Physical Chemistry B, 2001. 105(39): p. 9474-9486.
8. Delcorte, A., et al., *Sputtering kilodalton fragments from polymers.* Nuclear Instruments & Methods in Physics Research, Section B, 2002. 193: p. 768-74.
9. Bertrand, P., A. Delcorte, and B.J. Garrison, *Molecular SIMS for organic layers: new insights.* Applied Surface Science, 2003. 203(204): p. 160-5.
10. Postawa, Z., et al., *Molecular dynamic simulations of the sputtering of multilayer organic systems.* Nuclear Instruments & Methods in Physics Research Section B-Beam Interactions with Materials and Atoms, 2003. 202: p. 168-174.
11. Zhigilei, L.V., et al., *Computer simulations of laser ablation of molecular substrates.* Chemical Reviews, 2003. 103(2): p. 321-347.
12. Yingling, Y.G. and B.J. Garrison, *Photochemical ablation of organic solids.* Nuclear Instruments & Methods in Physics Research Section B-Beam Interactions with Materials and Atoms, 2003. 202: p. 188-194.
13. Delcorte, A., N. Medard, and P. Bertrand, *Organic secondary ion mass spectrometry: Sensitivity enhancement by gold deposition.* Analytical Chemistry, 2002. 74(19): p. 4955-4968.
14. Davies, N., et al., *Development and experimental application of a gold liquid metal ion source*. Applied Surface Science, 2003. 203(204): p. 223-7.
15. Delcorte, A., et al., *Sample metallization for performance improvement in desorption/ionization of kilodalton molecules: Quantitative evaluation, imaging secondary ion MS, and laser ablation.* Analytical Chemistry, 2003. 75(24): p. 6875-6885.

Acknowledgments. Sandia is a multiprogram laboratory operated by Sandia Corporation, a Lockheed Martin Company, for the United States Department of Energy under Contract DE-AC04-94-AL85000.

Reaction Mechanisms of Energetic Materials in the Condensed Phase: Long-term Aging, Munition Safety and Condensed-Phase Processes in Propellants and Explosives

Richard Behrens
Sandia National Laboratories
Combustion Research Facility
Livermore, CA 94551-0969
Project No: 43381CH
Reporting Period: Aug. 1, 2002 to July 31, 2003

Abstract

The main focus of this project is to develop mathematical models to characterize the reaction processes that control the thermal decomposition of RDX and HMX at low and moderate temperatures that are related to aging and safety issues (development materials for insensitive munitions). In 2003 the work has focused on developing a new surface analysis/FTICR mass spectrometry instrument to examine reaction chemistry on a microscopic scale (down to ~ 1 μm) and developing new mathematical tools to analyze the complex reaction processes that control the decomposition of energetic materials. We have also conducted a new set of thermal decomposition experiments on RDX in the solid phase. In these experiments we have utilized both pure RDX as well as insensitive RDX supplied by the U.S. Army, ARDEC. We have found that the outer layer of the particles that constitute the insensitive RDX powders is less stable, subliming more rapidly and decomposing faster. The results of our experiments along with data collected by ARDEC suggests that this altered outer layer may play a significant role in reducing the shock sensitivity of these materials. Understanding this behavior may be important for developing new RDX-based formulations.

Contents

Abstract 1
Contents 1
Summary 2
Publications 3

Summary

The focus of this project is to develop mathematical models of the reaction processes that control the thermal decomposition of energetic materials in the solid and liquid phase at low and moderate temperatures (room temperature to ~300°C). Understanding reactions of energetic materials in this temperature range is important for the development and characterization of insensitive munitions and the assessment of the effects of age on the performance and safety of munitions during their life cycle.

Our previous work examined the decomposition of a range of different types of energetic materials and found that in all cases the reaction processes are controlled by a set of complex nonlinear reactions that are often influenced by spatiotemporal effects at various length scales. In this project our focus is on developing a better understanding of spatiotemporal effects and developing mathematical models to characterize these processes.

To develop a better understanding of the spatiotemporal effects we are developing a new instrument to examine chemical reactions on a microscopic spatial scale. This instrument consists of a surface analysis system coupled to two types of mass spectrometers. Microscopic samples are removed from the surface and ionized using several different complementary methods: secondary ionization using a Ga^+ liquid metal ion source, ablation and ionization using high power UV and CO_2 lasers, and indirectly using low power CO_2 laser heating and photoionization of the evolved gas. The ions are detected and analyzed using either a reflectron TOF mass spectrometer or a high resolution FTICR mass spectrometer. The TOF mass spectra are recorded as a function of spatial location on the sample, allowing chemical maps of the sample surface to be measured. This spatially dependent spectral data is analyzed with new image analysis software, AXSIA (Automated expert Spectal Image Analysis), developed at Sandia by Kotula et.al.[1] This software uses both a principal component analysis (PCA) routine and an alternating least-squares-based multivariate curve resolution (MCR-ALS) routine, which provides more realistically interpretable spectra. AXSIA deconvolutes the TOF spectra into statistically relevant simplified spectra that represent all of the individual chemical 'phases' present in each image and also provides the chemical map for each represented phase. The FTICR mass spectrometer is used to maximize the likelihood of identifying the chemical composition of ions and determining their molecular structure through MS/MS or MS^n experiments. This chemical microprobe/FTICR mass spectrometry instrument is in its final stages of development and will be used next year to begin investigations of RDX decomposition processes.[2]

To develop mathematical models of the complex nonlinear spatiotemporal reaction processes that control the decomposition of energetic materials, we have conducted work in two areas. First, we have modified the temperature control system on the simultaneous thermogravimetric modulated beam mass spectrometry (STMBMS) instrument to allow data to be collected over wider temperature range using more complex thermal profiles. This provides data over a wider temperature range allowing more accurate parameters for the reaction models to be determined from the data. Second, we have continued to develop the reaction modeling and kinetics (REMKIN) compiler and analysis tool. REMKIN is designed to allow an analyst to postulate reaction models that characterize

the underlying physicochemical reaction processes that control the decomposition of energetic materials and to parameterize and test these models by using the STMBMS data. The experimental and analysis methods have been described in two recent publications[3, 4] and the application of these methods to characterize the decomposition of RDX has been presented at a recent JANNAF meeting.[5]

In our recent thermal decomposition experiments with RDX in the solid phase we have used both pure RDX and samples of insensitive RDX supplied by Dr. Barry Fishburn, U.S. Army, ARDEC. Insensitive RDX has reduced shock sensitivity and is of interest to the Army for the development of insensitive munitions. Comparing the results from our experiments on the decomposition of various samples of insensitive RDX to our previous work on pure samples of RDX shows that the insensitive RDX samples have a less stable outer layer. In our experiments, the RDX from this outer layer sublimes more rapidly and decomposes faster than the RDX in the core of the particles, suggesting that the manufacturing process creates RDX powders in which the outer layer is less stable than the interior.

These results correlate with the reduced shock sensitivity of these materials measured at ARDEC. In addition, we have also found that a sample of RDX that was prepared by one of these manufacturers using RDX made at the Holston Defense Plant, decomposes more rapidly than other samples of RDX we have examined. When compared to our extensive database on the decomposition of RDX, it appears that this sample may contain some contaminant, possibly hexahydro-1-nitroso-3,5-dinitro-s-triazine (ONDNTA), causing it to decompose faster than other samples of RDX. Accelerated aging studies, conducted at ARDEC, have shown that this material loses its reduced shock sensitivity after several months of accelerated aging and reverts to the shock sensitivity of normal Holston RDX. Coupling the fact that the decomposition of RDX in the solid phase occurs on the surface of the RDX particles with the results from ARDEC strongly suggests that the reduced shock sensitivity involves altering the outer layer of the RDX particles. In our future experiments with RDX in this project, we will utilize various samples of insensitive RDX in an effort to further our understanding of the characteristics that underlie its reduced shock sensitivity, while furthering our characterization of its underlying decomposition behavior.

Publications

[1] P. G. Kotula, M. R. Keenan, and J. R. Michael, Microscopy And Microanalysis **9**, 1 (2003).

[2] S. Maharrey, R. Bastasz, R. Behrens, et al., Applied Surface Science, Article in press (2004).

[3] R. Behrens, in *Overviews of Recent Research on Energetic Materials*, edited by R. W. Shaw, T. B. Brill and D. L. Thompson (To be published, 2004).

[4] R. Behrens, " Thermal Decomposition Processes in Energetic Materials in the Condensed Phase at Low and Moderate Temperatures ", edited by A. Weimer (AIChE, San Francisco, CA, 2003), Vol. 2, p. 1609

[5] R. Behrens and S. Maharrey, in *Proceedings of the 39th JANNAF Combustion Subcommittee Mtg.* (CPIA, Colorado Springs, CO, 2003).

Reaction Mechanisms of Energetic Materials in the Condensed Phase: Long-term Aging, Munition Safety and Condensed-Phase Processes in Propellants and Explosives

Richard Behrens
Sandia National Laboratories
Combustion Research Facility
Livermore, CA 94551-0969
Project No: 43381CH
Reporting Period: Aug. 1, 2003 to July 31, 2004

Abstract

The main focus of this project is to develop mathematical models to characterize the reaction processes that control the thermal decomposition of RDX and HMX at low and moderate temperatures that are related to aging and safety issues (development of materials for insensitive munitions). In the first half of 2004 the work has focused on developing a new surface analysis/FTICR mass spectrometry instrument to examine reaction chemistry on a microscopic scale (down to ~ 1 μm) and developing new mathematical tools to analyze the complex reaction processes that occur at low temperatures on the surface of particles of RDX and HMX. Based on our investigations of insensitive RDX materials in 2003, we have started a new series of thermal decomposition experiments focused on understanding the decomposition processes of RDX and HMX in the solid phase at temperatures below 185°C. The results for the decomposition of RDX show that reaction occurs on the surface of the particles and involves the formation of the mononitroso RDX intermediate (MNRDX) followed by the subsequent decomposition of MNRDX into gaseous products and nonvolatile residue (NVR). A film of NVR grows on the surface of the particles that leads to an increasing rate of reaction during the decomposition process. Reactions of RDX have been observed as low as 145°C.

Contents

Abstract 1
Contents 1
Summary 2
Publications 4

Summary

The focus of this project is to develop mathematical models of the reaction processes that control the thermal decomposition of energetic materials in the solid and liquid phase at low and moderate temperatures (room temperature to ~300°C). Understanding reactions of energetic materials in this temperature range is important for the development and characterization of insensitive munitions and the assessment of the effects of age on the performance and safety of munitions during their life cycle.

Our previous work examined the decomposition of a range of different types of energetic materials and found that in all cases the reaction processes are controlled by a set of complex nonlinear reactions that are often influenced by spatiotemporal effects at various length scales. In this project our focus is on developing a better understanding of spatiotemporal effects and developing mathematical models to characterize these processes.

To develop a better understanding of the spatiotemporal effects we are developing a new instrument to examine chemical reactions on a microscopic spatial scale. This instrument consists of a surface analysis system coupled to two types of mass spectrometers. Microscopic samples are removed from the surface and ionized using several different complementary methods: secondary ionization using a Ga^+ liquid metal ion source, ablation and ionization using high power UV and CO_2 lasers, and indirectly using low power CO_2 laser heating and photoionization of the evolved gas. The ions are detected and analyzed using either a reflectron TOF mass spectrometer or a high resolution FTICR mass spectrometer. The TOF mass spectra are recorded as a function of spatial location on the sample, allowing chemical maps of the sample surface to be measured. This spatially dependent spectral data is analyzed with new image analysis software, AXSIA (Automated expert Spectal Image Analysis), developed at Sandia by Kotula et.al.[1] This software uses both a principal component analysis (PCA) routine and an alternating least-squares-based multivariate curve resolution (MCR-ALS) routine, which provides more realistically interpretable spectra. AXSIA deconvolutes the TOF spectra into statistically relevant simplified spectra that represent all of the individual chemical 'phases' present in each image and also provides the chemical map for each represented phase. The FTICR mass spectrometer is used to maximize the likelihood of identifying the chemical composition of ions and determining their molecular structure through MS/MS or MS^n experiments. During the first half of 2004, a new reflectron TOF mass spectrometer has been installed in the instrument and tested. The operational mode of this new reflectron TOFMS is somewhat unusual in that the sample is grounded and the entire mass spectrometer floats at high voltage. This design allows for relatively simple switching between the TOFMS and the FTMS for analysis. A paper presented a the recent International SIMS conference outlines its design and operation and was selected for publication.[2]

To develop mathematical models of the complex nonlinear spatiotemporal reaction processes that control the decomposition of energetic materials, we have conducted work in two areas. First, we have modified the temperature control system on the simultaneous thermogravimetric modulated beam mass spectrometry (STMBMS) instrument to allow data to be collected over wider temperature range using more complex thermal profiles.

This provides data over a wider temperature range allowing more accurate parameters for the reaction models to be determined from the data. Second, we have continued to develop the reaction modeling and kinetics (REMKIN) compiler and analysis tool. REMKIN is designed to allow an analyst to postulate reaction models that characterize the underlying physicochemical reaction processes that control the decomposition of energetic materials and to parameterize and test these models by using the STMBMS data. The experimental and analysis methods have been described in two recent publications[3, 4] and the application of these methods to characterize the decomposition of RDX has been presented at a recent JANNAF meeting.[5] Developmental work on these numerical simulation tools during the first half of 2004 has focused on incorporating subgrid models to characterize reactions processes on the surface of particles. The ability to create reaction models of these surface related processes will be especially relevant for characterizing both the effects of age and reactions at interfacial regions of composite materials on the properties of propellants and explosives.

In our recent thermal decomposition experiments with RDX in the solid phase we have used both pure RDX and samples of insensitive RDX supplied by Dr. Barry Fishburn, U.S. Army, ARDEC. Insensitive RDX has reduced shock sensitivity and is of interest to the Army for the development of insensitive munitions. Comparing the results from our experiments on the decomposition of various samples of insensitive RDX to our previous work on pure samples of RDX shows that the insensitive RDX samples have a less stable outer layer. In our experiments, the RDX from this outer layer sublimes more rapidly and decomposes faster than the RDX in the core of the particles, suggesting that the manufacturing process creates RDX powders in which the outer layer is less stable than the interior.

These results correlate with the reduced shock sensitivity of these materials measured at ARDEC. In addition, we have also found that a sample of RDX that was prepared by one of these manufacturers using RDX made at the Holston Defense Plant, decomposes more rapidly than other samples of RDX we have examined. When compared to our extensive database on the decomposition of RDX, it appears that this sample may contain some contaminant, possibly hexahydro-1-nitroso-3,5-dinitro-s-triazine (ONDNTA), causing it to decompose faster than other samples of RDX. Accelerated aging studies, conducted at ARDEC, have shown that this material loses its reduced shock sensitivity after several months of accelerated aging and reverts to the shock sensitivity of normal Holston RDX. Coupling the fact that the decomposition of RDX in the solid phase occurs on the surface of the RDX particles with the results from ARDEC strongly suggests that the reduced shock sensitivity may involve altering the outer layer of the RDX particles.

To understand the behavior of RDX better we have started a new series of experiments focused on understanding and characterizing the reaction processes that occur on the surface of RDX and HMX particles. We have conducted thermal decomposition experiments with RDX powders in which the temperature of the sample is slowly cycled between 145°C and 185°C. In these experiments we observe that the decomposition occurs on the surface of the RDX particles. The main thermal decomposition pathway occurs via the mononitroso RDX intermediate, MNRDX. This pathway is by far the most dominant among the various pathway available in the overall decomposition scheme for RDX.[5, 6] The other reaction pathways have been observed in the

decomposition of RDX also occur on the surface of the particles. These pathways include the formation of a nonvolatile residue on the surface of the RDX that subsequently reacts with the remaining RDX. This reaction pathway manifests itself in an increased rate of decomposition in each subsequent thermal cycle in the experiment. In addition, when the temperature reaches the upper half of the temperature range during the heating cycle, the direct decomposition of RDX to oxy-s-triazine (OST) is observed indicating the surface of the RDX particle may liquefy due to localized interaction of RDX with its decomposition products on the surface of the particles.

Finally, we are interested in whether or not HMX when mixed with RDX will undergo the same reactions as those observed in the thermal decomposition of RDX. It seems reasonable to expect that if HMX particles are exposed to the decomposition products formed during the decomposition of RDX, they too will decompose in this lower temperature range. We plan to conduct experiments shortly to investigate this issue.

Publications

[1] P. G. Kotula, M. R. Keenan, and J. R. Michael, Microscopy And Microanalysis **9**, 1 (2003).

[2] S. Maharrey, R. Bastasz, R. Behrens, et al., Applied Surface Science **231-232**, 972 (2004).

[3] R. Behrens, in *Overviews of Recent Research on Energetic Materials*, edited by R. W. Shaw, T. B. Brill and D. L. Thompson (To be published, 2004).

[4] R. Behrens, in *AIChE Engineered Particle Systems: Synthesis, Processes and Applications Topical Conference*, edited by A. Weimer (AIChE, San Francisco, CA, 2003), Vol. 2, p. 1609

[5] R. Behrens and S. Maharrey, in *Proceedings of the 39th JANNAF Combustion Subcommittee Mtg.* (CPIA, Colorado Springs, CO, 2003).

[6] R. Behrens and S. Maharrey, in *Combustion of Energetic Materials*, edited by K. K. Kuo and L. T. DeLuca (Begell House, New York, 2002), p. 3

Reaction Mechanisms of Energetic Materials in the Condensed Phase: Long-term Aging, Munition Safety and Condensed-Phase Processes in Propellants and Explosives

Richard Behrens
Sandia National Laboratories
Combustion Research Facility
Livermore, CA 94551-0969
Project No: 43381CH
Reporting Period: Aug. 1, 2004 to July 31, 2005

Abstract

The main focus of this project is to develop mathematical models to characterize the reaction processes that control the thermal decomposition of RDX and HMX at low and moderate temperatures that are relevant to aging and safety issues of propellants and explosives (development of materials for insensitive munitions). In the past year (2004/2005) research has focused on the following areas; (1) developing mathematical models of the underlying reaction processes that control the thermal decomposition of RDX below and above its melting point, (2) collecting new data on the thermal decomposition of different types of HMX, (3) collecting new data on the decomposition of four different HMX-based explosives, PBX9501, LX-04, LX-14 and EDC-37 (UK/AWE) to evaluate the effects of other ingredients on the decomposition process, (4) examining the decomposition of the BDNPA/F plasticizer and (5) developing methods to examine propellants using the chemical imaging precision mass analyzer (ChIPMA) instrument.

Contents

Abstract....1
Contents....1
Summary....2
RDX Reaction Processes....2
HMX Reaction Processes....3
Decomposition of HMX-....5
based formulations....5
BDNPA/F plasticizer decomposition....6
Chemical Imaging Precision Mass Analyzer (ChIPMA) development....7
References....11

Summary

The focus of this project is to develop mathematical models of the reaction processes that control the thermal decomposition of energetic materials in the solid and liquid phase at low and moderate temperatures (room temperature to ~300°C). Understanding reactions of energetic materials in this temperature range is important for the development and characterization of insensitive munitions and the assessment of the effects of age on the performance and safety of munitions during their life cycle.

Our previous work examined the decomposition of a range of different types of energetic materials and found that in all cases the reaction processes are controlled by a set of complex nonlinear reactions that are often influenced by spatiotemporal effects at various length scales. In this project our focus is on developing a better understanding of spatiotemporal effects and developing mathematical models to characterize these processes. The spatial effects may be introduced into an energetic material as the constituent ingredients are mixed during the manufacturing process, creating interfaces between the various ingredients. Spatial effects may also develop during the course of the decomposition process itself, as the morphological features of the compound are transformed by the chemical reactions underlying the decomposition process. For example, the creation of new surfaces, as bubbles nucleate and grow, during the thermal decomposition of HMX below its melting point.

To address these issues we have focused our effort over the past year in three areas: (1) developing mathematical models of the underlying reaction processes that control the thermal decomposition of RDX, (2) collecting new data on HMX-based explosive formulations to understand how the various ingredients that comprise an explosive formulation may interact and affect its safety or long-term aging characteristics, (3) utilizing a new and unique instrument to probe the reaction processes at interfaces between different ingredients that comprise a propellant formulation.

RDX Reaction Processes.

The reaction processes that control the thermal decomposition of RDX in the condensed phase are complex, nonlinear and spatiotemporally dependent. The rate controlling processes are significantly different below[1] and above its melting point (~200°C).[2] A combination of simultaneous thermogravimetric modulated beam mass spectrometry (STMBMS) experiments and a new reaction modeling and kinetics (REMKIN) compiler and analysis tool have been used to probe the underlying reaction processes and develop mathematical models representing the reaction kinetics of RDX. First, a relatively simple model describing the decomposition of RDX below its melting point was developed. It incorporates both gas-phase reactions and reactions on the surface of the RDX particles. Parameters for this model are obtained from STMBMS experiments in which the RDX is cycled between 145°C and 185°C at a heating rate of ±0.05°C/min. Next, the underlying reaction processes that control the thermal decomposition of RDX above its melting point were developed. Results from experiments with RDX, in which the sample is heated at rates of 5 and 10°C/min, show clear temporal separation of the products associated with

different pathways in the RDX reaction scheme[3] and provide new insight into the underlying reaction processes. When combined with results on the thermal decomposition of hexahydro-1-nitroso-3,5-dintro-s-triazine (ONDNTA), an improved understanding of the reaction processes that control the creation and decomposition of the ONDNTA intermediate in the RDX decomposition process was obtained. The REMKIN compiler and analysis tool was used to incorporate these new reaction features into mathematical models that characterize the decomposition of RDX in the liquid phase. The issues associated with postulating and testing new reaction schemes and optimizing the parameters of the underlying reactions were discussed. The combination of STMBMS experiments and REMKIN analysis provide a new means to develop insight into the reaction processes that occur in the condensed phase.[4] This work forms the basis for examining reduced shock sensitivity RDX (RS-RDX) which is now of interest for the development of new insensitive DoD munitions.

HMX Reaction Processes.

Over the past several years, we have spent considerable effort to examine the reaction processes that control the decomposition of HMX below its melting point and have found that the reaction processes are dominated by (1) the nucleation and growth of micron-sized bubbles within the HMX particles and (2) the creation of a nonvolatile residue (NVR) whose interaction with the remaining HMX opens new reaction pathways in the overall decomposition scheme. While this work provides new insight into the underlying reaction processes, there remain several unresolved issues that require further experimental investigation. These issues can be divided into two general categories: (1) The relative rates of reaction of the main underlying reaction processes and the effect of material properties introduced by manufacturing processes and/or aging on these reaction rates. (2) The effects of other ingredients found in an explosive or propellant formulation on the reaction processes.

Other reaction pathways, in addition to the nucleation and growth of bubbles within HMX particles, may contribute to the overall decomposition process of HMX. For example, in the decomposition of RDX below its melting point, we have found that the formation of an NVR on the surface of the RDX particles opens a new reaction pathway.[1] Does this also occur in the decomposition of HMX? To examine this issue several different types of HMX were examined: Holston-grade 6μm and 600μm powders and HMX obtained from AWE,

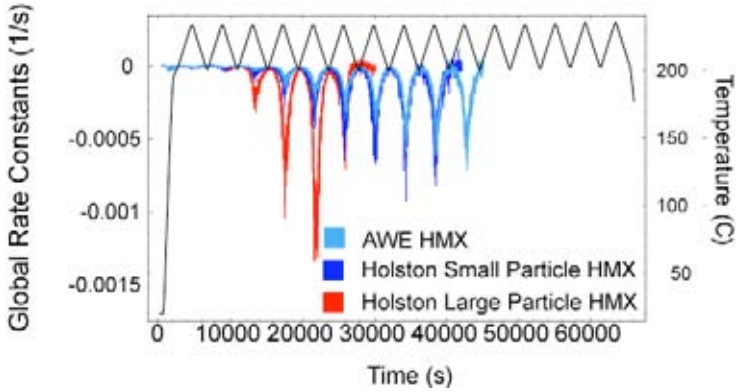

Figure 1. Global reaction rate constants, based on mass loss, from experiments with three different types of HMX powder. The sample is heated to 200°C and then cycles between 200 and 235°C at ± 1°C/min.

which was manufactured by Royal Ordnance. The results from experiments in which the HMX samples were cycled between 200 and 235°C at 1°C/min (Fig. 1) show that the global rate of decomposition of the 6μm Holston HMX and the Royal Ordnance HMX are quite similar. The reaction rate of the 600μm Holston material is initially quite similar to the other two samples, but its rate of decomposition accelerates more rapidly on subsequent thermal cycles. This result suggests that the reaction processes associated with the nucleation and growth of bubbles within the HMX particles accelerates more rapidly in larger HMX particles. (Note that the temperature of the sample is now slowly modulated during the course of the experiments to provide data on the temperature dependence of the constantly changing reaction processes within the sample.)

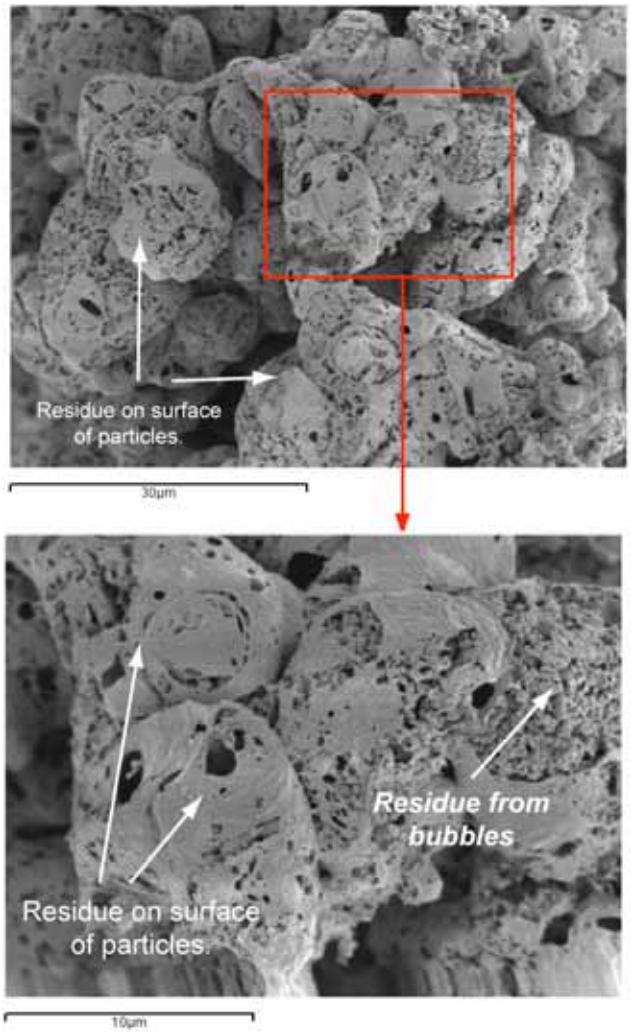

Figure 2. SEM pictures of nonvolatile residue that remains after the decomposition of 6μm diameter HMX particles. Note the formation of NVR on the surface of the particles and the shell-like structures from bubbles formed within the particles.

During the decomposition of HMX, the NVR remains behind in the sample and forms morphological features that provide insight into the location and development of the reaction process during the course of an experiment. In our past work with larger (600μm) HMX particles, these features were primarily associated with the nucleation and growth of bubbles within the HMX particles. The diameter of the shells, which are remnants from the bubbles, ranged in size from 0.2 to ~2μm in diameter. Whether these same types of processes occur in smaller (6μm) diameter HMX was investigated. The SEM results (Fig. 2) show that the NVR forms a coating on the outer surface of the 6μm HMX particles. However, the nucleation and growth of bubbles still occurs in these smaller particles as evidenced by the shell-like structures shown in the lower picture.

The new results on different types of HMX powders provide a broader basis for developing mathematical models to characterize the decomposition of HMX. Data is

now available to investigate the origins of particle size effects in the overall HMX decomposition scheme. The appearance of NVR on the surface of the HMX particles is similar to that observed in our studies of the decomposition of RDX below its melting point.[1] Thus, this new data provides a basis for developing reaction models of HMX and RDX decomposition that has a consistent basis for these two very similar compounds.

Decomposition of HMX-based formulations.

To characterize the decomposition processes that occur in propellants and explosives requires understanding the decomposition behavior of the individual ingredients, as well as the interactions that may occur between the various ingredients. To address these issues we have conducted new experiments to examine the decomposition of several different HMX-based explosives: PBX9501 (95%HMX, 2.5%BDNPA/F, 2.5% Estane), LX-04 (85%HMX, 15% viton), EDC-37 (AWE explosive, 91%HMX, 1%NC, 8% K10 – a mixture of dinitro- and trinitro-ethylbenzene), and LX-14 (95.5% HMX, 4.5% Estane).

Initial experiments focused on examining the decomposition of PBX9051 and LX-04 to address the issue of whether the BDNPA/F plasticizer may promote more rapid decomposition. The global rate contants from PBX9501, LX-04 and EDC-37 along with data on HMX by itself are presented in Figure 3. The results show that the global rate of decomposition of LX-04 and EDC-37 is very similar to that of smaller particle HMX (6μm). In contrast, the global decomposition rate of PBX9501 is significantly higher than the other materials. This suggested that the BDNPA/F plasticizer may increase the rate of decomposition of HMX as been previously suggested in the energetic materials community.

To test the role of the BDNPA/F plasticizer another set of experiments was conducted with LX-14, which contains Estane, but no plasticizer. The results (Fig. 4) show that the rate of decomposition of LX-14 is very similar to that of PBX9501 suggesting that the Estane binder may accelerate the rate of HMX decomposition and not the plasticizer. The results of experiments conducted to date suggest that the Estane binder may interact with HMX. This is likely to occur at the surface of the HMX particles since this is where the two compounds are in contact with each other.

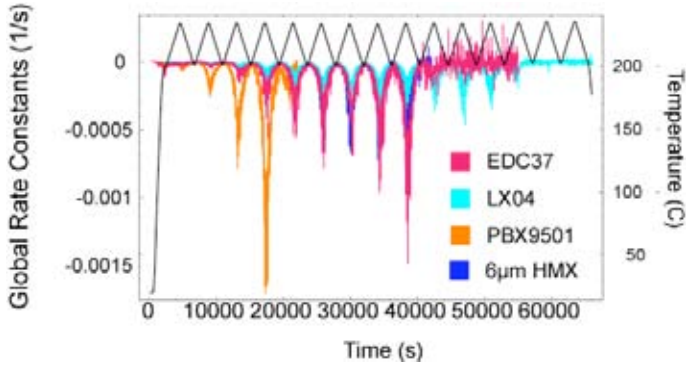

Figure 3. Global reaction rate constants, based on mass loss, from experiments with three different types of HMX-based explosives. The sample is heated to 200°C and then cycles between 200 and 235°C at ± 1°C/min.

To summarize the current state of our work with explosive formulations, we have collected thermal cycling data on four different types of explosive formulations. It appears that explosive containing Estane binder may decompose at a faster

rate. The data has been collected in thermal cycling experiments over temperature ranges of 200 to 235°C (as presented in the figures in this report) and 170 to 200°C. Examination of the global rate constant data shows that the rate of decomposition can be significantly altered by presence of other ingredients. The data collected to date has all of the information on the rates of evolution of various species that we collect in our STMBMS experiments. This data will be used to develop more detailed mathematical models of the reaction processes that occur in these composite materials.

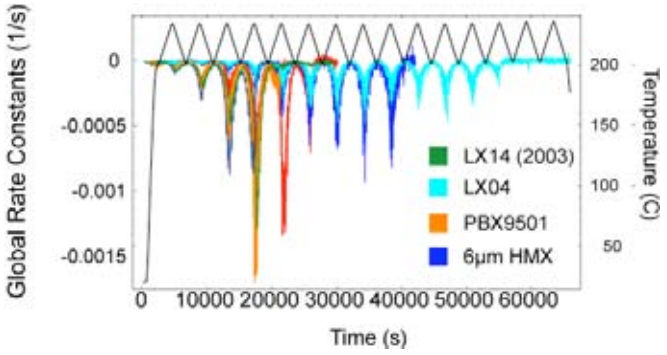

Figure 4. Global reaction rate constants, based on mass loss, from experiments investigating the effect of the Estane binder on the decomposition process. The sample is heated to 200°C and then cycles between 200 and 235°C at ± 1°C/min.

BDNPA/F plasticizer decomposition.

The vapor pressures and thermal decomposition chemistry of bis(2,2-dinitropropyl) acetal (BDNPA) and bis(2,2-dinitropropyl) formal (BDNPF) have been investigated with our STMBMS and Fourier Transform ion cyclotron resonance (FTICR) mass spectrometry methods.[5] BDNPA exhibits a heat of vaporization (ΔH_{vap}) of 22.23 ± 0.09 kcal/mol and a vapor pressure at 25 °C of 0.0109 + 0.003/ – 0.002 millitorr. The respective values of ΔH_{vap} and the vapor pressure at 25 °C for BDNPF are 20.26 ± 0.21 kcal/mol and 0.0165 + 0.014/ – 0.008 millitorr. The general features of the BDNPA and BDNPF decomposition chemistry are similar. STMBMS weight loss data strongly suggests the formation of a residue from each compound during the course of decomposition. The temporal behaviors and relative signal percentages of certain decomposition products support a nitro-nitrite ($-NO_2$ -> -O-NO) rearrangement mechanism. Upon rearrangement, both an NO and NO_2 product are cleaved from the structure, thus creating an unstable ketone radical. The ketone radical eventually rearranges into 1-(vinyloxy)propan-2-one in BDNPA and 1-methoxypropan-2-one in BDNPF. The nitro-nitrite rearrangement begins at appreciable rates between 160-180 °C. Additional decomposition products originate from evaporation/ decomposition of the residue as well as the formation of amines, imines and amides through reactions between nitroxyl and alkyl radicals. The major difference between BDNPA and BDNPF decomposition is the rate of reaction. In BDNPF, the ketone products from nitro-nitrite rearrangement are delayed in their release from the reaction cell. We postulate that the less sterically hindered formal carbon of

BDNPF subjects it to interactions with the residue. The interactions serve to maintain the product in a condensed phase, thus delaying its release.

Chemical Imaging Precision Mass Analyzer (ChIPMA) development.

To develop a better understanding of the spatiotemporal effects that control the reaction processes in propellants and explosives, requires examination of chemical reactions on a microscopic spatial scales. To acquire this type of data required designing and constructing a new type of instrument that would allow complex molecular compounds (e.g., organics, polymers) to be detected and identified as a function of spatial location. This instrument consists of a surface analysis system coupled to two types of mass spectrometers (Fig. 5). Microscopic samples are removed from a sample surface and ionized using several different complementary methods: secondary ionization directly from the sample surface using a Ga^+ liquid metal ion source, ablation and ionization using high power UV and CO_2 lasers, and indirectly using low power CO_2 laser heating followed by photoionization of the evolved gas. The ions are detected and analyzed using either a newly designed coaxial reflectron TOF mass spectrometer or a high resolution FTICR mass spectrometer. The TOF mass spectra are recorded as a function of spatial location on the sample, allowing chemical maps of the sample surface to be measured. This spatially dependent spectral data is analyzed with image analysis software, AXSIA (Automated expert Spectal Image Analysis).[6] The FTICR mass spectrometer is used to maximize the likelihood of identifying the chemical composition of ions and determining their molecular structure through MS/MS or MS^n experiments.

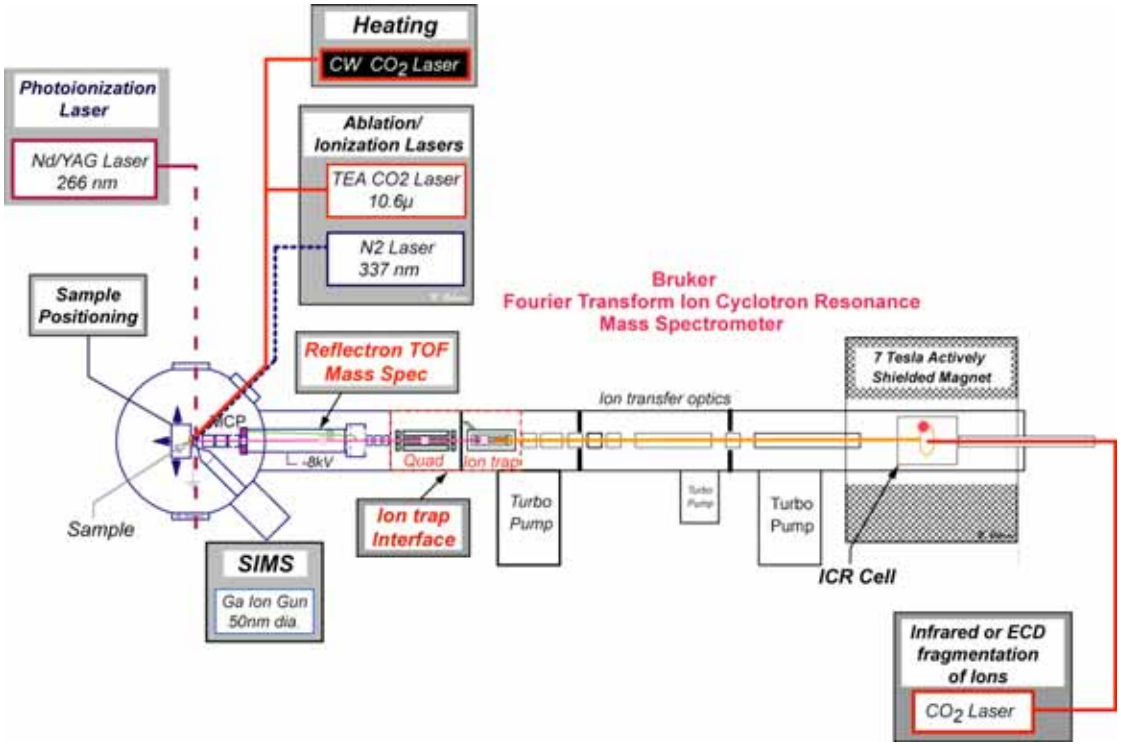

Figure 5. Schematic of ChIPMA instrument.

Over the past year our work with the ChIPMA instrument has focused on developing methods to examine lower molecular weight polymers using secondary ion mass spectrometry (SIMS) imaging methods. For example, films of various polymers have been prepared on silver and gold surfaces and examined with both TOF and FTICR mass spectrometry. The type of data obtained with a FTICR/SIMS is illustrated in Figure 6 with a spectrum of polystyrene coated on a silver surface. This illustrates the ability to remove higher molecular weight species from a sample surface using a Ga^+ ion beam and accurately identifying the species using the high resolution and high mass accuracy

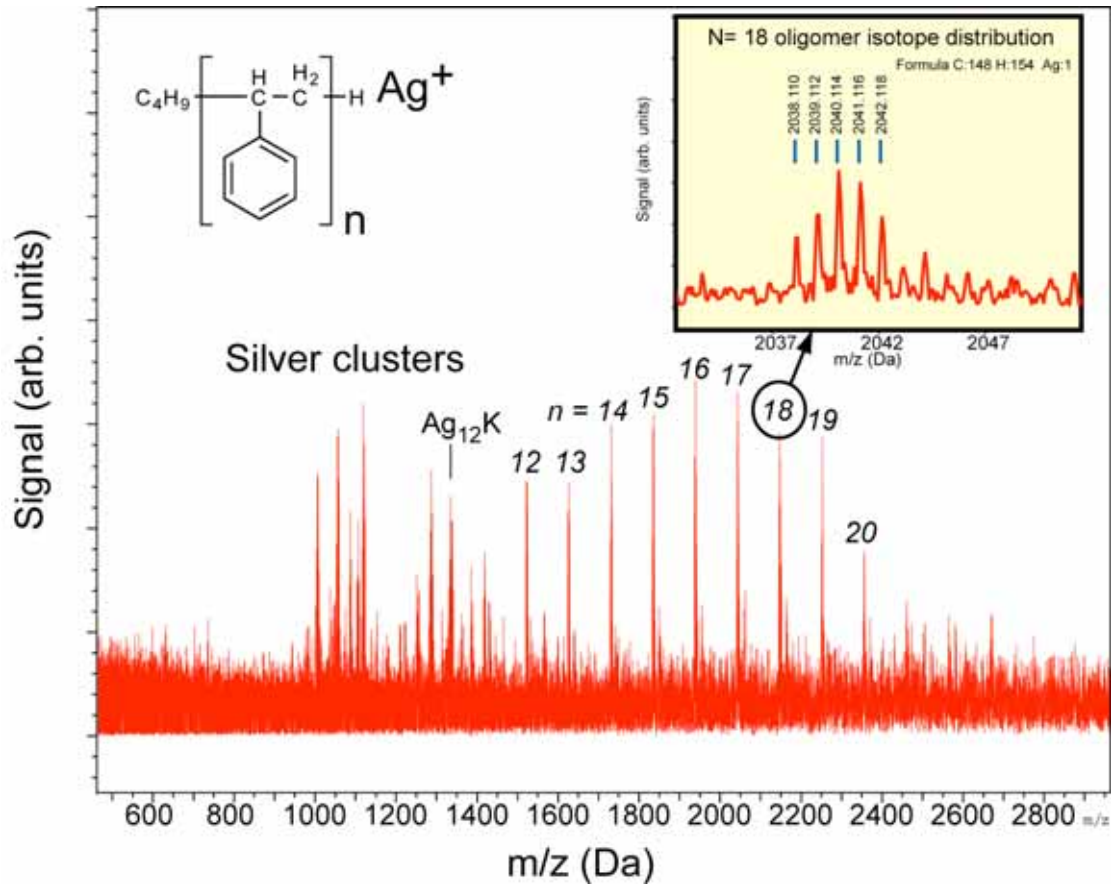

Figure 6. SIMS/FTICR mass spectrum of polystyrene film coated on a silver surface.

capabilities of the FTICR instrument.

We have also begun to develop methods to examine surfaces of propellants. Our initial focus has been on imaging the chemical constituents of an AP-based propellant. A Ga^+ induced secondary electron image of an AP-based propellant (Fig. 7) shows the morphological features of the interfaces between AP particles and the surrounding HTPB binder. The identities of the constituents in each region of the image are shown in Fig. 8, based on analysis of the ToFMS imaging data. The results show that a portion of the sample surface is pure AP (cyan) and another region is HTPB polymer (yellow). Part of the AP particle is covered by an organic coating (green), and the interface region between the AP particle and the HTPB (magenta) is a mixture of different compounds. Thus, in 2005 we have developed the ChIPMA instrument to a point in which chemical maps of

the location of chemical constituents on a sample surface can be measured using lower resolution ToFMS measurements and high resolution and high mass accuracy provided by the FTICR mass spectrometer can be used to identify the chemical constituents. The instrument will be used in the future to examine reaction processes in HMX and RDX and HMX-based formulations.

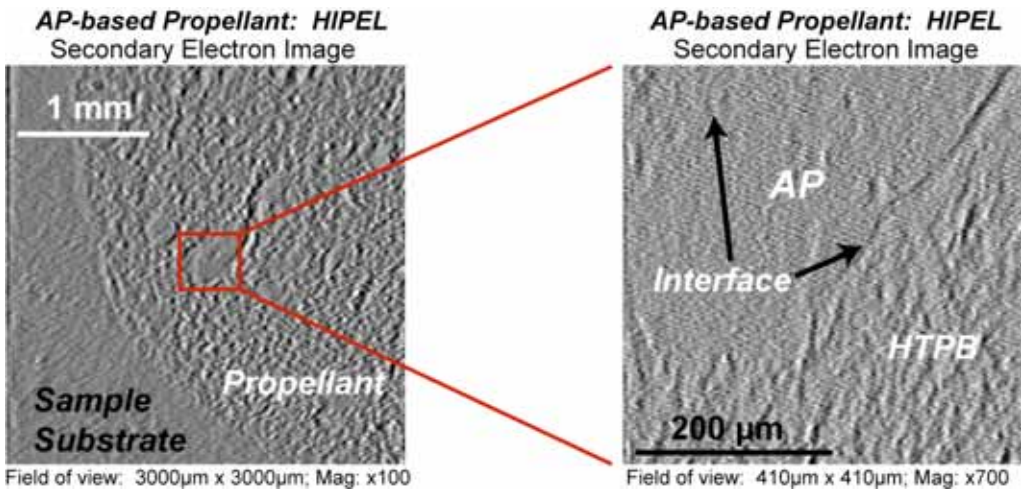

Figure 7. Ga^+ induced secondary electron images of the surface of an AP-based propellant. Higher magnification picture (right) shows an interface between an AP particle and the HTPB binder.

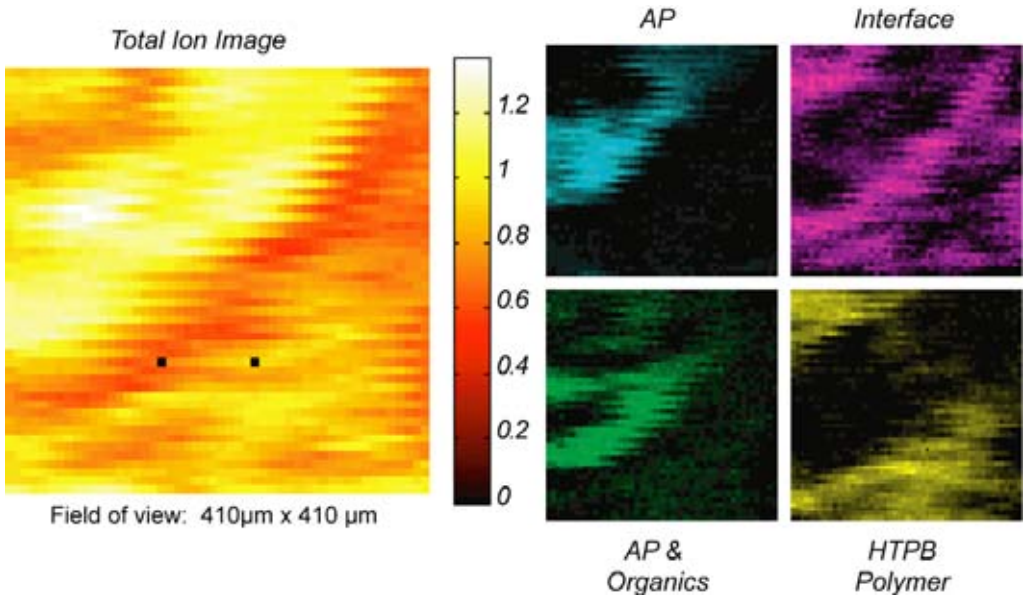

Figure 8. Images of various ingredients determined from ToFMS measurements recorded in the same area of the AP-based propellant sample shown in Figure 7. Image on left shows total ion signal recorded in the mass spectrum at each pixel location. Images at right show the principal components identified by AXSIA analysis of TOFMS data. Each image has a corresponding characteristic mass spectrum representing the compounds located in each image. Color intensity represents the relative amount of the compound located at each pixel location.

References

1. Maharrey, S. and R. Behrens, *Thermal Decomposition of Energetic Materials 5. Reaction Processes of 1,3,5-Trinitrohexahydro-s-triazine (RDX) Below Its Melting Point.* Journal of Physical Chemistry, 2005. **Submitted for publication**.
2. Maharrey, S. and R. Behrens, *Thermal Decomposition of Energetic Materials. 6. Development of a Physicochemical Reaction Network Describing the Thermal Decomposition Process in 1,3,5-Trinitrohexahydro-s-triazine (RDX).* Journal of Physical Chemistry, 2005. **In preparation**.
3. Behrens, R. and S. Maharrey, *Chemical and Physical Processes that Control the Thermal Decomposition of RDX and HMX*, in *Combustion of Energetic Materials*, K.K. Kuo and L.T. DeLuca, Editors. 2002, Begell House: New York. p. 3 - 21.
4. Behrens, R. and D. Wiese-Smith, *Reaction Kinetics of RDX in the Condensed Phase*, in *40th JANNAF Combustion Meeting*. 2005, CPIA Publication: Charleston, South Carolina. p. June 2005.
5. Rauch, R. and R. Behrens, *Vapor Pressures and Thermal Decomposition Processes of Bis(2,2-dinitropropyl) acetal (BDNPA) and Bis(2,2-dinitropropyl) formal (BDNPA).* Propellants Explosives Pyrotechnics, In preparation.
6. Kotula, P.G., M.R. Keenan, and J.R. Michael, *Automated analysis of SEM X-ray spectral images: A powerful new microanalysis tool.* Microscopy And Microanalysis, 2003. **9**: p. 1-17.

Publications

Maharrey, S. and R. Behrens, *Thermal Decomposition of Energetic Materials 5. Reaction Processes of 1,3,5-Trinitrohexahydro-s-triazine (RDX) Below Its Melting Point.* Journal of Physical Chemistry, 2005. **Submitted for publication**.

Maharrey, S. and R. Behrens, *Thermal Decomposition of Energetic Materials. 6. Development of a Physicochemical Reaction Network Describing the Thermal Decomposition Process in 1,3,5-Trinitrohexahydro-s-triazine (RDX).* Journal of Physical Chemistry, 2005. **In preparation**.

Behrens, R. and D. Wiese-Smith, *Reaction Kinetics of RDX in the Condensed Phase*, in *40th JANNAF Combustion Meeting*. 2005, CPIA Publication: Charleston, South Carolina. p. June 2005.

Rauch, R. and R. Behrens, *Vapor Pressures and Thermal Decomposition Processes of Bis(2,2-dinitropropyl) acetal (BDNPA) and Bis(2,2-dinitropropyl) formal (BDNPA).* Propellants Explosives Pyrotechnics, In preparation.

Behrens, R. *Understanding the Effects of Age on the Reaction Processes that Underlie Insensitive Munitions*. in *Insenstive Munitions – Proceedings of The Effect of Ageing Upon Lifecycle Workshop*. 2005. Helsinki, Finland: NATO MSIAC.

Reaction Mechanisms of Energetic Materials in the Condensed Phase: Long-term Aging, Munition Safety and Condensed-Phase Processes in Propellants and Explosives

Richard Behrens
Sandia National Laboratories
Combustion Research Facility
Livermore, CA 94551-0969
Project No: 43381CH
Reporting Period: Aug. 1, 2005 to July 31, 2006

Abstract

The main focus of this project is understand the complex reaction processes of the ingredients that comprise propellants and explosives and to develop mathematical models of these reaction processes that can be used to assess issues associated with their performance, safety, aging and detection. During the past year, our investigations have focused on three areas: (1) developing a better understanding of the complex set of nonlinear reaction processes that control the decomposition of RDX both below and above its melting point, (2) investigating the thermal decomposition of high-nitrogen compounds, such as triaminoguanidinium tetrazolate (TAGzT) and its interaction with other ingredients, such as RDX, which are used in gun propellant formulations, and (3) investigating the role of polymers and plasticizers on the thermal decomposition processes in HMX-based explosives. Investigations on the last topic lead to the discovery of an interesting complex formed between nitrocellulose (NC) and a K10 plasticizer. In addition, we have organized a workshop on "R&D Required to Implement New Energetic Ingredients in Munitions".

Contents

Abstract 1
Contents 1
Summary 2
RDX Reaction Processes. 3
High-nitrogen Compound Reaction Processes. 6
Initial TAGzT thermal decomposition scheme. 8
Evolution of decomposition products – low confinement. 10
Evolution of decomposition products – high confinement. 12
Thermal decomposition of a mixture of TAGzT with RDX. 14
Decomposition of HMX-based formulations. 15
BDNPA and BDNPF plasticizer mass spectra, vapor pressure and decomposition. 16
Interactions of Nitrocellulose with K10 Plasticizer 17
Workshop organization: "R&D Required to Implement New Energetic Ingredients in Munitions 19

Summary

The main focus of this project is to understand the complex reaction processes that occur in the ingredients that comprise propellants and explosives, and to develop mathematical models of these reaction processes that can be used to assess issues associated with their performance, safety, aging and detection. The investigations focus on reactions that occur between 20 and 300°C. Understanding the physical and chemical reaction processes in this temperature range will: (1) enable the development of new ingredients required to meet new performance requirements, (2) provide new insight into how to design new formulations that meet insensitive munition (IM) requirements, (3) provide insight into what may cause incompatibility between ingredients, and (4) provide data on the vapors that evolve from explosives that can be used to design explosive detection systems.

From the scientific point of view, the objective of this project over the years has focused on developing an understanding of the complex reaction processes that control the thermal decomposition of RDX and HMX. To accomplish this objective, new experimental methods had to be developed. This required: (1) the development of the simultaneous thermogravimetric modulated beam mass spectrometry (STMBMS) instrument and refinement of experimental protocols to accurately probe the rates of gas evolution during the thermal decomposition process, (2) the development of a reaction modeling and kinetics (REMKIN) compiler and analysis tool needed to develop models of complex reaction processes and determine their associated parameters from the STMBMS data, and (3) the development of a chemical imaging precision mass analysis (ChIPMA) instrument to probe the dependence of chemical reaction processes on microscopic spatial scales. This suite of instruments, experimental protocols, and modeling/simulation algorithms provides new capabilities to probe how the underlying physical processes, chemical reactions and their dependence on morphological structures and spatial location control reactions of materials in the condensed phase.[2] These types of complex reactions underlie the behavior of explosives and propellants over many of the conditions encountered during their life cycle.

The work on this project during the past year has focused in three areas: (1) developing a more detailed understanding the processes that control the decomposition of RDX and constructing mathematical models of these processes, (2) investigating the thermal decomposition of high nitrogen compounds such as triaminoguanidinium tetrazolate (TAGzT) and starting to investigate its interaction with other ingredients, such as RDX, which are used in gun propellant formulations, and (3) collecting data on the decomposition of several different types of HMX-based explosive formulations to ascertain the role of other ingredients in controlling the thermal decomposition of HMX-based explosives.

RDX Reaction Processes.

We have been investigating the thermal decomposition of RDX and HMX for the past 20 years. Over this period we have developed the experimental methods to collect data with a sufficient amount of information to enable us to identify and characterize many of the underlying reaction processes. This work has shown that the reactions of both compounds are controlled by a set of complex nonlinear reaction processes. The specific physical processes and chemical reactions from this set that dominate the overall thermal decomposition process for as specific experiment is very strongly dependent on the temperature, pressure and heating rates used in an experiment. The features of these processes have been characterized by a general reaction network describing the process.[3]

To develop mathematical models of these processes we have developed the REMKIN compiler and analysis tool that allows one to postulate physicochemical reaction models, automatically generate and numerically solve the associated set of differential equation and determine the parameters for the models by numerical optimization to the STMBMS data. This methodology has been demonstrated with initial models characterizing the decomposition of RDX both below and above it melting point.[4]

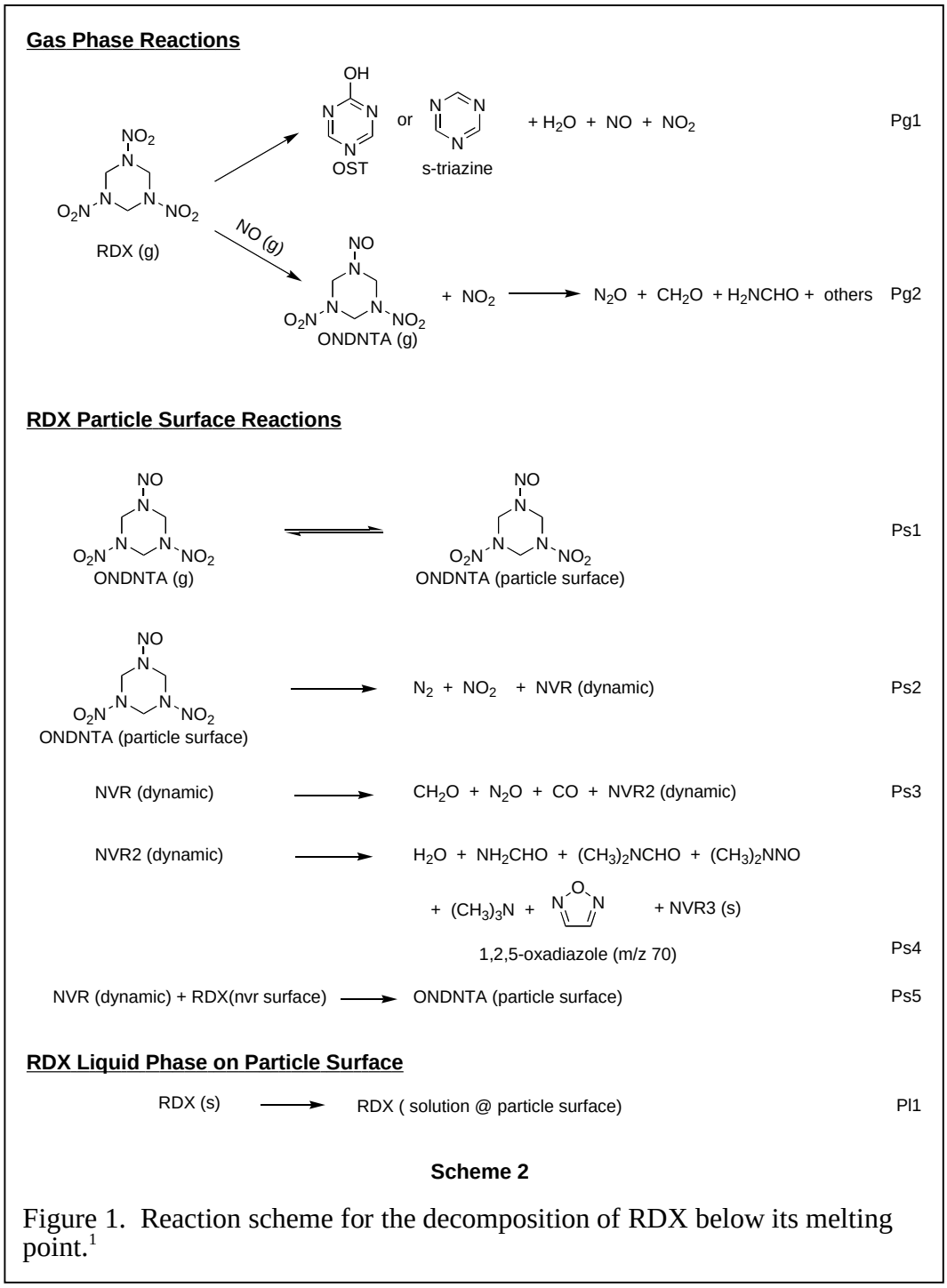

Figure 1. Reaction scheme for the decomposition of RDX below its melting point.[1]

Over the past year we have examined the decomposition of RDX in more detail below its melting point and have determined a more refined reaction scheme for this set of conditions (Fig. 1). Since the rate of reaction of RDX in the solid phase is very low (below our ability to measure it), making the decomposition of RDX in the gas phase the dominant process, these experiments allowed the reaction processes of RDX in the gas phase to be probed under low-pressure conditions. The data revealed that the direct decomposition of RDX in the gas phase forms more s-triazine than OST (Reaction Pg1).

This is opposite to the direct decomposition of RDX observed in experiments with RDX in the liquid phase,[5] which forms almost entirely OST. The gas-phase reactions also involve the replacement reaction of NO with RDX to form ONDNTA and NO_2 (Reaction Pg2).

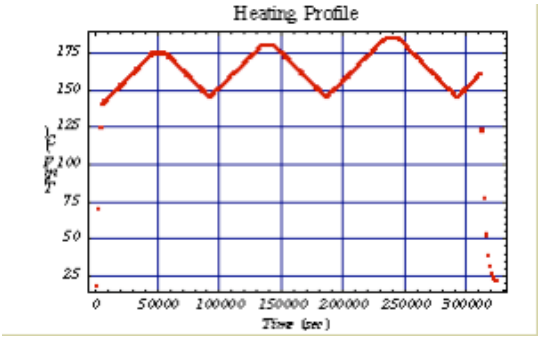

Figure 2. Heating profile for RDX experiments.

As the ONDNTA is formed in the gas phase within our reaction cell, it starts to deposit on the surface of the RDX particles, creating a new reaction environment and establishing a two phase equilibrium between the liquid phase on the surface of the RDX particles and the gas phase. On the surface of the RDX particles the ONDNTA decomposes releasing gaseous products such as CH_2O, N_2O, N_2, and NO_2 and leaving a nonvolatile residue (NVR) on the surface. This reaction process is summarized in reactions Ps1 through Ps5 in Figure 1.

To examine the direct gas-phase decomposition of RDX in more detail we have run several new STMBMS experiments in which the RDX was heated and cooled at ~ 0.03°C/min in cyclic manner (Fig. 2). To reduce contributions from reactions on the

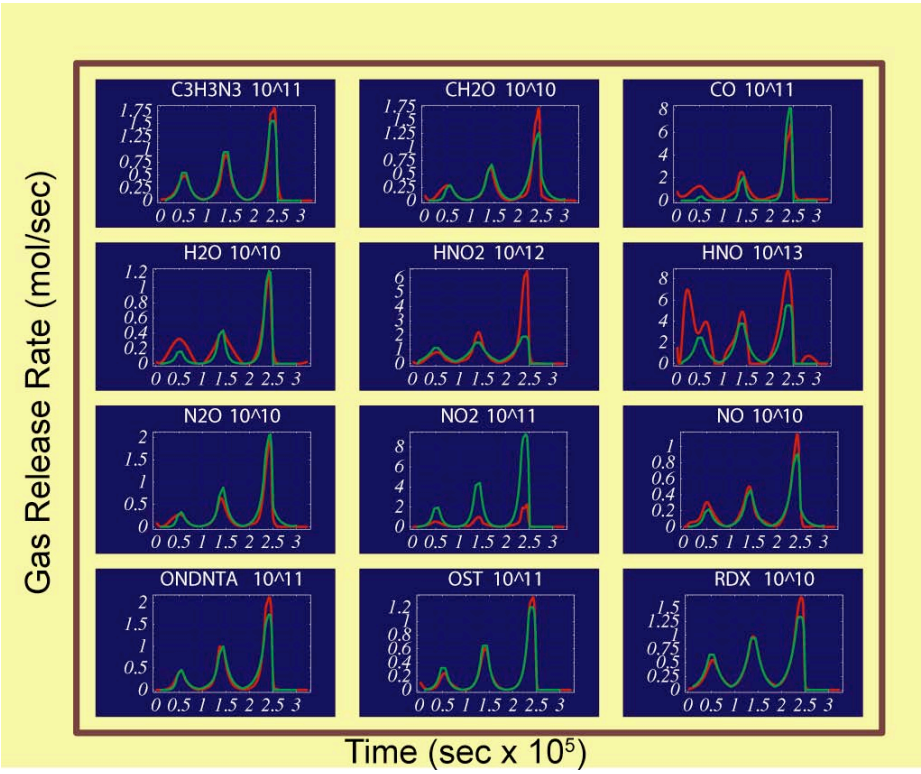

Figure 3. Gas release rates of decomposition products from RDX below its melting point. Red lines represent data, green lines represent the fit from the model. Parameters optimized to fit RDX, s-triazine, OST and ONDNTA data.

surface of the RDX particles, the maximum temperature during initial thermal cycle was 175°C. The rates of gas formation for the various products are represented by the red curves in Figure 3. The green curves are the results from the parameterized reaction model developed using REMKIN.

The relative rates of formation of s-triazine and OST from the direct decomposition of RDX were examined using the first thermal cycle from the data (Fig. 3). The reactions of RDX in the gas phase

$$RDX(g) \rightarrow \text{s-triazine} + 3\ HONO \qquad A = 2.35 \times 10^{4},\ Ea = 58\ kJ/mol \qquad (R1)$$

$$RDX(g) \rightarrow OST + 2\ HONO + HNO \quad A = 3.7 \times 10^{9},\ Ea = 105\ kJ/mol \qquad (R2)$$

suggest that the activation energy for the reaction forming s-triazine (58.4 kJ/mol) is significantly lower than the activation energy for the reaction forming OST (105 kJ/mol). Thus, by assuming that both s-triazine and OST originate from the direct decomposition of RDX in the gas phase, the formation of s-triazine will be more prevalent at lower temperature. However, in the liquid phase, we have observed that the reaction producing OST is predominant. Thus, the observed increase in the rate of formation of OST on subsequent thermal cycles (Fig. 3) may be due to the creation of a liquefied layer of RDX on the surface of the particles, and not due to the increase rate of reaction R2 in the gas phase at higher temperature. Further refinement of the reaction models for RDX and the parameters for the various reactions is currently in progress.

High-nitrogen Compound Reaction Processes.

The Army is investigating the use of high nitrogen (HiN) compounds for use in advanced gun propellants. To provide a basis for understanding the reaction processes of these materials and how they may affect gun propellant performance, safety and aging behavior we have started to investigate the reactions of several HiN compounds. The high nitrogen compounds are typically used by replacing a portion of the RDX in a conventional gun propellant with the HiN compounds. It was decided to investigate the HiN compounds instead of some of the compounds in the original ARO proposal (24DNI, NTO), since these compounds are of current interest to the Army in the development of new propellants. They also afford us the opportunity to develop our methods further by allowing us to investigate the reactions of mixtures of the HiN compounds with compounds that we have already studied (i.e., RDX and bis(2,2-dintropropyl)acetal (BDPNA) and bis(2,2-dintropropyl)formal (BDNPF)).

The HiN compounds under investigation are TAGzT and guanidinium tetrazolate (GUzT). In closed bomb combustion tests (Chris Walsh, NSWC/IH) in which new HiN compounds were used to replace a portion of the RDX in a gun propellant, it was found that TAGzT and GUzT had quite different effects. The burning rate of the propellant was increased much more by the addition of TAGzT compared to GUzT. Given the similarity of these two compounds, this was an interesting result. It suggests that TAGzT may somehow alter the burn rate of the RDX.

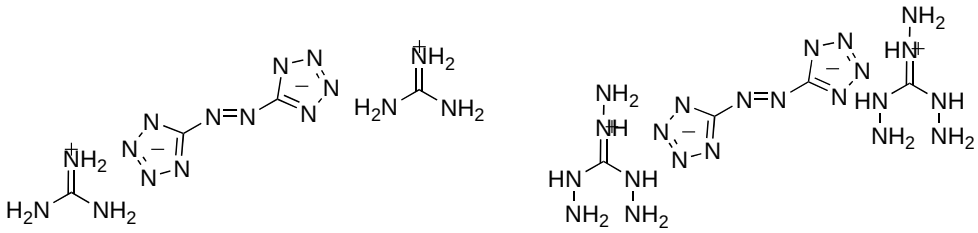

Guanidiium Azotetrazolate (GUzT) Triaminoguanidinium Azotetrazolate (TAGzT)

During the past year we have been investigating the thermal decomposition of TAGzT and its interaction with RDX. In this report we summarize our initial results on the decomposition of TAGzT.

TAGzT, like most energetic compounds we have studied, decomposes via a relatively complex reaction process that is dependent on the interaction of TAGzT with its own decomposition products. To examine these types of effects, experiments were conducted in which the extent of confinement of the gaseous decomposition products from TAGzT with the sample were varied. Higher confinement creates conditions in our experiments that increase the likelihood of secondary reactions of the decomposition products. To implement this, experiments were carried out using 25 µm and 1000 µm diameter orifices in our reaction cells.

General mass loss behavior. The mass loss during the decomposition of TAGzT under low and high confinement conditions are shown in Figure 4. Note the significant difference in the force measured in each experiment. In the lower confinement experiment (TAGzT010) there is a gradual increase in the mass loss starting at about 170°C and continuing up to about 204°C, where there is on onset of more rapid mass loss. In the higher confinement experiment, the mass loss up until the onset of rapid decomposition is small (and has been attributed to evolution of a water contaminant from the sample). Under higher confinement the rapid decomposition occurs at a temperature that is approximately 10°C lower than in the lower confinement case. In addition, about 40 wt.% of the TAGzT forms a relatively non-volatile product that decomposed between 200 and 250°C in our experiment. This type of product is not formed to an appreciable extent in the lower confinement experiment (TAGzT010). (Note: the apparent 0.2mg

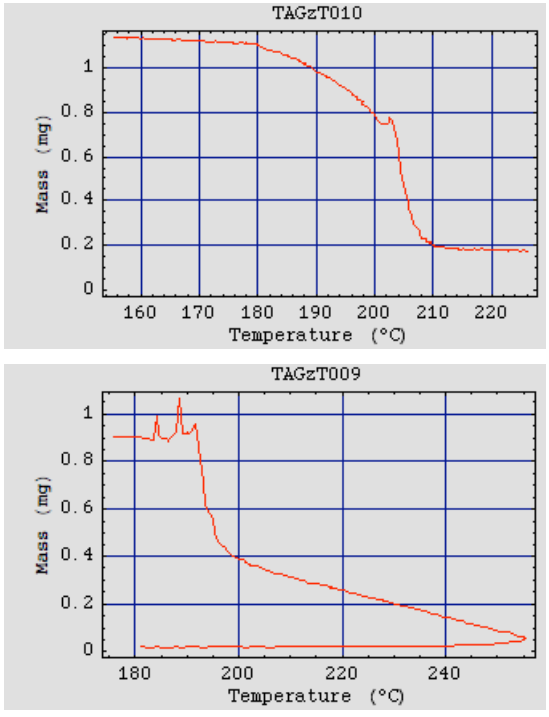

Figure 4. Mass loss during the decomposition of TAGzT under low (TAGzT010) and high (TAGzT009) conditions. Note: the apparent mass gain is due to the fact that the microbalance measures the force, which is composed of the mass of the sample and the thrust generate by the gas in the reaction cell.

of mass remaining in TAGzT is attributed to the loss of water that was adsorbed on the TAGzT within the reaction cell prior to the start of data collection in the experiment.)

Initial TAGzT thermal decomposition scheme.

Based on the results of approximately 15 STMBMS experiments with TAGzT and 10 thermal decomposition experiments using the chemical microanalysis reactor and the Fourier Transform ion cyclotron resonance (FTICR) mass spectrometer, the products formed during the thermal decomposition of TAGzT have been identified and the sequence of their evolution during the course of an experiment established. From this data we have created a reaction scheme (Fig. 5) to characterize the main features of the decomposition process. The ion signals formed in the mass spectrometer from the gaseous products that evolve during the thermal decomposition of TAGzT under low and high confinement conditions are shown in Figure 6.

The first seven steps of the reaction scheme were developed from data in lower confinement experiments, such as shown on the left in Fig. 6. The final two steps were developed based on higher confinement experiments, such as shown on the right in Fig. 6. Please note that secondary reactions, other than those listed in Figure 5, also occur during the course of the experiment. For example, it is likely that some of the hydrazine, N_2H_4, undergoes reaction prior to exiting the reaction cell.

The reactions may be summarized as follows:

1. Reaction R1 is the initial decomposition of TAGzT to form TAG (g) and tetrazolate. The transfer of hydrogen from the TAG cation to the tetrazolate anion appears to be the first step in the reaction. This is in agreement with Riad Manna's quantum chemistry calculations (LLNL).
2. Reaction R2 is the initial decomposition of TAG(g). This reaction is written to indicate that TAG forms hydrazine. Reaction R3 captures the subsequent reaction of the remaining part of the TAG molecule to form NH_3, HCN and N_2.
3. Reaction R4 represents the decomposition of the molecule formed from the tetrazolate ion. This tetrazolate molecular species (m/z=166) is not observed in the mass spectrometer. The largest fragment observed from the tetrazolate is observed at m/z=110 and has the formula, $C_2H_2N_6$. This species is formed from the central portion of the tetrazolate molecule – the region around the diazene group. Two possible structures for the $C_2H_2N_6$ species are shown. (Note: The ion signal measured at m/z=166 occurs during the latter part of the decomposition process and the FTICR data indicate this species has a formula of $C_4H_6N_8$. Thus, it is not the molecular ion of the tetrazolate.)
4. Reaction R5 captures the fact that the 110 species, or the decomposition of the tetrazolate anion that does not form the 110 species, is likely to form a nonvolatile "polymeric-like" product (NVPP) during the decomposition process. This NVPP has not been directly observed, but the identities of gaseous products that evolve after the TAGzT has decomposed suggest that this type of compound is formed during the decomposition of TAGzT.

5. Reaction R6 represents the decomposition of the NVPP. For example, one of the products observed after TAGzT has decomposed is at m/z=166.0711 and has a

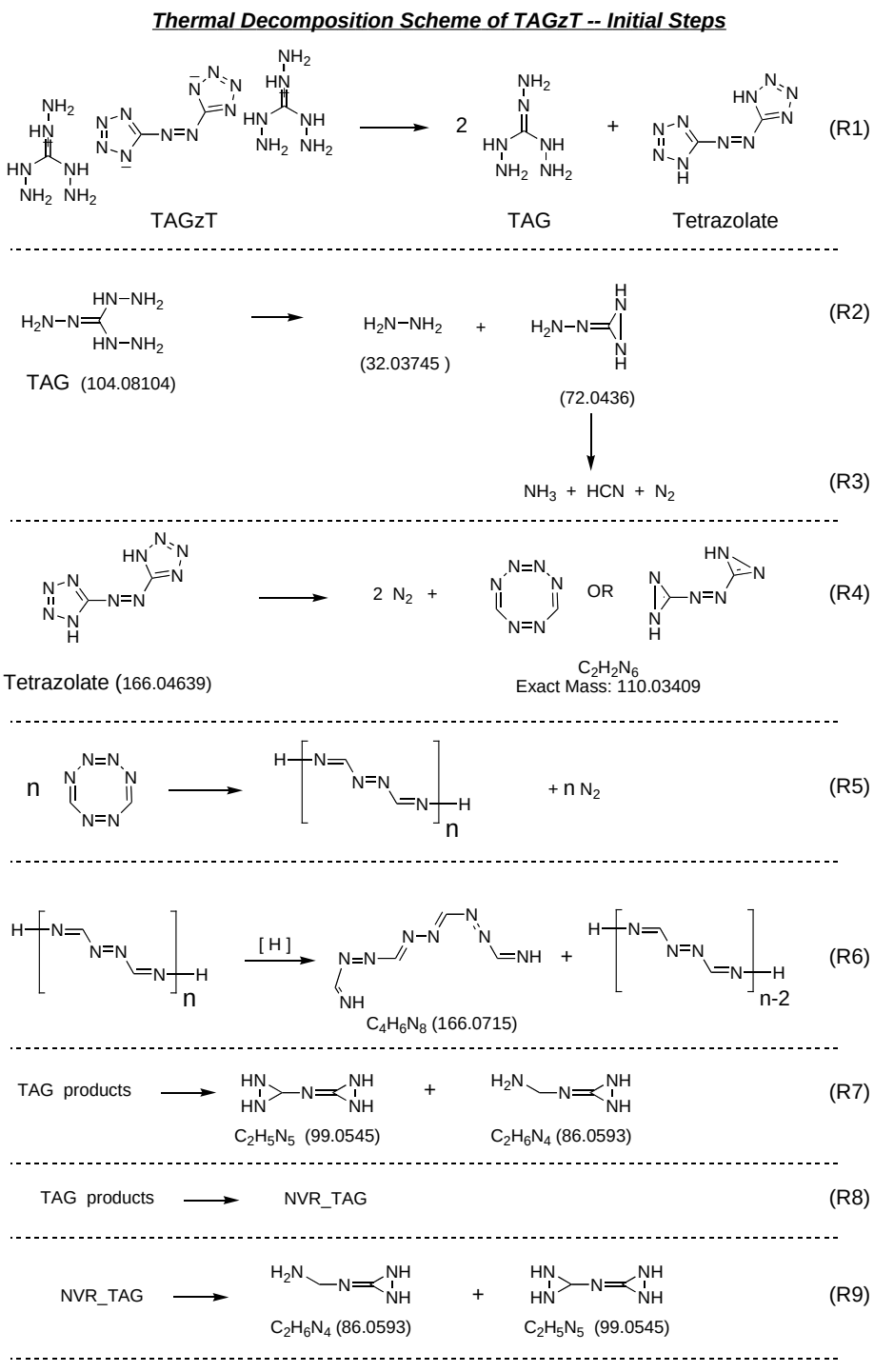

Figure 5. Reaction scheme that characterizes the main features of the thermal decomposition of TAGzT.

formula, $C_4H_6N_8$.

6. Reaction R7 represents a generic set of reactions that involve the secondary reactions of TAG and its decomposition products. From the lower confinement experiments the details of these secondary reactions are difficult to elucidate. Products are observed at m/z values of 99 and 86. Possible structures for these products are shown.
7. Reactions R8 and R9 represent the formation of a non-volatile product from the TAG decomposition products. These two steps are added to the reaction scheme based on results from the higher confinement experiment (Fig. 6).

Evolution of decomposition products – low confinement.

The temporal behaviors of the rates of evolution of the various gaseous products from TAGzT show that its decomposition involves a complex nonlinear process. This behavior, taken together with the fact that TAGzT is a relatively high molecular weight salt with low volatility, suggests that the reaction process may involve changing morphological features of the decomposing TAGzT particles.

The temporal behaviors of the ion signals associated with the major thermal decomposition products formed during a low confinement experiment are shown in Figure 6. Panel A shows the ion signals representing the evolution of TAG and the central portion of the product that originates from the tetrazolate ion. Note that the rate of increase of the TAG signal is similar to what is observed during a dissociative sublimation process. If the process was truly a dissociative sublimation, then the tetrazolate molecules should have the same temporal behavior as TAG. This is not the case. The product formed from the tetrazolate lags the TAG initially and then appears to overtake the TAG as the experiment progresses. From 170 to 195°C the TAG and tetrazolate product are proportional to each other. However, above 195°C the tetrazolate product increases more rapidly than the TAG. Given the formation of the lower molecular weight products, via Reactions R2 and R3, one expects less TAG to be observed due to its increasing rate of decomposition. Thus, the tetrazolate product provides a better characterization of the first step in TAGzT decomposition process.

The major lower molecular weight products formed as the sample decomposes, N_2H_4, NH_3, HCN, and N_2, are all temporally correlated in this experiment. The temporal behavior of the signals representing these four products are not directly correlated with the signals representing the dissociative sublimation, which suggests that the reaction process may be controlled by a complex process that has several distinguishing features.

First, the relatively abrupt jump in the rate of gas formation of the four products at ~175°C suggests that the sample has undergone some form of abrupt transformation that has “turned on” the reaction that controls the decomposition of TAG. If the source of the four products were from TAG in the gas phase within the reaction cell, then the rate of increase of these products should be more gradual and track the partial pressure of TAG within the reaction cell. The four products do not appear to do this. Once the products do appear, their rate of formation does not increase appreciably between 175 and 195°C.

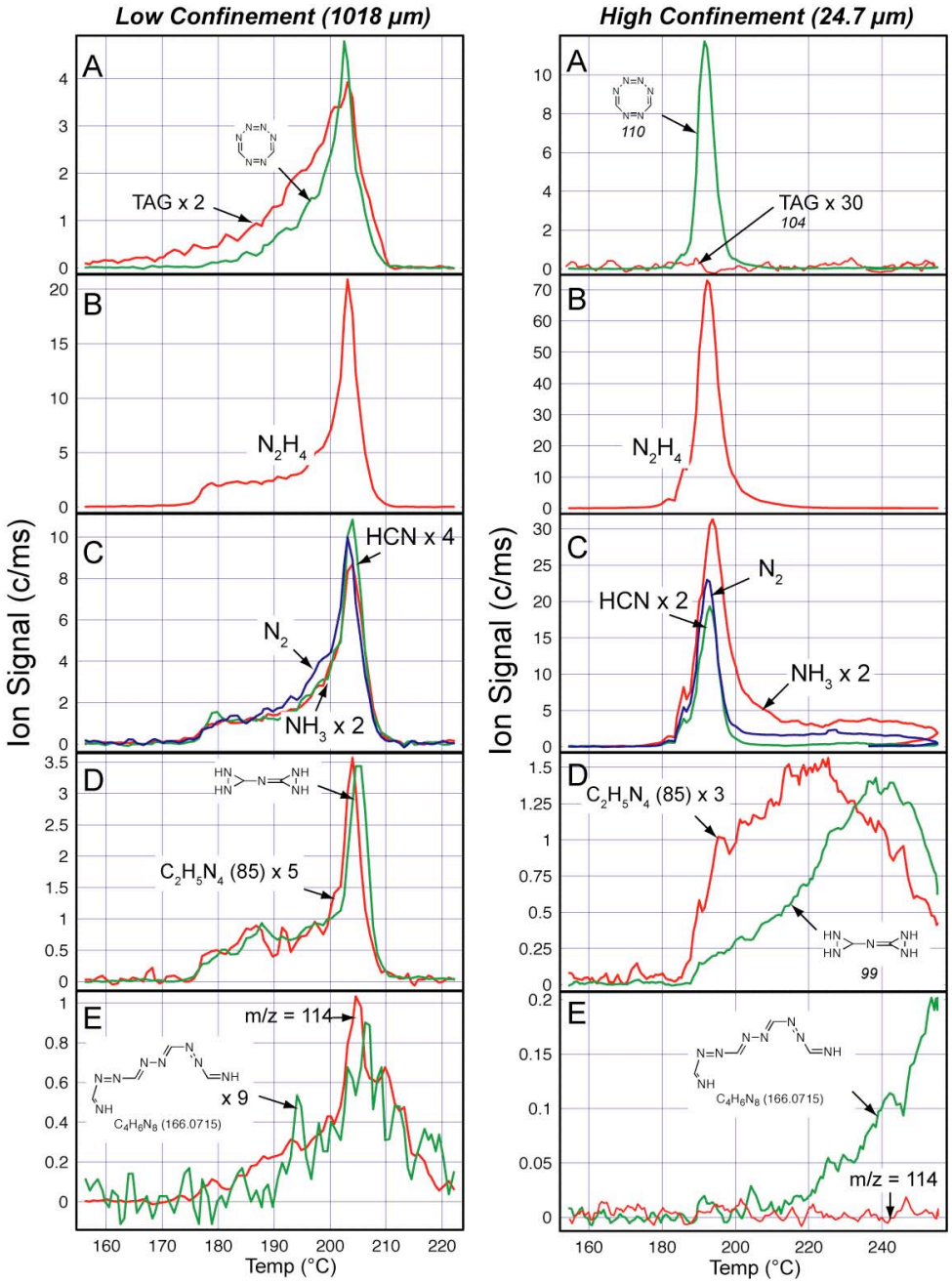

Figure 6. Ions signals created in the mass spectrometer from gaseous products that evolve during the thermal decomposition under low (TAGzT010) and high (TAGzT009) conditions.

This suggests that diffusion-like processes within the particles may limit the rate of gas formation in this temperature range.

Second, at ~195°C, the rate of formation of the four products increases quite rapidly. The rate of increase of the four lower molecular weight products in this region, N_2H_4, NH_3, HCN, N_2, correlate with the more rapid rise in the tetrazolate product (Panel A) in this

higher temperature region. This suggests that the decomposition process may be relatively simple. However, the formation of the NVPP (Reaction R5) within the particles would provide the means for the emergence of a new reaction pathway involving the NVPP.

The products that involve secondary reactions of intermediates formed in the decomposition of TAG are shown in Panel D. These products are temporally correlated with the four major TAG decomposition products as is expected. These higher molecular weight products contain two carbon atoms and significantly fewer hydrogen atoms than the TAG. Thus, the products appear to arise from the reaction of a guanidinium intermediate with either one of the lower molecular weight products (N_2H_4, NH_3) or another guanidinium intermediate.

Finally, the products formed from the NVPP are shown in Panel E. In this experiment the signals from these products are relatively small. Experiments conducted under higher confinement provide the information needed to clarify the reactions that are involved with the formation and subsequent decomposition of the NVPP.

Evolution of decomposition products – high confinement.

The temporal behaviors of the ion signals associated with the major decomposition products formed under high confinement are shown on the right in Figure 6.

Panel A shows the ion signals representing the evolution of TAG and the central portion of the product that originates from the tetrazolate ion. Note that the TAG signal is essentially zero compared to the lower confinement experiment. The data from the higher confinement experiment shows that the TAG molecule is unstable compared to the product formed from the tetrazolate product (represented by m/z=110).

Given the formation of the lower molecular weight products, via Reactions R2 and R3, one expects less TAG to be observed due to its increasing rate of decomposition. This is definitely the case with the higher confinement experiment, in which no TAG evolves from the reaction cell. Thus, the tetrazolate product is useful for characterizing the first step in TAGzT decomposition process.

The major lower molecular weight products formed as the sample decomposes, N_2H_4, NH_3, HCN, and N_2, are still temporally correlated with each other. However, in the higher confinement experiment, the N_2H_4, N_2 and HCN signals are more highly correlated with each other compared to the NH_3 signal. This is somewhat different from the results in the lower confinement experiment in which the HCN, N_2, and NH_3 were more highly correlated. In the higher confinement experiment the NH_3 appears to arise from two sources. The first is the decomposition process that also produces N_2H_4, HCN and N_2. Note the high correlation of the small shoulder at ~185°C in the higher confinement experiment. This part of the reaction is characterized by reactions R2 and R3. The second contribution is from the decomposition of a less volatile secondary product that was formed during the initial decomposition of TAGzT. Close examination of these four products shows that the evolution of the N_2H_4, HCN and N_2 are essentially complete by the time the sample reaches 200°C. In contrast the rate of evolution of NH_3 remains relatively high at 200°C and continues to evolve at an appreciable rate as the sample is heated to 250°C.

Examination of the evolution of N_2H_4, HCN, N_2 and the tetrazolate product (m/z=110) suggests that the TAGzT has completely decomposed by 200°C. At this point it is worthwhile to examine the mass loss data again. We find that at 200°C approximately 45% of the mass of the original sample remains in the reaction cell after the TAGzT has completely decomposed. Thus, to account for this fraction of the mass remaining as a non-volatile products requires a contribution from both the tetrazolate and TAG portions of the molecule.

The data from the higher confinement process provides more insight into the formation of the NVR and NVPP products, which were first observed in the lower confinement experiments. Examination of the products associated with m/z values 85 and 99 show a marked contrast between low and high confinement. The ion signals at m/z values 85 and 99 evolve over a broad range of temperature. The two ions signals are not temporally correlated. The rate of evolution of the product represented by m/z=85 rises to a high value as TAGzT nears depletions (~200°C) and then climbs slowly as the temperature continues to rise. In contrast, the rate of evolution of the product represented by m/z=99 is a relatively low value as the TAGzT nears depletion and rises by a factor of ~10 as the sample is heated.

The data on the products represented by m/z values 85 and 99 suggest that a non-volatile product is formed from the TAG decomposition products during the decomposition of TAGzT. This is supported by the following facts: (1) the products represented by m/z 85 and 99 evolve mostly after the decomposition of TAGzT is complete, (2) the products contain a relatively high mole fraction of hydrogen – suggesting TAG as the origin, (3) the molecular weight of the product is relatively low suggesting that their vapor pressure would be relatively high and they would evolve from the reaction cell as they were formed in the initial decomposition of TAGzT.

The sequence of evolution of the two products poses new questions regarding the nature of the NVR formed from TAG. For example, what is the chemical structure of the NVR? Does the product represented by m/z=85 evolve from a specific set of functional groups within the NVR? Does the product represented by m/z=99 represent a different structure within the NVR or is this structure formed within the NVR and the sample continues to be heated? The current data does not provide sufficient information to address these questions.

Finally, the products formed from the NVPP are shown in Panel E for each experiment. Large differences are observed between the behaviors of the ion signals at the m/z values associated with the NVPP under low and high confinement conditions. Under lower confinement conditions, there are correlated signals at several m/z values (114, 142, 166), whereas under higher confinement conditions the only signal remaining from the group is at m/z=166. In addition, the product represented by m/z=166 evolves at lower temperature in the lower confinement experiment compared to the higher confinement experiment. This suggests that a more stable NVPP is formed under higher confinement conditions. Furthermore, the mass loss after the TAGzT has decomposed is much larger under higher confinement (~ 40 to 45wt% after 200°C) than lower confinement (~3wt% after 210°C).

Higher confinement clearly produces more NVR and NVPP during the decomposition process. In the current experiment the NVR and NVPP represent 45wt% of the products formed during the decomposition of TAGzT. It is important to determine how the NVR and NVPP are formed during the decomposition of TAGzT.

Thermal decomposition of a mixture of TAGzT with RDX.

Over the past year we have started to examine the decomposition of mixtures of TAGzT and RDX to determine whether and how each ingredient may affect the decomposition process of the other ingredient. In our initial experiments we have found very strong interaction between the hydrazine, formed in the decomposition of TAGzT, and RDX. In the mixtures the ion signal from N_2H_4 drops to about 1 c/ms and we see a concomitant rise in the H_2O, NO and N_2O signals. This indicates that there is a very strong interaction between the hydrazine and the NO_2 groups on the RDX. We are currently collecting more data on this mixture and will report more results in the future.

Note: The work on high nitrogen compounds and HiN-based propellants was done in collaboration with Heather Hayden, NSWC/Indian Head. This work represents part of H. Hayden's doctoral thesis at George Washington University.

Decomposition of HMX-based formulations.

To characterize the decomposition processes that occur in propellants and explosives requires understanding the decomposition behavior of the individual ingredients, as well as the interactions that may occur between the various ingredients. To address these issues we have conducted experiments to examine the decomposition of several different HMX-based explosives: PBX9501 (95%HMX, 2.5%BDNPA/F, 2.5% Estane), LX-04 (85%HMX, 15% viton), EDC-37 (AWE explosive, 91%HMX, 1%NC, 8% K10 – a mixture of dinitro- and trinitro-ethylbenzene), and LX-14 (95.5% HMX, 4.5% Estane).

During the first few months of the project, which is covered by this interim report, we have completed our initial study of the thermal decomposition of BDNPA and BDNPF plasticizer and submitted it for publication.[6] We have also documented the data that we have collected on the decomposition of LX-04, LX-14, PBX9501 and EDC-37 and prepared several sets of data for development of decomposition models of HMX using REMKIN when we resume this task.

Our main findings with regard to how the ingredients in the binders affect the decomposition of HMX is that the Estane polymer appears to have the most significant affect on the process that controls the thermal decomposition of HMX. The data shown in Figure 7 illustrates this effect. The global rate constant for decomposition of PBX9501 and LX14 are much higher during the first three reaction cycles compared to the global rate constant for decomposition for LX04 and a 6µm HMX powder. This suggests that Estane may interact with the HMX more than the BDNPA/F plasticizer.

The reason for the increased rate of mass loss due to the release of thermal decomposition products in formulations that contain Estane has not yet been determined. There are two possible explanations. First, the Estane may chemically interact with at HMX on the surface of the HMX particles leading to the decomposition of HMX on the surface of the particles. The other possible explanation is that the Estane binds to the surface of the particles, forming a rigid structure. As the sample is heated and cooled in the thermal cycling the thermally induced stresses cause the HMX particles to fracture. This results in the gaseous products being formed within the HMX particles to be released earlier than is observed in experiments with only HMX particles or in the LX04 or EDC-37 formulations. Further experiments will be required to determine the correct explanation.

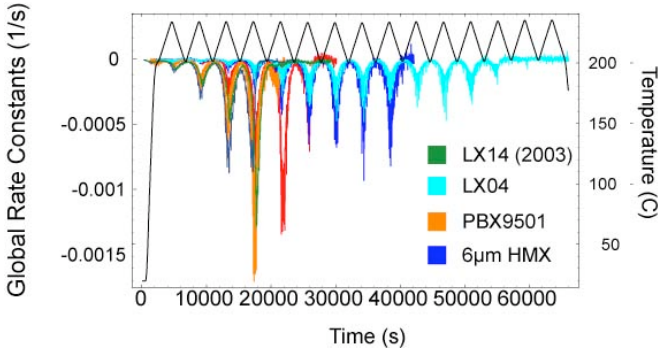

Figure 7. Global reaction rate constants, based on mass loss, from experiments investigating the effect of the Estane binder on the decomposition process. The sample is heated to 200°C and then cycles between 200 and 235°C at ± 1°C/min.

To summarize the current state of our work with explosive formulations, we have collected thermal cycling data on four

different types of explosive formulations. It appears that explosive containing Estane binder may decompose at a faster rate. The data has been collected in thermal cycling experiments over temperature ranges of 200 to 235°C (as presented in the figures in this report) and 170 to 200°C. Examination of the global rate constant data shows that the rate of decomposition can be significantly altered by presence of other ingredients. The data collected to date has all of the information on the rates of evolution of various species that we collect in our STMBMS experiments. This data will be used to develop more detailed mathematical models of the reaction processes that occur in these composite materials.

BDNPA and BDNPF plasticizer mass spectra, vapor pressure and decomposition.

A paper describing the mass spectra, vapor pressure and thermal decomposition processes in BDNPA and BDNPF has been prepared and accepted for publication.[6] The following few paragraphs summarize the findings.

The mass spectra of BDNPA and BDNPF are, for the most part, structurally analogous, but differ significantly in the relative abundance of some ion fragments. Each compound contains two ion fragments that make up more than 60 percent of the overall signal percentage. BDNPF exhibits a greater propensity to cleave a nitro group and forms smaller molecular weight fragments with greater abundance than BDNPA. The fragmentation pattern of the mass spectrum for each compound is sensitive to the internal energy of the molecules entering the mass spectrometer with the bond rearrangement process forming the daughter ions in the mass spectrum being similar to the bond rearrangements that occur during the thermal decomposition of each compound.

STMBMS data from 80-110 °C was used to measure the vapor pressure as a function of temperature for BDNPA and BDNPF. BDNPA exhibits a higher vapor pressure than BDNPF at temperatures higher than 56°C. For BDNPA, the enthalpy of vaporization (ΔH_{vap}) is 93.01 ± 0.38 kJ/mol and the vapor pressure at 25°C equals 0.0109 + 0.003/ – 0.002 millitorr. BDNPF has a lower enthalpy of vaporization, 84.77 ± 0.88 kJ/mol, but a higher vapor pressure at 25°C, 0.0165 + 0.014/ – 0.008 millitorr.

BDNPA and BDNPF undergo thermal decomposition at appreciable rates starting between 160-180 °C. The decomposition of each compound is characterized by a nitro-nitrite rearrangement mechanism and the formation of a low volatile residue (LVR). This decomposition pathway produces a high molecular weight alkyl radical, NO and NO_2 radicals, and a stable ketone identified as 1-(vinyloxy)propan-2-one in BDNPA and 1-methoxypropan-2-one in BDNPF. The remaining alkyl radicals begin to react and form an LVR that suppresses evaporation when the amount of pristine plasticizer left in the reaction cell reaches a critical minimum. The nitroxyl radicals react with alkyl reaction cell products to form amine, imide and amide decomposition products. Lower molecular weight decomposition products, such as H_2O and CO, appear at ~230 °C.

Some significant differences exist between BDNPA and BDNPF decomposition. The global weight loss rate of BDNPF is slower than that of BDNPA under the same experimental conditions. This, in part, can be attributed to a lower vapor pressure in BDNPF. Furthermore, the temporal behavior of the ketone product from nitro-nitrite

rearrangement in BDNPF (1-methoxypropan-2-one) is different than that of BDNPA (1-(vinyloxy)propan-2-one). The release of this product is delayed in the decomposition of BDNPF due to the formation of a low volatility reaction intermediate that resides in the condensed phase. This intermediate does not appear to form from secondary reactions in the decomposition of BDNPA, which is most likely due to steric hindrance from the acetal functional group.

Interactions of Nitrocellulose with K10 Plasticizer

In our thermal decomposition studies of HMX-based explosives, one of the explosives selected for study was EDC-37, an explosive developed by the Atomic Weapons Establishment (AWE, UK) for its low impact sensitivity. EDC-37 contains 91%HMX, 1% NC, and 8% K10 plasticizer by weight. The K10 plasticizer is comprised of equal proportions of 2,4-dinitroethylbenzene, 2,6-dinitroethylbenzene, and 2,4,6-trinitroethylbenzene.

K10:

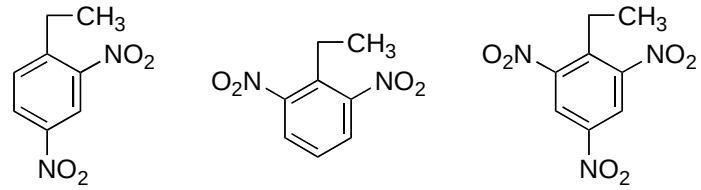

24DNEB 26DNEB TNEB

NC:

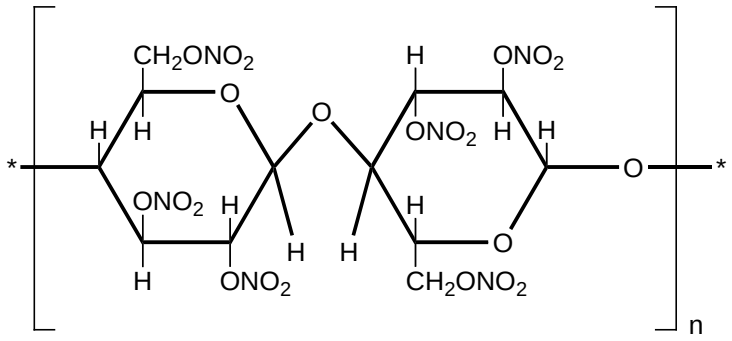

Examination of the data collected in thermal decomposition experiments with EDC-37 suggested that some of the K10 plasticizer might be more strongly bound in the explosive. It was expected that as the sample was slowly heated the plasticizer would quickly evaporate, leaving behind HMX and NC. To examine this unusual behavior mixtures of K10 and NC were prepared in ~8:1 ratio by weight and examined in STMBMS experiments.

The evolution of products from a mixture of 8:1 K10 to NC was compared to the evolution of products from K10 alone as the samples were heated through a series of heating and cooling cycles. The mass loss as the two samples were thermally cycled is shown in Figure 8 and the ion signals representing the different products that evolve from the samples are shown in Figures 9 and 10.

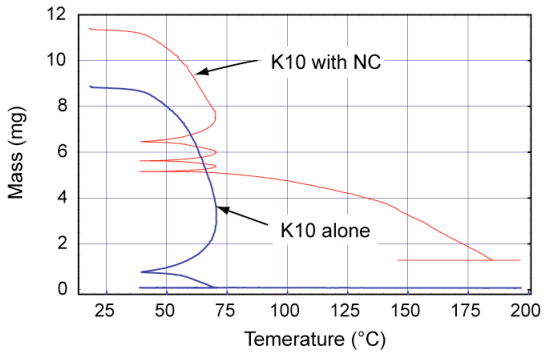

Figure 8. Mass of K10 (blue) and K10/NC (red) samples as the temperature is cycled between 40 and 72°C and finally heated to 200°C. Termination of red line at ~1.5mg is due to balance going off scale and not recording final mass loss.

The mass loss data shows that when the K10 plasticizer is heated by itself it loses all of its mass in the first two thermal cycles in which the maximum temperature was 72°C. In contrast, the mixture of K10 and NC loses approximately one-half of its mass in the first three thermal cycles. Only when the sample is heated up to 200°C does it lose the remaining mass.

Examining the evolution of the constituents from K10 (Fig. 9) shows that the DNEB isomers evolve from the sample faster than the TNEB, as is expected. In contrast, the evolution of the constituents from the K10/NC mixture (Fig. 10) shows several significant differences. First, some of the K10 constituents remain in the sample up until the NC starts to decompose (~170°C). Second, the rate of evolution of TNEB and the DNEB isomers are temporally correlated with each other after the initial loss of plasticizer in the first thermal cycle. This indicates that the release of TNEB and DNEB from the sample, during the later stage of the experiment, is controlled by the binding TNEB and DNEB to the NC. Third, the final portion of the K10 constituents evolves from the sample after the NC has started to decompose.

It is also interesting to note that the rate of decomposition of NC appears to be more gradual compared to several experiments we have run in the past to examine the decomposition of NC by itself.

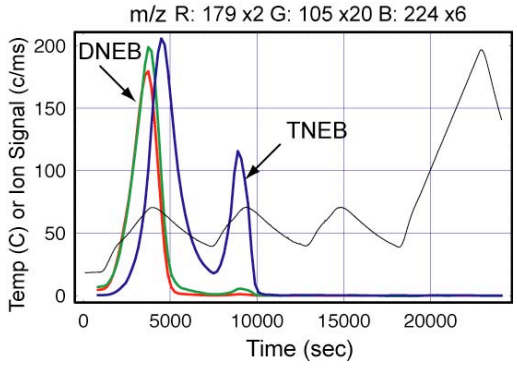

Figure 9. Ion signals representing the evolution of TNEB and DNEB isomers from K10.

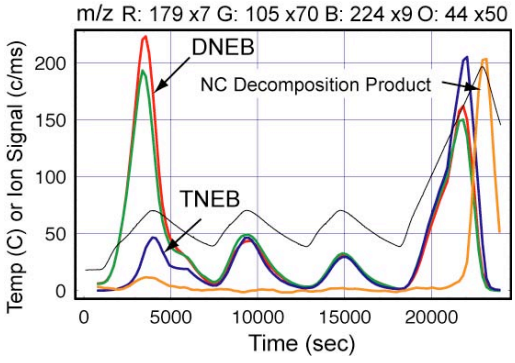

Figure 10. Ion signals representing the evolution of TNEB, DNEB isomers and products from the decomposition of NC/K10 mixture.

These initial results indicate that the constituents of the K10 plasticizer form a noncovalent complex with the NC. This complex may provide a means for the binder to absorb mechanical energy introduced into the sample by impact. For example, the mechanical energy may be dissipated by temporarily moving the K10 constituent from the K10/NC complex into the K10 liquid phase. Thus, the design of this type of complex between the polymer and plasticizers that constitute a binder may provide a means for reducing the impact sensitivity of munitions.

Note: The work on EDC-37 and the K10/NC binders was done in collaboration with Paul Deacon (AWE, UK).

Workshop organization: "R&D Required to Implement New Energetic Ingredients in Munitions.

A workshop has been organized to address the issues of R&D required to implement new ingredients in munitions. The workshop has been organized in cooperation with Bill Anderson (ARL), Brad Forch (ARL) and Bob Shaw (ARO) and will be coordinated through the CPIA/JANNAF organization. The workshop was held at the Battelle Eastern Science and Technology (BEST) Center, Aberdeen, Maryland, on 29 – 31 August, 2006.

The objective of the workshop was to create a plan for R&D investment strategies that will enable the rapid implementation of new energetic ingredients (e.g., high nitrogen compounds, energetic binders, and ionic liquids) needed to reach new munition performance goals, while meeting insensitive munition (IM), aging, quality assessment and cost requirements.

The following technical challenges were addressed.

1. Current development strategies for new ingredients focus on storing more energy in new types of molecules. This strategy targets new military performance goals. Most new molecules are never implemented in new munitions because they release their energy, or are modified in some way, prior to their intended use. This detrimental behavior may be manifested in (1) degradation due to material incompatibility, (2) failure to meet IM requirements (3) manufacturing and scale-up issues.
2. The experimental and modeling tools available to assess the properties of new materials that are the basis for detrimental behavior are: (1) primitive, (2) poor predictors of detrimental behavior, and (3) provide little insight into why new types of molecules fail.
3. New experimental and modeling methods must be developed to evaluate the long-term prospects for new ingredients more rapidly and at lower cost. This challenges most current research capabilities because it demands that we understand how new molecules react by themselves and with other ingredients. The reactions of interest occur at very small spatial scales (i.e., interfaces between ingredients) and at slow rates (i.e. for issues related to aging).
4. R&D is not focused to address these issues.

A select group of program managers and research scientists were assembled to assess the technical challenges, explore options and new ideas for addressing these challenges, and develop an R&D investment strategy that will enable a more successful and rapid implementation of new ingredients into munitions.

References:

(1) Maharrey, S.; Behrens, R. *Journal of Physical Chemistry* **2005**, *109*, 11236.

(2) Behrens, R. Thermal Decomposition Processes of Energetic Materials in the Condensed Phase at Low and Moderate Temperatures. In *Overviews of Recent Research on Energetic Materials*; Shaw, R. W., Brill, T. B., Thompson, D. L., Eds.; World Publications Inc: Singapore, 2005; pp 29.

(3) Behrens, R.; Maharrey, S. Chemical and Physical Processes that Control the Thermal Decomposition of RDX and HMX. In *Combustion of Energetic Materials*; Kuo, K. K., DeLuca, L. T., Eds.; Begell House: New York, 2002; pp 3.

(4) Behrens, R.; Wiese-Smith, D. Reaction Kinetics of RDX in the Condensed Phase. In *40th JANNAF Combustion Meeting*; CPIA Publication: Charleston, South Carolina, 2005; pp June 2005.

(5) Behrens, R.; Bulusu, S. *Journal Of Physical Chemistry* **1992**, *96*, 8877.

(6) Rauch, R.; Behrens, R. *Propellants Explosives Pyrotechnics* **2006**, *Submitted to Propellants, Explosives and Pyrotechnics*.

Publications:

Maharrey, S.; Behrens, R., *Thermal Decomposition of Energetic Materials 5. Reaction Processes of 1,3,5-Trinitrohexahydro-s-triazine (RDX) Below Its Melting Point*. Journal of Physical Chemistry 2005, 109, 11236-11249.

Rauch, R. and R. Behrens, *Vapor Pressures and Thermal Decomposition Processes of Bis(2,2-dinitropropyl) acetal (BDNPA) and Bis(2,2-dinitropropyl) formal (BDNPA) accepted for publication in* Propellants Explosives Pyrotechnics, 2006.

Presentations:

Richard Behrens, *Reaction Process of Energetic Materials at Low & Moderate Temperatures*, University of Missouri, Rolla, October 17, 2005 (*invited*).

Richard Behrens & Sean Maharrey, *Understanding the Reaction Chemistry of IEDs*, DARPA/MTO Workshop on Standoff Detection of IEDs, Chantilly, VA, 11/15/2005, (*invited*).

Richard Behrens, *Understanding the Reaction Chemistry of IEDs*, Department of Homeland Security Physics Methods Workshop, Lawrence Livermore Laboratory, Livermore, CA, 11/30/2005.

Richard Behrens, Using Experimental and Simulation Methods to Understand Reaction Processes in Energetic Materials, Gordon Research Conference, Tilton School, NH, 6/18/2006 (*invited*).

Swanson, R. L.; Thomas, B.; Sherlok, M.; Nock, L.; Behrens, R., Reduced Sensitivity RDX & Reduced Sensitivity RDX PBXN-109 Aging Study, 37th International Annual Conference of the Fraunhofer Institute for Chemical Technology (ICT), 2006; ICT: 2006 (*keynote address*).

Richard Behrens, Experimental Approaches to Assess and Predict Failure Modes of New Ingredients in Munitions, Workshop on R&D Required to Implement New Ingredients in Munitions, BEST Center, Aberdeen, MD, 8/29/2006.

Reaction Mechanisms of Energetic Materials in the Condensed Phase: Long-term Aging, Munition Safety and Condensed-Phase Processes in Propellants and Explosives

Richard Behrens
Sandia National Laboratories
Combustion Research Facility
Livermore, CA 94551-0969
Project No: 43381CH
Reporting Period: Aug. 1, 2006 to July 31, 2007

Abstract

The main focus of this project is understand the complex reaction processes of the ingredients that comprise propellants and explosives and to develop mathematical models of these reaction processes that can be used to assess issues associated with their performance, safety, aging and detection. During the past year, our investigations have focused on two areas: (1) developing a new conceptual framework to describe the complex reaction processes that control the reactions of RDX and HMX in the condensed phase, (2) investigating the thermal decomposition of high-nitrogen compounds, such as triaminoguanidinium tetrazolate (TAGzT) and its interaction with other ingredients, such as RDX, which are used in gun propellant formulations. Investigations of TAGzT has shown that hydrazine is formed during its decomposition and that the hydrazine survives for a sufficiently long time to enable its interaction with RDX. This provides new insight into how to design new molecules that can be used to alter the combustion process in propellants. Based on a workshop held in August 2006, a new conceptual framework has been developed that would enable the creation of a new R&D paradigm for the successful implementation of new energetic ingredients in future munitions.

Contents

Abstract 1
Contents 1
Summary 2
Conceptual Framework for Characterizing Complex Reaction Processes in the Condensed Phase. 4
Reaction Processes of High-nitrogen Compounds. 7
TAGzT Decomposition 10
Low Temperature & Morphological Aspects of TAGzT Decomposition 12
Reaction of TAGzT with RDX 23
Workshop organization: "R&D Required to Implement New Energetic Ingredients in Munitions 32

Summary

The main focus of this project is to understand the complex reaction processes that occur in the ingredients that comprise propellants and explosives, and to develop mathematical models of these reaction processes that can be used to assess issues associated with their performance, safety, aging and detection. The investigations focus on reactions that occur between 20 and 300°C. Understanding the physical and chemical reaction processes in this temperature range will: (1) enable the development of new ingredients required to meet new performance requirements, (2) provide new insight into how to design new formulations that meet insensitive munition (IM) requirements, (3) provide insight into what may cause incompatibility between ingredients, and (4) provide data on the vapors that evolve from explosives that can be used to design explosive detection systems.

From the scientific point of view, the objective of this project over the years has focused on developing an understanding of the complex reaction processes that control the thermal decomposition of RDX and HMX. To accomplish this objective, new experimental methods were developed. This required: (1) the development of the simultaneous thermogravimetric modulated beam mass spectrometry (STMBMS) instrument and refinement of experimental protocols to accurately probe the rates of gas evolution during the thermal decomposition process, (2) the development of a reaction modeling and kinetics (REMKIN) compiler and analysis tool needed to develop models of complex reaction processes and determine their associated parameters from the STMBMS data, and (3) the development of a chemical imaging precision mass analysis (ChIPMA) instrument to probe the dependence of chemical reaction processes on microscopic spatial scales. This suite of instruments, experimental protocols, and modeling/simulation algorithms has been used to probe how the underlying physical processes, chemical reactions and their dependence on morphological structures and spatial location control reactions of materials in the condensed phase.[1] These types of complex reactions underlie the behavior of explosives and propellants over many of the conditions encountered during their life cycle. During the early years of this project, data were collected on RDX, HMX and a number of different HMX-based formulations.

The work on this project during the past year has focused in two areas: (1) creating a series of papers to describe our work on investigating the complex reaction processes that control the behavior of RDX and HMX, and (2) applying our methods to probe the decomposition of new high-nitrogen (HiN) compounds and their interaction with other ingredients in gun propellants. The latter represents the extension of our methods to examine the more complex processes associated with reactions of mixtures of compounds, which typically comprise propellants and explosives.

In our work with HiN compounds we discovered that TAGzT decomposes to form substantial quantities of hydrazine, N_2H_4. When TAGzT is mixed with RDX, the hydrazine reacts rapidly with the RDX. In our experiments the rate of reaction of hydrazine with RDX was faster than the decomposition of RDX by itself. Thus, this reaction pathway provides a means for introducing a reaction path into the initial stages of RDX combustion that is faster than the decomposition of the nitramine itself. This additional reaction pathway should provide a means to adjust the burn rate of propellants.

The reaction processes that control the decomposition of TAGzT and its interaction with RDX have been investigated from reaction onset at ~ 110 to 120°C, through its rapid decomposition at ~ 180°C, and up to the decomposition of the nonvolatile residues formed in the decomposition process. A reaction scheme including spatial features that are dependent on sample morphology has been developed. The interaction of hydrazine formed from TAGzT with RDX has been examined using isotopic crossover experiments with RDX-d6 and RDX-$^{15}N_6$.

Based on a JANNAF workshop on "R&D Required to Implement New Energetic Ingredients in Munitions" a conceptual framework has been developed that forms a basis for a new paradigm to implement new energetic ingredients in munitions. The new paradigm moves away from old trial and error type "Edisonian" development to a more modern science-based development that relies on rapid evaluation of new compounds and materials. This new paradigm envisions new super-small scale experimental diagnostics that derive large quantities of information on underlying reaction processes from very small quantities of material, coupled with modeling and simulation algorithms that can translate this information into new design concepts to meet future munition requirements.

Conceptual Framework for Characterizing Complex Reaction Processes in the Condensed Phase.

We have been investigating the thermal decomposition of RDX and HMX for the past 20 years. Over this period we have developed the experimental methods to collect data with a sufficient amount of information to enable us to identify and characterize many of the underlying reaction processes. This work has shown that the reactions of both compounds are controlled by a set of complex nonlinear reaction processes. The specific physical processes and chemical reactions from this set that dominate the overall thermal decomposition process for as specific experiment is very strongly dependent on the temperature, pressure and heating rates used in an experiment. The features of these processes have been characterized by a general reaction network describing the process.[2, 3]

To create mathematical models of these processes we have developed the REMKIN compiler and analysis tool that allows one to postulate physicochemical reaction models, automatically generate and numerically solve the associated set of differential equation and determine the parameters for the models by numerical optimization to the STMBMS data. This methodology has been demonstrated with initial models characterizing the decomposition of RDX both below and above it melting point.[4]

Based on this work, this year we embarked on writing a series of papers describing the investigation of complex reactions in the condensed phase, using our investigations and modeling of RDX and HMX reaction processes as a basis, and example, of how to characterize these types of processes. In examining the reactions of HMX and RDX in the light of other investigations of complex reaction mechanisms in chemical, biological and genetic systems,[5] it became apparent that we are dealing with a level of complexity that is beyond the scope of most investigations of complex chemical mechanisms. To adequately characterize the complex reactions that occur in compounds such as RDX or HMX in the condensed phase requires the introduction of new terms and concepts.

Most investigations of complex chemical systems deal with systems of reactions in which the concept, and characterization, of an elementary reactions remains valid. For example, complex reaction mechanisms characterizing gas-phase combustion rely on the fact the individual reactions in the overall combustion process are independent of each other at the instant of time when reaction occurs. They typically involve either the unimolecular decomposition of isolated molecules, or the reaction and exchange of atoms in a bimolecular collision event. The reactions are independent of each other and their surrounding environment. A similar situation exists for reactions that take place in dilute solution. Except in this case the surrounding environment is characterized by the properties of the solvent molecules surrounding the reactants, rather than free space, as is the case for the combustion environment. In either case competition between elementary reactions determine the evolution of the system in time.

From our studies with RDX and HMX in the condensed phase, it is clear that the evolution of the system is not determined by *isolated* elementary reactions. The close proximity of the molecules to each other (i.e., varying combinations of reactant and products) in the condensed phase of these organic compounds dynamically alters the

reaction environment on a range of spatial scales. Thus, the application of concepts based on elementary reactions is likely to be inadequate in these situations. The reaction process will depend on the chemical nature of the surrounding spatial environment. The range of spatial scales that we are considering in the development of reaction models for RDX and HMX are illustrated in Figure 1. For example, the variation in the reaction environment ranges from molecular dimensions (S5), through dimensions that may be associated with a grain structure (S3), up to larger dimensions associated with the experimental configuration (the solid/vapor of solid/liquid phase boundaries).

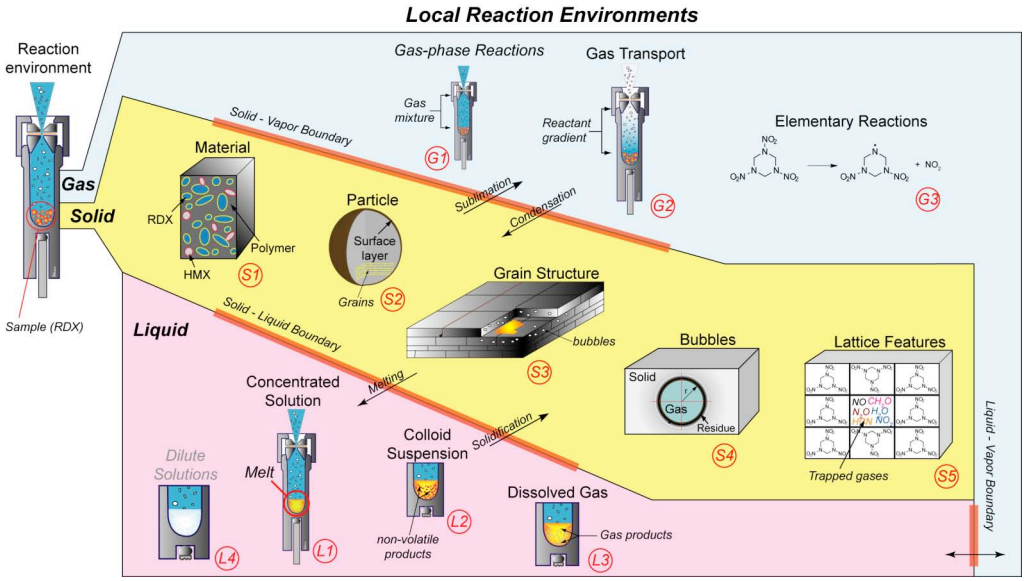

Figure 1. Illustration of local reaction environments (LRE) that play a role in determining the decomposition of RDX or HMX in the condensed phase.

Our experimental methods coupled with our modeling/simulation methods provide the means to determine the reaction scheme of complex processes, such as those illustrated for HMX in Fig. 1, and develop mathematical models to represent the main underlying reaction processes. We are currently working to describe and characterize the various aspects of the complex processes that control the decomposition of HMX and RDX and the methods we use to accomplish this task in a series of six or seven papers summarizing this work.

This fundamental research into complex processes provides the basis for enabling the development of energetic materials in two areas; (1) the development of mathematical models of the underlying rate controlling processes that can be used to predict the behavior of formulations of energetic materials over a range of life cycle conditions, and (2) the opportunity to identify and understand the underlying behavior of new energetic ingredients at a level of detail that will enable the logical design of new energetic compounds and materials.

In addition, it should be pointed out that the understanding that we have derived from our experiments with RDX and HMX require very small quantities of material and do not

preclude experimental investigations due to hazards presented by working with larger quantities of these materials. The ability to conduct meaningful experiments and tests is one of the main features of the new paradigm for R&D required to develop new energetic materials as outlined below.

Reaction Processes of High-nitrogen Compounds.

The Army and Navy are investigating the use of high nitrogen (HiN) compounds for use in advanced gun propellants. These materials have the potential to improve gun performance and reduce barrel corrosion. To provide a basis for understanding the reaction processes of these materials and how they may affect gun propellant performance, safety and aging behavior we are investigating the reactions of several HiN compounds. The high nitrogen compounds are typically used by replacing a portion of the RDX in a conventional gun propellant with the HiN compounds. In 2006, we decided to investigate the HiN compounds rather than some of the compounds in the original ARO proposal (24DNI, NTO), since the HiN compounds are of current interest to the Army in the development of new propellants.

The objectives of our research on high-nitrogen compounds focus on developing new propellants. These objectives may be divided into three general areas: (1) Understand how to modify the burn rates of nitramine (min. smoke) propellants by probing the initial stages of the combustion process; (2) Provide assessment of reactions that may compromise the safety or stability of propellants by probing reactions of and between ingredients at temperatures related to safety and aging issues; and (3) Determine how to design better ingredients by a) understanding how new ingredients, such as TAGzT and GUzT, react and interact with other ingredients and b) using this insight to design new compounds that are targeted at desired properties.

To address these objectives we selected two HiN compounds that exhibited opposite effects on the burn rate of nitramine-based propellants in closed bomb measurements.[6, 7] GUzT had little effect on altering the burn rate of the baseline propellant, while the addition of TAGzT resulted in the significant increase its burn rate. Given the similarities of the molecular structure of these two compounds, they are good candidates for our experimental investigation to determine the underlying reaction mechanisms of their decomposition and interaction with the other ingredients in the propellant.

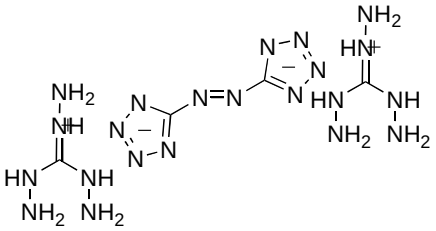

Triaminoguanidinium Azotetrazolate (TAGzT)

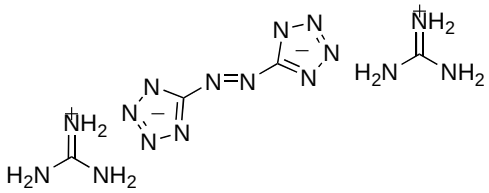

Guanidiium Azotetrazolate (GUzT)

Last year we reported the initial results from our experiments investing the decomposition of TAGzT (the compound that enhances the propellant burn rate). Over the past year, we expanded our efforts in this area to address our three primary objectives. The work to be described was carried in our research group at Sandia, with the assistance of Ms. Heather Hayden (Navy/Indian Head) who is participating in this project as the basis for her Ph.D. thesis at George Washington University. Ms. Hayden's efforts are funded by the Office of Naval Research.

While the instrumentation, numerical algorithms to create reaction models and simulate the reaction processes, and the general nature of the complex reaction processes have been described previously,[1] the general experimental protocol that we use to determine the complex reaction mechanism and to obtain the data necessary to create the models has not been specifically defined. The general experimental protocol that we use to investigate the reactions of energetic materials is shown in Figure 2. This protocol includes six primary activities whose purpose is to provide the different types of information required to determine reaction mechanisms, to identify spatial features that influence the reaction process, and to provide the reaction rate data needed to construct models of the reaction process. For example, the identification of species, followed by the determination of their evolution sequence, provides the information needed to create a reaction mechanism.

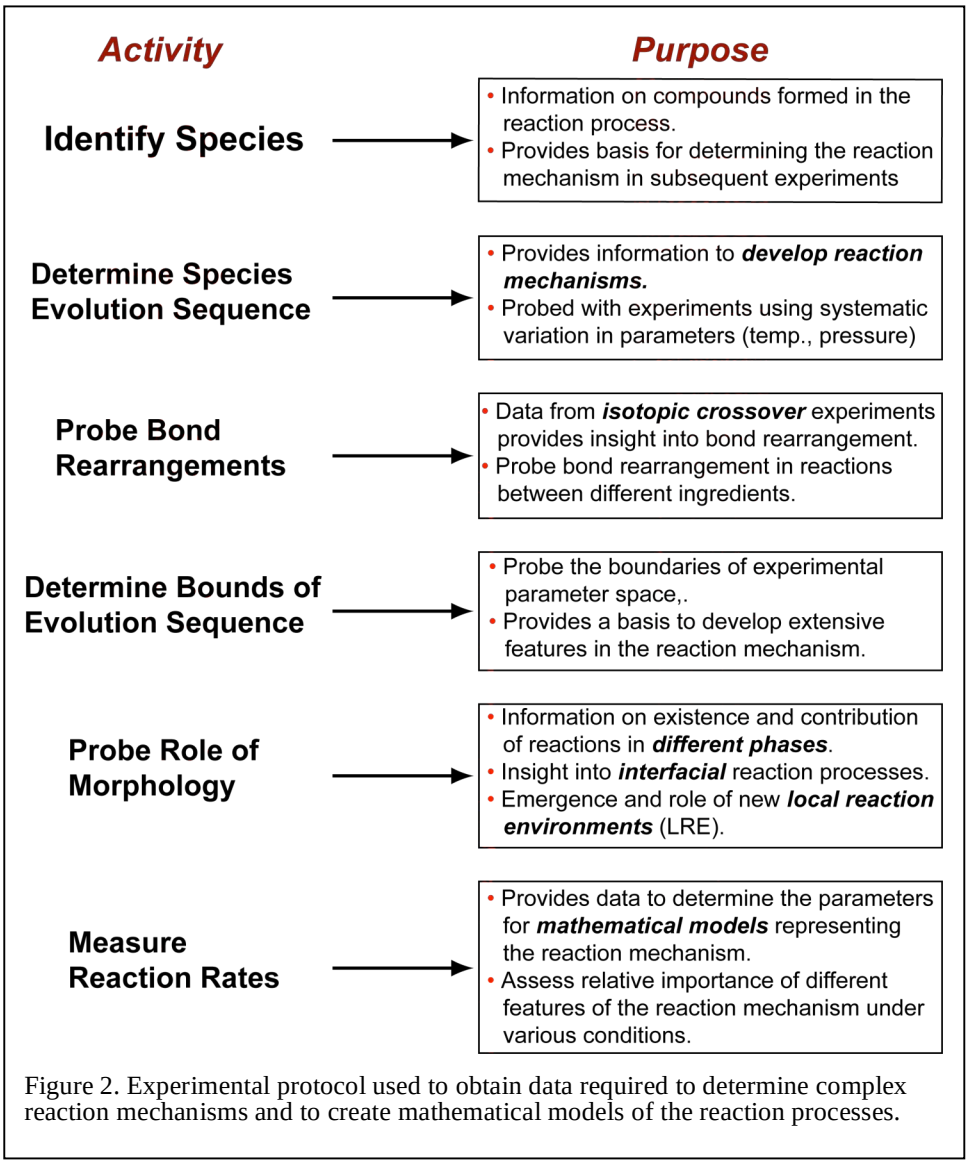

Figure 2. Experimental protocol used to obtain data required to determine complex reaction mechanisms and to create mathematical models of the reaction processes.

In the previous year we had collected data in the first two steps of our protocol for TAGzT. In the past year we have accomplished the following:

1. Collected and analyzed data on TAGzT through step 5 of the protocol. This provides additional insight into the spatial aspects of the decomposition process that play a role in the decomposition of TAGzT.
2. Collected data on the interaction of TAGzT with RDX through step 5 of the protocol. This has provided new insight into why TAGzT accelerates the burn rate of nitramine-based propellants. It also provides new information to assess compatibility issues between TAGzT and RDX.
3. Collected data on the decomposition of GUzT through the first two steps of the protocol.

A summary of our findings on the decomposition of TAGzT and its interaction with RDX are presented next in this report.

Experimental method. A short overview of the STMBMS instrument and experimental methods are presented here for readers who are not familiar with the methods. Further details may be found in several publications.[1, 8-10] A schematic illustration of the instrument is shown in Fig. 3. In a typical experiment a 1 to 5 mg sample is loaded in the reaction cell that is sealed with a cap containing an orifice of a measured diameter through which gases in the cell may exit. The loaded reaction cell is placed on top of a thermocouple probe that is mounted in a microbalance. Once the reaction cell is loaded the instrument is evacuated. The typical pressure in different sections of the instrument are listed in the figure. As the sample is heated gas exits the reaction cell and transitions to molecular flow ~1mm downstream of the orifice. The gas is then formed into a molecular beam and the mass spectra of the gases in the beam measured with a quadrupole mass spectrometer. The simultaneous measurement of the rate of force change with the microbalance and the mass spectra allow the identities and number density of each gaseous species within the reaction cell to be determined as a function of time during the course of an experiment.

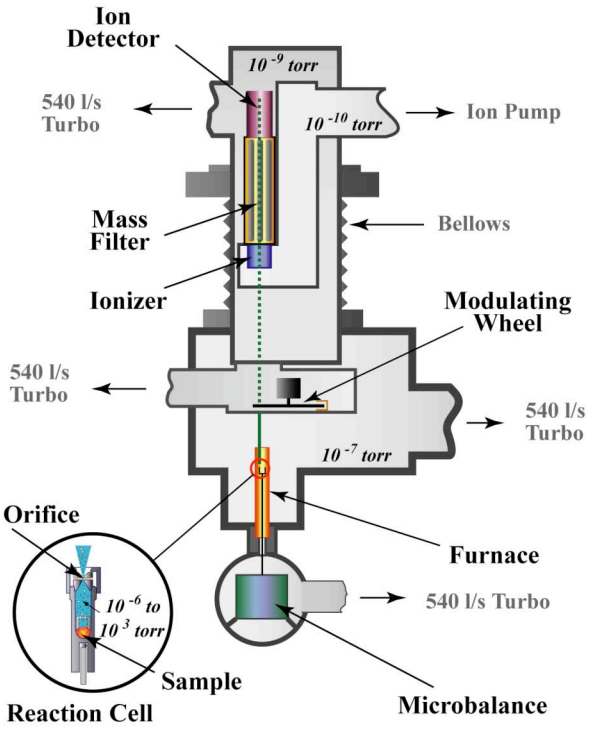

Figure 3. Illustration of the STMBMS instrument. Reaction cell in which thermal decomposition of a sample takes place is shown in lower left.

The formulas of the ions in the mass spectra are determined by conducting a set of analogous thermal decomposition experiments with a Bruker Apex II FTICR mass spectrometer. The high resolution (m/Δm ~100,000) and high mass accuracy (<1ppm) of this instrument allow the formulas of the ion signals at each m/z value in the mass spectrum to be determined. Temporal correlations of ion signals from the mass spectra measured with the STMBMS instrument provide highly correlated groups of m/z values that most likely arise from the fragmentation of a thermal decomposition product in the mass spectrometer. The formulas of each of the m/z values in each group are checked to see if they are all consistent with originating from a single compound.

These data are eventually used in a quantification procedure that provides the number density (or any other measure of the gases within the cell that depend on number density) as a function of time during the course of an experiment. We are currently approaching this point of analysis with the TAGzT work. These results are not presented in this report.

TAGzT Decomposition

General decomposition behavior of TAGzT. In our initial thermal decomposition experiments, conducted last year, we found that TAGzT releases relatively small quantities of gaseous products until it reaches a temperature where it undergoes a rapid decomposition (i.e., rapid compared to what we have observed with most other energetic materials such as RDX, TNAZ, NTO…). The rapid decomposition occurs between 180 and 200°C and depends on the extent of confinement of decomposition products with the sample. In our initial experiments we identified the decomposition products and measured the sequence of the evolution under both low and high confinement conditions. The ion signals representing the various products from two typical experiments are shown in Figure 4.

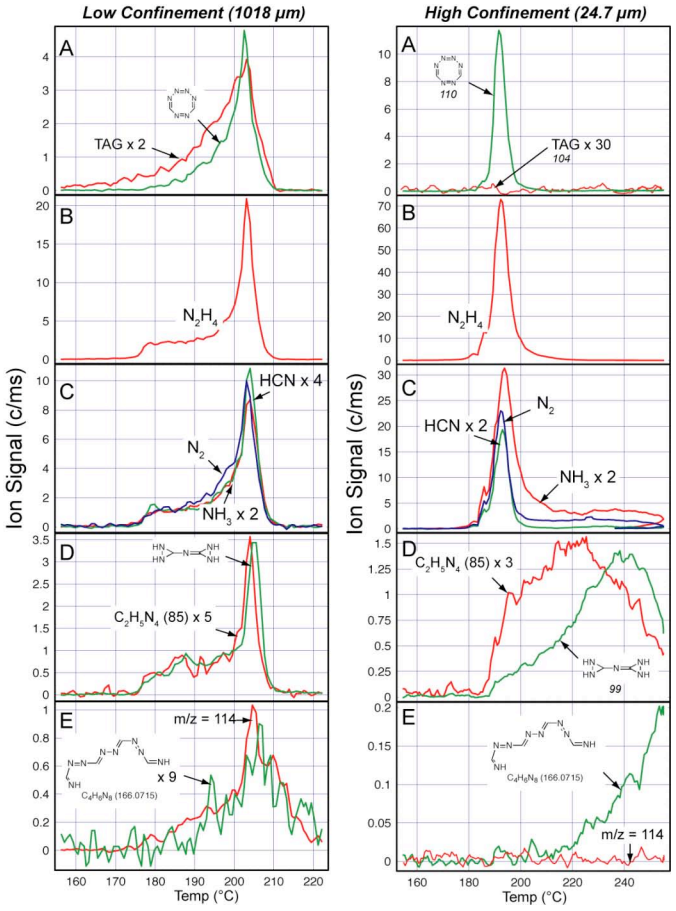

Figure 4. Ion signals at m/z values representing thermal decomposition products that evolve from TAGzT under low and high confinement conditions. Heating rate: 2.5°C/min

Based on this data a reaction mechanism was created. A

nine-step mechanism is shown in Figure 5. The first seven steps of the reaction scheme were developed from data in lower confinement experiments, such as shown on the left in Fig. 4. The final two steps were developed based on data from higher confinement experiments, such as shown on the right in Fig. 4. Please note that secondary reactions, other than those listed in the reaction scheme, also occur during the course of the

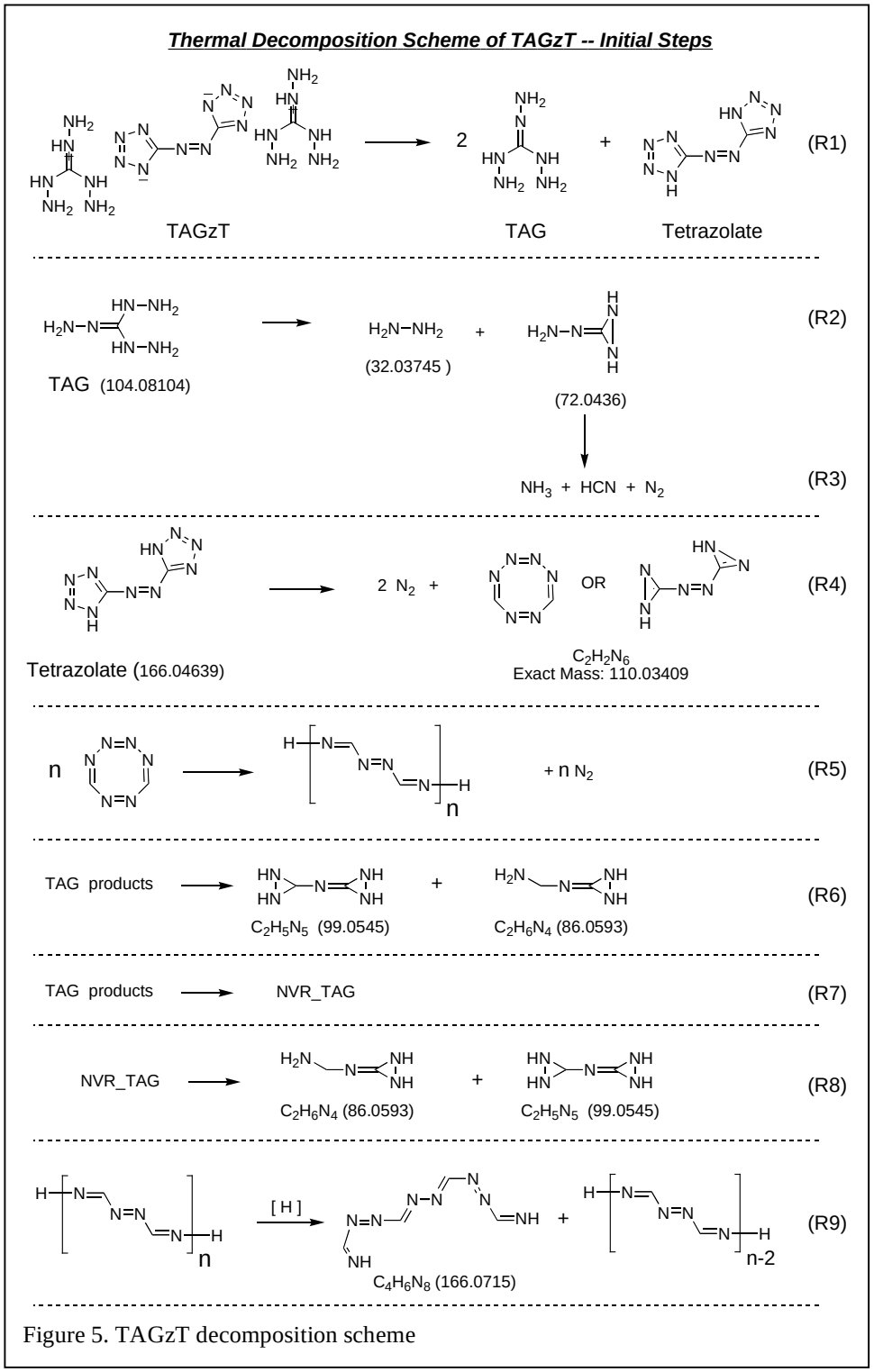

Figure 5. TAGzT decomposition scheme

experiment. For example, it is likely that some of the hydrazine, N_2H_4, undergoes reaction prior to exiting the reaction cell.

The reactions may be summarized as follows:

1. Reaction R1 is the initial decomposition of TAGzT to form triaminoguanidine (g) (TAG) and azobitetrazolate (ABT). The transfer of hydrogen from the TAG cation to the ABT anion appears to be the first step in the reaction.
2. Reaction R2 is the initial decomposition of TAG(g). This reaction is written to indicate that TAG forms hydrazine. Reaction R3 captures the subsequent reaction of the remaining part of the TAG molecule to form NH_3, HCN and N_2. The exact sequence of evolution of this group of products cannot be determined from our experiments because this part of the reaction process if faster than the temporal resolution of our experiments.
3. Reaction R4 represents the decomposition of the molecule formed from the azobitetrazolate (ABT). This azobitetrazolate molecular species (m/z=166) is not observed in the mass spectrometer. The largest fragment observed from the tetrazolate is observed at m/z=110 and has the formula, $C_2H_2N_6$. This species is formed from the central portion of the ABT molecule – the region around the diazene group. Two possible structures for the $C_2H_2N_6$ species are shown. (Note: The ion signal measured at m/z=166 appears during the latter part of the decomposition process and the FTICR data indicate this species has a formula of $C_4H_6N_8$. Thus, it is not the molecular ion of the tetrazolate.)
4. Reaction R5 captures the fact that the 110 species, or the portion of the azobitetrazolate anion that does ***not*** form the 110 species, is likely to form a nonvolatile "polymeric-like" product (NVPP) during the decomposition process. This NVPP has not been directly observed, but the identities of gaseous products that evolve after the TAGzT has decomposed suggest that this type of compound is formed during the decomposition of TAGzT.
5. Reaction R6 represents the decomposition of the NVPP. For example, one of the products observed after TAGzT has decomposed is at m/z=166.0711 and has a formula, $C_4H_6N_8$.
6. Reaction R7 represents a generic set of reactions that involve the secondary reactions of TAG and its decomposition products. From the lower confinement experiments the details of these secondary reactions are difficult to elucidate. Products are observed at m/z values of 99 and 86. Possible structures for these products are shown.
7. Reactions R8 and R9 represent the formation of a non-volatile product from the TAG decomposition products. These two steps are added to the reaction scheme based on results from the higher confinement experiment (Fig. 4).

Low Temperature & Morphological Aspects of TAGzT Decomposition

The initial experiments explored the decomposition of TAGzT over a limited temperature range. To develop a broader characterization of the decomposition processes and derive deeper insight into the rate controlling reaction processes, experiments were designed to

provide data over a broader temperature range. Several experiments were performed to identify appropriate temperature ranges and develop a thermal profile to use for conducting the experiments. Data from one such experiment using this profile is shown in Figure 6. In this experiment the sample is first heated from 90 to 140 and back to 90°C in steps of 10°C to examine the first steps in the decomposition process. Next, the sample is heated and held at 150°C for a period of time to examine the initial point where TAG decomposes to NH_3, HCN, N_2 and N_2H_4. The sample is then cooled to 90°C and then heated to 150°C in steps of 10°C again. This is done to determine whether the initial decomposition of TAG to its decomposition products affects the subsequent decomposition process of TAGzT. Next, the sample is cycled between 150 and 165°C six times to investigate the more rapid decomposition process of TAGzT, which in faster heating rate experiments is observed at ~180°C. After the cycling process the sample is heated to 190°C in steps of 5°C to provide data on the decomposition of the NVPP formed during the decomposition of TAGzT. Finally the sample is heated to 500°C to decompose any remaining residue. An experiment using a similar thermal profile, but conducted under higher confinement (38µm vs 1000µm diameter orifice) is shown in Figure 7.

Examination of different temperature regions of each experiment and comparison of these regions between experiments conducted under low and high confinement provides additional insight into the thermal decomposition process. Several of these insights are illustrated next.

The initial results suggested that TAGzT decomposed to triaminoguanidine (TAG) prior to the evolution of NH_3, HCN, N_2 and N_2H_4. We wanted further evidence as to whether this was true and if so, at what temperature it started. We also want to know whether the decomposition of TAGzT to TAG + ABT was reversible (i.e., in dissociative equilibrium). Examination of the data during the early segments of the experiment provides the required information.

The data shown in graph [3, 2] (i.e., [row 3, column 2]) at m/z values of 58, 73, and 104 originate from TAG. Close examination of the data during the first set of temperature steps shows that the first discernible signals appear at 120°C. Close examination of the data also shows that the main decomposition products NH_3, HCN, N_2, N_2H_4 and $C_2H_2N_6$ (from ABT) are *not* observed along with TAG in this temperature region. The signal at m/z=31 that we use to characterize N_2H_4 also is present as a small peak in the mass spectrum of TAG. In this temperature region it is highly correlated with the other ion signals in the mass spectrum of TAG. Thus, we attribute its presence in this region to TAG.

Based on these results it appears that when TAGzT is heated to temperatures up to 140°C the dominant decomposition step is the dissociation of TAGzT to TAG and ABT. The decomposition product associated with ABT, $C_2H_2N_6$, is not observed in this temperature region. This suggests that the ABT remains intact on the surface of the TAGzT particles. Given the relatively complex molecular structures of TAG and ABT it was not obvious whether TAGzT would be in dissociative equilibrium with TAG and ABT.

$$\text{TAGzT (s)} \quad \Leftrightarrow \quad \text{TAG (g)} \quad + \quad \text{ABT (s)}$$

Close examination of the data in the experiment with TAGzT under higher confinement (Fig. 7) shows no evidence of TAG evolving from the reaction cell. If TAGzT is in dissociative equilibrium with TAG and ABT, then the rate of evolution of TAG in the higher confinement experiment should be a factor of ~750 below that observed in the lower confinement experiment. This is below the detection limit for this species in the experiment. Thus, the data is consistent with a dissociative equilibrium between TAGzT, TAG and ABT.

Examination of data from an experiment using an intermediate confinement condition (Fig. 9) shows that the TAG signal (m/z=58) is a factor of ~14 lower in this experiment using intermediate confinement (108μm diameter orifice). While estimating the relative effusive flow rate of the gas from the reaction cell in each experiment suggests that the relative flow rates should differ by a factor of ~90, the observed reduction in signal intensity is a factor of ~6 below this value. While the relative difference in effusive flow rates is typically proportional to the cross sectional area of the orifice being used, in the two experiments used in our comparison the larger orifice has a cross sectional area that is a significant fraction of the surface area of the sample. Thus, the ability of the sample to maintain the near equilibrium condition plays a role in these measurements. For these types of measurements, this change in apparent measured vapor pressure due to the use of larger size orifices can be employed to determine the sticking probability of a molecule striking a surface. In our case this would be analogous to the TAG undergoing the reverse reaction with ABT to form TAGzT. Thus, the fact that the measured value is a factor of ~6 lower than expected from a quasi-equilibrium assumption is consistent with (1) TAGzT being in dissociative equilibrium with TAG and ABT and (2) the relatively complex structure of TAG and ABT requiring substantial time to complete the reverse reaction.

The final item we will address, before presenting our current overall scheme describing TAGzT decomposition, is the first point at which TAGzT decomposes. The first main decomposition products from TAGzT start to appear as the sample nears 150°C. The portion of the data in the low confinement experiment in which the sample was heated from 90 to 150 and back to 90°C is shown in Figure 10. As the sample is heated to 150°C the rate of evolution of TAG rises and reaches a constant value when the reaction cell temperature reaches 150°C (graph [3,2]). This is as expected for a dissociative equilibrium.

It is reasonable to expect that NH_3, HCN, N_2 and N_2H_4 are formed from the decomposition of TAG (g). Thus, it is expected that their signals should rise and track the TAG signal. Close examination of the ion signals associated with TAG (58, 104) and the decomposition products NH_3 (17), HCN (27), N_2 (28), N_2H_4 (31), and $C_2H_2N_6$ (110) in Fig. 10 show a lag of approximately 1500 seconds of the ion signals from the main products behind those from TAG. Thus, the reaction of TAG depends on the formation of some other compound or feature in the sample that promotes its decomposition to the lower molecular weight products at 150°C. This delay is not observed the second time the sample is heated to 150°C. Hence, we postulate that a residue of some type is formed on the surface of the TAGzT particles that promotes the decomposition of TAG.

Comparison of the data from the high confinement experiment (Fig. 7) to the data from the low confinement experiment (Fig. 6) shows the very clear effect of confining the

gaseous decomposition products with the sample. The overall rate of reaction is clearly increased by the presence of TAGzT decomposition products.

The following diagram illustrates our current understanding of TAGzT decomposition.

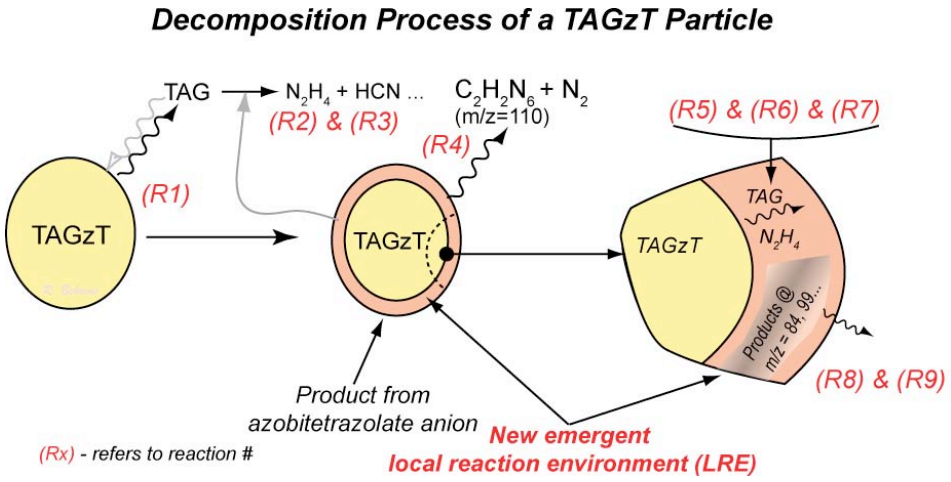

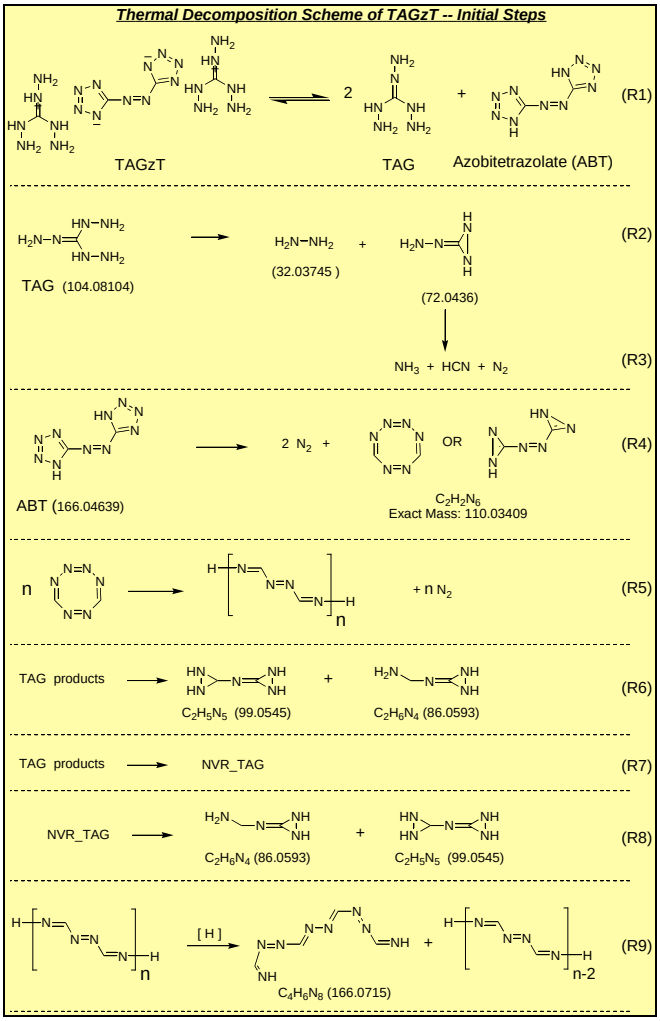

The reaction diagram indicates how the various reactions in the thermal decomposition scheme are related to the morphological features of the sample. The graphic on the left illustrates the dissociative sublimation of TAGzT to TAG and ABT via Reaction R1. The TAG then decomposes to NH_3, HCN, N_2 and N_2H_4 via Reactions R2 and R3. During the initial stage of TAGzT decomposition at 150°C the decomposition of TAG apparently involves other products that are most likely present on the surface of the TAGzT particles.

As TAG and its decomposition products evolve from the sample, the ABT appears to initially remain on the sample. The ABT then appears to decompose via Reaction R4 to N_2 and $C_2H_2N_6$, which most likely originates from the central portion of the ABT molecule after a nitrogen molecule has evolved from each of the tetrazolate rings.

As a "crust" or "film" builds on the surface of the TAGzT particles, the TAG must travel through greater amounts of this material. The products from TAG and the ABT now undergo secondary reactions via Reactions R5, R6, and R7 to form the observed products. After products that are associated with the decomposition of TAGzT cease to evolve from the sample, products formed from the decomposition of the crust continue to evolve as represented by Reactions R8 and R9. The formation and decomposition of relatively nonvolatile products is evident in all of the experiments. However, it is readily apparent in the high confinement experiment (Fig. 7) in which the ion signals representing the TAGzT decomposition products (graphs [1, 1] and [2, 1]) are distinctly separated from those associated with products from the crust (graph [1, 2]).

The decomposition of TAGzT is another example of a decomposition process that is controlled by a complex reaction process that takes place in the condensed phase. As is the case for the cyclic nitramines, any realistic reaction model will need to identify the local reaction environments and characterize the elementary reaction manifold that controls the behavior in each of the LREs.

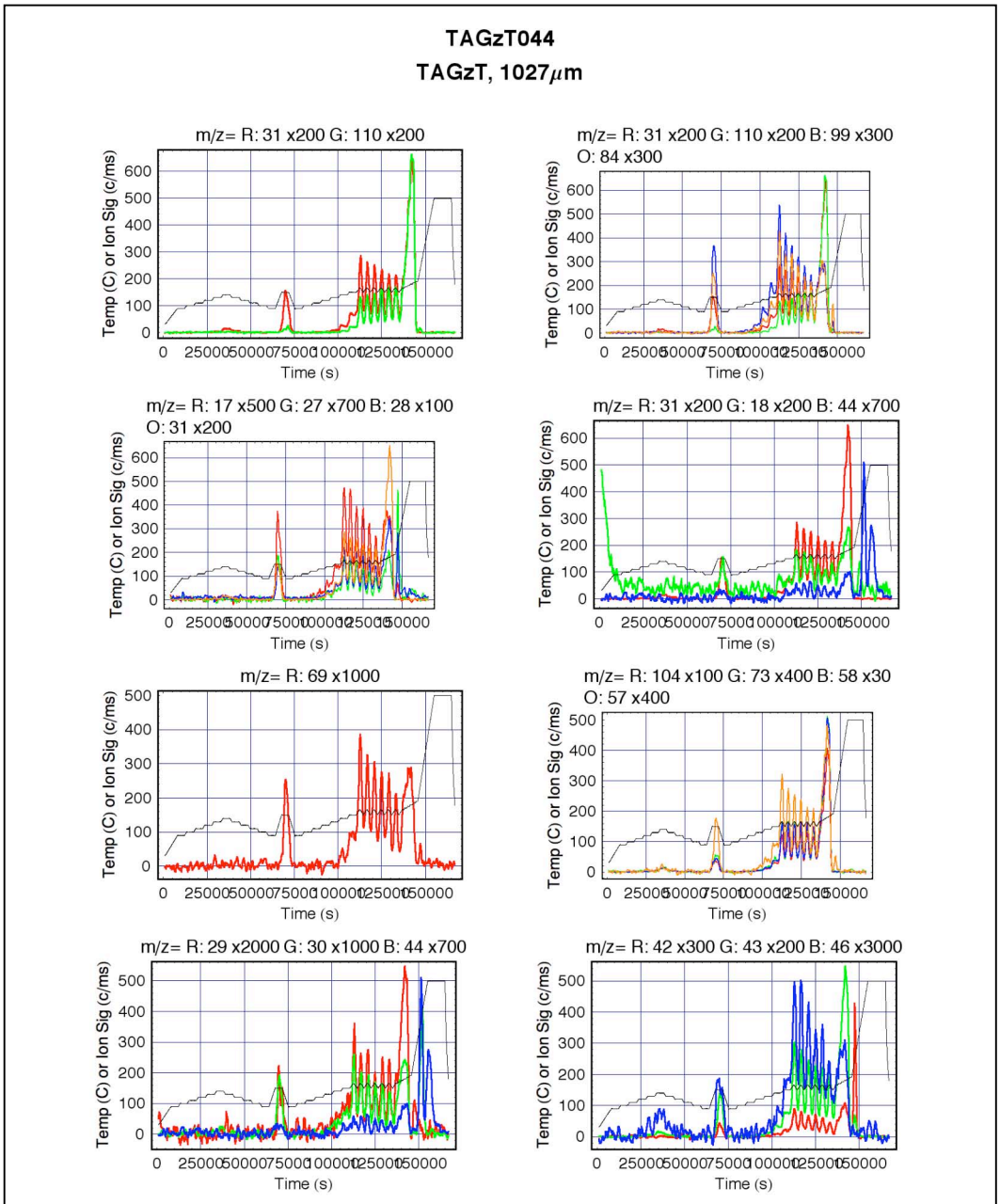

Figure 6. Ion signals representing various products formed during the thermal decomposition of TAGzT under low confinement. The black curve on each plot shows the reaction cell temperature. The colored curves are associated with the m/z values and scaling factors listed above each graph. For example the m/z values at 58, 73, and 104 in graph [3,2] originate from TAG. Experiment duration ~175,000 seconds.

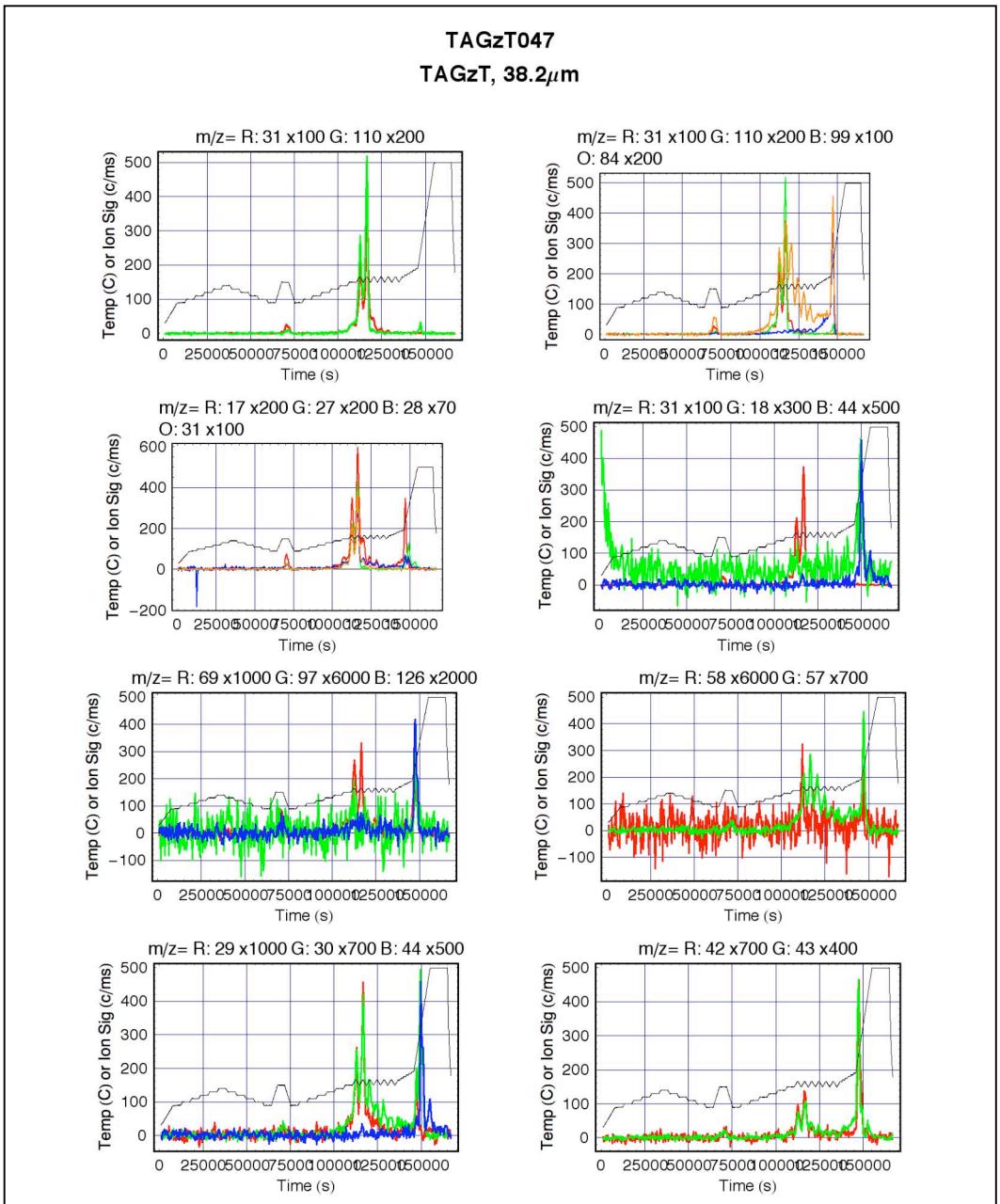

Figure 7. . Ion signals representing various products formed during the thermal decomposition of TAGzT under high confinement. The black curve on each plot shows the reaction cell temperature. The colored curves are associated with the m/z values and scaling factors listed above each graph. For example the m/z values at 17, 27, 28, 31 represent NH_3, HCN, N_2 and N_2H_4, respectively. Experiment duration ~175,000 seconds.

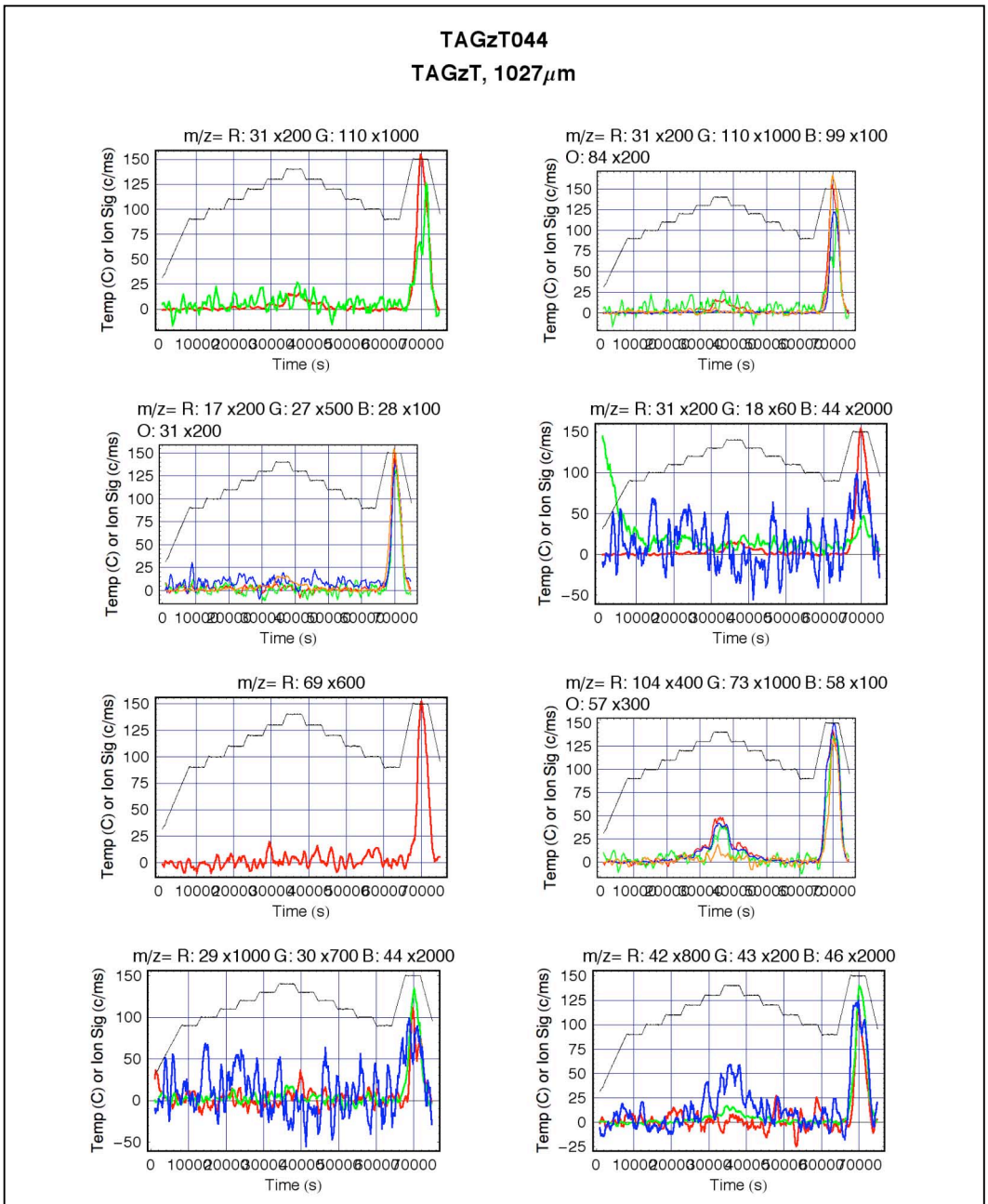

Figure 8. Ion signals representing various products formed during the thermal decomposition of TAGzT under low confinement. The black curve on each plot shows the reaction cell temperature. The ion signals at m/z values of 58, 73, and 104 shown in graph [3,2] represent TAG evolving from the reaction cell. Duration of data shown: ~75,000 seconds.

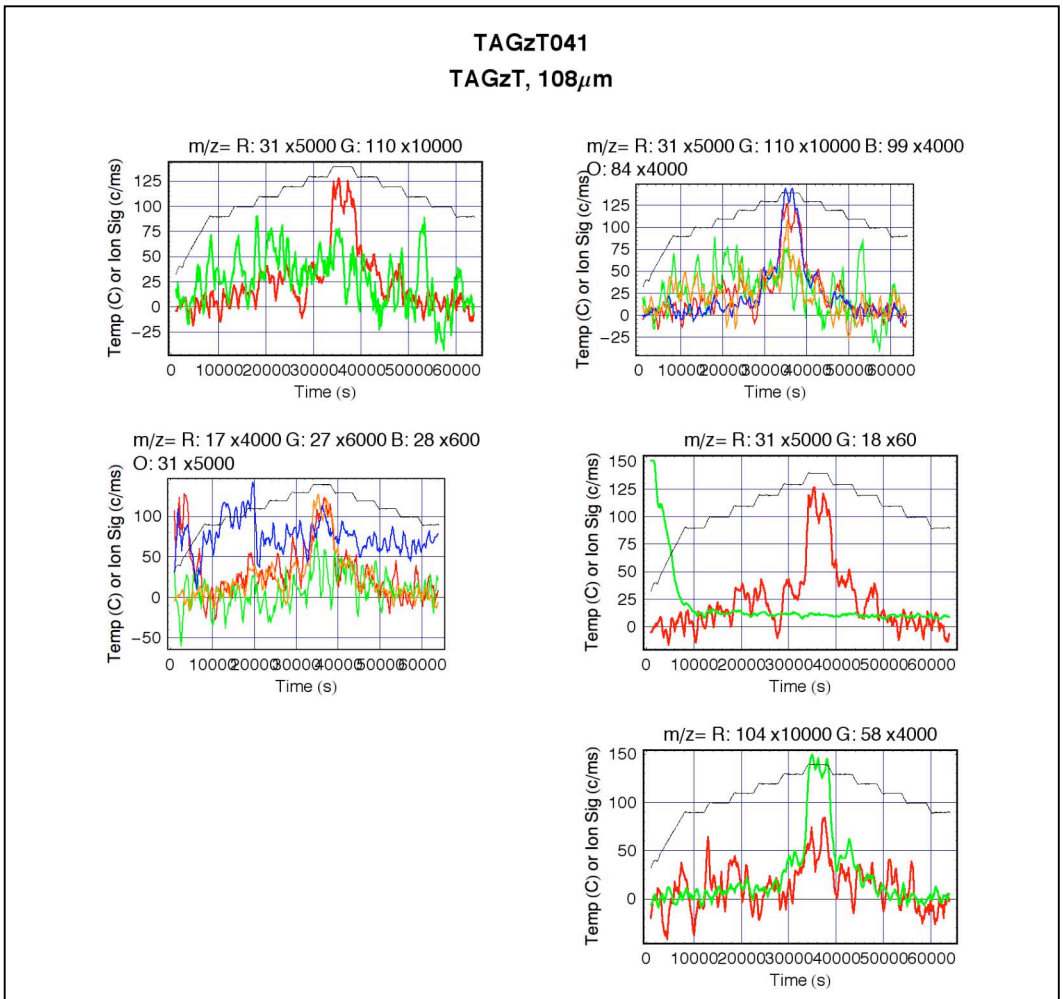

Figure 9. Ion signals representing various products formed during the thermal decomposition of TAGzT under intermediate confinement. The black curve on each plot shows the reaction cell temperature. The ion signals at m/z values of 58, and 104 shown in graph [3,2] represent TAG evolving from the reaction cell. Duration of data shown: ~65,000 seconds.

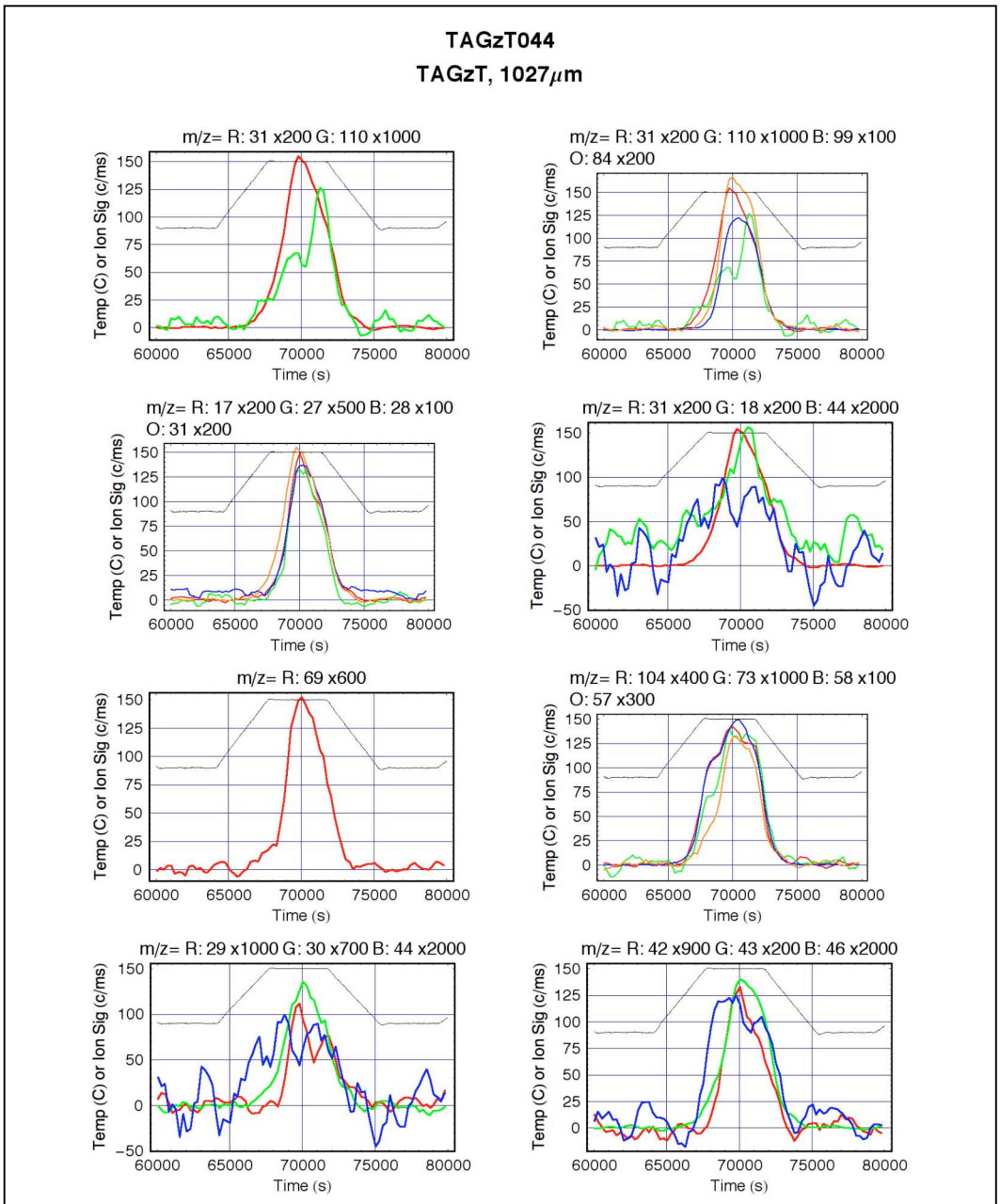

Figure 10. Ion signals representing various products formed during the thermal decomposition of TAGzT under low confinement. The black curve on each plot shows the reaction cell temperature. This data shows the sequence of evolution of the main decomposition products from TAGzT (graphs [1, 1], [1, 2] and [2, 1]) and their relationship to the evolution of TAG (graph [3, 2]).

Reaction of TAGzT with RDX

Thermal decomposition experiments of mixtures of TAGzT with RDX have shown that hydrazine formed in the decomposition of TAGzT reacts with RDX. This reaction first occurs below the melting point of RDX and results in a reaction with RDX that is faster than the decomposition of RDX by itself. This finding suggests that molecules such as TAGzT can be designed and used to adjust the burn rates of nitramines such as RDX.

The interactions between TAGzT and RDX are of interest in two areas: (1) the initial stages of the combustion process, and (2) at lower temperatures related to aging and safety of propellants. Insight into the reactions that occur during the first stages of combustion is derived from comparison of data from experiments with RDX, TAGzT and mixtures of TAGzT with RDX. For reference, the products formed from the thermal decomposition of RDX and their rates of formation are shown in Figure 11. The onset of rapid evolution of the products occurs upon melting of RDX (mp ~200°C), which happens when the reaction cell is at ~210°C in this experiment.

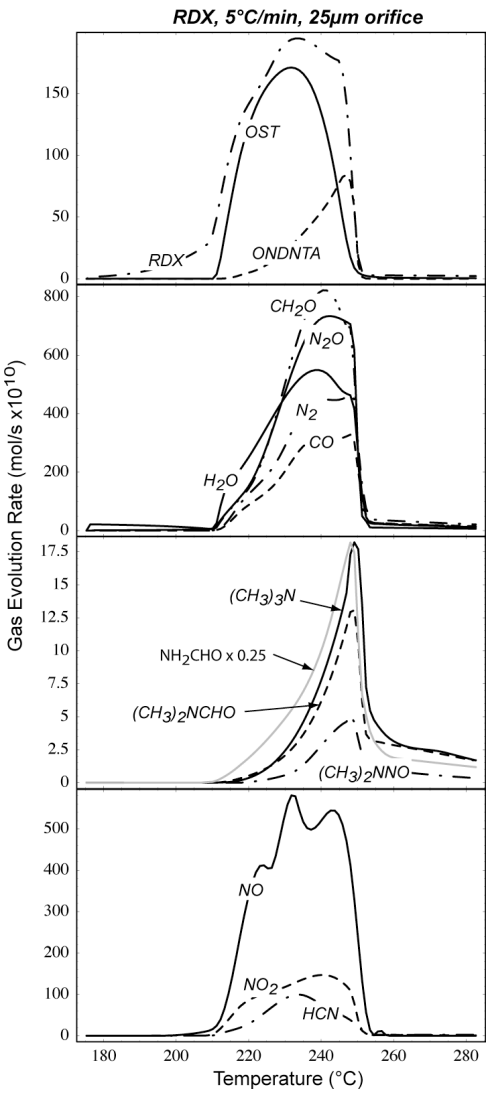

Figure 11. Products formed during the decomposition of RDX.

Examination of the ion signals associated with the various compounds formed in the decomposition of TAGzT, RDX and a mixture of TAGzT with RDX (Figs. 12 & 13) shows that ion signals typically representing H_2O, NO, N_2O and N_2H_4 have new features in the decomposition of the mixture of TAGzT with RDX that are not observed in the decomposition of either compound by itself.

These features appear during the main decomposition process of TAGzT, which occurs between 165 and 180°C in the mixture. New peaks are observed in the ion signals at m/z values of 18, 30 and 44, which are tentatively assigned to H_2O, NO and N_2O. At the same time, the hydrazine (m/z=32) signal intensity drops from a maximum of 80 c/ms in the TAGzT by itself to 2 c/ms in the mixture of TAGzT and RDX. There are also new, but smaller, signals at m/z values of 29 (CHO fragment from CH_2O), 47 (HONO), 84 and 121.

The primary conclusions that can be derived from these initial results are:

1. Hydrazine formed from TAGzT

interacts with RDX.

2. In an oversimplified explanation, hydrazine may be thought to react with the RDX nitro groups to form H_2O and N_2O. However, the ion signals representing NO, CH_2O and HONO that evolve at the same time as these other products suggest the reaction process is more complex than

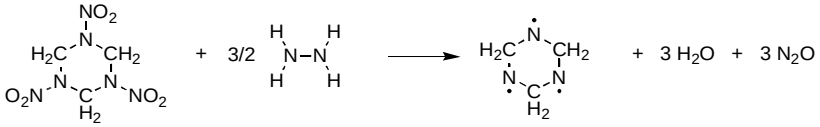

Subsequent isotopic crossover experiments with TAGzT and RDX-d6 and RDX-^{15}N6 also indicate the reaction process is more complex.

3. The decomposition of TAGzT to form hydrazine occurs before RDX melts in our experiments. This implies

    a. Reactions between hydrazine and RDX in the gas phase are a major contributor to this process

    RDX (s) ←→ RDX (g) (R1)

    RDX (g) → CH_2O + N_2O + other products (R2)

    RDX (g) + N_2H_4 (g) → H_2O + N_2O + other products (R3)

    since the sublimation rate of RDX is quite fast (R1) compared to its rate of decomposition (R2), as determined from simulations of our RDX decomposition experiments.

    b. Reactions are likely to occur on the surface of the RDX and the TAGzT particles.

4. After TAGzT has decomposed and the hydrazine is consumed, further heating leads to melting of the remaining RDX, which then undergoes decomposition in a manner similar to RDX by itself.

5. The reactions that occur on the surface of RDX particles to create a new local reaction environment may occur faster in the presence of TAGzT.

Based on these observations, compounds that form hydrazine in their decomposition process are likely to be good candidates for ingredients to serve as burn rate modifiers in nitramine-based propellants. An example of how this may be accomplished is illustrated in Figure 14. The burn rates may be tailored by adjusting the extent of interaction of hydrazine with the nitramine. By altering the relative particle sizes of the ingredients, using nitramines that have different physical properties, such as melting point and vapor pressure that will modify their interaction with the hydrazine, or using other compounds that may generate hydrazine, the burn rates of nitramine-based propellants may be modified.

One of the key features of the compound that generates hydrazine is that the hydrazine does not readily react with the product from the anion in the TAG compound. For example, it is unlikely that TAG nitrate would work since the hydrazine is likely to undergo a very rapid reaction with the nitric acid formed from the nitrate anion. Thus, it would be unavailable to react with the nitramines in a formulation.

Reaction of TAGzT with RDX at lower temperatures. The temperature range over which the products from TAGzT evolve are lower when TAGzT is in the presence of RDX. For example ammonia, NH_3, evolves from TAGzT between 182 and 210°C when it is decomposed by itself, whereas it evolves between 165 an 182°C when it is in the presence of RDX (Fig. 12). This is most likely due to the transport of RDX vapor to a region in the vicinity of the surface of the TAGzT particles. In this region, the RDX may react in the gas phase with decomposition products formed from TAGzT or it may deposit on the surface of the TAGzT particles. The heat generated by the reaction of RDX with the TAGzT products may create localized hotter regions on the surface of the particles, leading to an apparent reaction at lower temperatures. Careful examination of the vapor pressure of RDX in the region where TAGzT products interact with RDX indicate that its vapor pressure is higher than at corresponding reaction cell temperatures in the experiment with only RDX (Fig. 12). This is consistent with the RDX within the reaction cell being at a higher temperature than is expected.

To examine the interaction of TAGzT and its decomposition products with RDX, a mixture of TAGzT with RDX was cycled repeatedly between 135 and 155°C (Fig. 15). The signals associated with RDX (m/z=128) and its products CH_2O (29) and N_2O (44) are shown in graphs [1, 3] and [1, 4]. The pressure of RDX rises and falls as the temperature of the sample is cycled. No TAG is observed in this experiment. New products appear that were not observed in the decomposition of TAGzT by itself at m/z values of 18, 30, and 44, as was observed in the higher temperature experiments.

Comparison of data from experiments with TAGzT by itself and TAGzT mixed with RDX (Fig. 16) show that the presence of RDX causes the TAGzT to decompose more rapidly. In the experiment with TAGzT alone, the products evolve at a relatively uniform rate during the course of the experiment. While the evolution of the various products from TAGzT is relatively uniform, it is important to note that very small quantities of products evolve during the first two heating cycles. Thus, *the TAGzT must be altered in some way so as to enable the decomposition process* that we observe in these experiments.

When RDX is present with TAGzT, the rate of decomposition increases in each subsequent cycle in the thermal decomposition process (graphs [1, 1] and [1, 2] in Fig. 16). This is consistent with a changing local reaction environment on the surface of the TAGzT particles. The introduction of RDX into this LRE clearly alters its associated elementary reaction manifold in such a way that increases the rate of reaction. This change in the LRE brought about by the introduction of RDX into the reaction environment is also evident by a comparison of the rate of decomposition of TAGzT before and after the sample is heated to 150°C (Fig. 17). In these experiments the rate of evolution of products from TAGzT (e.g., NH_3, HCN, N_2 and N_2H_4 in graph [1, 2]) is clearly faster at the same isothermal temperature after the sample has been heated to 150°C, the temperature at which the TAG first decomposes to NH_3, HCN, N_2 and N_2H_4.

Based on these results we are currently creating qualitative models that capture the LREs that control the reactions of mixtures of TAGzT with RDX. The LREs we have currently identified are captured in the following schematic.

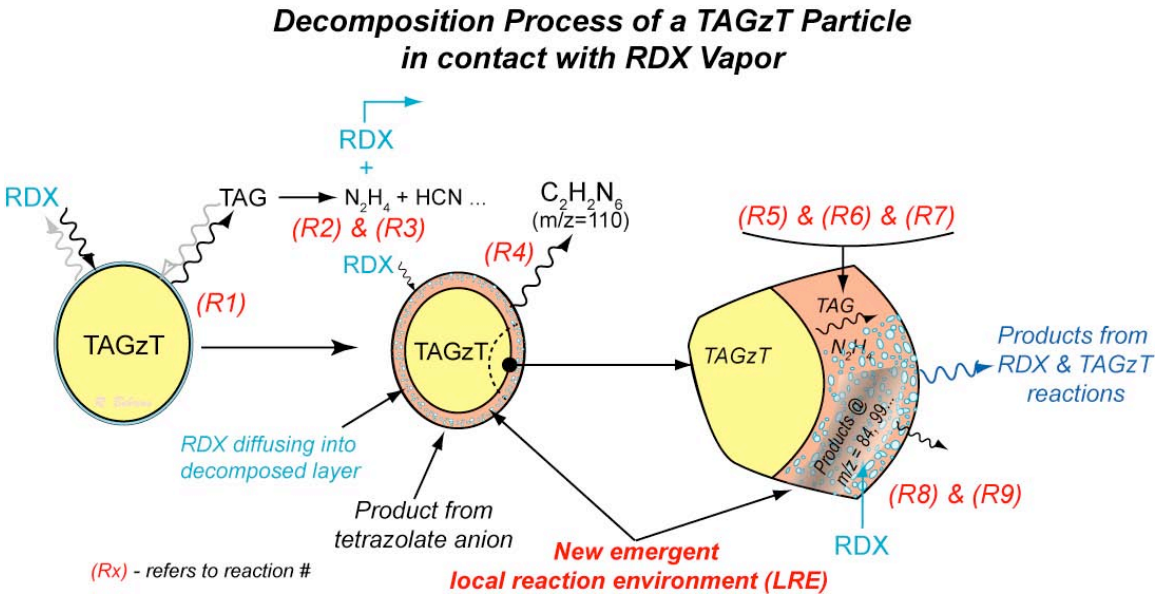

There are two new local reaction environments introduced and one altered when RDX is introduced into the reaction environment with TAGzT. The first new LRE is the deposition of RDX on the surface of the TAGzT particles. It may be anticipated that this may decrease the onset time to more rapid decomposition of TAGzT. However, comparing the induction time to the release of products from TAGzT in thermal cycling experiments with and without RDX (Fig. 16) does not show a particularly significant effect. The second new LRE is the reaction of RDX in the gas-phase with hydrazine. This is clearly a very significant reaction in the decomposition of mixtures of TAGzT with RDX.

A very significant effect of RDX is the alteration of the LRE that develops on the surface of the TAGzT particles and apparently establishes a reaction manifold that enables a more rapid decomposition of TAGzT. The much more rapid increase in the rate of decomposition of TAGzT with RDX present suggests that RDX diffuses into the LRE on the surface of the TAGzT particles and promotes the decomposition of TAGzT (Fig. 16). The extent of RDX that decomposes in this surface LRE compared to the decomposition of RDX through it reaction with N_2H_4 in the gas phase is difficult to discern from the current experiments. For example, the rate of formation of N_2O (44) from RDX increases as the amount of hydrazine in the reaction cell increases (compare graphs [1, 1] and [4, 1] in Fig 16). This is consistent with hydrazine reacting with RDX in the gas phase. However, the rate of reaction in the LRE on the TAGzT surface is also reacting at a faster rate to form the TAGzT decomposition products. The RDX may also be reacting in this environment to a significant extent.

We are currently examining our data and carrying out further experiments to probe these issues.

Isotopic Crossover Experiments. We have also conducted isotope crossover experiments with TAGzT and RDX-d6 and RDX-15N6 to develop further insight into the reactions between TAGzT, hydrazine and RDX. Preliminary analysis of the data indicates that

simple reaction of N_2H_4 with the NO_2 groups of RDX, leaving the ring behind is too simple an explanation of the interaction. The reaction involves attack of the hydrazine on the RDX molecule that leads to reactions of both the ring and NO_2 groups. For example, in reactions of TAGzT with RDX-d6 we observe a shift in some of the signal at m/z=44 to m/z=46. This indicates some of the signal at m/z=44 arises from a compound that contains two hydrogen atoms. The most likely formula is H_2CNO. Further analysis of the results from isotopic crossover experiments is in progress.

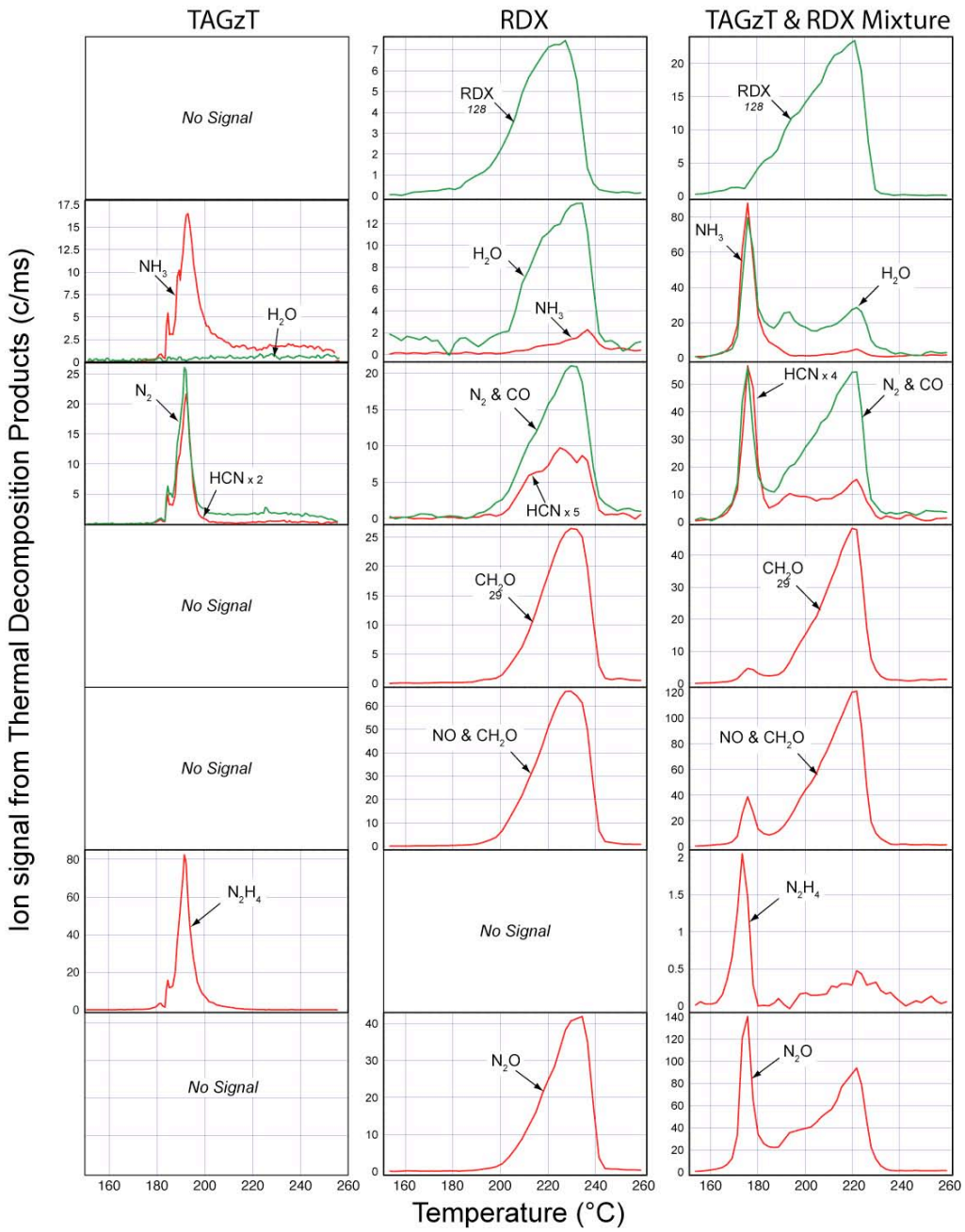

Figure 12. Comparison of ion signals from gaseous compounds formed during the thermal decomposition of TAGzT, RDX and a mixture of RDX with TAGzT.

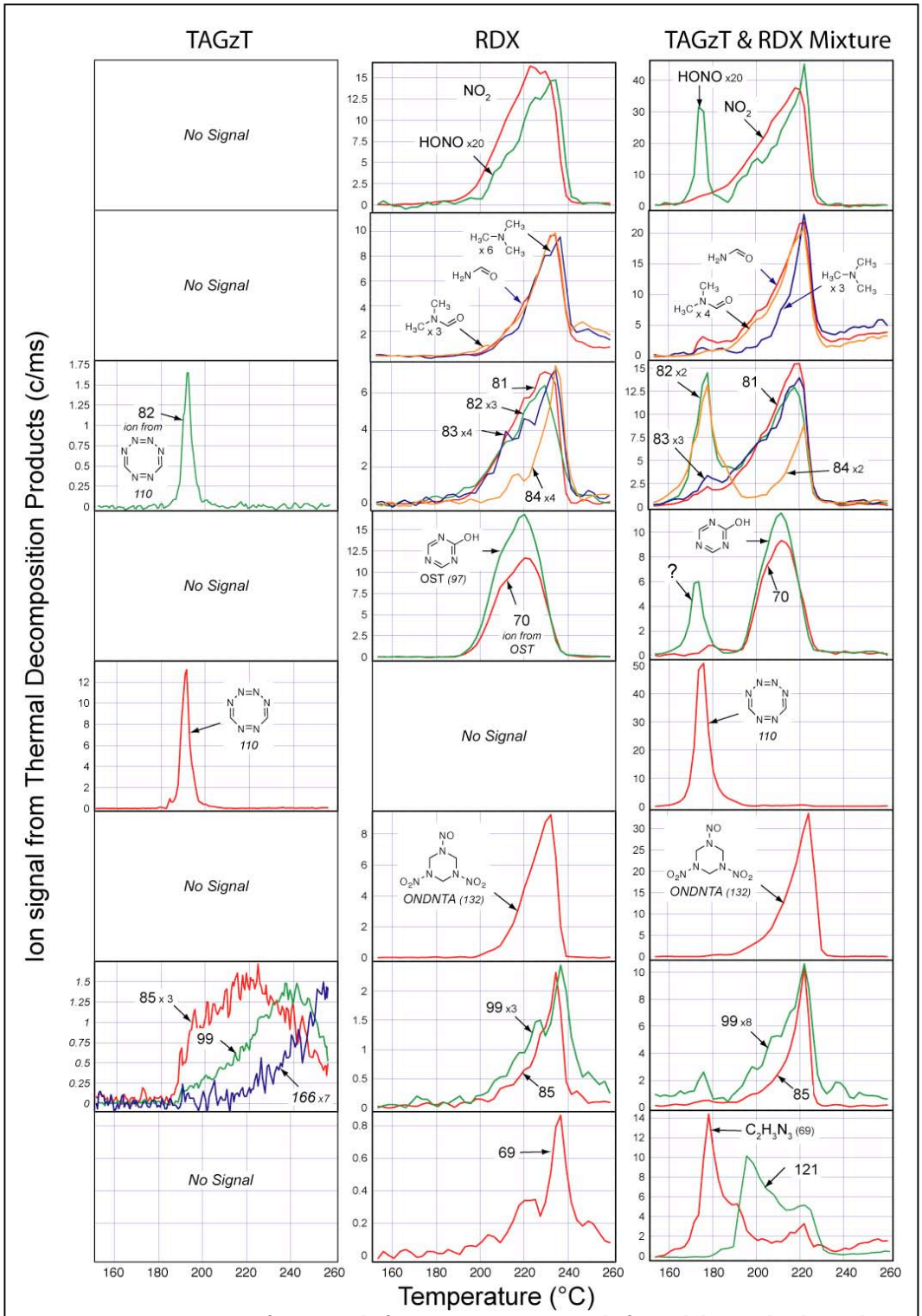

Figure 13. . Comparison of ion signals from gaseous compounds formed during the thermal decomposition of TAGzT, RDX and a mixture of RDX with TAGzT.

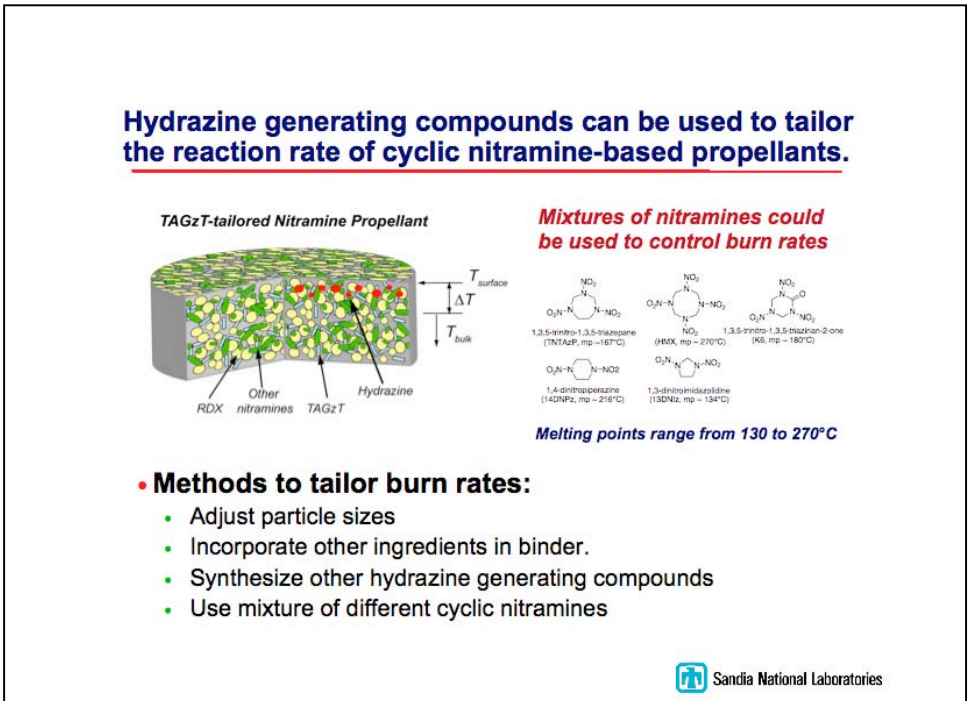

Figure 14. Method to use hydrazine-generating compounds to modify burn rates of nitramine-based propellants.

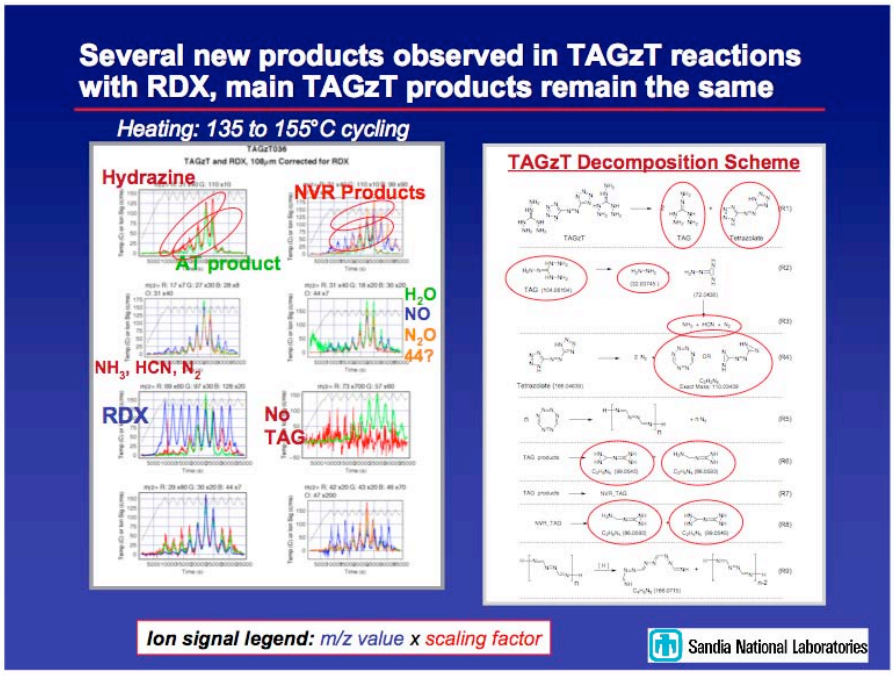

Figure 15. Ion signals from compounds formed in the decomposition of a mixture of TAGzT with RDX as the sample is cycled in temperature between 135 and 155°C.

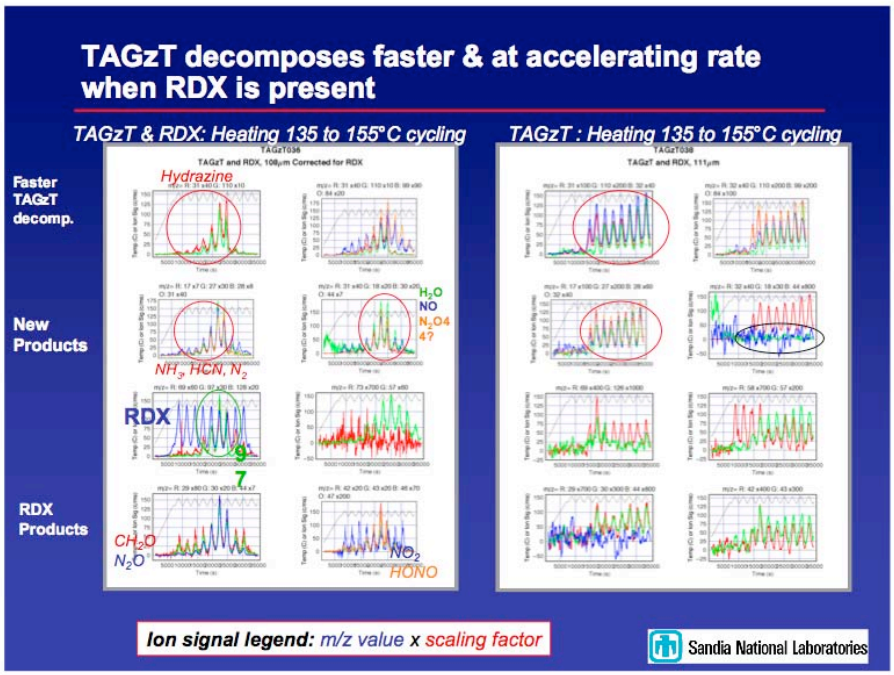

Figure 16. Comparison of the ion signals from compounds formed in the thermal decomposition of TAGzT (right) and TAGzT mixed with RDX(left).

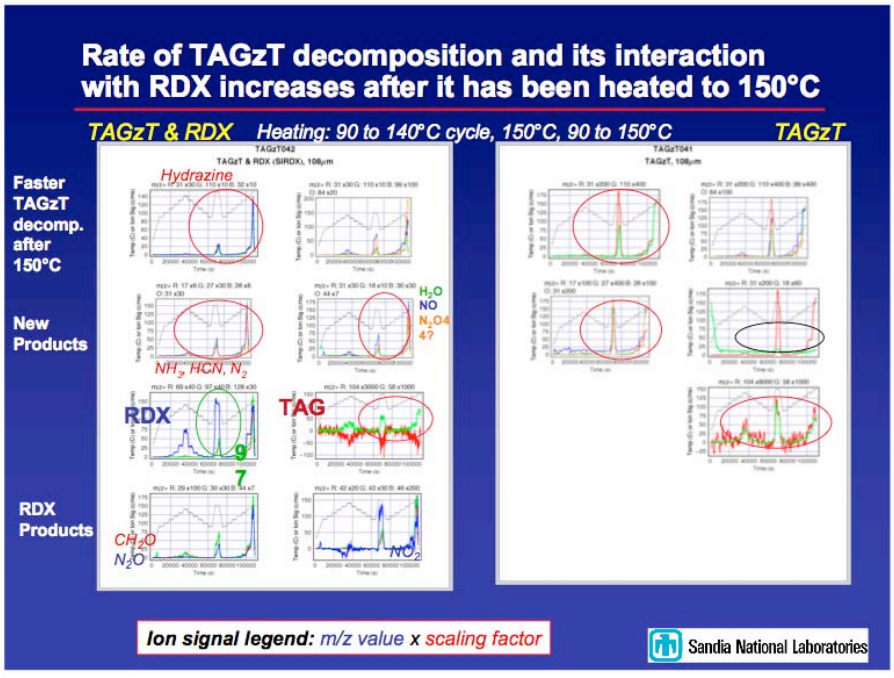

Figure 17. Comparison of ion signals from compounds formed in the thermal decomposition of TAGzT (right) and TAGzT mixed with RDX (right before and after the sample is heated to 150°C.

Workshop organization: "R&D Required to Implement New Energetic Ingredients in Munitions.

A workshop was held to address the issues of R&D required to implement new ingredients in munitions. The workshop has been organized in cooperation with Bill Anderson (ARL), Brad Forch (ARL) and Bob Shaw (ARO) and was coordinated through the CPIA/JANNAF organization. The workshop was held at the Battelle Eastern Science and Technology (BEST) Center, Aberdeen, Maryland, on 29 – 31 August, 2006.

The workshop on "R&D Required to Implement New Energetic Ingredients in Munitions" has succeeded in establishing the groundwork for developing a new conceptual framework for what will be required to implement new energetic ingredients in munitions. One of the main issues that limit progress in the development of new energetic materials and formulations is the perceived high risk of investing in this area.

This perception of high risk is felt to originate primarily from limited success in developing new ingredients and implementing new energetic materials in munitions. This limited success is due to the complexity of the processes that control the reactions of these materials, and the broad range of performance, safety, environmental compliance, health and cost issues that must be met.

To reduce the risk of developing new energetic materials will require (1) increasing our ability to monitor and understand the reactions that control the various critical performance, safety and aging behaviors of energetic materials, (2) using this understanding to guide the design of better energetic ingredients and energetic materials, (3) developing new diagnostic tools and super-small scale experiments to gain an understanding of the reaction processes underlying performance, safety and aging, and (4) the ability to synthesize, formulate and test new materials at rate that are 100 times faster and use 100 times less materials than current methods.

To achieve these goals will require using today's scientific understanding and technology to develop a new integrated system for energetic material development.

Teams have been assembled to address the details of the issues for implementing this general R&D investment strategy.

An interim report on the workshop was presented at the JANNAF Combustion Subcommittee Meeting in December 2006.[11] A report containing proceedings of the workshop is currently in the final stages of preparation by CPIAC.

References:

1. Behrens, R., *Thermal Decomposition Processes of Energetic Materials in the Condensed Phase at Low and Moderate Temperatures,* in *Overviews of Recent Research on Energetic Materials*, R.W. Shaw, T.B. Brill, and D.L. Thompson, Editors. 2005, World Scientific Publishing Co.: Singapore. p. 29 - 74.
2. Behrens, R. and S. Maharrey, *Chemical and Physical Processes that Control the Thermal Decomposition of RDX and HMX,* in *Combustion of Energetic Materials*, K.K. Kuo and L.T. DeLuca, Editors. 2002, Begell House: New York. p. 3 - 21.
3. Maharrey, S. and R. Behrens, *Thermal Decomposition of Energetic Materials 5. Reaction Processes of 1,3,5-Trinitrohexahydro-s-triazine (RDX) Below Its Melting Point.* Journal of Physical Chemistry, 2005. **109**: p. 11236-11249.
4. Behrens, R. and D. Wiese-Smith, *Reaction Kinetics of RDX in the Condensed Phase*, in *40th JANNAF Combustion Meeting.* 2005, CPIA Publication: Charleston, South Carolina. p. June 2005.
5. Ross, J., I. Schreiber, and M.O. Vlad, *Determination of Complex Reaction Mechanisms - Analysis of Chemical, Biological, and Genetic Networks.* 2006, Oxford University Press: New York City. p. 136.
6. Knott, C., C. Walsh, and S. Prickett, *TPE Based Gun Propellants with High Nitrogen Modifiers,* in *Propellant Development and Compatibility Subcommittee Meeting.* 2004, CPIA.
7. Walsh, C. and C. Knott, *Gun Propellant Formulations with High Nitrogen Modifiers,* in *Propellant Development & Compatibility Subcommitte Meeting*. 2003, CPIA.
8. Behrens, R., Jr., *New simultaneous thermogravimetry and modulated molecular beam mass spectrometry apparatus for quantitative thermal decomposition studies.* Review of Scientific Instruments, 1987. **58**(3): p. 451-461.
9. Behrens, R., Jr., *Identification of Octahydro-1,3,5,7-tetranitro-1,3,5,7-tetrazocine (HMX) Pyrolysis Products by Simultaneous Thermogravimetric Modulated Beam Mass Spectrometry and Time-of-Flight Velocity-Spectra Measurements.* International Journal of Chemical Kinetics, 1990. **22**: p. 135-157.
10. Behrens, R., Jr., *Determination of the Rates of Formation of Gaseous Products from the Pyrolysis of Octahydro-1,3,5,7-tetranitro-1,3,5,7-tetrazocine (HMX) by Simultaneous Thermogravimetric Modulated Beam Mass Spectrometry.* International Journal of Chemical Kinetics, 1990. **22**: p. 159-173.
11. Behrens, R., et al. *Interim Report: Workshop on R&D Required to Implement New Energetic Ingredients in Munitions*. in *41st JANNAF Combustion Subcommitte Meeting*. 2006. San Diego, California: CPIA.

Publications:

Rauch, R.; Behrens, R., Vapor Pressures and Thermal Decomposition Processes of Bis(2,2-dinitropropyl) acetal (BDNPA) and Bis(2,2-dinitropropyl) formal (BDNPA). *Propellants Explosives Pyrotechnics* **2007,** 32, (2), 97-116.

Hayden, H.; Behrens, R.; Wiese-Smith, D.; Maharrey, S. In *Thermal Decomposition of High Nitrogen Compounds: TAGzT*, 41st JANNAF Combustion Subcommittee Meeting, San Diego, California, December 4-8, 2006, 2006; CPIAC: San

Behrens, R.; Wiese-Smith, D.; Hayden, H. In *Reaction Processes that Control the Thermal Decomposition of Mixtures of TAGzT and RDX*, 41st JANNAF Combustion Subcommittee Meeting, San Diego, California, December 4-8, 2006.

Behrens, R.; Anderson, W. R.; Forch, B.; Shaw, R. W. In *Interim Report: Workshop on R&D Required to Implement New Energetic Ingredients in Munitions*, 41st JANNAF Combustion Subcommittee Meeting, San Diego, California, December 4-8, 2006.

Presentations:

R. Behrens, "Overview of Research in Our Energetic Materials Group at CRF", Army Research Lab, July 17-18, 2006, invited by Brad Forch, Propulsion Branch Chief.

R. Behrens "Using Experimental and Simulation Methods to Understand Complex Reaction Processes in Energetic Materials", Auburn University, January 25, 2007 (invited by Rik Blumenthal).

R. Behrens, "Experimental Approaches to Assess and Predict Failure Modes of New Ingredients in Munitions", Workshop on R&D Required to Implement New Ingredients in Munitions, Aberdeen MD, Aug 29-31, 2006.

R. Behrens. D.Wiese-Smith, H. Hayden, "Investigation of Reaction Processes of TAGzT & Its Interaction with Propellant Ingredients (RDX, BDNPA/F)", Workshop on HiN Ingredients, Army Research Lab, June 5-6, 2007.

Thermal Decomposition Processes of Energetic Materials in the Condensed Phase at Low and Moderate Temperatures*

Richard Behrens
Sandia National Laboratories
Combustion Research Facility
Livermore, California 94551-0969

* Published in Advanced Series in Physical Chemistry: Overviews of Recent Research on Energetic Materials, Editors: R.W. Shaw, T.B. Brill and D.L. Thompson, World Scientific Press, 2005, pp. 29-74.

ABSTRACT

A new conceptual framework to examine and communicate the ideas needed to characterize the thermal decomposition processes of energetic materials in the condensed phase at low and moderate temperatures is described. This framework uses a new experimental protocol,

primarily based on mass spectrometry, to examine the complex irreversible and spatiotemporal reactive processes that underlie the decomposition of energetic materials.An outline of the type of information that is required, a discussion of experimental methods for obtaining the information, an overview of new numerical simulation methods for extracting reaction mechanisms and chemical kinetics from the data, an illustration of these methods with recent results on the decomposition of RDX and HMX, and a discussion of future directions for research on the thermal decomposition of energetic materials in the condensed phase is presented.

TABLE OF CONTENTS

I. INTRODUCTION

A. Scientific Issues: Understanding Processes Far From Equilibrium

II. REACTIVE PROCESSES: EXPERIMENTAL METHODS

A. Experimental Challenges

B. Experimental Requirements

1. Experimental Design Principles
2. Analysis of Data From High-Level Information Content Experiments

C. New Mass Spectrometry-Based Experimental Protocol

1. Qualitative Models Require Both Chemical and Spatial Information
2. Development of Mathematical Methods

D. Comparison Of Conventional Thermal Decomposition Experiments

1. Global Measurements
2. Product Identification Measurements

III. CONDENSED-PHASE REACTIVE PROCESSES

A. Evidence For Complex Processes

B. HMX Decomposition Processes

1. General Nature of Condensed-Phase Reactions in Energetic Materials
2. Decomposition of Composite Materials

C. Characterization of Decomposition Processes: RDX and HMX Case

1. Development of A Conceptual Framework to Represent and Analyze Decomposition Processes

2. Reaction Pathways: Solid-Phase Reactions, Non-linear Processes, Feedback Loops and Autocatalysis

3. Emergent Phenomena

D. Effects of Experimental Conditions on Observed Decomposition Processes

1. Reaction-Coordinate Vectors

2. Environmental Conditions Determine Location of Reaction-Coordinate Vector

3. Conditions Probed by Various Experiments

IV. REACTION KINETICS

A. Extracting Reaction Kinetics From Condensed-Phase Experiments

1. Simple Kinetics – Direct Inversion From Experiment

2. Kinetics of Complex Reaction Networks

V. CONCLUSIONS AND FUTURE RESEARCH

VI. ACKNOWLEDGEMENTS

VII. REFERENCES

VIII. TABLES

IX. FIGURE CAPTIONS

I. INTRODUCTION

The processes that control the thermal decomposition of energetic materials in the condensed phase at low and moderate temperatures present a challenge to the chemical kineticist in the 21st century. Meeting this challenge will provide new means to develop improved propellants and explosives and to assess the safety and aging characteristics of existing ones. Currently, there is great interest in developing less sensitive munitions and extending the shelf life of existing ones. The development of new insensitive munitions will require understanding how reactive processes that occur at temperatures associated with fires or other abnormal environments will alter the characteristics of the energetic ingredients and lead to violent reactions.[1, 2] A more fundamental understanding of the underlying reactive processes, which occur in these environments, can guide the development of new compounds, or the development of new formulations, that will mitigate the violence of the reactions and lead to less sensitive munitions.

The underlying reactive processes are also related to safety, aging, and performance in propulsion and explosive applications. Slow reactions related to aging behavior clearly involve spatiotemporal controlled reactions. They are also influenced by interfacial reactions with other ingredients. Safety issues related to slow and fast cook-off behavior are influenced by changes in the chemical, physical and morphological properties of the material. Finally, performance issues related to the combustion process that occurs on the surface of a burning propellant are dependent on condensed phase reactive processes. To develop the understanding required to address these issues demands a more fundamental understanding of the processes that occur in the condensed phase, at low and moderate temperatures, than is currently available.

A. Scientific Issue: Understanding Processes Far From Equilibrium

As the temperature at which reactions occur in energetic materials are lowered from those that are associated with combustion (600º to 3000ºC), new types of processes start to play a more dominant role in controlling their decomposition. As the temperature decreases, the rates of reaction of individual molecules decrease and transport processes become more important. In the temperature range from room temperature up to approximately 400ºC, most energetic materials are present as solids or liquids so that reactions in the liquid and solid phases can play the major role in the decomposition processes.

This transition in the types of physical and chemical processes that control the decomposition of energetic materials creates reaction systems that are difficult to characterize. At lower temperatures the focus for examining the reactions shifts from the molecular spatial scale to larger spatial scales associated with thermal and mass transport processes that give rise to nonhomogeneities in the system. In the liquid phase, localized reactions may form in the vicinity of bubbles and gaseous products may diffuse into the surrounding liquid, creating gradients of the gaseous products in the liquid phase. In the

solid phase, reactions may occur preferentially on the surface of particles or complex processes may occur within the solid phase via nucleation and growth processes. In addition, lower temperatures allow reactions to occur that create compounds that may have higher molecular weights and be more complex than the energetic materials themselves. Growth of these more complex compounds in the reaction environment opens new "catalytic-like" reaction pathways, where the secondary and tertiary structure of the complex compounds may play a role in controlling the reactive process. This type of process is analogous to the catalytic behavior of enzymes in living systems.

Each new type of process that may occur during the decomposition of energetic materials in the condensed phase at low and moderate temperatures is irreversible and may occur far from equilibrium conditions. Thus, to understand the decomposition of energetic materials under these lower temperature conditions, one must work within the framework of the physics of nonequilibrium processes, which uses concepts such as self-organization and dissipative structures.

Reactive systems that evolve under conditions far from equilibrium are characterized by processes that become unstable at some distance from equilibrium and bifurcate along multiple reaction pathways. When systems pass this bifurcation point, a set of new phenomena arises in which nonequilibrium spatial structures, chemical waves, or oscillating chemical reactions are observed. These spatiotemporal organizations are known as dissipative structures. The conditions usually necessary for this type of behavior and the creation of dissipative structures are: 1.) reactions that occur far from equilibrium and; 2.) catalytic-like reactions. Many experiments that have examined the decomposition of energetic materials in the condensed phase involve reactive processes that meet the criteria required for the creation of dissipative structures. In some cases, direct visual evidence of the evolution of the spatial structures is observed as will be described below.

The complex nature of the reactive processes that control the thermal decomposition of energetic materials in the condensed phase at low and moderate temperatures present a great challenge to the chemical kineticist. The conventional methods available to the kineticist focus on characterizing reactions at the molecular level. While this is an important component of understanding the thermal decomposition process in the condensed phase, it does not address many of the issues associated with the irreversible processes that control their decomposition behavior.

Given the complex nature of these reactive processes, how can a better understanding and characterization of these processes be achieved? This is the main question that I address in this chapter.

To address this question, an analogy to the development and use of elementary reactions for characterizing gas-phase reactions may be posed, and then the ability to develop a similar understanding for condensed phase reactions examined. Elementary reactions[3] are fundamental to our ability to characterize and predict the behavior of complex physicochemical processes, such as gas-phase combustion. *Can the concept of elementary reactions also be applied to the characterization of complex processes in the condensed phase? If so, how?*

A range of different types of reactions can control the decomposition process in the condensed phase. *What are the reactions? How do the types of reactions change with increasing temperature and pressure?* At low temperatures, reactions may occur at interfacial boundaries, reaction rates may be limited by transport processes, nucleation and growth processes may play a role, or enzymatic reactions may be involved.[4] For reactions at higher temperatures, the materials are heated more rapidly, thus, transport processes and the development of spatiotemporal features are less important, and reactions at the molecular level become dominant. In this realm, unimolecular decomposition and elementary bimolecular reactions control the reactive processes.

Roles of different types of physical and chemical processes will change with experimental conditions (temperature and pressure). *How does the transition from low temperature spatiotemporal controlled reactions to high temperature molecularly focused reactions occur? How rapid and how distinct is the transition?* Reactions that are initiated by thermal heating, and occur in the solid and liquid phase, are likely to be controlled by more complex spatiotemporal processes. For this reason, compounds with lower rates of vaporization are more likely to remain in the condensed phase and react. Thus, condensed phase processes may be relevant up to ~100°C above the melting point of a material, which would correspond to a temperature range from 200° to 400°C for energetic materials.

There is a wide range of different types of processes that must be considered in condensed phase reactions. The processes include the following:

1) Phase transitions: solid-solid, solid-liquid;
2) Reactions on the surface of particles;
3) Nucleation and growth of reaction regions (bubbles) within the solid;
4) Creation of other condensed-phase products within the sample;
5) Reactions between the reactant and its gas and condensed phase reaction products;
6) Creation of new morphological structures within the sample that can form new reaction zones with localized temperature and pressure environments;
7) Reactions at surfaces and interfacial boundaries.

The challenge is to unravel and understand these underlying processes. The scientific community has generally avoided this challenging problem. The main difficulty stems from the inability to divide the system (*i.e.*, decomposition of the material in the condensed phase) into its individual components for independent examination.

This standard "divide and examine" methodology has been used extensively to understand reactions in the gas phase, but it is difficult, perhaps impossible, to apply to organic materials in the condensed phase. For example, one could consider examining the decomposition of an energetic compound, say RDX, in the gas phase.[5] Done properly, this provides basic information on the elementary unimolecular decomposition of RDX. Unfortunately, this provides only one of several possible rate-limiting reaction pathways that may occur in the condensed phase. For example, a more rapid reaction may involve the interaction between RDX and one or more of its gas-phase or condensed-phase reaction products. Thus, the RDX unimolecular decomposition kinetics, while a useful piece of basic information, may not play a significant role in the

rate-limiting processes that control its decomposition in the condensed phase. Therefore, we are left with the problem of how to extract information from a set of different processes that occur simultaneously during the course of an experiment.

Given the complex and irreversible nature of reactions that occur in energetic materials in the condensed phase, and the limited experimental methods available to probe these reactions, a new conceptual framework is required to understand and communicate the ideas that are needed to address these issues. This framework must provide the basis for examining and understanding reactive processes in the condensed phase, in a way that is similar to the framework used to examine complex reaction processes in the gas phase. It must incorporate features that 1.) allow discovery of underlying reactive processes, 2.) relate underlying features to materials properties, 3.) assess the competition between underlying processes as a function of experimental conditions, and; 4.) provide a basis for mathematical characterization of the underlying processes. With these features, the conceptual framework will provide a basis for creating new knowledge of the underlying processes that occur in energetic materials in the condensed phase and building a roadmap, based upon this knowledge, that can be used to examine each of these underlying processes in more detail.

This chapter focuses on the development and application of an experimental protocol to understand and characterize the reactive processes that occur in the condensed phase of energetic materials and how this work has lead to the development of a new conceptual framework to examine and communicate the details of these processes. It presents an outline of the type of information that is required, a discussion of experimental methods for obtaining the information, an overview of new numerical simulation methods for extracting reaction mechanisms and chemical kinetics from the data, an illustration of these methods with recent results on the decomposition of RDX and HMX, and a discussion of future directions for research on the thermal decomposition of energetic materials in the condensed phase.

II. REACTIVE PROCESSES: EXPERIMENTAL METHODS

To obtain better understanding of the reactive processes of energetic materials in the condensed phase, we have developed a new experimental protocol. This section describes the development of the experimental protocol and compares it with more standard measurement methods, which have been used in the past to examine the decomposition of energetic materials. First the experimental challenges are described. Next the experimental requirements needed to address these challenges are outlined. This is followed by a brief description of the experimental protocol. Finally, the protocol is compared to other methods.

A. Experimental challenges

Four general features of thermal decomposition reactions of energetic materials in the condensed phase pose significant experimental challenges:

1. A wide range of reactive processes controls the thermal decomposition of energetic materials.
2. Chemical, physical and morphological (spatial) features can play significant roles in controlling the decomposition process. The experimental method must be capable of capturing the nature and roles of these spatiotemporal processes.
3. The different reactive processes are often nonlinearly coupled. The experimental methods must enable us to characterize these nonlinearities.
4. The state of the sample is a function of the extent of decomposition. Consequently, the state of the reaction conditions changes continuously during the course of an experiment making steady-state experiments infeasible. This behavior makes it difficult, if not impossible, to isolate specific individual reactions to study in an independent manner. Hence, traditional chemical kinetics methods, which isolate and control the concentration of specific reactants and measure their rates of reaction, have limited applicability. These four general features of condensed-phase energetic material reactions are characteristic of nonequilibrium processes, which involve self-organization and the development of dissipative structures,[6] and require new methods to understand and characterize the underlying reactions.

B. Experimental requirements

Given the general features of the thermal decomposition process, guidelines for developing the experimental methods can be defined as follows:

1. Assume it is not feasible to isolate reactive processes to study them individually. Furthermore, assume that the development of dissipative structures are important and develop as a result of interactions between reactive components of the entire system.
2. Focus on identifying and characterizing underlying physicochemical processes. Experiments must identify and characterize the underlying physicochemical processes that control the decomposition.
3. Develop experiments that provide a high level of information content. The overall approach must use experiments that provide a high level of information on the underlying reactive processes over a wide range of controllable conditions.

1. EXPERIMENTAL DESIGN PRINCIPLES. Several general principles are used to guide the development of new instrumental methods that will provide the high information content needed to study the reactions of energetic materials in the condensed phase. These principles may be summarized as follows:

1. Maximize simultaneous measurements. Design new experimental methods using the general principle that the greatest amount of information will be obtained by measuring as many different properties of a sample as possible, with the widest range of measurement methods, at the same time. This allows direct comparison of different types of information. Otherwise the data represents reactions

collected under different reaction conditions and makes interpretation of the results more difficult.

2. Collect chemical information as a function of spatial location. Chemical reactions in the solid or liquid phase can occur in localized regions or at interfacial boundaries associated with the development of dissipative structures. Thus, their reaction rates are often controlled by both the rate of chemical reaction and the transport of reactants and products in the localized region. Development of instruments to provide detailed molecular information, as a function of spatial location in a material, will provide insight into how chemical reactions are coupled with transport processes in these materials. For example, a microscope that provides molecular information as a function of location, in a manner analogous to reflected light for optical images or secondary electrons for SEM images.

2. ANALYSIS OF DATA FROM HIGH-LEVEL INFORMATION CONTENT EXPERIMENTS. The overall objectives of experimental work with energetic materials are: 1.) to develop a qualitative understanding of the underlying reactive processes and 2.) to create mathematical models of the reactive processes. To achieve these objectives requires the extensive development and use of numerical algorithms.

High-level information content experiments provide large amounts of data that must be analyzed to glean relevant information on the underlying reactive processes. This requires both the application of transformation algorithms to convert raw data to the desired information format, and the use of analysis algorithms to extract the chemical, physical, and temporal information from the data. Developing mathematical models of the underlying reactive processes and comparing these models to data collected from the high information content experiments provide a test of the postulated reactive processes. The optimized models that characterize the underlying reactive processes provide a basis for development of models that can be used to characterize the response of materials in larger scale systems.

To summarize, the experiments must provide information that can track the chemical and physical state of the sample as a function of time. They must also provide information that can be used to identify and track the progress of the rate-controlling reactions in the decomposition process. The experiments should also provide information on the identities and amounts of condensed-phase products and morphological changes that occur in the sample during the course of an experiment. To extract an understanding of the underlying reactive processes and the associated reaction kinetics, a numerical simulation method must be used to analyze the data. The method must allow one to postulate various reaction schemes, numerically simulate the reaction rates for the postulated reaction scheme, and compare the numerical results with the data from the experiments. Feedback between experiments and numerical simulations provide guidance to select new experimental conditions.

C. New mass spectrometry-based experimental protocol

A mass spectrometry based experimental protocol, developed in our laboratories, addresses the experimental requirements for examining the decomposition of energetic materials in the condensed phase. The protocol uses new instrumental methods and numerical algorithms for data analysis and simulation of physicochemical processes in the condensed phase. A schematic diagram outlining the experimental methods and numerical algorithms and the types of information obtained by each is shown in Figure 1. As illustrated in the diagram, the overall goal is to develop a model of the thermal decomposition processes based on the underlying fundamental reactions and the associated reaction kinetics.

1. QUALITATIVE MODELS REQUIRE BOTH CHEMICAL AND SPATIAL INFORMATION.

   To understand the underlying reactive processes requires identifying the compounds and determining how fast they are formed as a function of experimental conditions. For reactions in the condensed phase, the development of dissipative structures may play a significant role in determining the rates of reaction. Therefore, it is important to determine the spatial characteristics of these features and how they may change during the course of an experiment. This requires determining the morphological characteristics of the samples during the course of an experiment in addition to the time-dependent chemical information on the reactants and products.

   <u>The Simultaneous thermogravimetric modulated beam mass spectrometry instrument</u>.

   The simultaneous thermogravimetric modulated beam mass spectrometry (STMBMS) instrument provides the main source of information on the thermal decomposition processes. It was designed to conduct experiments that would provide information on both the identities and rates of formation of the compounds involved in the reactive processes that control the decomposition of energetic materials.

   The instrument and the obstacles presented by using mass spectrometry has been described in detail previously[7-9]; the STMBMS enables:

   1. Identification of compounds in a mixture
   2. Quantitative measurement of each of the identified compounds
   3. Control of rate of vaporization of condensed phase species
   4. Control of the pressure of gaseous compounds formed in the reactions and contained in the reaction environment
   5. Collecting data that provides simultaneous information on all compounds.

   The STMBMS instrument (Figure 2) incorporates several features to provide the desired information. The decomposition experiment is conducted in a reaction cell that is fitted with well-characterized exit orifice that can be used to control the rate of flow of gases out of the reaction cell. Varying the size of the orifice allows the pressure of gases within the reaction cell to be controlled. The simultaneous measurement of the rate of force change (mass loss and thrust) and the mass spectra of the gases exiting the reaction cell provides the rates of formation of compounds formed during thermal decomposition. The time-of-flight velocity spectra of the

neutral gases that exit the reaction cell are used to determine whether ion signals measured with the quadrupole mass spectrometer are parent or daughter ions. Thus ion signals at a specific m/z value, measured with the mass spectrometer, can be associated with a compound that evolves from the reaction cell.

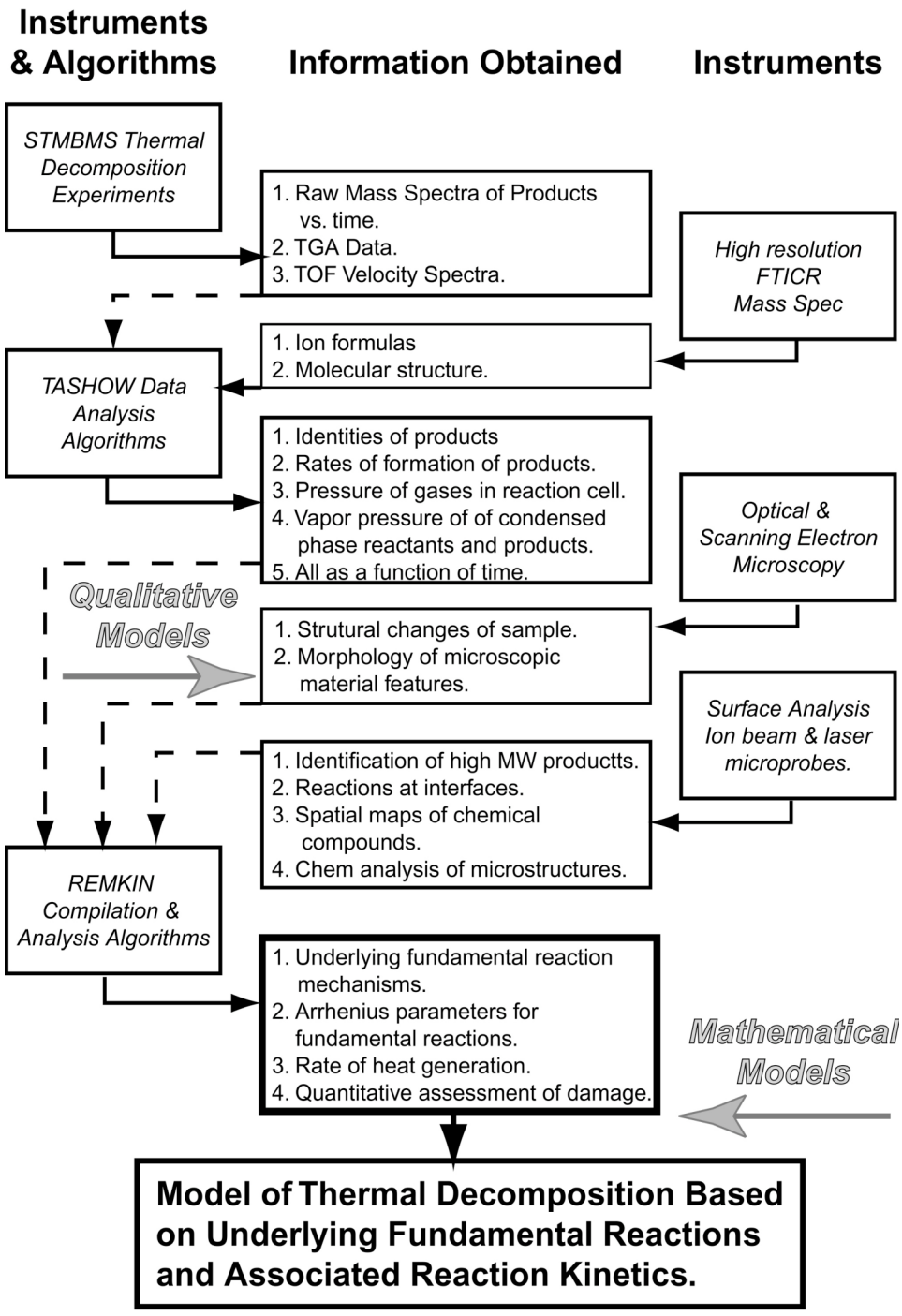

Figure 1. Experimental protocol used to study thermal decomposition processes of energetic materials in the condensed phase.

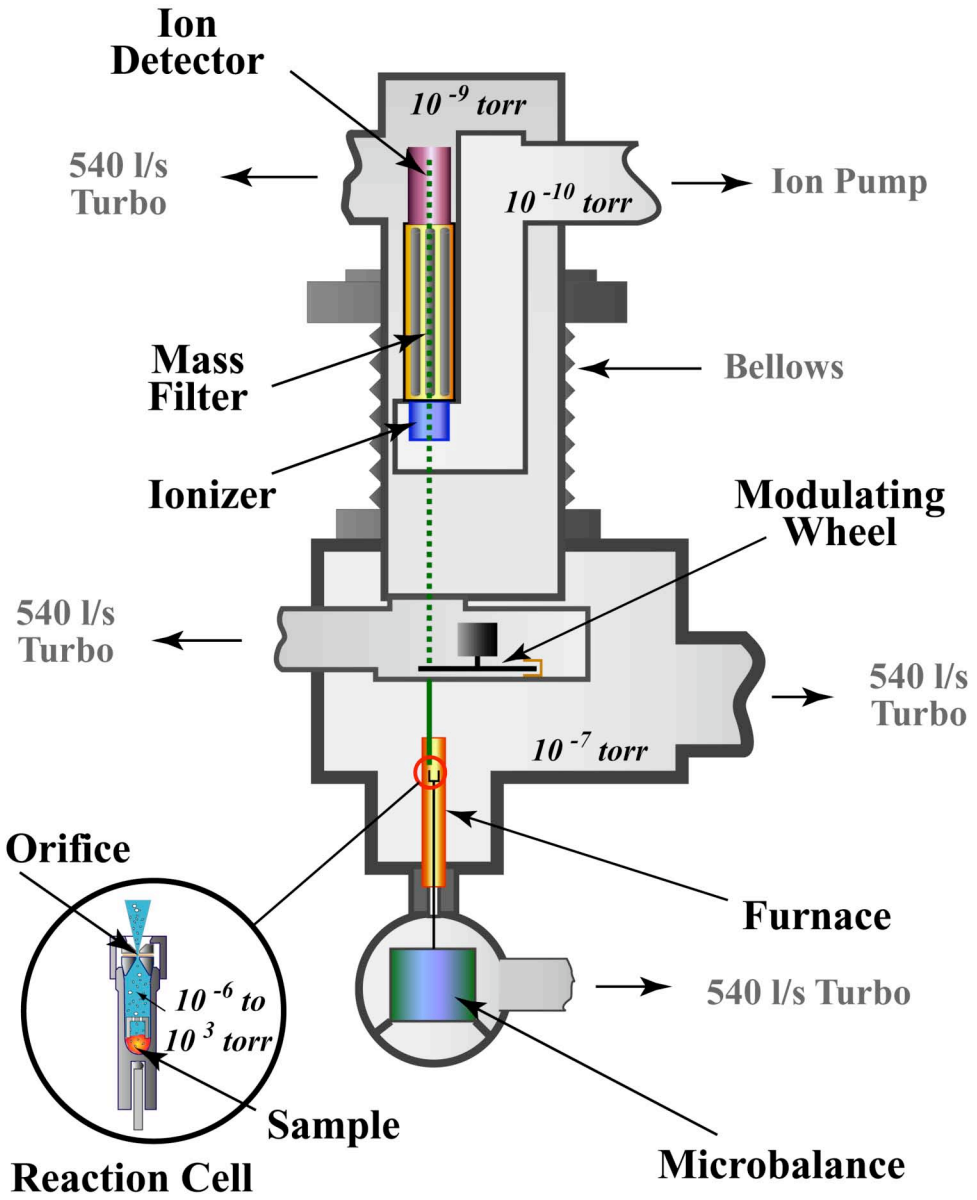

Figure 2. Schematic of STMBMS instrument. An experiment is conducted with the STMBMS instrument by placing the sample in the reaction cell, closing the reaction cell with a cover containing an orifice of desired diameter, mounting the reaction cell in the instrument on top of the thermocouple probe that is seated in a microbalance, and then evacuating the instrument. The data is collected by heating the sample and collecting data on the rate of force change due to gas exiting the cell with the microbalance and collecting the mass spectra of the mixture of gaseous compounds exiting the cell with a modulated beam quadrupole mass spectrometer. The pressure of the gaseous compounds in the reaction cell may range from 10^{-6} to 10^{3} torr, depending on experimental conditions.

Enhanced Product identification and molecular structure determination.

Three methods are used to help identify the compounds that evolve from the reactive processes. Two of these provide additional information to assign formulas to the ions that make up the mass spectra of the evolving compounds. The third method sorts ion signals into groups of m/z values that are associated with each compound.

In the first method, isotopically labeled analogues of the energetic materials are synthesized (deuterium, ^{13}C, ^{15}N, and ^{18}O) and the corresponding isotopic shifts, recorded in the STMBMS experiments, are used to determine the formulas of the ions. In the second method, high resolution and high mass accuracy measurements are made using a Fourier Transform Ion Cyclotron Resonance (FTICR) mass spectrometer. These two methods provide the information needed to determine the formulas of the ions in the mass spectra. The FTICR mass spectrometer provides a more rapid means of determining the formulas, eliminating the need to synthesize isotopically labeled analogues.

The third method employs a correlation analysis of the temporal dependence of the ion signals in the mass spectra to sort the ion signals into groups whose m/z values represent the mass spectra of the individual compounds that evolve from the reaction cell.

Quantitation of the data.

After the compounds are identified and ion signals from the mass spectra are assigned to represent each compound, the data are quantitated using the TASHOW analysis algorithm. The ion signals, measured with the mass spectrometer, and the rate of force change, measured with the microbalance, are used to determine the sensitivity parameters that relate the measured ion signals to the number density of the corresponding compound in the reaction cell as a function of time.[7, 9] This analysis may be used to calculate rates of reaction, partial pressures, and other related properties. At this point in the analysis, the following information is available to construct a qualitative model of the decomposition process:

1. Identities of the compounds involved in the decomposition process
2. Rates of formation of the compounds
3. Pressure of gases in the reaction cell
4. Vapor pressure of condensed phase compounds
5. All data as a function of time.

Morphological features.

Morphological features of the condensed-phase samples: surface roughness, grain structure, bubbles can play an important role in the decomposition process. Because these features cannot be examined *in situ* during the course of a decomposition experiment, the morphological characteristics are determined by stopping the reaction at various stages of the decomposition process and removing the

sample for examination by optical microscopy and scanning-electron microscopy (SEM).

Some energetic materials form products that are nonstoichiometric, polymeric-like and have a low volatility; these are called nonvolatile residue (NVR). In many cases the NVR reacts with the remaining reactant or other decomposition products. Optical and SEM examination has shown that these NVRs may be located on the surface of particles, in reactive regions within solid grains, or on the walls of the reaction cell. Knowing the geometrical characteristics of these morphological features is often important for understanding and modeling the reactive process.

While optical and SEM pictures provide valuable information about the structures created during the decomposition process, they do not provide information about the chemical compounds that are involved in the reactions at these localized regions. To improve our understanding of the role that interactions between chemical reactions and morphological features play in the decomposition process, we must probe the nature of the chemical reactions that occur at the boundaries of these morphological features. We are developing surface analysis methods such as secondary ion mass spectrometry (SIMS) and laser desorption mass spectrometry (LDMS) to examine these features in energetic materials.[10]

2. DEVELOPMENT OF MATHEMATICAL MODELS. Once a qualitative understanding of the underlying processes that control the thermal decomposition of an energetic material is obtained, the next task is to formulate this understanding into a set of mathematical expressions to characterize the thermal decomposition process. This task requires using the qualitative model of the decomposition process to construct the set of differential equations that represents the reaction rates of the underlying reactive processes, then solving this set of differential equations, and finally, determining the values of the parameters for the reaction model by comparing the results of the calculations to experimental data.

   This method is basically a numerical simulation method in which a reaction scheme is postulated, a mathematical representation of the reaction scheme is constructed, a guess for the reaction parameters in the model is made, and the model is solved. The model simulates a decomposition experiment. The reaction scheme and its associated parameters are iterated to capture the various features of the reactions that appear in the data from the thermal decomposition experiments. Further details are provided below.

D. Comparison of Conventional Thermal Decomposition Experiments

So far we have 1.) summarized the scientific issues that must be addressed to understand the underlying reactive processes of energetic materials in the condensed phase, 2.) outlined the experimental challenges that must be addressed and described the development of one experimental protocol intended to meet these experimental challenges. Later in this chapter, I will show how this work has led to new understanding of reactions in the condensed phase. While this experimental protocol provides new opportunities to understand the underlying reactive processes in energetic materials, it is relatively expensive and unique. The highly specialized equipment is not as accessible as

the other methods previously used to examine the thermal decomposition of energetic materials in the condensed phase. In this section we provide a brief summary of the other methods and assess their strengths and weaknesses in meeting the experimental challenges for studying the thermal decomposition of energetic materials.

Thermal decomposition experiments have been used extensively to probe the reactions of energetic materials. In general the various experimental methods may be grouped according to the type of data provided. One group focuses on measuring the overall behavior of a sample by measuring a global property, such as heat flow or mass loss. The second group focuses on identifying the products formed during a decomposition experiment.

1. GLOBAL MEASUREMENTS.

Standard thermal analysis methods such as thermogravimetric analysis (TGA), differential thermal analysis (DTA) and differential scanning calorimetry (DSC) have been used extensively to characterize the thermal behavior of energetic materials in the condensed phase.[11-14] The DTA and DSC methods track the heat flow as a sample is heated and are useful for detecting phase changes and the onset of decomposition of an energetic material. TGA measures the mass of the sample as it is heated and reveals when reactions occur that release gaseous decomposition products and result in a loss of sample mass.

Thermal analysis methods are excellent for characterizing the behavior of simple, well-defined processes such as phase transitions or simple chemical transformations. However, for complex processes, such as those that occur during the decomposition of energetic materials, thermal analysis methods do not provide sufficient information to unravel the underlying processes as discussed by Pinhiero *et al.* The global nature of the measurement (*i.e.*, total heat flow or total mass loss) is determined by the summation of all the underlying processes at any particular time during an experiment, providing a limited amount of information on the underlying processes.

The thermal behavior of propellants and explosives has also been characterized by time to explosion experiments. In these experiments, such as the one-dimensional time to explosion (ODTX) experiment,[15] a sample is heated using a predefined isothermal boundary condition, and the time until the sample explodes is recorded. This has provided useful information for handling explosives, but, due to the limited amount of information collected during an experiment, this method has been of limited value in determining the underlying reactive processes that occur during the thermal decomposition process.

2. PRODUCT IDENTIFICATION MEASUREMENTS.

To complement the global experiments and provide insight into the reactive processes that occur during the decomposition of energetic materials, a number of different types of spectroscopic methods have been used over the years. Some methods, such as mass spectrometry, have identified a broad range of different compounds formed during the decomposition process; other methods, such as electron spin resonance,[16, 17] have identified a more limited range of species, such as radicals.

Infrared spectroscopy(IR) and mass spectrometry (MS) have been used extensively to identify products formed during the decomposition of energetic materials. MS has been used to identify the gaseous products that evolve during the decomposition process, while IR has mostly been used to probe the products formed in the condensed phase. IR spectroscopy can be applied over a wide range of experimental conditions: high-pressure,[18,19] in thin films, [20, 21]during combustion,[22-24] in shocked materials,[25] and at very low temperatures.[26, 27]

Depending on the specific experiment, IR may provide information ranging from individual steps in a decomposition reaction,[28] to a more detailed set of reaction kinetics.[19] While this information is often useful, the extent of the data is somewhat limited, making it difficult to develop complete reaction schemes and the associated reaction kinetics from the data. For applications to experiments focused on understanding the underlying reactive processes in the condensed phase at low and moderate temperatures, IR lacks some of the molecular specificity provided by mass spectrometry-based methods.

Mass spectrometry measurements were some of the first experiments to identify the products formed in the thermal decomposition of energetic materials.[29-31] Analyzing gaseous thermal decomposition products with mass spectrometry can be done by either admitting the gas mixture directly into the mass spectrometer or by first chromatographically separating the mixture before introducing the gas into the mass spectrometer.

Both methods have limitations. If the mixture of the reactant and its decomposition products is admitted into the mass spectrometer, it is difficult to associate individual ions with the corresponding decomposition products. For example, it has been shown[8] that using appearance potential measurements developed to examine hydrocarbons[32] is not adequate to distinguish ions that originate from products formed in the thermal decomposition of HMX from ions formed by the fragmentation of sublimed HMX in the mass spectrometer. HMX fragments into daughter ions using electron energies of 12.5 eV (~ 3 eV above its estimated appearance potential).[8, 33]

If the mixture is chromatographically separated prior to entering the mass spectrometer, it is difficult to obtain time-dependent information to characterize the behavior of the sample. The sensitivity of the mass spectrometer varies for different species, which also makes it difficult to obtain quantitative data.

Finally, depending on the type of mass spectrometer used for the measurements, there can be uncertainty in the identification of ions because of uncertainties in the exact mass of the ion: N_2O= 44.0083 and CO_2=43.9898 would both be measured as m/z= 44 with most types of mass spectrometers, making the two compounds indistinguishable.

Mass spectrometry provides useful information for identifying products, but may not clearly identify the thermal decomposition products.

III. CONDENSED-PHASE REACTIVE PROCESSES

A. Evidence for Complex Processes

In examining the decomposition of energetic materials, one may ask, what evidence suggests that their decomposition is controlled by a complex set of coupled reactive processes. The answer may be found in the general features of experimental results from two sources: a historical examination of the results from a wide range of different experiments and the results from STMBMS experiments on a number of different compounds.

During the 1980s, Schroeder undertook an extensive examination of the entire literature on the thermal decomposition of energetic nitramine compounds.[34-36] This review of the wide range of results from both nominally similar and different types of experiments revealed a high degree of variation in the results. For example, in some decomposition experiments with RDX and HMX the major products were CH_2O and N_2O. In other types of experiments, HCN and NO_2 were the major products. Similarly, an accelerating type of "autocatalytic" behavior was reported in some cases but not in others.

To describe the reactive processes in these older experiments, a unimolecular decomposition framework was used, and the experimental observations were attributed to a particular bond-breaking sequence of the reactant. For example, in experiments in which HCN and NO_2 were observed, it was argued that N-NO_2 bond fission was the rate-limiting step; whereas in experiments in which CH_2O and N_2O was observed, it was argued that fission of a C-N bond in the ring of the molecule was the rate limiting step. These arguments also assumed that once the first bond in the molecule ruptured, the remaining bonds would rearrange rapidly and lead to the final reaction products. Additionally, in many experiments the temperature dependence of the experimental observable (*i.e.*, weight loss, heat generation) was determined and reported as an activation energy, assuming that an Arrhenius expression described the underlying reaction. Schroeder reported[36] that the activation energies from these experiments varied widely.

This variation in activation energies is not surprising if the decomposition process is controlled by an underlying set of coupled nonlinear reactive processes. For these types of processes, even slight variations in experimental conditions (*e.g.*, the extent of confinement of gaseous decomposition products with the sample) can lead to variations in the identities of the products, as well as how fast the products are formed. This complex behavior was examined in the early 1970's by Batten for the case of RDX decomposition,[37-41] in which it was found that the decomposition of RDX below its melting point was controlled by a complex autocatalytic-like process. The results showed that a nonvolatile residue is formed during the decomposition and the addition of gases such as CH_2O increase the reaction rate. Batten also demonstrated that the past decomposition history of the sample can affect the subsequent decomposition processes.

Our STMBMS experiments performed on a range of different types of energetic materials provide more detailed evidence for the complex nature of the thermal decomposition process. The compounds that we have investigated using STMBMS are listed in Table I.

We have studied the nitramines, RDX and HMX, most extensively. The thermal decomposition of all these compounds exhibits two common features, which show that their thermal decomposition is controlled by a complex set of coupled reactions.

Table I. Compounds studied with STMBMS methods.

Nitramines		C-Nitro, azoles, and others	
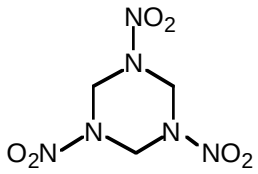 RDX	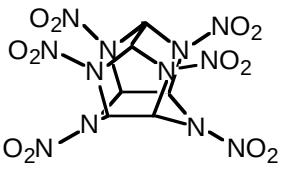 CL-20	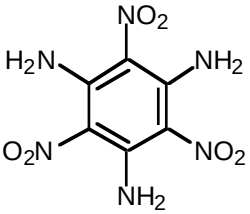 TATB	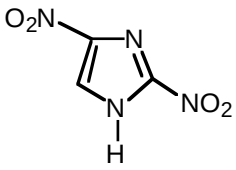 24DNI
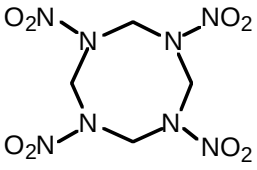 HMX	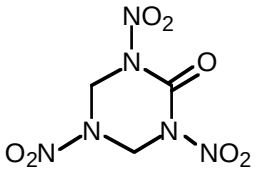 K6	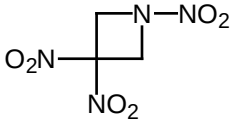 TNAZ	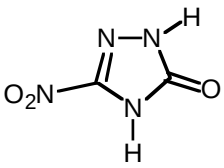 NTO
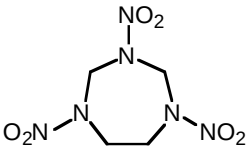 TNCHP	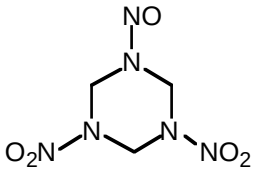 ONDNTA	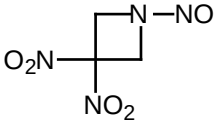 NDNAZ	Ammonium perchlorate,

First the temporal behaviors of the rate of evolution of the gaseous decomposition products are never what is expected for a simple first order decomposition reaction, in which the rate of reaction falls as the sample is depleted. Indeed, for most of the compounds listed in Table I, there is an induction period, characterized by low rates of evolution of gaseous products, followed by an accelerating rate of reaction. In addition, the identities of the products and their rates of evolution are very sensitive to the extent of confinement of gaseous decomposition products in the reaction environment; higher pressures typically increase the rate of reaction. Second, a nonvolatile residue is always created during the decomposition process. Its presence is usually associated with higher rates of reaction. These two general features clearly indicate that the thermal decomposition behavior of these materials in the condensed phase is controlled by a set of complex nonlinear reactive processes.

B. HMX decomposition processes.

The decomposition of HMX provides a good example of the types of processes that occur in the condensed phase. An illustration of the features that are observed using the experimental protocol, outlined above, is shown in Figure 3. The temporal behavior of the rates of formation of two of the main decomposition products (CH_2O and N_2O) indicates a complex process and is completely different from the exponential decay that is expected for a simple first order reaction. Their behavior is more indicative of a nucleation and growth reaction or what is commonly referred to as an "autocatalytic" reaction.

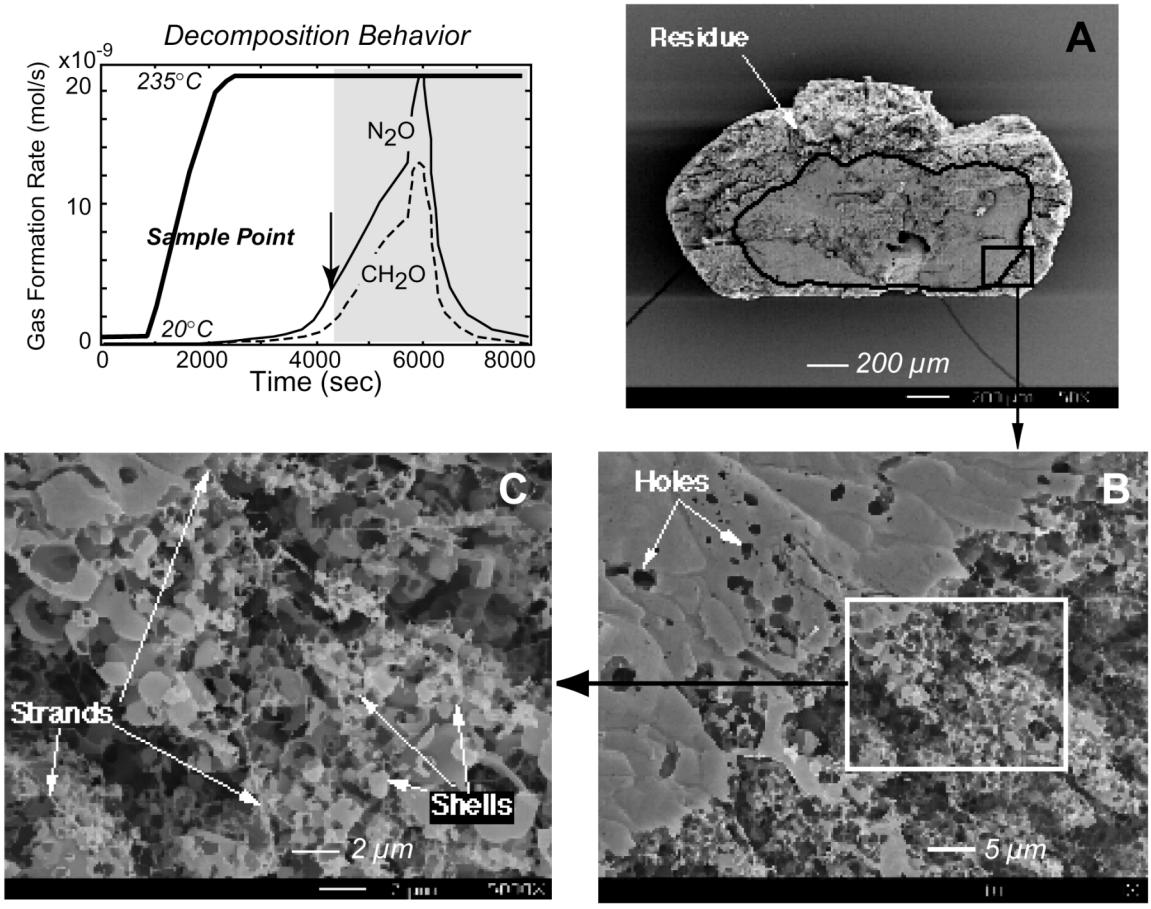

Figure 3. Illustration of the gas evolution rates and the morphological structures created during the thermal decomposition of an HMX particle. The graph shows the rate of evolution of two products formed during the decomposition of a single particle of HMX that was heated to and held at 235°C. To examine the morphological structures that are created during the decomposition, the reaction was stopped at the "sample point". To expose the morphological structures that grow within the particle, about half of the HMX remaining after decomposition was stopped is removed by sublimation. The particle was cut in half to expose the interior of the particle for SEM analysis. Pictures A through C show increasing magnifications of the particle interior. In picture B the material in the upper left portion of the picture is the HMX that remains in the particle (note the granular structure). The lower right portion shows the structures of nonvolatile residue that is formed via reactions within the HMX grains. Picture C shows that the NVR forms both strands and shell-like structures.

The temporal behaviors of the rates of evolution of the products can be divided into three stages: an induction period, an acceleratory period, and a late stage (2000 to 3800s, 3800 to 5800s, and 5800 to 7000s, respectively in Figure 3). The identities of the products and the temporal behaviors of their rates of formation provide information that can be used to guide the development of models of the reactive processes that control decomposition.

The SEM pictures in Figure 3 illustrate how spatial features can play an important role in controlling the decomposition process. The micron-size shell-like structures formed during the decomposition of HMX in the solid phase are remnants from reactive regions that were formed during the decomposition process. Localized decomposition within these regions suggests that several types of spatially dependent processes may play a role in the overall reactive process.

The rate of transport of products within the condensed phases can play an important role in controlling the rates of reaction. For example, in the localized micron-size reaction regions in solid HMX, which appear to be bubbles contained within the solid HMX, the gaseous decomposition products from the bubble may diffuse into the surrounding lattice. As a result, this process may control the reaction rate by transforming crystalline HMX into a molten solution in which the HMX may react more rapidly.

The SEM pictures of HMX also illustrate the role that interfacial boundaries may play in controlling the decomposition process. New surfaces are created at interfacial boundaries within the HMX particle. Initially, a grain structure is created within the particle (upper left of Picture B), which forms a new reaction environment on the surface of the grains. As the decomposition progresses, another type of reaction environment is created at the interfacial boundaries in the micron-size reaction regions, associated with the formation of bubbles within the grains. The formation of strands of NVR (Picture C) appear to be associated with reactions that occur at the grain boundaries, whereas the shell-like structures appear to be associated with the formation of bubbles within the grains.

Both the development of the morphological features associated with the creation of interfacial boundaries and the transport of reactants and products in the vicinity of these boundaries illustrate the important role that spatial features can play in controlling the underlying nature of the reactive processes and the rates at which these processes occur.

Isotopic scrambling experiments and deuterium kinetic isotope effects (DKIE) using isotopically labeled analogues of HMX[42] and RDX[43] have provided further information on the sequence of bond-breaking steps that occur in the various reaction channels during the decomposition process. This provides further evidence of the complex nature of the decomposition process.

1. GENERAL NATURE OF CONDENSED-PHASE REACTIONS IN ENERGETIC MATERIALS.

   The experimental protocol developed to investigate the decomposition of energetic materials in the condensed phase has been applied to examine a relatively wide range

of different types of energetic compounds, which are listed in Table I. Data with the level of detail shown above for HMX has been collected on most of these compounds.

All of the compounds listed in Table I exhibit complex nonlinear reaction behavior. The degree of complexity varies from compound to compound. The most complex processes are observed in HMX[14, 42, 44, 45] and AP.[46-48] The decomposition of both materials involve tightly coupled interactions between the chemical reactions and the spatial aspects of the morphological features created in the particles during the thermal decomposition process. The least complex processes are observed in the decomposition of K6 and TNCHP.[49, 50] The presence of the keto group in K6 appears to promote a more direct reaction to the gaseous decomposition products.

Decomposition of TNCHP has a number of similarities to the decomposition of RDX and HMX in terms of the chemical reactions involved, but is not complicated by morphological issues associated with the solid phase, since it melts at approximately 170°C and is relatively stable in the liquid phase. The complexity of the decomposition process for the other compounds falls somewhere in between these two groups.

Types of Processes that control decomposition in the condensed phase

Examination of the data from experiments with the compounds listed in Table I show that a wide range of processes can be a factor in the decomposition process. The types of processes that may contribute to the overall decomposition behavior include the following:

1. Phase changes. Solid-solid, melting, and vaporization all may play a role in controlling the rate of decomposition.
2. First order reactions. The direct reaction to the gaseous decomposition products can play a role, but it is unlikely to be the sole reaction pathway in the condensed phase.
3. Formation of solutions. Mixtures of the reactant with its decomposition products may occur in either the solid or liquid phase, creating solutions of the components.
4. Reactions of parent compounds with decomposition products. These appear to be the main rate-limiting reactions for decomposition in the condensed phase.
5. Secondary reactions of products. All of the decomposition processes involve secondary reactions of the products. For nitramines, the creation and decomposition of the mononitroso analogue of the reactant appears to play an important role in their decomposition.
6. Nucleation and growth of bubbles. For compounds that remain solid at higher temperatures, such as HMX, AP, and TATB, the nucleation and growth of reaction regions within the solid, which forms microscopic bubbles, can be very important in controlling the decomposition process.

7. Reactions on surfaces and interfacial boundaries. Several compounds that remain solid at relatively high temperatures (> 170°C) react on the surface of the particles by nucleating and growing an NVR on the surface of the particles. This behavior has been observed for 24DNI[51, 52] and RDX.[53, 54]
8. Formation and growth of new morphological structures. For compounds that remain solid at higher temperatures, such as HMX, AP, and TATB, the growth of new morphological features creates dissipative structures that play a role in controlling the rates of reaction.

The relative importance of these different processes depends on the intrinsic properties of the energetic compound and raises an interesting question: How do the molecular structure, crystal structure, and morphological characteristics of these materials determine which types of reactive processes will play a role in the overall decomposition process?

Spatial dimensions of reactivity

Is it possible that the physicochemical properties of the material may determine spatial dimensions of reactivity? The development of spatiotemporal structures is associated with some of the underlying decomposition processes in an energetic material. The spatial structures may be characterized by cellular units: volumes of material in which a physicochemical reactive process occurs within the volume and is controlled by a combination of chemical reactions, transport of species within the volume, and the development and growth of interfacial boundaries. This concept is similar to a unit cell used to represent crystal structure or a grain structure in a metal, except the volume contains a reactive system on a microscopic scale. This concept is also similar to nucleation and growth concepts used to describe solid-state reaction chemistry of inorganic compounds.[55]

Using this concept of a reactive unit-cell, it may be possible to characterize and categorize the underlying reactive processes in an energetic material with a set of reactive cellular units with several different discrete and representative dimensions. For example, for HMX there may be one cellular unit to represent the reactions in bubbles and another to represent reactions at grain boundaries, essentially forming a hierarchy of cellular subunits.

Within this framework, a reactive unit-cell may be defined as a volume of material that contains a reactive system with self-contained chemical, physical and morphological features. Thus, characterizing the reactions in a reactive unit-cell can be used to describe the overall behavior of any size sample, assuming appropriate heat-and mass-transfer processes can be properly characterized.

2. DECOMPOSITION OF COMPOSITE MATERIALS.

Up to this point, discussion has focused on reactive processes in energetic compounds, however, the same general ideas can be applied to the reactions of composite energetic materials such as propellants and explosives. In this case, the chemical nature of the reactants, the morphological structure of the material, and interfacial boundaries are determined by the material design and manufacturing processes. For example, a binder or plasticizer that may be included with the

energetic compound will: 1.) Create new boundaries between the binder and energetic compounds, and 2.) Create potential interactions between the plasticizer and its decomposition products with the energetic compound or the binder. Understanding these processes requires the same type of information that is required for the individual energetic compounds. Hence the framework developed to examine and characterize energetic compounds may be used to characterize more complex propellants and explosives, which are composite materials with a cellular structure.

C. Characterization of Decomposition Processes: RDX and HMX case

1. DEVELOPMENT OF A CONCEPTUAL FRAMEWORK TO REPRESENT AND ANALYZE DECOMPOSITION PROCESSES.

Characterization of the complex processes that control the thermal decomposition of energetic materials requires a framework on which to build and test new concepts. Historically, a basic concept has been used to represent, analyze, and understand the experimental observations from thermal decomposition experiments. This concept may be expressed as "the harder you drive something the more likely it will happen." This concept was formulated into a model to characterize chemical reactions by Arrhenius,[56] in which the amount of energy available drives a chemical reaction.

We have established a new framework to integrate the data derived from high information content experiments with concepts derived from everyday, anecdotal, and scientific experience. The framework consists of a suite of concepts that are built on parallel representations of two types of natural phenomena. The resulting framework is designed to achieve two main objectives:

1. Develop an understanding of the underlying processes
2. Form the basis for predicting the behavior of the decomposition processes over a range of physical conditions

The suite of concepts borrows from two widely used models: Darwinian evolution of biological systems and physicochemical control of high-temperature combustion. While both models characterize complex reactive systems, they are quite different, focusing on substantially different phenomena, but providing complementary means to represent and analyze thermal decomposition processes.

The Darwinian evolution model provides a means to represent sets of interacting processes, which are not necessarily elementary reactions, and analyze how these processes compete and spawn new processes over a range of controllable environmental conditions.

In contrast, the high-temperature combustion model provides a framework to represent the physical processes and chemical reactivity at a more fundamental level, associated with elementary processes, and creates mathematical representations of the underlying behaviors.

A conceptual framework being developed to represent, analyze, and understand the decomposition of energetic materials draws from general features of the models for both metabolic pathways and high-temperature combustion. The general

Darwinian approach used to characterize metabolic pathways forms the basis for describing the general competitive nature of the reactions that occur in the condensed phase of energetic compounds at low and moderate temperatures. Once the general nature of the underlying reactive processes is determined, physical and mathematical features, similar to those used in the high-temperature combustion model, are applied to further test the original reaction concepts and to develop a deeper understanding of the reactions.

Many details of this conceptual framework are still under development. However, in the course of its development, the underlying concepts have been used to represent and analyze the decomposition of four energetic compounds: 24DNI, NDNAZ, RDX, and HMX. The use of the conceptual framework is illustrated with a discussion of the decomposition of the cyclic nitramines: RDX and HMX.

3. REACTION PATHWAYS: SOLID-PHASE REACTIONS, NONLINEAR PROCESSES, FEEDBACK LOOPS AND AUTOCATALYSIS.

The Darwinian model has been used to construct a qualitative depiction of the competing processes that control the thermal decomposition of RDX and HMX over a range of conditions. It is based on data collected using the mass spectrometric experimental protocol and is illustrated in Figure 4. The competing reaction pathways are gleaned from the analysis of extensive sets of experimental data on the decomposition of RDX[43, 53, 54, 57, 58] and HMX[42, 44, 45] in the condensed phases. Typical data for HMX is shown in Figure 3.

The representation of the decomposition process for RDX/HMX, shown in Figure 4, describes the general set of reactions and interconnections between the main reaction pathways. It also contains a set of pressure and temperature scales, whose purpose is described below.

Illustrations of how the reactive processes were gleaned from the data have been described previously[53] for several of the pathways.

The reactants are listed in the upper left corner. The products detected using the experimental protocol are listed in the two boxes. The species that are denoted as "Exit Products" are compounds that have been involved in the reactive processes within the reaction environment, but eventually leave the reaction environment and are detected without undergoing further reaction. Several of these products (*i.e.*, H_2O, CO, N_2O) are considered nonreactive under the conditions of the experiment, whereas the others can continue to react. The amount of each reactive species observed depends on the competition between the various reaction pathways that dominate under different sets of reaction conditions.

The species listed as "minor products" are also formed in reactive processes, but represent only a small fraction of the total amount of products formed during decomposition. While only minor species, these compounds provide valuable insight into the nature of the underlying processes, since their time-dependent rates of formation track the various underlying behaviors, such as the decomposition of the NVR.

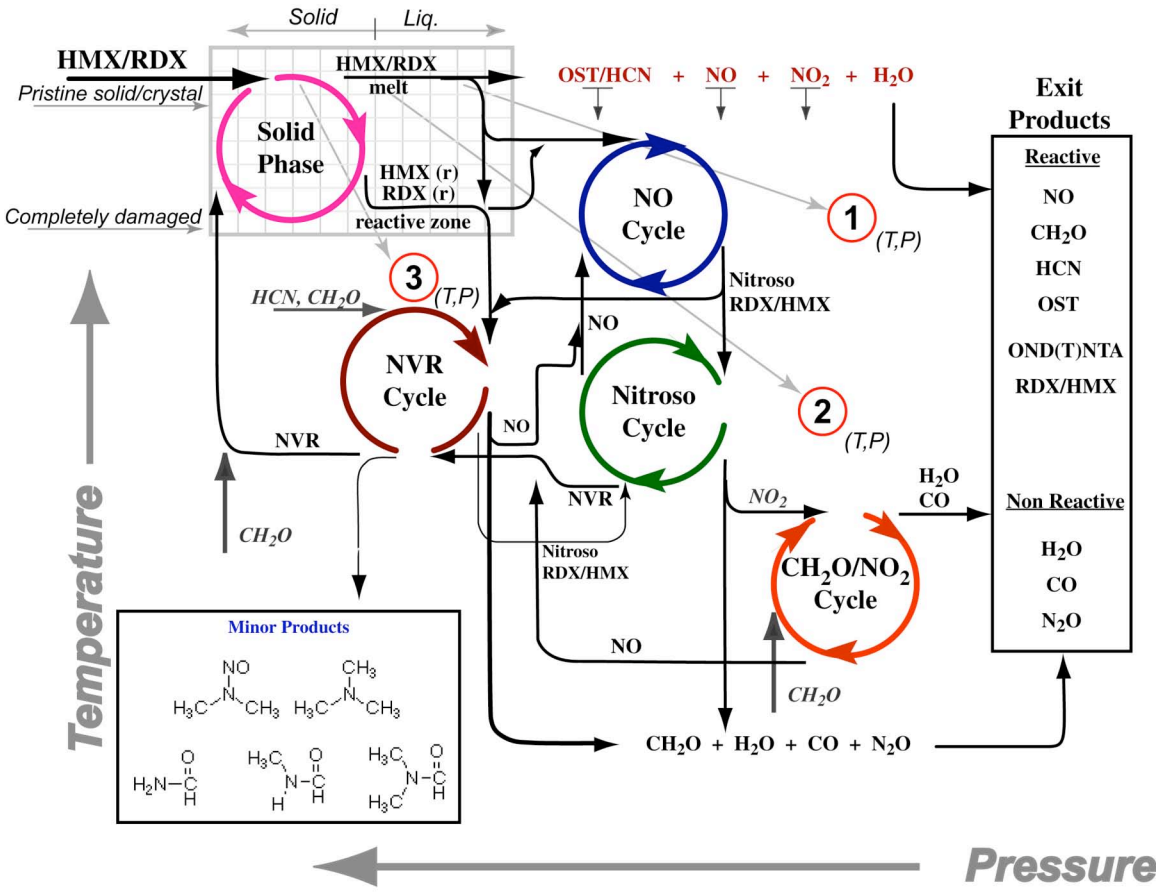

Figure 4. Reaction diagram showing the underlying reactive processes that control the decomposition of HMX and RDX.

The reaction at the top of the diagram represents a relatively direct reaction pathway between the reactants and exit products. This reaction represents the elimination of HONO from the RDX or HMX to form oxy-s-triazine in the case of RDX, and the subsequent reaction of these products to HCN, NO, NO_2 and H_2O. This reaction is first order in the amount of reactant, and is the only pathway whose reaction rate is consistent with a unimolecular decomposition process. The bond-breaking sequence of this reaction has been determined via DKIE and isotope scrambling experiments.[43]

The five circles shown in the reaction diagram represent the main nonlinear reactive processes that occur in RDX and HMX. These reactions are described as cycles, as is done for biochemical pathways, in order to track and illustrate how the different reaction pathways are interrelated. The arrows connecting the different reaction cycles show how various compounds move between the different reaction cycles. This movement of compounds between reaction cycles also illustrates the coupling and extent of nonlinearity that occurs during decomposition.

The five reaction cycles can be divided into two groups with similar features. One group represents chemical reactions at the molecular level. The second group

represents complex physicochemical processes involving multiple phases, reactions at interfacial boundaries, and emergent phenomena.

The three reaction cycles representing the chemical reactions play a major role in the decomposition of RDX and HMX in the molten or liquid phase. The chemical reaction cycles include the NO Cycle, the Nitroso Cycle and the CH_2O/NO_2 Cycle.

The NO Cycle involves the reaction of NO with RDX or HMX to form the mononitroso analogue of these compounds. Isotope scrambling experiments[43] have shown that this is the primary reaction leading to the formation of hexahydro-1-nitroso-3,5-dinitro-s-triazine (ONDNTA) from RDX in the liquid phase. NO can originate from several different sources. For example, during the decomposition of RDX in the liquid phase, NO produced by the direct reaction (OST/HCN) provides the initial source of NO to form ONDNTA. Note that, as the DKIE lowers the rate of the direct reaction, the rates of the NO Cycle and Nitroso Cycle may also be reduced if the direct reaction is the primary source of NO.

The Nitroso Cycle is more complex. The mononitroso analogues of RDX and HMX may be formed initially by reacting with NO. Once formed, the decomposition of the mononitroso analogue can itself be quite complex. Thermal decomposition studies of ONDNTA[59, 60] have shown that N_2O, H_2O, and CH_2O are the major products formed during its decomposition. However, a large portion of each ONDNTA molecule is incorporated into the nonvolatile residue.

Once the NVR is present, a new pathway leading to the formation of the mononitroso analogue is created. In this case, the isotope-scrambling experiments indicate that the reaction involves the removal of an oxygen atom from the NO_2 group, rather than the replacement of the NO_2 groups with NO, since there is no scrambling in the N-NO bond.

The CH_2O/NO_2 Cycle is a facile reaction that involves reactants formed from different reaction pathways and results in the generation of a substantial amount of heat (ΔH = -185 kJ/mol). This type of behavior shows how the extent of self-heating of the sample may be influenced by the relative rates of the different reaction cycles since separate reaction cycles produce the CH_2O and NO_2 reactants in this heat-generating cycle.

The two remaining cycles represent complex physicochemical processes, play a major role in solid-phase decomposition, and are responsible for morphological damage created in the material that can lead to sensitized explosives and propellants.

The NVR Cycle is characterized by the creation of an amorphous higher molecular weight material that has a low volatility. Infrared spectra and thermal decomposition of the NVR indicate it has amide and cyano groups. The NVR is formed during the decomposition of HMX, RDX, and ONDNTA. In each case, the same minor products, shown in the box, are either associated with its formation or decomposition.

The location in the sample where the NVR is formed differs for ONDNTA, RDX, and HMX. ONDNTA becomes molten at relatively low temperatures (125°C to 165°C, depending on experimental conditions), and the NVR is formed in the molten mass of the sample. In contrast, the NVR nucleates and grows on the surface of the

RDX particles when the sample is maintained below the melting point of RDX (~ 170° to 190°C). In these experiments, it is clear that the rate-controlling reaction involves the interaction between the NVR and the RDX at the surface of the RDX particle.[58]

Formation of the NVR during the decomposition of HMX occurs in micron-size reaction centers, which are distributed homogenously throughout an HMX particle (the strand and shell-like structures shown in Figure 3). In HMX, formation of the NVR may involve the reaction of HCN with CH_2O under high-pressure conditions, since both of these compounds are observed at lower rates when the sample remains solid compared to when the sample is allowed to liquefy. Given the range of physical conditions under which the NVR is formed in these three compounds, it is remarkable that the reaction products associated with its formation are the same in each case. This again emphasizes the nonlinear and cyclic nature of the processes involved in the formation and decomposition of the NVR.

The Solid-phase Cycle is the most complex of the five cycles. The processes involved in the Solid-phase Cycle are quite different, depending on whether the reactant is RDX or HMX.

In RDX, the surface of the particles appears to roughen and undergo a morphological change. This is accompanied by the formation of the "reddish" NVR on the surface of the particle. Once the NVR is formed on the surface of the RDX particle, the rate of reaction accelerates, leading to an increase in the amount of NVR and the continued acceleration of the reaction rate.

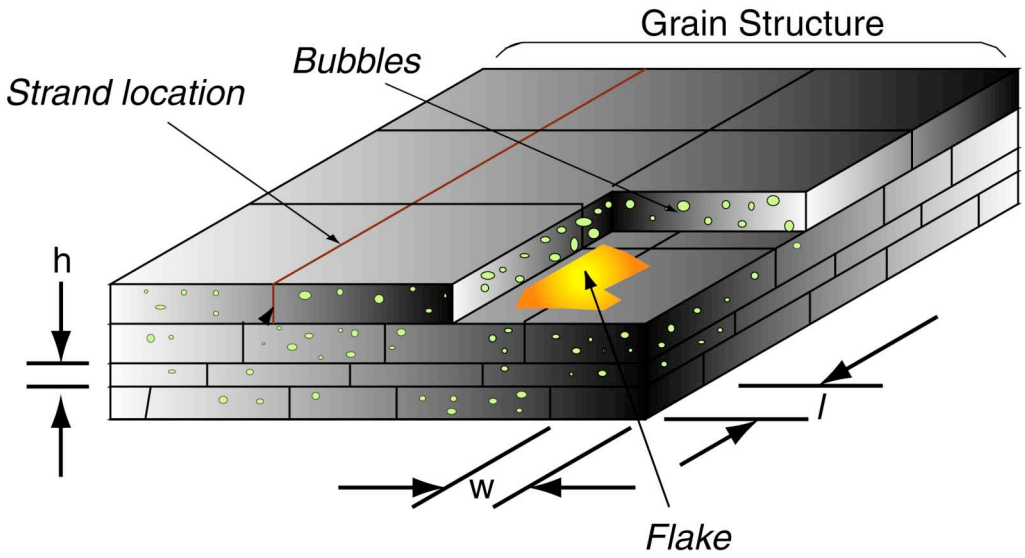

Figure 5. Illustration of the morphological features created in an HMX particle during the thermal decomposition process.

In HMX, the solid-phase processes are more complex, creating a set of morphological features as illustrated in Figure 5. HMX first undergoes the β --> δ phase transition, which creates a granular structure within the particles. This is followed by the nucleation and growth of reaction centers within the grains of HMX.

The gaseous products formed in the reaction centers create bubbles, which grow in size as the reaction progresses. The smallest dimension of the HMX grains limits their maximum size, since the gas is released from the bubbles as they intersect the grain boundaries. The high-pressure conditions within the bubbles appear to favor the formation of the NVR within the bubbles as the bubbles grow. The NVR remains behind as a remnant of the reactions that have occurred within the bubble. Once a substantial amount of decomposition has occurred (~ 30%), the particle becomes relatively porous, allowing HMX and its decomposition products to flow within the porous structure and interact with the sample surfaces during the later stages of the decomposition process, forming flakes of NVR in the intergranular regions. What is especially intriguing about the processes involved in the Solid-phase Cycle is that there is no *a priori* way to anticipate their emergence from the properties of either RDX or HMX.

4. EMERGENT PHENOMENA.

The concept of emergence has been developed to describe the behaviors of complex systems and may be defined as a set of interacting components whose collective behaviors cannot be predicted from the behavior of the individual parts.[61] In examining the decomposition behavior of energetic compounds, we are confronted with similar issues. For example, can the behaviors that emerge on a larger spatial scale during the decomposition process of HMX be predicted from its underlying physical and chemical properties? If so, how?

At this point, we do not have the answers to these questions. However, further examination of these systems may provide new insights into how basic chemical reactions and physical phenomena may be coupled to create systems that exhibit new and independent behaviors.

From the chemical point of view, energetic materials are comprised of carbon, hydrogen, nitrogen and oxygen. From the physical point of view, energetic compounds are relatively easy to characterize. Their molecular crystal structures are readily measured and known. Calculations on the energetics and dynamics of their reactions at the molecular level have been made,[62-64] and calculation of their interactions at larger spatial scales are now possible[65, 66] Thus, the main question becomes how do we determine the rules that control the evolution of these systems in time?

D. Effects of Experimental Conditions on Observed Decomposition Processes

The complex physicochemical thermal decomposition reaction network, described above for HMX and RDX, can be used to understand the rules that control the competition between the various reaction pathways. This, in turn, will provide insight into the apparent discrepancies observed in experiments conducted using different experimental techniques. The reaction network can be interpreted as a diagram that illustrates the set of possible reaction channels by which a sample of HMX or RDX may decompose during an experiment. The entire set of channels is active for any given decomposition experiment; however, what is observed for a particular experiment is

simply the subset of reaction channels that successfully compete and dominate the reactive process under a given set of experimental conditions. The most successful pathways will consume the RDX/HMX the fastest.

1. REACTION-COORDINATE VECTORS.

To provide a framework to represent and discuss the details of the reactive process, we introduce the concept of a reaction-coordinate vector. The reaction-coordinate vector represents the progress of a reaction through a set of conditions defined by an experiment. Graphically, a vector joining two points on the reaction network represents the reaction-coordinate vector. Thus, the dominant rate-limiting steps encountered, and therefore measured, by an experiment conducted under a specific set of conditions, will correspond to the reaction cycles and coupling pathways directly intersected by the reaction-coordinate vector. Reaction cycles not intersected by the vector will play only a minor role under the given conditions; the extent of contribution decreases for reaction cycles that lie farther away from the vector. For example, the line between the solid-phase cycle and point 1 represents one such reaction-coordinate vector.

2. ENVIRONMENTAL CONDITIONS

Determine Location of Reaction- coordinate Vector. Figure 4 shows the global thermal decomposition reaction network for HMX and RDX. Depicted, are the different reactive processes: no, ondnta, ch_2o/no_2, nvr, and the solid-phase cycles. The complex interaction pathways connecting these distinct reaction cycles are also shown. The extent that each reaction cycle contributes to the overall decomposition process is dependent on several 'environmental' factors. These factors include: (1) pressure of gas in contact with the RDX/HMX, which is represented by a vertical line and increases qualitatively as one moves to the left in the diagram; (2) temperature of the RDX/HMX, which is represented by the horizontal line and increases qualitatively as one moves up in the diagram; (3) heating rate of the RDX/HMX, which is depicted by the horizontal axis in the grid surrounding the solid-phase cycle, with heating rates increasing from left to right in the grid; and (4) initial state of the RDX/HMX, qualitatively depicted by the two horizontal lines (labeled "pristine solid /crystal" and "completely damaged") to the left of the solid-phase cycle, with initial 'damage' to the RDX/HMX sample increasing as one goes down between the lines.

Qualitatively, a vector connecting the "starting point" of the RDX/HMX sample with a point formed by the intersection of the relative pressure and temperature lines can be thought of as a reaction-coordinate vector. The starting point is a point within the grid located in the upper left region of the reaction network that represents the initial state of the sample, which is determined by the heating rate in an experiment. The heating rate controls the relative amount of initial 'damage' created in the sample, with slower heating rates being associated with the creation of more damage.

In this context, the reaction cycles and 'coupling' pathways that are intersected by this reaction-coordinate vector are indicative of the dominant decomposition processes followed during a specific thermal decomposition event.

This is not to say that any processes not intersected are inactive for this specific set of circumstances. Indeed, due to the coupling of the different reaction cycles, all processes must play some role. A correct interpretation of this vector is that it depicts the dominant processes during the thermal decomposition under this specific set of circumstances, and therefore, these processes will be the ones observed during an experiment that is conducted under these same conditions.

With this interpretation of the decomposition process, the apparent discrepancies observed by previous experiments may be addressed. As mentioned above, different experimental investigations have shown different sets of products. Until now, this discrepancy was thought to indicate that different unimolecular decomposition mechanisms were at play under different thermal decomposition conditions. The decomposition diagram shows that each of these different experimental results (*i.e.* product distributions) is correct. One may use this framework based on different "simplified" (*i.e.*, unimolecular) reaction mechanisms to interpret the results from experiments collected under different sets of conditions to account for the apparent discrepancy. The reaction network expresses the idea that a single complex reactive process, with interactions between the distinct reaction cycles, is responsible for the overall decomposition. The varied experimental conditions simply serve to 'shift' the reaction coordinate vector to regions of the reaction mechanism where different reaction cycles dominate the reactive process and lead to different distributions of the observed products.

3. CONDITIONS PROBED BY VARIOUS EXPERIMENTS.

The three numbers in red circles (Figure 4) depict the regions of the global thermal decomposition reactive process network probed by several different experimental techniques.

The initial state of the sample is of significant importance when determining the dominant reaction pathway. The initial state of the RDX or HMX sample at the onset of decomposition in the STMBMS and other experiments can be mapped to a point within the region formed by the initial state and heating rate parameters. This region essentially encompasses the solid-phase reaction cycle and accounts for the possible states of RDX/HMX powders or single crystals used in various experiments (grid region).

At the upper left of the region is pristine RDX/HMX solid or single crystals. Rapid heating moves the sample to the right through the upper portion of the grid, corresponding to an experiment in which there is minimal damage in the solid due to nucleation and growth in the Solid-phase Cycle.

Continuing towards the right in the grid, liquid-phase RDX/HMX is formed in experiments that start with pristine, undamaged RDX/HMX and rapidly heat the sample above its melting point, to again minimize the extent of 'damage' due to the solid-phase reaction cycle.

The bottom left is a 'fully damaged' solid/single crystal, liquid-or melt-phase RDX/HMX, (*i.e.* RDX/HMX where the solid-phase nucleation and growth process has fully developed and an NVR has been produced). The bottom right depicts

solid/single crystal, liquid-or melt-phase RDX/HMX that has become fully 'reactive' (*i.e.* the nucleation and growth process is fully developed, and the condensed-phase RDX/HMX is completely saturated with intermediate stage decomposition products). Within this region, the possible initial states of RDX/HMX used in the thermal decomposition studies can be 'mapped'.

Region 1 in Figure 4 is occupied by TGA/DSC and vacuum laser-pyrolysis experiments. In a typical TGA/DSC experiment, a fast heating rate is used to obtain temperatures above the melting point of RDX/HMX, thereby minimizing the amount of time spent in the solid-phase reaction cycle during the heat ramp and resulting in essentially pristine liquid-phase RDX/HMX as the isothermal temperature is reached. Decomposition then proceeds in parallel by unimolecular liquid- and gas-phase processes, typically accompanied by significant RDX/HMX sublimation. The lack of high gas-confinement near the condensed-phase surface minimizes the contributions of secondary reactions between the condensed-and gas-phase decomposition products in the TGA/DSC measurements.

The vacuum laser-pyrolysis experiments[67] also generate rapid heating of the solid surface, again leading to essentially pristine liquid-phase RDX/HMX at the sample surface and consistent with the reaction-coordinate vector for Region 1. There is a significant contribution to the decomposition through the OST/HCN decomposition pathway and also contributions from the NO Cycle. Interactions between these two channels are controlled by the coupling pathways. Contributions to the overall decomposition process by reaction cycles and coupling pathways that are not directly intersected by the reaction-coordinate vector decrease the farther removed from the reaction-coordinate vector the individual process lies.

The parameter space depicted by Region 1 in Figure 4 does not include all variations of the space encountered by current ongoing TGA/DSC and laser-pyrolysis experiments; it simply maps the relative parameter space that is typical of the majority of work in these types of experiments.

Region 2 (Figure 4) is the relative parameter space occupied by flash-heating mass spectrometry and FTIR experiments.[68] In these experiments, very fast heating rates are used to 'flash' the solid sample to isothermal temperatures ranging from just below to significantly above the melting point of RDX/HMX. This flash heating produces a sample surface-temperature that initially falls within the transition region between pristine solid-phase and pristine liquid-phase RDX/HMX. This creates a surface that exists as a melt or 'froth' prior to the onset of significant decomposition, with minimal 'damage' created by the solid-phase reaction cycle before decomposition initiates.

The visual indications of a residue in these experiments, along with measurements of a mononitroso derivative of RDX (ONDNTA) indicate that there is a contribution to these experiments from the ONDNTA and NVR reaction cycles. Thus, results from these experiments can be mapped to Region 2, with the dominant processes lying along the reaction-coordinate vector and minor processes falling farther away from the vector.

A comparison of the reaction-coordinate vectors for regions 1 and 2 shows that ONDNTA and solid-phase decomposition contribute to Region 2 processes[41], while the first order OST and NO channels contribute more to region 1 processes.

Region 3 depicted in Figure 4 is the experimental parameter space filled by the slow-heating rate sealed bulb type experiments such as those by Batten [37-40] and Cosgrove and Owen.[69, 70] In these experiments, the slow heating allows the Solid-phase Cycle to contribute significantly to the decomposition. Thus, the NVR reaction cycle is the major contributor to the rate-limiting processes controlling the overall decomposition for the solid-phase experiments and plays a contributing role in the melt-phase experiments.

Summarizing: one unified picture captures the overall decomposition process. This picture is a network of complex interactions amongst different reactive processes with multiple pathways coupling the individual processes. This network captures all of the seemingly contrary results obtained in many different investigations in one unified picture. The network also provides a framework where most experiments can be mapped to distinct regions within the network. Differences among experiments can be attributed to variations in the experimental parameters which shift the dominant, rate-limiting steps to different reaction paths within one overall reaction network.

IV. REACTION KINETICS

While the reaction network provides a qualitative picture of the decomposition process and illustrates how various reaction pathways may compete under different sets of conditions and lead to the emergence of different observed behaviors, it falls short of the ultimate goal: predicting the behaviors of propellants and explosives over a wide range of conditions. To achieve this goal requires applying the second aspect of our conceptual framework: physicochemical control of high-temperature combustion reactions. The various reactive pathways in the reaction network must be individually characterized and represented by a set of mathematical expressions in a manner analogous to use of elementary reactions to characterize gas-phase reactions in high-temperature combustion processes. This requires new numerical algorithms that can be used to characterize the reaction kinetics associated with reaction networks that characterize the decomposition of the different energetic compounds and various energetic materials.

A. Extracting Reaction Kinetics from Condensed-Phase Experiments

1. SIMPLE KINETICS – DIRECT INVERSION FROM EXPERIMENT.

For simple reactive processes, the reaction kinetics can be determined directly from experiments by means of an Arrhenius-type analysis. Inversion of the data from the experiment provides the required reaction rate constant and its temperature dependence. If this type of analysis is applied to thermal decomposition results from

experiments with energetic compounds, the rate constant will only represent the reaction rate along the reaction-coordinate vector that represents the conditions of the particular experiment in the overall reaction network. The obvious limitation of this approach is that each reaction-coordinate vector requires its own set of reaction rate parameters.

3. KINETICS OF COMPLEX REACTION NETWORKS.

The development of mathematical models to represent combustion processes is a good example of how the kinetics of complex reaction networks has been developed. In this case the reaction kinetics have been determined by two different approaches. In the first approach, experiments are conducted to investigate and measure the rate of elementary reactions, thus providing pieces to be used in the overall reaction network. In the second approach, the distribution of reactants, intermediates, and final products are measured as a function of spatial location in a flame. Then the reaction rate parameters of the elementary reactions that represent the reaction network are optimized to match the details of the experimental measurements.

The conceptual framework that has been developed to investigate reactions of energetic materials in the condensed phase incorporates an approach to characterize the reaction kinetics that is analogous to the one used to characterize reaction kinetics in flames. In this approach, the time-dependent rates of formation of the reactants, intermediates, and products are measured using the experimental protocol. Next, reaction schemes are postulated, sets of differential equations representing the underlying processes constructed, solved, and compared to the experimental data (Figure 6). The analysis procedure is divided into two primary tasks. First the reaction scheme is postulated and refined and then the kinetics parameters are optimized.

Sets of differential equations are constructed to characterize the various processes in the reaction network that represent the decomposition of an energetic compound, such as the one above for RDX and HMX. The procedure used to build the model starts with a small set of differential equations that represent specific aspects of the decomposition process. The parameters for these processes are optimized by minimizing the difference between the calculations and the corresponding experimental measurements. If the differential equation for a specific aspect of the reaction network captures the features observed in the experimental measurements, it is retained in the model. If not, it is discarded and another process is postulated and tested. Using this procedure, a model of the reaction network is built.

Once the reaction scheme is developed to a point where it captures most, if not all, of the features observed in the data, it is then used to assess its ability to capture the features observed in experiments collected over a range of experimental conditions. When the model can capture the behavior over a range of experimental conditions, the parameters used in the model are then optimized to provide the kinetic parameters for the different pathways in the reaction network.

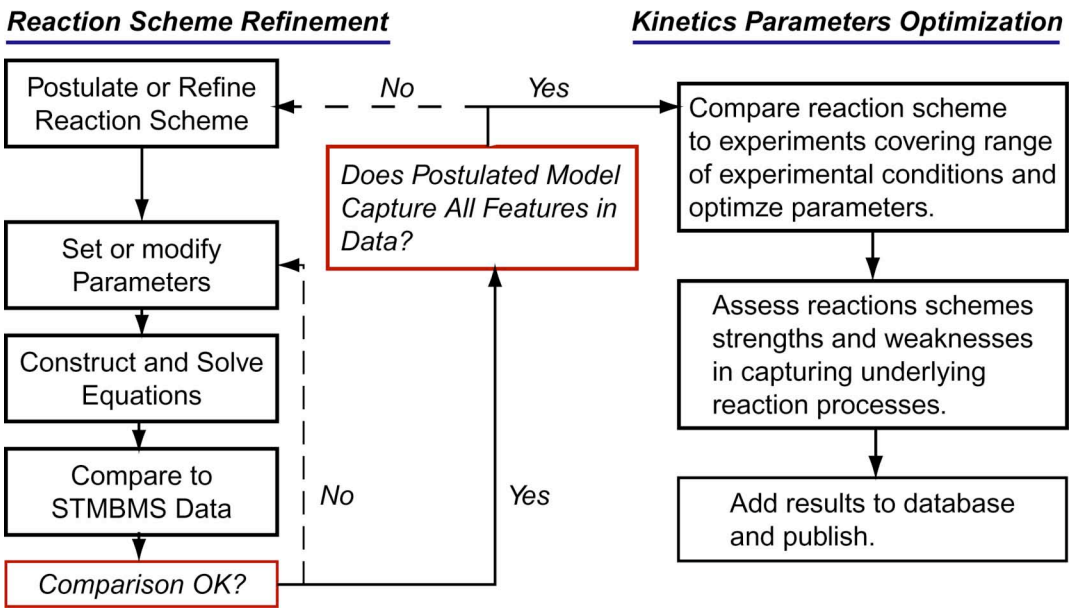

Figure 6. Algorithm used to create mathematical models to represent the reaction kinetics of thermal decomposition processes.

The modeling aspects of the conceptual framework for investigating the thermal decomposition of energetic materials are still under development. A higher level programming language, *Mathematica*©, has been used to develop the analysis methods. Papers on the decomposition of 24DNI[52] and NDNAZ,[71]illustrate how models of the reaction networks are developed for complex reactive processes in the condensed phase.

A new reaction modeling and kinetics (REMKIN) compiler and analysis tool is currently under development. The design goal for REMKIN is to provide a set of numerical algorithms to facilitate the development of mathematical representations of the reaction networks that control the decomposition of energetic materials. With the completion of the REMKIN compiler and analysis tool, the conceptual framework for investigating the thermal decomposition of energetic materials will be complete and new advances in our understanding of reactive processes in energetic materials in the condensed phase at low and moderate temperatures will be possible.

V. CONCLUSIONS AND FUTURE RESEARCH

Understanding the physicochemical processes that control the thermal decomposition of energetic materials in the condensed phase will help to characterize the safety and aging behavior of existing explosives and propellants. This understanding will also provide new insight for designing and developing new energetic compounds. Obtaining this understanding is a challenge due to the complex nature of the decomposition processes in these materials, which occur far from equilibrium conditions.

The development of a new experimental protocol to examine the complex processes associated with the thermal decomposition of energetic materials in the

condensed phase has been described. The fundamental concept of the new protocol is to maximize the extent of information obtained from the experiments so as to reveal the greatest insight into the underlying reactive processes.

The protocol described in this chapter is primarily based on mass spectrometric methods. However, the general concepts of using multiple instrumental methods to make simultaneous measurements on a system, with the goal of obtaining the maximum amount of temporally correlated information, is a general principal that provides guidance for creating other types of experiments to probe reactive processes in the condensed phase.

The new experimental protocol has been used to examine a range of different types of energetic materials and has revealed new insight into the underlying reactive processes. It has been found that the decomposition of most energetic compounds is controlled by a set of coupled nonlinear physical and chemical reactive processes.

These features create complex reactive systems whose behavior is characterized by the emergence of dissipative structures that play a major role in controlling the overall decomposition. Several different types of spatiotemporal structures have been observed for different materials. For example, reactions on the surface of 24DNI and RDX particles control the decomposition of these compounds in the solid phase, whereas nucleation and growth of sub-micron size reaction regions within HMX particles control its decomposition in the solid phase.

The experiments have also provided new insight into the multiple reaction pathways that compete to control the evolution of the decomposition process in time. This competition and interaction between the underlying processes has been illustrated with results from the decomposition of RDX and HMX. It has been shown how the effects of temperature and pressure of the contained gaseous decomposition products can alter the reaction pathways and lead to divergent results. It has also been shown which reaction pathways are likely to dominate the decomposition process using a variety of the more conventional thermal analysis methods. These methods typically provide insufficient information to identify and characterize the underlying processes.

The complex reaction behavior poses a challenge to develop new a conceptual framework that can be used to represent, develop, and convey understanding of the underlying behavior of energetic materials. While this is a new challenge in the field of energetic materials, understanding similar types of processes have been of great interest in the more general scientific community.

The entire set of behaviors observed in the decomposition of energetic materials in the condensed phase falls under the new science, born over the past several decades, of non-equilibrium processes. This new science uses concepts such as dissipative structures and self-organization and describes processes in terms of unidirectional time and irreversibility.[6] This context has been used to characterize a range of different phenomena, including complex chemical systems, such as the well-known Belousov-Zhabotinski chemical oscillator reaction. Use of these concepts will most likely play an important role in the characterization of decomposition processes of energetic materials in the future.

More recently, Wolfram has developed a description of complex processes in his book "A New Kind of Science".[72] It uses cellular automata to explore the behavior of complex systems and categorizes the evolution of these systems using a set of rules to guide the evolutionary progress. Some rules lead to the rapid development of simple, repetitive and predictable structures; others evolve as complex unpredictable patterns. This behavior illustrates that, for some set of rules, one can develop mathematical representations that predict the future state of the system, but with other sets of rules this is not possible and the system is not computationally reducible. Thus, the only way to characterize the evolution of the computationally irreducible system is to let it evolve and examine its structure at the time of interest.

These concepts developed by Wolfram[72] for cellular automata may be applied to the characterization of the decomposition processes in energetic materials by allowing the physicochemical processes to represent the rules that guide the evolution of the system and using the corresponding set of differential equations to compute the evolution of the system. This is essentially the process that has been developed for the numerical simulation features of the experimental protocol described in this chapter. A set of chemical reactions and physical processes are postulated (the rules to control the process), the evolution of the system is computed, and the results are then compared to the experimental results to determine if the chemical reactions and physical processes (the rules) describe the observed results.

From one point of view, the high-information content experiments developed in the experimental protocol can be considered an experimental implementation of the computational processes (rules), which guides the evolution of a system. Basically, a non-silicon analogue computer.

One of the main challenges remaining from the scientific viewpoint is connecting the behavior of the nonequilibrium reactive processes to the chemical and physical properties of the compounds (*i.e.*, chemical functionality, molecular and crystal structure, and constitutive properties). The ability to meet this challenge is in its infancy, for it requires first identifying the underlying reactive processes and then determining how these underlying processes are linked to the molecular, physical, and constitutive properties of the material. Currently, this is being approached by collecting data from high-information content experiments on a diverse set of different compounds and carefully examining the data to uncover correlations between decomposition behavior and the properties of the compounds.

Until now, most experiments that have examined the underlying detail of reactions of energetic materials in the condensed phase at low and moderate temperatures have focused on individual pure compounds. However, development of new experimental methods now allow the interactions of ingredients that make up explosive and propellant formulations to be examined in more detail. This should provide a more fundamental understanding of how the ingredients interact and what effects these interactions have on the mesoscale mechanics and aging behavior of these materials.

VI. ACKNOWLEDGEMENTS

The development of the new experimental protocol and its applications to the examination of energetic materials is the result of contributions of many people at Sandia National Laboratories over the past twenty years. Contributors include: Mr. N. Toly, Mr. J. Collins, Mr. J. Damico, Mr. M. Mitchell, Mr. D. Puckett, Dr. T. Land, Dr. L. Minier, Dr. K. Anderson, Mr. R. Hannush, Ms. L. Johnston, Ms. J. Wood, Ms. S. Mack, Ms. D. Wiese-Smith, Ms. E. Cooper and Dr. S. Maharrey. Many advances in our understanding were through discussions and collaborations with Dr. Surya Bulusu (U.S. Army, ARDEC; deceased). The work has been supported over the years by U.S Army/DOE Memorandum of Understanding (MOU), the Army Research Office, DoD Office of Munitions/DOE MOU, and United States Department of Energy's National Nuclear Security Administration under Contract DE-AC04-94-AL85000. The author thanks Dr. G. Anderson, Dr. W. Alzheimer, Mr. P. Gildea, Mr. Tom Hitchcock, Dr. S. Johnston, Dr. R. Carling, Dr. A. Ratzel, Dr. F. Tully, and Dr. D. Hardesty for support and encouragement for this work within Sandia. Finally, we thank Dr. R. Shaw for his long-term support and encouragement in our efforts.

VII. REFERENCES

1. B. Asay, *et al.* Large Scale Annular Cookoff Experiment (LASC). in PSHS Meeting, Coca Beach, Florida, CPIA (1999).

2. S. K. Chidester, *et al.*, On the violence of thermal explosion in solid explosive, *Combustion and Flame* **110** (1-2), 264-280 (1997).

3. H. S. Johnston, Gas Phase Reaction Rate Theory, Modern Concepts in Chemistry, edited by J. Crawford, B., W. D. McElroy, and C. Price, 1966, New York: The Ronald Press Company.

4. B. Bhushan, *et al.*, Biotransformation of hexahydro-1,3,5-trinitro-1,3,5-triazine catalyzed by a NAD(P)H: Nitrate oxidoreductase from Aspergillus niger, *Environmental Science & Technology* **15** (36), 3104-3108 (2002).

5. X. E. Zhao, E. J. Hintsa, and Y. T. Lee, Infrared Multiphoton dissociation of RDX in a molecular beam, *J. Chem. Phys.* **88** (2), 801-810 (1987).

6. I. Prigogine, The End of Certainty: Time, Chaos and the New Laws of Nature, First Edition: The Free Press, 57-72 (1996).

7. Behrens, R., Jr., New simultaneous thermogravimetry and modulated molecular beam mass spectrometry apparatus for quantitative thermal decomposition studies, *Review of Scientific Instruments* **58** (3), 451-461 (1987).

8. R. Behrens, *Jr.,* Identification of Octahydro-1,3,5,7-tetranitro-1,3,5,7-tetrazocine (HMX) Pyrolysis Products by Simultaneous Thermogravimetric Modulated Beam Mass Spectrometry and Time-of-Flight Velocity-Spectra Measurements, *International Journal of Chemical Kinetics* **22**, 135-157 (1990).

9. R. Behrens, Jr., Determination of the Rates of Formation of Gaseous Products from the Pyrolysis of Octahydro-1,3,5,7-tetranitro-1,3,5,7-tetrazocine (HMX) by Simultaneous Thermogravimetric Modulated Beam Mass Spectrometry, *International Journal of Chemical Kinetics* **22**,159-173 (1990).

10. Maharrey, S., et al., *High mass resolutions SIMS.* Applied Surface Science, 2004. **231-232**: p. 972-975.
11. R. N. Rogers, Differential Scanning Calorimetric Determination of Kinetics Constants of Systems that Melt with Decomposition, *Thermchimica Acta* **3**, 437-447 (1972).

12. S. L. Rodgers, *et al*., Comparative Mechanistic Thermochemical Decomposition Analyses Of Liquid Hexahydro-1 ;3 ;5-Trinitro-1 ;3 ;5-Triazine (Rdx) Using the Kinetic Deuterium-Isotope Effect Approach, *Thermochimica Acta* **177**, 151-168 (1991).

13. G. T. Long, *et al*., Competitive vaporization and decomposition of liquid RDX, *J. Phys.Chem. B* **23** (104), 2570-2574 (2000).

14. G. F. M. Pinheiro, V. L. Lourenco, and K. Iha, Influence of the heating rate in the thermal decomposition of HMX, *Journal Of Thermal Analysis And Calorimetry* **67**, 445-452 (2002).

15. C. M. Tarver, *et al*. The Thermal decomposition of Explosives with Full Containment in One-Dimensional Geometries. in Seventeenth Symposium (International) on Combustion, Pittsburgh: The Combustion Institute (1978).

16. M. D. Pace, Thermal Decomposition of RDX: Evidence of a Nitronylnitroxyl Free Radical Intermediate, *Journal of Energetic Materials* **3**, 279-291 (1985).

17. M. D. Pace, EPR-Spectra of Photochemical No_2 Formation in Monocyclic Nitramines and Hexanitrohexaazaisowurtzitane, *J. Phys. Chem* **95**, 5858-5864 (1991).

18. E. Catalano, and C. E. Rolon, On the Solid State Products of the Thermal Decomposition of Confined and Unconfined Triaminotrinitrobenzene, *Thermochmica Acta* **61**, 53-71 (1983).

19. P. J. Miller, S. Block, and G. J. Piermarini, Effects Of Pressure On the Thermal-Decomposition Kinetics ; Chemical-Reactivity and Phase-Behavior Of Rdx. *Combustion and Flame* **83** (1-2), 174-184 (1991).

20. T. R. Botcher, *et al.*, Thermal-Decomposition Mechanism Of NTO, *J. Phys. Chem.* **100** (21), 8802-8806 (1996).

21. K. L. Erickson, W. M. Trott, and A. M. Renlund, Thin-Film Methods for Examining the Decomposition Chemistry of Explosives, in Proceeding of the Tenth International Detonation Symposium, J.M. Short, Editor, Office of Naval Research: Boston Massachusetts, 340 - 346 (1993).

22. T. B. Brill, *et al.*, Condensed Phase Chemistry of Explosives and Propellants at High-Temperature - Hmx, Rdx and Bamo, Philosophical Transactions Of The Royal Society Of London Series A Physical Sciences And Engineering, **15** (339), 377-385 (1992).

23. S. T. Thynell, P. E. Gongwer, and T. B. Brill, Condensed-Phase Kinetics Of Cyclotrimethylenetrinitramine By Modeling the T-Jump/Infrared Spectroscopy Experiment, *J. Prop. and Power* **12** (5), 933-939 (1996).

24. J. Wormhoudt, P. L. Kebabian, and C. E. Kolb, Embedded Infrared Fiber Optic Absorption Studies Of Nitramine Propellant Strand Burning, *Combustion and Flame* **111**(1-2), 73-86 (1997).

25. W. M. Trott, and A. M. Renlund, Single-pulse Raman Scattering Studies of Heterogeneous Explosive Materials, Applied Optics **24** (10), 1520-1525 (1985).

26. L. R. Ryzhkov, and J. M. McBride, Low-temperature reactions in single crystals of two polymorphs of the polycyclic nitramine N-15-HNIW, *J. Phys. Chem.* **100** (1), 163-169 (1996).

27. L. R. Ryzhkov, and J. M. McBride, Structure, motion, and exchange coupling of (NO2)-N-15/(NO2)-N-15 radical pairs occupying adjacent solvent cavities of alpha-HNIW, a nitramine hydrat, *J. Am.Chem. Soc*. **119** (21), 4826-4833 (1997).

28. T. R. Botcher, and C. A. Wight, Transient Thin-Film Laser Pyrolysis Of RDX, *J. Phys. Chem.* **97** (36), 9149-9153 (1993).

29. A. J. B. Robertson, The Thermal Decomposition of Explosives, *Transactions of the Faraday Society* **45** 85-93 (1949).

30. S. Bulusu, and R. J. Graybush. Thermal Decomposition of 1,3,5,7-Tetranitro-1,3,5,7-tetrazacyclooctane (HMX): A Mass Spectrometric Study of the Products from β-HMX. in 39th Congress on Industrial Chemistry, Brussels, Belgium (1966).

31. W. L. Ng, J. E. Field, and H. M. Hauser, Study of the Thermal Decomposition of Pentaerythritol Tetranitrate, J. *Chem. Soc. (Perkin II)* 637-639 (1976).

32. F. W. Lampe, J. L. Franklin, and F. H. Field, Cross Sections for Ionization by Electrons **79,** 6129-6132 (1957).

33. M. Farber, and R. D. Srivastava, Mass Spectrometric Studies of the Thermal Decomposition of 1,3,5,7-Tetranitro-1,3,5,7-tetraazacyclooctane (HMX). *Chemical Physics Letters* **80,** 345-349 (1981).

34. M. A. Schroeder, Critical Analysis of Nitramine Decomposition Data Preliminary Comments on Autoacceleration and Autoinhibition in HMX and RDX Decomposition, US Army Ballistic Research Laboratory (1984).
35. M. A. Schroeder, Critical Analysis of Nitramine Decomposition Data: Product Distributions from HMX and RDX Decomposition, U. S. Army Ballistic Research Laboratory (1985).

36. M. A. Schroeder, Critical Analysis of Nitramine Decomposition Data: Activation Energies and Frequency Factors for HMX and RDX Decomposition, U. S. Army Ballistic Research Laboratory (1985).

37. J. J. Batten, and D. C. Murdie, The Thermal Decomposition of RDX at Temperatures Below the Melting Point I. Comments on the Mechanism, *Australian Journal of Chemistry* **23,** 737-747 (1970).

38. J. J. Batten, and D. C. Murdie, The Thermal Decomposition of RDX at Temperatures Below the Melting Point II. Activation Energy, *Australian Journal of Chemistry* **23,** 749-755 (1970).

39. J. J. Batten, The Thermal Decomposition of RDX at Temperatures Below the Melting Point III. Towards the Elucidation of the Mechanism, *Australian Journal of Chemistry* **24,** 945-954 (1971).

40. J. J. Batten, The Thermal Decomposition of RDX at Temperatures Below the Melting Point IV. Catalysis of the Decomposition by Formaldehyde, *Australian Journal of Chemistry* **24,** 2025-2029 (1971).

41. J. J. Batten, The Thermal Decomposition of RDX at Temperatures Below the Melting Point V. The Evolution of Occluded Volatile Matter Prior to the Decomposition, and the Influence of Past History of the Sample on the Rate of Decomposition, *Australian Journal of Chemistry* **25,** 2337-2351 (1972).

42. R. Behrens, and S. Bulusu, Thermal-Decomposition Of Energetic Materials .2. Deuterium-Isotope Effects and Isotopic Scrambling In Condensed-Phase Decomposition Of Octahydro-1,3,5,7-Tetranitro-1,3,5,7-Tetrazocine, *J. Phys. Chem.* **95** (15), 5838-5845 (1991).

43. R. Behrens, and S. Bulusu, Thermal-Decomposition Of Energetic Materials .4. Deuterium-Isotope Effects and Isotopic Scrambling (H/D; C-13/O-18; N-14/N-15) In Condensed-Phase Decomposition Of 1,3,5-Trinitrohexahydro-S-Triazine, *J. Phys. Chem*. **96** (22), 8891-8897 (1992).

44. R. Behrens, Jr., Thermal Decomposition of Energetic Materials: Temporal Behaviors of the Rates of Formation of Gaseous Pyrolysis Products from Condensed-Phase Decomposition of Octahydro-1,3,5,7-tetranitro-1,3,5,7-tetrazocine, *J. Phys. Chem*. **94,** 6706-6718 (1990).

45. R. Behrens, S. Mack, and J. Wood, Thermal Decomposition Mechanisms of HMX: The Interrelationship of Chemical and Physical Processes, JANNAF 17th Propulsion Systems Hazards Subcommittee Meeting, CPIA Publication 681
(Vol. 1), 21-44 (1998).

46. R. Behrens, and L. Minier, The Thermal Decomposition Behavior of Ammonium Perchlorate and an Ammonium-Perchlorate-Based Composite Propellant, in 33rd JANNAF Combustion Meeting, CPIA Publicaton 653, Monterey, CA. 1-19 (1996).

47. L. Minier, and R. Behrens, Thermal Decomposition Characteristics of Orthorhombic Ammonium Perchlorate (o-AP) JANNAF 17th Propulsion Systems Hazards Subcommittee Meeting, in 17th JANNAF Propulsion Systems Hazards Subcommittee Meeting, CPIA, Editor, CPIA Publication 681, Tucson, AZ, 57-72 (1998).

48. A. I. Atwood, *et al*., Thermal Decomposition Characteristics of Ammonium Perchlorate (AP) and an AP Based Propellant, in 49th JANNAF Propellant System HazardsSubcommittee Meeting, CPIA, Editor, Tucson, AZ, (1999).

49. J. Behrens, R. and S. Bulusu, Thermal Decomposition of HMX, Mononitroso-RDX, TNCHP and K6 in the Liquid Phase: Results from Simultaneous Thermogravimetry Modulated Beam Mass Spectrometry Measurements. 29th JANNAF Combustion Meeting, CPIA Publication 573 (Vol. II), 453 - 463 (1992).

50. R. Behrens, Jr. and S. Bulusu, Recent Advances in the Thermal Decomposition of Cyclic Nitramines. Fall 1992 Meeting of the Materials Research Society, **296,** 13 - 24 (1992).

51. L. Minier, R. Behrens, and S. Bulusu. Solid-Phase Decomposition of 2,4-Dinitroimidazole (2,4-DNI). in Decomposition, Combustion and Detonation Chemistry of Energetic Materials, Boston, MA: Material Research Society (1996).

52. R. Behrens, L. Minier, and S. Bulusu, Coupling Experimental Data and a Prototype Model to Probe the Physical and Chemical Processes of 2,4-Dintiroimidazole Solid-Phase Thermal Decomposition, in 34th JANNAF Combustion Subcommittee

Meeting, CPIA, Editor, CPIA Publication 662, West Palm Beach, FL, 549-567 (1997).

53. R. Behrens, and S. Maharrey, Chemical and Physical Processes that Control the Thermal Decomposition of RDX and HMX, in Combustion of Energetic Materials, K.K. Kuo and L. T. DeLuca, Editors, Begell House, New York, 3-21 (2002).

54. S. Maharrey, D. Wiese-Smith, and R. Behrens, Development of a Physicochemical Model for the Thermal Decomposition of RDX, in Proceedings of the 38th JANNAF Combustion Meeting, Chemical Propulsion Information Agency, Destin, Florida, 373-386 (2002).

55. W. E. Brown, D. Dollimore, and A. K. Galwey, Reactions in the Solid State. Comprehensive Chemical Kinetics, edited by C. H. Bamford and C. F. H. Tipper. (Vol. 22), Amsterdam, Elsevier Scientific Publishing, **340,** (1980).

56. S. Arrhenius, *Z. Phys. Chem*. **1,** 110 (1887).

57. R. Behrens, and S. Bulusu, Thermal-Decomposition Of Energetic Materials .3. Temporal Behaviors Of the Rates Of Formation Of the Gaseous Pyrolysis Products From Condensed-Phase Decomposition Of 1,3,5-Trinitrohexahydro-S-Triazine, *J. Phys. Chem.* **96** (22), 8877-8891 (1992).

58. S. Maharrey, R. Behrens, and L. Johnston, Physical and Chemical Processes Controlling the Solid-Phase Thermal Decomposition of hexahydro-1,3,5-trinitro-s-triazine (RDX), in 19th PSHS Meting, Chemical Propulsion Information Agency, Monterey, CA, 17 - 32 (2000).

59. R. Behrens, Jr. and S. Bulusu, Recent Advances in the Thermal Decomposition of Cyclic Nitramines, *Materials Research Society Proceedings* **296,** 13-24 (1993).

60. R. Behrens, and S. Bulusu, The Importance of Mononitroso Analogues of Cyclic Nitramines to the Assessment and the Safety of HMX-Based Propellants and Explosives, in Challenges in Propellants and Combustion 100 Years after Nobel, K. K. Kuo, Editor, Begell House, Inc., New York, 275 - 289 (1997).

61. J. Bickle, Understanding neural complexity: A role for reduction, *Minds And Machines* **11,** 467-481 (2001).

62. C. C. Chambers, and D. L. Thompson, Further-Studies Of the Classical Dynamics Of the Unimolecular Dissociation Of RDX, *J. Phys. Chem*. **99** (43), 15881-15889 (1995).

63. D. Chakraborty, *et al*., A detailed model for the decomposition of nitramines: RDX and HMX, *Journal Of Computer Aided Materials Design* **8,** 2-3 (2002).

64. C. J. Wu, and L. E. Fried, Ab initio study of RDX decomposition mechanisms, *J. Phys. Chem. A* **13** (101), 8675-8679 (1997).

65. D. C. Sorescu, B. M. Rice, and D.L. Thompson, Theoretical studies of the hydrostatic compression of RDX ; HMX ; HNIW ; and PETN crystals, *J. Phys. Chem B* **103** (32) 6783-6790 (1999).
66. D. Bedrov, *et al.*, Molecular dynamics simulations of HMX crystal polymorphs using a flexible molecule force field, *Journal Of Computer Aided Materials Design* **8,** 2-3 (2002).

67. T. R. Botcher, and C. A. Wight, Explosive Thermal-Decomposition Mechanism Of RDX, *J. Phys. Chem*. **98** (21), 5441-5444 (1994).

68. P. E. Gongwer, and T. B. Brill, Thermal decomposition of energetic materials 73: The identity and temperature dependence of "minor" products from flash-heated RDX, *Combustion and Flame* **115** (3), 417-423 (1998).

69. J. D. Cosgrove, and A. J. Owen, The Thermal Decomposition of 1,3,5-Trinitro-hexahydro-1,3,5-triazine (RDX)--Part I: The Products and Physical Parameters, *Combustion and Flame* **22**13-18 (1974).

70. J. D. Cosgrove, and A. J. Owen, The Thermal Decomposition of 1,3,5-Trinitro-hexahydro-1,3,5-triazine (RDX)--Part II: The Effects of Products, *Combustion and Flame* **22,** 19-22 (1974).

71. K. Anderson, *et al.*, Modeling the Thermal Decomposition of TNAZ and NDNAZ, 11th International Detonation Symposium, **1,** 239-245 (1998).

72. S. Wolfram, A New Kind of Science, First Edition, Wolfram Media, Inc., (2002).

Thermal Decomposition of Energetic Materials. 5. Reaction Processes of 1,3,5-Trinitrohexahydro-*s*-triazine below Its Melting Point

Sean Maharrey and Richard Behrens, Jr.*

Combustion Research Facility, Sandia National Laboratories, Livermore, California 94551-0969

Received: July 28, 2005; In Final Form: October 6, 2005

Through the use of simultaneous thermogravimetry modulated beam mass spectrometry, optical microscopy, hot-stage time-lapsed microscopy, and scanning electron microscopy measurements, the physical and chemical processes that control the thermal decomposition of 1,3,5-trinitrohexahydro-*s*-triazine (RDX) below its melting point (160−189 °C) have been identified. Two gas-phase reactions of RDX are predominant during the early stages of an experiment. One involves the loss of HONO and HNO and leads to the formation of H_2O, NO, NO_2, and oxy-*s*-triazine (OST) or *s*-triazine. The other involves the reaction of NO with RDX to form NO_2 and 1-nitroso-3,5-dinitrohexahydro-s-triazine (ONDNTA), which subsequently decomposes to form a set of products of which CH_2O and N_2O are the most abundant. Products from the gas-phase RDX decomposition reactions, such as ONDNTA, deposit on the surface of the RDX particles and lead to the development of a new set of reaction pathways that occur on the surface of the RDX particles. The initial surface reactions occur on surfaces of those RDX particles in the sample that can accumulate the greatest amount of products from the gas-phase reactions. Initial surface reactions are characterized by the formation of islands of reactivity on the RDX surface and lead to the development of an orange-colored nonvolatile residue (NVR) film on the surface of the RDX particles. The NVR film is most likely formed via the decomposition of ONDNTA on the surface of the RDX particles. The NVR film is a nonstoichiometric and dynamic material, which reacts directly with RDX and ONDNTA, and is composed of remnants from RDX and ONDNTA molecules that have reacted with the NVR. Reactions involving the NVR become dominant during the later stage of the decomposition process. The NVR reacts with RDX to form ONDNTA via abstraction of an oxygen atom from an NO_2 group. ONDNTA may undergo rapid loss of N_2 and NO_2 with the remaining portion of the molecule being incorporated into the dynamic NVR. The dynamic NVR also decomposes and leads to the formation of H_2O, CH_2O, N_2O, NH_2CHO, $(CH_3)_2NCHO$, $(CH_3)_2NNO$, $C_2H_2N_2O$, and $(CH_3)_3N$ or CH_3NCH_2-CH_3. The competition between reaction of the dynamic NVR with RDX and its own thermal decomposition manifests itself in a rapid increase in the rate of evolution of the NVR decomposition products as the amount of RDX remaining in the sample nears depletion. The reactions between the NVR film and RDX on the surface of the RDX particles leads to a localized environment that creates a layer of molten RDX on the surface of the particles where reactions associated with the liquid-phase decomposition of RDX may occur. The combination of these reaction processes leads to an acceleration of the reaction rate in the later stage of the decomposition process and creates an apparent reaction rate behavior that has been referred to as autocatalytic in many previous studies of RDX decomposition. A reaction scheme summarizing the reaction pathways that contribute to the decomposition of RDX below its melting point is presented.

Introduction

A major challenge for today's chemical kineticist is to understand and characterize the complex nonlinear spatiotemporal reaction processes that control the decomposition of explosive organic compounds, such as 1,3,5-trinitohexahydro-*s*-triazine (RDX, Scheme 1) in reaction environments that are relevant for assessing their aging, safety, and combustion characteristics. While many studies of this compound over the past 50 years have focused on characterizing its thermal decomposition and reactions in combustive environments, an understanding of the underlying reaction process has been difficult to develop.[1−6] Most experimental studies have focused on examining its thermal decomposition at temperatures (20−300 °C) well below those associated with combustion due to experimental feasibility and expediency. The initial reaction schemes used to characterize the reaction processes that control its decomposition have been based on gas-phase reaction rate concepts in which unimolecular decomposition theory may be used to estimate reaction rates based on the calculation of

SCHEME 1. Decomposition Pathways of RDX above Its Melting Point

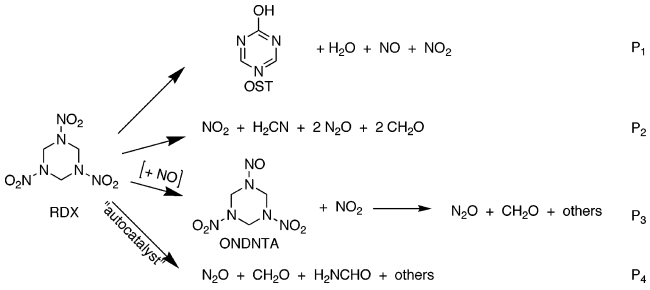

* To whom correspondence may be addressed. E-mail: rbehren@sandia.gov. Phone: (925) 294-2170. Fax: (925) 294-2170.

10.1021/jp054188q CCC: $30.25
Published on Web 11/18/2005

activation energies for various decomposition pathways using various forms and levels of theory.[7,8] Examination of the literature reveals few experimental studies on the decomposition of RDX that are limited to examining exclusively gas-phase, single-molecule aspects of its decomposition. An infrared multiphoton dissociation (IRMPD) study of RDX[9] provides the only experimental results on its gas-phase, single-molecule decomposition pathways. The results obtained in most other studies involve contributions from reactions that occur in the condensed phase.

Simultaneous thermogravimetric modulated beam mass spectrometry (STMBMS) experiments with RDX above its melting point[10,11] revealed how additional complexity, beyond single-molecule reaction processes, is introduced into the reaction processes that control the thermal decomposition of RDX. The results showed that four different primary reaction pathways control the decomposition of RDX in the liquid phase (Scheme 1). The first pathway (P1) is the direct decomposition of RDX via loss of HONO and HNO from RDX, which results in the formation of oxy-*s*-triazine (OST). Subsequent reactions of HONO produce the H_2O, NO, and NO_2 products. The mechanistic aspects of this pathway were strongly supported by the experimental results. The second pathway (P2) is consistent with a concerted ring fragmentation leading to the formation of three methylenenitramine (H_2CNNO_2) moieties, which undergo subsequent reactions to form NO_2, H_2CN, N_2O, and CH_2O. The experimental evidence supporting the mechanistic details of the pathway P2 is limited and cannot explicitly verify the formation of the observed products via the concerted ring fragmentation mechanism. The third pathway (P3) involves a substitution reaction in which an RDX NO_2 group is replaced by NO and results in the formation of 1-nitroso-3,5-dinitrohexahydro-*s*-triazine (ONDNTA), the mononitroso analogue of RDX. Subsequent reaction of this intermediate is quite complex and results in the formation of N_2O and CH_2O and a set of other products. This intermediate has been synthesized and its decomposition examined in STMBMS experiments.[12] The results revealed that a complex process controls the decomposition of ONDNTA and that this process is consistent with the behavior observed in the decomposition of RDX. The fourth pathway (P4) involves an "autocatalytic-like" reaction of RDX with a product that accumulates in the sample as an experiment progresses and produces N_2O, CH_2O, NO_2, and NH_2CHO. Subsequent experiments with ONDNTA suggest that pathway P4 may also involve the ONDNTA reaction intermediate, in which the ONDNTA leads to the formation of a nonvolatile residue (NVR) that interacts with RDX and leads to a time-dependent change in the rate of decomposition that could be interpreted as being autocatalytic.

The four reaction pathways include two direct decomposition reactions of RDX, similar to the

$$\mathrm{RDX} \rightarrow 3\mathrm{HCN} + 3\mathrm{HONO} \qquad \text{(R1)}$$

$$\mathrm{RDX} \rightarrow 3\,\mathrm{CH_2O} + 3\,\mathrm{N_2O} \qquad \text{(R2)}$$

reactions used to characterize RDX decomposition at high heating rates[13] and two additional pathways that are more complex. If only reactions such as R1 and R2 controlled the decomposition of RDX, then the associated reaction kinetics would be simple and relatively easy to characterize. However, reaction pathway P3 involves interactions with a gaseous decomposition product, creating a coupling between reaction pathways and introducing nonlinear effects into the underlying reaction kinetics. Furthermore, in reaction pathway P4, a nonvolatile reaction product accumulates in the sample and reacts with the remaining RDX. This behavior introduces an " arrow of time" into the reaction process and imposes a temporal dependence in which the relative contributions from the underlying reaction pathways change during the course of an experiment. Careful comparison of the rates of evolution of the various decomposition products from STMBMS experiments with RDX[10,11] shows that contributions from the underlying reactions change continuously during the course of an experiment. This variation in reaction features also has been observed in thermogravimetric analysis (TGA) and differential scanning calorimetry (DSC) experiments with RDX as evidenced by changes in the activation energies during the course of an experiment.[14] Hence, the reaction processes that control the decomposition of RDX are at least complex, nonlinear, and temporally dependent.

In this paper, the processes that control the decomposition of RDX below its melting point and how they are related to the four reaction pathways observed in its liquid-phase decomposition are examined. The thermal decomposition of RDX below its melting point has been examined previously by Cosgrove and Owen,[15,16] Batten,[17−21]and Bradley et al.[22] Their results provide qualitative insight into the features of the solid-phase decomposition process, show the effects of varying the pressure and types of gases confined with the sample, and demonstrate that higher gas confinement promotes an "auto-catalytic-like" decomposition process. In this paper, we address the following outstanding issues regarding the decomposition of RDX: (1) How the reaction pathways observed in the liquid-phase decomposition of RDX are related to the physicochemical processes that control its decomposition below the melting point. (2) The role of gas-phase reactions in the decomposition process. In experiments with RDX above its melting point, reactions in the liquid dominate and contributions from gas-phase RDX decomposition processes are difficult to distinguish. Below its melting point, contributions from the decomposition of gaseous RDX are more readily observed. (3) Reactions that control the decomposition of RDX in the particles. Whether or not reactions occur directly in the solid phase or if reactions in the gas phase are required to create new reaction pathways in the solid are examined.

To address these issues, results from experiments that focus on identifying the main chemical reactions and physical processes that control its decomposition between 170 and 189 °C are presented. The results show that the underlying reaction processes that control the decomposition are complex and involve reactions that occur in both the gas phase and on the surface of the RDX particles.

Experimental Methods

Instrument Description. An overview[23] describes the experimental methods and numerical algorithms used to examine and characterize the reactions of energetic materials in the condensed phase at low and moderate temperatures and details of the STMBMS instrument and analysis methods have been described previously.[24−26] The experimental methods utilize: (1) the STMBMS instrument to conduct thermal decomposition experiments and an associated set of numerical algorithms to transform the raw data to rates of formation of the decomposition products, (2) isotopically labeled analogues or a Fourier transform ion cyclotron resonance (FTICR) mass spectrometer to aid in identifying the products, and (3) scanning electron microscopy (SEM) to examine the morphological aspects of the reaction processes. Qualitative models of the spatiotemporal-

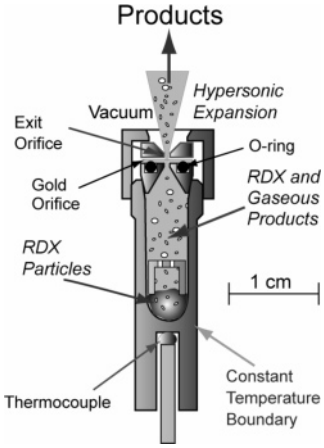

Figure 1. Cross section of reaction cell. Reaction cell is constructed from aluminum oxide, 99.8% purity. Reaction cell is sealed with ground fit cone and elastomer O ring beneath gold foil orifice. Baffle above sample reduces splatter onto gold orifice.

dependent reaction processes that control the decomposition of RDX are developed from data collected with these three methods. The methods also provide quantitative data that may be used to develop mathematical models of the underlying reaction processes.[27,28]

The basic features of a thermal decomposition experiment using the STMBMS instrument are illustrated in Figure 1. A small sample of RDX (2−10 mg) is placed in an alumina reaction cell (free volume of 0.227 cm^3), which is sealed with a cap assembly containing a disk of gold foil (25μm thick) that contains a hole with a specific diameter (2.5−50 μm) through its center. The reaction cell is heated in a controlled manner, using the thermocouple to measure and control the temperature of the cell. As the reaction cell is heated, vapor from RDX, and any other compounds within the cell, fills the free volume. The vapor flows through the orifice, and each constituent is identified and its rate of flow through the orifice is determined. The measurements provide the time-dependent *rate of formation* of each gaseous species that is present *solely* in the gas phase within the reaction cell. The measurements also provide the *vapor pressure* of gaseous species that are in *quasi-equilibrium* with material in condensed phases. For example, during the decomposition of RDX above its melting point, ONDNTA forms a solution with RDX, and the amount of ONDNTA vapor present in the gas phase is proportional to its mole fraction in the liquid. Thus, data on the rate of formation of both gas and condensed phase species are obtained during the course of an experiment.

The pressure of gases confined within the reaction cell, at a given temperature, may be varied by using orifices with different diameters and/or varying the mass of the sample. The gas pressure within the cell is governed by a steady-state balance between the rate of gas formation from the sample and the rate of exhaust through the orifice. Smaller orifices will result in higher pressures for a given gas formation rate from the sample. For compounds in a two-phase quasi-equilibrium, the pressure is governed by the temperature of the reaction cell and the properties of the compounds. In this case, a smaller orifice results in a lower rate of the gas exiting the reaction cell.

The data used to characterize the thermal decomposition processes are the identities and rates of formation of the different vapors that flow through the orifice and out of the reaction cell over a range of experimental conditions. The reaction conditions are controlled by altering the sample size, temperature, heating rate, orifice diameter, and volume of the reaction cell. For experiments with powders, the average particle diameter may be altered to assess effects of surface area on the rates of reaction.

Two modifications have been made to the original experimental and data analysis procedures.[24−26] First, to contain higher pressures of gas within the reaction cell during an experiment, the cap assembly of the reaction cell assembly now includes a gold orifice fitted with an elastomer O-ring seal and a thin bead of Krytox ultrahigh vacuum grease is applied to the ground cone to obtain a reproducible seal. After loading the sample, the reaction cell assembly is checked with a Balzers model HLT 160 helium leak detector to verify that the cell is properly sealed and gases will only evolve through the orifice. Second, a new procedure has been developed to calibrate the flow rate through the gold orifices and provide an accurate representation of the pressure within the reaction cell. In this procedure a standard set of orifices was created to relate the pressure within the reaction cell to the flow rate of gas through the ionization region of the mass spectrometer, which is used to detect the gases. The standard set of orifices was calibrated using naphthalene as the source of vapor in the reaction cell. This calibration provides a measure of the fraction of gas that exits the cell and flows through the ionization volume of the mass spectrometer as a function of pressure within the cell. To relate the flow characteristics of a gold orifice used in individual experiments to the flow characteristics of an orifice in the standard set of calibration orifices, a flow test system is used to measure the flow rate of nitrogen through the orifices. Pressure correction factors for each experiment are obtained by comparing the nitrogen flow rates through the orifice used in an experiment with the nitrogen flow rates measured for the corresponding calibration orifice. The measurements are made before and after each experiment to check whether the flow rate through the orifice has been altered during the course of an experiment. The equivalent "choked" flow orifice diameter and gas holding time within the fixed reaction cell volume are also calculated from the nitrogen flow tests, which allows orifices to be matched as closely as possible for given experiments and allows for better control of orifice diameter as an experimental variable.

The mass range of the quadrupole mass spectrometer is calibrated using perfluorotributylamine. The resolution is set so that the peak widths in the 20−300-amu region are approximately 0.7 amu full width at 10% maximum. The ionizer is operated in the linear electron-emission range at 1.0 mA. The electron energy is calibrated using the appearance potential of H_2O and set to 20 eV for all experiments, to reduce ion fragmentation in the mass spectrometer.

Hot-Stage Time-Lapse Microscopy. The hot-stage microscopy system used to examine the morphological changes in RDX particles as they decompose is shown in Figure 2. The system consists of a nitrogen gas convective hot-stage (Fluid Inc.), an Olympus SZH stereo optical microscope, a Polaroid model DMC digital microscope camera with DMC Direct 1.0 image acquisition software, and a G4 Macintosh computer for image acquisition. Individual particles of RDX were placed in a quartz sample cell (0.026 cm^3 free volume). The quartz cell was mounted in a thermally insulated cooling block and a methane/oxygen mini-torch was used to neck-down the end of the cell to a small throat diameter (<50 μm). The complete microreactor was then mounted under the thermocouple probe tip within the optically accessible hot-stage. The microreactor was heated and held at an isothermal temperature

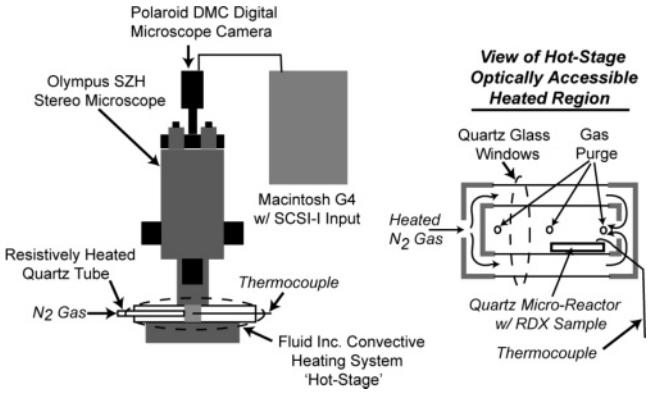

Figure 2. Schematic illustration of hot-stage microscope apparatus used for time-lapse microscopy measurements. The RDX sample is placed in the quartz microreactor, which is then placed in the optically accessible convective heating system and heated with N_2 at a pressure of 0.237 MPa.

below the melting point of RDX, and time-lapse photographs of the RDX particle were recorded at set intervals during the experiment.

Sample Preparation. Warning RDX is a High Explosive and Must Be Handled in an Appropriate Manner. The pure RDX samples used in these experiments were prepared by oxidation of hexahydro-1,3,5-trinitroso-*s*-triazine.[11] The mean RDX particle size used in these experiments was 194 μm, as measured with particle-sieving methods. The RDX particles for hot-stage microscopy were grown by dissolving pure (>99%) RDX powders in high-purity acetone and slowly recrystallizing the RDX over 7−10 days. This recrystallization process produced single large particles of RDX ranging from 1 to 6 mg.

Results

To probe the decomposition of RDX below its melting point, a set of experiments was conducted over a range of experimental conditions. Results from these experiments provide insight into reaction processes associated with sublimation and decomposition of RDX in the gas-phase, condensed-phase decomposition, and the reaction processes that lead to the development of complex nonlinear spatiotemporal processes on the surface of the RDX particles. First, the identities of the products formed during the decomposition are presented. Next, the temporal dependence of the rates of decomposition over a range of different experimental conditions is described. The variation in the rates of decomposition is illustrated with both simple TGA results and the rates of evolution of the various gas products during the course of each experiment. The TGA results illustrate the overall trends in the reaction processes over a range of different conditions, and the rates of gas evolution of individual products provide insight into contributions from the underlying reaction pathways. After describing the various processes revealed by the TGA data, optical and SEM pictures of RDX taken during different stages of the decomposition processes are presented to illustrate the morphological features associated with the reaction processes. Next, the products associated with the various underlying thermal decomposition processes are described. Finally, data illustrating the interaction of RDX with the NVR is presented. Table 1 lists five representative experiments conducted over a range of experimental conditions.

Product Identities. The identities of the products formed during the decomposition of RDX in these experiments are listed in Table 2. Products are listed by the *m*/*z* values used to measure each product with the mass spectrometer. The identities of the products associated with each *m*/*z* value have been determined from molecular weights derived from previous time-of-flight velocity spectra (TOFVS) experiments[29] and their corresponding molecular formulas, as derived from previous STMBMS experiments with isotopically labeled analogues of RDX.[11] In addition to the gaseous products listed in Table 2, a dark-red to orange colored remnant from the dynamic NVR remains in the reaction cell at the conclusion of the experiments. The amount of NVR remaining at the end of each experiment is listed in Table 1. Elemental analysis of two NVR samples shows that it is enriched in carbon and hydrogen compared to RDX and has a molecular formula of C, 3; H, 5; N, 1.7−1.8; O, 2−2.3.

TGA Data. Trends in the temporal dependence of the total sample mass vs time curves provide a global overview and initial insight into the general behavior and the degree of complexity of the decomposition process under a particular set of experimental conditions. The temporal behavior of the TGA data is correlated with the evolution of specific products, which provides insight into the chemical reactions associated with the underlying reaction processes. To depict the primary underlying reaction processes that contribute to the overall decomposition behavior of RDX below its melting point, data is presented from a series of experiments in which temperature and pressure of the gaseous products confined with the sample are varied (parts A and B of Figure 3). The role of the NVR is depicted by

TABLE 1: Experimental Parameters

exp. no.	temperature (°C)	orifice diameter (μm)	Choked-flow diameter (μm)	sample mass (mg)	decomp.[a] time (s)	residue mass (mg)
I	179	10	10.65	8.12	85 896	0.65[c]
II	179	5	7.28	8.33	73 595	0.79[d]
III	184	5	5.20	9.41	50 695	0.93[d]
IV	189	5	na	8.01	41 665	0.61[d]
V	179	5	6.29	14.3[b]	42 042	1.86[c]

[a] Time measured from start of isothermal condition. [b] Added onto 0.33 mg of residue from a 5 μm, 180 °C experiment. [c] Residue mass measured by Mettler balance in STMBMS apparatus. [d] Residue recovered from reaction cell and weighed.

TABLE 2: Decomposition Products from RDX

ion *m*/*z* value[a]	STMBMS-derived molecular formula ($C_xH_yN_zO_w$)[b]
18	H_2O
27	HCN
28	CO, N_2, RDX[c]
29	CH_2O, RDX[c]
30	CH_2O, NO, RDX[c]
43	C_2H_5N
44	N_2O
45	H_2NCHO
46	NO_2, RDX[c]
47	HONO
58	C_3H_9N[d]
59	CH_3NHCHO[e]
70	$C_2H_2N_2O$[f]
73	$(CH_3)_2NCHO$
74	$(CH_3)_2NNO$
81	$C_3H_3N_3$
97	$C_3H_3N_3O$ (OST)
132	$C_3H_6N_6O_5$ (ONDNTA)
128	$C_3H_6N_6O_6$ (RDX[c])

[a] *m*/*z* values of ions formed in mass spectrometer from the products formed in the reaction cell during an experiment. [b] Neutral products represented by the measured *m*/*z* values. [c] Electron bombardment fragment of RDX. [d] May be either $(CH_3)_3N$ or $CH_3NCH_2CH_3$. [e] Time-of-flight analysis indicates this product formed as a dimer.[10] [f] Originates from a product formed in NVR reactions and from ion fragment of OST.

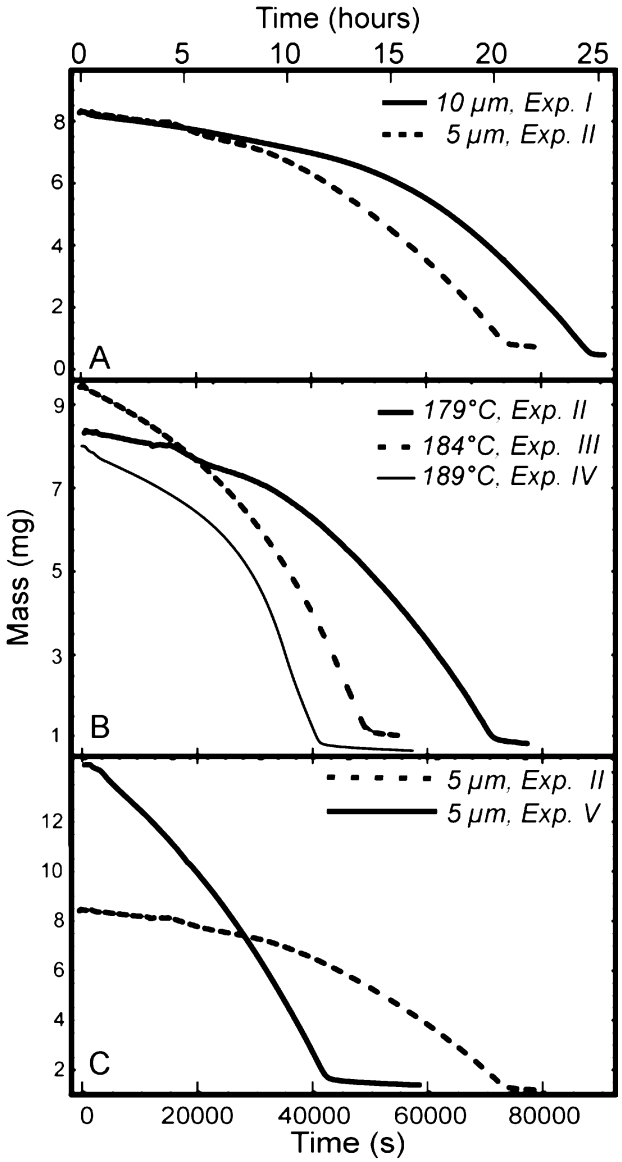

Figure 3. Mass of sample vs time for Exps I−V. Panel A shows results illustrating the effect of pressure of the gaseous decomposition products on the rate of mass loss. Panel B shows results illustrating the effect of temperature on the rate of mass loss. Panel C shows results illustrating the effect of the NVR on the rate of mass loss.

comparing the decomposition behavior from an experiment with a mixture of NVR and RDX (Exp. V, Figure 3C) with a similar experiment using only RDX (Exp. II).

The effect of gas confinement on the decomposition process is illustrated in Figure 3A with data from two experiments in which the orifice diameter is decreased from 10 to 5μm (Exps. I and II). While RDX does decompose in the gas phase, as indicated in the results from STMBMS measurements described below (Figure 7), the isothermal TGA results are unable to distinguish mass loss due to RDX vapor exiting the reaction cell from mass loss due to the RDX gas-phase decomposition products exiting the reaction cell.

At the lower gas confinement, the mass loss rate from Exp. I (10-μm orifice) is approximately constant during the first 20 000 s of the experiment (~0.09 mg/h) and then accelerates through the remainder of the experiment, reaching a final rate of mass loss of 0.70 mg/h when the RDX is near depletion at ~86 000 s. Mass loss due to both decomposition products formed from RDX in the gas phase and RDX vapor exiting the reaction cell is consistent with the constant rate of mass loss observed during the first 20 000 s of the experiment. The accelerating rate of mass loss, starting at ~20 000 s, indicates that additional reaction processes occur, other than RDX sublimation or decomposition of RDX in the gas phase. These additional processes involve reactions associated with the condensed phase of RDX and indicate a change in the rate controlling mechanism during the course of the experiment. The continually increasing rate of mass loss during the course of the experiment indicates that the reaction rates associated with the condensed phase reaction processes do not depend solely on the mass of RDX available for reaction.

At higher gas confinement, the qualitative features of the mass loss from Exp. II with the 5-μm orifice are similar to Exp. I with the 10-μm orifice. In this case, the mass loss rate is again approximately constant during the first 20 000 seconds of the experiment (~0.10 mg/h) and then accelerates through the remainder of the experiment, reaching a final rate of mass loss of 0.72 mg/h when the RDX is near depletion at ~74 000 s. The almost identical mass loss rates during the first 20 000 s of Exps. I and II indicate that most of the mass loss during this stage of the experiment arises from evolution of lower molecular weight products formed in the gas-phase decomposition of RDX, rather than the evolution of RDX itself from the reaction cell. On the basis of the effective choked flow diameters of the orifices used in each experiment (Table 1), the pressure of the gaseous decomposition products within the reaction cell should be about twice as high in Exp. II compared to Exp. I. In contrast to Exp. I, the acceleration in the rate of decomposition is faster in Exp. II, indicating a faster build up of the contributions from reactions associated with condensed phase processes. The similar time to onset of the acceleratory reaction rates in each experiment suggests that the reactions that lead to the nucleation conditions required for condensed phase processes to commence is similar in both experiments. However, once the nucleation conditions are established, higher pressure of one, or more, of the decomposition products results in the more rapid development of the reactions that control the condensed phase processes. Furthermore, the nearly identical final mass loss rates of Exps. I and II (0.70 vs 0.72 mg/h) indicate that, once the condensed-phase processes are developed, the rate-limiting steps may no longer be dependent on the products formed via the decomposition of RDX in the gas phase.

Further insight into reaction processes that occur below the melting point of RDX has been obtained by examining its decomposition between 179 and 189 °C (Exps. II, III, and IV). The TGA results are shown in Figure 3B, and the corresponding gas evolution rates (GERs) of the decomposition products from the reaction cell are described below and shown in Figure 8. The TGA results at 179 °C (Exp. II) and 184 °C (Exp. III) exhibit an initial constant rate of decomposition followed by an accelerating rate of decomposition. In Exp. III, the duration of the initial constant rate of decomposition is shorter and difficult to distinguish from the TGA data. (However, reaction products associated with primarily gas-phase decomposition during the early stage of decomposition are apparent in the corresponding data presented in Figure 8.) In Exp. III (184 °C) the mass loss rate is approximately constant during the first 5 000 s of the experiment (~0.28 mg/h) and then accelerates through the remainder of the experiment, reaching a final rate of mass loss of 1.10 mg/h when the RDX is near depletion at ~51 000 s. The fractions of residue formed in Exps. II and III are approximately equal (0.094 and 0.099, respectively, Table 1). Thus, the general behavior of the decomposition processes at 179 and 184 °C is similar.

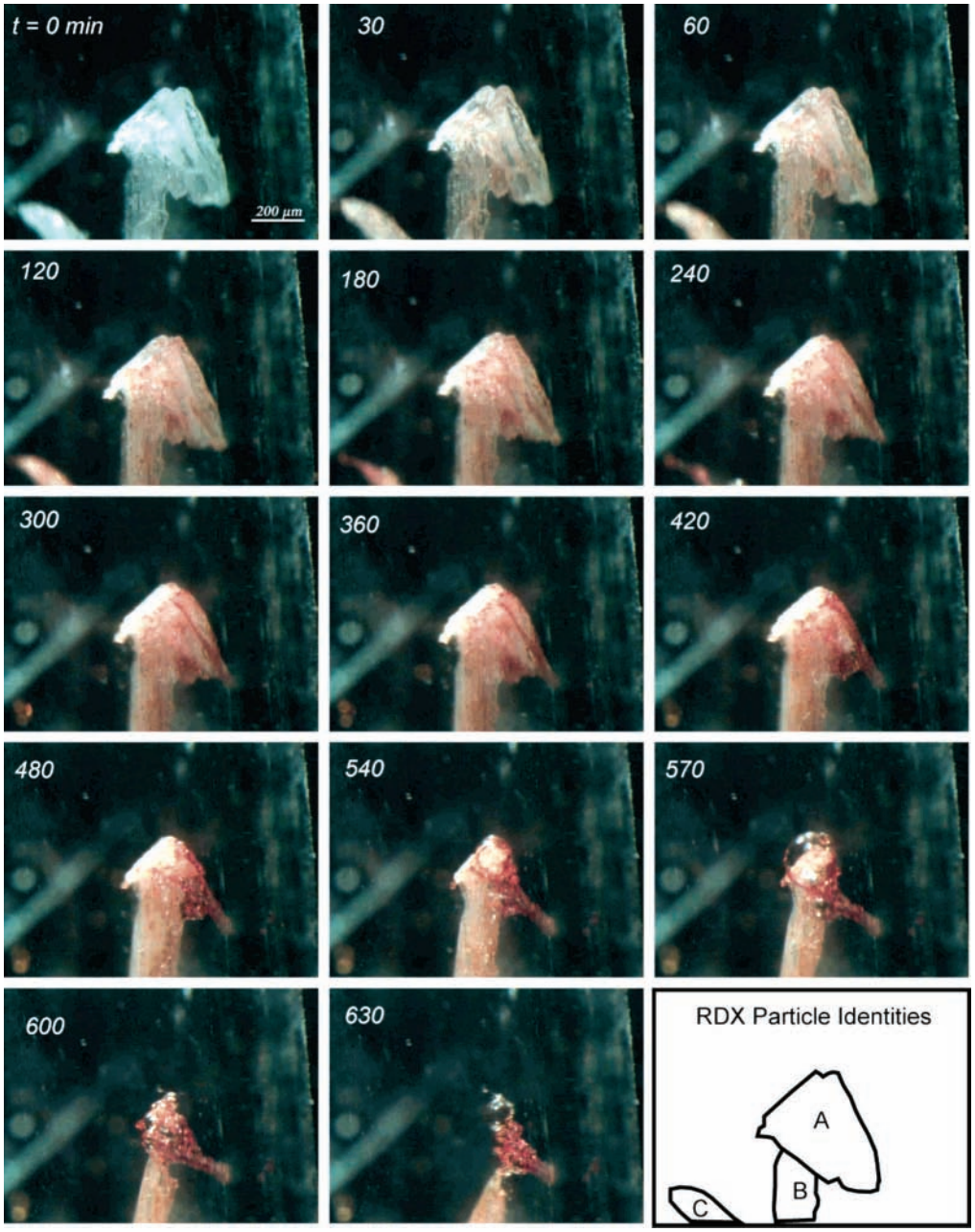

Figure 4. Hot-stage time-lapse images of a 1.6-mg RDX single particle decomposing at 180 °C in a quartz microreactor with a 10-μm diameter exhaust orifice. Time in minutes is listed on each image. $T = 0$ is when the sample first reaches 180 °C.

The temporal behavior of the TGA data from Exp. IV (189 °C) is more complex than the data from the experiments at 179 and 184 °C. In Exp. IV, the decomposition behavior over the first 20 000 s of the experiment is similar to the behavior observed in Exp. III (185 °C). The initial rate of mass loss is 0.24 mg/h, compared to 0.28 mg/h in Exp. III. However, in Exp. IV there is a rapid acceleration in the rate of reaction starting at about 20 000 s. This behavior suggests that at 189 °C another type of condensed phase process may develop and contribute to the overall decomposition rate. It is interesting to note that the fraction of residue formed at 189 °C is 0.076, significantly lower than the fraction formed in the two experiments at lower temperatures.

To probe the interaction between RDX and the NVR, experiments were conducted in which RDX was combined with NVR, formed in a previous experiment, and the decomposition of this mixture was examined (Exp. V). The sample for Exp. V was prepared by placing RDX on top of a solid mass of NVR that was formed in a previous experiment at 180 °C using a reaction cell fitted with a 5-μm orifice. The TGA results from Exp. V are shown in Figure 3C, and the corresponding gas evolution rates are shown in Figure 7C. In this case the initial mass loss rate starts at a relatively high value ($\sim$0.77 mg/h) and accelerates slightly through the remainder of the experiment, reaching a final rate of mass loss of 1.55 mg/h when the RDX is near depletion at $\sim$42 000 s. Comparing the results from Exps. V and II (Figure 3C) shows that the initial decomposition rate is higher and the total decomposition time is significantly shorter than in the corresponding experiments with starting samples containing only RDX. This experiment demonstrates that reaction between RDX and the NVR is a dominant reaction pathway below the melting point of RDX. By consideration of the geometric relationship between the RDX and the NVR in Exp. V and the fact that RDX remains a solid during the experiment, the higher initial reaction rate is most likely due to the transport of RDX through the gas phase to the surface of

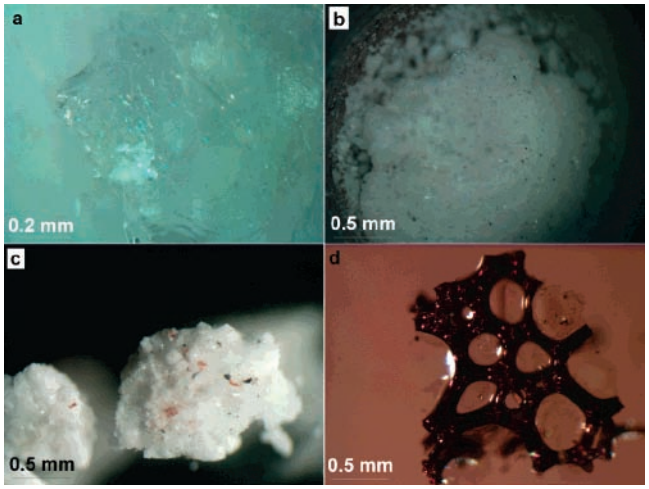

Figure 5. Optical images of RDX samples taken at different stages during the decomposition process. The pictures show the pristine RDX (a), a sample after 3% mass loss (b), as sample after 30% mass loss (c), and the dark-red translucent NVR sample remaining after complete decomposition (d). Background colors differ due to different lighting conditions.

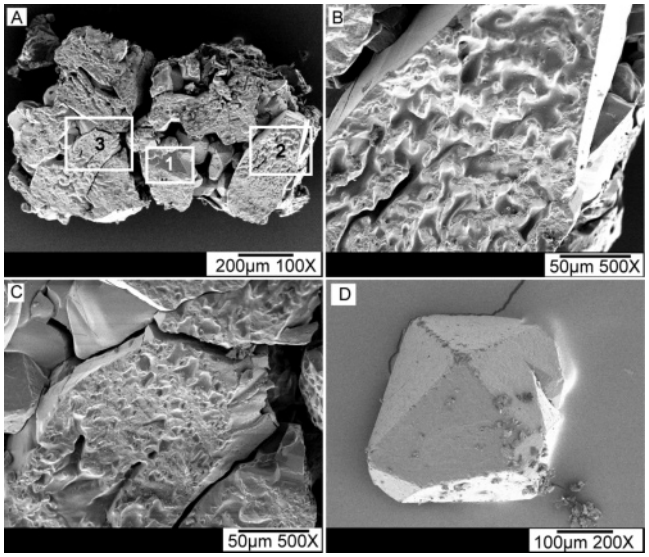

Figure 6. SEM pictures of a partially decomposed agglomerate of RDX particles (A, B, and C) and an inner surface of a fractured pristine RDX particle (D). The agglomerate of RDX was decomposed at 160 °C in a reaction cell with a 5-μm orifice. The sample was quenched after ~35% mass loss. Picture A shows the outer surface of the agglomerate of RDX particles. Higher magnification pictures of regions 2 and 3 are shown in pictures B and C, respectively. In region 1 the agglomerate has fractured during handling and reveals a view into the subsurface of the sintered material, showing an RDX particle with a smooth surface.

the NVR, where it reacts to form the decomposition products. However, it is also possible that as the mixture is heated the NVR in the bottom of the reaction cell becomes molten and interacts with the RDX on the surface of the RDX particles.

Although the relative increase in the rate of reaction in Exp. V is smaller compared to the experiments with samples containing only RDX, the absolute change in the rate of mass loss (1.55 − 0.77 = 0.78 mg/h) is similar to the final rate of mass loss observed in the corresponding experiment (Exp. II). Thus, the accelerating rate of decomposition in Exp. V is most likely due to the nucleation and growth of NVR on the surface of the RDX particles as was the case for Exps. I−IV. In Exp. V, the growth of the reaction rate due to reactions on the surface of RDX particles is masked by the relatively high rate of reaction between RDX and the NVR included from the previous experiment.

Hot-Stage Time-Lapse Microscopy. The TGA and GER results show that the NVR plays a significant role in the controlling the decomposition of RDX. Hot-stage microscopy is used to investigate how and where the NVR is formed during the decomposition of RDX. Results from the hot-stage microscopy experiments provide information on the spatiotemporal features of the underlying reaction processes. A set of time-lapse photographs of a 1.6-mg particle decomposing at 180 °C in a quartz reaction cell is shown in Figure 4. The duration of the experiment was approximately 10 h. The elapsed time in minutes is listed on each picture and a legend identifying particles A, B, and C in each picture is shown.

The first image (t = 0 min) shows the pristine RDX particles at 180 °C. At t = 30 min, the red-colored NVR has started to form on the right side of the particles. The RDX underlying the NVR remains translucent. The red NVR continues to grow (t = 60 and 120 min) until it covers the entire surface of particles A and B and has consumed most of particle C (180 min). Correspondingly, there is little NVR covering the upper left side of the particle A and the left side of particle B. Particle C disappears at 240 min. From 180−360 min, the NVR film is seen to substantially darken and thicken on particles A and B, while not spreading significantly. From 30−360 min a substantial portion of the RDX on the right side of particle A has been consumed in the reaction. At 360 min, a small spot of NVR has formed on the lower right underside of particle A. The region of particle A that is more heavily coated with NVR (right side) reacts more rapidly, as this portion of the RDX particle disappears more rapidly, moving from right to left in the images from t = 360−540 min. When it reaches the unaltered RDX, a bubble rapidly forms and grows while the NVR consumes the unaltered RDX (t = 540−630 min). At 630 min, the NVR bubble ruptures upon depletion of the RDX that formed particle A, leaving an NVR that is morphologically similar to that remaining from the STMBMS experiments. While particle B has formed a thick film coating, it has not fully decomposed during this same time period. The total decomposition time for this experiment was ~37 000 s. The more rapid decomposition of the RDX sample in the hot-stage experiment, compared to a nominally similar STMBMS experiment (Exp. II, 86 000 s), is most likely due to the higher pressure (~0.237 MPa) of the gaseous products contained in the vicinity of the RDX sample in the hot-stage experiments.

Optical Microscopy. The morphology of the NVR that grows on the RDX sample during the STMBMS experiments is less uniform than that observed in the hot-stage decomposition experiments. The growth and development of the NVR during the STMBMS experiments was probed by quenching STMBMS experiments at various extents of decomposition and taking high-magnification optical images of the remaining sample. Figure 5 shows a pristine RDX sample (a), samples that have undergone 3% (b) and 30% (c) mass loss, and the residue remaining after full decomposition (d). The pictures of partially decomposed samples were taken from experiments run at 160 °C using a 5-μm reaction cell exit orifice. During the initial stages of the decomposition (Figure 5B), the individual RDX particles have sintered and formed a white, opaque, rigid matrix. The individual RDX particles are still visible in the surface of the sintered material and upon removal, not shown, from the agglomerate, appear unchanged from the pristine RDX. The next stage of the NVR formation, not shown in Figure 5, involves the

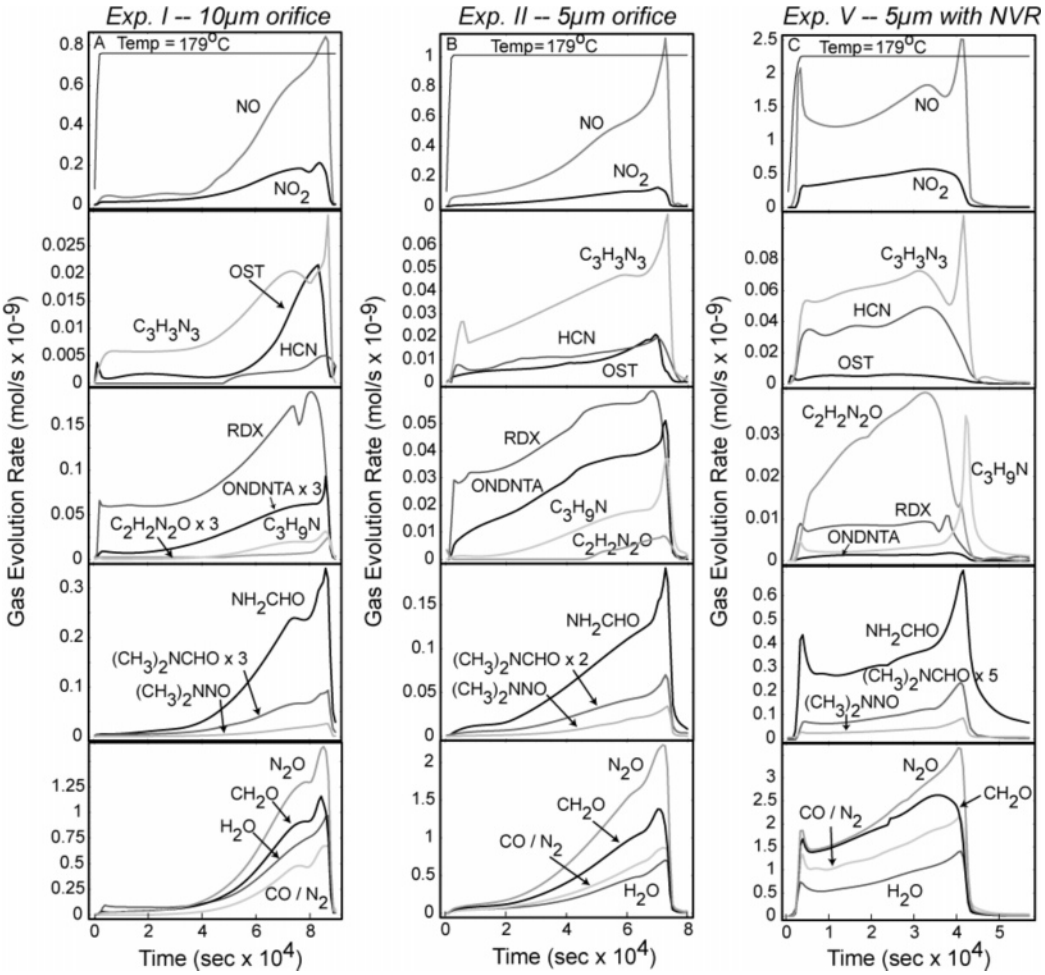

Figure 7. Gas evolution rates of products formed during the decomposition of RDX in three separate experiments conducted under isothermal conditions at 179 °C. Temperature profile is shown in upper panel. The starting temperature for each experiment is 20 °C. (A) Decomposition of RDX using a 10-μm diameter orifice (Exp. I). (B) Decomposition of RDX using a 5-μm diameter orifice (Exp II). (C) Decomposition of mixture of RDX and NVR using a 5-μm diameter orifice (Exp V). Experimental conditions are listed in Table 1.

formation of small, isolated, black "decomposition" spots on the sintered surface. At this stage of the process, the RDX particles are still visible in the sintered surface and appear as pristine RDX. Figure 5c shows the sample at the next stage of the NVR formation process. The RDX particles, which were still visible in the sintered surface of Figure 5b, have been completely covered by the sintered surface and the black spots have grown in size and number. An orange-colored NVR grows in the vicinity of the black spots. The RDX particles lying beneath the sintered surface can be recovered and still appear translucent and unaltered, with no black spots or orange patches growing on them. At the onset of the final stage of the NVR formation, the individual orange-colored regions coalesce into large, reddish-orange-colored translucent fibers that grow together to form the red, translucent NVR, shown in Figure 5D.

While the development of the NVR in the hot-stage and STMBMS experiments is similar, the details of the growth of the morphological characteristics differ and suggest a possible reaction process leading to its formation. The NVR forms a relatively uniform red-colored film on the surface of the particle in the hot-stage experiment (Figure 4, $t = 30$ and 60 min), whereas it forms localized islands situated in RDX that was redeposited in regions between the particles during the ST-MBMS experiments (parts b and c of Figure 5). Although there are differences in the volume and type of materials used to construct the reaction cells used in the hot-stage and STMBMS experiments, the main difference is the pressure of the gaseous decomposition products that are contained in the vicinity of the sample in each type of experiment. The hot-stage experiments are conducted at a constant pressure of 0.237 MPa (1775 Torr). In the STMBMS experiments, the pressure of the products in the reaction cell is determined by the steady-state balance between their rate of formation and their rate of flow out of the reaction cell. For the experiments conducted at 160 °C, using a 5-μm orifice, the pressure during the experiment ranges from 270−9300 Pa (2−70 Torr).

The higher pressure of the gaseous products contained in the quartz microreactor used in the hot-stage experiments will increase the rate of gas-phase reactions and limit the transport of material by diffusion. Thus, in the hot-stage experiments, the gas-phase reactions will be confined more to a layer adjacent to the surface of the particle and less volatile products, formed in gas-phase reactions, are likely to deposit more uniformly on the surface of the particle. In the STMBMS experiments, material transport is greater as evidenced by the deposition of RDX in the sintered regions of the sample, due to relatively rapid sublimation and condensation processes and greater diffusion distances at lower pressure. The products from the gas-phase decomposition reactions apparently deposit and undergo more rapid condensed-phase reactions in the sintered regions of the RDX sample in the STMBMS experiments.

The growth of the dynamic NVR in the hot-stage and STMBMS experiments is consistent with the following general reaction scheme: (1) RDX decomposes in the gas phase, (2)

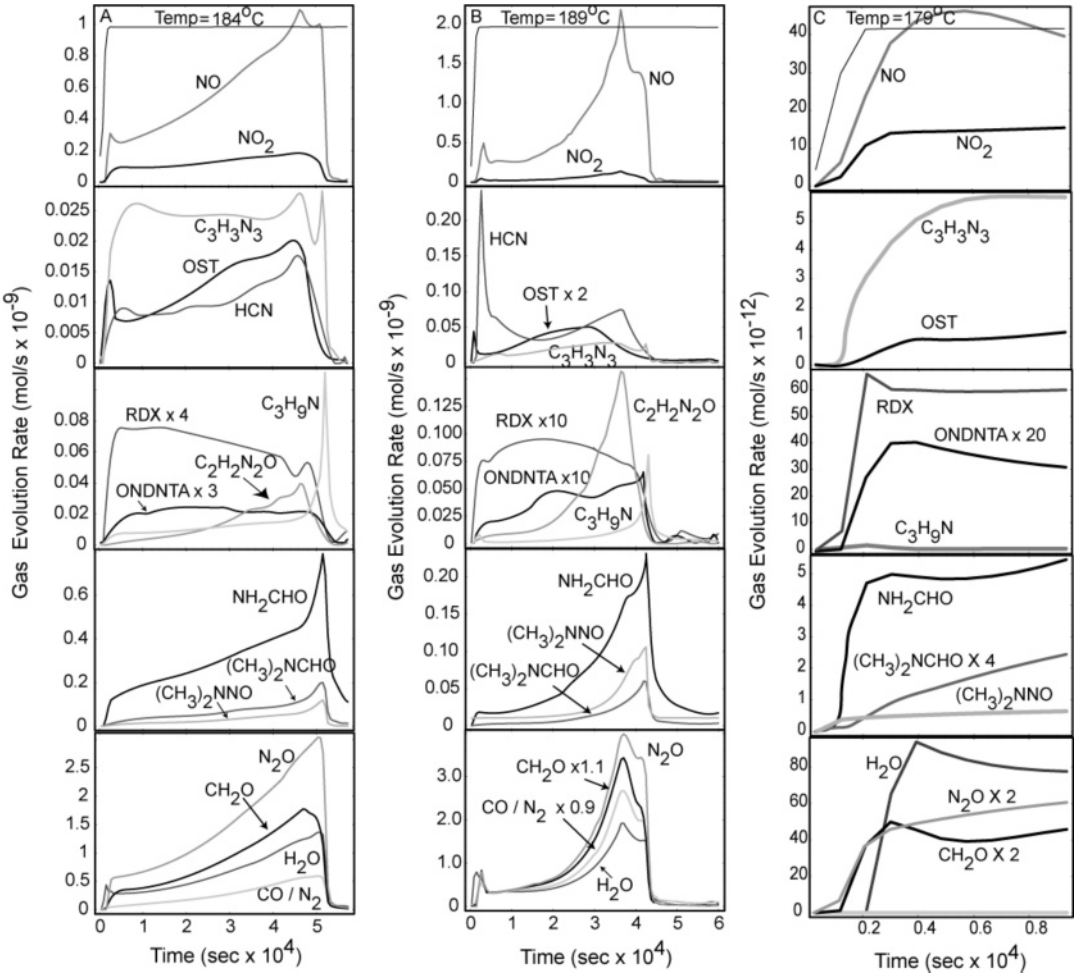

Figure 8. Gas-evolution rates of products formed during the decomposition of RDX at isothermal temperatures of 184 °C (A, Exp. III) and 189 °C (B, Exp IV). Temperature profile is shown in upper panel. The starting temperature for each experiment is 20 °C. The gas evolution rates of products during the early stage in the experiment using the 10-μm diameter orifice (Exp. I) are shown in C. Experimental conditions are listed in Table 1.

products from the gas-phase reactions are codeposited along with condensing RDX on the surface of the particles or sintered regions of the sample, and (3) some of these codeposited decomposition products initiate new reaction pathways in the condensed phase. The results also suggest that the rate of reaction of the condensed phase processes is more rapid in the sintered regions of RDX than on the surface of the original crystalline RDX particles.

SEM Microscopy. SEM pictures of a partially decomposed agglomerate of RDX particles (Figure 6) provide further insight into the processes involved in the decomposition of RDX below its melting point. Figure 6A shows a low magnification picture of the outer surface of a partially decomposed agglomerate of RDX particles. The particles separated slightly when removed from the reaction cell but maintained their relative positions and orientations. The surfaces of the particles located on the outer surface of the agglomerate have a rough appearance compared to the surface of the pristine RDX particles (Figure 6D). Closer inspection of region 2 (Figure 6B) and region 3 (Figure 6C) shows that the surface of the RDX particles that were on the outer surface of the agglomerate are roughened, whereas the surface of the RDX particles in the interior of the agglomerate remain smooth and similar to the surface of a pristine particle (Figure 6D). The surfaces of the particles that are located on the outer surface of the agglomerate, but are not directly exposed to the free volume of the reaction cell (6B), are also smooth. The sides of the largest particle in Figure 6B are smooth compared to its outer surface. The black and orange regions observed in optical micrographs are located in the roughened regions observed in the SEM pictures.

The location of the roughened surfaces in the RDX sample provides further insight into the reaction processes that control the decomposition of RDX below its melting point. The fact that the roughened surfaces are only observed on the outside of the sample agglomerate, which is exposed to the relatively large free volume of the reaction cell above the RDX sample, suggests that products formed in the gas-phase decomposition of RDX interact with the surface of the RDX particles and lead to the roughened surfaces. The location of the different morphological features also suggests that roughening is not simply due to sublimation and recondensation of RDX on the surface of the particles. For if this were the cause of the roughening, it would be expected to occur in a similar manner on the surface of particles located in both the interior and outer surface of the agglomerate, which it does not. Likewise, the location of the roughened surface also suggests that reactions that occur on the surface of the RDX particles are not due solely to RDX being located on the surface of the particle, but must involve the creation of some other compound, formed via reactions in the gas phase, that interacts with, and may deposit on, the surface of the RDX particles. In our STMBMS experiments this occurs preferentially on the outer surface of the agglomerate, because most of the volume in which the gas-phase reactions occur is in the free volume of the reaction cell

located above the surface of the agglomerate. In comparison, the free volume within the agglomerate is less, so the amount of RDX decomposition products available to react with the surface of the particles in the interior of the agglomerate will be less than those on its surface.

The roughened surfaces of the RDX particles located on an outer surface of the agglomerate, together with the accelerating rate of mass loss during the course of the decomposition experiments, indicates that the increasing rates of reaction are due to new reaction pathways developing on the surface of the RDX particles. From this perspective, the roughened surface would be created by decomposition occurring more rapidly at some locations than at others. Thus, the dimensions of the pockets in the roughened surface would suggest that the reaction regions may vary in size from 1 up to $\sim 20\mu$m at the point in time when the sampled was cooled and the reactions stopped.

Evolution Rates of Decomposition Products. Examining the identities and time-dependent rate of evolution of the products formed during an experiment provides further insight into the underlying processes that control the decomposition of RDX. The data collected in each of the STMBMS experiments listed in Table 1 has been quantified according to previously published procedures,[24,26] and the time-dependent rate of gas evolution from the reaction cell of each product has been calculated and is presented in Figures 7 and 8. The same type of relative ion formation probability and elemental mass balance constraints are used for quantification of the data presented in this paper as was used for previous analysis of RDX data.[10] The elemental mass balance for each experiment is within 4% of the nominal value. Table 2 lists the decomposition products measured during the STMBMS experiments (Exps. I−V).

Products associated with different reaction pathways are identified by separating their rates of gas evolution into temporally correlated groups. Some products may be associated with several different reaction pathways. The general temporal behavior of the GERs of products in Exps. I−IV may be characterized by a period of a relatively constant rate of evolution followed by a period of increasing rate of gas evolution. Closer examination of the temporal behavior of the GERs as the RDX nears depletion shows significant variation in the rates of evolution of the various products. During this period the GER of RDX decreases and the GERs of most of the other products increase. This increase in GER is more pronounced for some products (e.g., C_3H_9N) than others.

The relatively constant rate of formation of decomposition products during the earlier stage of each experiment persists for the longest period of time in Exp. I (Figures 7A and 8C). During this period most of the various products are formed at relatively low rates. The products not formed, or formed at very low rates, during this early period are those compounds with relatively high fractions of carbon and hydrogen: $(CH_3)_2NCHO$, $(CH_3)_2NNO$, and C_3H_9N. The constant rate of formation of H_2O, CO/N_2, CH_2O, NO, N_2O, NO_2, *s*-triazine, OST, and ONDNTA in Exp. I over a long period of time is proportional to the partial pressure of RDX vapor in the cell and indicates that these products are formed via reaction of RDX in the gas phase.

The GER of one of the products, *s*-triazine ($C_3H_3N_3$), is roughly proportional to the amount of RDX present in the gas phase during the entire course of each experiment (the GER of RDX is proportional to its partial pressure in the reaction cell). This indicates that *s*-triazine, formed during the early stage of the experiment, originates solely from the decomposition of RDX in the gas phase. The rate of evolution of OST during the early stage of each experiment is lower than that of *s*-triazine (the temporal behavior of the GERs of the products during the early stage of Exp. I is shown in Figure 8C). This behavior differs from the decomposition of RDX in the liquid phase in which OST is the major product formed in the direct decomposition of RDX.[10] Thus, elimination of 3HONO from RDX appears to be one of the main decomposition pathways of RDX in the gas phase. This is consistent with one of the low energy reaction pathways predicted by recent ab initio quantum chemistry calculations.[8] Decomposition of RDX in the liquid phase alters the direct decomposition of RDX and leads to the formation of OST. An example of this behavior is illustrated by comparing the *s*-triazine and OST GERs in Exp. I (Figure 7A). In the later stage of Exp. I, the OST GER grows and eventually becomes as large as the *s*-triazine GER. The GERs of the products formed by secondary reactions of HONO, H_2O, NO, and NO_2 are also constant during the early stage of the experiments (Figure 8C).

The other gas-phase reaction that occurs during the early stage of Exp. I leads to the formation of ONDNTA. The direct decomposition of RDX to form *s*-triazine provides the NO required for reaction with RDX to form ONDNTA via a substitution reaction, similar to its formation in experiments with RDX in the liquid phase (Pathway P3, Scheme 1).[11] Examination of the early stage of Exp. I (Figure 8C) shows that the GER of ONDNTA from the reaction cell lags the GERs of RDX and several of the more volatile decomposition products. This behavior is due to the ONDNTA that is formed in the very early stage of the experiment condensing on the RDX particles in the sample. As more ONDNTA accumulates on the surface of the RDX sample, its partial pressure within the reaction cell increases until it attains its quasi-equilibrium vapor pressure value. The dominant products formed in the decomposition of ONDNTA,[12] CH_2O and N_2O, are also formed at relatively constant rates during the early stage of the experiments, suggesting that ONDNTA decomposes in the gas phase in these experiments. However, previous studies on the decomposition of ONDNTA[12] show that it decomposes in the condensed phase at temperatures between 100 and 150 °C. Thus, the evolution of decomposition products from ONDNTA may occur from ONDNTA present in either the gas phase or on the surface of the RDX particles.

The GERs of the products associated with the two primary gas-phase reactions have similar behaviors under both higher confinement (Exp. II, Figure 7B) and higher temperature (Exps. III and IV, parts A and B of Figure 8) conditions. In each of these experiments the duration of the early stage is less than it is in Exp. I, but the general behavior of the products associated with each of these reaction pathways, *s*-triazine and ONDNTA, is similar.

At the end of the early stage, associated with gas-phase reactions, the gas evolution rates of all the products start to accelerate. This increasing rate of reaction coincides with the formation of the NVR on the surface of the RDX particles. The major products formed in the accelerating reaction process are: H_2O, N_2/CO, CH_2O, NO, and N_2O. The rates of evolution of the minor products such as NH_2CHO, $(CH_3)_2NCHO$, $(CH_3)_2NNO$, and C_3H_9N also increase continuously until the RDX is depleted. This behavior, taken together with the growth of the film of NVR on the surface of the particles in the hot-stage microscopy experiment, indicates that the rate of reaction during the later stages of each experiment is controlled by the reaction and growth of the NVR during the course of the experiment. Thus, the NVR may be considered a dynamic mixture of products formed by reaction with RDX. This dynamic NVR

mixture both reacts with RDX and itself decomposes to release gaseous products and form new reaction intermediates that remain in the NVR. The rapid increase in the GERs of most of the products as the amount of RDX present in the sample nears depletion is indicative of the competition between the reaction of the NVR with RDX and the decomposition of the NVR by itself.

The overall behavior of the GERs for the products from Exps. I−III is similar, whereas the GERs from Exp. IV (Figure 8B) in which the sample is closer to the melting point of RDX have additional features. One difference is the rapid evolution of a small amount of HCN when the sample first reaches its isothermal temperature. This may be due to differences in the chemical characteristics of the outer subsurface regions of the RDX particles compared to the inner portion of the particles. A similar effect on the initial decomposition rate of 2,4-dinitroimidazole (24DNI), due to water absorbed in the subsurface of the particles, has been observed.[27] The other difference is the delayed, but more rapid, increase in the rate of evolution of major decomposition products: H_2O, CO/N_2, CH_2O, NO, and N_2O. This delayed onset of gas evolution and the similarity of the products to those observed in the liquid-phase decomposition of RDX suggests that at 189 °C the RDX on the surface of the RDX particles in the vicinity of the NVR may liquefy. This would open the liquid-phase reaction pathways, previously reported[10] and listed in Scheme 1.

Interaction of the Dynamic NVR with RDX. To examine the interaction between RDX and the dynamic NVR in more detail, an experiment (Exp. V) was conducted in which RDX was mixed with NVR produced in a previous experiment and decomposed under conditions similar to those used for Exp. II. Comparison of the results from these two experiments shows that RDX decomposes more rapidly in the experiment with the mixture of RDX and NVR (Exp. V, Figure 7C) than in the experiment with RDX by itself (Exp. II, Figure 7B). The most obvious difference in the GERs of the products is the relatively high rate of evolution of products when the experiment with the RDX/NVR mixture first reaches the isothermal temperature of 179 °C. For example, the GER of N_2O in Exp. V is $\sim 1.5 \times 10^{-9}$ mol/s when the sample first reaches the isothermal temperature. This value is high compared to the similar period in Exp. II in which the GER for N_2O is $\sim 0.02 \times 10^{-9}$ mol/s. However, as Exp. II progresses the GER of N_2O just prior to depletion of RDX rises to a value of 2×10^{-9} mol/s, which is approximately the same as its initial rate of evolution in Exp. V. This is very strong evidence that reaction between RDX and the NVR becomes the dominant reaction process as the dynamic NVR accumulates in the sample during the course of an experiment.

The high GERs of the decomposition products in Exp. V when the sample first reaches its isothermal temperature indicates that the reaction process may involve the transport of RDX through the gas phase to the surface of the NVR where it reacts. The relatively modest growth in the GERs during Exp. V (e.g., the GER of N_2O rises from 1.5 to 3.5×10^{-9} mol/s) suggests that the rate of reaction may be limited by amount or exposed surface area of the dynamic NVR available during the course of an experiment.

Further insight into the nature of the reaction of RDX with the dynamic NVR and the decomposition of the NVR itself may be obtained by examining the GERs of RDX and the various products just prior to, and after, the depletion of RDX in each experiment. There are four distinguishing temporal features of the GERs during this period of each experiment. First, two of the products (NH_2CHO and C_3H_9N) have small, but significant, GERs after the RDX is depleted. This suggests that these products originate directly from decomposition of the dynamic NVR. Second, most of the products exhibit a rapid rise in their GER as the RDX nears depletion. Products with this characteristic include: NO, N_2O, NH_2CHO, $(CH_3)_2NCHO$, and $(CH_3)_2NNO$. Third, the GERs of RDX and $C_2H_2N_2O$ decrease as the RDX nears depletion. This suggests that the formation of $C_2H_2N_2O$ is related to vapor phase RDX and the presence of the dynamic NVR. The higher rate of formation of $C_2H_2N_2O$ in the experiment with the mixture of NVR and RDX (Figure 7C) is consistent with this idea. Thus, $C_2H_2N_2O$ may be formed via a reaction between RDX and the NVR on the surface of the NVR. Fourth, there is a shorter period during this final stage of the decomposition process in which the GER of one of the products (C_3H_9N) increases rapidly and the GER of another product (CH_2O) falls off as the other lower molecular weight products are still increasing (see CH_2O in Figure 7C). This suggests that during the final stage of the decomposition CH_2O may react with the dynamic NVR to form several of the other products (i.e., NH_2CHO and $(CH_3)_2NCHO$). These features of the temporal behaviors of the GERs during the final stage of the decomposition process provide some further qualitative understanding of the reactions that involve the NVR.

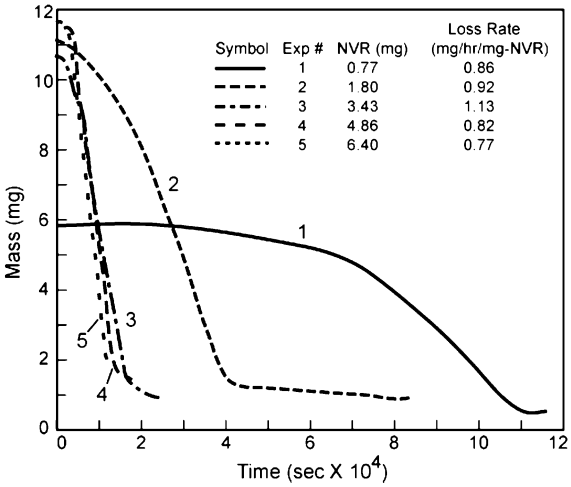

Figure 9. Sample mass vs time data from a series of five experiments in which RDX was added to the NVR remaining in the reaction cell from the previous experiment. The experiments were run at 180 °C using a reaction cell fitted with a 5-μm diameter orifice. The NVR formed in each experiment accumulated as a solid mass in the bottom of the reaction cell. The mass loss rates and amount of NVR present at the end of each experiment are listed in the table.

To examine the reactivity of the dynamic NVR a series of five experiments were run in which RDX was added to the NVR remaining in the reaction cell from the previous experiment. TGA data from the series of five experiments (Figure 9) shows that after accumulating NVR from two experiments the delay until onset of the rapid reactions associated with the dynamic NVR is essentially eliminated. After the first two experiments the bottom of the reaction cell was coated with dark-red islands of NVR. After the third experiment the bottom of the reaction cell was coated with a dark-red solid mass of NVR, whose effective exposed surface area did not increase further with the addition of residue from the fourth and fifth experiments. The NVR did not accumulate on the sides of the reaction cell above the location of the RDX sample, as had been observed for experiments using the larger 10- and 25-μm diameter orifices. The higher pressure of gases in experiments using smaller diameter orifices appears to confine the reactions involving RDX

SCHEME 2. Decomposition Pathways of RDX below Its Melting Point

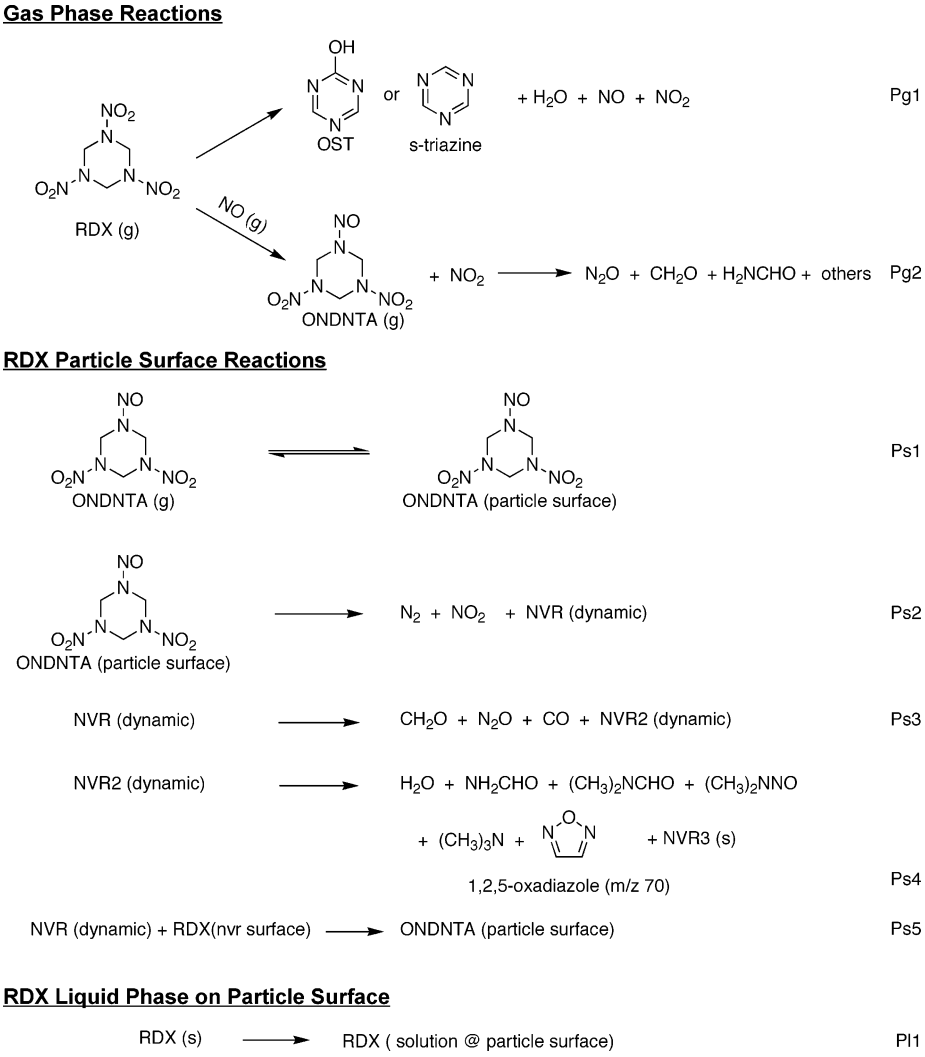

to regions near the sample. The accumulation of NVR during the first experiment had the biggest effect on changing the reaction rate, as would be expected, since the NVR must first nucleate via gas-phase reaction processes. In the final two experiments the surface area of the NVR located in the bottom of the reaction cell remained approximately the same. Thus, in the last two experiments the depth of the NVR sample grew by approximately 40% in each experiment.

Examining the data from the last three experiments shown in Figure 9 shows that the rate of mass loss due to RDX reacting with the NVR does not increase in proportion to the increase in the amount of NVR present in the bottom of the reaction cell. This indicates that reaction between the RDX and NVR involves reactions on the surface and/or subsurface of the NVR but not with the entire mass of NVR. Thus, one of the factors limiting the rate of reaction between RDX and the NVR may be the solubility of RDX in the NVR.

Discussion

The results from the STMBMS experiments with RDX below its melting point show that thermal decomposition reactions occur in three principal regions. These regions include: (1) RDX in the gas phase, (2) the surface of the RDX particles, and (3) in a liquid film formed on the surface of the RDX particles. Several different reaction pathways, as summarized by Scheme 2, control the decomposition process in each region.

Two reaction pathways account for the primary decomposition processes in the gas phase. One pathway is the direct reaction of RDX to form either OST or *s*-triazine and the corresponding decomposition products formed via the elimination of HONO and HNO from RDX: NO, NO_2, and H_2O. This reaction is similar to the direct reaction of RDX observed in the liquid-phase decomposition of RDX (Scheme 1). Elimination of 3 HONO to form *s*-triazine appears to be the more dominant reaction in the gas phase. One of these products, NO, is involved in the second reaction pathway in which NO replaces an NO_2 group to form the mononitroso analogue of RDX, ONDNTA. This reaction pathway is also similar to Pathway P3 in the liquid-phase decomposition (Scheme 1), in which ONDNTA decomposes to form CH_2O, N_2O, NH_2CHO, and several other gaseous products. The ONDNTA, having a vapor pressure similar to RDX, condenses on the surface of the RDX particles. During the initial stage of the experiment, the rate of evolution of ONDNTA from the reaction cell is quite low until a quasi-equilibrium is established between ONDNTA in the condensed and gas phases (Pathway Ps1, Scheme 2).

The deposition of ONDNTA from gas-phase reactions onto the surface of the RDX particles opens new reaction pathways (Pathways Ps2−Ps5). Previous studies on the decomposition of ONDNTA[12] have shown that it decomposes in a series of steps. First, N_2 and NO_2 are eliminated rapidly from ONDNTA to form an intermediate, NVR(dynamic). Next, CH_2O, N_2O, and

CO are gradually eliminated from the NVR(dynamic) intermediate to form a second intermediate, NVR2(dynamic) (Pathway Ps3). This second intermediate eventually is transformed to a state in which a new set of reactions occur, leading to the formation of H_2O, $(CH_3)_2NCHO$, $(CH_3)_2NNO$, and $(CH_3)_3N$ and another nonvolatile residue, NVR3, that remains at the completion of an experiment (Pathway Ps4). The same set of products is observed during the decomposition of RDX below its melting point in the STMBMS experiments as was observed in the STMBMS experiments with ONDNTA. In each of the STMBMS experiments with RDX, this set of products is observed during the later stage of each experiment when the rates of reaction are increasing in an "autocatalytic-like" manner. During the later stages of the STMBMS experiments reactions are observed to occur on the surface of the RDX particles. This is consistent with the growth of an orange-colored film on the surface of the RDX particles (Figures 4 and 5) and the roughened appearance of the surface of the RDX particles located on the outer surface of the agglomerated sample (SEM pictures, Figure 6). Thus, the reaction process during the later stages of each experiment is dominated by the reactions of ONDNTA and its decomposition intermediates on the surface of the RDX particles.

The reaction intermediates formed in the decomposition of ONDNTA, NVR(dynamic) and NVR2(dynamic), are referred to as dynamic because these intermediates are not true compounds but are actually mixtures of remnants from decomposed RDX and ONDNTA molecules that most likely link to form a nonvolatile residue. The nature of these NVR intermediates changes during the course of the decomposition process and thus may be referred to as dynamic.

The NVR(dynamic) intermediate located on the surface of the RDX particles can react with RDX at the interface to form more ONDNTA and lead to an accelerating rate of reaction (Pathway Ps5), as observed during the STMBMS experiments. As the decomposition process progresses this reaction pathway leads to the accumulation of NVR(dynamic) on the surface of the RDX particles. The accumulation of NVR(dynamic) on the surface of the RDX particles and the accelerating rate of reaction observed during the course of an experiment leads to the question of how NVR(dynamic) interacts with the RDX.

To answer this question, an experiment in which RDX was transported through the gas phase to the surface of the NVR was conducted. In a sequence of RDX decomposition steps, NVR was accumulated on the bottom of the STMBMS reaction cell. Once the exposed surface area of the NVR achieved a constant value the rate of reaction also attained a constant value (Figure 9). Thus, the rate of reaction of RDX with the NVR is limited by the surface area of the NVR. The increasing depth of the NVR does not result in an increased rate of reaction with RDX, indicating that the reaction between the NVR and the RDX occurs either on the surface of the NVR or in a near subsurface region of the NVR. These results confirm that the accelerating rate of reaction is due to the accumulation of NVR(dynamic) on the surface of the RDX particles. However, the results also suggest that the dissolution of RDX into the NVR film may be limited to a thin layer of the NVR(dynamic) near the NVR/RDX interfacial boundary.

The formation of the NVR(dynamic) film on the surface of the RDX particles leads to the formation of new region on the surface of the RDX particles, located between the NVR(dynamic) film and a boundary of the RDX particle that still retains its crystalline properties. This region can be considered a thin film of RDX mixed with decomposition products to form a liquid solution. A new set of reaction pathways may occur in this thin film region as indicated by Pathway Pl1 in Scheme 2. The reaction pathways available for decomposition of RDX in this region are those associated with the decomposition of RDX in the liquid phase (Scheme 1). The accelerating rate of reaction that is expected from the liquefaction of the RDX is most pronounced in the experiment in which the temperature of the sample approaches the melting point of RDX (Exp. IV).

The reaction processes outlined in Scheme 2 can be affected by the pressure of gases surrounding the RDX particles. This difference may be observed by comparing the location of the growth of the NVR in the STMBMS experiments (Figure 5) with its growth in the hot-stage experiment (Figure 4). In the STMBMS experiment the lower gas pressure allows greater movement of both RDX and its decomposition products in the sample. This leads to the redeposition of RDX and its decomposition products in regions between original RDX particles. Decomposition via the RDX particle surface reactions (Pathways Ps1−Ps5) occurs initially in these regions. In contrast, the higher gas pressure (0.237 MPa of gaseous decomposition products in the microreactor) used in the hot-stage experiments limits gas-phase transport of RDX and its decomposition products, resulting in a more uniform formation of the NVR(dynamic) film on the surface of the RDX particles.

In the series of experiments conducted by Batten[17−21] the rate and kinetics of the decomposition of RDX below the melting point were influenced by the RDX sample geometry. The effect was attributed to interactions between gaseous decomposition products and the remaining solid RDX sample. At later stages in the decomposition, localized liquefaction of the remaining RDX is also noted for samples originally packed within small sample tubes, while for samples initially spread over the bottom of the large reaction flask, uniform liquefaction is observed throughout the sample. In both cases, the samples are maintained below the melting point of RDX and the liquefaction is attributed to formation of an intermediate that combines with RDX to form a solution with a lower melting point than RDX. Results from these experiments also indicated formation of a colored NVR that acted as a positive catalyst for the decomposition. Experiments using NO as a backfilling gas also showed a positive catalyst effect. These results are consistent with the decomposition pathways determined in the present experiments and summarized in Scheme 2. The increased rate of reaction due to the addition of NO can be attributed to increased rate of reaction Pg2 and a more rapid accumulation of ONDNTA on the RDX sample. Their observation of the appearance of a colored residue is consistent with reactions that occur on the surface of the RDX particles via pathways Ps2−Ps5. The observed liquefaction late in the experiments can be attributed to the pathway Pl1 in Scheme 2 that opens the reaction pathways associated with decomposition of RDX in the liquid phase (Scheme 1). Once the RDX becomes molten, NO may dissolve in the molten mixture and increase the rate of decomposition of the sample via reaction pathway P3 in Scheme 1.

Conclusions

The decomposition of RDX below its melting point has been examined. Gas-phase reactions are predominant in the early stages of an experiment. Reactions in the gas phase are similar to those previously observed for RDX in the liquid phase above its melting point. These reactions include the formation of OST, *s*-triazine, H_2O, NO, and NO_2 via the elimination of HONO and HNO from an RDX molecule and the formation of ONDNTA and NO_2 via an NO replacement reaction with RDX.

ONDNTA decomposes to form predominantly CH_2O and N_2O. NH_2CHO may also be formed in the gas-phase decomposition of ONDNTA.

In our STMBMS experiments, products from the gas-phase reactions, such as ONDNTA and formamide, condense along with RDX on the surface of the RDX particles and in regions between the RDX particles. This mixture of compounds on the surface of the RDX particles opens new reaction pathways that occur on the surface of the particles. The deposited material initially nucleates and grows in reactive islands on the surface of the particles. Reactions are more likely to occur on the surface of particles located in areas of the sample surface that are exposed to larger volumes containing RDX vapor, which can decompose.

The reactions on the surface of the particles lead to the formation of a colored nonvolatile residue on the surface of the RDX particles. At lower pressures, diffusion in the gas phase is greater and leads to the deposition of RDX and the decomposition products in regions separate from the original particles, where the NVR is observed to grow first. At higher pressures (0.1−0.2 MPa), diffusion of RDX and the decomposition products is limited due to the surrounding gas and they are confined in a region close to the RDX surface, which results in the growth of a more uniform film of NVR on the surface of the RDX particles.

The NVR reacts directly with RDX and leads to a range of different decomposition products, of which CH_2O and N_2O are the most prevalent. RDX decomposes most rapidly when it is contact with the NVR. Reaction between RDX and the NVR can occur via either transport of RDX through the gas phase to the surface of the NVR or at the boundary between the NVR and the RDX on the surface of the RDX particles. It is possible that the RDX may react not only at the surface of the NVR but may also dissolve and react within a layer below the NVR surface.

The NVR is a dynamic mixture in which its constituents change during the course of the decomposition process. During the course of an experiment, RDX reacts with the NVR to form ONDNTA, which in turn decomposes to form gaseous products and add more material to the NVR. There is competition between reaction processes involving RDX and the NVR and the decomposition of the NVR by itself. This competition manifests itself in the increased rate of release of compounds with high levels of hydrogen, such as $(CH_3)_2NNO$, $(CH_3)_2$-NCHO, and $(CH_3)_3N$, when the RDX nears depletion at the end of an experiment. This suggests that the structures in the NVR that lead to the formation of these compounds may be involved in the reaction between RDX and the NVR.

As the temperature of the RDX powder nears the melting point of RDX, regions of the sample become molten, probably in the vicinity of the NVR, and the reaction process more closely resembles that observed during the decomposition of RDX in the liquid phase. Thus, at temperatures well below its melting point, the decomposition of RDX is controlled initially by sublimation of RDX and its decomposition in the gas phase and later by reactions with the NVR in localized regions on the surface of the RDX particles.

Acknowledgment. The authors thank L. Johnston for assistance with running experiments and collecting the data, D. Wiese-Smith and G. A. Goelzer for assistance in quantifying the experimental data. J. Woods, S. Mack, and K. Anderson for assistance in developing the modified reaction cell and flow rate calibration procedures. M. Kennedy for collecting the hot-stage microscopy data, N. Yang and J. Chames for the SEM micrographs, and Huffman Laboratories of Golden, CO, for the quantitative C/H/N microanalysis of the RDX NVR. This research was supported by the U.S. Army Research Office Project 43381-CH and a joint Memorandum of Understanding between the Department of Defense Office of Munitions and the U.S. Department of Energy.

References and Notes

(1) Robertson, A. J. B. *Trans. Faraday Soc.* **1949**, *45*, 85.
(2) Cosgrove, J. D.; Owen, A. J. *Chem. Commun.* **1968**, 286.
(3) Schroeder, M. A. Critical Analysis of Nitramine Decomposition Results: Some Comments on Chemical Mechanisms. In *16th JANNAF Comb. Mtg.*; Chemical Propulsion Information Agency, 1979; Vol. 308, II., p 17.
(4) Schroeder, M. A. Critical Analysis of Nitramine Decomposition Data: Activation Energies and Frequency Factors for HMX and RDX Decomposition. In *17th JANNAF Comb. Mtg.*; Chemical Propulsion Information Agency, 1980; Vol. 329 , II., p 493.
(5) Schroeder, M. A. Critical Analysis of Nitramine Decomposition Data Product Distributions From HMX and RDX Decomposition. In *18th JANNAF Mtg.*; Chemical Propulsion Information Agency, 1981; Vol. 347, II., p 395.
(6) Adams, G. F.; Shaw, R. W. *Annu. Rev. Phys. Chem.* **1992**, *43*, 311.
(7) Melius, C. F. *J. Phys.* **1987**, *c4*, 341.
(8) Chakraborty, D.; Muller, R. P.; Dasgupta, S.; Goddard, W. A. *J. Phys. Chem. A* **2000**, *104*, 2261.
(9) Zhao, X.; Hintsa, E. J.; Lee, Y. T. *J. Chem. Phys.* **1987**, *88*, 801.
(10) Behrens, R.; Bulusu, S. *J. Phys. Chem.* **1992**, *96*, 8877.
(11) Behrens, R.; Bulusu, S. *J. Phys. Chem.* **1992**, *96*, 8891.
(12) Behrens, R.; Bulusu, S. The Importance of Mononitroso Analogues of Cyclic Nitramines to the Assessment and the Safety of HMX-Based Propellants and Explosives. In *Challenges in Propellants and Combustion 100 Years after Nobel*; Kuo, K. K., Ed.; Begell House, Inc.: New York, 1997; p 275.
(13) Brill, T. B.; Brush, P. J.; Kinloch, S. A.; Gray, P. *Philos. Trans. R. Soc. London, Ser. A* **1992**, *15*, 377.
(14) Long, G. T.; Vyazovkin, S.; Brems, B. A.; Wight, C. A. *J. Phys. Chem. B* **2000**, *23*, 2570.
(15) Cosgrove, J. D.; Owen, A. J. *Combust. Flame* **1974**, *22*, 13.
(16) Cosgrove, J. D.; Owen, A. J. *Combust. Flame* **1974**, *22*, 19.
(17) Batten, J. J. *Austr. J. Chem.* **1972**, *25*, 2337.
(18) Batten, J. J.; Murdie, D. C. *Austr. J. Chem.* **1970**, *23*, 737.
(19) Batten, J. J.; Murdie, D. C. *Austr. J. Chem.* **1970**, *23*, 749.
(20) Batten, J. J. *Austr. J. Chem.* **1971**, *24*, 945.
(21) Batten, J. J. *Austr. J. Chem.* **1971**, *24*, 2025.
(22) Bradley, J. N.; Butler, A. K.; Capey, W. D.; Gilbert, J. R. *J. Chem. Soc., Faraday Trans. I* **1977**, *73*, 1789.
(23) Behrens, R. Thermal Decomposition Processes of Energetic Materials in the Condensed Phase at Low and Moderate Temperatures. In *Overviews of Recent Research on Energetic Materials*; Shaw, R. W., Brill, T. B., Thompson, D. L., Eds.; World Publications Inc., 2005.
(24) Behrens, R., Jr. *Rev. Sci. Instr.* **1987**, *58*, 451.
(25) Behrens, R., Jr. *Int. J. Chem. Kinet.* **1990**, *22*, 135.
(26) Behrens, R., Jr. *Int. J. Chem. Kinet.* **1990**, *22*, 159.
(27) Behrens, R.; Minier, L.; Bulusu, S. Coupling Experimental Data and a Prototype Model to Probe the Physical and Chemical Processes of 2,4-Dintiroimidazole Solid-Phase Thermal Decomposition. In *34th JANNAF Combustion Subcommittee Meeting*; CPIA, Ed.; CPIA Publication # 662: West Palm Beach, FL, 1997; Vol. 1, p 549.
(28) Anderson, K.; Homsy, J.; Behrens, R.; Bulusu, S. *11th International Detonation Symposium* **1998**, *1*, 239.
(29) Behrens, J., R.; Bulusu, S. *29th JANNAF Combustion Meeting* **1992**, *CPIA Publ. 573, Vol. II*, 453.

Presented at the JANNAF Combustion Subcommittee & Propulsion Systems Hazards Subcommittee Meetings, Charleston, South Carolina, June, 2005.

Reaction Kinetics of RDX in the Condensed Phase. *

Richard Behrens and Deneille Wiese-Smith
Combustion Research Facility
Sandia National Laboratories
Livermore, CA 94551-0969

Abstract

The reaction processes that control the thermal decomposition of RDX in the condensed phase are complex, nonlinear and spatiotemporally dependent. The rate controlling processes are significantly different below and above its melting point (~200°C). A combination of simultaneous thermogravimetric modulated beam mass spectrometry (STMBMS) experiments and a new reaction modeling and kinetics (REMKIN) compiler and analysis tool are used to probe the underlying reaction processes and develop mathematical models representing the reaction kinetics of RDX. First, a relatively simple model describing the decomposition of RDX below its melting point is described. It incorporates both gas-phase reactions and reactions on the surface of the RDX particles. Parameters for this model are obtained from STMBMS experiments in which the RDX is cycled between 145°C and 185°C at a heating rate of ±0.05°C/min. Next, the underlying reaction processes that control the thermal decomposition of RDX above its melting point are described. Results from experiments with RDX, in which the sample is heated at rates of 5 and 10°C/min, show clear temporal separation of the products associated with different pathways in the RDX reaction scheme[1] and provide new insight into the underlying reaction processes. When combined with results on the thermal decomposition of hexahydro-1-nitroso-3,5-dintro-s-triazine (ONDNTA), an improved understanding of the reaction processes that control the creation and decomposition of the ONDNTA intermediate in the RDX decomposition process is obtained. Finally, the REMKIN compiler and analysis tool is used to incorporate these new reaction features into mathematical models that characterize the decomposition of RDX in the liquid phase. The issues associated with postulating and testing new reaction schemes and optimizing the parameters of the underlying reactions are discussed. The combination of STMBMS experiments and REMKIN analysis provide a new means to develop insight into the reaction processes that occur in the condensed phase.

INTRODUCTION

One of the unresolved challenges in the propellant community has been to understand the reaction processes that control the decomposition of nitramine-based propellants in the condensed phase. An improved understanding of these processes will provide a sound technical basis for developing better performing and safer propellants. Two specific areas of propellant development will benefit. One area is the development of new ingredients that can be used as burn rate modifiers to tailor the pressure dependence of propellant burn rates. The other area is safety assessment of propellants in fires and other abnormal thermal environments.

Developing burn rate modifiers for nitramine-based propellants has been a largely unmet challenge. The ingredients that have been used successfully as burn rate modifiers for double-base propellants have also been examined for use in nitramines-based propellants and were found ineffective. Development of burn rate modifiers for nitramine-based propellants will require understanding the reaction processes that

* Research supported in part by the U.S. Army Research Office, under contract No. 43381-CH, and the U.S. Department of Energy under Contract No. DE-AC0494AL85000.

occur on the surface of burning propellants and how these processes may be altered with the addition of other ingredients. The main scientific issue involves understanding the reaction processes that occur in the liquid phase that is created on the surface of a burning propellant and how these processes relate to and influence the overall combustion process.

In the area of propellant safety, the main issue focuses on the physical and chemical changes that occur in the propellant when it is heated and how these changes affect the time to ignition of the propellant and the nature of the subsequent combustion processes in the thermally damaged material. For example, it has been shown that as AP-based propellants undergo thermal decomposition in an elevated thermal environment,[2-4] there are significant changes that occur in the morphological structure of the propellant that accompany the thermal decomposition process. The main scientific issues in this case involve understanding the decomposition processes that occur in the solid phase of the ammonium perchlorate (AP) and reactions of its decomposition products with the binder.

While these issues have been at the forefront of concerns in the propellant community over the past several decades, limited progress has been made on understanding these issues due to the high level of difficulty in probing reaction processes in the condensed phase. This difficulty arises for several reasons.

First, the processes that occur during the decomposition of energetic materials in the condensed phase are most often complex, coupled and nonlinear. The close proximity of the reactants with their decomposition products create conditions in which spatiotemporal features can play an important role in determining the rates of reaction. These spatiotemporal features may range from creation of bubbles of gaseous products dispersed in a liquid on the surface of a burning propellant to the nucleation and growth of reactive regions in solid ingredients such as AP or HMX. In addition, more traditional spatiotemporal effects associated with diffusion-limited reactions are more likely to play a role in condensed-phase reactions.

Second, it is difficult to create experiments that can probe the details of reactions that occur in the condensed phase. In many cases only the global thermal behavior of the condensed phase can be monitored, leaving the nature of the underlying chemical reactions and physical processes to speculation and hypotheses. Furthermore, it is quite difficult to isolate the underlying physical or chemical processes for individual studies, as is often done in the study of gas phase reactions (e.g., examination of reactions in flow tubes, flames or shock tubes). Thus, progress on understanding the decomposition of energetic materials in the condensed phase has been slow.

We have developed new methods over the past 20 years to examine the thermal decomposition of energetic materials in the condensed phase. A summary discussing the main issues and our approach to understanding these complex processes will appear in the near future.[5] These methods utilize a unique combination of mass spectrometry and thermogravimetric analysis measurements and employ a set of numerical algorithms to extract basic information on the underlying decomposition processes from the data.[6-8]

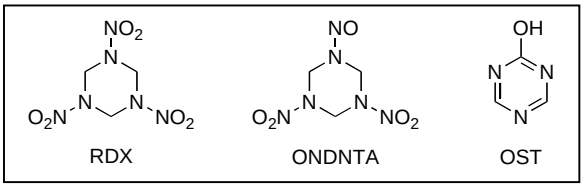

The ultimate goal of our studies of energetic materials is to identify the set of underlying rate-limiting processes that control their decomposition and to formulate mathematical representations of these processes that can be used to predict their behavior over a range of environmental conditions. Most of our previous work has focused on identifying the underlying reactions and physical processes that control the decomposition of different types of energetic materials. For almost all of the compounds examined, the decomposition was controlled by a set of complex coupled nonlinear reaction processes. In all cases, spatiotemporal processes played an important role in controlling the decomposition of these materials.

An example of the reaction processes that occur in the thermal decomposition of RDX and HMX is illustrated in Figure 1. The experimental results that form the basis for the conceptual framework developed to characterize the decomposition processes have been described previously[1]. After the initial conceptual framework was developed, a notional framework of environmental conditions (pressure

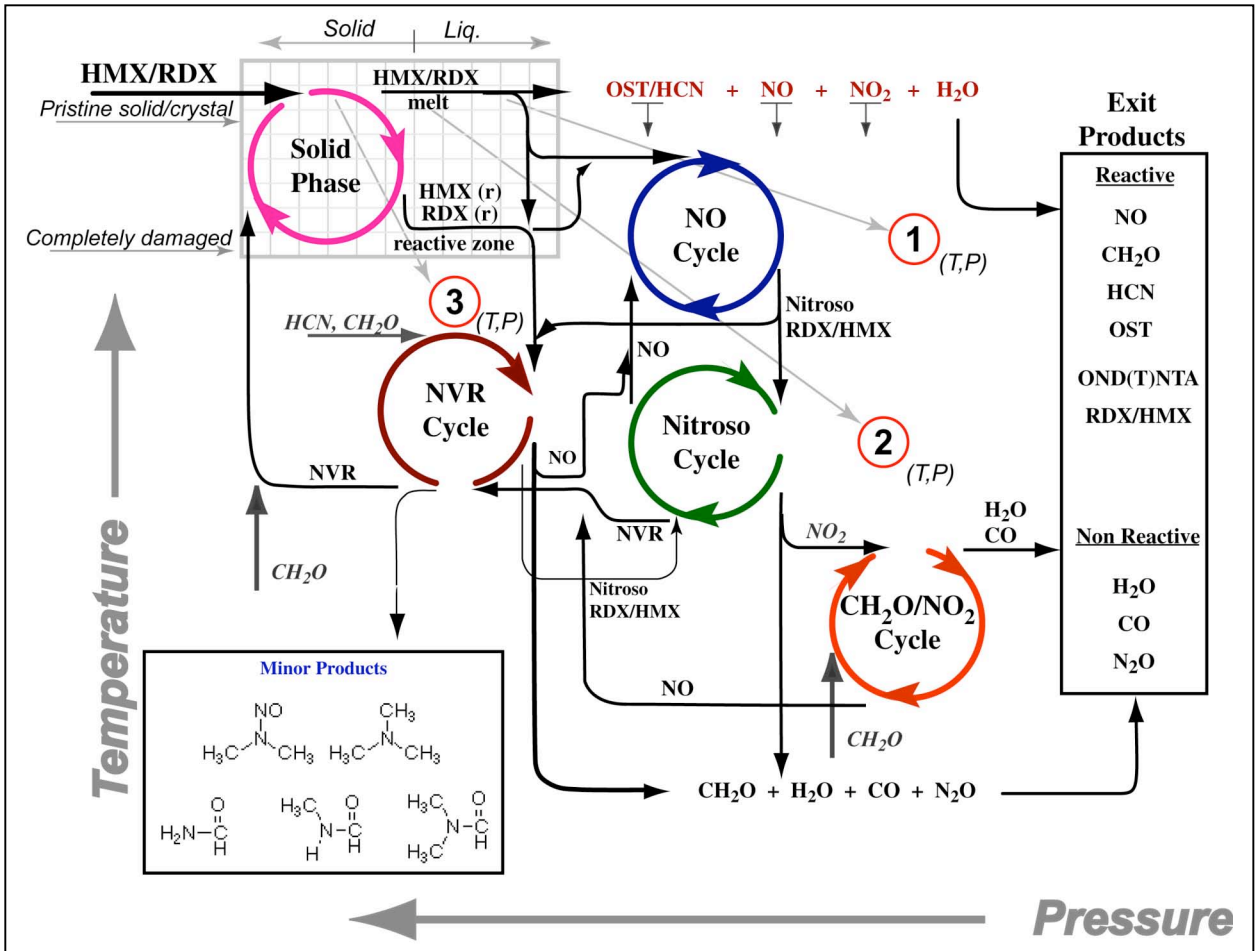

Figure 1. Reaction scheme representing the processes that can control the decomposition of RDX and HMX over a range of conditions. The temperature and pressure coordinates provide a notional view of which reactions will contribute most significantly under different sets of pressure and temperature conditions. Exit and minor products are measured in STMBMS experiments.

and temperature) was superimposed on the reaction network, which provides insight into how different experimental conditions will affect the dominant reaction pathways[9]. Once this notional framework describing the main processes involved in the thermal decomposition of RDX and HMX was established, a new reaction modeling and kinetics (REMKIN) compiler and analysis tool was developed to enable the creation and refinement of mathematical model to characterize these processes[10]. Initially, REMKIN was used to develop a relatively simple model of RDX decomposition in the liquid phase[11]. While this model captured the general features of the main reaction cycles shown in Fig. 1, it did not include reactions of RDX in the gas or solid phase, or the more specific details of the ONDNTA and NVR reaction cycles. Furthermore, in developing mathematical models of the decomposition of RDX in the liquid phase in the previous paper, it became readily apparent that the reactions of RDX, under the reaction conditions of the selected STMBMS experiments (i.e., isothermal, approximately 5 to 15°C above the melting point), involved contributions from two separate liquid phase regions. One region is the RDX sample when it melts. The other region is the accumulation of a liquid mixture of RDX and its decomposition products that adhere to the wall of the reaction cell.

In this paper we examine the details of the processes that control the decomposition of RDX beyond our previous efforts[11]. First, new results on the decomposition of RDX below its melting point are presented. The low reaction rates associated with the decomposition of RDX in the solid phase allow contributions from gas-phase reactions to be observed and characterized. Second, results from higher heating rate experiments with RDX in the liquid phase are presented. These results clearly illustrate the

reaction sequence as captured in Fig. 1 and demonstrate that the reaction process at higher heating rates is not significantly influenced by the accumulation of a separate liquid phase as observed in lower temperature isothermal experiments. The results from these higher heating rate experiments with RDX clearly show the major role that the NO cycle, ONDNTA cycle and NVR cycle play in controlling the decomposition of RDX. The minor products (Fig. 1) have clear and distinct behaviors in the liquid phase experiments and raise the question of how they are formed in the reaction process. To address this question, we draw on results from STMBMS experiments examining the decomposition of ONDNTA, by itself. Finally, we present an initial REMKIN model characterizing these new aspects of the decomposition process.

RDX DECOMPOSITION PROCESSES

The reaction network shown in Fig. 1 illustrates the complex and coupled nature of the processes that control the decomposition of RDX and HMX. The five circles on the diagram represent major decomposition processes that may occur. The main chemical reaction pathways include the direct reaction to form oxy-s-triazine (OST), the reaction of NO to form the mononitroso analogue of the reactant (RDX or HMX) and the reaction of CH_2O and NO_2 (the main exothermic reaction). The other two cycles, the nonvolatile residue (NVR) cycle and the solid phase cycle are more complex and represent chemical, physical and spatial (morphological) features that play roles in controlling the decomposition processes. Details on the nature of the these reaction cycles and the experimental basis for these results have been reported previously[12, 13].

DECOMPOSITION OF RDX BELOW ITS MELTING POINT

The decomposition of RDX below its melting point provides insight into two issues: (1) reactions of RDX in the gas phase, and (2) how reactions start and propagate in the condensed phase[14]. The experiments are conducted with pure reduced sensitivity RDX (RS-RDX) manufactured by SME Groupe SNPE, France. The experiments were conducted using the standard STMBMS experimental procedures.

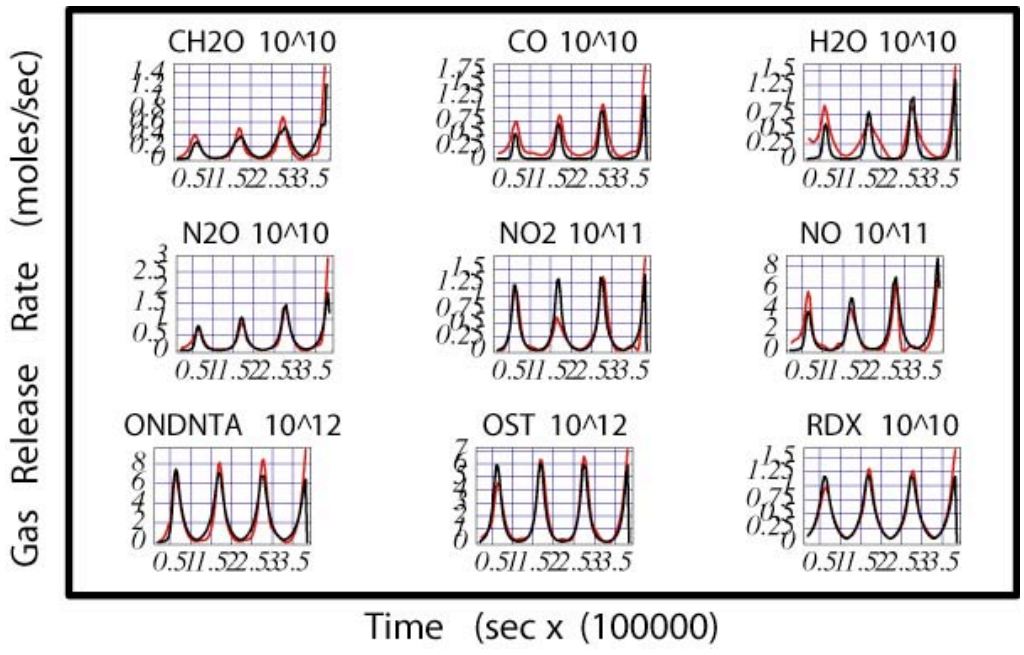

Figure 2. Rate of release of gaseous products during the decomposition of an RDX sample as it is heated between 145°C and 185°C at ±0.05°C/min. Data from STMBMS experiments (red); model (black). Species and scaling factor listed above each graph.

To provide more information on the temperature dependence of the underlying reaction processes, the temperature of the sample is cycled between two temperature limits in the STMBMS experiments. For experiments with RDX below its melting point, the sample is cycled between 145°C and 185°C at a heating rate of ±0.05°C/min. The sample is maintained at a temperature of 185°C for 1000 seconds between heating and cooling cycles. The rate of evolution of the various products from a decomposition experiment using a 6.17 mg sample of RDX in a reaction cell fitted with a 10.5 µm diameter orifice is shown in Fig. 2.

A relatively simple model (Fig. 3) has been created to characterize the main decomposition processes that occur in RDX below its melting point. The reaction conditions for the experiment are illustrated in the cross section of the reaction cell. The sample decomposes within the reaction cell and gaseous products evolve and are detected in the STMBMS experiments. The model includes reactions that occur in both the gas phase and on the surface of the RDX particles. Reactions on the surface of the RDX particles commence only after products formed in the gas phase deposit on the surface of the RDX particles. Reaction processes that are related to the gas phase include: (1) sublimation and condensation of RDX (R1 & R2), (2) decomposition of RDX to oxy-s-triazine (OST), H_2O, NO, NO_2 and N_2O via loss of HONO and HON (R3), (3) formation of hexahydro-1-nitroso-3,5-dinitro-s-triazine (ONDNTA) by the reaction of NO with RDX (R4), (4) the decomposition of ONDNTA (R5), and the reaction of CH_2O and NO_2 (R6). The polyH2CN species made in reaction R5 deposits on the surface of the RDX particles along with ONDNTA. The ONDNTA establishes a quasi-two-phase equilibrium between the gas phase and surface of the RDX particles (R6 & R7). Reaction between the non-volatile residue (NVR), which in this case is denoted as polyH2CN, and RDX lead to the formation of more ONDNTA on the surface of the RDX particles (R8). Finally, the ONDNTA is allowed to decompose on the surface of the RDX particles (R9) forming gaseous products and more NVR. This relatively simple reaction scheme captures the main reaction cycles previously identified in the RDX decomposition process (Fig. 1). The differential equations representing the rate of formation of each species in the model are created and solved

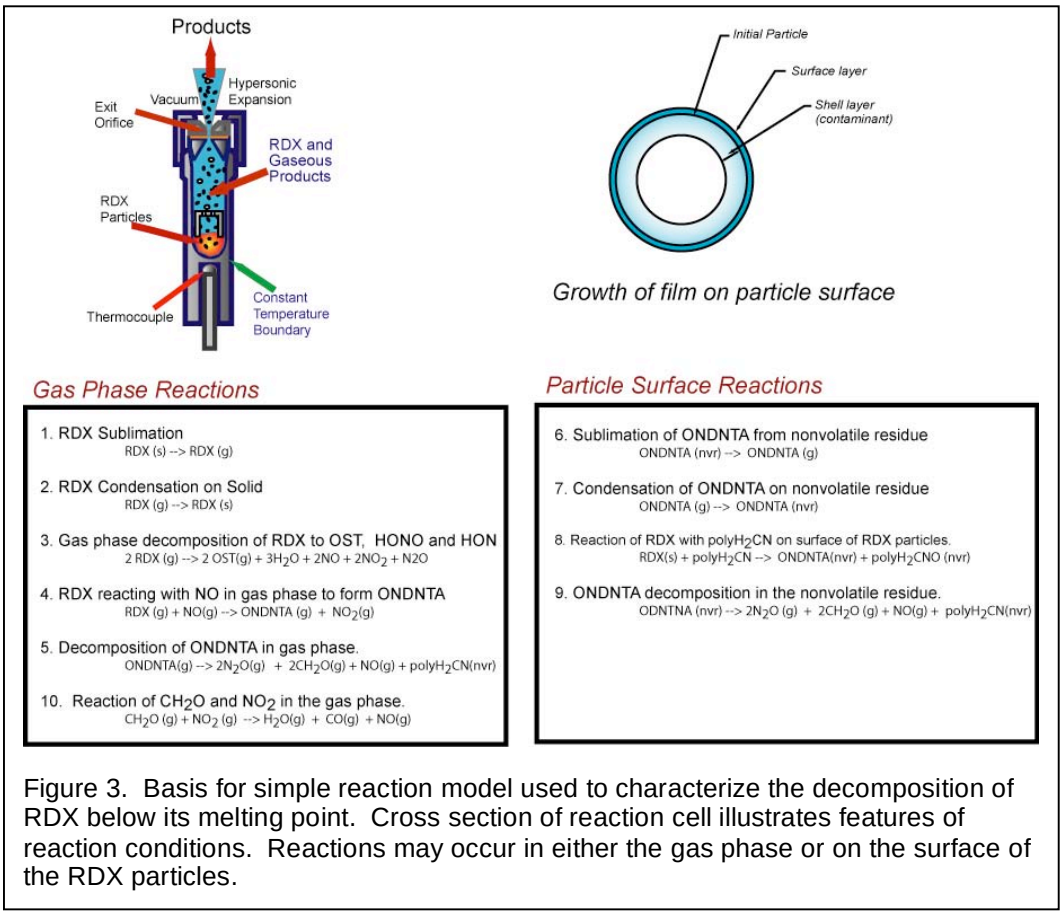

Figure 3. Basis for simple reaction model used to characterize the decomposition of RDX below its melting point. Cross section of reaction cell illustrates features of reaction conditions. Reactions may occur in either the gas phase or on the surface of the RDX particles.

numerically. The parameters, which represent the kinetics for each reaction, are optimized by minimizing the difference, in a least-squares sense, between values predicted by the model and the STMBMS data for each species.

This simple model fits the experimental results relatively well. The model captures the sublimation of RDX and the direct decomposition of RDX in the gas phase to OST and the associated HONO/HON products very well. The model also captures: (1) the formation of ONDNTA and its decomposition products and (2) the development of spatiotemporal reactions on the surface of RDX particles, which cause the reaction rate of the sample to increase as time progresses in the experiment. The features not captured very well are the rates of evolution of CH_2O, N_2O and ONDNTA as the sample is first heated to 185°C. This suggests that something may be different about the RDX located on the outer layers of the particles comprising these RS-RDX powders.

These measurements may be the first to have resolved the direct thermal decomposition of RDX in the gas phase (R3). The Arrhenius parameters for this reaction were optimized using the second and third heating cycles and the values are: A3 = 2.0×10^7 and Ea3 = 93 kJ/mol. The other parameters used in the model are listed in Table I.

Table I. Parameters for model of RDX decomposition below melting point.

Number	Reaction	A	Ea or B
1	RDX Sublimation*	16.075	6600
2	RDX Condensation on Solid RDX		
3	Gas phase RDX Decomposition to OST + HONO + HON	1.98E+07	92.6
4	Reaction of RDX with NO to form ONDNTA in the gas	2.00E+11	40
5	Decomposition of ONDNTA (g) to N2O, CH2O, NO & polyH2CN	1.00E+16	146.5a
6	Sublimation of ONDNTA from residue*	17.406	7617
7	Condensation of ONDNTA on the Nonvolatile residue		
8	Reaction of RDX with NVR	4.00E+16	146.5a
9	ONDNTA Decomposition in NVR to CH2O, N2O, NO and POLYH2CN	7.90E+11	146.5a
10	CH2O + NO2 gas phase reaction	9.20E+16	80

* Log10 (P) = A - B/T(K); pressure in Pascals
a: Parameter not optimized.

DECOMPOSITION PROCESSES OF RDX IN THE LIQUID PHASE

While examining reactions of RDX below its melting point provides new insight into the gas phase reactions of RDX and how products from these gas-phase reactions open new reaction pathways on the surface of the RDX particles, better insight into the details of the various cycles in the reaction process (Fig. 1) is gleaned by examining the reaction of RDX above its melting point, using experiments with higher rates of heating than we have used in the past. The rates of evolution of the gaseous products from RDX heated at 5°C/min and 10°C/min are shown in Fig. 4. Pure RS-RDX, manufactured by SNPE, is also used in these experiments.

The results from all three experiments (Fig. 4) show distinct temporal behaviors for different sets of gaseous species evolving from the reaction cell during the course of each experiment. RDX forms the first set. The slope break in the RDX gas evolution rate occurs when the RDX sample melts. In each experiment the slope break occurs at a temperature above the RDX melting point (~200°C) indicating that the temperature of the RDX powder lags the temperature of the reaction cell.

The second set of gases includes: OST, NO, NO_2 and water. This set is characterized by a rapid rate of rise after the RDX melts. The OST product is most representative of this group. The products in this group come from the unimolecular decomposition of RDX. This reaction is similar to the direct decomposition of RDX in the gas phase.

The third set of products includes: ONDNTA, H_2O, N_2, CO, CH_2O, and N_2O. The temporal behavior of this set is different from the first order reaction of RDX that forms OST and the other lower molecular weight products. The rate of evolution of the products in this group rises more slowly than OST after the RDX melts. For example, the rate of evolution of ONDNTA rises gradually as its mole fraction in the liquid solution (consisting of RDX, ONDNTA and other less volatile species) increases. Note that the rate of evolution of RDX decreases as its mole fraction in the liquid phase decreases during the course of the experiment. The major products formed during the decomposition, H_2O, N_2, CO, CH_2O and N_2O, also grow gradually during the course of the experiment. This indicates that they are not formed directly from a unimolecular decomposition of RDX, but instead involve the formation of a reaction intermediate and/or reaction of RDX with other products. In general, the temporal behavior of these major gaseous products is correlated with the formation of ONDNTA.

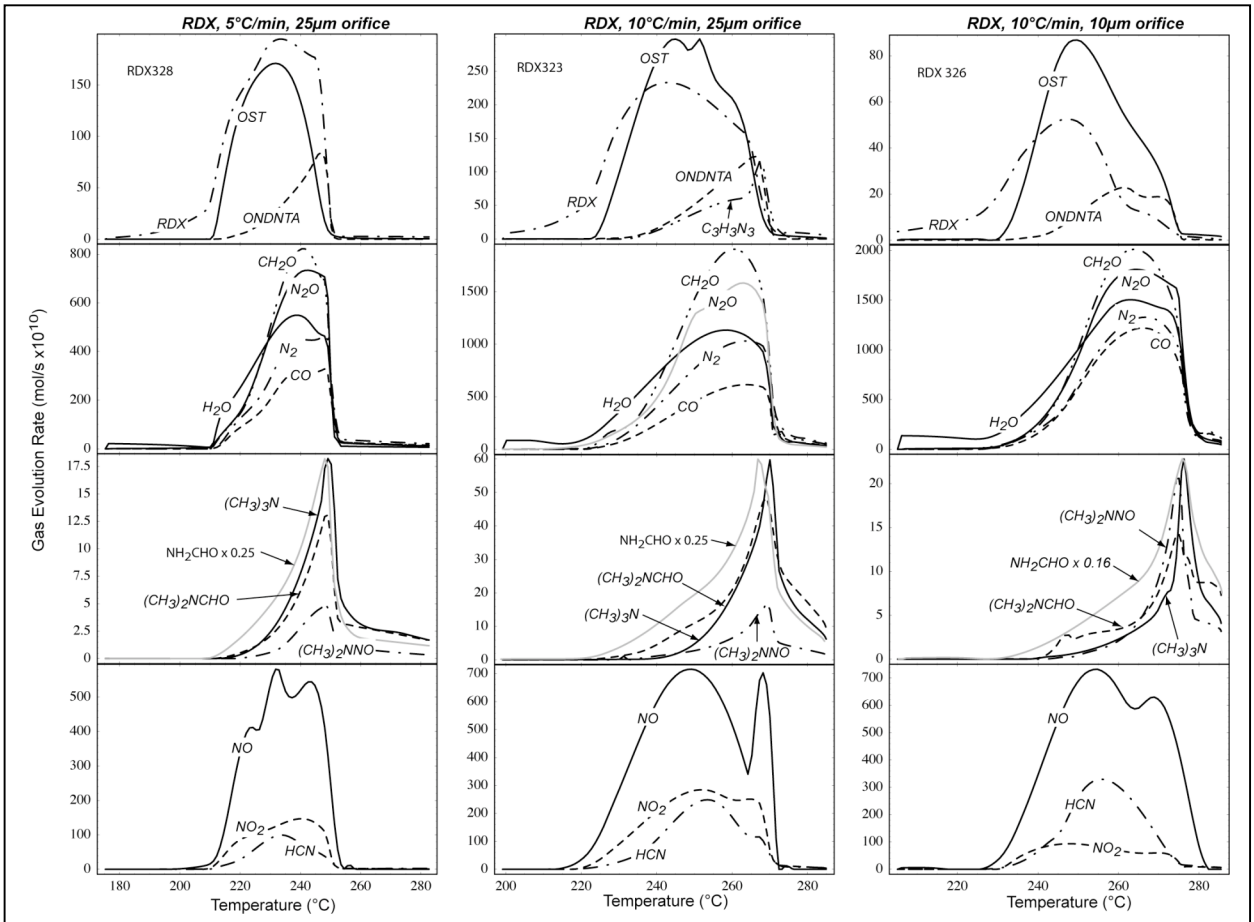

Figure 4. Gas evolution rates of products formed during the decomposition of RDX above its melting point (m.p.~ 200*C). The reaction cell was heated at rates of 5 and 10°C/min in these experiments.

The fourth set of products includes, aziridine (C_2H_5N), formamide (H_2NCHO), N-methylformamide (CH_3NHCHO), N,N-dimethylformamide ($(CH_3)_2NCHO$), dimethylnitrosamine ($(CH_3)_2NNO$) and trimethylamine ($(CH_3)_3N$) or ethylmethylamine ($CH_3CH_2NCH_3$), which are considered the minor products in the overall reaction network (Fig. 1). The temporal behaviors of the products in this group dominate the later stages of the decomposition process during an experiment. These products only start to appear well after the RDX has melted and started to decompose via the direct unimolecular reaction. Furthermore, the rate of evolution of these products from the reaction cell increase most rapidly during the final stage of the experiment. This behavior suggests that these products are engaged in a rather complex reaction scheme involving RDX and/or ONDNTA, in which the intermediate that leads to the formation of the products in this set also interacts, in a competitive fashion, with RDX and/or ONDNTA. Hence, when the amount of RDX, ONDNTA or their decomposition products diminish, the rate of decomposition of the intermediate to form the products in this set increases until the intermediate is also depleted. This behavior is observed in all three experiments. When the pressure of the gases contained in the reaction cell is higher (10°C/min experiment with 10.5μm orifice), the rate of decomposition of the intermediate to the minor products is faster.

It is interesting to examine the temporal behavior of compounds such as HCN or s-triazine ($C_3H_3N_3$) whose structures are similar to OST. One might expect that these compounds are also formed directly from RDX in a manner analogous to OST. However, in these higher heating rate experiments, HCN and s-triazine appear later in the decomposition process along with the other major products (i.e., ONDNTA, CH_2O, N_2O, etc.) and are not correlated with OST. This suggests that either OST may react with the

intermediate products that accumulate during the experiment to form HCN, or the intermediates may react with RDX to form HCN.

DETAILS OF THE NO, ONDNTA AND NVR CYCLES

While the sequence of product evolution in the higher heating rate RDX experiments is captured by the overall reaction scheme shown in Fig. 1, the specific chemical reactions, which are associated with the NO, ONDNTA and NVR cycles and lead to major products (e.g., CH_2O and N_2O) and minor products (e.g., H_2NCHO or $(CH_3)_2NCHO$), require further definition. Furthermore, a pathway to form N_2 is not part of the reaction scheme. To provide further insight into the origin of these species, we examine the decomposition of ONDNTA itself. The details of the methods used to examine its decomposition have been presented previously along with a few examples of selected results[15].

The temporal behavior of the rates of evolution of the gaseous products from the decomposition of ONDNTA under high confinement conditions provides additional insight into the details of the ONDNTA and NVR reaction cycles. The results from two experiments with ONDNTA are shown in Figure 5. In one experiment ONDNTA was heated at 2°C/min and in the other the sample was heated to 120°C and held isothermally.

The evolution sequence of the gaseous products is similar in both experiments. In each case the sample loses most of its original mass in a short period of time. This rapid mass loss is followed first by a more gradual mass loss and then by a short period of more rapid mass loss. The thermogravimetric analysis (TGA) data shows each of these regions for both experiments.

Examination of the ion signals representing each of the decomposition products in these three regions reveals additional detail about the decomposition of ONDNTA. In both experiments the ion signals representing N_2, NO_2, CH_2O, NO, and N_2O all rise very rapidly in the first region. However, the N_2 and NO_2 signals fall off very rapidly compared to the CH_2O, NO and N_2O signals. This behavior suggests that N_2 and NO_2 are rapidly eliminated from ONDNTA, which results in the formation of a new intermediate product. This intermediate then continues to release CH_2O and N_2O. Eventually, it has decomposed to a point at which its rate of decomposition increases and another set of products are formed. This set includes H_2O, N,N-dimethylformamide ($(CH_3)_2NCHO$), dimethylnitrosamine ($(CH_3)_2NNO$) and either

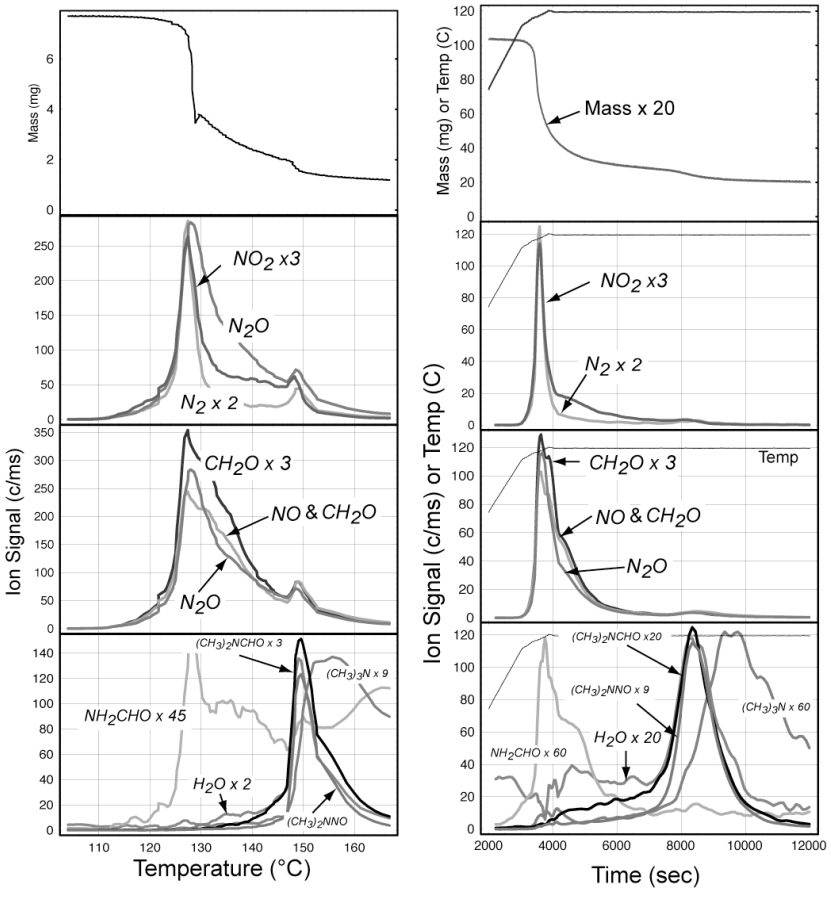

Figure 5. Ion signal from the various products formed during the decomposition of ONDNTA. Reaction cell fitted with 2.5μm diameter orifice.

trimethylamine ($(CH_3)_3N$) or ethylmethylamine($CH_3CH_2NCH_3$). These are the same products observed during the final stage of RDX decomposition above its melting point.

Closer examination of the temporal behaviors of this last set of products in both the decomposition of ONDNTA and RDX shows further similarities. In each case formamide, N,N-dimethylformamide, and dimethylnitrosamine all gradually increase toward the end of the experiments. In each case, as the signals from these products start to decrease the rate of formation of the trimethylamine species increases. Thus, in this stage of the decomposition process there appears to be a competition between the formation of the trimethylamine or methylethylamine product and the formation of the other minor products.

Based on the results from experiments with ONDNTA and RDX, a reaction sequence leading from ONDNTA to the various decomposition products observed in the experiments may be postulated.

The ONDNTA results suggest that the first step in its decomposition is the elimination of N_2 and NO_2. This would leave behind several different types of biradicals as follows:

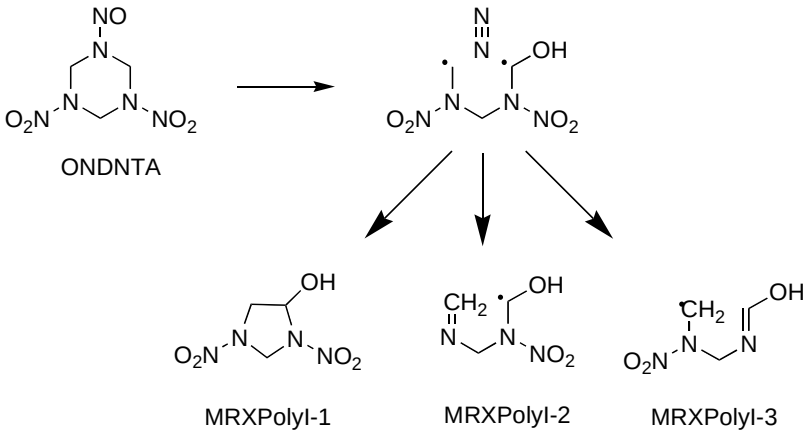

The biradical could possibly reform a ring structure, such as MRXPolyI-1. However, after the rapid release of N_2 and NO_2 from ONDNTA there is no evidence of more complex molecules being released from the sample until later in the experiment. This suggests that the intermediate formed after the elimination of N_2 and NO_2 may link to form a higher molecular weight “polymeric-like” intermediate whose features may be represented as

Polymer-like Intermediate formation

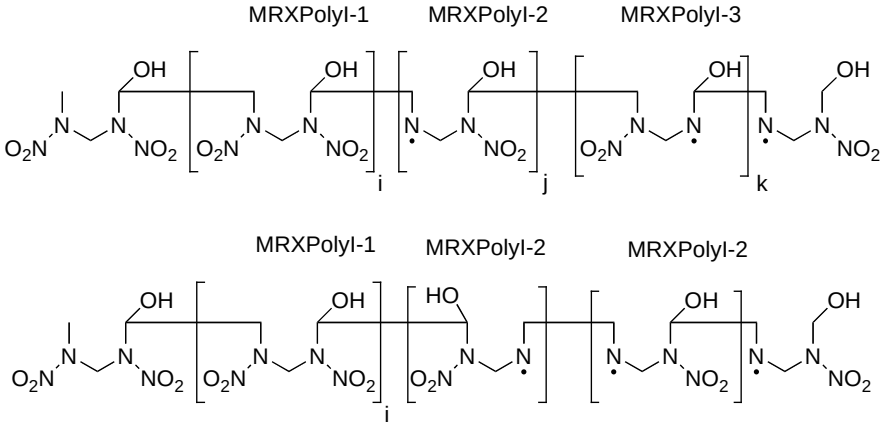

This intermediate provides the means to form more CH_2O and N_2O as it decomposes, as well as provide the molecular framework to form the more complex minor products, which are observed during the final stages of the

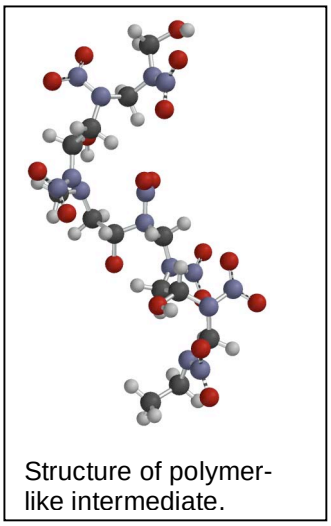

Structure of polymer-like intermediate.

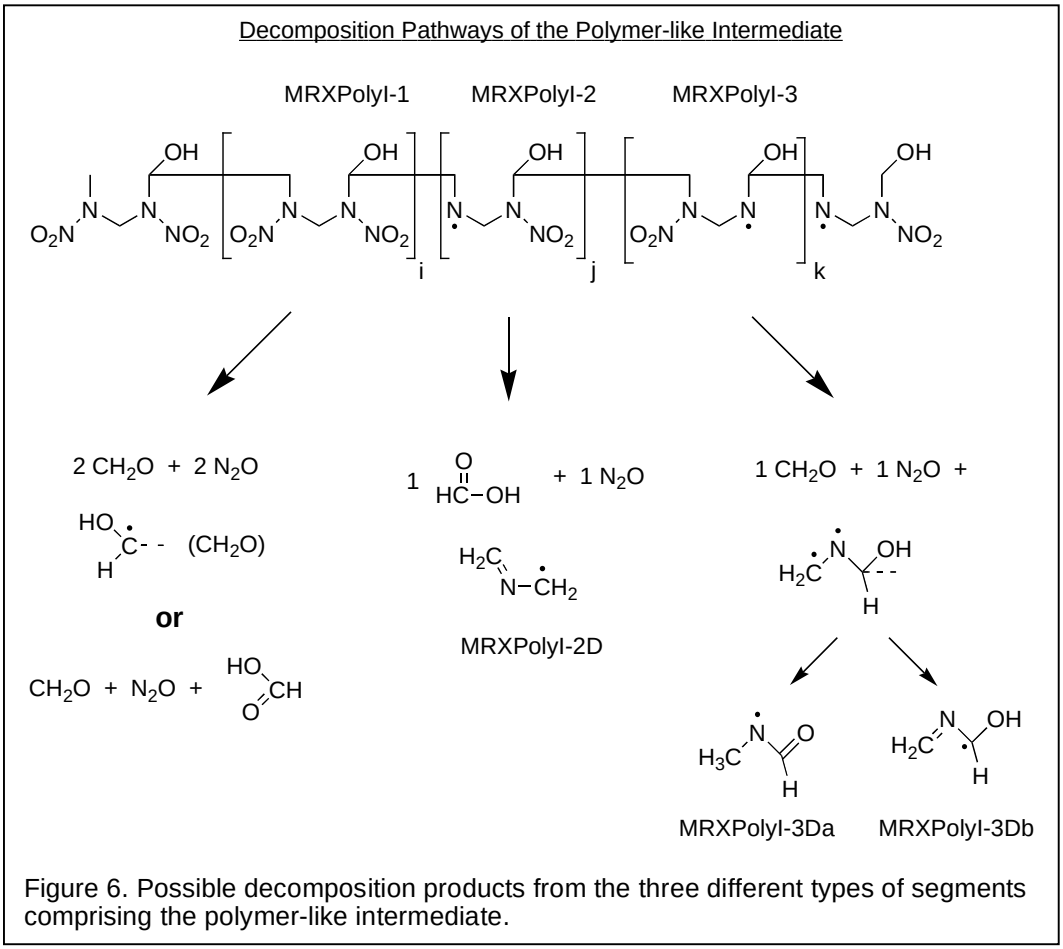

Figure 6. Possible decomposition products from the three different types of segments comprising the polymer-like intermediate.

ONDNTA and RDX decomposition. The various fragments formed from ONDNTA are simply listed at MRXPolyI-1, MRXPolyI-2, and MRXPolyI-3. These fragments may join in various combinations and sequences, creating an intermediate that could readily decompose to the more complex minor products observed in both the ONDNTA and RDX experiments. Molecular mechanics energy minimization[16] provides a structure for the intermediate and illustrates how the intermediate may assume a number of configurations that may lead to many of the observed products. For example, the reaction of CH_2O or NO at the nitrogen radical could lead to the formation of N,N-dimethylformamide or dimethylnitrosamine, respectively. Possible decomposition reactions of each type of segment in the polymer-like intermediate are shown in Figure 6. Each segment may decompose to CH_2O and N_2O plus other types of fragments, such as MRXPolyI-2D or MRXPolyI-3Da.[17] MRXPolyI-3Da may abstract a hydrogen atom to form the N-methylformamide product. In a similar manner, one can envision how these segments may lead to the formation of other minor products formed in the decomposition of ONDNTA and RDX.

Results from isotopic-scrambling experiments using mixtures of ^{14}N and ^{15}N labeled RDX show that there is complete scrambling of the N-NO bond in ONDNTA during the early stages of the experiments, but incomplete scrambling of the bond during the later stages.[18] This suggests that as the NVR accumulates during the course of an experiment, it reacts with RDX to form ONDNTA. The fact that the N-NO bond is not completely scrambled in ONDNTA after NVR is present in the reaction cell indicates that another reaction also leads to ONDNTA, namely the abstraction of an oxygen atom from the NO_2 group by the NVR. A possible mechanism for this reaction, based on one of the polymer-like intermediate fragments, is shown in Fig. 7.

The formation of ONDNTA by reaction with an intermediate segment, such as MRXPolyI-2, involves the transfer of an oxygen atom from an RDX NO_2 group to the relatively reactive CH_2 group on MRXPolyI-2. This results in the formation of a new intermediate, MRXPolyI-2DB. This intermediate may

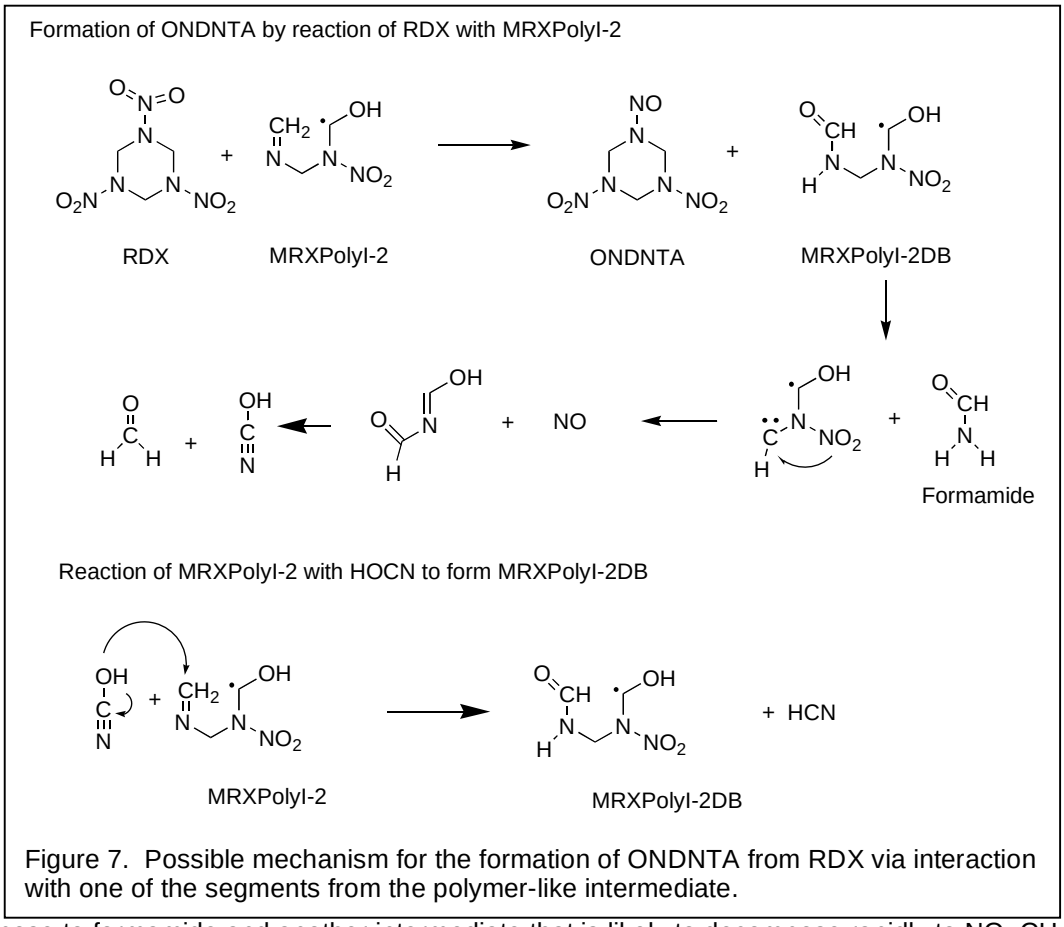

Figure 7. Possible mechanism for the formation of ONDNTA from RDX via interaction with one of the segments from the polymer-like intermediate.

decompose to formamide and another intermediate that is likely to decompose rapidly to NO, CH_2O and HOCN (Fig. 7). This mechanism is consistent with the correlation between the increasing rates of formation of ONDNTA and formamide (H_2NCHO) during the decomposition of RDX (Fig. 4). Formamide is also the most abundant of the minor products that evolve during the later stages of the RDX experiments. The HOCN product may react relatively rapidly with the polymer-like intermediate to form HCN. This reaction pathway may account for the relatively late appearance of HCN during the decomposition of RDX in our experiments.

In summary, the decomposition of ONDNTA via the rapid release of N_2 and NO_2 and the formation of a polymer-like intermediate provides additional features that characterize the non-volatile residue and can be used to construct models of the underlying reaction processes that control the decomposition of RDX.

REACTION MODELS OF RDX IN THE LIQUID PHASE

The REMKIN compiler and analysis tool provides the means to postulate reaction schemes, construct the associated set of differential equations that characterize the reaction scheme, optimize parameters for individual reactions and processes, and compare the results of the simulation with the data from the STMBMS experiments. A schematic overview of this process is shown in Fig. 8 and a general overview of the REMKIN compiler and analysis tool has been presented previously [10, 11].

Using the new results on the decomposition of RDX and ONDNTA, a more comprehensive model of the RDX reaction processes is being developed. Our initial REMKIN modeling effort [11] focused on creating a reaction scheme to characterize the decomposition of RDX in the liquid phase, based on results from RDX experiments conducted at isothermal temperatures 5 to 15°C above the melting point. While these experiments characterized the basic features of RDX decomposition in the liquid phase, a significant portion of the decomposition process involved the formation of material in a separate phase that had reaction characteristics that differed from the liquid phase. Since our initial effort, REMKIN has been expanded to account for reactions in this second phase. However, before tackling this more

complex set of reaction conditions, we focus on characterizing the underlying reactions that control the thermal decomposition of RDX in the liquid phase more thoroughly.

The effort to construct a model of the underlying processes of the decomposition of RDX in the liquid phase is currently in progress. The results presented here summarize the current state of these efforts. The methods used to capture the features of the reaction processes of RDX and ONDNTA, which we have described, show how mathematical models of the underlying reaction processes may be created. Careful comparison of the results of the REMKIN simulations with the results from the STMBMS experiments illustrate how the details of the underlying reactions can be examined and how details of the experimental conditions may be assessed.

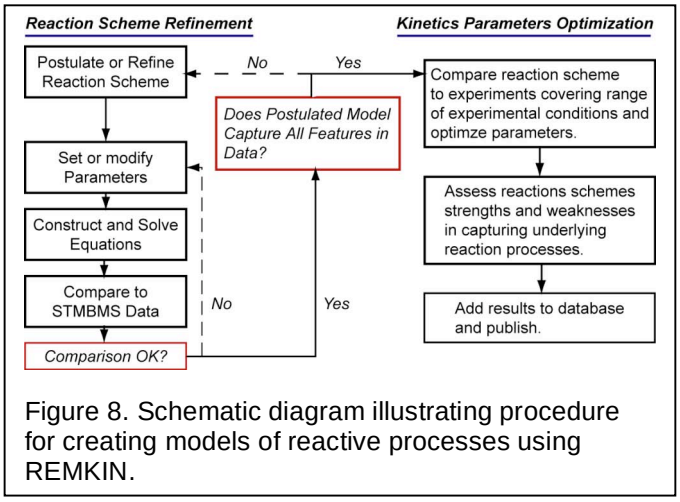

Figure 8. Schematic diagram illustrating procedure for creating models of reactive processes using REMKIN.

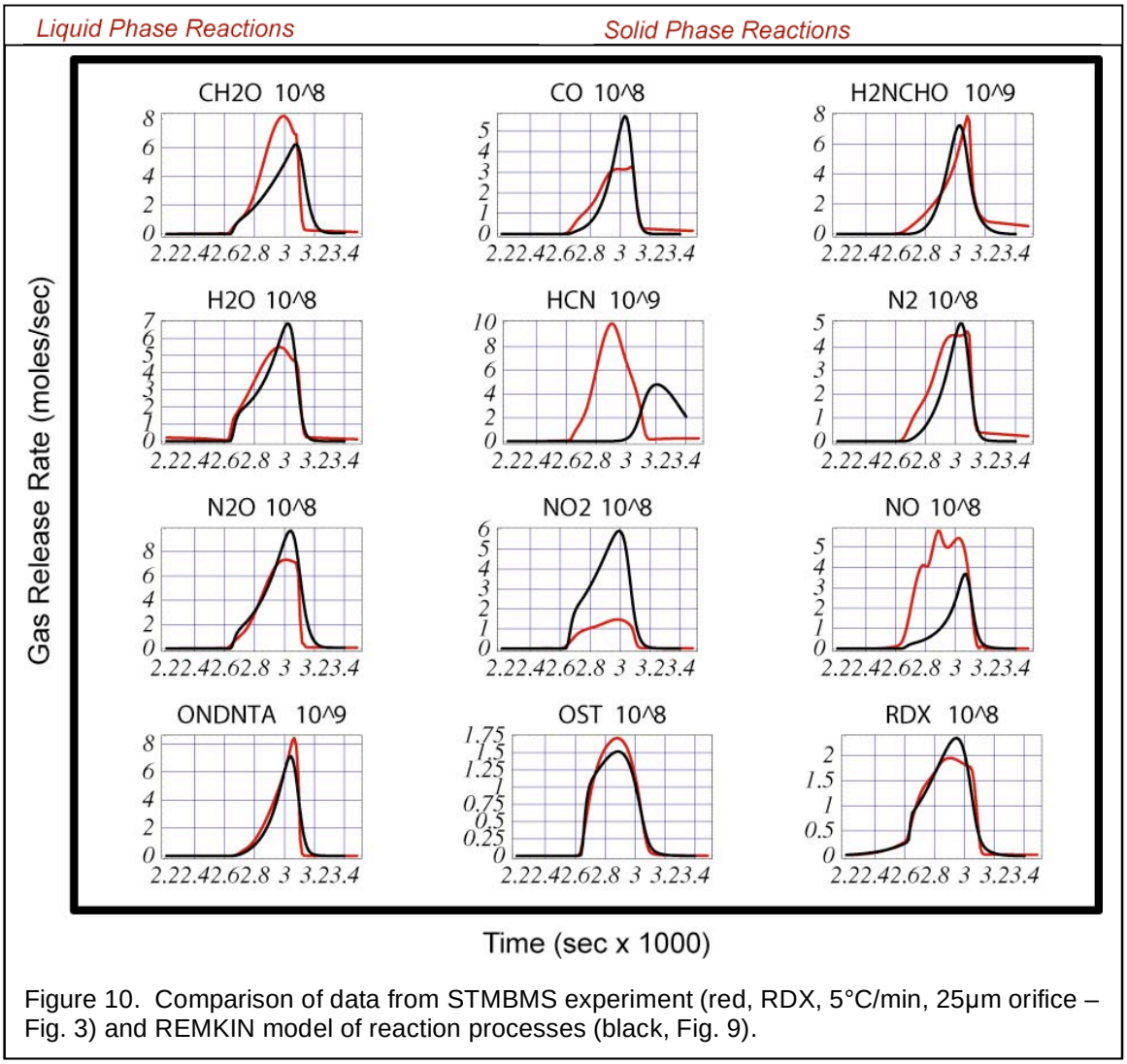

Figure 10. Comparison of data from STMBMS experiment (red, RDX, 5°C/min, 25μm orifice – Fig. 3) and REMKIN model of reaction processes (black, Fig. 9).

The reaction scheme for the model under development is listed in Fig. 9. The model captures reactions that occur in three phases: solid, liquid and gas. The main focus of the model is on the reactions that occur in the liquid phase. The solid phase processes are quite simple. Two processes maintain the quasi-equilibrium between gas and solid RDX (R1 and R2) up until the time that the RDX melts (R3). Once the RDX melts, the RDX vapor pressure is controlled by the vaporization and condensation of gaseous RDX on the surface of the liquid phase sample (reactions R3 and R4). A comparison of the calculated and measured rate of RDX release from the reaction cell is shown in the panel for RDX in Fig. 10. The current values for the vapor pressure of solid and liquid RDX are listed in Table II (Log10 P = A – B/T(K), P in Pascals). The model captures the behavior of the RDX vapor quite well. The increase in the vapor pressure as the RDX melts occurs when the reaction cell temperature is at 208°C, approximately 7 to 8°C above the melting point of RDX. This indicates that the temperature of the solid RDX lags the temperature of the reaction cell due to a low rate of heat transfer into the RDX powder [19]. The calculated RDX exhaust rate from the reaction cell continues to track the data reasonably well as its mole fraction in the liquid decreases, due to the accumulation of other products in the liquid. For example, as the amount of ONDNTA in the liquid increases the amount of RDX decreases (Fig. 11).

The model also captures the direct decomposition of RDX in the liquid phase to form OST and the associated products (R7, Fig. 10). This reaction is first order with respect to the amount of liquid RDX. The contribution to the overall decomposition from this reaction falls off early in the experiment as can be seen from the temporal behavior of the rate of OST evolution (Fig. 10) and the amount of liquid RDX remaining in the sample (Fig. 11) as the experiment progresses. A corresponding reaction for the direct decomposition of RDX to OST in the gas phase is also included in the model (R6).

Development of the parameters for the reactions associated with ONDNTA formation and decomposition is less straightforward than for the OST reaction, due to the coupled nature of the reactions. Comparison of the present state of the RDX model to the STMBMS data illustrates several of the issues involved in developing the model. The NO cycle is one of the more challenging to construct and optimize. NO is involved in both the formation and decomposition of ONDNTA, as well as several other reactions. NO is produced in reactions R6, R7, R12, R14, R16 and R22, and consumed in reactions R9, and R15. Reaction R8 represents a process that establishes a relationship between the pressure of NO in the reaction cell and the concentration of NO in the liquid. The equilibrium is established with a solubility constant based on Henry's Law (AhenryLiquid8, deltaGHenryLiquid8). Deviation from the equilibrium condition is controlled by a kinetic expression that determines the rate of movement NO through the surface of the liquid (ATransferLiquid8, EaTransferLiquid8). Adjusting the equilibrium value for NO in the liquid phase, and how fast NO can be transferred between the liquid and gas phases, affect the coupling of the reactions that generate and consume NO. Comparison of the predicted rate of NO leaving the reaction cell with the actual STMBMS data (Fig. 10) shows a large difference in the temporal behavior using the current parameter values. However, the amount of NO dissolved in the liquid phase (Fig. 11) has a temporal behavior more closely resembling the rate of NO evolution from the reaction cell. Thus, the parameters controlling the rate of movement of NO between the gas and liquid phase require adjustment.

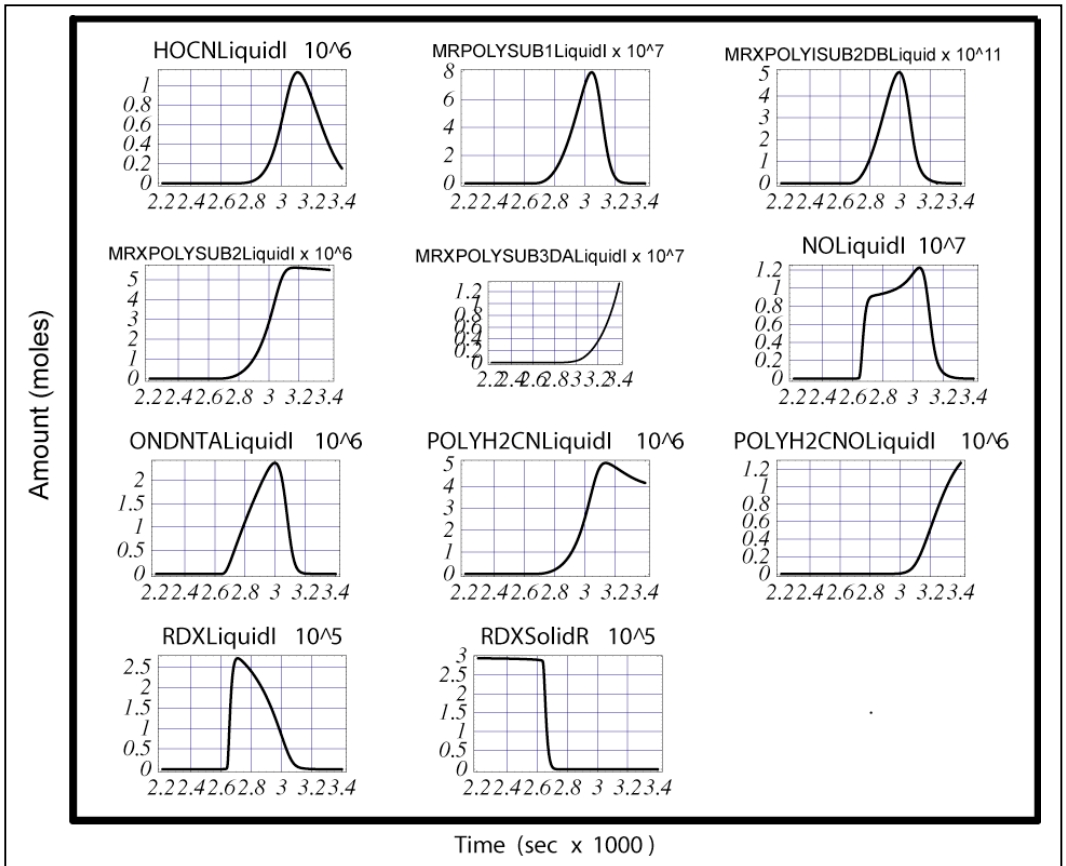

Figure 11. Amount of various non-volatile species tracked in the reaction model of RDX. Scaling factor shown in title above each graph. For example, RDXSolidR, RDXLiquidI, and ONDNTALiquidI show the amount of solid RDX, liquid RDX and liquid ONDNTA in the liquid phase during the course of the experiment, respectively.

The model also captures the rate of ONDNTA evolution from the reaction cell (Fig. 10). This is controlled by the rate of vaporization and condensation on the liquid phase (R10, R11 and the mole fraction of ONDNTA in the liquid phase see Fig. 11). The A and B terms in the vapor pressure expression for RDX and ONDNTA are quite similar (Table II) as would be expected, given the similar molecular structures of these two compounds.

Table II. Parameters for RDX liquid phase model.

Reaction #	A Name	A factor	Ea Name	Ea (kJ/mol)
1*	avpRDX1	A=16.99	bvpRDX1	B= 7133
2				
3*	avpRDX3	A=15.55	bvpRDX3	B=6233
4				
5	meltingPointRDXCon1	481	meltingRateCon1	100
6		4.10E+03	Ea6	63
7	A7	1.00E+06	Ea7	94
8	AHenryLiquid8	5.60E+06	deltaGHenry	90
8	ATransferLiq*	1.00E+08	EaTransferLiq8	90
9	A9	5.00E+07	Ea9	118
10*	avpONDNTA10	A=15.6	bvpONDNTA10	B=6253
11				
12	A12	1.10E+10	Ea12	120
13	A13	7.80E+01	Ea13	80
14	A14	4.60E+13	Ea14	80
15	A15	2.00E+10	Ea15	40
16	A16	4.00E+12	Ea16	128.9
17	A17	4.00E+12	Ea17	146.5a
18	A18	1.00E+13	Ea18	146.5a
19	A19	1.00E+13	Ea19	146.5a
20	A20	1.29E+10	Ea20	146.5a
21	A21	5.22E+11	Ea21	146.5a
22	A22	1.00E+16	Ea22	146.5a
23	A23	2.00E+08	Ea23	146.5a

* Log10 (P) = A - B/T(K); pressure in Pascals
a: Parameter not optimized.

The model captures the rate of formation of most of the major gaseous products: H_2O, CO, N_2, CH_2O, and N_2O. For the most part CH_2O and N_2O are formed via the decomposition of ONDNTA (R12) and the decomposition of the ONDNTA decomposition intermediates (MRXPolyI_1 and MRXPolyI_2 in reactions R18 and R20). The formation of CH_2O and N_2O only through ONDNTA or its decomposition intermediate could not account for the initial rapid rise in the rate of release of CH_2O and N_2O after the RDX melts. To account for this rapid rise a reaction for the direct decomposition of RDX to CH_2O and N_2O is included in the model (R21). The rate of N_2O gas evolution is characterized fairly well by the model. However, the rate of CH_2O evolution predicted by the model deviates significantly from the data. The lower rate of CH_2O evolution predicted by the model is due to the consumption of CH_2O via reaction with NO_2 (R14). This requires further adjustment as part of the NO cycle.

The model currently incorporates several features of the reactions associated with the decomposition of RDX via the ONDNTA decomposition intermediate (Figures 6 and 7). The current model includes the formation of two forms of the ONDNTA intermediate, MRXPolyI_1 (R17) and MRXPolyI_2 (R19). The model also incorporates the formation (R13) and decomposition (R22) of one of these intermediates, MRXPolyI_2DB, to form one of the minor products, formamide (H_2NCHO). The parameters in the model have been adjusted to provide a reasonable fit to the rate of evolution of H_2NCHO in the experiment. The reaction of HOCN to form HCN in reaction R23 does not capture the rate of HCN evolution in the experiment. To capture the behavior of the other minor products formed in the decomposition of RDX, more details of the reaction of the ONDNTA decomposition intermediate must be incorporated into the model. This will require incorporating competitive reactions between the ONDNTA intermediate reacting with RDX, CH_2O, NO and the direct decomposition of the ONDNTA intermediate itself.

The current state of the model to characterize the decomposition of RDX in the liquid phase illustrates how REMKIN is used to create models of these complex condensed-phase reaction processes. Postulating and testing possible reaction mechanisms is enabled by optimizing parameters for individual reactions using least squares differences between the model and the STMBMS data. Once a set of parameters is roughly optimized, the contributions of each reaction to the overall rate of generation of each species is graphed and evaluated. An example is shown in Fig. 12. Careful examination of the contribution of each reaction to the rate of generation of various species provides insight into how to improve the model.

In summary, a model of the decomposition of RDX in the liquid phase is under development. The REMKIN compiler and analysis tool allows models to be postulated and refined in a timely manner. Parts of the RDX decomposition process that are less complex and less coupled are more easily characterized. The more complex aspects of the decomposition, involving the NO cycle and the formation and decomposition of ONDNTA, require more effort to develop a reaction scheme and optimize the associated parameters.

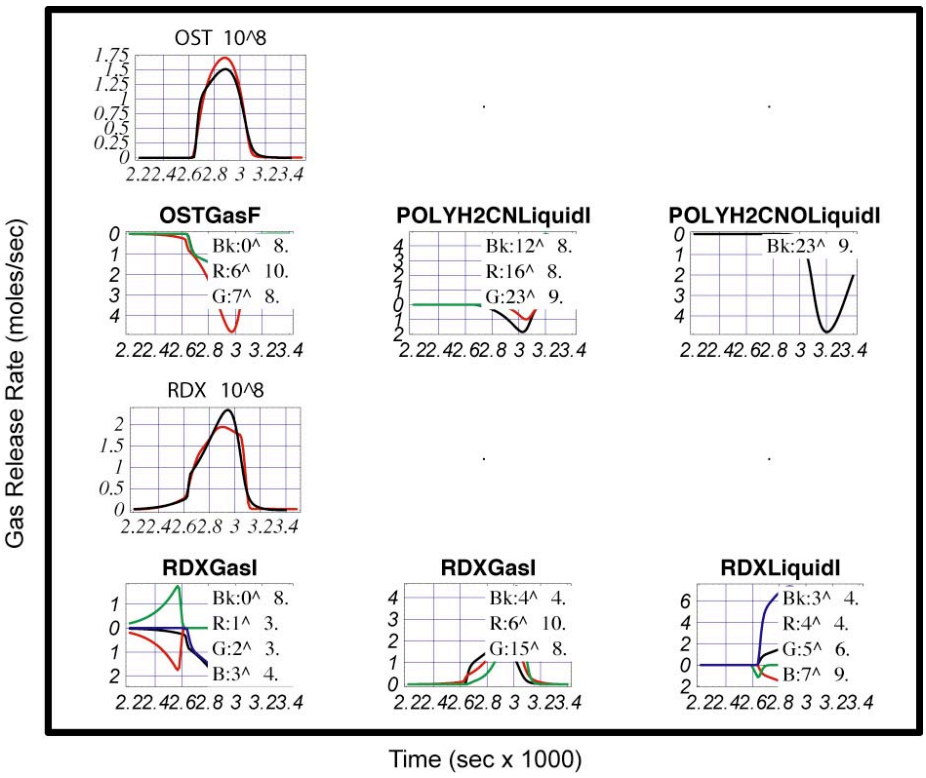

Figure 12. Illustration of REMKIN graphics used to assess the contribution of each reaction to the rate of gas release for each species. The reaction number and scaling factor are listed for each plot on a graph. Reaction number zero is the rate of evolution of the species through the reaction cell orifice. Graphs showing comparison of model and STMBMS data are in first and third rows. Graphs showing contribution from each reaction are in second and fourth rows.

CONCLUSIONS

Understanding the processes that control the reactions on the surface of burning propellants in the condensed phase has been an outstanding issue in the chemical propulsion community for several decades. Having a better understanding of these processes will provide a better framework for creating new burn rate modifiers that can be used to tailor the combustion characteristics, allowing the system designer to use more rational methods to create new propulsion designs.

Progress in understanding reactions in the condensed phase has been limited for a number of reasons. First, probing the reaction environment on the surface of a burning propellant is a very difficult experimental task [20, 21]. To circumvent the problems of examining reactions on the surface of burning propellants, researchers have turned to thermal analysis methods to examine the thermal decomposition behavior of these materials. These experiments have revealed the second reason for limited progress in this area, namely the complex nature of the underlying reaction processes that control the decomposition behavior in the condensed phase at low and moderate temperatures (up to ~ 400°C).

Over the years our research on these materials has uncovered the many different underlying physical and chemical processes that control their decomposition behavior [1, 18, 22, 23]. This general understanding is captured in a reaction diagram that shows the dominant reaction pathways and how these pathways are interrelated under a range of environmental conditions. While this provides new

insights into the reaction mechanisms, it does not provide the quantitative understanding required to capture the reaction kinetics that controls these underlying processes.

Through the most recent set of experiments, we have probed the reactions of RDX both below and above its melting point and have improved our understanding of the underlying reaction processes that control its decomposition. The results show clear differences in the dominant reaction process in each temperature range. Below its melting point, the dominant reactions occur in the gas phase, with new reactions pathways opening as products from the gas phase decomposition start to accumulate and react on the surface of the RDX particles. Above its melting point, reactions in the liquid phase dominate the decomposition process.

The underlying reaction processes in the liquid phase are quite complex. The direct decomposition of RDX to form OST, NO, NO_2 and H_2O is a significant contributor to the overall decomposition, but not the most dominant process. The most dominant process involves the formation and decomposition of the mononitroso analogue of RDX, ONDNTA. This reaction intermediate is formed by several different pathways (Fig. 1). Results from higher heating rate RDX experiments suggest that ONDNTA may itself decompose to form another reaction intermediate that goes on to itself decompose and release the more common decomposition products (i.e., CH_2O and N_2O). Separate experiments with ONDNTA indicate that this process involves the rapid release of N_2 and NO_2 from ONDNTA to form the new reaction intermediate. This reaction intermediate is likely to recombine to form a higher molecular weight polymer-like product. This polymer-like product gradually decomposes releasing CH_2O, N_2O and the minor products (e.g., formamide, N,N-dimethylformamide) and accounts for the non-volatile residue remaining at the end of an experiment. Eventually the reaction diagram (Fig. 1) will be modified to include this new intermediate in the reaction scheme.

Mathematical models of the underlying reaction processes for RDX below and above its melting point have been developed using the REMKIN compiler and analysis tool. The reaction model of RDX decomposition below its melting point is relatively simple and captures the most dominant features of the reaction process. However, careful comparison of the reaction model with the STMBMS data revealed that an additional reaction process occurs in the reduced sensitivity RDX particles when they are first heated to 185°C. This provides an example of the level of detail that can be discerned about the decomposition processes from the STMBMS experiments and associated REMKIN analysis.

The reaction model of RDX above its melting point is more complex and illustrates the level of complexity that can be considered when developing reaction models with REMKIN. The distinct and relatively independent reaction processes, such as RDX or ONDNTA vaporization and the direct decomposition of RDX to OST, are rather easy to characterize. The more complex nonlinear reaction processes, such as the ONDNTA formation and decomposition, are more difficult to address, due to multiple reaction pathways and coupling of the chemical and physical processes. These processes require more effort to develop a reaction scheme that accounts for all of the relevant results from the STMBMS experiments.

At present STMBMS experiments and REMKIN analysis have been used to develop detailed models of the reaction processes that underlie the thermal decomposition of RDX. Currently new STMBMS data is being collected on HMX, HMX-based formulations and new high-nitrogen compounds being considered for new advance propellants[24, 25]. Results from these experiments will provide a basis for examining the reaction between ingredients in existing propellants and explosives and evaluating the interaction of new ingredients with RDX for use in new propellant formulations.

REFERENCES

1. Behrens, R. and S. Maharrey, *Chemical and Physical Processes that Control the Thermal Decomposition of RDX and HMX*, in *Combustion of Energetic Materials*, K.K. Kuo and L.T. DeLuca, Editors. 2002, Begell House: New York. p. 3 - 21.

2. Behrens, R. and L. Minier, *The Thermal Decomposition Behavior of Ammonium Perchlorate and an Ammonium-Perchlorate-Based Composite Propellant*, in *33rd JANNAF Combustion Meeting*. 1996, CPIA Publicaton # 653: Monterey, CA. p. 1-19.

3. Minier, L. and R. Behrens, *Thermal Decomposition Characteristics of Orthorhombic Ammonium Perchlorate (o-AP) JANNAF 17th Propulsion Systems Hazards Subcommittee Meeting*, in *17th JANNAF Propulsion Systems Hazards Subcommittee Meeting*, CPIA, Editor. 1998, CPIA Publication #681: Tucson, AZ. p. 57-72.

4. Atwood, A.I., K.J. Kraeutle, T.P. Parr, D.M. Hanson-Parr, R. Behrens, L. Minier, and A. Ratzel, *Thermal Decomposition Characteristics of Ammonium Perchlorate (AP) and an AP Based Propellant*, in *49th JANNAF Propellant System HazardsSubcommittee Meeting*, CPIA, Editor. 1999, CPIA: Tucson, AZ.

5. Behrens, R., *Thermal Decomposition Processes of Energetic Materials in the Condensed Phase at Low and Moderate Temperatures*, in *Overviews of Recent Research on Energetic Materials*, R.W. Shaw, T.B. Brill, and D.L. Thompson, Editors. 2005, World Publications Inc. p. in press.

6. Behrens, R., Jr., *New simultaneous thermogravimetry and modulated molecular beam mass spectrometry apparatus for quantitative thermal decomposition studies.* Review of Scientific Instruments, 1987. 58(3): p. 451-461.

7. Behrens, R., Jr., *Identification of Octahydro-1,3,5,7-tetranitro-1,3,5,7-tetrazocine (HMX) Pyrolysis Products by Simultaneous Thermogravimetric Modulated Beam Mass Spectrometry and Time-of-Flight Velocity-Spectra Measurements.* International Journal of Chemical Kinetics, 1990. 22: p. 135-157.

8. Behrens, R., Jr., *Determination of the Rates of Formation of Gaseous Products from the Pyrolysis of Octahydro-1,3,5,7-tetranitro-1,3,5,7-tetrazocine (HMX) by Simultaneous Thermogravimetric Modulated Beam Mass Spectrometry.* International Journal of Chemical Kinetics, 1990. 22: p. 159-173.

9. Maharrey, S., D. Wiese-Smith, and R. Behrens, *Development of a Physicochemical Model for the Thermal Decomposition of RDX*, in *Proceedings of the 38th JANNAF Combustion Meeting*. 2002, Chemical Propulsion Information Agency: Destin, Florida. p. 373 - 386.

10. Behrens, R., *Thermal Decomposition of HMX: Morphological and Chemical Changes Induced at Slow Decomposition Rates*, in *Proceedings of the 38th JANNAF Combustion Subcommittee Mtg.* 2002, CPIA: Destin, Florida. p. 397-408.

11. Behrens, R. and S. Maharrey, *Reaction Kinetics of RDX in the Condensed Phase*, in *Proceedings of the 39th JANNAF Combustion Subcommittee Mtg.* 2003, CPIA: Colorado Springs, CO.

12. Behrens, R., S. Mack, and J. Wood, *Thermal Decomposition Mechanisms of HMX: The Interrelationship of Chemical and Physical Processes.* JANNAF 17th Propulsion Systems Hazards Subcommittee Meeting, 1998. CPIA Publication #681, Vol. 1: p. 21-44.

13. Maharrey, S., R. Behrens, and L. Johnston, *Physical and Chemical Processes Controlling the Solid-Phase Thermal Decomposition of hexahydro-1,3,5-trinitro-s-triazine (RDX)*, in *19th PSHS Mtg*. 2000, Chemical Propulsion Information Agency: Monterey, CA. p. 17 - 32.

14. It is important to define the nomenclature for describing condensed phase processes. Although experiments may be conducted well below the melting point of RDX where the material may be considered crystalline solid, there may be regions within the sample in which the RDX is no longer in a well-defined crystal structure. These regions could be solid or liquid solutions of RDX with its decomposition products or contaminants left behind in the synthesis or manufacturing process. Reaction may occur preferentially in these regions rather than in the crystalline RDX regions.

15. Behrens, R. and S. Bulusu, *The Importance of Mononitroso Analogues of Cyclic Nitramines to the Assessment and the Safety of HMX-Based Propellants and Explosives*, in *Challenges in Propellants and Combustion 100 Years after Nobel*, K.K. Kuo, Editor. 1997, Begell House, Inc.: New York. p. 275 - 289.

16. *Spartan'04 for Macintosh*. 2004, Wavefunction, Inc.: Irvine, CA.

17. The letter "D" is appended to the name of the original segment to indicate that it is an associated decomposition product.

18. Behrens, R. and S. Bulusu, *Thermal-Decomposition Of Energetic Materials .4. Deuterium-Isotope Effects and Isotopic Scrambling (H/D; C-13/O-18; N-14/N-15) In Condensed-Phase Decomposition Of 1,3,5-Trinitrohexahydro-S-Triazine.* Journal Of Physical Chemistry, 1992. 96(#22): p. 8891-8897.

19. Note: REMKIN can track heat generation and heat transfer between the reaction cell wall and the different phases present in the reaction cell. These thermal parameters are optimized after the basic reaction chemistry model has been developed and optimized.

20. Wormhoudt, J., P.L. Kebabian, and C.E. Kolb, *Infrared Fiberoptic Diagnostic Observations Of Solid-Propellant Combustion.* Combustion and Flame, 1997. 108(#1-2): p. 43-60.

21. Wormhoudt, J., P.L. Kebabian, and C.E. Kolb, *Embedded Infrared Fiber Optic Absorption Studies Of Nitramine Propellant Strand Burning.* Combustion and Flame, 1997. 111(#1-2): p. 73-86.

22. Behrens, R. and S. Bulusu, *Thermal-Decomposition Of Energetic Materials .3. Temporal Behaviors Of the Rates Of Formation Of the Gaseous Pyrolysis Products From Condensed-Phase Decomposition Of 1,3,5-Trinitrohexahydro-S-Triazine.* Journal Of Physical Chemistry, 1992. 96(#22): p. 8877-8891.

23. Behrens, R. and S. Bulusu, *Thermal decomposition of HMX: low temperature reaction kinetics and their use for assessing response in abnormal thermal environments and implications for long-term aging.* Materials Research Society Symposium Proceedings, 1996. 418: p. 119-126.

24. Hiskey, M.A., N. Goldman, and J.R. Stine, *High-Nitrogen Energetic Materials Derived from Azotetrazolate.* J. Energetic Mat., 1998. 16: p. 119-127.

25. Son, S.F., H.L. Berghout, C.A. Bolme, D.E. Chavez, D. Naud, and M.A. Hiskey, *Burn rate measurements of HMX, TATB, DHT, DAAF, and BTATz.* Proceedings Of The Combustion Institute, 2000. 28: p. 919-924.

Full Paper

Vapor Pressures, Mass Spectra and Thermal Decomposition Processes of Bis(2,2-Dintropropyl)acetal (BDNPA) and Bis(2,2-Dinitropropyl)formal (BDNPF)

Rory B. Rauch, Richard Behrens*

Combustion Research Facility, Sandia National Laboratories, Livermore, CA 94551-0969 (USA)
DOI: 10.1002/prep.200700012

Abstract

Simultaneous thermogravimetric modulated beam mass spectrometry (STMBMS) and Fourier-transform ion cyclotron resonance (FTICR) instruments have been used to measure the mass spectra, measure vapor pressures and evaluate the thermal decomposition mechanism of bis(2,2-dinitropropyl)acetal (BDNPA) and bis(2,2-dinitropropyl)formal (BDNPF). The high mass accuracy FTICR mass spectra provide the chemical formulas of the ion fragments formed in the mass spectra of BDNPA, BDNPF and their decomposition products, and provide a basis for predicting possible structures of the ion fragments. The heat of vaporization ($\Delta_{vap}H$) and vapor pressure at 25 °C are 93.01 ± 0.38 kJ/mol and $1.4532 + 0.40/-0.27$ mPa for BDNPA, and 84.77 ± 0.88 kJ/mol and $2.20 + 1.87/-1.07$ mPa for BDNPF. STMBMS data support a nitro-nitrite ($-NO_2 \rightarrow -O-NO$) rearrangement mechanism for both compounds. Upon rearrangement, both NO and NO_2 are cleaved from the structure, thus producing a ketone radical. The nitro-nitrite rearrangement begins to occur at appreciable rates between 160 and 180 °C. Additional decomposition products include amines, imines and amides, as well as CO_2 and H_2O at higher temperatures. STMBMS mass loss data suggest the formation of a residue during the decomposition of BDNPA and BDNPF. The major difference between the decomposition of the two compounds is the slower reaction rate of BDNPF. We postulate that the less sterically hindered formal carbon of BDNPF subjects it to interactions with an intermediate, thus forming a complex and delaying its release. Methods to elucidate complex thermal decomposition mechanisms from STMBMS data are illustrated.

Keywords: Bis(2,2-Dinitropropyl)acetal, Bis(2,2-Dinitropropyl) formal, BDNPA, BDNPF, Decomposition, Nitro-Nitrite Rearrangement, Vapor Pressure, Mass Spectra, FTICR Mass Spectrometry, Thermal Decomposition, Reaction Mechanism, STMBMS

1 Introduction

Bis(2,2-dinitropropyl)acetal (BDNPA) and bis(2,2-dinitropropyl)formal (BDNPF) are used as energetic plasticizing agents in explosive and propellant composite systems. The compounds are most commonly utilized as a BDNPA/F 50/50 wt% eutectic mixture. Table 1 [1, 2] gives the physical properties of BDNPA, BDNPF and the BDNPA/F eutectic.

Specific applications of BDNPA/F are reflected in past studies. The majority of these reports focus on mixtures of BDNPA/F and polymer binders, such as glycidyl azide polymer (GAP) [3–6], poly-bisazidomethyl oxetane (poly-BAMO) [4, 5, 7], polyethylene glycol (PEG) [1, 3], and poly(caprolactone) (PCL) [8]. Several thermoanalytical techniques, such as differential scanning calorimetry (DSC), thermogravimetry (TG), differential thermogravimetry (DTG), and differential thermal analysis (DTA), have been used to estimate the potential effect of these binder-plasticizer systems on the performance and safety of gun or rocket propellants [1, 3–8]. Nair et al. evaluated BDNPA/F as a substitute co-plasticizer in a new composite modified double-base propellant (CMDB) that incorporates hexanitro-hexaazaisowurtzitane (CL-20) as a new ingredient [9]. BDNPA/F was also used as a basis for comparison during the development of a new energetic plasticizer, 2,2-dinitro-1,3-bis-nitrooxy-propane (NPN) [2].

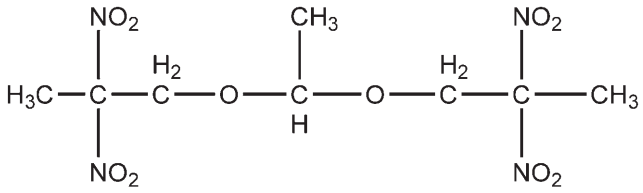

BDNPA

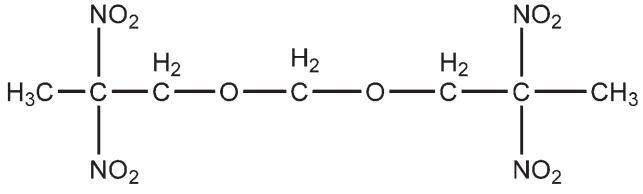

BDNPF

Scheme 1.

* Corresponding author; e-mail: rbehren@sandia.gov

Table 1. Physical properties of BDNPA, BDNPF and BDNPA/F.

Compounds	Boiling Point[a] (°C)	Melting Point (°C)	Density at 25 °C (g ml^{-1})
BDNPA	150	33 – 34	1.366
BDNPF	152	31	1.411
BDNPA/F[b]	150	– 15	1.383, 1.397

[a] At 1.33 Pa. [b] $\Delta_f H$ = -1942 kJ/ 100 kg

A number of studies have also been performed on plastic bonded explosive (PBX) materials. Many have centered around the properties of the explosive formulation PBX-9501 (95 wt% octahydro-1,3,5,7-tetranitro-1,3,5,7-tetrazocine (HMX), 2.5 wt% BDNPA/F, 2.5 wt% Estane binder) [10, 11]. The effect of BDNPA/F on the cure conditions, tensile strength and stabilities of other PBXs has also been addressed [12]. In the case of both propellant and PBX-related studies, the vast majority of experiments assessed *global* properties of the composite system, making it difficult to glean relevant pure-component BDNPA/F characteristics from the literature. BDNPA/F has not been studied extensively in its pure form. Shen et al. [3] report a DSC onset temperature (T_o) of 220 °C and a maximum reaction temperature (T_m) of 255 °C for the BDNPA/F eutectic. The same group later reports an auto-ignition temperature of 204 °C and a T_m of 265 °C [4].

Compounds with chemical structures that are similar to BDNPA/F (i.e. polynitro aliphatic compounds) have been examined previously. A number of studies have focused on bis(2-fluoro-2,2-dinitroethyl)formal (FEFO), a relatively insensitive energetic liquid with applications as a component in paste-extrudable explosives. Minier and Behrens analyzed FEFO using STMBMS methods [13] and reported six major pathways in the thermal decomposition of FEFO. The initial decomposition (~ 150 °C) is characterized by a nitro-nitrite rearrangement (−NO_2 to −O−NO) and subsequent cleavage of NO. Prior literature [14] had detailed the nitro-nitrite rearrangement as the dominant rate-determining mechanism for gem-dinitro compounds such as FEFO.

The primary objective of our work on BDNPA/F is to characterize its thermal decomposition for future use in assessing the performance, safety, and aging behavior of propellants and explosives. Specifically, reaction kinetics models of BDNPA and BDNPF decomposition will provide important baseline information to assess the safety and aging behavior of PBX and propellant formulations that utilize a BDNPA/F plasticizer. To achieve this objective requires: (1) determining the underlying reaction mechanism, (2) collecting and analyzing data on the rate of reaction, and (3) developing a mathematical model to characterize the reaction mechanism and determine the associated kinetic parameters.

Determining the underlying reaction mechanisms of BDNPA and BDNPF is difficult due to the complexity of their mass spectra, and the similarity of these mass spectra to those of their thermal decomposition products. Thus, this paper presents the results of our work focused on determining the underlying reaction mechanisms that control the thermal decomposition of BDNPA and BDNPF. To do this requires determining the vapor pressures of BDNPA and BDNPF, and carefully examining the mass spectra of BDNPA, BDNPF, and their decomposition products. Based on these results, we also address the effect of the formal and acetal functionality on the thermodynamic properties and decomposition mechanism of BDNPF and BDNPA.

STMBMS and Fourier-transform ion cyclotron resonance (FTICR) mass spectrometry instruments have been used to identify the decomposition products of each compound and examine the temporal dependence of their thermal decomposition behavior. A plausible thermal decomposition mechanism is then presented. The structures and stoichiometry of the decomposition products are estimated from careful consideration of the STMBMS ion signal data and how it may logically relate to the proposed mechanism. These results form the basis for future work to determine the rates of reaction and develop mathematical models to characterize the underlying reaction processes.

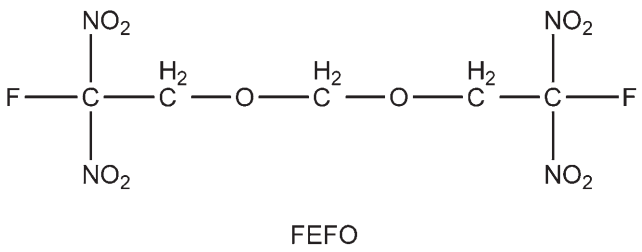

FEFO

Scheme 2.

2 Experimental

2.1 STMBMS Apparatus

The STMBMS apparatus, and basic experimental and data analysis procedures, have been described previously [15 – 17]. A schematic diagram of the instrument is shown in Figure 1. This instrument allows the concentration and rate of formation of each gas-phase species in a reaction cell to be measured as a function of time by correlating the ion signals at different m/z values measured with a mass spectrometer with the force measured by a microbalance at any instant.

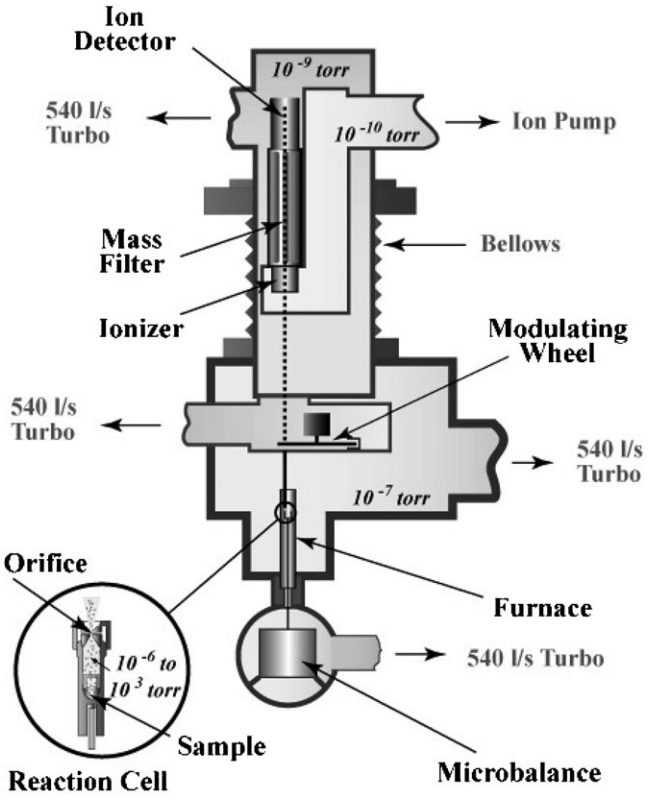

Figure 1. Schematic cross section of STMBMS apparatus.

2.2 BDNPA and BDNPF Purity

The pure component BDNPA and BDNPF samples were received from Lawrence Livermore National Laboratory. The BDNPA/F eutectic composition was obtained from ATK Thiokol. All samples were used as received. The sample purity for BDNPA, BDNPF and the BDNPA/F eutectic are greater than 99%, as analyzed by mass spectrometry.

2.3 Data Collection Protocols

2.3.1 Mass Spectra Protocol

The mass spectra are measured with two different instruments. The STMBMS apparatus is used to collect low-resolution mass spectra by heating the sample in the reaction cell to temperatures that generate a sufficient amount of vapor but do not cause decomposition, which is confirmed by the high degree of temporal correlation ($R >$ 0.98) between the ion signals at the various m/z values in the mass spectrum. Larger diameter orifices (~1000 μm for low vapor pressure substances such as HMX to ~100 μm for high vapor pressure substances such as BDNPA/F or FEFO) are used to reduce the temperature required to achieve a sufficient ion count rate in the mass spectrometer. Selecting the appropriate combination of sample size, confinement level and temperature is a critical step in all forms of STMBMS analysis (i.e. mass spectra, vapor pressure and decomposition). The appropriate balance for BDNPA and BDNPF mass spectra and vapor pressure experiments is achieved with sample sizes of 1–3 mg, ~100 μm orifice confinement, and temperatures $\leq 110\,^{\circ}C$.

A Bruker-Apex II FTICR mass spectrometer is used to collect high resolution ($m/\Delta m > 50{,}000$) and high mass accuracy (< 1 ppm) mass spectra of the samples using a direct insertion probe (DIP) and electron bombardment ionization (70 eV). These data are used to assign the stoichiometry of the ions in the mass spectra.

2.3.2 Vapor Pressure Protocol

The vapor pressures of the compounds are measured with the STMBMS apparatus, based on a Knudsen effusion cell method. In these experiments, the sample is placed in a reaction cell with a larger diameter orifice (~250 to 1000 μm with lower vapor pressure substances, ~100 μm with a higher vapor pressure substance). The sample is heated through a set of isothermal temperature steps, and the mass spectra and rate-of-force change are measured with the STMBMS apparatus. The data are analyzed with the STMBMS thermal analysis algorithms and the vapor pressure of the compound at each temperature step is determined. The measurements are typically obtained by collecting data in a series of increasing temperature steps followed by a series of decreasing temperature steps. These two sets of isothermal data are compared and used to check for the evolution of volatile contaminants that may influence the initial vapor pressure measurements.

The vapor pressures are measured over a temperature range in which molecular flow controls the rate of mass loss from the reaction cell (Knudsen number > 10). The mass loss is described by the following expression:

$$\frac{dm(t)}{dt} = \frac{C A_0 M \bar{v}(t) n(t)}{4N_A}$$

where C is the Clausing factor, A_0 is the area of the orifice, N_A is Avogadro's number, M is the molecular weight, $\bar{v}$ is the average velocity of the gas, and n is the number density of the gas within the reaction cell [15]. The vapor pressures are related to the number density through the ideal gas law.

The vapor pressure measurements are based on the evolution of gas from the reaction cell in which there is a "quasi-equilibrium" established between the condensed phase and gas phase of the compound within the reaction cell. The quasi-equilibrium value converges toward the equilibrium value when the surface area of the sample is much larger than the area of the exit orifice. For the larger diameter orifices (~1000 μm), the measured quasi-equilibrium value may deviate from the equilibrium condition by up to a factor of 3. A set of correction factors were developed by performing a series of vapor pressure experiments at varying orifice diameters and extrapolating these results to a zero-diameter orifice. However, these correction factors

Table 2. STMBMS and FTICR mass spectra experimental parameters.

Experiment	Type	Sample Mass (mg)	Orifice Diameter (μm)	Temperature Range (°C)
BDNPA1	STMBMS	8.41	106.5	60 – 110
BDNPA2	STMBMS	1.32	96.5	110 – 160
BDNPF1	STMBMS	8.36	96.5	60 – 110
BDNPF2	STMBMS	3.09	95.0	110 – 160
BDNPF3	FTICR	~1	na	50 – 177
BDNPAF1	FTICR	~1	na	50 – 190

were not applied because the resultant changes in vapor pressure were much smaller than experimental error. The enthalpy of vaporization ($\Delta_{vap}H$) is calculated using the form of the Clausius-Clapeyron equation assuming negligible contribution from the volume of the condensed phase:

$$LogP = -\frac{\Delta H_{vap}}{RT} + C$$

2.3.3 Decomposition Protocol

BDNPA and BDNPF decomposition experiments require smaller orifice diameters (~10 μm) to preclude the sample from vaporizing too rapidly at higher temperatures (>180 °C). The sample size is limited to 2 – 3 mg in these experiments to prevent the orifice from clogging. The ion signals at various m/z values in decomposition experiments may arise from either evaporation of the reactant, its decomposition products, or the evolution of contaminants. Samples were heated under low confinement to check for the evolution of impurities. No impurities were found in the samples used in these experiments. The contribution from evaporation of BDNPA or BDNPF to the ion signal at each m/z value was removed by applying the fragmentation ratios measured from the mass spectra of the reactant. This results in a collection of ion signals at various m/z values that originate from compounds formed during the thermal decomposition of the reactant in the reaction cell. These corrected signals are sorted into temporally correlated groups and plotted. For BDNPA and BDNPF, fragmentation patterns of the mass spectra are sensitive to the temperature of the sample in the reaction cell, thus making it difficult to apply corrections. In this case, a characteristic evaporation signal was selected and the ion signals were grouped by judgment through visual inspection of their evaporative contribution. A plausible reaction mechanism may then be formulated through careful consideration of these groupings, the relative ratios of m/z signals, temperature and mass loss data.

3 Results and Discussion

3.1 Mass Spectra

Formulation of a decomposition mechanism from the STMBMS data requires identifying the thermal decomposition products from the ion signals formed in the mass spectrometer. While the ionizer is operated with a low electron energy to reduce fragmentation of molecular ions formed from each species evolving from the reaction cell into daughter ions, a number of ion signals still contain such contributions from fragmentation. Resolving the contribution to each ion signal, particularly the evaporative contribution (mass spectrum), is a critical step in the formulation of a decomposition mechanism.

Mass spectra of BDNPA and BDNPF were obtained from both STMBMS and FTICR experiments. The conditions for the STMBMS and FTICR mass spectral experiments are summarized in Table 2.

It is important to note two differences when comparing STMBMS and FTICR data. First, the FTICR ionizer energy was 70 eV versus 20 eV for the STMBMS measurements, thereby creating additional fragmentation pathways for the FTICR experiments. Second, experiment BDNPAF1 used the BDNPA/F eutectic mixture as opposed to a pure form of either compound. The potential impacts of these differences were well understood during data analysis and neither ultimately affected the mass spectra assignment process. The empirical formulae for the various m/z values from FTICR data are summarized in Table 3. The relative abundance of BDNPA and BDNPF fragments from STMBMS low-temperature (≤ 110 °C) data are presented in Tables 4 and 5. The ion structures in Tables 4 and 5 are based on likely fragmentation pathways and stoichiometry of the ions determined from the FTICR data. Note that the molecular ion does not appear in the fragmentation pattern of either BDNPA or BDNPF.

The fragmentation patterns for BDNPA and BDNPF are similar. The ion signals with the largest relative abundance, m/z = 177 in BDNPA and m/z = 163 in BDNPF, are analogous as they are both formed through fragmentation of the acetal/formal C–O bond. Many of the remaining fragments are structurally analogous, but vary dramatically in relative abundance. This trend begins with the second most abundant fragments; m/z = 133 in BDNPA results from cleavage of the C–O bond beta to the acetal carbon. By contrast, the formation of m/z = 117 in BDNPF requires nitro group cleavage. This apparent propensity towards nitro group fragmentation is further demonstrated by the larger relative abundance of m/z = 88, 87, 59, 58, and 57 in the BDNPF mass spectrum. BDNPF also has a higher percentage of its ion signal at lower m/z values, indicating a greater proclivity towards producing smaller ion fragments. BDNPA exhibits a larger signal at m/z = 43, which may be

Table 3. FTICR/MS data summary.

Ion Signal (m/z)	Primary Formula[a]	Relative Signal Intensity[b]	Meas. Mass (u)	Theoretical Mass (u)	Secondary Formula	Relative Signal Intensity	FTICR Mass (u)	Theoretical Mass (u)
177	$C_5H_9N_2O_5$	0.06	177.058	177.051				
163*	$C_4H_7N_2O_5$	0.3	163.039	163.035				
133*	$C_3H_5N_2O_4$	0.1	133.028	133.028				
131	$C_5H_9NO_3$	0.006	131.062	131.060				
117*	$C_4H_7NO_3$	0.4	117.045	117.045				
102*	$C_3H_4NO_3$	0.1	102.020	102.019				
101	$C_5H_9O_2$	0.045	101.062	101.060				
88*	$C_3H_6NO_2$	0.03	88.041	88.040				
87*	$C_4H_7O_2$	0.05	87.046	87.044	$C_3H_5NO_2$	0.007	87.033	87.032
86*	$C_3H_4NO_2$	0.015	86.025	86.024				
74	$C_2H_4NO_2$	0.6	74.025	74.024				
73*	$C_3H_5O_2$	0.01	73.026	73.027				
70[c]*	C_3H_4NO	0.004	70.030	70.029				
60*	CH_2NO_2	0.075	60.009	60.008				
59*	C_2H_5NO	0.5	59.037	59.037	C_3H_7O	0.075	59.050	59.049
58*	C_2H_4NO	0.03	58.029	58.029	C_3H_6O	0.015	58.042	58.041
57*	C_3H_5O	0.125	57.021	57.021				
48*	NH_2O_2	0.015	48.008	48.008				
46*	NO_2	0.015	45.992	45.992				
45	C_2H_5O	0.03	45.034	45.034				
43*	C_2H_3O	0.175	43.018	43.018				
41*	C_3H_5	0.04	41.039	41.039	C_2H_3N	0.015	41.026	41.026
31*	CH_3O	0.04	31.018	31.018				
30*	NO	0.2	29.997	29.997				
29*	C_2H_5	0.05	29.039	29.039	CHO	0.006	29.002	29.002

[a] Primary formula designation based on larger relative intensity signal. [b] Signals with a relative intensity < 0.001 were not considered. [c] Signals with a relative intensity < 0.005 are considered suspect. * Signal in BDNPF mass spectrum (from experiment BDNPF3); does not necessarily exclude it from BDNPA mass spectrum

attributed to the potential formation of the ion from *either* an end carbon *or* acetal carbon source.

The mass spectra of BDNPA and BDNPF exhibit a change in the relative ion formation probability (RIFP) at various m/z values as the temperature of the molecules emanating from the reaction cell increases. For example, the ratio of ion signals at m/z values of 133:177 in BDNPA grows from 0.75 under lower temperature conditions (Table 4), to 3.0 at 250 °C for experiment BDNPA4, which will be discussed below. This sort of increase in relative abundance is normally due to contributions from decomposition products appearing at the same m/z values as those observed in the mass spectra of the reactant. For example, BDNPA could potentially form a thermal decomposition product with an ion fragment appearing at $m/z = 133$. There are strong indications, however, that these ion signals only originate from evaporation of BDNPA or BDNPF. In each of the thermal decomposition experiments with BDNPA and BDNPF, which will be described below, there is a high degree of temporal correlation between the higher molecular weight ion fragments from the mass spectra of BDNPA and BDNPF at both lower temperature and higher temperature regions of the experiment, as illustrated in Figure 2 for the decomposition of BDNPA (experiment BDNPA3). These include signals at $m/z = 177$, 133, 131, and 74 in BDNPA and $m/z = 163$, 133, 117 and 102 in BDNPF. This high degree of temporal correlation at both lower temperatures, prior to the onset of thermal decomposition, and higher temperatures, where substantial amounts of decomposition products are observed, indicates that the given set of signals originates from either a) the fragmentation of a single reaction cell species (as with evaporation of BDNPA) in the ionizer or b) the creation of a decomposition product that has ion signals in its mass spectrum that are identical in m/z values and RIFPs to that of the reactant. The latter explanation is highly unlikely. Thus, the data indicate that the temperature of BDNPA and BDNPF affects the RIFPs of ions at various m/z values in their mass spectra. Experiments BDNPA2 and BDNPF2 were performed to specifically address the potential temperature dependence of the fragmentation pattern for each compound. Table 6 compares the RIFPs at low temperatures (60 – 110 °C) and those predicted at 210 and 250 °C by an extrapolation of a first-order polynomial fit to the temperature-dependent ion signal data collected in experiments BDNPA2 and BDNPF2. The first-order fit was performed on data from 110 – 160 °C and extrapolated to predict values at 210 and 250 °C.

While the values at 210 and 250 °C are not exact (the first-order polynomial fit and subsequent extrapolation does not predict the observed $m/z = 133 : m/z = 177$ ratio of 3:1 at 250 °C), they do provide support for the application of the following trends during decomposition analysis:

- The second most abundant ion signal overtakes the most abundant ion signal by a significant margin at higher

Table 4. BDNPA mass spectrum summary.

Ion (m/z)[a]	Relative Abundance[b]	Formula	Possible Ion Fragment Structures[d]
326	Not seen	$C_8H_{14}N_4O_{10}$	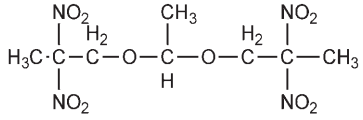
177	100.0	$C_5H_9N_2O_5$	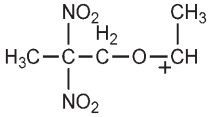
133	75.3	$C_3H_5N_2O_4$	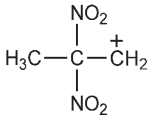
30	18.3	NO, CH_2O[c]	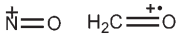
43	9.9	C_2H_3O	
57	9.3	C_3H_5O	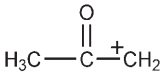
74	6.6	$C_2H_4NO_2$, $C_3H_6O_2$[c]	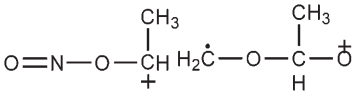
131	5.4	$C_5H_9NO_3$	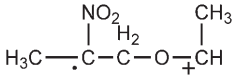
101	3.5	$C_5H_9O_2$	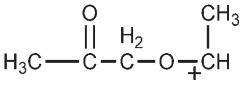
88	3.4	$C_3H_6NO_2$	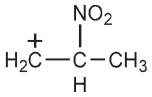
41	1.8	C_3H_5	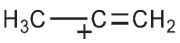
45	1.6	C_2H_5O	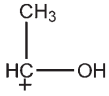
58	1.1	C_2H_4NO, C_3H_6O	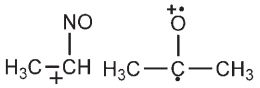

[a] Isotopic analog signals such as m/z = 178, 179, 134, and 135 were not included in the table. [b] Signals with a relative abundance < 1.0 from STMBMS (20 eV) data were not included. [c] Fragmentation structure does not match FTICR formula but could be plausible based on structure. [d] Likely ion structures based on ion formula and structure of BDNPA. FTICR MS/MS measurements have not been performed to determine ion structures.

temperatures. This larger relative abundance is not interpreted as an additional contribution from decomposition processes.

- The increase in relative abundance of some lower molecular weight ion signals at higher temperatures can be attributed to a change in RIFP and thus a change in the evaporative contribution to the signal intensity.

Closer examination of the m/z values whose ion signals increase most rapidly at higher temperatures indicate that the molecular rearrangement processes that lead to forma-

Table 5. BDNPF mass spectrum summary.

Ion (m/z)[a]	Relative Abundance[b]	Formula	Possible Ion Fragment Structures [d]
312	Not seen	$C_7H_{12}N_4O_{10}$	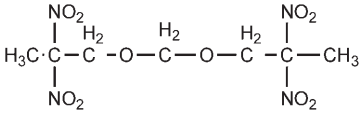
163	100.0	$C_4H_7N_2O_5$	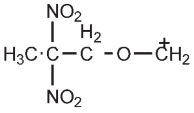
117	95.1	$C_4H_7NO_3$	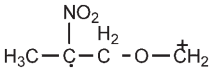
88	20.1	$C_4H_8O_2$[c], $C_3H_6NO_2$	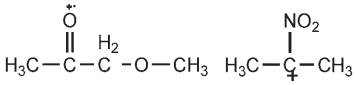
57	14.0	C_3H_5O	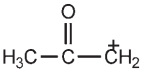
133	12.5	$C_3H_5N_2O_4$	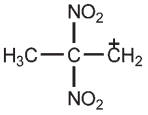
30	12.5	NO, CH_2O[c]	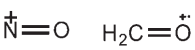
59	7.7	C_2H_5NO, C_3H_7O	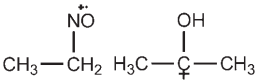
87	6.9	$C_4H_7O_2$, $C_3H_5NO_2$	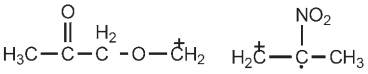
58	5.1	C_2H_4NO, C_3H_6O	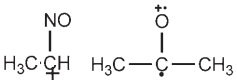
102	4.4	$C_3H_4NO_3$	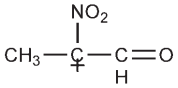
43	3.9	C_2H_3O	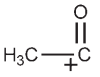
29	3.4	C_2H_5, CHO	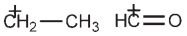
70	3.3	C_3H_4NO	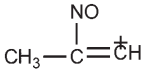
60	3.1	$C_2H_4O_2$[c], CH_2NO_2	
41	2.7	C_3H_5	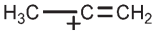
48	2.3	NH_2O_2, CH_4O_2[c]	

[a] Isotopic and protium analog signals such as m/z = 164, 165, 116, 118, and 119 were not included in the table. [b] Signals with a relative abundance < 1.0 from STMBMS (20 eV) data were not included. [c] Fragmentation structure does not match FTICR formula but could be plausible based on structure. [d] Likely ion structures based on ion formula and structure of BDNPF. FTICR MS/MS measurements have not been performed to determine ion structures.

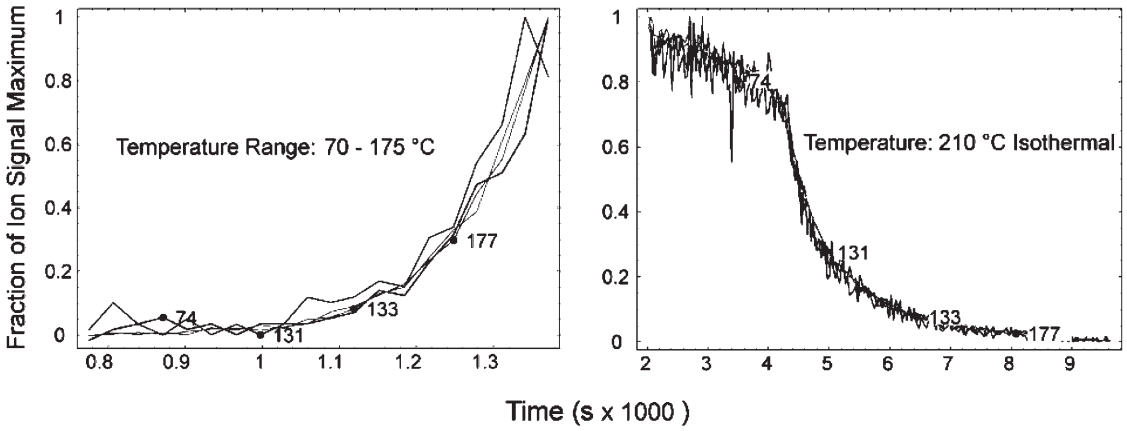

Figure 2. Correlated higher molecular weight BDNPA ion fragments. Ion fragments are correlated at both lower temperature (left figure) and higher temperature (right figure) conditions.

tion of daughter ions in the mass spectrometer are similar to those observed in the decomposition of BDNPA and BDNPF. The ions whose signals increase the most at higher temperatures (e.g. have ratios in the range of 3.0 at 210 °C and greater than 4.0 at 250 °C) are primarily ions that have a carbonyl group at the carbon atom in BDNPA and BDNPF that was originally part of the gem-dinitro group. These ions are at m/z values of 43, 57 and 58 in BDNPA and m/z values of 43, 57, 58, 59 and 60 in BDNPF. The elimination of the gem-dinitro groups and the formation of a carbonyl group in

Table 6. Comparison of mass spectral relative ion formation probabilities values of BDNPA and BDNPF at 60 – 110 °C[a] to extrapolated values at 210 and 250 °C[b].

Signal (m/z)	Relative Abundance from 60 – 110 °C	Extrapolated to 210 °C		Extrapolated to 250 °C	
		Relative Abundance	Ratio	Relative Abundance	Ratio
BDNPA Data					
177	100.0	100.0	1.0	100.0	1.0
133	75.3	114.7	1.5	157.7	2.1
30	18.3	46.2	2.5	77.5	4.2
43	9.9	23.1	2.3	38.7	3.9
57	9.3	25.9	2.8	44.5	4.8
74	6.6	15.1	2.3	25.3	3.8
131	5.4	15.6	2.9	26.9	5.0
101	3.5	5.5	1.6	7.3	2.1
88	3.4	6.1	1.8	9.9	2.9
41	1.8	5.9	3.3	10.7	5.9
45	1.6	3.5	2.2	5.8	3.6
58	1.1	2.7	2.5	4.6	4.2
BDNPF Data					
163	100.0	100.0	1.0	100.0	1.0
117	95.1	130.1	1.4	129.0	1.4
88	20.1	40.1	2.0	55.0	2.7
57	14.0	39.9	2.9	60.8	4.3
133	12.5	31.6	2.5	47.0	3.8
30	12.5	35.1	2.8	52.5	4.2
59	7.7	23.9	3.1	36.8	4.8
87	6.9	17.2	2.5	25.6	3.7
58	5.1	14.7	2.9	22.2	4.4
102	4.4	8.3	1.9	11.6	2.6
43	3.9	10.3	2.6	15.5	4.0
29	3.4	11.6	3.4	18.3	5.4
70	3.3	7.6	2.3	11.7	3.5
60	3.1	9.6	3.1	14.8	4.8
41	2.7	9.4	3.5	15.3	5.7
48	2.3	7.5	3.3	11.4	5.0

[a] Data obtained from experiments BDNPA1 and BDNPF1. [b] Extrapolation based on first-order polynomial fit to ion signal data at 110 – 160 °C from experiments BDNPA2 and BDNPF2. Data is collected over a temperature range in which the thermal decomposition of BDNPA is negligible.

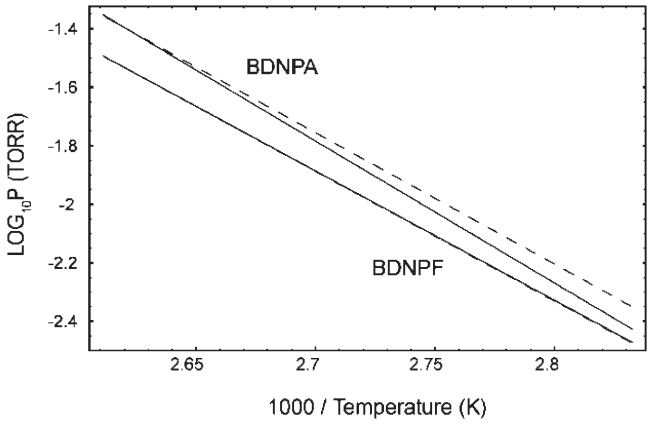

Figure 3. Vapor pressure of BDNPA and BDNPF as a function of 1/temperature (K). Dashed lines indicate the vapor pressures of BDNPA and BDNPF upon initial heating from 80 to 110 °C.

the dissociation of the molecular ion are similar to the thermal decomposition reactions as described below.

3.2 Vapor Pressure

The vapor pressures of BDNPA and BDNPF were determined by stepping the sample temperature in 10 °C increments through two cycles of 60 – 110 – 60 °C. An orifice diameter of ~100 μm was used in each experiment (BDNPA1 and BDNPF1). The vapor pressure as a function of temperature for each compound is illustrated in Figure 3. The heat of vaporization ($\Delta_{vap}H$) and vapor pressures at 25 °C of each compound are reported in Table 7. The temperature dependence of the vapor pressures of BDNPA and BDNPF are expressed as:

BDNPA:

$$Log_{10}P(Pa) = 13.440(\pm.051) - 4851.4(\pm19.8)/T_k$$

BDNPF:

$$Log_{10}P(Pa) = 12.175(\pm.114) - 4420.7(\pm46.1)/T_k$$

Both relationships were calculated from the average slope and intercept from three temperature intervals: the second increasing temperature intervals from 80 – 110 °C and the two decreasing temperature intervals from 110 – 80 °C. The first temperature interval was excluded from the calculation because of water and minor contaminants in the sample that increase the vapor pressure of BDNPA, and to a lesser extent in BDNPF, as they are initially heated to 100 °C (dashed lines in Figure 3). The error values given are the standard deviation of the data from the final three ramps.

The vapor pressure of BDNPA, as depicted in Figure 3, is larger than that of BDNPF within the temperature range of interest for plasticizer decomposition. STMBMS experiments performed with the BDNPA/F eutectic at low temperature (< 150 °C) and low confinement (> 100 μm diameter orifice) conditions corroborate this trend as they exhibit faster BDNPA evolution.

Table 7. $\Delta_{vap}H$ and vapor pressure for BDNPA and BDNPF.

Compound	$\Delta_{vap}H$ (kJ/mol)	Vapor Pressure at 25° (mPa)
BDNPA	93.01 ± 0.38	$1.4532 + 0.40 - 0.27$
BDNPF	84.77 ± 0.88	$2.20 + 1.87 - 1.07$

3.3 Thermal Decomposition

BDNPA and BDNPF decomposition processes are not identical, but do share several similar features. An analysis of the temporal behavior of ion signals at the various m/z values reveals features that point to a blend of contributions from evaporation, decomposition, and residue formation. The salient portion of the decomposition mechanism includes a nitro-nitrite ($-NO_2$ to $-O-NO$) rearrangement followed by cleavage of the NO and paired gem NO_2 to form a carbonyl functional group. A low volatility residue (LVR) forms through the course of an experiment and may arise from reaction of alkyl radicals formed during the decomposition process. The parameters of the experiments used to characterize the decomposition of BDNPA and BDNPF are summarized in Table 8.

3.3.1 Residue formation

Given the structural similarity and relative compatibility of the two compounds, one would expect the decomposition of BDNPA and BDNPF to progress in a similar manner. For the most part, this expectation holds true. One feature in particular, the formation of a low volatility residue, warrants immediate discussion as it sets the stage for the remainder of

Table 8. Experimental parameters for BDNPA and BDNPF decomposition.

Experiment	Sample Mass (mg)	Orifice Diameter (μm)	Heating Rate (°C/min)	Plateau Temperature (°C)
BDNPA3	2.29	10.6	10	210
BDNPF4	2.83	10.2	10	210
BDNPA4	2.44	10.9	10	250
BDNPF5	2.77	10.6	10	250
BDNPA5	2.54	23.84	stepped/ varied	210

this analysis. The mass loss data from BDNPA2, BDNPA3 and BDNPA5 (held isothermally at 210 °C, but with a different temperature ramp to the isothermal temperature) are illustrated in Figure 4.

Examination of Figure 4 reveals three trends. First, as confinement of the gases in the reaction cell is increased (c to a), the amount of material remaining in the reaction cell asymptotically approaches a larger value. In the case of the two extremes, experiment BDNPA2 (c) has almost no material remaining in the reaction cell, whereas BDNPA3 (a) contains approximately 0.3 mg (13% of the original sample). Second, as the confinement level increases, the global mass loss rate decreases and the experiment requires more time to complete. Third, each experiment displays an increasingly sharper transition to its late stage (indicated by the placement of the (a), (b), and (c) labels on Figure 4) as the orifice diameter is changed from 10 μm to 100 μm. The preceding three trends are repeated in analogous experiments with BDNPF. When one considers these trends, and their meaning as it relates to the physical transformation of the material in the reaction cell, the most logical explanation is the formation of a residue from the decomposition of BDNPA. The differences in the temporal behaviors of the experiments performed with 100 μm and 10 μm diameter orifices are due to the fraction of the sample that decomposes under the different experimental conditions of each experiment. The mass loss from the experiment using the 100 μm orifice (BDNPA2, c) is the most rapid and is mostly due to evaporation of the sample and loss of BDNPA vapor from the reaction cell under low-confinement conditions. At this point, no observable residue has been formed in the reaction cell and the mass-loss profile experiences a sharp transition to a zero slope as the BDNPA in the reaction cell is depleted. In the experiment using a 10 μm orifice (BDNPA3, a), a significant amount of BDNPA decomposition occurs because the sample is confined to the reaction cell at higher temperatures and pressures. The rate of mass loss of this experiment is smaller than that of the experiment with the 100 μm diameter orifice because the rate of BDNPA molecules exiting the reaction cell is reduced by the smaller cross-sectional area of the 10 μm diameter orifice. Under higher confinement conditions, decomposition is promoted and the decomposition process produces an LVR in the reaction cell. The mass loss profile eventually experiences a smooth transition to the later stages of the experiment when only residue is left to evaporate and/or decompose. The weight loss profile for the experiment with the 25 μm diameter orifice contains intermediate features that support the trends of the experiments with 100 and 10 μm diameter orifices.

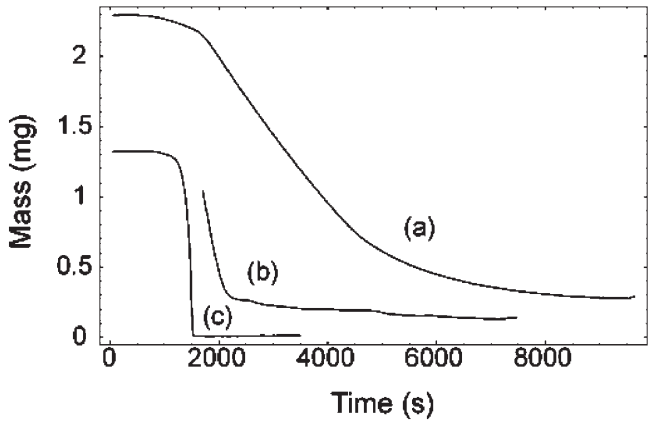

Figure 4. Comparison of temporal behavior of the mass of the sample vs. time for BDNPA experiments with (a) 10 μm, (b) 25 μm and (c) 100 μm orifice diameters. The data for the 25 μm confinement experiment has been shifted to the point at which its temperature profile coincides with the profiles of the other experiments. Each experiment reaches an isothermal temperature of 210 °C at 1900 s.

3.3.2 BDNPA Decomposition

STMBMS mass spectrometry data indicate that BDNPA decomposition reaches appreciable rates between 160–180 °C. The m/z = 100 ion signal, which is not observed in the BDNPA mass spectrum, begins to increase from its baseline value in this temperature range. The ion signal associated with the BDNPA decomposition products and their total ion signal percentages from experiments BDNPA2, BDNPA3 and BDNPA4 are presented in Table 9. The empirical formulae presented in this table, as well as the structures of the decomposition products (presented later in Figure 10), were fashioned from an iterative process. First, best guess estimates of the stoichiometry and structures of the more abundant STMBMS ion signals were made. The temporal behaviors of these ions were then used to formulate a decomposition mechanism (found later in this section). The mechanism was then used to validate the previously estimated structures and create the stoichiometry and structures for the less abundant ion signals. Ion structures were changed, if necessary. This process was repeated until temporal behaviors and relative abundance of the STMBMS data logically agreed with the proposed mechanism.

The data in Table 9 were not corrected for evaporation of the BDNPA. The change in fragmentation pattern of the BDNPA mass spectrum with changing sample temperature and the rapid evaporation of BDNPA at higher temperatures made it difficult to accurately obtain and apply correction factors to the BDNPA ion signals. Comparison of the fraction of the total ion signal at each m/z value from the three experiments shows the ion signals that are associated with the more significant BDNPA decomposition products. The ion signals that exhibit the largest relative decrease in fraction of total ion signal from BDNPA3 to BDNPA2 (10 μm confinement to 100 μm confinement) are more likely associated with decomposition products (e.g. m/z = 44, 100). Those ion signals that exhibit the largest relative increase from BDNPA3 to BDNPA4 (210 °C to 250 °C) may be associated with a change in the decomposition process (e.g. 18, 28) at higher temperature.

Table 9. BDNPA decomposition products and relative abundance[a].

Ion (m/z)	Ion Empirical Formulae[c]	% Total Ion Signal from BDNPA2 (100 μm confinement, 210 °C max)	% Total Ion Signal from BDNPA3 (10 μm confinement, 210 °C max)	% Total Ion Signal from BDNPA4 (10 μm confinement, 250 °C max)
18[b]	H_2O	< 0.01	1.93	2.78
27	HCN, C_2H_3	< 0.01	< 0.2	0.48
28[b]	CO	0.04	0.61	1.28
29	C_2H_5, CH_3N	0.29	1.34	2.47
30	NO	11.22	10.96	14.13
41	C_3H_5, C_2H_3N	1.14	2.15	4.21
43	C_2H_3O	5.14	6.16	10.00
44	C_2H_4O, C_3H_8	0.17	1.96	3.84
45	C_2H_5O	0.85	0.98	1.88
46	NO_2	0.33	0.58	1.07
57	C_3H_5O	5.59	4.81	4.82
58	C_3H_6O	0.66	1.43	2.90
59	C_2H_5NO	0.29	0.45	0.73
100	$C_5H_8O_2$	0.07	0.54	1.20
101	$C_5H_9O_2$	1.78	1.47	2.74
177[d]	$C_5H_9N_2O_5$	61.26	25.78	5.83

[a] Signals not corrected for evaporation. [b] Signals skewed to higher values due to noise from background corrections. [c] Formulae selected from structures that were likely to result from the plausible reaction schemes discussed in this section (i.e. iterative method). [d] Signal representative of BDNPA evaporation.

The ion signals from the BDNPA decomposition experiments contain features characteristic of evaporation, decomposition, and residue formation. Data from experiment BDNPA3 demonstrates these features as it differentiates the temporal behaviors of the signals associated with these processes.

The m/z = 177 ion signal best exemplifies the temporal behavior associated with evaporation of BDNPA. As discussed in the mass spectra section, the m/z = 177 ion maintains a high degree of temporal correlation with several of the other higher m/z value signals in every experiment performed. Experiment BDNPA3 is no exception. The temporal behavior of m/z = 177 and other correlated signals such as m/z = 133, 131, 88 and 74 are illustrated in Figure 5. The decay of the signals starting at ~4300 s is unusual and likely corresponds to the point at which the evolution of BDNPA transitions from that dominated by evaporation from BDNPA in a liquid phase to evolution of the BDNPA confined within a separate residue phase. Normally, the ion signals associated with evaporation of a reactant will fall rapidly to zero as the pristine sample is depleted. In this case, the residue formed in the reaction cell may create a separate phase that slowly releases BDNPA in a diffusion-limited process.

Mass spectra from experiment BDNPA3 contain ion signals at various m/z values with temporal behaviors that arise from differing extents of contribution from decomposition, residue formation and evaporation. The relative contributions from each process are conveniently assessed by dividing the temporal behavior of the ion signals into an induction/acceleration stage (0–1800 s), a decomposition stage (1800–4300 s), and a residue stage (4300 s completion). The three stages are represented in Figure 6. Ion signals at m/z values that exemplified different extents of contribution from decomposition, residue formation, and evaporation were selected as a baseline for comparison of the different processes. The range of temporal behaviors for these exemplary signals is shown in Figure 7a–d (full evaporative character is presented in Figure 5). M/z = 100 (Figure 7a) exhibits full decomposition character with no contributions from either residue formation or evaporation. Note how the signal falls as the amount of BDNPA in the reaction cell decreases and falls to near zero at the same time (~4300 s) as the signals associated with the BDNPA start to decay (Figure 5). M/z = 44 (Figure 7d) is an example of a product that evolves principally from the LVR, with little contribution from direct decomposition or evaporation of BDNPA. The signals at the other two m/z values fall somewhere within this range of temporal behaviors. M/z = 100 (decomposition), m/z = 44 (residue), and m/z = 177

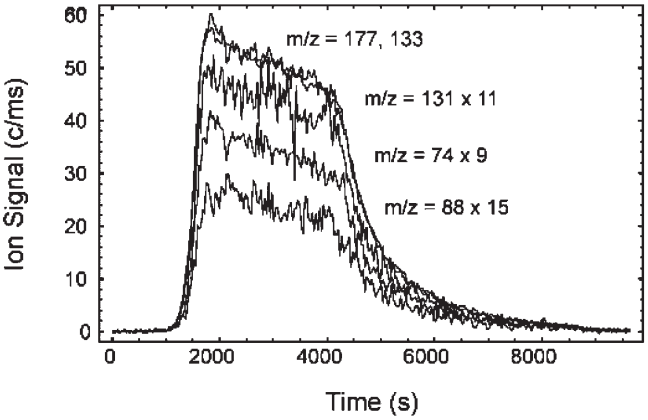

Figure 5. Temporal behavior of ion signals associated with BDNPA evaporation. Lower intensity signals are scaled for visual comparison.

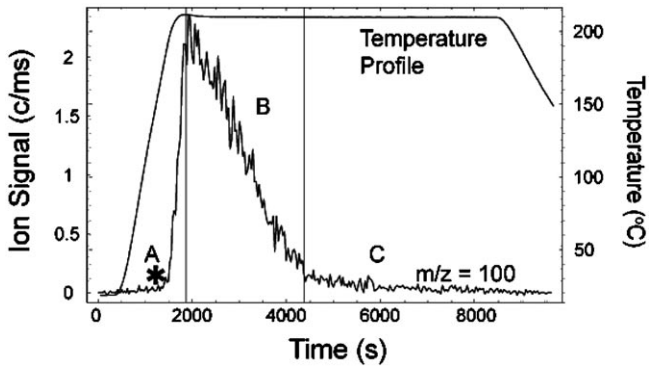

Figure 6. The three stages of BDNPA decomposition as represented by m/z = 100; A. Induction/Acceleration, B. Decomposition, C. Residue; * Indicates start of appreciable decomposition.

(evaporation) present the baseline by which all other signals are judged. For example, ion signals with major evaporative contributions tend to increase at earlier times (or temperatures) during the induction/acceleration stage and maintain relatively constant signal intensities during the decomposition stage. Ion signals with a decaying temporal behavior similar to that of m/z = 100 are associated with direct decomposition of BDNPA. Finally, those signals that maintain a large fraction of their signal intensity during the residue formation stage are associated with the residue.

A plausible BDNPA reaction mechanism was formulated based on careful consideration of mass loss data, temperature data, the postulated structures of the ions at different m/z values, and the m/z values of ion signals with similar temporal behaviors. Specifically, the temporal behavior and logical structures of m/z = 46, 100, and 101 (Figure 8) lead to the conclusion that BDNPA decomposes through nitro-nitrite rearrangement (Figure 9). Nitro-nitrite rearrangement is a commonly recognized reaction pathway for condensed phase gem-dinitro compounds with bonded alkyl groups [14]. During the induction stage, BDNPA molecules begin to evaporate. As the temperature increases, the acetal C–O bond homolytically cleaves to form a radical. The radical undergoes nitro-nitrite rearrangement, cleaving an NO (m/z = 30) and NO_2 (m/z = 46) group and forming a carbonyl functional group in the process. The remaining structure is that associated with the ion signal at m/z = 101, which may rearrange to the more stable m/z = 100 (1-(vinyloxy)propan-2-one). The LVR may be created through the reaction of the alkyl radicals that remain after the nitro-nitrite rearrangement to form a higher molecular weight "polymeric-like" species.

The remaining ion signals may originate from either fragmentation of nitro-nitrite rearrangement products in the ionizer, the formation of amines, imines or amides through nitroxyl radical reactions in the reaction cell, or evaporation/decomposition of the residue. The likely structures are summarized in Figure 10. As a reminder, these structures were crafted from careful consideration of the ion signal temporal behaviors as they relate to proposed decomposition processes. The ions with a carbonyl functional group likely stem from fragmentation of the m/z = 100 or m/z = 101 decomposition products in the ionizer. These

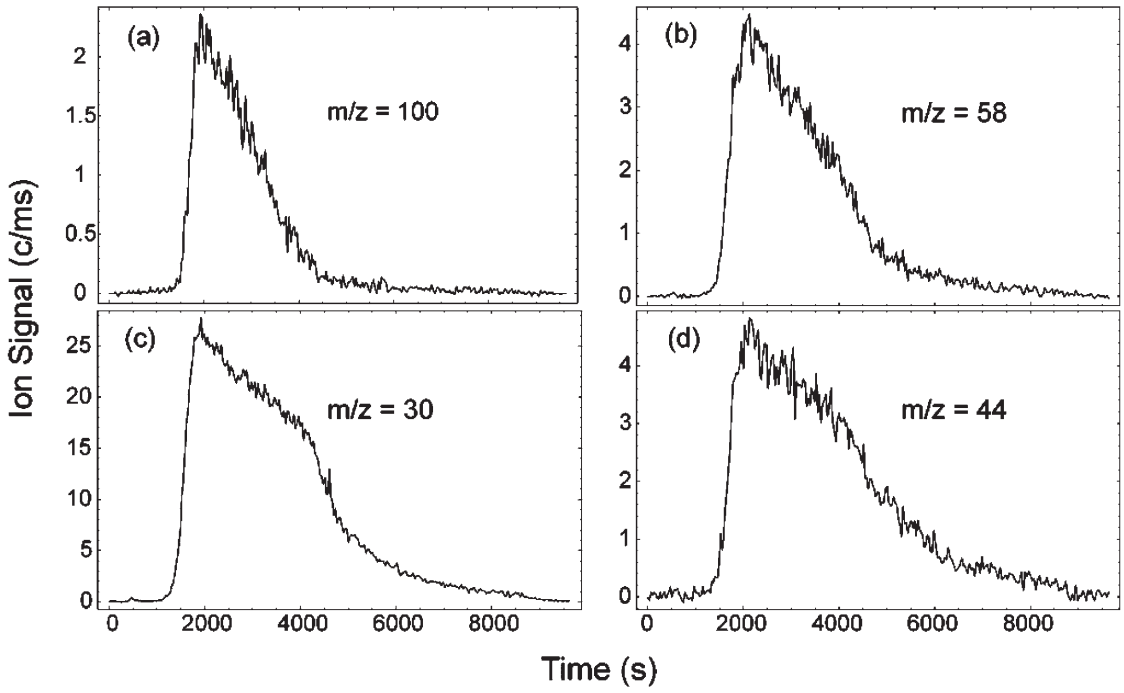

Figure 7. Ion signals representing a range of temporal behaviors that are observed in the decomposition of BDNPA. (a) m/z = 100; large fraction of decomposition, no evaporation, minimal residue. (b) m/z = 58; moderate fraction of decomposition, low evaporation, low residue. (c) m/z = 30; low fraction of decomposition, moderate evaporation, moderate residue. (d) m/z = 44; moderate fraction of decomposition, minimal evaporation, large residue. All ion signals were taken from experiment BDNPA3.

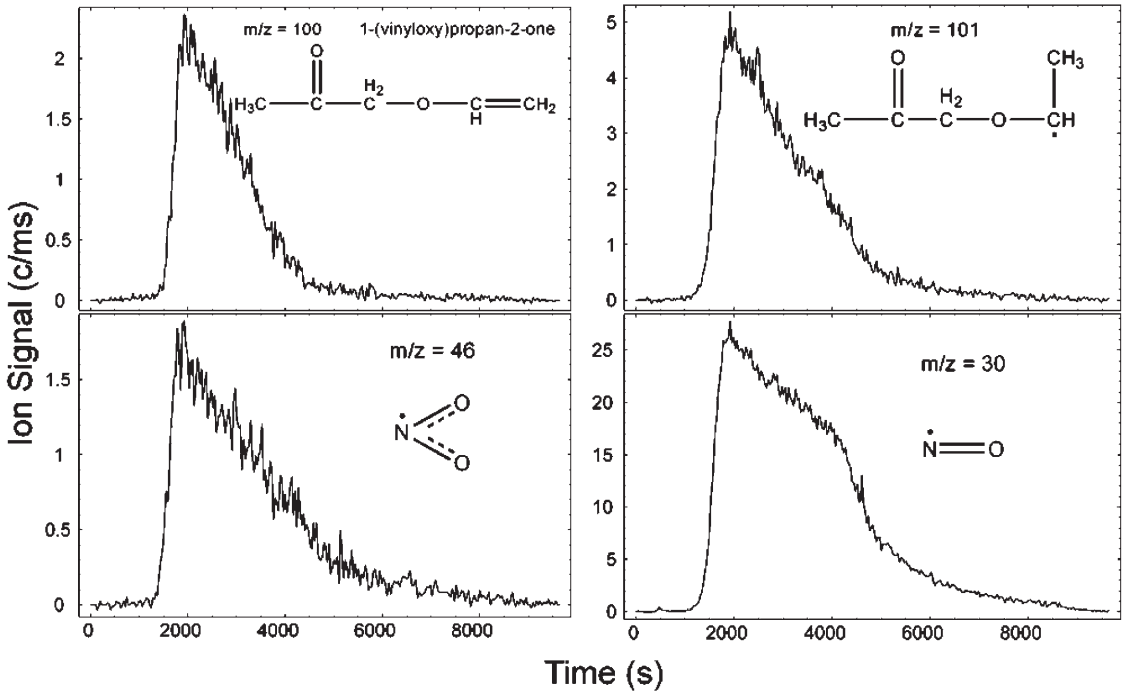

Figure 8. Temporal behavior of ion signals originating from products formed via the nitro-nitrite rearrangement mechanism in BDNPA. Differences in temporal behavior can be attributed to different extents of contribution from BDNPA evaporation, with m/z = 100 influenced the least and m/z = 30 influenced the most.

include ion structures such as m/z = 41, 43, 44 (acetaldehyde), 45, 57, and 58 (acetone). A plethora of radicals remain in the reaction cell after nitro-nitrite rearrangement. These radicals likely react to form a variety of decomposition products. For example, alkyl radicals may interact to produce the LVR. M/z = 29, 41, and 44 appear to originate from the residue as they maintain the intensity of their signal throughout the residue stage of experiment BDNPA3. Nitroxyl radicals may react with the alkyl radicals remaining in the reaction cell and produce amine, imine and amide structures.

Three new low molecular weight ion structures appear in the higher temperature BDNPA decomposition experiment (BDNPA4). The m/z = 18 (H_2O), 27 (HCN or alkyl radical) and 28 (CO) ions appear in appreciable quantities at ~230 °C, indicating contribution from other reaction pathways at higher temperature. At these higher temperatures, it is difficult to reach specific conclusions regarding origin of these new products because the reactions occur too rapidly to differentiate between subtle ion signal temporal behaviors from the current experimental results. These particular ion signals may originate from either decomposition of the residue, or fragmentation and rearrangement of the BDNPA backbone.

3.3.3 BDNPF Decomposition

BDNPF decomposition contains many features similar to that of BDNPA. As with BDNPA, BDNPF decomposition starts to occur at appreciable rates between 160 – 180 °C (Figure 12c). The characteristic BDNPF evaporation signals include m/z = 163, 133, 117, and 102; their temporal behaviors are presented in Figure 11. BDNPF also exhibits residue formation and decomposes through nitro-nitrite rearrangement. Many of the products formed in the thermal decomposition of BDNPF are analogous, if not identical, to those observed in BDNPA. The BDNPF decomposition products as well as their total ion signal percentage from experiments BDNPF2, BDNPF4 and BDNPF5 are given in Table 10. The stoichiometry and structures of the BDNPF decomposition products were developed in the same manner as that used for BDNPA.

The decomposition of BDNPF and BDNPA differs in two major ways. First, the decomposition rate of BDNPF is less than that of BDNPA. BDNPF does exhibit a lower vapor pressure than BDNPA at temperatures higher than 56 °C, which may play a role in suppressing the initial stages of decomposition. It appears, however, that other factors may also slow the rate of BDNPF decomposition. Three key comparisons between the decomposition of BDNPA and BDNPF are presented in Figure 12. As with BDNPA, BDNPF decomposition is conveniently analyzed in three temporal stages. The induction/acceleration (0 – 1800 s), decomposition (1800 – 6300 s), and residue stages (6300 s completion) are illustrated in Figure 12c. BDNPA and BDNPF have similar, if not identical, behavior during the induction/acceleration stage. Furthermore, both compounds appear to transition to the residue stage with approximately the same amount of relative sample mass

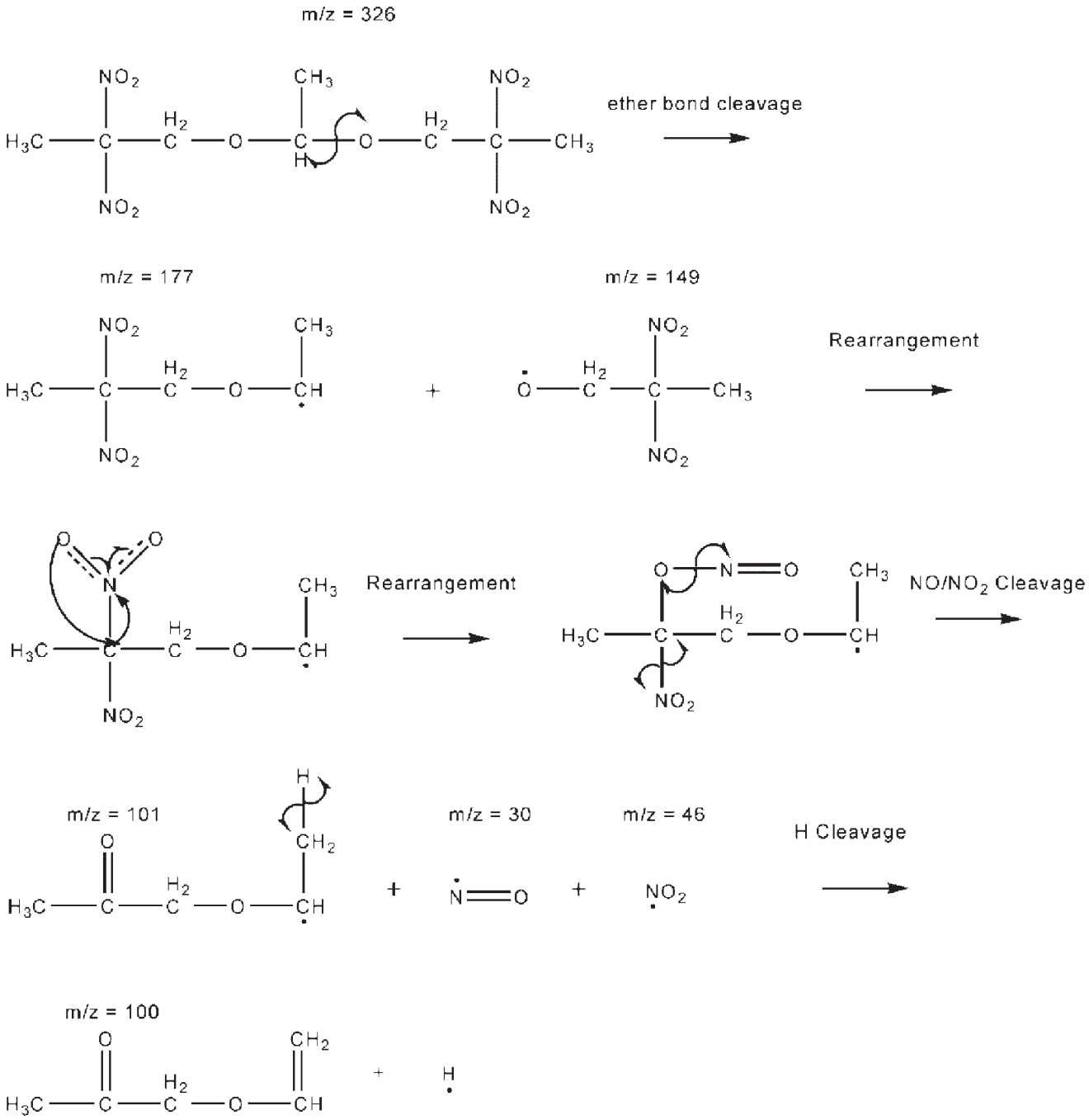

Figure 9. Nitro-nitrite rearrangement mechanism for BDNPA.

remaining. The mass-loss data from experiments BDNPA3 and BDNPF4 are presented in Figure 12a. These data, scaled to a range that represents the extent of reaction, indicate a lower rate of mass loss during the decomposition stage, but a faster decay during BDNPF's residue stage. A comparison of the m/z = 46 ion signal from BDNPA3 and BDNPF4 is given in Figure 12b. The m/z = 46 ion signal, with the exception of the point at which the signal transitions to its residue stage, exhibits the same temporal behavior for each compound. The similar temporal behavior of the m/z = 46 ion signal strongly suggests that nitro-nitrite rearrangement also occurs in BDNPF. The greater count rate in the BDNPF m/z = 46 ion signal is due to a larger initial sample mass. The question remains: if the characteristic nitro-nitrite rearrangement signal (m/z = 46) maintains a similar temporal behavior from BDNPA to BDNPF, then why does BDNPF exhibit a slower decomposition rate? Clearly, there is a mass-loss pathway that has not yet been accounted for. We postulate that this pathway manifests itself in the temporal behavior of the ketone products from nitro-nitrite rearrangement.

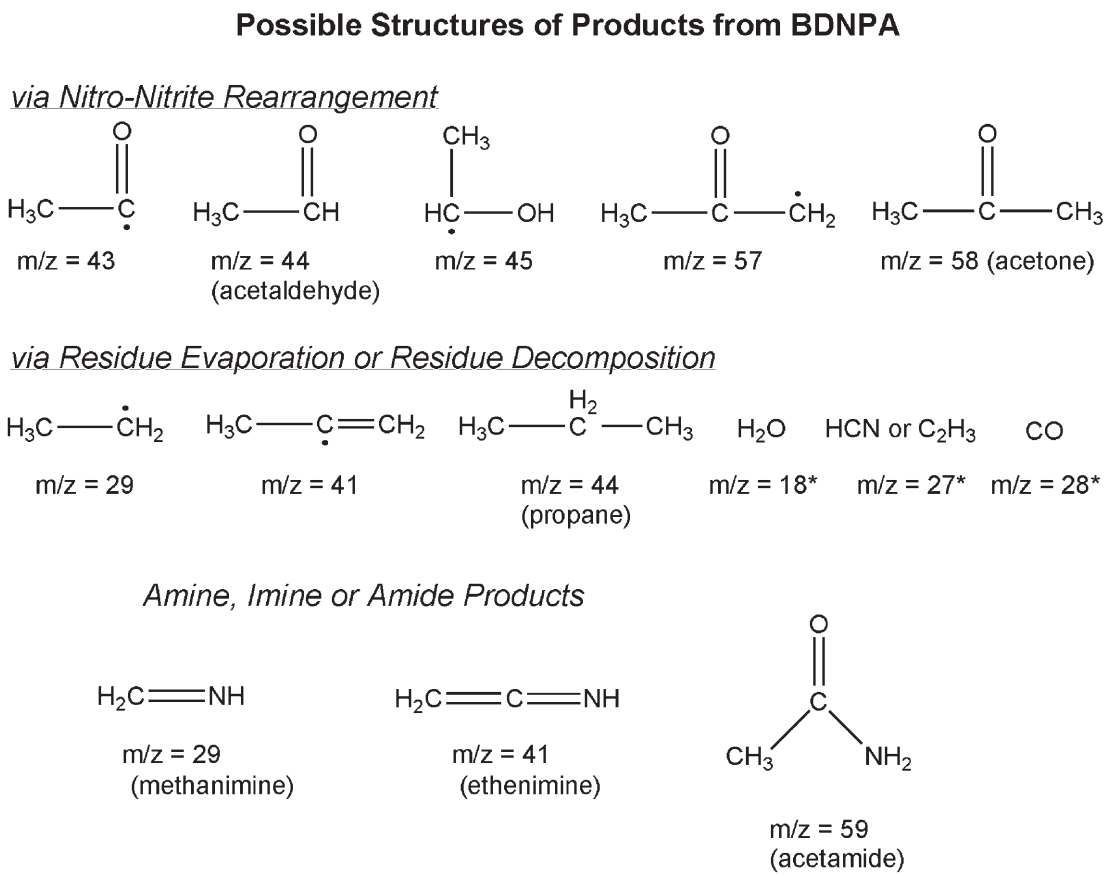

Figure 10. Possible BDNPA decomposition products. Structures are based on STMBMS ion signals at the listed m/z values and proposed reaction schemes. * Appreciable quantities only observed in 250 °C experiment (BDNPA4).

The second difference between the decomposition of BDNPA and BDNPF is the temporal behavior of some of the nitro-nitrite rearrangement decomposition products. The set of ion signals for BDNPF, with ion signals at individual m/z values representing various levels of contribution from decomposition, evaporation and residue formation, is presented in Figure 13a – e. The decrease in signal intensity of the m/z = 46 ion shown in Figure 13a has been discussed previously for the case of BDNPA. The m/z = 30 signal, presented in Figure 13b, originates from several different sources, which display a mix of temporal behaviors. The signal initially decays (like m/z = 46), but also appears to have contributions from evaporation (Figure 11) and a new source that is characterized by the signal at m/z = 87 (Figure 13c). Contributions from evaporation and the new source are also displayed in Figure 13d by m/z = 88. M/z = 44 in Figure 13e, much as it did with BDNPA, retains a large fraction of its signal intensity during the residue stage. The remaining decomposition products contain a mix of the aforementioned features and fall somewhere within the range of signals illustrated in Figure 13. The new temporal behavior, characterized by m/z = 87 in Figure 13c, is representative of products from the decomposition of BDNPF that originate from nitro-nitrite rearrangement. The signal is rounded in nature, which contrasts significantly with the m/z = 46 ion signal and those decomposition products from BDNPA that are formed via nitro-nitrite rearrangement. The BDNPF decomposition mechanism is presented in Figure 14. Note the additional step in the decomposition mechanism. We postulate that the m/z = 87 product, which is structurally analogous to the m/z = 101 larger molecular weight ketone product in BDNPA, is delayed in its release from the reaction cell by forming a complex through interactions with an unidentified intermediate species. The

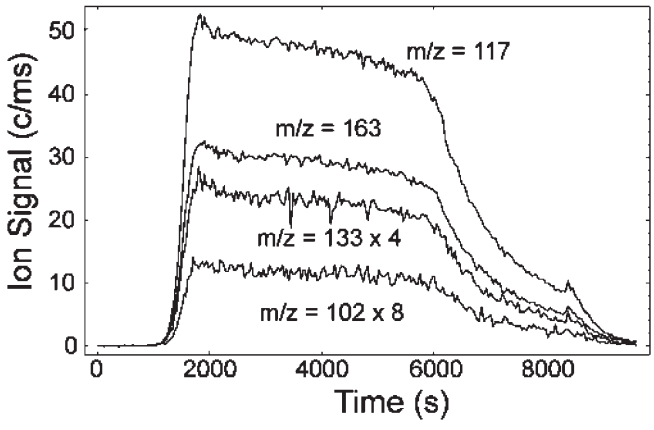

Figure 11. Temporal behavior of ion signals from BDNPF evaporation. Lower intensity signals scaled for visual comparison.

Table 10. BDNPF decomposition products and relative abundance[a].

Ion (m/z)	Ion Empirical Formulae[d]	% Total Ion Signal from BDNPF2 (100 μm confinement, 210 °C max)	% Total Ion Signal from BDNPF4 (10 μm confinement, 210 °C max)	% Total Ion Signal from BDNPF5 (10 μm confinement, 250 °C max)
18[b]	H_2O	< 0.1	2.15	3.91
27	HCN, C_2H_3	< 0.1	0.13	0.29
28[b]	CO	< 0.1	0.45	1.26
29	CHO, C_2H_5	2.04	1.75	2.10
30	NO, CH_2O	6.31	8.05	10.57
31	CH_5N	0.40	0.50	1.09
41	C_3H_5, C_2H_3N	1.64	2.56	4.18
43	C_2H_3O	1.87	5.04	8.18
44	C_2H_4O, C_3H_8	< 0.1	1.09	2.39
46	NO_2	0.33	0.73	1.23
57[c]	C_3H_5O	6.31	5.47	4.81
58	C_3H_6O	2.48	4.03	5.66
59[c]	C_2H_5NO	3.88	3.00	2.83
60[c]	CH_2NO_2	1.60	1.10	1.13
73	$C_3H_5O_2$	< 0.1	0.27	0.50
87	$C_4H_7O_2$	2.97	5.18	7.69
88[c]	$C_4H_8O_2$	7.15	4.70	3.72
103	$C_4H_7O_3$	0.16	0.38	0.76
118[c]	$C_5H_{10}O_3$	2.85	2.19	2.00
163[e]	$C_4H_7N_2O_5$	50.48	16.12	6.78

[a] Signals not corrected for evaporation. [b] Signals skewed to larger values due to noise from background corrections. [c] Signals contain significant evaporation contributions (Table 6), which skew trends in ion signal percentage. [d] Formulae selected from structures that were likely to result from the plausible reaction schemes discussed in this section. [e] Signal representative of BDNPF evaporation.

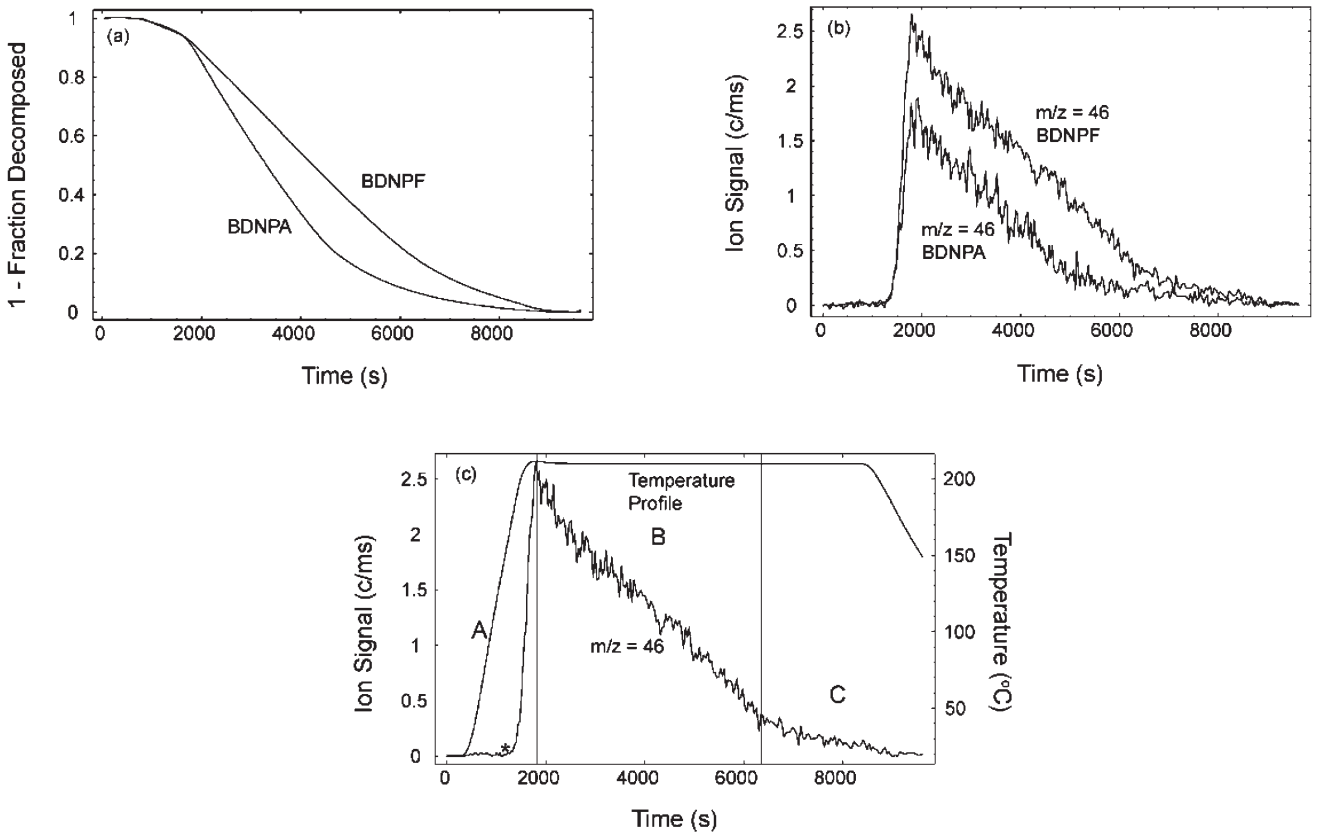

Figure 12. Comparison of BDNPF and BDNPA decomposition. (a) weight loss data (scaled to the fraction of decomposable mass remaining). (b) m/z = 46 ion signal for both compounds. (c) temperature profile for the experiment and three stages of decomposition in BDNPF; A. Induction/Acceleration, B. Decomposition, C. Residue. The * (~1800 s in 13c) indicates start of appreciable decomposition.

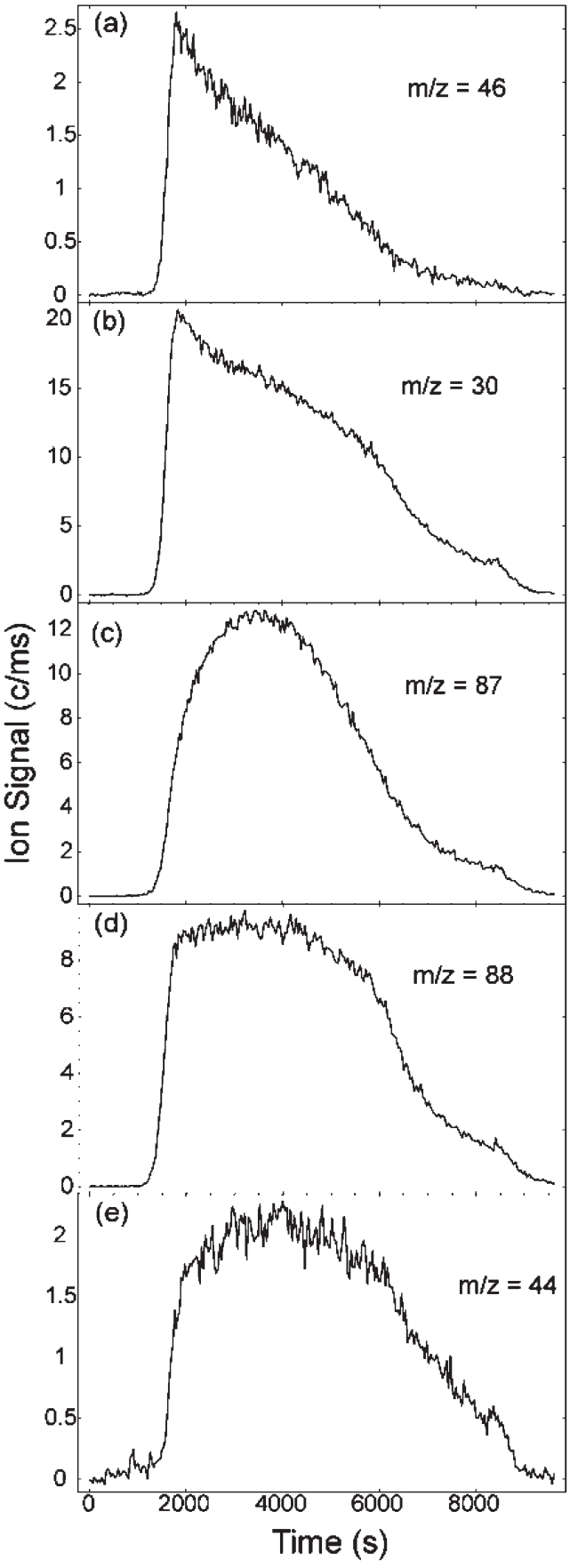

ketone product eventually disengages from the complex as the BDNPF decomposition progresses, possibly due to interactions with the residue that is formed during decomposition. The ketone products from BDNPA nitro-nitrite rearrangement do not exhibit the same "delayed release" temporal behavior. There are two possible explanations for this behavior: (1) BDNPA may not form an intermediate that interacts with the ketone products from nitro-nitrite rearrangement, or (2) the more likely scenario, m/z = 101 in BDNPA does not interact with the intermediate because steric hindrances reduce the reactivity of the acetal carbon.

The remaining structures from BDNPF decomposition are presented in Figure 15. Most of the BDNPF decomposition products are analogous to those of BDNPA, however BDNPF decomposition appears to produce a greater number of products. The most notable of these products is 1-(dimethoxy)propan-2-one (m/z = 118). The structure requires a reaction at the formal carbon point of reactivity or unimolecular cleavage of the C–O bond beta to the formal carbon. BDNPA decomposition does not produce an analogous structure. The reactivity of the acetal carbon may be sufficiently reduced through steric means.

3.4 Future Work

Additional experiments can be performed to develop more concrete conclusions. Time-of-flight velocity spectra experiments [16] will aid in definitively differentiating between reaction cell products and ionizer fragmentation products. This technique would be particularly beneficial in identifying those lower molecular weight products that have been produced through direct decomposition and not through fragmentation of higher molecular weight decomposition products in the ionizer of the mass spectrometer. The FTICR instrument may be used to examine samples at higher temperatures and provide confirmation of the empirical formulae presented in the BDNPA and BDNPF decomposition tables (Tables 9 and 10). Finally, the experiments performed with pure component BDNPA and BDNPF may also be repeated with the BDNPA/F eutectic to identify any aggregate effects from the coexistence of the two materials.

4 Conclusions

The mass spectra of BDNPA and BDNPF are, for the most part, structurally analogous, but differ significantly in the

Figure 13. Temporal behaviors of ion signals representing different aspects of the BDNPF decomposition process. (a) m/z = 46; almost entirely decomposition. (b) m/z = 30; mix of "delayed release" and "immediate cleavage" decomposition products and some evaporation. (c) m/z = 87; decomposition. (d) m/z = 88; even mix of decomposition and evaporation. (e) m/z = 44; decomposition and large residue formation. The representative temperature profile is shown in 12c.

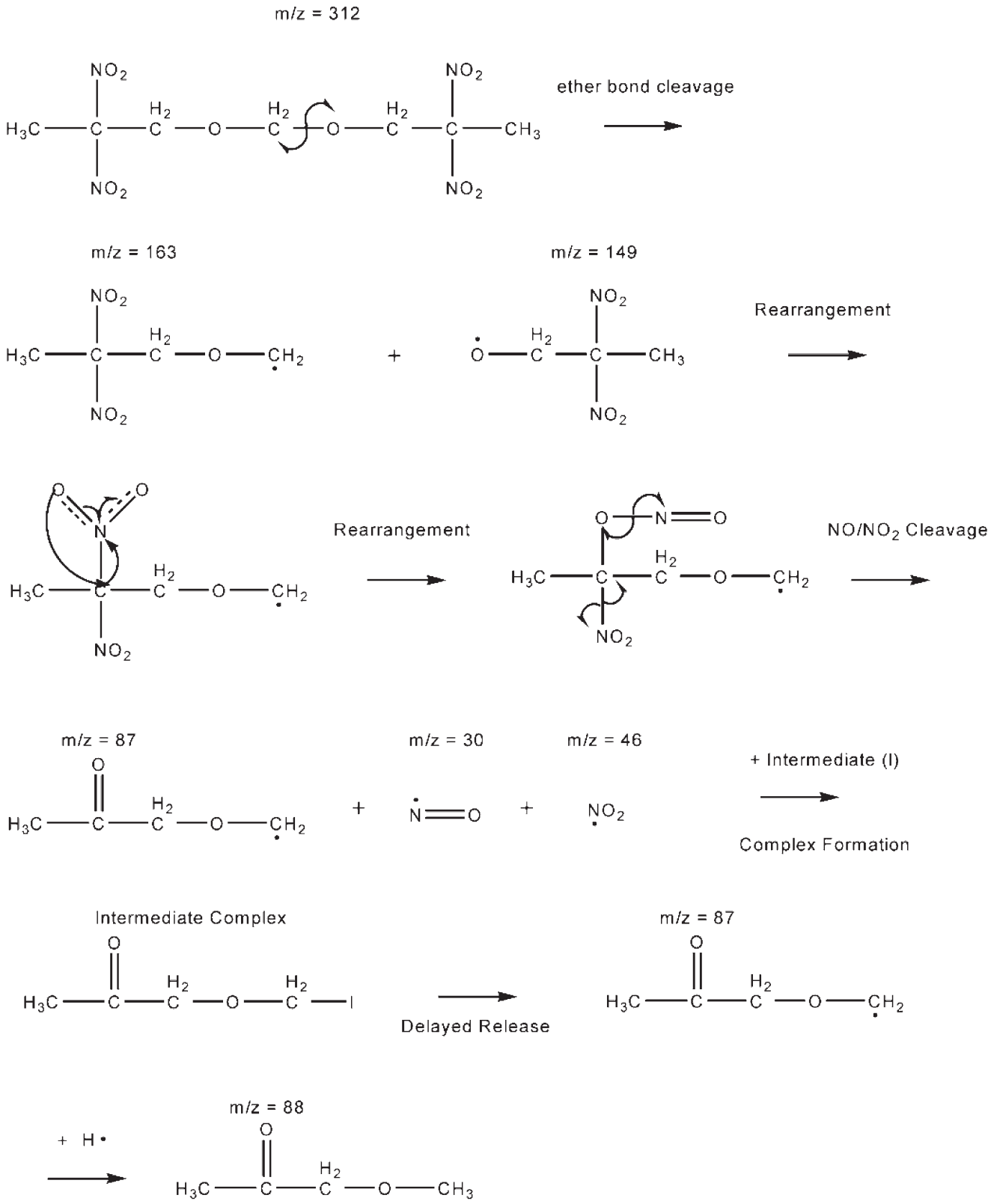

Figure 14. Proposed reaction mechanism for the thermal decomposition of BDNPF.

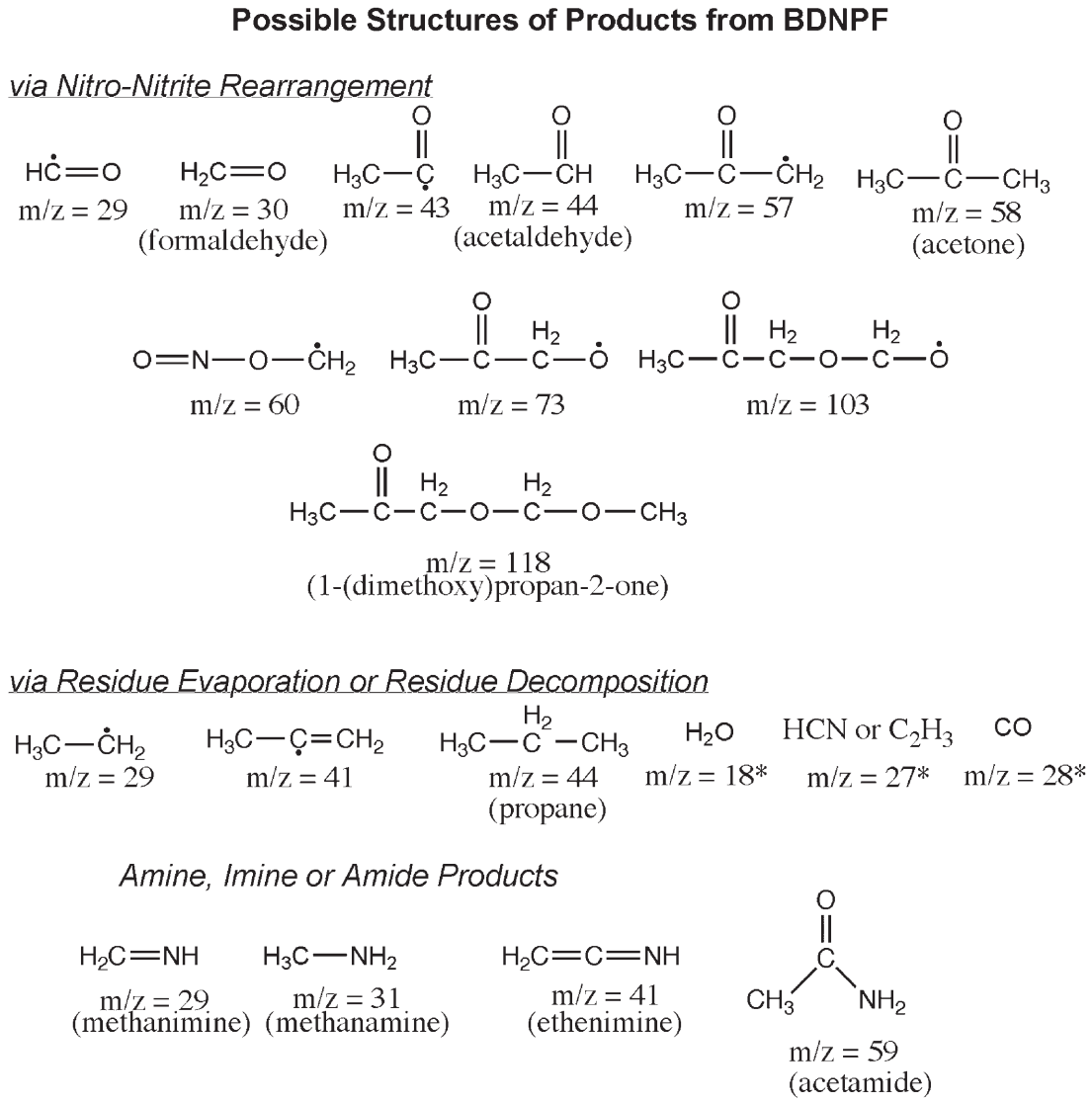

Figure 15. Possible BDNPF decomposition products. Structures are based on STMBMS ion signals at the listed m/z values and proposed reaction schemes.

relative abundance of some ion fragments. Each compound contains two ion fragments that make up more than sixty percent of the overall signal percentage. BDNPF exhibits a greater propensity to cleave a nitro group and forms smaller molecular weight fragments with greater abundance than BDNPA. The fragmentation pattern of the mass spectrum for each compound is sensitive to the internal energy of the molecules entering the mass spectrometer, with the bond rearrangement process forming the daughter ions in the mass spectrum being similar to the bond rearrangements that occur during the thermal decomposition of each compound.

STMBMS data from 80 – 110 °C were used to measure the vapor pressure as a function of temperature for BDNPA and BDNPF. BDNPA exhibits a higher vapor pressure than BDNPF at temperatures higher than 56 °C. For BDNPA, the enthalpy of vaporization ($\Delta_{vap}H$) is 93.01 ± 0.38 kJ/mol and the vapor pressure at 25 °C equals 1.45 + 0.40/– 0.27 mPa. BDNPF has a lower enthalpy of vaporization, 84.77 ± 0.88 kJ/mol, but a higher vapor pressure at 25 °C, 2.20 + 1.9/– 1.1 mPa.

BDNPA and BDNPF undergo thermal decomposition at appreciable rates starting between 160 – 180 °C. The decomposition of each compound is characterized by a nitro-nitrite rearrangement mechanism and the formation of an LVR. This decomposition pathway produces a large molecular weight alkyl radical, NO and NO_2 radicals, and a stable ketone identified as 1-(vinyloxy)propan-2-one in BDNPA and 1-methoxypropan-2-one in BDNPF. The remaining alkyl radicals begin to react and form an LVR that suppresses evaporation when the amount of pristine plasticizer left in the reaction cell reaches a critical minimum. The nitroxyl radicals react with alkyl reaction cell products to form amine, imide and amide decomposition products. Lower molecular weight decomposition products, such as H_2O and CO, appear at ~ 230 °C.

Some significant differences exist between BDNPA and BDNPF decomposition. The global weight loss rate of BDNPF is slower than that of BDNPA under the same experimental conditions. This, in part, can be attributed to a lower vapor pressure in BDNPF. Furthermore, the temporal behavior of the ketone product from nitro-nitrite rearrangement in BDNPF (1-methoxypropan-2-one) is different than that of BDNPA (1-(vinyloxy)propan-2-one). The release of this product is delayed in the decomposition of BDNPF due to the formation of a low volatility reaction intermediate that resides in the condensed phase. This intermediate does not appear to form from secondary reactions in the decomposition of BDNPA, which is most likely due to steric hindrance from the acetal functional group.

This work forms the basis for collecting and analyzing additional data needed to develop models of the reaction kinetics underlying the reaction mechanisms of BDNPA and BDNPF presented in this paper.

5 References

[1] S. M. Shen, A. L. Leu, H. C. Yeh, Thermal Characteristics of Polyurethane PEG and BDNPA F-Blends, *Thermochim. Acta* **1991,** *176*, 75.

[2] N. Wingborg, C. Eldsater, 2,2-Dinitro-1,3-Bis-Nitrooxy-Propane (NPN): A New Energetic Plasticizer, *Propellants, Explos., Pyrotech.* **2002**, *27*, 314.

[3] S. M. Shen, A. L. Leu, S. I. Chen, H. C. Yeh, Thermal Characteristics Of GAP, GAP/BDNPA/BDNPF and PEG/BDNPA/BDNPF and the Energetic Composites thereof, *Thermochim. Acta* **1991,** *180*, 251.

[4] S. M. Shen, Y. S. Chiu, S. W. Wang, S. I. Chen, The Thermal Decomposition of Azide Polymers Containing Ferruginous Compounds, *Thermochim. Acta* **1993**, *221*, 275.

[5] K. Sugimori, M. Shimoda, T. Yamaya, K. Hori, T. Saito, The Combustion Characteristics of BAMO-THF/AN Propellants, *Kayaku Gakkaishi/Journal of the Japan Explosives Society* **2001,** *62*, 80.

[6] K. Selim, S. Ozkar, L. Yilmaz, Thermal Characterization of Glycidyl Azide Polymer (GAP) and GAP-based Binders for Composite Propellants, *J. Appl. Polym. Sci.* **2000**, *77*, 538.

[7] S. M. Shen, Y. S. Chiu, S. I. Chen, Thermal-Characteristics of Poly-BAMO and Poly-BAMO/BDNPA/BDNPF Blends, *Thermochim. Acta* **1993**, *213*, 151.

[8] S. M. Shen, A. L. Leu, S. I. Chen, H. C. Yeh, Thermal Behavior and Compatibility of Polyurethane PCL/BDNPA/F and PCL/TMETN Blends, *Thermochim. Acta* **1991**, 181, 277.

[9] U. R. Nair, G. M. Gore, R. Sivabalan, C. N. Divekar, S. N. Asthana, H. Singh, Studies on Advanced CL-20-Based Composite Modified Double-Base Propellants, *J. Propulsion and Power* **2004**, *20*, 952.

[10] C. K. Saw, C. M. Tarver, Binder/HMX Interaction in PBX 9501 at Elevated Temperatures, *Conference of the American Physical Society Topical Group on Shock Compression of Condensed Matter*, Portland, Oregon, USA, July 20 – 25, **2003**, AIP Conference Proceedings 706, p. 1029.

[11] P. D. Peterson, J. T. Mang, B. W. Asay, Quantitative Analysis of Damage in an Octahydro-1,3,5,7-Tetranitro-1,3,5,7-Tetrazonic-Based Composite Explosive Subjected to a Linear Thermal Gradient, *J. Appl. Phys.* **2005**, *97*, 1.

[12] J. I. Sato, M. Shibaura, Y. Yonemura, K. Nakamura, S. Nakahara, Explosive Properties of Urethane-based PBXes Containing HMX and BDNPA/F (II), *Explosion and Explosives (English translation of Kogyo Kayaku)* **1992**, *53,* 268.

[13] L. M. G. Minier, R. Behrens, Jr., Thermal Decomposition Mechanisms of Bis(2-Fluoro-2,2-Dinitroethyl) Formal (FEFO) and Bis(2-Fluoro-2,2-Dinitroethyl) Difluoroformal from Simultaneous Thermogravimetric Modulated Beam Mass Spectrometry (STMBMS) Measurements, *Propellants, Explos. Pyrotech.* **1997**, *22*, 23.

[14] Y. Oyumi, T. B. Brill, Thermal Decomposition of Energetic Materials 11. Condensed Phase Structural Characteristics and High Rate Thermolysis of Di- and Trinitroaliphatic Carboxylic Acids and Carbonates, *Combust. Flame* **1986**, *65*, 103.

[15] R. Behrens, Jr., New Simultaneous Thermogravimetry and Modulated Molecular Beam Mass Spectrometry Apparatus for Quantitative Thermal Decomposition Studies, *Rev. Sci. Instrum.* **1987**, *58*, 451.

[16] R. Behrens, Jr., Identification of Octahydro-1,3,5,7-Tetranitro-1,3,5,7-Tetrazocine (HMX) Pyrolysis Products by Simultaneous Thermogravimetric Modulated Beam Mass Spectrometry and Time-of-Flight Velocity-Spectra Measurements, *Int. J. Chem. Kinet.* **1990**, *22*, 135.

[17] R. Behrens, Jr., Determination of the Rates of Formation of Gaseous Products from the Pyrolysis of Octahydro-1,3,5,7-Tetranitro-1,3,5,7-Tetrazocine (HMX) by Simultaneous Thermogravimetric Modulated Beam Mass Spectrometry, *Int. J. Chem. Kinet.* **1990**, *22*, 159.

Acknowledgements

This work was supported in part by the U.S. Army Research Office Project 43381-CH and a joint Memorandum of Understanding between the Department of Defense Joint Munitions Program and the U.S. Department of Energy. Rory Rauch was supported by the Defense Nuclear Facilities Safety Board Professional Development Program.

(Received July 17, 2006; Ms 2006/129)

To be presented at the 41st JANNAF Combustion Subcommittee Meeting, December 4-8, 2006, San Diego, CA.

REACTION PROCESSES THAT CONTROL THE THERMAL DECOMPOSITION OF MIXTURES OF TAGZT AND RDX

Richard Behrens, Deneille Wiese-Smith
Combustion Research Facility, Sandia National Laboratories
Livermore, CA 94551-0969

Heather Hayden
Naval Surface Warfare Center, Indian Head Division
101 Strauss Avenue
Indian Head, MD 20640-5035

ABSTRACT

To determine why TAGzT acts as a good burn rate modifier in RDX-based composite propellants, simultaneous thermogravimetric modulated beam mass spectrometry (STMBMS) and Fourier Transform ion cyclotron resonance (FTICR) mass spectrometry methods were used to examine the thermal decomposition of mixtures of bis(triaminoguanidinium) 5,5'-azotetrazolate (TAGzT) and hexahydro-1,3,5-trinitro-s-triazine (RDX). Hydrazine that is formed in the decomposition of TAGzT undergoes a very strong and rapid reaction with RDX. At temperatures near the melting point of RDX, the reaction rate of hydrazine with RDX is faster than the rate of decomposition of RDX by itself. The main interaction between hydrazine and RDX involves the removal of the NO_2 groups from RDX and their reaction with hydrazine to form primarily H_2O and N_2O. The other gaseous products formed during the decomposition of TAGzT, NH_3, HCN and N_2 do not react with RDX to a significant extent when compared to the reaction of hydrazine with RDX. Since the reaction of hydrazine with RDX is rapid compared to the decomposition of RDX alone, compounds that decompose to form hydrazine at a temperature near the decomposition temperature of the nitramine ingredient should be good candidates for burn rate modifiers for nitramine-based composite propellants.

INTRODUCTION

Munition systems of the future will be required to achieve new performance objectives while meeting insensitive munition (IM), safety, environmental compliance, and health requirements. Performance objectives will require increasing the energy deposited on target, and doing it in controlled and field-tailored manner. This will require chemical propulsion systems with features that go beyond current design capabilities. Meeting these objectives will require new solid propellants whose combustion behavior can be tailored to meet specific needs.

For example, in a quest to improve the performance of its gun systems, the Army and Navy are exploring advanced propellant formulations. Tailoring the burn rate of nitramine propellants through the use of high-nitrogen energetic compounds is an approach to achieve that goal. The advantage is an increase in the energy or work delivered to the projectile that won't exceed the hardware limitations of the gun system.[1] High-nitrogen compounds are also attractive in that they have high heats of formation, they lower the flame temperature of propellants and their high nitrogen content is favorable for mitigating gun barrel erosion.[2-4]

High performance, smokeless propellants often employ nitramines, such as RDX, as a primary ingredient. While nitramines provide significant energy enhancements in solid propellants, until recently there has been little success in developing burn rate modifiers that can be used to tailor their combustion behavior to meet more demanding design requirements. The

conventional formulation and test methods used to development burn rate modifiers for double-base propellants have been unsuccessful, when applied to nitramine-based propellants.[5]

In the Navy's program to examine the use of high-nitrogen compounds to develop advanced gun propellants, closed bomb combustion results revealed that triaminoguanidinium azotetrazolate (TAGzT) significantly increases the burn rate of the nitramine-based propellant, EX-99 (76.0% RDX, 12.0%CAB, 4.0%NC, 7.6%BDNPA/F, 0.4%EC).[1, 6] This result shows that TAGzT can be an effective burn rate modifier for nitramine-based propellants.

If an understanding of why TAGzT is an effective burn rate modifier can be determined, then this information may be used to guide the design of other molecules with a range of different properties that may also be effective burn rate modifiers.

To address this issue we examined the interaction of TAGzT, RDX and their decomposition products to determine (1) whether the decomposition behavior of RDX is altered by the presence of TAGzT and (2) if it is, the nature of the underlying reaction process that controls the interaction.

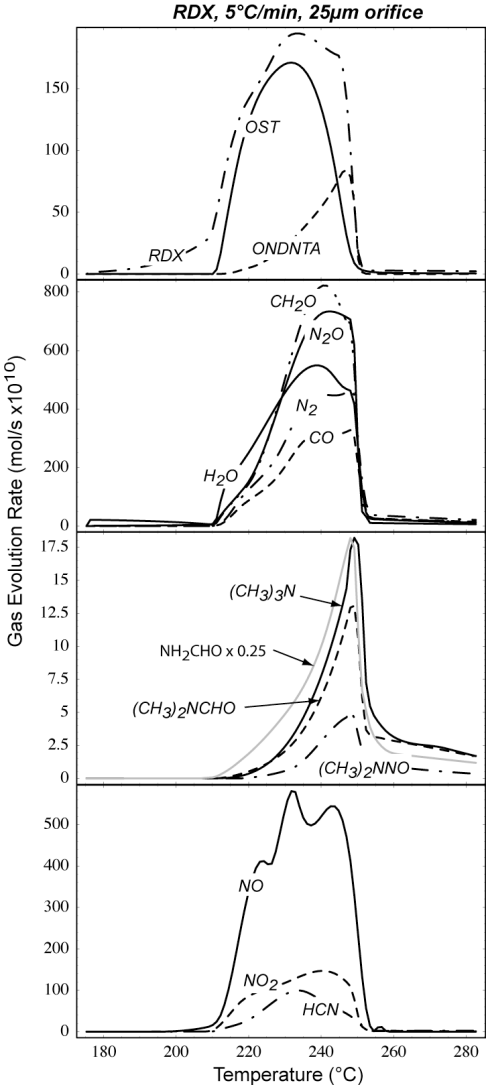

Figure 1. Gas evolution rates of products formed during the thermal decomposition of RDX.

RDX Decomposition. Previously, we have examined the decomposition of RDX[7-11] and TAGzT[12]. The reaction process that controls the decomposition of RDX is nonlinear and complex. This behavior is illustrated in Figure 1 by the different temporal behaviors of the rate of formation of the products formed during its decomposition. For example, the rate of evolution of RDX increases as the sample melts (~200°C). As the sample melts there is a rapid increase in the rate of formation of oxy-s-triazine (OST), which is formed via the direct decomposition of RDX. In contrast, many of the decomposition products (e.g., CH_2O and N_2O), formed via the mononitroso intermediate of RDX, hexahydro-1-nitroso-3,5-dinitro-s-triazine (ONDNTA), appear later in the decomposition process. A non-volatile residue (NVR) also forms during the decomposition process. Once NVR has formed, it too reacts directly with RDX, opening new reaction pathways. Some features of the NVR have been determined by monitoring the gaseous products formed as the NVR decomposes (e.g., trimethylamine, $(CH_3)_3N$).

RDX Decomposition Model. The data from a series of experiments probing the decomposition of RDX below and above its melting point have been used to construct a reaction scheme characterizing the main features of its decomposition process (Fig. 2). Mathematical models of this reaction scheme have been presented previously.[11] The reaction scheme is composed of reactions that occur in four separate phases that are present during the thermal decomposition experiments: solid phase, liquid phase, gas phase and a separate phase of the NVR. The reactions in the solid phase are limited to sublimation and melting of RDX. Note that reactions occur on the surface of RDX particles as products from the decomposition of RDX,

formed in the gas phase, deposit on the surface of the particles. Reactions in the gas phase occur in RDX that has evaporated from solid or liquid RDX. At temperatures above the melting point of RDX, reactions in liquid phase RDX will dominate the reaction process, since most of the RDX is present in the liquid phase during the course of an experiment. It is also important to note the role of NO and NO_2 in coupling several different reaction pathways in the overall reaction scheme.

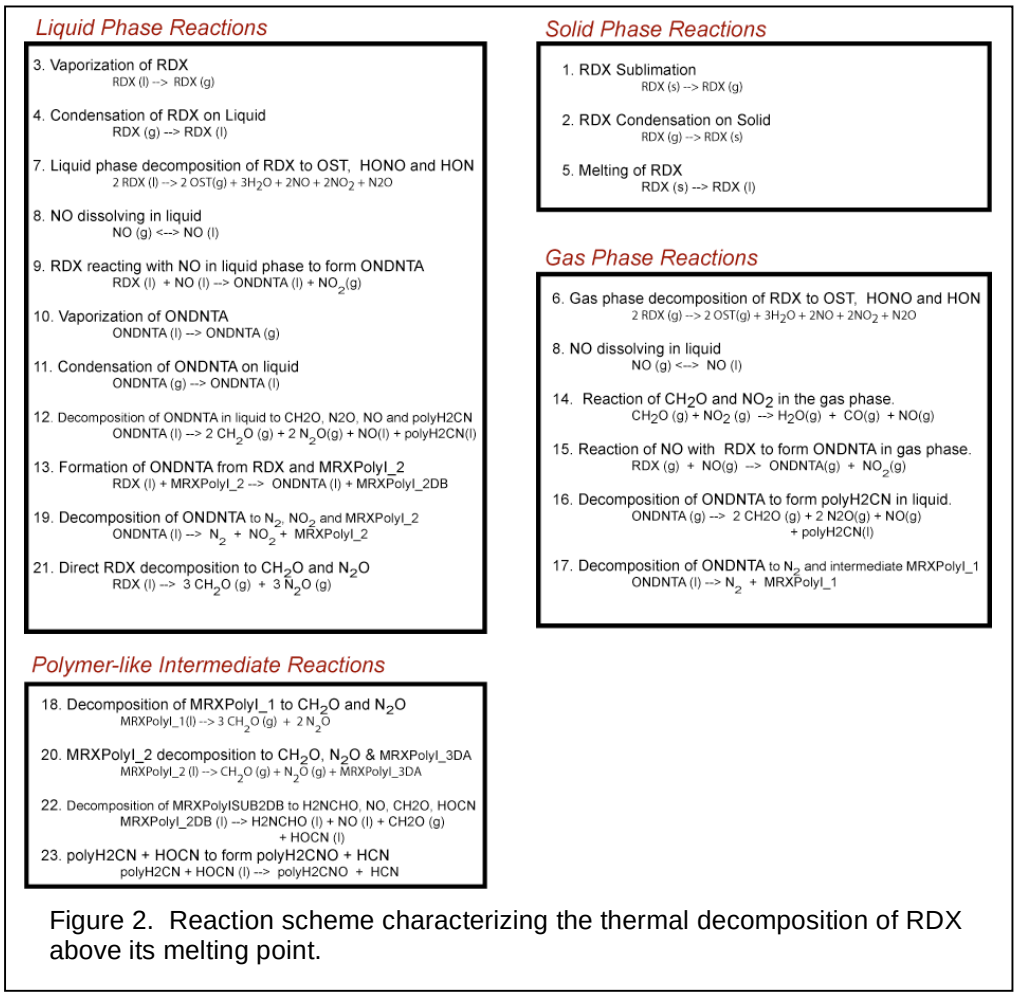

Figure 2. Reaction scheme characterizing the thermal decomposition of RDX above its melting point.

Burn Rate Modification. In order for a compound to be an effective burn rate modifier of an RDX-based propellant, it must either (1) react with RDX and effectively compete with the reactions that control the decomposition of RDX by itself, or (2) it must form gaseous products that interact and alter the combustion of the flame above the propellant surface. The first type of interaction will alter the pyrolysis processes on the surface of the burning propellant. The second type of interaction will alter the flame properties and affect the heat transfer to the propellant surface.

To most effectively alter the burn rate of RDX, a burn rate modifier should affect the first stages of the RDX decomposition process. As suggested by the reaction scheme shown in Fig. 2, a burn rate modifier may affect reactions at different steps in the RDX decomposition scheme.

The decomposition of TAGzT is currently being probed using simultaneous thermogravimetric modulated beam mass spectrometry (STMBMS) and Fourier Transform ion cyclotron resonance (FTICR) mass spectrometry methods. To date we have identified the products formed during its decomposition and developed a reaction scheme based on their

identities and temporal behavior of their evolution during the course of an experiment.[12] The current reaction scheme is shown in Figure 3.

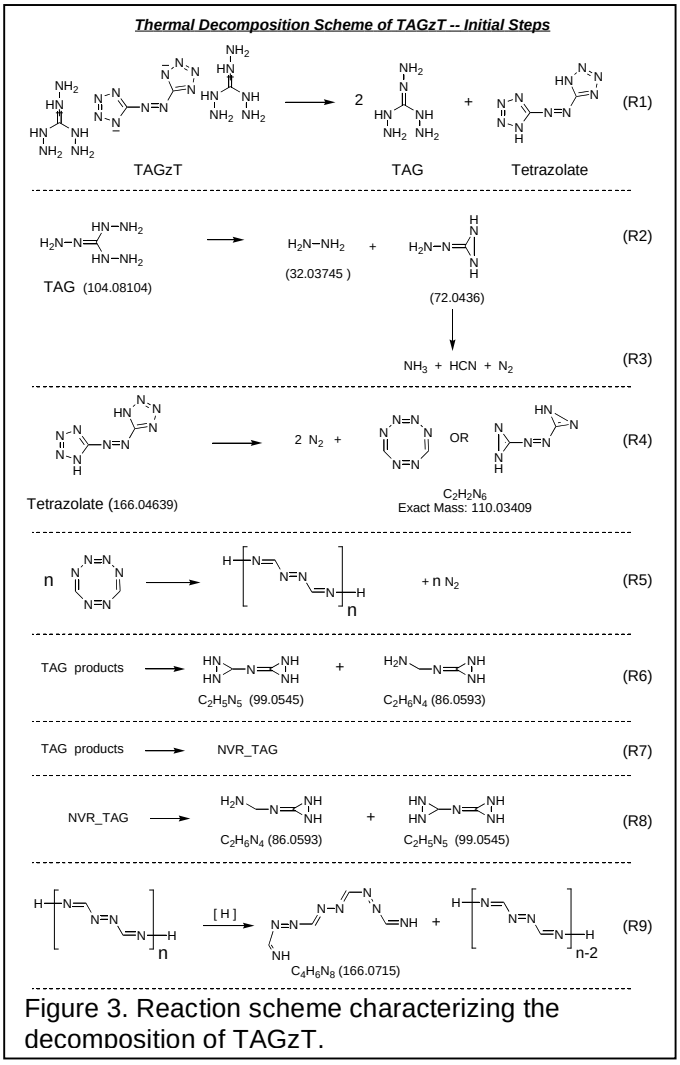

Figure 3. Reaction scheme characterizing the decomposition of TAGzT.

The first step involves the transfer of hydrogen from the triaminoguanidinium (TAG) cation to the azotetrazolate (AT) anion resulting In the formation of TAG and AT (R1). The TAG then decomposes to form hydrazine, N_2H_4, and an intermediate (R2) that may either decompose to lower molecular weight products (R3), HCN, N_2 and NH_3, or form higher molecular weight products, which may be volatile (R6) or (R7). The azotetrazolate decomposes releasing two N_2 molecules and forms a product with a molecular weight of 110, which may have a structure shown in R4. Higher confinement of the decomposition products promotes secondary reactions between the intermediate formed in the decomposition of TAGzT, which results in ~40wt% of the sample remaining as relatively non-volatile products after the TAGzT has decomposed. Further heating of this residue releases higher molecular weight gaseous products shown in Reactions R8 and R9.

Thus, there are two main features of the TAGzT decomposition process that may provide for interactions with RDX: (1) reaction with one or more of the gaseous products, NH_3, HCN, or N_2H_4, or (2) interaction of RDX with the non-volatile product. Hydrazine is the most reactive species formed in the decomposition of TAGzT.

The objective of the work presented in this paper is to determine the nature of the interactions that occur, if any, between TAGzT and RDX. The results from our experiments showing how TAGzT interacts with RDX are presented in this paper. In the future quantified data of the decomposition process will be acquired and mathematical models will be developed to represent the reaction kinetics of the decomposition process.

RESULTS AND DISCUSSION

EXPERIMENTAL METHODS

Instruments. Mass spectrometry is used to identify the compounds formed during the decomposition of mixtures of TAGzT and RDX. Simultaneous thermogravimetric modulated beam mass spectrometry (STMBMS) methods are used to measure the time and temperature dependence of the evolution of the decomposition products during the course of an experiment. The variables in an experiment (i.e., temperature, heating rate, pressure of the confined gaseous decomposition, extent of mixing of the compounds in the mixture) are altered in a controlled

manner to provide data that can be used to elucidate the details of the reaction scheme. In this paper the formulas and temporal behaviors of the ions signals formed during the course of the decomposition experiments are used to develop our understanding of the interactions that occur between TAGzT and RDX.

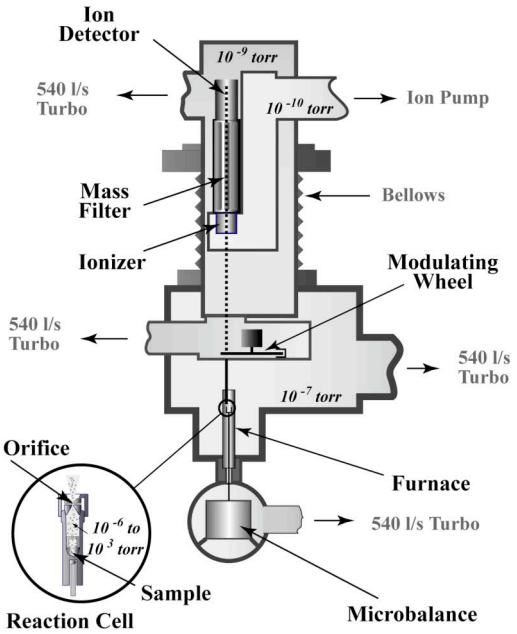

Figure 4. Schematic diagram of the STMBMS instrument.

The design and operation of the STMBMS instrument and details of the methods used to analyze the data have been descibed previously.[13-16] A schematic diagram of the instrument is shown in Figure 4. In a typical experiment a ~1 to 5 mg sample is placed in the reaction cell, which is then placed in the STMBMS instrument. The reaction cell is heated radiatively by the furnace. As the temperature of the sample in the cell rises, vapors from the sample fill the reaction cell. The vapor then exits through an orifice located in the top of the reaction cell. The mass loss of the vapor exiting the cell is recorded with the microbalance. The vapor exiting the cell is formed into a molecular beam, which is then modulated and the molecules in the modulated beam are detected with a quadrupole mass spectrometer. Analysis of the data allows the concentration of each gaseous product within the reaction cell to be determined as a function of time during the course of an experiment. Since the aim of this paper is to determine how TAGzT may interact with RDX, effort has not been expended to quantify the data at this time. Ion signals formed in the mass spectrometer from the various gaseous products that evolve from the reaction cell are presented. Note that some of the ion signals may arise from multiple sources (i.e., different decomposition products).

Since the quadrupole mass spectrometer that is used in the STMBMS instrument has limited resolution ($m/\Delta m$ ~ 200 to 1000) and can measure only nominal mass values (i.e., integer values of atomic mass), it is difficult to determine the formulas of the ion signals found at the various m/z values in the data. To circumvent this problem, we also conduct thermal decomposition experiments using a Bruker Daltonics Apex II Fourier Transform ion cyclotron resonance (FTICR) mass spectrometer to measure the decomposition products. The FTICR mass spectrometer has a mass resolution greater than 100,000 and a mass accuracy of < 1.0 ppm. This allows the formulas of the ions formed in the mass spectrometer to be determined and the presence of ions with different formulas that occur at the same nominal m/z value to be identified (e.g., CO^+ = 27.99437 and N_2^+ = 28.00560). To collect mass spectra of the gases that evolve during the decomposition of TAGzT and RDX, approximately 1mg of the mixture is placed in a glass capillary tube and inserted into the instrument using a direct insertion probe (DIP). The DIP is heated in a controlled manner from room temperature to ~300°C and mass spectra are recorded as the sample is heated.

Materials. TAGzT and RDX are used in these experiments. The TAGzT used for these experiments were synthesized by the by Naval Surface Warfare Center at Indian Head (NSWC IHD). The material is a bright yellow, needlelike crystalline solid and is made by reacting triaminoguanidine hydrochloride (TAG-HCl) with sodium azotetrazolate (NaZT) and has an average particle size of about 200µm. Elemental analyses show the TAGzT is 98% pure. The RDX was procured from Holston Defense Plant. The mean particle diameter of RDX is 5µm. It contains approximately 8.0 wt% HMX.

Sample preparation. The mixtures of TAGzT and RDX used in the experiment were prepared by mixing approximately 3 mg of RDX with 0.8mg of TAGzT. The powders were placed in the

reaction cell and then mixed with a spatula. The reaction cells are fabricated from aluminum oxide. They are cleaned between each experiment by heating the reaction cell parts in air at 800°C for at least three hours. The reaction cells are kept in a desiccator prior to use. After the sample is loaded into the reaction cell, it is fitted with a cap that contains an orifice of a desired size for an experiment. For orifice diameters > 50 μm a cap fabricated from alumina is used. For orifice diameters ≤ 50 μm an orifice of the desired size located in a gold foil (25 μm thickness) is used. For experiments using an orifice in gold foil, the reaction cells are leak checked, using a He leak detector, prior to use in each experiment.

RESULTS

To illustrate the interactions that occur between RDX and TAGzT, the results from three decomposition experiments are presented: (1) TAGzT, (2) RDX, and (3) a TAGzT/RDX mixture. A ~25 μm diameter orifice and a heating rate of 2.5°C/min were used in each experiment.

Mass loss data. Comparison of the mass loss data from each experiment (Fig. 5) shows that there is an interaction between RDX and TAGzT. The TAGzT is characterized by a rapid weight loss commencing at ~190°C, followed by a more gradual weight loss proceeding from ~200 to 250°C. As described in the previous paper on TAGzT decomposition,[12] under the confinement conditions using a ~25μm diameter orifice about 60% of the TAGzT decomposes to volatile gases, NH_3, HCN, N_2, N_2H_4 and a product from the AT portion of TAGzT. The remaining 40% forms a nonvolatile product that subsequently decomposes as it is heated to higher temperatures. (Note: The apparent gain in mass observed in the experiments with TAGzT and TAGzT/RDX is due to the fact that the microbalance measures a force that has two components. One is the mass of the sample. The other is the thrust term due to the presence of the orifice and gases confined within the reaction cell. When gases are produced rapidly from material within the reaction cell, the thrust term becomes significant and forces the cell in a downward direction. The multiple peaks in the TAGzT data are most likely due to the formation of gas within the reaction cell and temporary blockage of the orifice.)

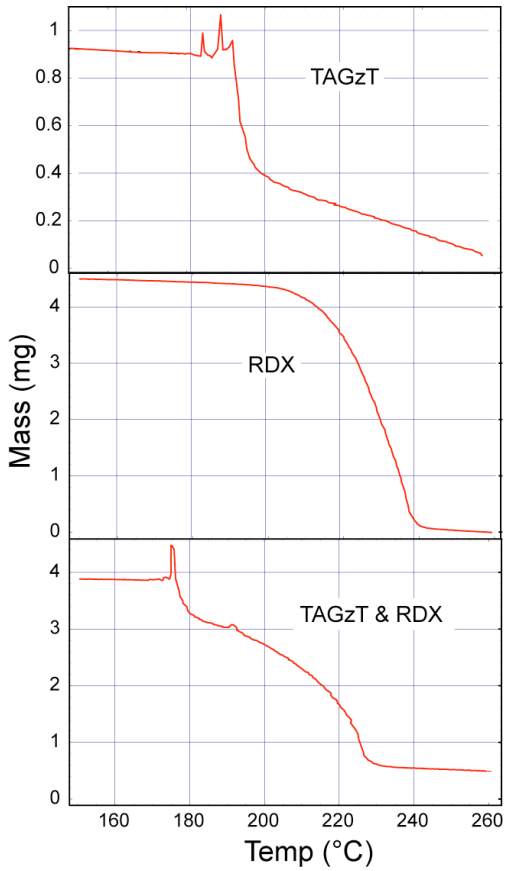

Figure 5. Mass loss data from experiments with TAGzT, RDX and a mixture of TAGzT and RDX.

RDX usually starts to decompose when it melts at ~200°C. However, since we are using a Holston grade RDX in these experiments, HMX dissolved in the RDX particles creates a lower melting eutectic mixture. The properties of the eutectic mixture control the rate of liquefaction of the sample, which in turn controls the rate of decomposition of RDX. Thus, the onset of RDX decomposition will start at a lower temperature and be more gradual when less pure Holston grade RDX is used.[7]

Comparison of the mass loss from the mixture of TAGzT and RDX with the mass loss from TAGzT and RDX individually shows: (1) The rapid mass loss, observed in the decomposition of TAGzT, commences at a temperature that is approximately 15°C lower in the mixture. (2) The mass loss attributable to the decomposition of

RDX also starts at a lower temperature. (3) Some form of non-volatile residue that does not decompose significantly at temperatures up to 260°C may be formed. Thus, the mass loss data indicates that there is significant interaction between TAGzT and RDX. Examination of the temporal behavior of the decomposition products formed during the process provides further insight into the reactions that control the interaction of these two compounds.

Identities and rates of evolution of reaction products. The ion signals formed in the STMBMS mass spectrometer from the products that evolve from the reaction cell during the decomposition of TAGzT, RDX and a mixture of TAGzT and RDX provide the data that is used to determine how TAGzT interacts with RDX. The data comparing ion signals representing the temporal behaviors of various products are shown in Figures 6 and 7.

The data shows that there is a very strong interaction between hydrazine formed via reactions R1 and R2 in the decomposition of TAGzT and RDX as characterized by the following global reaction

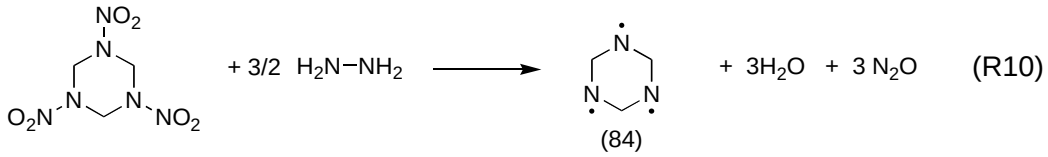

(R10)

in which the hydrazine extracts NO_2 from the RDX and forms H_2O and N_2O. Close examination of the signals representing N_2H_4, H_2O, N_2O and a product represented by m/z=84 show the following: (1) The ion signal representing hydrazine, N_2H_4, drops from ~80 to ~2 c/ms. (2) As the TAGzT decomposes, which is characterized by the ion signal at m/z=110, the ion signals representing water, N_2O and 84 are much higher than during the decomposition of RDX by itself. (3) The rapid rate of H_2O and N_2O evolution diminishes after the TAGzT is consumed in the decomposition process. (4) These reactions occur prior to the onset of the main decomposition process of RDX, characterized by the evolution of oxy-s-triazine (OST, 97) and hexahydro-1-nitroso-3,5-dinitro-s-triazine (ONDNTA). *These features demonstrate that hydrazine, formed in the decomposition of TAGzT, interacts strongly and rapidly with RDX prior to onset of the main RDX decomposition processes*.

Two of the other gaseous products formed during the decomposition of TAGzT, HCN and N_2, do not appear to interact strongly with RDX or its decomposition products. Comparing the data from TAGzT with the data from the mixture of TAGzT and RDX shows that the ion signals representing HCN and N_2 do not change to a significant extent.

There appears to be more ammonia, NH_3, formed during the decomposition of the mixture of TAGzT with RDX than in TAGzT by itself. The peak of the NH_3^+ signal in the experiment with TAGzT/RDX is about 85 c/ms compared to about 16 c/ms in the experiment with TAGzT by itself. After accounting for the slightly higher ion formation probability in the mass spectrometer in the experiment with TAGzT/RDX, the higher value suggests that more ammonia is formed from the mixture of TAGzT and RDX than from TAGzT alone. This may be due to the interaction of the hydrazine with the RDX, or possibly presence of elementary reactions other than those that comprise the global reaction R10.

The main product formed from the azotetrazolate portion of the TAGzT molecule ($C_2H_2N_6$, m/z= 110, 82) appears to evolve at a greater rate in the experiment with the mixture of TAGzT and RDX than in TAGzT alone. This suggests that less non-volatile polymeric product (NVPP) may be formed via reaction R5. This is also consistent with the fact that the ion signal from the product (m/z=166) formed from the dissociation of the NVPP via reaction R9 is not observed in the experiment with the mixture of TAGzT and RDX.

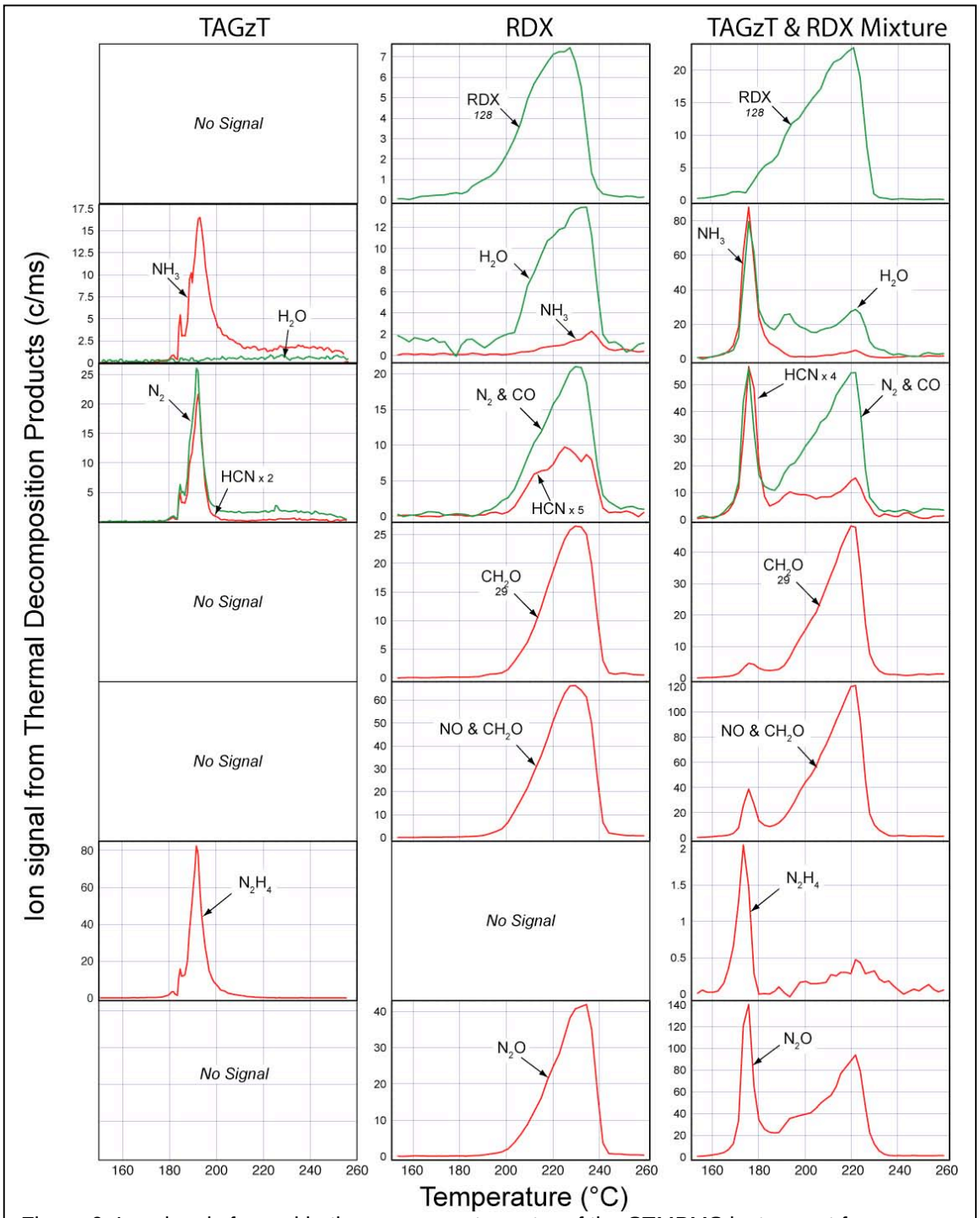

Figure 6. Ion signals formed in the mass spectrometer of the STMBMS instrument from products that evolve from the reaction cell during the decomposition of TAGzT, RDX, and a mixture of TAGzT and RDX. The data was collected in the same experiments for which the mass loss data is shown in Fig. 5. Ion signals representing higher molecular weight products are shown in Fig. 7. (Note: the efficiency for creating ions at a specific m/z value from a gaseous product varies from experiment to experiment. For example, the efficiency of forming ions in the experiment with a mixture of TAGzT and RDX is ~50% higher than in the experiment with RDX.)

Although there is a strong interaction between hydrazine and RDX, the main features

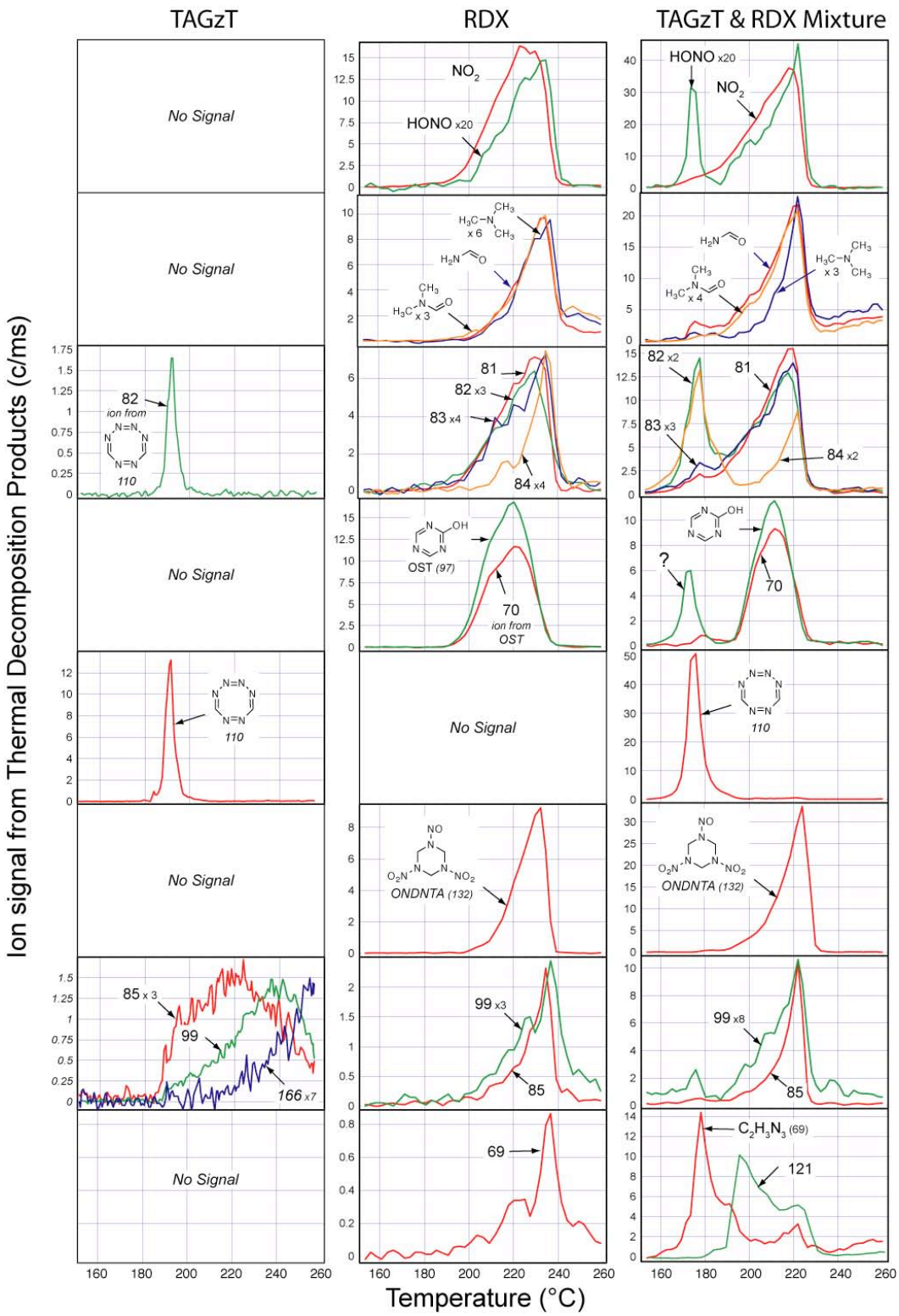

Figure 7. Ion signals formed in the mass spectrometer of the STMBMS instrument from products that evolve from the reaction cell during the decomposition of TAGzT, RDX, and a mixture of TAGzT and RDX. The data was collected in the same experiments for which the mass loss data is shown in Fig. 5. Ion signals representing lower molecular weight products are shown in Fig. 6.

characterizing the decomposition of RDX, after there has been an interaction with hydrazine, are

quite similar to RDX by itself. The primary reactions that control the decomposition of RDX are reactions 7, 9 and 12, which are listed in Fig. 2. These reactions are characterized by the ion signals for OST (m/z= 97 & 70), ONDNTA (m/z=132), and the main gaseous decomposition products, H_2O, N_2/CO, CH_2O, and N_2O, which are shown in Figures 6 and 7.

The OST tracks the direct decomposition of RDX in the liquid phase. Comparison of the OST signals from the experiment with pure RDX to those from the experiment with the TAGzT/RDX mixture show similar behavior. The evolution of OST starts at ~192°C and it climbs gradually as the eutectic mixture of RDX and HMX in the RDX particles gradually melts. The ion signals formed from OST are at m/z values of 97 and 70 and usually have a ratio of ~ 1.5:1, as is observed during the initial portion of the RDX decomposition process. The increase in the signal at m/z=70 relative to the signal at m/z-=97 originates from the formation of an additional product during the later stages of the RDX decomposition process as described previously.[10] This occurs in both the RDX and TAGzT/RDX experiments.

The formation of ONDNTA occurs through the reaction of RDX with NO (reaction 9 in Fig. 2) and is similar for experiments with RDX and TAGzT/RDX. However, closer examination shows that the evolution of ONDNTA starts at a slightly lower temperature in the mixture of TAGzT and RDX than it does in RDX alone (~192°C vs. ~198°C). This is also supported by the earlier appearance of signals representing the decomposition products from ONDNTA (e.g., CH_2O and N_2O, reaction 12 in Fig. 2) in the mixture of TAGzT and RDX than in RDX alone.

Products formed during the later stages of the decomposition of RDX appear to be relatively unaffected by the TAGzT. For example the signals representing formamide, N,N-dimethylformamide, and trimethylamine (Fig. 7) are quite similar in the experiments with RDX and the mixture of RDX and TAGzT.

Based on these observations of the similarities and differences in the evolution of products from experiments with TAGzT, RDX, and a mixture of TAGzT and RDX, we draw the following conclusions regarding the nature of the interaction of TAGzT and RDX:

1. Hydrazine, formed in the decomposition of TAGzT, interacts directly with RDX.
2. The hydrazine reacts with RDX by abstracting the NO_2 groups, forming water and N_2O as the main products of the reaction.
3. The decomposition of TAGzT, and resulting generation of hydrazine, occurs before the RDX melts in our experiments. Thus, the reaction of hydrazine and RDX must occur in the gas phase and on the surface of the RDX particles.
4. After the available hydrazine is consumed, the RDX melts and undergoes decomposition in a manner that is similar to RDX by itself.
5. The reaction on the surface of RDX particles is accelerated and is most likely due to the previous interaction of RDX on the surface with hydrazine. However, it is also possible that the NVPP formed in the decomposition of TAGzT may affect the early stages of the RDX decomposition. The products formed in the affected region on the surface are those typically associated with the decomposition of RDX via the ONDNTA reaction intermediate.

Thus, the new dominant interaction is a very strong reaction between hydrazine and RDX.

The interaction of the TAGzT with RDX is somewhat more complex than the simple reaction scheme that has been outlined. Further examination of the data in Figures 6 and 7 shows signals at several other m/z values that are indicative of interactions between the TAGzT decomposition products and RDX. These signals are associated with NO, HONO, $C_2H_3N_3$ (69), and unidentified products at m/z values of 97 and 121. The signals representing NO and HONO would appear to be minor products formed in the interaction of hydrazine with RDX. This would be expected. The signal at m/z=97 is not OST since there is not a corresponding signal in the mass spectral data at m/z=70. The signal at m/z=121 appears after the TAGzT has decomposed and during the early phase of the RDX decomposition. This suggests that it is associated with a

product formed on the surface of the RDX particles during the interaction with TAGzT. More careful FTICR mass spectrometry measurements will be made to identify these currently unknown products.

Finally, it should be noted that the TAGzT decomposes at a temperature that is 15 to 20°C lower when it is in the presence of RDX than when it is by itself. This suggests that RDX is transported to the surface of the TAGzT particles, reacts on the surface of TAGzT, and results in the onset of decomposition of TAGzT at a lower temperature.

BURN RATE MODIFIERS FOR NITRAMINE PROPELLANTS

While burn rate modifiers for *double-base* propellants have been available for many decades, the development of burn rate modifiers for *nitramine-based* composite propellants had been an elusive quest.[5] Various lead salts have been shown to catalyze the reactions of the nitrate esters used to fabricate double-base propellants. But until recently, there has been little success in finding compounds that will alter the reaction process of the nitramine ingredients, RDX or HMX. Normally, the decomposition of RDX and HMX is controlled by their own self-contained reaction processes. However, advances over the past several years in the synthesis of high nitrogen energetic ingredients has provided a means to increase the burning rates of RDX propellants. These materials, which include TAGzT, have been used successfully as burning rate modifiers for RDX propellants by the Department of Defense.[1] Why some high nitrogen compounds modify the burn rate of RDX-based propellants, while others do not, has been an unresolved question.

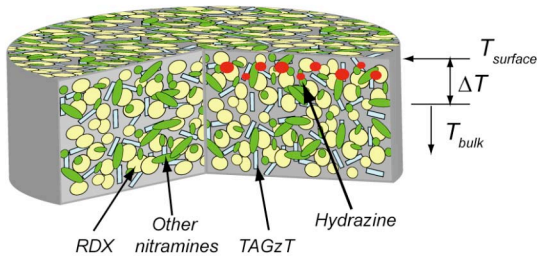

Figure 8. Illustration of hydrazine formed in the decomposition of TAGzT acting as a burn rate modifier in nitramine composite propellant. Relative sizes of RDX and TAGzT are illustrative. Previously measured burn rates used needle shaped TAGzT (~20µm w x ~ 100 µm l) and 5µm RDX powders.[1]

The results of our current experiments with TAGzT and RDX show that the hydrazine formed in the decomposition of TAGzT will react with RDX faster than RDX can decompose on its own. Thus, the ability to create hydrazine within a nitramine-based propellant, provides a reaction pathway that can be adjusted to control the rate of reaction of RDX. This is a key feature that should allow propellants to be designed to have desired burning rate characteristics.

A conceptual design for a burn rate modified nitramine-based propellant is shown in Figure 8. The temperature gradient established below the surface of the burning propellant (temperature: $T_{surface} > T_{bulk}$) can be used to control the interaction between the hydrazine formed in the decomposition of TAGzT and the RDX. In this case, since the TAGzT decomposes at a lower temperature than RDX, the hydrazine should be generated at a depth further from the surface of the burning propellant than the RDX. Thus, the hydrazine should flow up through the RDX particles. In a steep temperature gradient, the RDX will melt and the hydrazine should flow through a melted layer of RDX.

The fact that hydrazine reacts rapidly with RDX compared to the decomposition of RDX itself opens a wide range of methods that could be employed to tailor the burn rate of RDX-based propellants. Several possible approaches include:

1. Adjustment of the particle sizes and particle size distributions of RDX and the hydrazine-generating compound (e.g., TAGzT) to obtain an appropriate balance between the rate of formation of hydrazine and the rate of decomposition of RDX by itself.
2. The use of a mixture of different nitramines that have a range of different melting points and rates of reaction. Possible nitramine that may be used are listed in Fig. 9.
3. Incorporation of other ingredients in the propellant binder that would moderate the generation of hydrazine in the pressure range that is required to create a plateau burning propellant.
4. Synthesis of other compounds that generate hydrazine at various rates over a wide range of temperatures. These would enhance the ability to tailor the burn rates by providing a broader selection of ingredients.
5. The use of HMX instead of RDX if a larger temperature difference is required between the hydrazine generating compound (e.g., TAGzT) and the energetic nitramine.
6. Utilization of other nitramines in conjunction with RDX or HMX to effectively tailor the interaction with TAGzT. For example1,3,5-trinitro-1,3,5-triazirane-2-one (K6) has a lower melting point (~180°C) and decomposes more rapidly than RDX.[17]

These are a few examples of how compounds that generate hydrazine could be used to advantage to modify the burn rate behavior of propellants.

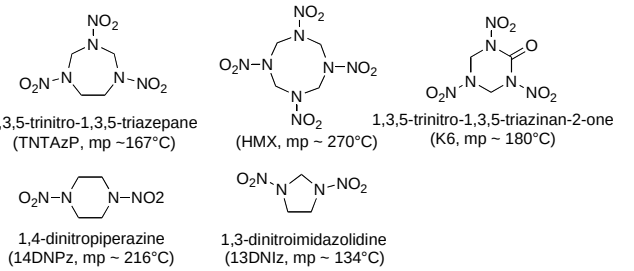

Figure 9. Molecular structure of cyclic nitramines that may be used in TAGzT-tailored (or other hydrazine forming compounds) nitramine propellants.

SUMMARY AND CONCLUSIONS

STMBMS experiments with mixtures of TAGzT and RDX provide insight into the decomposition of the individual ingredients, as well as the interactions between the two compounds and their decomposition products. This information provides insight into reactions that are likely to play an important role in the initial steps in the combustion of TAGzT/RDX-based propellants.

The two compounds decompose over the same temperature range of 170 to 250°C which allows reactions between the each compound and their decomposition products to occur.

TAGzT decomposes via a relatively complex multistep nonlinear reaction process, which has been described in another paper presented at this meeting.[12] However, for considering its interaction with RDX the components of this complex process may be divided into two branches: (1) the formation of volatile gaseous products, NH_3, HCN, N_2 and N_2H_4 and (2) the formation of non-volatile products that remain in the condensed phase of the sample and decompose at higher temperatures. Thus, the decomposition of RDX may be altered by TAGzT in two ways: (1) the gaseous products may interact with RDX in the gas phase or may diffuse into the RDX and react with RDX within the condensed phase, or (2) the RDX may be transported to the non-volatile TAGzT product and react.

The dominant interaction occurs between RDX and N_2H_4. This reaction is very rapid and results in the formation of H_2O, N_2O and various forms of remnants from the RDX ring. The amount of N_2H_4 that evolves from the reaction cell during the course of an experiment is

approximately a factor of 100 lower when RDX is present in the reaction cell compared to when it is not present. By comparison, NH_3 does not react appreciably with RDX under similar conditions.

The products that evolve due to the interaction of N_2H_4 with RDX indicate that the reaction involves reaction with the NO_2 groups on RDX. The fact that products that are associated with the decomposition of the RDX ring, HCN and CH_2O, are not observed to an appreciable extent suggests that removal of one NO_2 group from an RDX molecule does not trigger a rapid decomposition of the remaining intermediate. The data indicates that hydrazine removes all three nitro groups from an RDX molecule.

TAGzT can effectively alter the decomposition process of RDX. This occurs primarily via the formation of N_2H_4 in the decomposition of TAGzT and its subsequent rapid interaction with RDX.

Thus, this explains why TAGzT is a good burn rate modifier. The key feature is the formation of hydrazine during the decomposition process. Since formulating a propellant will involve developing a composite material that includes powders of RDX and TAGzT, it should be possible tailor the burn rate of a TAGzT/RDX-based propellant by controlling the transport of N_2H_4 between ingredients in the propellant. For example, mixtures of very fine powders may have a higher degree of burn rate enhancement than mixtures of larger particles.

Finally, the key feature of TAGzT that enables its interaction with RDX is the formation of hydrazine during its decomposition. Thus, other compounds that form hydrazine during their thermal decomposition may also be good candidates for burn rate modifiers.

FUTURE WORK

Results from our initial experiments on the decomposition of TAGzT and RDX mixtures have been presented. To build on this effort further work is planned in the following areas: (1) Deuterium and ^{15}N-labeled RDX will be used to elucidate the mechanism of reaction between N_2H_4 and the NO_2 groups on RDX. (2) Further refinement of the reaction mechanism to describe the interaction of TAGzT with RDX. (3) Investigation of the reaction of TAGzT with other types of nitramines and the ingredients used in propellant binders. (4) Development of mathematical models to describe the reaction processes that control the decomposition of RDX, TAGzT and their interaction. (5) The examination of TAGzT/RDX-based propellants.

ACKNOWLEDGMENTS

This work was supported in part by the Joint Munition Program memorandum of understanding, the Army Research Office under contract # 43381-CH, and the Office of Naval Research. We thank Aaron Highley and Sean Maharrey for assistance in collecting the FTICR mass spectrometry data. This work is part of H. Hayden's graduate thesis research at George Washington University.

REFERENCES

1. Walsh, C. and C. Knott, *Gun Propellant Formulations with High Nitrogen Modifiers*, in *Propellant Development & Compatibility Subcommitte Meeting*. 2003, CPIA.
2. Hiskey, M.A., N. Goldman, and J.R. Stine, *High-Nitrogen Energetic Materials Derived from Azotetrazolate.* J. Energetic Mat., 1998. **16**: p. 119-127.
3. Hammerl, A., et al., *Azidoformamidinium and guanidinium 5,5'-azotetrazolate salts.* Chemistry Of Materials, 2005. **17**(14): p. 3784-3793.
4. Tappan, B.C., et al., *Decomposition and ignition of the high-nitrogen compound triaminoguanidinium azotetrazolate (TAGzT).* Propellants Explosives Pyrotechnics, 2006. **31**(3): p. 163-168.

5. Fifer, R.A., *Chemistry of Nitrate Ester and Nitramine Propellants*, in *Fundamentals of Solid-Propellant Combustion*, K.K. Kuo and M. Summerfield, Editors. 1984, American Institute of Aeronautics and Astronautics, Inc.: New York N.Y. p. 177-237.
6. Knott, C., C. Walsh, and S. Prickett, *TPE Based Gun Propellants with High Nitrogen Modifiers*, in *Propellant Development and Compatibility Subcommittee Meeting*. 2004, CPIA.
7. Behrens, R. and S. Bulusu, *Thermal-Decomposition Of Energetic Materials.3. Temporal Behaviors Of the Rates Of Formation Of the Gaseous Pyrolysis Products From Condensed-Phase Decomposition Of 1,3,5-Trinitrohexahydro-S-Triazine.* Journal Of Physical Chemistry, 1992. **96**(#22): p. 8877-8891.
8. Behrens, R. and S. Bulusu, *Thermal-Decomposition Of Energetic Materials.4. Deuterium-Isotope Effects and Isotopic Scrambling (H/D; C-13/O-18; N-14/N-15) In Condensed-Phase Decomposition Of 1,3,5-Trinitrohexahydro-S-Triazine.* Journal Of Physical Chemistry, 1992. **96**(#22): p. 8891-8897.
9. Behrens, R. and S. Maharrey, *Chemical and Physical Processes that Control the Thermal Decomposition of RDX and HMX*, in *Combustion of Energetic Materials*, K.K. Kuo and L.T. DeLuca, Editors. 2002, Begell House: New York. p. 3 - 21.
10. Maharrey, S. and R. Behrens, *Thermal Decomposition of Energetic Materials 5. Reaction Processes of 1,3,5-Trinitrohexahydro-s-triazine (RDX) Below Its Melting Point.* Journal of Physical Chemistry, 2005. **109**: p. 11236-11249.
11. Behrens, R. and D. Wiese-Smith, *Reaction Kinetics of RDX in the Condensed Phase*, in *40th JANNAF Combustion Meeting*. 2005, CPIA Publication: Charleston, South Carolina. p. June 2005.
12. Hayden, H., et al. *Thermal Decomposition of Triaminoguanidinium azotetrazolate (TAGzT)*. in *41st JANNAF Combustion Subcommittee Meeting*. 2006. San Diego, California: CPIAC.
13. Behrens, R., Jr., *New simultaneous thermogravimetry and modulated molecular beam mass spectrometry apparatus for quantitative thermal decomposition studies.* Review of Scientific Instruments, 1987. **58**(3): p. 451-461.
14. Behrens, R., Jr., *Identification of Octahydro-1,3,5,7-tetranitro-1,3,5,7-tetrazocine (HMX) Pyrolysis Products by Simultaneous Thermogravimetric Modulated Beam Mass Spectrometry and Time-of-Flight Velocity-Spectra Measurements.* International Journal of Chemical Kinetics, 1990. **22**: p. 135-157.
15. Behrens, R., Jr., *Determination of the Rates of Formation of Gaseous Products from the Pyrolysis of Octahydro-1,3,5,7-tetranitro-1,3,5,7-tetrazocine (HMX) by Simultaneous Thermogravimetric Modulated Beam Mass Spectrometry.* International Journal of Chemical Kinetics, 1990. **22**: p. 159-173.
16. Behrens, R., *Thermal Decomposition Processes of Energetic Materials in the Condensed Phase at Low and Moderate Temperatures*, in *Overviews of Recent Research on Energetic Materials*, R.W. Shaw, T.B. Brill, and D.L. Thompson, Editors. 2005, World Publications Inc: Singapore. p. 29 - 74.
17. Behrens, J., R. and S. Bulusu, *Thermal Decomposition of HMX, Mononitroso-RDX, TNCHP and K6 in the Liquid Phase: Results from Simultaneous Thermogravimetry Modulated Beam Mass Spectrometry Measurements.* 29th JANNAF Combustion Meeting, 1992. **CPIA Publ. 573, Vol. II**: p. 453 - 463.

REACTIONS OF TAG-BASED ENERGETIC MATERIALS

Richard Behrens, Jr. and Deneille Wiese-Smith
Combustion Research Facility, Sandia National Laboratories
Livermore, CA 94551-0969

Heather Hayden
NAVSEA, Indian Head Division
Indian Head, MD

ABSTRACT

A new paradigm, "Concepts, Methods and Protocols for Reaction Hierarchy and Network Development" (CoMPReHND) is under development and has been applied to investigate the thermal decomposition of TAG-based salts and their interaction with RDX over a range of conditions that are relevant to performance, safety, and long-term aging behavior of gun propellants. Four TAG-based salts have been examined to investigate the role of the anion in the reaction network. The four salts include: TAGzT, TAG-TATTz, TAG nitrate, and TAG chloride. The reaction network of TAG-TATTz and TAGN have features similar to those found in our previous studies of TAGzT. The relative fraction of hydrazine observed from the four salts when examined by themselves has the following sequence: TAGzT>TAG-TATTz>TAGN>TAGCl, indicating that the smaller inorganic anions, Cl^- and NO_3^-, are more reactive than the organic anions. Reactions of TAGzT, TAG-TATTz, and TAGN with RDX show that the extent of reaction of hydrazine with RDX is comparable for each salt. This suggests that even though the inorganic anions react more readily with hydrazine than the organic anions, the rate of reaction of hydrazine with RDX is faster than its rate of interaction with the anions. This effectively overcomes the differences in the reaction rate of hydrazine with the different anions. The results also indicate the reaction of hydrazine with RDX occurs primarily in the gas phase. Experiments investigating the onset of decomposition of TAGzT, TAG-TATTz and TAGN show that the initial reaction for each salt is dissociation to TAG and an associated product from the anion. The observed onset temperature for decomposition is between 110 and 120°C for TAGzT and TAGN and 165°C for TAG-TATTz.

INTRODUCTION

High nitrogen compounds are of interest for the development of advanced gun propellants. For example, it has been shown that replacing ingredients such as RDX with triaminoguanidinium nitrate (TAGN) or triaminoguanidinium azobitetrazolate (TAGzT) in gun propellants increases their burn rate.[1, 2] In addition, the high nitrogen content of the expanding gaseous products of propellants formulated with these ingredients will reduce gun barrel erosion and increase the service life of guns.

To introduce new ingredients into gun formulations requires addressing standard life cycle issues: (1) the ability to manufacture the new formulation safely; (2) the ability of the new formulation to meet safety and insensitive munition (IM) requirements; and (3) the long-term stability of the material during deployment and storage. The reactivity of the new ingredients and their interactions with other ingredients in the formulation underlies the ability to successfully develop a new propellant that will meet these standard life cycle requirements.

To address life cycle issues for new formulations, the conventional development paradigm utilizes a synthesize-and-test approach. A new compound is synthesized, usually based on target goals based on performance (i.e., higher energy content, larger fraction of

Approved for public release; distribution is unlimited.

nitrogen). If it meets the expected performance requirements, is thermally stable, and has acceptable impact sensitivity, the synthesis process is scaled up to create enough material for testing. With sufficient material available, tests to measure performance, such as burn rate for a propellant, and safety characteristics, such as shock sensitivity, and IM characteristics are conducted. The results from these are often in the form of go/no-go information and provide limited information. Thus, the amount of insight that can be gained on how to design the next molecule to meet the performance and life cycle requirements is limited. Furthermore, it is costly and time consuming to do the scale up and conduct the required tests.

To overcome these limitations, we are developing a more scientific approach for evaluating new ingredients. In this approach, we first recognize that the reaction behavior of a propellant or explosive formulation, over the many different environments encountered during its life cycle, is determined by a network of reactions and reaction processes. How a material behaves will depend on which parts of the reaction network play a dominant role in the reaction process for the set of conditions that are defined by a particular reaction environment. For example, it is quite likely that the parts of the reaction network that are important for controlling the first steps in the combustion processes will be different from those that are important in the manufacturing process, which in turn are likely to be different from those that are important for long-term aging. Thus, the scientific approach requires determining and understanding the reaction network that characterizes a new ingredient and its interaction with other ingredients in a formulation.

To determine the network that controls the reaction processes of an energetic material is difficult and cannot be accomplished using commercially available instruments and methods. To develop a scientific approach has required: (1) Understanding and defining the concepts needed to characterize complex reaction mechanism of compounds in the condensed phase. (2) Devising instrumental methods and numerical algorithms to identify chemical species and measure their concentrations as a function of time during the course of an experiment. (3) Creating the protocols needed to design the experiments, analyze the data and interpret the results in order to determine and characterize the reaction network. The instruments and experimental methods have been described previously.[3] Currently, we are developing a manuscript[4] to describe how these methods are used to determine the networks that characterize these complex processes. The new paradigm we have created is known as “Concepts, Methods and Protocols for Reaction Hierarchy and Network Development” (CoMPReHND). All of the features of CoMPReHND have been developed through our extensive work over the years on RDX, HMX and other energetic compounds.

Examination of new HiN compounds and their interaction with other ingredients in gun propellants is our first application of CoMPReHND to determine the reaction networks of new formulations. This class of compounds was selected for investigation based on previous results that showed that some HiN compounds, such as TAGzT, increased the burn rate of nitramine-based gun propellants, whereas similar compounds such as guanidinium azobitetrazolate (GUzT) did not. The reason for this difference was unknown.

In our initial work, the decomposition of TAGzT and GUzT, and their interactions with RDX, was investigated. During the thermal decomposition of TAGzT large quantities of hydrazine are formed,[5] whereas this compound is not observed in the decomposition of GUzT.[6] In addition, in experiments with mixtures of TAGzT and RDX,[7] it was discovered that hydrazine formed from TAGzT interacts with, and leads to the decomposition of, RDX faster than RDX can react by itself. Thus, the generation of N_2H_4 from TAGzT and its interaction with RDX

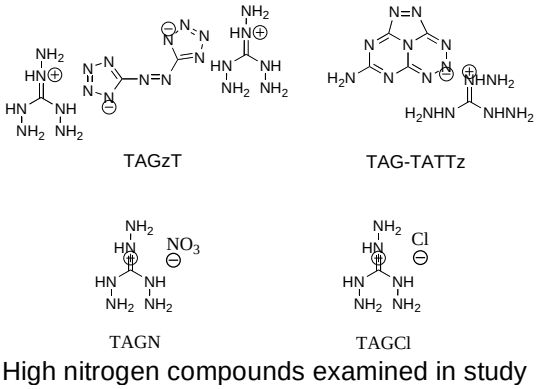

High nitrogen compounds examined in study

is a likely reason for the observed increase in burning rate of TAGzT modified propellant.[2]

Recent work on the development of gun propellant formulations containing TAGzT has raised concern regarding the thermal stability of TAGzT and its compatibility with other ingredients. This raised a number of questions that are addressed in this paper: (1) At what temperature does TAGzT first decompose? (2) What molecular properties determine the initial decomposition? (3) How does TAGzT, or its decomposition products, interact with other ingredients? (4) How can other TAG-based molecules be designed that are more stable than TAGzT, but will produce hydrazine in sufficient quantity to interact with RDX in the propellant?

To address these questions, we focus on the role that the anion may play in the decomposition process of TAG-based compounds. Since TAG-based compounds are salts, their stability may depend on the barrier that limits their transition from an ionic to neutral form. Once the neutral compounds are formed from the cation and anion, then the reaction network will depend on how each compound reacts individually and how they, and their decomposition products, interact with each other. For example, in our previous work it was observed that hydrazine, formed from TAGzT, reacted with RDX. This process requires that the N_2H_4 must persist for a length of time that is sufficient to encounter, and react with, an RDX molecule. If the anion formed in the initial decomposition process reacts rapidly with hydrazine, then transport of hydrazine from its point of origin at a TAGzT particle to the region where RDX is located will be limited. This would limit any enhanced rate of reaction of the RDX by hydrazine.

To examine these aspects of the reaction of TAG-based compounds, the reactions of four TAG salts have been investigated. They include TAGzT, triaminoguanidinium triazoloaminotriazinyltetrazine (TAG-TATTz),[8] TAGN, and TAG chloride (TAGCl). The experiments examine the initial decomposition reactions, the relative amount of hydrazine that evolves from each compound, and the effect of each compound on the reaction process of RDX.

METHODS

CoMPReHND has been used previously to determine the elements and linkages in the networks that control the thermal decomposition of TAGzT,[5] RDX[9, 10] and their interaction.[7] The instruments and methods used to conduct the thermal decomposition experiments are described elsewhere.[3, 11-13]

To investigate the role of the anion in the decomposition of TAG salts, we initially examine important

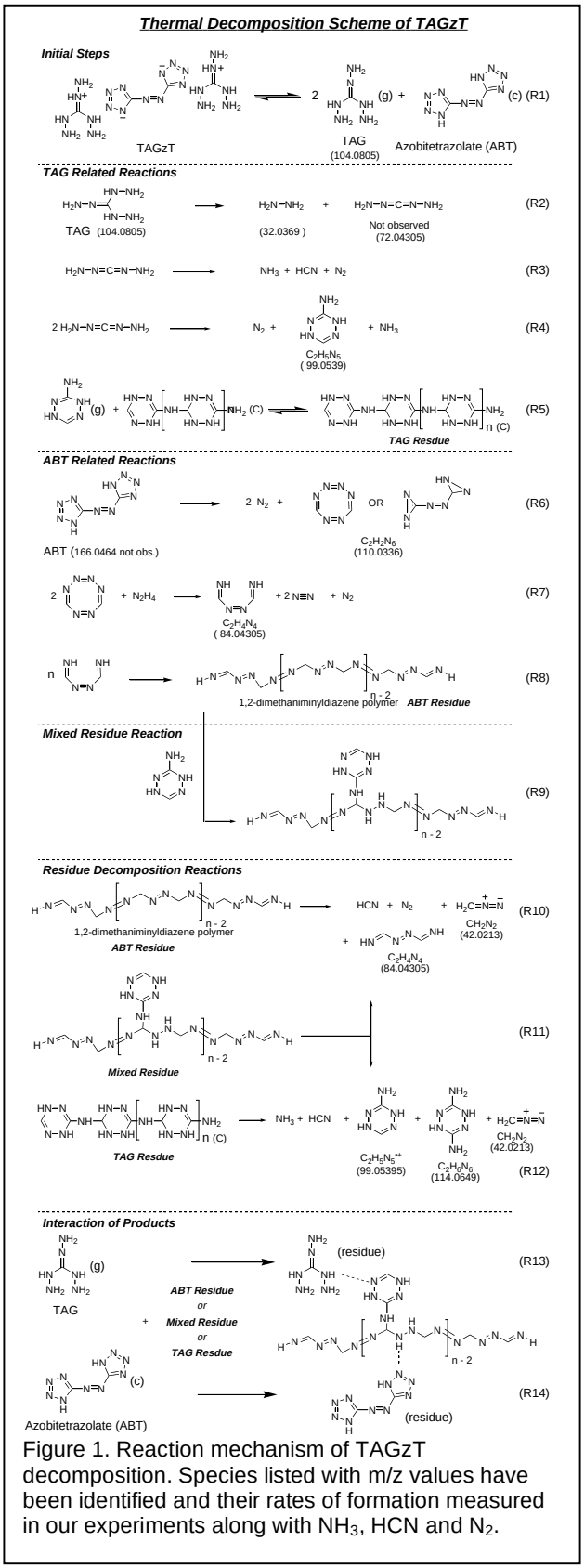

Figure 1. Reaction mechanism of TAGzT decomposition. Species listed with m/z values have been identified and their rates of formation measured in our experiments along with NH_3, HCN and N_2.

features in the reaction mechanism of TAGzT (Fig. 1).[5] The first step of the decomposition process involves the dissociative sublimation of TAGzT to TAG and azobitetrazolate (ABT) via R1. TAG is a volatile product while ABT is not. The TAG then decomposes into hydrazine (R2) and an intermediate that decomposes to NH_3, HCN and N_2 (R3). Diaminocarbodiimine is a known reactive intermediate, but it is not observed directly in our experiments. ABT decomposes to two moles of N_2 and $C_2H_2N_6$ (R6). The decomposition products from TAG and ABT may undergo further reaction to form compounds such as $C_2H_5N_5$ (99) or $C_2H_4N_4$ (84), via reactions R4 and R7, respectively. These compounds may in turn form less volatile, polymeric-like, compounds via reactions such as R8 and R9. These compounds may either decompose via reactions such as R10 through R12, or form a feedback loop and react with TAGzT via reactions such as R13 and R14 in an "autocatalytic-like" manner.

To design new high nitrogen ingredients, such as TAG salts, that will meet future munition requirements, it is necessary to identify critical steps in the reaction network that determine the behavior of the ingredient under various lifecycle conditions. These include performance, manufacturability, safety and IM characteristics, and long-term aging behavior. For the TAG salts the following steps may be considered critical:

1. Performance. Hydrazine formed from TAGzT has been shown to react more rapidly with RDX than RDX can decompose by itself.[7] Thus, compounds that decompose to form substantial amounts of hydrazine (via R2 for TAGzT) are likely to be good burn rate modifiers, if the hydrazine can survive transport to a region in which it can encounter and react with RDX (or other nitramine compound). On the other hand, if hydrazine is formed, but undergoes secondary reactions prior to encountering RDX then it is not likely to be a good burn rate modifier.
2. Manufacturability & long-term aging. To be useful, compounds must be thermally stable. Compounds must be stable at the elevated temperatures often used in the manufacturing process. Thus, it is important to understand the initial steps of the decomposition process (R1) as well as processes that may have an "autocatalytic effect" (R13 and R14).
3. Safety and IM behavior. Compounds that form larger more stable molecules versus

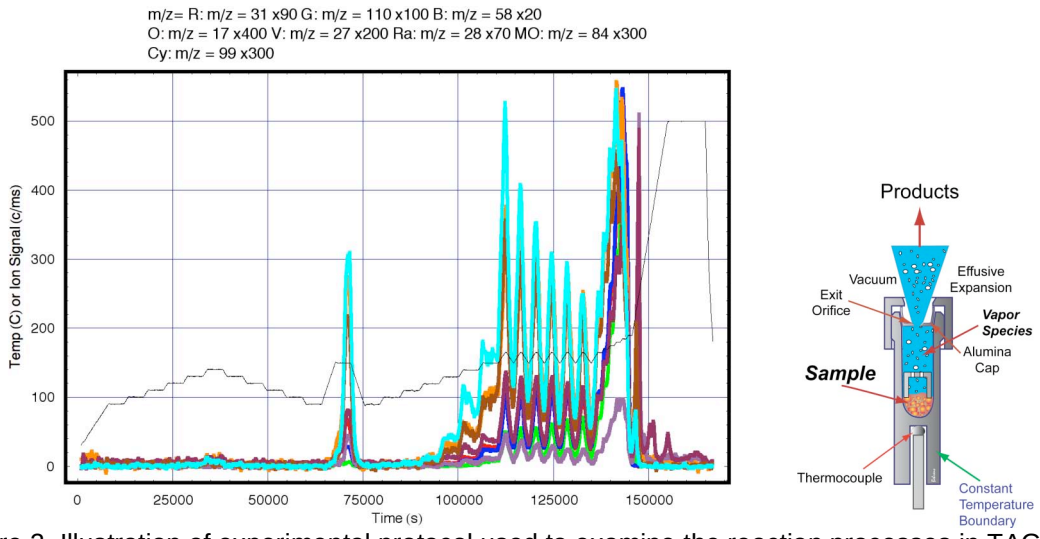

Figure 2. Illustration of experimental protocol used to examine the reaction processes in TAG based salts. Data from decomposition of TAGzT. Black curve indicates temperature profile for experiment. Other curves are ion signals, measured with a mass spectrometer, representing the various products shown in the TAGzT reaction scheme (Fig. 1). Color codes for m/z values and scaling factors are listed on top of graph. Data collected under low confinement, sample mass 2.49 mg. Cross section of reaction cell used in STMBMS experiments is shown on right. Confinement is altered by using exit orifices with various diameters (~50 to 1000μm).

smaller gaseous molecules when they decompose are likely to be safer and more likely to meet IM requirements. Thus, compounds that form intermediate products such as those shown in reactions R4, R5, R8, and R9 may result in safer munitions.

To screen new compounds we have developed a new experimental protocol using our simultaneous thermogravimetric modulated beam mass spectrometry (STMBMS) instrument that evaluates various aspects of important reactions (e.g. R1, R2, R6 and R13/R14) in one experiment. The protocol is illustrated in Figure 2 with data from the decomposition of 2.49mg of TAGzT under low confinement. The temperature of the sample is varied in a controlled manner over a temperature range from 20 to 500°C. The first set of heating/cooling steps is set to identify the first steps in the decomposition process and determine the onset temperature of decomposition. The next interval is a heat and hold section to determine if there is a delay time associated with the onset of secondary reactions. This provides insight into the complexity of the reaction process and whether the reaction network contains coupled reactions or feedback loops (often referred to as autocatalysis). The next set of temperature steps is to determine the onset of different secondary reactions in the network. This is followed by a series of heating/cooling cycles. This provides temperature-dependent data on a sample whose characteristics are changing with time due to the complex reaction process occurring in the sample. Finally, the sample is heated to 500°C to decompose any relatively non-volatile species that were formed during the decomposition process. This provides insight to the nature of the condensed-phase species formed in the decomposition processes and allows closure on the elemental mass balance for quantification of the data. The products are represented by the ion signals at the following m/z values: N_2H_4 (m/z = 31), $C_2H_2N_6$ from azobitetrazolate (ABT) (110), TAG (58, daughter ion), NH_3 (17), HCN (27), N_2 (28), $C_2H_4N_4$(84), and $C_2H_5N_5$(99).

The data in Fig. 3 illustrates how changing the extent of confinement of gaseous species within the reaction cell is used to control the reaction process and provide insight used to construct a reaction network to characterize the thermal decomposition of a compound. The three graphs in the left column of Fig. 3 compare ion signals representing the rate of formation of various species under low, high and medium confinement. Under low confinement (3a), the species evolve gradually over the course of the entire experiment. The rates of evolution of the various species rise and fall as the sample is heated and cooled during the cycling stage. This is followed by their increasing rate of evolution in the sequence of isothermal steps that follow the cycling stage. In contrast, the signals representing the same species when the experiment is conducted under high confinement (3b) is quite different. The more volatile products evolve only during the first two cycles of the cycling stage and the evolution of the species from the non-volatile residue falls through the remaining cycles. The rate that species evolve from the residue formed in the decomposition of TAGzT rises as the sample is heated to 500°C.

The complex behavior that controls the decomposition of TAGzT between the low and high confinement conditions can be investigated in more detail with an experiment run under medium confinement conditions as illustrated with the data in Fig. 3c and 3f. In this experiment, one observes the evolution of TAG (blue) in each stage of the experiment and an increasing rate of evolution of the thermal decomposition species during each subsequent heating/cooling cycle during the thermal cycling stage of the experiment. This shows that a portion of the reaction network for the decomposition of TAGzT consists of a feedback loop in which products formed earlier in the process accumulate and lead to an increasing rate of reaction as the experiment progresses. The rate of this feedback loop depends on the pressure of the confined gases. In our lower confinement case this feedback loop contributed only slightly to the overall reaction of the sample whereas in the higher confinement case it led to a much more rapid decomposition of the sample.

The protocol provides data to determine the reaction that initiates the decomposition of the compound of interest and to provide data to determine how fast this occurs as a function of temperature. The data illustrating this feature for TAGzT is shown in Fig. 3d. For TAGzT the initial reaction involves the reversible decomposition of TAGzT to TAG (green) and ABT (the reversibility was determined in experiments not presented here). The data collected at set of isothermal steps can be used to determine the parameters that determine the pressure of TAG

formed from the dissociative sublimation of TAGzT. In our experiments the first decomposition of TAGzT is observed at ~110°C. It is also worthwhile to note that if the reaction conditions are altered in such a way that TAG decomposes, or reacts with another ingredient, then the reaction rate of TAGzT will increase to satisfy the equilibrium conditions.

Finally, the complex nature of the decomposition of TAGzT is further illustrated with the data in Fig. 3e. If the decomposition of TAG to N_2H_4, NH_3, HCN, and N_2 as summarized by reactions R2 and R3, then their rate of formation should be proportional to the concentration of TAG in the gas phase (characterized by green curve in Fig. 3e). This is not the case. There is a delay of approximately 2000 seconds from the time the TAG reaches a stable concentration in the reaction cell at 150°C and the time that the four gaseous species start to evolve from the sample. This suggests that some species is being formed in the condensed phase (most likely

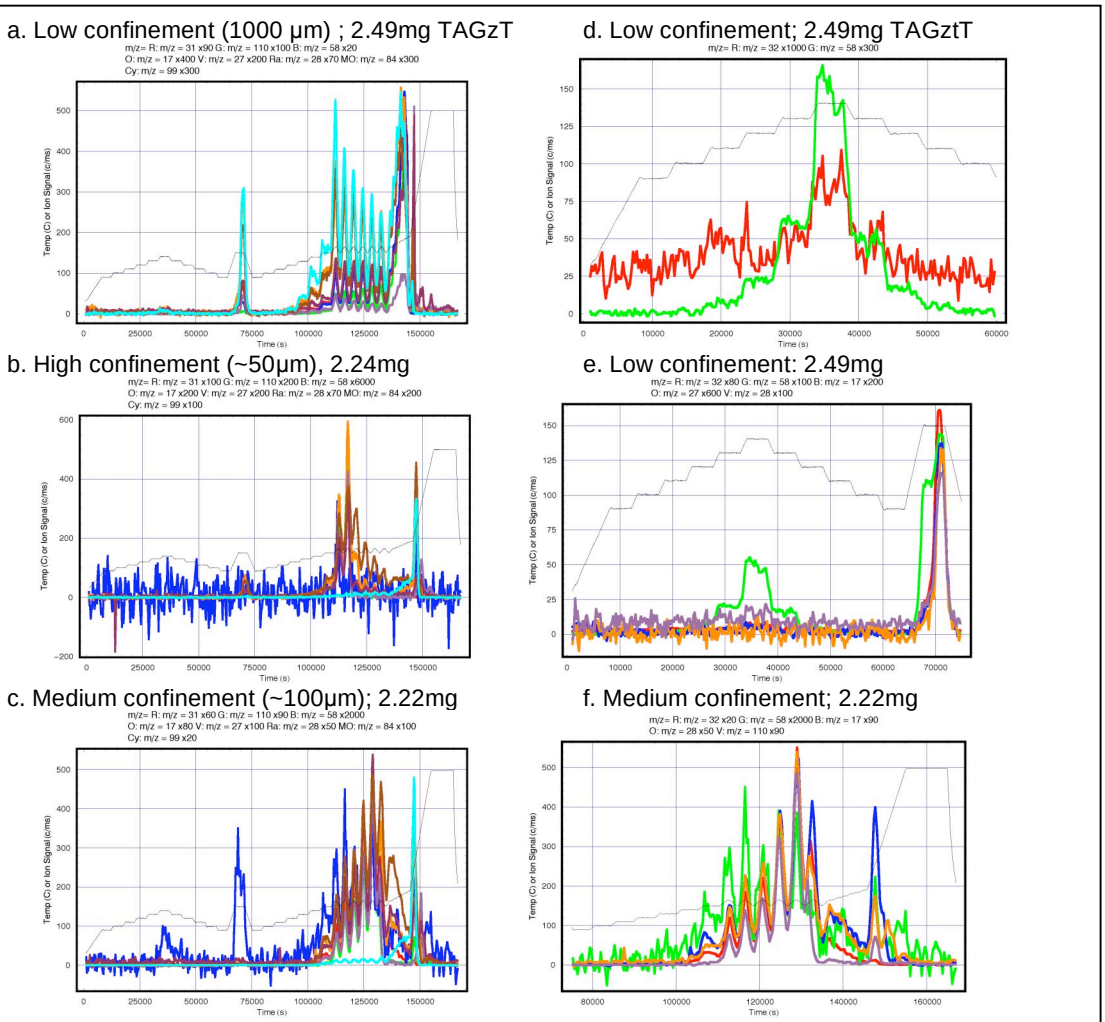

Figure 3. Comparison of ion signals representing different products formed during the thermal decomposition of TAGzT under three different confinement conditions. The temperature profile for each experiment is the same as shown in Fig. 2. The graphs in the left column compare the decomposition of TAGzT under low, high and medium confinement. The graph in the upper right shows that evolution of TAG (green) in the initial decomposition step. The second graph in the right column shows the delay between the evolution of TAG (grn) and the evolution of its four main decomposition products: NH_3, HCN, N_2, and N_2H_4. The graph in the lower right shows that evolution of the various products under medium confinement. The increase in reaction rate in each subsequent thermal cycle illustrates the complex reaction network of the TAGzT decomposition.

on the surface of the TAGzT particles) that catalyzes the decomposition of TAG to the lower molecular weight gaseous species.

The protocol illustrated here for TAGzT is applied to evaluate other TAG-based compounds to assess reactions in the network that are relevant to performance, safety, manufacture, and long-term stability change as a function of molecular and physical properties of the various TAG compounds. The compounds examined in to date are TAGCl, TAGN and TAG-TATTz (supplied by Bill Koppes -- Navy/IH). The entire evaluation performed here was done with small quantities of material, less than 20 mg total for all experiments with each compound.

RESULTS AND DISCUSSION

In our evaluation of TAGzT, TAGN, TAG-TATTz and TAGCl, we assessed relative amounts of hydrazine formed from the decomposition of each compound, the extent of reaction of each compound with RDX, and the onset of decomposition to assess relative stability. A summary of these results is presented in Table I.

Table I. Hydrazine formation rates & Interaction with RDX

#	Experiment	Compound	NH3 m/z =17	N2H4 m/z= 32	N2H4/ (NH3+N2H4)	H2O m/z=18	N2O.. m/z=44	burning rate (% increase)
1	TAGzT009	TAGzT	15	46.4	75.57%	1.14	0.00	
2	TAGTATT004	TAG-TATTz	20.36	21.7	51.59%	10.30	1.47	
3	TAGN002	TAG nitrate	34.6	10.4	23.11%	19.40	2.20	
4	TAGzT013	TAG Chloride	27.18	3.31	10.86%	1.89	0.12	
5	TAGzT024	TAGzT/RDX	11.62	0.24	2.02%	12.62	16.1	226
6	TAGTATTz003	TAG-TATTz/RDX	14.67	0.23	1.54%	9.95	14.73	165
7	TAGN003	TAG nitrate/RDX	9.44	0.11	1.15%	16.7	14.55	
8	TAGzT051	TAG Chloride/RDX	6.25	0.042	0.67%	16.59	19.62	

* Units for ion signal value columns are percent of total ion signal in the time region associated with decomposition of the TAG salt.

\# The numbers are the ratio of N_2H_4 signal to the sum of N_2H_4 and NH_3.

The fraction of the total ion signal representing NH_3, N_2H_4, H_2O and N_2O are shown for each experiment. To assess the production rate of hydrazine from each compound, the ratio of N_2H_4 to the total nitrogen containing compounds released from TAG (NH_3 and N_2H_4) is shown in column 6. The results from experiments with the four TAG salts by themselves are shown in lines 1 through 4 and the results from experiments in which each TAG salt is mixed with RDX is shown in lines 5 through 8.

DECOMPOSITON OF TAG SALTS

The experiments with the TAG salts by themselves show that TAGzT yields the largest fraction of hydrazine (~76%) and TAG chloride yields the least (~11%). The yield of hydrazine from TAG-TATTz is ~52% and the yield from TAGN is ~ 23%. Thus, the two TAG salts with simple anions yield a significantly lower fraction of hydrazine than the salts with more complex organic anions. Reaction of hydrogen from the TAG with the chloride anion to form HCl from TAGCl and with the nitrate anion to form H_2O from TAGN is observed in these experiments. This suggests that either (1) a significant portion of the hydrazine formed from the decomposition of TAG may react with the chloride or nitrate anions to reduce the amount of measured hydrazine, or (2) the anions react directly with the TAG, reducing the amount of N_2H_4 formed from the decomposition of TAG.

The results on the amount of hydrazine observed in the decomposition of the four TAG salts indicate that the Cl^- and NO_3^- anions may either react more readily with TAG than the ABT or TATTZ anions to reduce the amount of N_2H_4 formed, or they may react more rapidly with hydrazine via secondary reactions to reduce the net amount of measured hydrazine. In the first case, more hydrazine should be available from TAGzT and TAG-TATTz to react with RDX than from TAGCl and TAGN. In the second case, if hydrazine is formed in significant quantities from

all four salts, and the lower amounts of measured hydrazine from the TAGN and TAGCl salts are due to secondary reactions, then it is possible that the reaction of hydrazine with RDX will be more rapid than its reaction with the anions. In this case, all of the salts may undergo significant interactions with RDX. This is examined in the next section.

REACTION OF TAG SALTS WITH RDX

Data illustrating the reactions of mixtures of RDX with TAGzT, TAG-TATTz, and TAGN are shown in Figures 4 and 5. Ion signals formed in the mass spectrometer and representing various species formed in the reaction of each TAG salt with RDX are shown in two graphs for each mixture (TAGzT/RDX in Fig. 4A and 4B, TAG-TATTz/RDX in Fig. 4C and 4D, and TAGN/RDX in Fig. 5A and 5B). The first graph in each set shows four signals that illustrate the decomposition of the TAG salt and its interaction with RDX. The signals represent N_2H_4 (m/z=32), NH_3 (17), H_2O (18), N_2O (44) and CH_2NO (44). The N_2O and CH_2NO species, formed in the reaction of TAGzT with RDX, have the same nominal m/z value. They were identified from isotopic crossover experiments using mixtures of TAGzT with the deuterium and ^{15}N isotopomers of RDX. The second graph in each set shows N_2H_4 and four of the main species observed in the thermal decomposition of RDX: oxy-s-triazine (OST), CH_2O, hexahydro-1-nitroso-3,5-dinitro-s-triazine (ONDNTA) and RDX, which have been described in previous publications.[9, 10, 14]

The ion signals representing the species can be divided into two groups of temporally related signals. One group occurs after RDX melts at ~202°C, which is indicated by the onset of evolution of OST from the sample (orange curve in Fig. 4B, 4D, and 5B). The other group occurs prior to the melting of RDX and is associated with the onset of the decomposition of the TAG salt to form N_2H_4, NH_3, HCN and N_2 (not shown). The onset of decomposition of the TAG salt is best illustrated by the signal representing N_2H_4, since its scaling factor is higher than the other

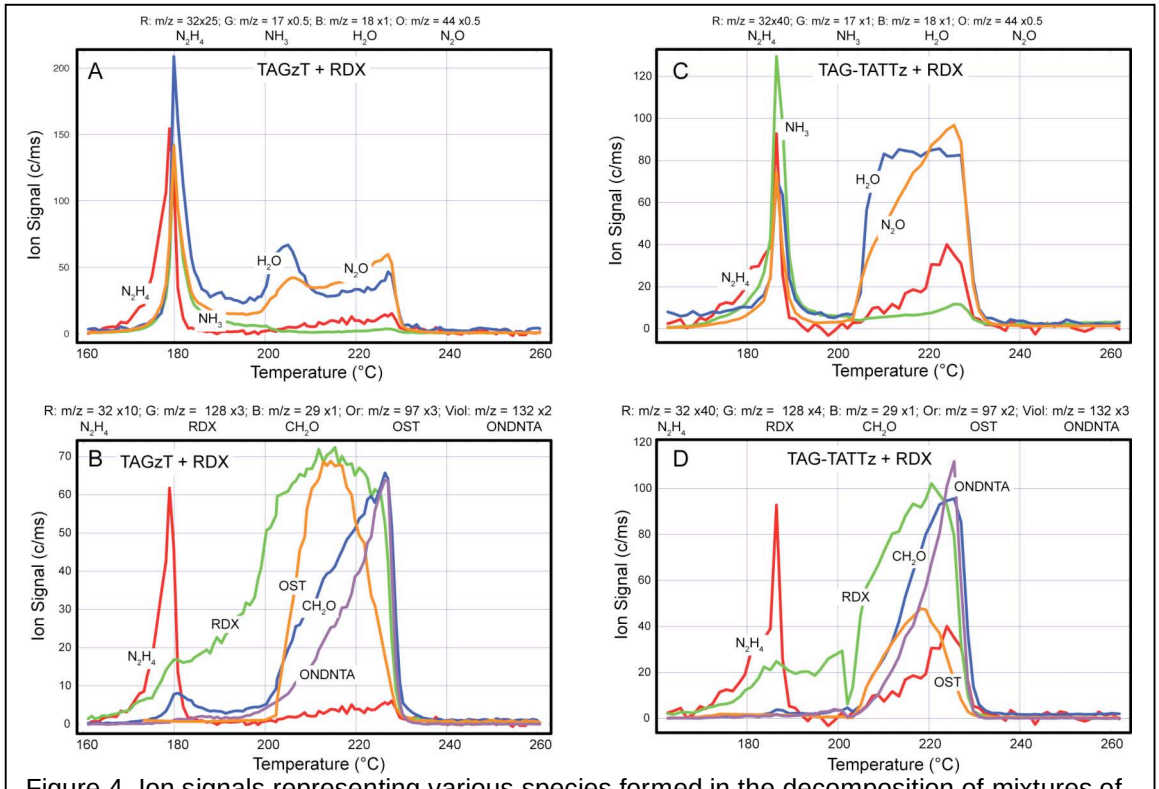

Figure 4. Ion signals representing various species formed in the decomposition of mixtures of TAGzT with RDX (A & B) and TAG-TATTz with RDX (C & D). The scaling factors and m/z values associated with each species are shown at the top of each graph. Heating rate: 2.5°C/min

species. For example, the onset of hydrazine evolution from TAGzT/RDX starts slightly above 160°C (Fig. 4B). The scaling factor for N_2H_4 is high due to its low concentration in the reaction cell caused by its interaction with RDX.[7] When RDX is not present, the signals from N_2H_4 and NH_3 are comparable.

The reaction of hydrazine with RDX is observed for the three TAG salts. In each case, signals representing H_2O (18), N_2O (44), CH_2NO (44) and NO (30, not shown) increase rapidly at the same time that the N_2H_4 signal is decreasing. These signals illustrate the reaction of hydrazine with RDX for each TAG salt. In each case, the signals representing H_2O, NH_3, N_2O/CH_2NO are large and comparable in intensity. Correspondingly, the signals representing N_2H_4 are small and comparable in each case. These results suggest that hydrazine is formed in comparable quantities from all three TAG salts and its interaction with RDX is similar in each case. This indicates that reaction of hydrazine with RDX is more rapid than its reaction with any of the three different anions. Thus, even though the amount of hydrazine observed from the thermal decomposition of TAGN is less than the other two TAG salts, its rate of reaction with any of the anion is slow compared to its reaction with RDX and its performance should not be affected by the anion in these three cases.

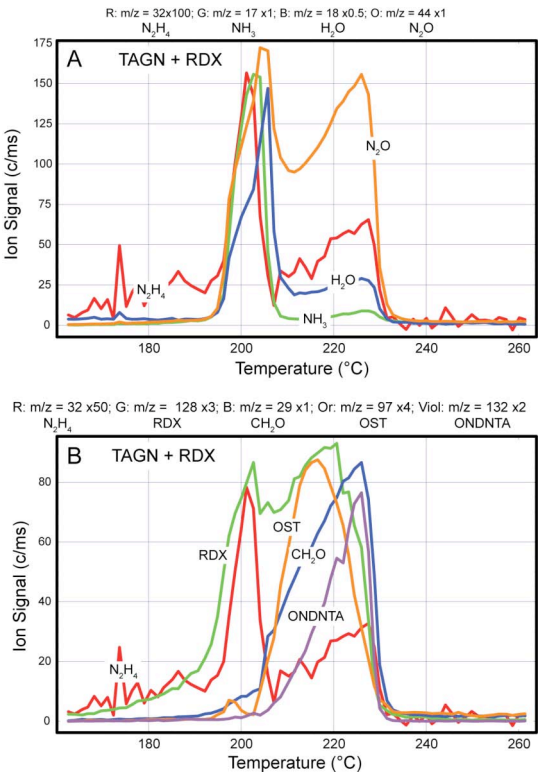

Figure 5. Ion signals representing various species formed in the decomposition of a mixture of TAGN with RDX. The scaling factors and m/z values associated with each product are shown at the top of each graph. Heating rate: 2.5°C/min.

Although the interactions of each TAG salt with RDX have many similarities, there are significant differences. The reaction with TAGzT starts at the lowest temperature (~175°C), the reaction with TAG-TATTz starts at a slightly higher temperature (~182°C), and reaction with TAGN starts at the highest temperature (~193°C). The duration of the interaction of hydrazine with RDX is the shortest for TAG-TATTz (ΔT~4°C) and greatest for TAGN (ΔT~10°C). While the reaction of hydrazine with RDX starts and finishes prior to melting of RDX for TAGzT and TAG-TATTz, it starts just prior to melting of RDX and continues past the melting point of RDX for TAGN. This behavior coupled with the similar intensities of the N_2H_4, NH_3, H_2O and N_2O/CH_2O signals for all three salts suggests that the interaction between hydrazine and RDX occurs in the gas phase.

Reaction of hydrazine with RDX in the gas phase is consistent with models of RDX decomposition in the condensed phase that show that the rate of sublimation of RDX from either the solid or liquid is four to five orders of magnitude greater than its decomposition rate in either the gas or liquid phase (see Fig. 12 in reference[9]). When RDX is present by itself, its slow reaction in the gas phase compared to its rate of sublimation and recondensation on the surface of RDX allows a quasi two-phase equilibrium to be established between the gas and condensed phases. This effectively eliminates the sublimation process as a rate limiting step in the reaction process. However, in the presence of hydrazine from the thermal decomposition of the TAG salts, reaction of RDX in the gas phase is more rapid. Thus, quasi two-phase equilibrium between RDX in the gas and condensed phases is significantly altered and the rapid rate of sublimation of RDX supplies ample amounts of RDX to react with the hydrazine.

The reaction of hydrazine with gaseous RDX does not appear to alter the subsequent decomposition of the remaining RDX from that observed when RDX is decomposed by itself.[9] In one reaction channel, RDX decomposes in the liquid phase to OST, H_2O, NO and NO_2, which start to evolve when RDX melts. In the other main reaction channel, RDX reacts with NO to form ONDNTA, which then decomposes to form CH_2O, N_2O and several other products. Both of these main reaction channels are illustrated with the data shown in Figures 4 and 5. This normal decomposition behavior is observed in the experiments with all three TAG salts.

One slight difference between the decomposition of RDX by itself and its decomposition after having been exposed to the reaction of hydrazine with the RDX is the evolution of H_2O from the RDX. In the experiments with all three TAG salts that rate of evolution of water from the sample as the RDX melts is higher than is observed in the decomposition of RDX by itself. The origin of this behavior is currently unknown. It is possible that some of the water formed in the reaction of hydrazine with RDX is absorbed by the remaining RDX and is later released upon melting.

STABILITY OF TAG SALTS

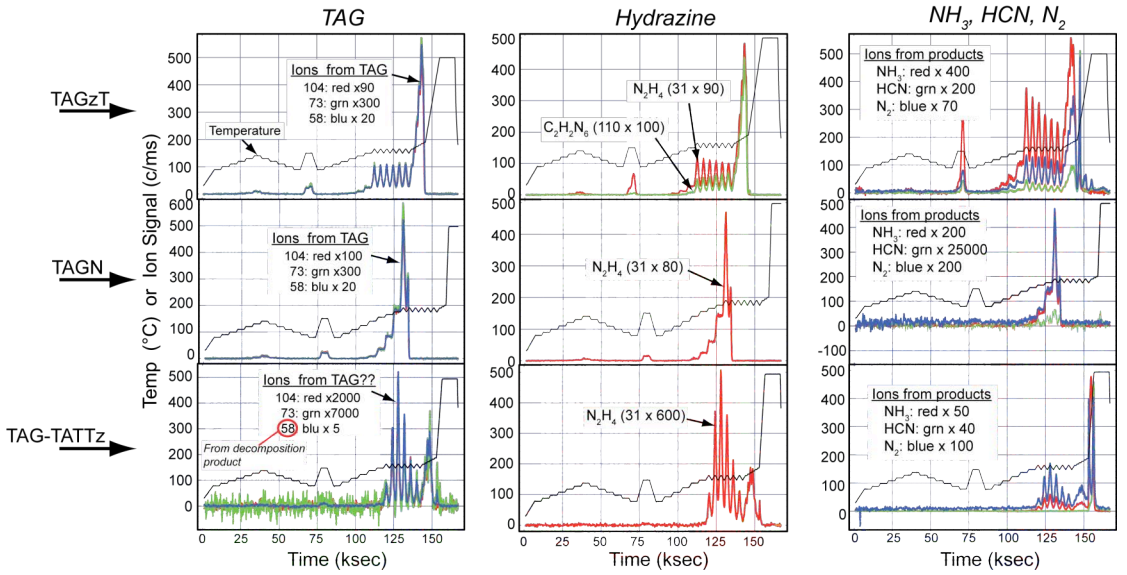

Figure 6. Comparison of TAG, hydrazine and TAG decomposition products NH_3, HCN and N_2 from three TAG salts: TAGzT, TAGN, and TAG-TATTz. The samples are analyzed using the protocol described in the methods section. Note that the lower and upper temperature limits for the thermal cycles in the TAGN experiment is higher than for the other two compounds.

Understanding the thermal stability of TAG salts and their possible interaction with other ingredients is important for assessing possible production issues and long-term aging properties of formulations. We have screened TAGzT, TAG-TATTz and TAGN. The results are shown in Figure 6. Three aspects of the thermal decomposition are examined and compared for each compound: (1) The initial decomposition step, R1 in the TAGzT mechanism (Fig. 1); (2) The decomposition of TAG to N_2H_4, NH_3, HCN and N_2, reactions R2 and R3; and (3) Whether feedback loops are established in the reaction mechanism to create an “autocatalytic-like” effect. These are examined using the thermal profiles outlined in the methods section. Comparison of ion signals representing the rates of evolution of TAG, N_2H_4 and NH_3/HCN/N_2 are shown in Fig. 6.

The results for TAGzT show the following:

1. TAG evolves from the sample (represented by ion signals at m/z values of 58, 73 and 104). 104 is the molecular ion of TAG. 73 and 58 are daughter ions in its mass spectrum. The first significant TAG signal is observed at the step to 110ºC in lower confinement conditions and at the step to 120ºC in the higher confinement conditions.

2. Under both high and low confinement conditions, hydrazine and the other TAG decomposition products, NH_3, HCN and N_2, first evolve at the 150°C step.
3. The rate of evolution of TAG does not accelerate dramatically under lower confinement, as indicated by the signals in the thermal cycling region shown in Fig 6. However, increasing the confinement of gaseous products causes the reaction to accelerate in the thermal cycling region (data not shown). This indicates that feedback loops, as indicated by reactions R13 and R14, are established in the decomposition process.

This data suggests that any processes associated with the manufacturing of propellant near the temperature range of 120 to 140ºC should be carefully evaluated for compatibility and safety issues, as this is the temperature region at which TAG decomposes. Furthermore, the reaction of TAG with other compounds will affect the equilibrium condition established in R1 and lead to a more rapid decomposition of TAGzT. Possible compounds may include either other ingredients used in a formulation or the emergence of new species in the reaction of TAGzT itself.

The results for TAG-TATTz show the following:

1. There is no significant mass loss or evolution of TAG from the sample as it is heated in isothermal steps to 140ºC, back down to 80ºC and then up to 150ºC.
2. TAG evolves from the sample as seen with the TAGzT. TAG is represented by ion signals at m/z values of 104, 73 and 58. The first significant TAG signal is observed at 165ºC.
3. Subsequent decomposition of the TAG to form the major lower molecular weight products, N_2H_4, NH_3, N_2 and HCN occur approximately 1000 seconds after the appearance of TAG.
4. The temporal behavior of the rate of evolution of the products in the thermal cycling region indicate the establishment of a feedback loop in the reaction mechanism that leads to an increasing rate of reaction.

The onset of the initial decomposition step in TAG-TATTz occurs at a temperature 45ºC higher than TAGzT. Thus, TAG-TATTz is more thermally stable than TAGzT.

The results for TAGN show the following:

1. The thermal decomposition of TAGN is different from the thermal decomposition of the other compounds in that the TAG and the major lower molecular weight product, N_2H_4 evolve simultaneously. In experiments with TAGzT and TAG-TATTz, the evolution of TAG and its decomposition products were separated by 1000 to 2000 seconds. This is not the case with TAGN. The products appear to be evolving at the same time.
2. The first significant TAG and hydrazine signal is observed at the step to 120ºC. Thus, the onset of decomposition of TAGN is comparable to TAGzT.
3. The rate of decomposition of TAGN in the thermal cycling region of 150 to 165°C used for TAGzT and TAG-TATTz was slower. To obtain data in the thermal cycling region of the experiment, the TAGN sample was cycled between 175 and 190°C.

The onset of decomposition of TAGN occurs at approximately the same temperature as TAGzT, 120°C.

Use of TAGzT or TAGN in a propellant that requires processing near 100°C during its production may present compatibility and possibly safety issues. In contrast, TAG-TATTz is more stable than the other two compounds and its compatibility with other ingredients may be less of a concern.

SUMMARY AND CONCLUSIONS

Reactions of compounds used as ingredients in propellant formulations play a central role in determining their performance, manufacturability, safety, IM properties and long-term aging behavior. The decomposition of individual compounds and the interaction of various ingredients in a propellant formulation form a reaction network that will determine the behavior of a propellant over the range of conditions it encounters during its life cycle. Methods to identify the elements and linkages in the reaction network and quantitatively characterize its behavior have not been available to the energetic materials community.

We are developing a new paradigm, known as “Concept, Methods and Protocols for Reaction Hierarchy and Network Development” (CoMPReHND) to address a range of reactivity issues that underlie propellant performance, safety, IM behavior and long-term aging. The CoMPReHND paradigm has been used to evaluate the thermal decomposition of four TAG-based salts and their reaction with RDX.

Previous results from experiments examining the thermal decomposition of TAGzT and its interaction with RDX showed that hydrazine is formed in abundance in the thermal decomposition of TAGzT and it reacts more rapidly with RDX than RDX can decompose by itself. In addition, it was found that onset of decomposition occurs at ~110°C and involves the dissociative sublimations of TAGzT to TAG and ABT. This presents concerns if production of the propellant requires the use of elevated temperatures.

To develop new ingredients that meet performance requirements while satisfying compatibility, safety and long-term aging issues, we are in the process of investigating a range of different compounds, which are likely to form hydrazine, to determine essential features of their reaction networks. The data presented in this paper focuses four TAG-based salts and the role that the anion plays in the net production of hydrazine from TAG, its interaction with RDX, and the onset of decomposition reactions. Four TAG-based salts were investigated: TAGzT, TAG-TATTz, TAGN, and TAGCl.

In experiments with each TAG-based salt by itself, it was found that the relative fraction of N_2H_4 observed from the four compounds ranged from 11% for TAGCl, 23% for TAGN, 52% for TAG-TATTZ, up to 76% for TAGzT. The results show that the smaller inorganic anions react more readily with the hydrazine and/or TAG than the organic anions, as may be expected.

In experiments with mixtures of each TAG-based salt and RDX, it was found that the extent of interaction of TAGzT, TAG-TATTz, and TAGN were similar (TAGCl was not included in the experiments with RDX). Thus, it is likely that each compound forms comparable amounts of hydrazine that is able to react with RDX faster than it reacts with any of the three anions. In addition, the reaction of hydrazine from TAGzT and TAG-TATTz occurs below the melting point of RDX, whereas the reaction of hydrazine from TAGN occurs near and above the melting point of RDX. The similarity in the observed rates of reaction in all three cases indicates that the hydrazine reacts with RDX in the gas phase. It is interesting to note that consumption of RDX in the gas phase by reaction with hydrazine will reduce the rate of condensation of RDX from the gas to solid or liquid, which has the effect of increasing the net rate of transport of RDX from the condensed phase to the gas phase.

The onset of decomposition of TAGzT, TAG-TATTZ, and TAGN was examined. TAGzT and TAGN both decompose to form TAG with an observed onset temperature for each between 110 and 120°C. The onset temperature for onset of reaction of TAG-TATTz occurs at about 165°C, which is approximately 45°C above the other two compounds.

The results illustrate the utility of using the CoMPReHND paradigm to examine the reaction networks that control the decomposition and interactions of energetic compounds used in propellant formulations. In this paper CoMPReHND has been used to identify and probe the initial reactions that control the behavior of a group of related compounds. It is effectively used as a screening tool. Once more promising compounds are identified, CoMPReHND can be used to more fully understand the reaction network and quantitatively characterize its behavior over a range of environmental conditions encountered during its life cycle.

FUTURE WORK

A series of new compounds targeted at forming hydrazine, synthesized by Phil Pagoria (LLNL) and David Chavez (LANL), will be examined in future work.

ACKNOWLEDGMENTS

This work was supported in part by the DoD Joint Munition Program/DOE Memorandum of Understanding, the Army Research Office under contract # 43381-CH, and the Office of Naval Research. We thank Bill Koppes for supplying the TAG-TATTz sample used in these experiments.

REFERENCES

1. Flanagan, J.E., M.B. Frankel, and D.O. Woolery, *HMX Combustion Modification*. 1984, Rockwell International, Rocketdyne Division: Edwards Air Force Base, California. p. 57-71.
2. Walsh, C. and C. Knott, *Gun Propellant Formulations with High Nitrogen Modifiers*, in *Propellant Development & Compatibility Subcommittee Meeting*. 2003, CPIA.
3. Behrens, R., *Thermal Decomposition Processes of Energetic Materials in the Condensed Phase at Low and Moderate Temperatures*, in *Overviews of Recent Research on Energetic Materials*, R.W. Shaw, T.B. Brill, and D.L. Thompson, Editors. 2005, World Scientific Publishing Co.: Singapore. p. 29 - 74.
4. Richard Behrens, J. and D. Wiese-Smith, *Investigating Reactions of Cyclic Nitramines in the Condensed Phase: 1. Concepts, Methodology, Protocols for Reaction Hierarchy and Network Development*. In preparation.
5. Hayden, H., et al. *Thermal Decomposition of High Nitrogen Compounds: TAGzT*. in *41st JANNAF Combustion Subcommittee Meeting*. 2006. San Diego, California: CPIAC.
6. Hayden, H., R. Behrens, and D. Wiese-Smith, *Thermal Decomposition of Bis(triaminoguanidinium)-5,5'-azotetrazoloate and Bis(guanidinium)-5,5'-azotetrazolate(GUzT)*, in *JANNAF PEDCS Meeting*. 2007, Chemical Propulsion Information Agency: Reno, NV.
7. Behrens, R., D. Wiese-Smith, and H. Hayden. *Reaction Processes that Control the Thermal Decomposition of Mixtures of TAGzT and RDX*. in *41st JANNAF Combustion Subcommittee Meeting*. 2006. San Diego, California: CPIA.
8. Personal communication. Koppes, W., M. Sitzman, and D. Rosenberg, *Synthesis of TAG-TATTz*,.
9. Behrens, R. and D. Wiese-Smith, *Reaction Kinetics of RDX in the Condensed Phase*, in *40th JANNAF Combustion Meeting*. 2005, CPIA Publication: Charleston, South Carolina. June 2005.
10. Maharrey, S. and R. Behrens, *Thermal Decomposition of Energetic Materials 5. Reaction Processes of 1,3,5-Trinitrohexahydro-s-triazine (RDX) Below Its Melting Point.* Journal of Physical Chemistry, 2005. **109**: p. 11236-11249.
11. Behrens, R., Jr., *New simultaneous thermogravimetry and modulated molecular beam mass spectrometry apparatus for quantitative thermal decomposition studies.* Review of Scientific Instruments, 1987. **58**(3): p. 451-461.
12. Behrens, R., Jr., *Identification of Octahydro-1,3,5,7-tetranitro-1,3,5,7-tetrazocine (HMX) Pyrolysis Products by Simultaneous Thermogravimetric Modulated Beam Mass Spectrometry and Time-of-Flight Velocity-Spectra Measurements.* International Journal of Chemical Kinetics, 1990. **22**: p. 135-157.
13. Behrens, R., Jr., *Determination of the Rates of Formation of Gaseous Products from the Pyrolysis of Octahydro-1,3,5,7-tetranitro-1,3,5,7-tetrazocine (HMX) by Simultaneous Thermogravimetric Modulated Beam Mass Spectrometry.* International Journal of Chemical Kinetics, 1990. **22**: p. 159-173.
14. Behrens, R. and S. Bulusu, *Thermal-Decomposition Of Energetic Materials .3. Temporal Behaviors Of the Rates Of Formation Of the Gaseous Pyrolysis Products From Condensed-Phase Decomposition Of 1,3,5-Trinitrohexahydro-S-Triazine.* Journal Of Physical Chemistry, 1992. **96**(#22): p. 8877-8891.

INTERIM REPORT: WORKSHOP ON R&D REQUIRED TO IMPLEMENT NEW ENERGETIC INGREDIENTS IN MUNITIONS

Richard Behrens
Combustion Research Facility, Sandia National Laboratories,
Livermore, CA 94550

William Anderson and Brad Forch
Army Research Laboratory, Ballistics and Weapons Concepts Division,
Aberdeen Proving Ground, MD 21005-5066

Robert Shaw
Army Research Office
4300 South Miami Blvd, Box 12211,
Research Triangle Park, NC 27709-2211

ABSTRACT

This is an interim report on a workshop that was held at the Battelle Conference Center, Aberdeen, MD on 29-31 August 2006 to assess the R&D required to implement new energetic ingredients in munitions. The participants discussed: (1) conventional methods for evaluating ingredients, (2) system requirements for new energetic materials, (3) what technically limits the implementation of new ingredients in munitions, (4) new experimental concepts for evaluating performance and deleterious features of new ingredients, and (5) new modeling/simulation methods for evaluating and predicting performance and deleterious features of new compounds and materials. From these discussions it became apparent that the perceived risk for investing in the development of new energetic materials was high due to limited success over the past fifty years in implementing new ingredients in munitions. To reduce this perceived risk, it is important to have (1) programmatic efforts focused in the areas of controlled chemical propulsion, interaction at targets, and meeting IM requirements and (2) new experimental and theoretical methods that provide more insight into the reactive processes and can provide meaningful data 100 times faster and use 100 times less energetic material. Several teams have been formed to develop detailed research plans in the areas of synthesis and scaleup, formulations, super-small scale testing, modeling/simulation, new diagnostics, data mining, health and environmental compliance issues, and material design parameters. From these efforts a new R&D paradigm is being developed to meet future munition requirements.

INTRODUCTION

A workshop on “R&D Required to Implement New Energetic Ingredients in Munitions” was held at the Battelle Conference Center, Aberdeen, MD from 29 – 31, August, 2006. Approximately 55 people from DoD and DOE laboratories, industry and academia participated in the workshop. The background of participants was broad, drawing on people with backgrounds in basic research, formulation development, manufacturing, systems development and program management. The workshop was supported by the Army Research Laboratory, the Army Research Office, the Office of Naval Research, the Air Force Office of Scientific Research,

Sandia National Laboratories, CPIAC and other DoD and DOE organizations who provided resources to allow staff to participate in the workshop.

This is an interim report that summarizes many of the general conclusions of the workshop and provides a guideline for the follow on work needed to define individual research areas more specifically.

RESULTS AND DISCUSSION

OBJECTIVE

The objective for the workshop was to create a plan for R&D investment strategies that will enable the rapid implementation of new energetic ingredients (e.g., high nitrogen compounds energetic binders, and ionic liquids) needed to reach new munition goals, while meeting insensitive munition (IM), aging, quality assessment and cost requirements. To accomplish this objective we brought together a group of people with expertise in diverse areas of energetic materials R&D. Participants in the three-day workshop included about 55 people whose responsibilities involve basic research, material development, munition development, and management of a range of DoD interests.

To construct strategies for future R&D investments, we discussed many aspects concerning future requirements for new munitions, the role for new ingredients, and the R&D required for their development. Discussions focused on two themes: (1) the requirements for munition systems of the future, and (2) scientific and technical issues that will enable the rapid development of new energetic materials that can be used for the development of new munition systems. By the end of the workshop we had (1) developed a strategy for assessing future munition requirements, (2) reviewed the current state of capabilities used for munition development, (3) identified gaps in our R&D capabilities that limit the development of new energetic materials, (4) initiated discussions on research approaches that can be used to develop technology that will close these gaps and enable rapid development of new energetic materials.

To build on the ideas developed in the workshop, teams were formed to develop detailed plans in nine specific areas identified in the workshop. This is currently underway and will be completed in the Winter of 2007.

DEFINITION OF TERMS

Historically, the energetic materials community has used the term *energetic materials* to describe all forms of materials, ranging from pure energetic compounds to explosive or propellant formulations. To provide a specific framework with which to describe the reaction processes that control the behavior of these materials and to avoid confusion, we present the following definitions:

Energetic ingredient: a pure energetic compound whose properties are determined at the molecular level. For example, compounds such as RDX, TNT, HMX, etc. Properties such as bond energies, crystal structure, and vapor pressure would be associated with the energetic ingredient. Herein, energetic ingredients are considered homogenous except at very small (molecular) scales. If crystalline, the structure is considered to be perfect. If amorphous, it is considered to be perfectly mixed and packed (no voids).

Energetic material: (1) a mixture of ingredients, some of which are energetic ingredients, of a given spatial structure (e.g., features of grain structure/size, solvent inclusions, crystal defects, interfaces between ingredients, etc. are significant; such physical features may differ between two energetic materials composed of exactly the same ratio of pure molecules and may make large-scale properties such as responses to stimuli differ). (2) a relatively pure energetic compound whose properties are determined at spatial scales larger than the molecular

level (that is, spatial structures matter, as in part 1). New forms of molecular interactions that are not present in an energetic ingredient may determine the properties of an energetic material.

Formulation: a mixture of ingredients, some of which are energetic, that is used as an explosive or propellant and has a given spatial structure. Note: two formulations could be composed of exactly the same ratios of molecules but differ because of spatial organization.

GENERAL SUMMARY

The following is a general summary of the workshop and the central themes of the discussions.

The participants were asked to present a short summary of their ideas on a specific topic in one of the following five areas: (1) conventional methods for evaluating ingredients, (2) system requirements for new energetic materials, (3) what technically limits the implementation of new ingredients in munitions, (4) new experimental concepts for evaluating performance and deleterious features of new ingredients, and (5) new modeling/simulation methods for evaluating and predicting performance and deleterious features of new compounds and materials. The diverse perspectives of the participants from academia, government laboratories and industry on both the programmatic and technical issues provided a basis for assessing the issues that will control the path forward in the development of new energetic materials for future munition requirements.

Following the short presentations, the participants were divided into three groups. Each group spent one day discussing the issues and developing a strategy for future R&D investments. The chairs of each group presented a summary of each group's discussions and R&D plans to all workshop participants. At the conclusion of these presentations, the participants identified nine areas that required further definition and selected leaders to assemble teams to address the issues in each area.

The brief overviews provided insight into the wide range of issues that underlie the development of new energetic ingredients, materials, and formulations. The summaries outlined the performance, safety, IM, reliability, service life, environmental compliance, and health requirements that must be met to successfully introduce a new energetic material. The number of different, stringent requirements that must successfully be met in order to implement a new ingredient in energetic materials and the difficulty in meeting these requirements struck a number of workshop participants as being somewhat analogous to the difficulty of developing new drugs in the pharmaceutical industry. The discussions provided an overview of the many issues that must be confronted to develop new materials to meet future munition requirements. The number and diverse aspects of these issues account for the general perception of weapons development program managers within the DoD of the high risk associated with introducing new ingredients into munitions.

The perceived high degree of risk limits the investment of funds in this area. Limited funding, in turn, restricts the development of new tools needed to understand and design new materials. Thus, a self-fulfilling cycle that limits the development of new energetic materials is created. To assess whether it is feasible to exit this cycle, the participants in the workshop discussed the programmatic requirements that drive the procurement of new munitions. Two themes emerged: (1) The drivers for the procurement of new munitions range from procurement of munitions based on well-established and tested designs to procurement of new munitions to meet new system requirements. The perceived benefits derived from the development of new energetic materials for the well-established munitions are very low, and consequently investment is nil. In contrast, the perceived benefits from investment in the development of new energetic materials for new systems are high because current materials cannot meet the design objectives. (2) The demand by the DoD that new munition procurements meet IM requirements will require investment in new energetic materials for both new and well-established munition systems. While waivers have been granted in recent years for new noncompliant munitions, international defense agreements will require that future acquisitions meet IM requirements. Thus, there are both

national and international drivers pushing for IM compliant munitions. Much of the current effort to develop IM compliant munitions is occurring outside of the US, thus increasing the likelihood that future munition procurements may come from foreign countries. Thus, the R&D investment strategy must be focused to (1) enable the design of new energetic materials for systems to meet new operational requirements, (2) enable the development of IM compliant munitions for both new and well-established systems, and (3) provide materials that meet health and environmental compliance issues.

PROGRAMMATIC DRIVERS FOR NEW MATERIALS

To move forward in introducing new ingredients to enhance munitions will require demonstration of significant, not marginal, improvement in performance, while meeting new requirements for safety, IM, environmental compliance and health.

In discussions of what constitutes significant improvements, the development of advanced energetics requiring improvement factors ranging from 5 to 10 times current CHNO materials was mentioned. For a number of participants, the development of materials with this degree of improvement seemed forbidden by thermodynamics for classic combustion systems. More exotic energy sources may be allowed by physical laws but are not practical. For example, one could conceive of creating materials that store energy in excited electronic states, but implementation of this concept seems impractical. Furthermore, the nuclear option with improvements ranging from 10^4 to 10^6 already exists. Thus, simply specifying a need for new energetic materials with some factor of enhancement in energy storage seems a less than adequate concept to guide the development of new energetic materials.

A number of participants also presented issues associated with the development of new weapons systems driven by cost. For example, a number of new energetic ingredients have been synthesized and small-scale testing (less than one gram total) suggests their possible utility, but synthesis scale-up and large-scale testing would be quite expensive. In most of these weapons systems, the demands to meet IM requirements may drive the development and implementation of new energetic ingredients, but cost will still be the primary driver. Program managers consider risk of introducing new ingredients too high for this type of procurement. Thus, it is unlikely that funds will be available from this source until either (1) the perceived risk of new EM development is reduced or (2) the demand for IM compliance limits procurement.

So what drives the current needs in new munition development? *Having a desired effect on a target*. This was the underlying idea of the workshop discussions on this topic. For example, asymmetric warfare presents situations in which the use of current munitions, designed for symmetric warfare, are ineffective or detrimental to the overall situation. In these situations it may be important to neutralize a limited target without inflicting collateral damage. Thus, a munition system specifically tailored for this purpose may be required. For example, propulsion may need to be controlled and modified in flight, or the type of interaction with a target may need to be determined as a munition nears its target and acquires updated information. While old ingredients may be useful in designing new formulations to meet these types of requirements, it is likely that new ingredients will be required in order to tailor the performance of new formulations to meet the new requirements.

Thus, to identify what will be required of energetic materials in the future, the system-level requirements of new weapons should be used as a guide. Consideration of system level requirements will establish a conceptual framework that can be used to define energetic material requirements. The successful implementation of new system designs is likely to depend on the ability to procure materials that meet the design requirements in a short period of time. Hence, the ability to design a wide range of different types of materials will enable the development of more viable munitions systems that can meet a more demanding range of objectives.

In summary, the features of new munition systems that will require new energetic materials are : (1) Munitions designed for specific strategic or tactical objectives, (2) Those designed to deposit a controlled amount of energy on target especially to limit collateral damage.

While meeting new performance requirements, these systems will also be required to meet IM, safety, environmental, health and cost requirements.

REQUIREMENTS FOR THE EM COMMUNITY

This conceptual framework sets the stage for what is required from the EM community:

1. The ability to provide a range of different types of energetic *materials*, not simply ingredients.
2. These materials must provide for
    a. Propulsion – precise guidance
    b. Controlled interaction with target
        i. Fragments
        ii. Blast
        iii. Reaction with target.
3. Agile development and manufacturing capability.
    a. Low cost and fast deployment.
4. Must meet safety, IM, service life, reliability, environmental compliance & health requirements.

Thus, the *main requirement* is for the capability to design a wide range of different types of energetic materials that will broaden our ability to design new munitions to meet specific mission needs.

Many of the discussions at the workshop suggest that the current infrastructure and paradigm used for the development of energetic materials cannot meet these needs. In reviewing the presentations and summaries of the three breakout groups these insufficiencies stem from:

1. An infrastructure for the development of munitions built in WWII or earlier.
2. A Cold War focused on counteracting a single, strong adversary, which has created an infrastructure not well suited to today's needs.
3. A mindset and standards for developing and testing energetic ingredients and energetic materials based on scientific methods developed early in the twentieth century (before 1950).
    a. Many methods used to evaluate new ingredients are:
        i. Over 50 years old
        ii. Provide only global measurements
        iii. Provide little information on chemical reactions.
        iv. Require large amounts of materials to assess properties.
        v. Do not provide knowledge that can be used to guide the design of new ingredients
        vi. Are not well-standardized.
    b. Current focus is on ingredients, not materials and formulations actually used.
4. Formulations are made from ingredients using *trial and error*. We should instead design new systems for specific missions, then build them based on our knowledge of the ingredients and their reactions. Better ways to determine the properties of the materials are needed to enable this approach.

Thus, to meet future needs we need to be able to design new energetic materials using modern scientific methods, many of which need to be better developed.

R&D REQUIRED TO EXPEDITE ENERGETIC MATERIAL DEVELOPMENT

While the *development* of energetic materials is still mired in the use of old technology, research over the past 30 years has provided much new insight into the behavior of energetic ingredients and provides a basis for developing new strategies for improving our ability to design new energetic materials more rapidly. Successes have included:

1. The ability to model the physicochemical processes that control the combustion of propellants.
2. The ability to assess the thermochemistry of new formulations (e.g. Cheetah code)
3. The ability to design new molecules using quantum chemistry calculations.
4. New experimental methods to understand complex reactions in the condensed phase.

Each of these advances provides us with the ability to link performance with the underlying chemical features of the molecules.

The challenge that lies ahead of us is to determine how the properties of a material or formulation, not an ingredient, depend on the underlying chemical reactivity. We need to know:

1. How materials respond to mechanical, thermal and electrical stimuli
    a. These underlie their safety and IM response.
2. How to design materials that minimize their response to these stimuli.
3. How to tailor and control the release of energy from a material.

The underlying knowledge required, from a materials point of view, is how the constituents used to make these materials react in the condensed phase. Historically, scientific investigations of reactions of organic materials in the condensed phase have been deemed too difficult to warrant significant effort. However, advances in instrumentation, computational resources, and scientific methods over the past twenty years have opened new avenues for investigating these complex systems. Hence, it is now feasible to investigate the reactions in energetic materials at a level of sophistication not available during the most recent intense development cycle (1980s).

Thus, our current capabilities that have been developed to examine the reaction of energetic molecules over the past 30 years must be extended to probe the issues of chemical reactivity at the larger spatial scales that are relevant to the reactions in *energetic materials*.

FOCUS AREAS

Examination of the reactions of energetic materials and formulations will be difficult with current experimental and testing capabilities. While single ingredients only require one set of tests to be conducted on the ingredient, the development of new materials will require tests on may different combinations of ingredients. Thus, methods will be required to *rapidly* prepare, test, characterize and model many different ingredients and combination of ingredients. This will require new approaches to be developed in the following areas:

1. **Synthesis and scale up**. How to make the new materials rapidly and in sufficient quantity.
    a. Any technical issues that limit synthesis should be highlighted. Are there types of compounds that we would like to make, but no synthesis route exists?
    b. What is required to make sufficient quantities for rapid testing?
2. **Formulation design**: How to control and vary material properties.
    a. To simulate manufacturing scaleup issues.
    b. To provide a range of materials with different properties for testing.
    c. To address issues such as particle morphology & manufacturing defects.
3. **Super-small scale tests/experiments**: How to design tests that will provide the greatest amount of information about material behavior with the smallest amount of material.
    a. Reduce synthesis scale up requirements.
    b. Work with samples that reduce safety issues and enable high throughput.
    c. Provide data on reactions at spatial scales that can be simulated in molecular-based models of reactive systems.
4. **Modeling/simulation**: Develop models that can be used in conjunction with super-small scale experiments and new diagnostics, and/or via *a priori* methods to provide predictive tools to guide material design.

5. **New diagnostics**: Develop new instruments and testing devices that will enable a better understanding of the response of energetic materials to thermal, mechanical and electrical stimuli.
    a. These will allow rapid testing of new material formulations.
    b. Replace current testing methods: drop hammer, etc.
    c. Provide high-level of information feedback at the molecular level to guide the design of new materials.
6. **Data mining and analysis**: Need methods to determine the critical factors in the design of new energetic materials.
    a. Methods to determine critical features from large data sets will be required.
7. **Health and environmental compliance issues**: Methods to rapidly screen new compounds will be required.
    a. Must use limited amount of material to provide confidence in health hazard for new compound.
    b. Is it sufficient to conduct these tests on the individual ingredients and not the materials? This reduces the total number of tests compared to those required for materials development.
8. **Material design parameters**: Strategies for the design of new materials must be developed.
    a. The conceptual framework needed to guide the design of new materials must be constructed. This should be built on the analysis of the types of *effects on target* that will be required in future munition systems.
    b. General ideas on the types of materials that may be needed in the future.
9. **Testing protocols**: Methods to assess the critical design parameters in new materials must be developed in parallel with materials design.
    a. Must enable service life evaluations of munitions to meet design criteria.

The requirements in these nine areas span basic research, applied research, and development. To successfully enable the design of new energetic materials to meet future munition system objectives clearly requires a tighter coupling and feedback between basic research, applied research and development.

BASIC RESEARCH, APPLIED RESEARCH, DEVELOPMENT PARADIGM

Areas of inquiry for basic research must be focused and prioritized to maximize the likelihood of success of future applied research & development. While *curiosity* driven basic research may lead to groundbreaking discoveries, *directed* basic research provides the conceptual framework to develop the tools needed for applied research and development. Without significant investment in *directed basic research* in several areas, it is unlikely that the tools will be available to enable the development of new energetic materials.

Areas of applied research must build on and test basic research concepts. Applied research must provide feedback and a definition of future needs to the basic research community. The applied research community must also develop the tools needed to make the development process highly efficient.

Areas of development must define the critical steps in the development process. The efficiency and cost of development must be improved by at least an order of magnitude (probably two orders of magnitude). To accomplish this goal will require definition of the technical requirements for each critical step. The definition of these technical requirements will provide the feedback necessary to focus the basic and applied research needs.

To accomplish these goals will require a much tighter coupling in the

basic ↔ applied ↔ development

paradigm. Close, interactive coupling of DoD 6.1, 6.2 and 6.3 programs is not the norm and changes have been recommended by the National Academies.[1] So success in establishing an R&D program will require organization focused on the primary goals.

A CONCEPTUAL FRAMEWORK FOR DEVELOPING R&D STRATEGIES

To create a conceptual framework for developing R&D strategies requires (1) carefully defining the main underlying requirements and (2) planning the integration of research to development to application (R→D→A) functions. To focus our thoughts on these two issues a *hypothetical* organization focused on EM development is put forth as a means for developing concepts and defining the details required to build an R&D strategy for implementing new energetic ingredients in munitions.

To develop and focus these thoughts, a *hypothetical organization* called the National Energetic Materials Research & Development Institute (NEMReDI) has been created to guide our analysis of the relevant issues. This hypothetical organization has all the components to do high throughput materials development. NEMReDI may be physical location, a virtual institute, or a combination of physical location & virtual institute. It incorporates members from government laboratories, academia, and industry. It does precompetitive R&D. It has members from industry and licenses intellectual property to its partners.

NEMReDI is a *conceptual framework* that outlines requirements for EM development. It is used to identify existing capabilities and highlights where investment is required. An illustration of NEMReDI is shown in Figure 1. The main feature of NEMReDI is that it contains all of the resources required to develop new energetic materials and implement them in new munition concepts. A brief description of each of these resources is listed in Table 1. Its main focus is to provide an agile resource for developing new munition systems, in small quantity, to meet critical strategic needs. Spin-offs from this work will form the basis for modernizing older, more conventional munition systems.

The hypothetical organization is divided into three conceptual wings:

1. Research and development – small-scale experiments and testing.
2. Medium scale testing.
3. New system design and testing.

Each wing is divided into laboratories. Each laboratory is associated with properties of the materials that need to be assessed. We use the requirements for each laboratory to judge our current capabilities for evaluating materials.

The *research and development – small-scale experiments and testing wing* is where new energetic materials are created to meet new performance objectives. The laboratories that comprise this wing are required to provide the means to enable high throughput material development.

The *medium scale testing wing* is where promising materials are scaled up and tested with modified versions of the tests now commonly in use. The purpose of this wing is to provide the testing to demonstrate the efficacy of a new material and provide the knowledge base required for incorporating the material into a new munition system.

The *new system design and testing wing* is where new munition concepts are created, developed and tested. It is likely that work in this wing will develop small-scale proof of concept tests. It will coordinate the development and testing of larger-scale devices at remote facilities.

IDENTIFYING AND BRIDGING CAPABILITY GAPS

To implement the hypothetical NEMReDI concept, specific capabilities for each laboratory must be in place. The capabilities for each laboratory are those functions required to measure, model and characterize specific properties of the materials. The successful implementation of the concept requires the successful implementation of each of the pieces. In

considering the requirements for each individual laboratory, *gaps* between what can currently be done and what needs to be done must be identified, and a plan to bridge each gap developed. Each laboratory must incorporate all needed requirements: (1) basic understanding, (2) instrument development, and (3) required models, simulation, data analysis, database integration. The perceived size of the gap for each laboratory capability has been estimated and color-coded in Fig. 1. The laboratories listed in *red* have the largest technical gaps. The laboratories listed in *black* have the smallest technical gaps, or may have not technical gaps at all. (Note: The gaps in the laboratory capabilities in the new system design and testing wing have not been estimated.)

The final product for each laboratory is a viable capability that meets the NEMReDI requirements for the needed capability and achieves the knowledge generation & throughput goals for NEMReDI.

The requirements for impact sensitivity are used to illustrate the issues and define the approach required for each laboratory (laboratory # 10 for impact sensitivity).

Requirement: Information must be gathered that will allow the physical processes and chemical reactions that lead to ignition of an energetic material due to impact to be determined from a sample with a mass of less than 500 mg.

Technical challenges:

1. Current impact test methods do not provide information on where ignition occurs in a sample.
2. Methods have not been developed to probe the time-dependent reaction chemistry that occurs in response to mechanical stimuli associated with an impact event.
3. Ignition may occur over a range of spatial scales, depending on the characteristics of the material.

Approach: Focus on developing a new diagnostic instrument that will provide the information required to assess the impact response of a material. Integrate the instrument with data analysis and modeling/simulation codes. Use basic research projects to develop an understanding of the physicochemically driven reaction process and the appropriate spatial scales needed to design the instrument and codes.

Details: Three areas of investigation are required.

- One involves systematically exploring the relative importance of reactions at different spatial scales. These scales range from the molecular level (i.e., dislocations, voids) to dimensions associated with individual particles or clusters of particles. It includes reactions that may occur at grain boundaries or other defects of this nature.
- The second involves developing models to characterize the new understanding how reaction processes at larger spatial scales are related to properties of the molecules.
- The third involves the development of fast (probably optical) diagnostics that can be used to probe the time-dependent reaction processes in an impact event.

This analysis is required for each laboratory in the NEMReDI and will be carried out by each of the teams assembled to address the various issues. General ideas regarding the issues associated with each laboratory are listed in Table 1.

TASKS FOR DEVELOPING R&D INVESTMENT STRATEGIES

The hypothetical NEMReDI concept provides a framework for creating a plan for R&D investment strategies that will enable the rapid implementation of new energetic ingredients (e.g., high nitrogen compounds energetic binders and ionic liquids) needed to reach new munition goals, while meeting insensitive munition (IM), aging, quality assessment and cost requirements.

During the final discussions at the workshop, teams were formed to address the issues in the areas listed in Table 2. Note the first nine areas follow the technical areas/issues described in more detail earlier in the 'focus areas' section. The last two areas are more programmatic in nature, but were determined to be very important by the workshop participants.

The workshop subgroups will develop R&D plans to ensure that laboratory or required capability is a viable part of the NEMReDI. For each laboratory or capability the following is needed (*for items in the following list that ask for places and people, generic, not specific, sources will be provided*):

1. A statement of what constitutes the gap(s)
2. Objectives that must be met to fill the gap(s)
3. What is needed to fulfill the objectives.
    a. Technical challenges
    b. Approach to meet each technical challenge
        i. Type of research
        ii. Type of development
        iii. Where should it be done (generic, not specific location)?
4. Strategy for filling the gap ('who' below is generic, not a specific person)
    a. Who builds the scientific framework?
    b. Who implements the framework into instruments/models?
    c. Who implements the tools into the NEMReDI?
        i. Verifies knowledge generation.
        ii. Verifies throughput capabilities
    d. How to balance academic, government, industry responsibilities
5. An estimate of the resources required to fill the gap
    a. Manpower, funds, facilities
        i. Do they exist?
        ii. If not, how can they be developed?

SUMMARY AND CONCLUSIONS

The workshop on R&D Required to Implement New Energetic Ingredients in Munitions has succeeded in establishing the groundwork for developing a new conceptual framework for what will be required to implement new energetic ingredients in munitions. One of the main issues that limit progress in the development of new energetic materials and formulations is the perceived high risk of investing in this area.

This perception of high risk is felt to originate primarily from limited success in developing new ingredients and implementing new energetic materials in munitions. This limited success is due to the complexity of the processes that control the reactions of these materials, and the broad range of performance, safety, environmental compliance, health and cost issues that must be met.

To reduce the risk of developing new energetic materials will require (1) increasing our ability to monitor and understand the reactions that control the various critical performance, safety and aging behaviors of energetic materials, (2) using this understanding to guide the design of better energetic ingredients and energetic materials, (3) developing new diagnostic tools and super-small scale experiments to gain an understanding of the reaction processes underlying performance, safety and aging, and (4) the ability to synthesize, formulate and test new materials at rate that are 100 times faster and use 100 times less materials than current methods.

To achieve these goals will require using today's scientific understanding and technology to develop a new integrated system for energetic material development.

Teams have been assembled to address the details of the issues for implementing this general R&D investment strategy.

FUTURE WORK

Teams are currently working develop details of the R&D required to implement new energetic ingredients in munitions. The reports from these teams will be integrated into a final document and used to develop a national consensus to invest in the development of new energetic materials for future munition needs.

ACKNOWLEDGMENTS

Funding for the workshop has been provided by the Army Research Laboratory, the Army Research Office, the Office of Naval Research, the Air Force Office of Scientific Research and Sandia National Laboratories. Funds for R. Behrens have been provided by a Memorandum of Understanding between the DoD Joint Munitions Program and the DOE. We thank Nicole Metzger and Battelle for providing use of the Battelle Conference Center and personnel to support running the workshop and Debbie Eggleston and Ron Fry for support from CPIAC.

REFERENCES

1. Welch, L.D., ***Assessment of Department of Defense Basic Research***. 2005, National Academies Press. p. 70.

Figure 1. Layout of the ***hypothetical*** NEMReDI organization.

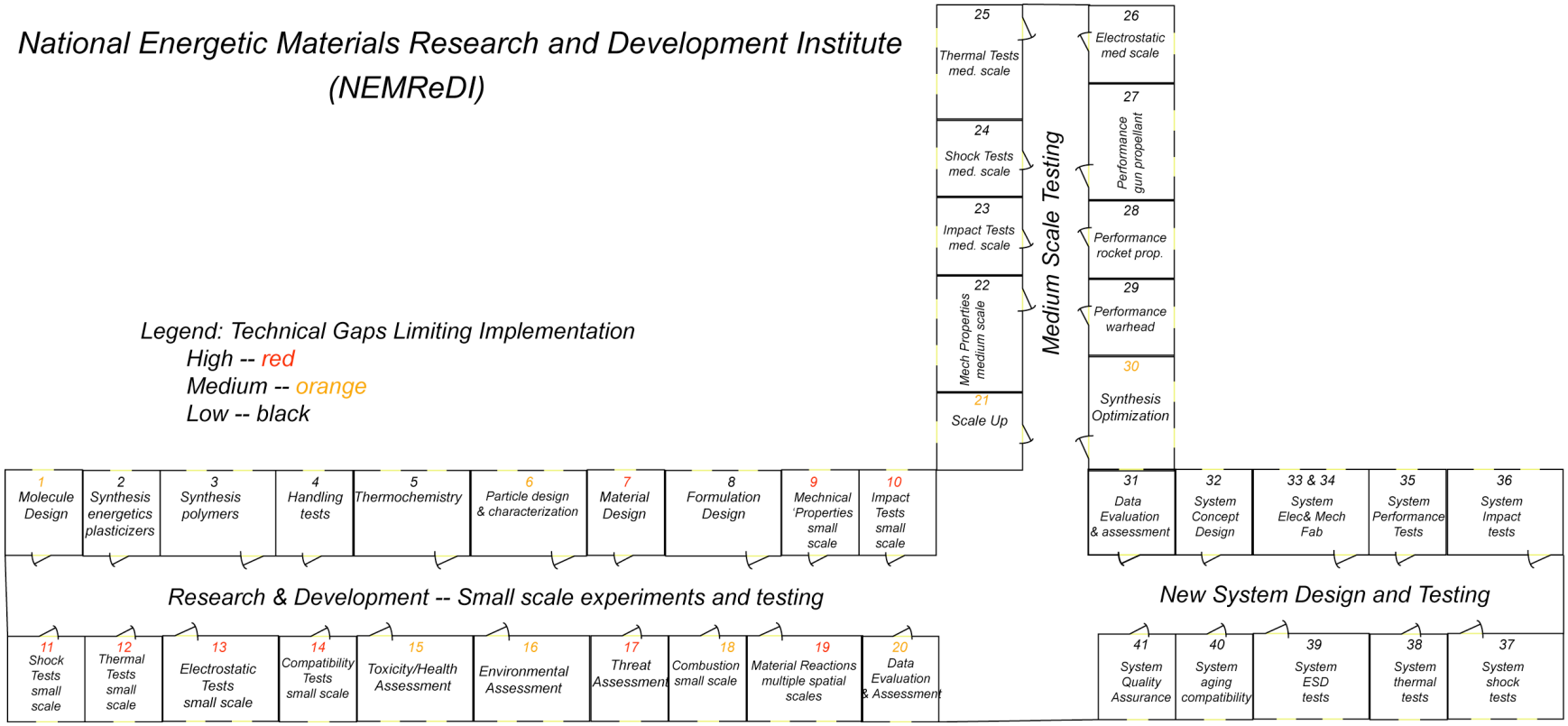

Table 1 Laboratories that comprise the National Energetic Materials Research and Development Institute (NEMReDI)

Lab #	*Topic*	*Description*	*Category*	*Design Level*	*New technology?*
1	Molecule Design	Computer design of new molecules. Quantum chemistry design of molecules,	Model/ simulation	Molecular	medium
2	Synthesis - energetics, plasticizers	Laboratory for synthesis of new energetic ingredients, energetics, plasticizers.	Synthesis/ scaleup	Molecular	low
3	Synthesis - polymers	Laboratory for synthesis of new polymers.	Synthesis/ scaleup	Molecular	low
4	Handling tests	Tests required for safe handling of new compounds: DSC, drop hammer, etc.		Molecular	low
5	Thermochemistry	Laboratory for measurement of thermochemical properties. Heat of formation, heat of combustion, heat of detonation.		Molecular	low
6	Particle design & characterization	Laboratory to develop methods for powder production: 1. Crystallization processes for morphology. 2. Methods to reduce byproducts and contaminants.	Formulation design	Molecular	medium
7	Material Design	Material design – theoretical approach. 1. Reactive force fields to model larger systems. 2. Molecular dynamics simulations.	Model/ simulation	Material	high
8	Formulation design	Laboratory to prepare and test mechanical properties of formulations for new energetic materials.	Formulation design	Material	medium
9	Mechanical properties - small scale	Laboratory to determine mechanical properties. 1. Standard mechanical testing instruments. 2. New instruments to relate mechanical properties of composite materials to chemical interfacial bonding. 3 Information feedback to guide the design of stronger materials (mostly issue for rocket propellants).	small tests/ new diagnostics	Material	high
10	Impact test - small scale	Laboratory to provide high information feedback on impact sensitivity of new materials. 1. Provide information on ignition process -- where?, what chemical reactions? 2. Reactions in individual ingredient -- effects of defects, impurities. 3. Reactions at interfaces -- design on binders that moderate sensitivity. 4. Information feedback to guide design of less impact sensitive materials.	small tests/ new diagnostics	Material	high
11	Shock test - small scale	Laboratory to provide high information feedback on shock sensitivity of new ingredients and materials with very small samples. 1. Provide	small tests/ new	Material	high

Lab #	Topic	Description	Category	Design Level	New technology?
		information on ignition process -- where?, what chemical reactions?. 2. Reactions in individual ingredient -- effects of defects, impurities. 3. Reactions at interfaces -- design on binders that moderate sensitivity. 4.	diagnostics		
12	Thermal tests - small scale	Laboratory to provide high information feedback on the reactions that occur in slow and fast cookoff. 1. Provide insight on how materials change. 2. Provide insight into whether the chemically induced changes will make the material more or less sensitive to other stimuli (mechanical, electrical). 3. Provide feedback to guide the design of new materials that will moderate the cookoff response.	small tests/ new diagnostics	Material	high
13	Electrostatic tests – small scale	Laboratory to provide high information feedback on the electrostatic sensitivity of ingredients and materials. 1. Methods must determine how electrons and ions interact with individual ingredients and materials. 2. The location of the interactions that lead to ignition must be determined from the tests. 3. How the ions/electrons lead to chemical reaction must be determined. 4. Tests must provide feedback that will guide the design of new ingredients and materials that will be less sensitive to ESD.	small tests/ new diagnostics	Material	high
14	Compatibility tests – small scale	Laboratory to provide information on what causes incompatibility between ingredients. 1. Use instruments that provide information on what chemical reactions cause incompatibility. 2. Use information to design ingredients that will not be incompatible.	small tests/ new diagnostics	Material	high
15	Toxicity/health assessment - small	Laboratory and QSAR models to predict possible toxicity of new compounds.	health & env	Molecular	medium
16	Environmental assessment - small	Laboratory and QSAR models to predict possible environmental effects.	health & env	Molecular	medium
17	Threat assessment	Laboratory to analyze threats and how they will affect the response of energetic materials. 1. What physical and chemical environment does an energetic material encounter in bullet impact, fragment impact, shaped charge impact, cookoff, ESD. 2. Provide information needed to design new energetic materials.	new diagnostics	Material	high
18	Combustion assessment -- small scale	Laboratory to assess combustion processes of new energetic materials. 1. Low pressure kinetics measurements. 2. Assess rocket motor combustion. 3. Assess gun propellant combustion.	small tests/ new diagnostics	Material	medium
19	Material reactions -	Laboratory to analyze reaction processes in energetic materials over	small tests/	Material	high

Lab #	Topic	Description	Category	Design Level	New technology?
	multiple spatial scales	range of relevant spatial scales. 1. Defects, grain boundaries, solvent inclusion in ingredients. 2. Interfacial boundaries in energetic materials. 3. Provide feedback on how to design materials.	new diagnostics		
20	Data evaluation & assessment - small	Facility to collect, analyze, evaluate and assess all data collected from laboratories in NEMReDI. 1. Collect and store all data from experiments, testing, modeling/simulation in form for further analysis and use. 2. Cluster analysis to select ingredients based on chemical properties. 3. Data for design of materials. 4. Data to assess correlation of results from different scale tests.	Model/ simulation	Material	medium
21	Scale up	Facility to scale up ingredient production. 1. Scale up to levels for medium scale tests (need to determine how much is typically required).	Synthesis/ scaleup	Molecular	medium
22	Mech properties - medium scale	Laboratory with standard mechanical testing equipment.	new diagnostics	Material	low
23	Impact tests - medium scale	Laboratory with larger scale impact tests. 1. Ability to retrieve samples with partially reacted material for analysis. 2. Retrieved samples should provide insight into where reactions occur that lead up to ignition.	new diagnostics	Material	med/high
24	Shock tests - medium scale	Standard shock tests. Card gap, etc. 1. Retrieve sample for analysis to determine how energy transfer through material leads to ignition.	new diagnostics	Material	med/high
25	Thermal tests - medium scale	Laboratory with medium scale test. 1. Instrumented cookoff tests. 2. Sample retrieval from specific locations. 3. Time to ignition. 4. Ignition of damaged material to assess change in sensitivity.	new diagnostics	Material	med/high
26	Electrostatic tests -- medium scale	Laboratory to evaluate ESD environment. Define these tests in a manner similar to thermal and mechanical stimuli.	new diagnostics	Material	med/high
27	Performance tests -- gun propellant	Similar to current testing methods – burn rate measurements, etc	new diagnostics	Material	???
28	Performance tests -- rocket propellant	Similar to current testing methods – burn rate measurements, etc	new diagnostics	Material	???
29	Performance tests - warhead explosive	Similar to current testing methods – cylinder test, etc	new diagnostics	Material	???
30	Synthesis optimization	Laboratory to develop new synthetic pathways to reduce cost.	Synthesis/ scaleup	Molecular	medium
31	Data evaluation & assessment -	Facility to collect, analyze, evaluate and assess all data collected from laboratories in NEMReDI. 1. Collect and store all data from	Model/ simulation	Material	medium

Lab #	Topic	Description	Category	Design Level	New technology?
	medium	experiments and tests. 2. Integrate with analysis of data from small scale experiments. 3 Provide basis for development of QA tests.			
32	System concept design	Computational laboratory to design new systems by drawing on the range of materials available for design. (For example, explosives contained with reactive liners.) 1. Propulsion design codes. 2. Explosive design codes.	New system concepts	System	high
33	System -- mechanical fabrication	Mechanical fabrication facility for making designs for tests.	New system concepts	System	low/med
34	System - electrical fab	Electrical lab to provide electronics for test designs.	New system concepts	System	low
35	System - performance tests	Lab to test performance. 1. Evaluate the range of different types of test that may need to be done. 2. Provide definition of facilities that may be needed to conduct these different types of tests.	New system concepts	System	???
36	System - impact tests	Facility to conduct impact related tests on new systems.	New system concepts	System	???
37	System - shock tests	Facility to conduct shock related tests on new systems.	New system concepts	System	???
38	System - thermal tests	Facility to conduct thermal tests on new systems.	New system concepts	System	???
39	System - ESD tests	Facility to conduct ESD tests on new systems.	New system concepts	System	???
40	System – aging/compatibility	Facility to conduct aging and compatibility tests.	New system concepts	System	???
41	System - quality assurance tests	Laboratory to develop the quality assurance tests needed to evaluate the system.	New system concepts	System	???
	Munition Design	Design of munitions to achieve specific effect. This may be done within NEMReDI.	Large scale		
	Large scale tests	Done outside NEMReDI??			

PARARI 2007
8th Australian Explosive Ordnance Symposium
November 13 – 15, 2007

A NEW PARADIGM FOR R&D TO IMPLEMENT NEW ENERGETIC MATERIALS IN MUNITIONS

Technical Paper

By
Richard Behrens Jr. PhD, Sandia National Laboratories
&
Roger L. Swanson, Naval Ordnance Safety & Security Activity

Introduction:

The future position of our Nations and their well-being in the world will be challenged on many fronts in the coming decades and perhaps the foreseeable future. There are several current issues that may or will bring about changes in the world in the near future, from what we know today. These include: (1) the economic development of the third world, (2) the global competition for energy and natural resources, (3) the tensions between societies with different ethnic and cultural histories, (4) the tensions between several different cultures as we move towards a more interconnected and global world, (5) the potential stark realities and tensions of an effectively ever smaller world brought about by an increasing human population, (6) the tensions that can result from global climate changes whether warming or cooling, and (7) the resulting environmental and social positive and negative effects of these issues.

While addressing these issues does not directly involve a military component, history suggests that societies will develop military capabilities that may be used to influence the global balance of power on many of these issues. Much as all of our Nations and all world powers have done since World War II and are continuing to do. A cornerstone of the U.S. military strength of the last half of the twentieth century, and it continues today, was the development and superiority of U.S. munitions. These munitions encompass both conventional and nuclear ordnance. Superiority ranging from advanced chemical propulsion systems for rockets motors and guns to advanced nuclear warheads provided superpower status for the U.S. in the twentieth century. As larger fractions of the world's population moves into the modern technically interconnected world, both global and regional balances of power will surely change. Whether for the positive or negative is to be debated in the political arena, not in the domain of engineering and science. As such, this paper does not advocate, endorse, or support any specific political viewpoint or agenda. We are here to address technology and the improvement thereof.

In this paper, we attempt to address the issue of how to maintain technologically viable munitions in the 21st century from strictly the point of view of the energetic materials used for the propellants and explosives in those munitions. In attempting to address these issues; one must ask: Will maintaining the status quo be sufficient?, Will using technology developed in the years following WWII be sufficient for providing energetic materials, propellants and explosives, for future munition/weapon needs to meet new threats and provide for defenses?, Will investment in new sensors and electronics be sufficient or will new energetic materials be required?, Will the existing paradigm used for the development of energetic materials be sufficient, or will a new paradigm be required?

History of R&D and EM Developments:

This section provides a thorough description of energetic materials research and development history and concludes with a philosophical/policy discussion of the importance of developers, among other things, to implement new design concepts that enable systems to meet new military requirements. Historical statements regarding the degree that emerging military requirements resulted in new propellant and explosive material could reveal an important limitation in the current development process and another basis for a shift in strategy. The modern development of energetic materials for chemical propulsion and warheads can be traced back to the mid to late 19th century and beginning of to the middle of the 20th century with the development of nitroglycerine, nitrocellulose, and other energetic organic nitrate/nitramine compounds such as RDX, HMX, TATB, etc.

Most sophisticated plastic bonded explosives and propellants were developed just before and during the WWII timeframe. A great majority of "new" solid rocket motor propellants were developed during the first two decades of the cold war. Most of the developments after those timeframes are in essence follow-on work to the earlier research and development. A large part of that development can be characterized as; trial and error or what is commonly referred to as "Edisonian", although, that characterization disfavors Edison.

The current paradigm of an empirical "Edisonian" approach to develop new propellants and explosives is perceived by some as being too slow (lacking time responsiveness), largely unsuccessful, or

providing limited successes and is thus considered high risk and unworthy of significant investment. In some circles, it is disparagingly referred to as "tweaking molecules". Given the large number of different requirements that must be satisfied to make a new propellant or explosive that meets very high performance goals while being as intrinsically safe and as stable as possible; i.e., insensitive, it is not surprising that the slow empirical "Edisonian" approach has not been as successful as most would desire. Similar challenges are encountered in the development of new drugs. This paper considers the pharmaceutical industries' approach to addressing similar research and development issues and how that approach may serve as a guide for the development of a new paradigm for energetic material R&D. We considered the pharmaceutical industries' approach not only because of their similar research and developmental issues but also the fact that many of their precursor compounds are, or can be, very energetic in nature and they test to identify and exclude[1], where we desire to identify and include via test.

To circumvent the perceptions and/or limitations associated with the current "Edisonian" approach will require the development of a new R&D paradigm that can facilitate the creation of new propellants and explosives much more rapidly, with orders of magnitude less material, and at the same time providing new data that can be used to guide the design of new compounds, composite materials, and applications. The paper also addresses the requirement or need for new experimental methods and diagnostics tools. The primary objective being to provide the material scientist/engineer with the experimental tools needed to design new formulations required to meet the system requirements of the future.

Many of the ideas presented and discussed in this report are based on ideas and discussions from the Joint Army, Navy, NASA, and Air Force (JANNAF) and the Chemical Propulsion Information Analysis Center (CPIAC) sponsored workshop on "R&D Required to Implement New Energetic Ingredients in Munitions". The workshop was held at the Battelle Conference Center, Aberdeen, MD from 29-31, August 2006. Fifty-five individuals from various DoD (Army, Air force, and Navy) and DOE (Sandia, LLNL, and LANL) laboratories, US energetics and munitions industry, and academia participated in the workshop. The backgrounds of the participants were broad: with expertise in basic research, formulation development, manufacturing, systems development, and program management.

The primary objective for the workshop was to create a plan for R&D investment strategies that would enable the rapid implementation of new energetic ingredients (e.g., high nitrogen compounds energetic binders, and ionic liquids) needed to reach new munition goals, while meeting insensitive munition (IM), aging, quality assessment and cost requirements. To construct strategies for future R&D investments, we discussed many aspects concerning future requirements for new munitions, the role for new ingredients, and the R&D required for their development. Discussions focused on two themes: (1) the requirements for munition systems of the future, and (2) scientific and technical issues that will enable the rapid development of new energetic materials that can be used for the development of new munition systems. By the end of the workshop the following was achieved: (1) developed a strategy for assessing future munition requirements; (2) reviewed the current state of capabilities used for munition development; (3) identified gaps in our R&D capabilities that limit the development of new energetic materials; (4) initiated discussions on research approaches that can be used to develop technology that will close these gaps and enable rapid development of new energetic materials.

One theme, that was repeatedly discussed, was the perceived high degree of risk, by individuals inside this field, of investing in energetic materials R&D in a national environment of limited funding, which in effect also self limits funding in this area. Limited funding, also in turn, restricts the development of new tools needed to understand and design new materials. Thus, a self-fulfilling feedback cycle that limits the development of new energetic materials is created. The immediate ramifications of this situation are (1) a lack of excitement and enthusiasm about future science and engineering directions, (2) the lack of state of the art tools and instruments, (3) the inability to attract some of the best and brightest students to the field, and (4) a growing disparity between the availability of new technology and the need for increased functionality and preparedness.

This limited funding, in part, has been addressed by the US Department of Defense, OSD (AT&L), in the development and programming of a budget line for the Joint Insensitive Munitions Technology Program (JIMTP). As good an advance as this development of a budget line is, and it is a good advance, the overall funding picture is still quite limited in real dollar and in historical terms.

This lack of investment of R&D dollars in research on energetic materials, which is resulting in the current downward spiral in the U.S. capabilities to develop new energetic materials for propulsion systems and warheads, may simply be seen as a prudent investment decision by some individuals and corporations. However, it may also be a shortsighted investment decision based on a lack of knowledge, resulting in the inability to foresee future requirements and opportunities. In this paper, and the report of the August 2006 JANNAF meeting, we provide our assessment of the requirements for energetic ingredients for future munitions and the research and development opportunities that may enable the U.S. to maintain viable munitions to support our military responsibilities throughout the 21st century. The main themes addressed in the JANNAF report are: (1) Why should any individual, nation, or corporation invest in energetic material R&D, (2) A brief history of energetic material development, (3) Assessment of a need for a new paradigm, (4) Technical opportunities, (5) Implementation strategy, (6) Why investing in energetic material R&D is a sound future policy?

Some of the answers proffered to the first and main question above; "Why should anyone individual, nation, or corporation invest in energetic material R&D?" were: (a) World societies, friendly and not friendly, will continue to invest in military technology, (b) Other societies may develop threats using new propellants and explosives, as well as new defenses, even with today's limit R&D tool set, (c) Other societies may have more manpower to devote to these efforts, (d) These efforts may provide marginal improvements in materials that will translate into significant military advantage vis-à-vis our current capabilities.

If other nations or international groups develop offensive or defensive capabilities using new propellants or explosives, how will our advantages be maintained with conventional munitions? How does one conduct or advance R&D in conventional ordnance that will facilitate quick responses to actual or perceived threats? To stay competitive will require the agility to design, develop, and consistently (reproducible cost and quality) produce new materials rapidly. This must be coupled together with tight integration to implement those new energetic materials in new system designs. A scientific approach is therefore needed to design those energetic materials to meet new insensitive munition (IM), safety, aging, quality, health, and environmental compliance issues.

Environmental compliance issues or the development and fielding of "green" energetic materials raises additional questions such as; what is the measure of "green", by what/whose definition, how much is enough or too much, and at what cost in terms of resources (money and time) and in terms of safety and performance? These issues must be addressed by any energetic materials development paradigm. The second theme noted above from the JANNAF report was; "A brief history of energetic material development" and its relation to where the state of the art is today. That theme is tightly coupled with the third theme "Assessment of a need for a new paradigm". Current methods for development of new propellants and explosives are based on an empirical "Edisonian" approach developed in the early decades of the cold war. This approach requires large quantities of materials for tests, provides little insight beyond "go/no go" results, and takes several years to go through one testing cycle. An honest assessment is this approach has provided very limited successes in implementing new ingredients in the last 60 years. The results of using this approach has created the current perception that investing in the further development of new energetic material is fraught with risk and warrants little, or no, investment.

New instruments, new experimental methods, and new computational capabilities (theme of "technological opportunities" noted in the JANNAF report) will allow and facilitate the investigation of complex reactive systems that heretofore have not been available for use in investigating energetic materials. These tools have been applied to address complex issues in biological & biochemical systems and have revolutionized opportunities in these areas. These tools have not been applied in our overall

industry; remember the "black art" philosophy, to address the complex reaction issues that underlie the behaviors of propellants and explosives. Our "Implementation strategy" has to be a new paradigm whereby we not reject, but minimize, trial and error and maximize our current "technological opportunities" while continuing to develop new instruments, methods, and capabilities.

The ultimate goal of the scientific and engineering communities is to understand, measure, model, and predict the forces; i.e., the quantitative and qualitative mechanics that act upon the bonds between independent atoms, between intra-molecular atoms, and between molecules of complex molecular formulations. If these forces (chemical, mechanical, and electrical) can be understood and modeled from the molecular/atomic to macroscopic spatial scales (Fig. 1), the future performance or behavior of macro sized, orders of magnitude, infinitely more complex systems have the potential to be modeled with the advanced computational capabilities now available and perhaps understood and predicted[2].

The answer to the question/theme; "Why investing in energetic material R&D is a sound future policy" is the sustainment of leading edge capabilities in chemical propulsion systems and warheads. The table below projects the major payoffs that can be expected as additional focused research is accomplished.

Table 1: R&D Expectations

Research Area	*Energetic System*	*Major Payoff Projected*
Propulsion		
	Rocket Motors	Enhanced energy in heavy lift systems.
		Energetic binders to increase I_{sp}.
	Guidance Systems	Tailorable burn rates to provide in flight control resulting in more precise target interdiction.
	Guns	Tailorable burn rates to permit reduced gun weight, erosion, corrosive products, and extended gun life.
Warheads	Micro-propulsion	Programmable on-board micro-propulsion devices to steer warheads for increased accuracy/lethality.
	Energetic Payload	Use of controlled payload output utilizing different types of energetic material to permit a desired type of reaction with a particular target.
High Energy IM Systems	Propulsives & Warheads	Enhanced energetics knowledge to optimize tradeoffs between insensitivity and system requirements
	Propulsives & Warheads	Enhanced IM knowledge to provide safer- high performance systems that are less costly to transport, store and maintain.
Surveillance (Aging)	Propulsives & Warheads	New evaluation methods that can provide a better means for understanding aging behavior to optimize the life expectancy, assure safe continued performance and overall lowest life cycle cost.

Propulsion & Warhead Development:

If one reflects on the state of other technologies, such as optical and mass spectrometers and computers, which are ubiquitous and commonplace in our present-day laboratories, it is apparent that these tools were not available to the scientists and engineers who developed our original propulsion and warhead systems. To develop these energetic materials and their application articles at the time, testing protocols were created to enable engineers to develop safe munitions. Those tests typically provided limited information and for the most part simply provided an assessment of whether or not an energetic formulation would meet limited, and in most cases gross, laboratory and/or production line, safety and handling specifications. Further, in many cases the formulation, configuration, and subsystem specifications were based not on system requirements or the quest for optimum performance but merely on preproduction/production test results.

For example, drop or fall hammer tests were developed to assess impact sensitivity and various types of card gap tests (it seems most laboratories have their own favorite) were developed to assess shock sensitivity. This methodology continues in use today in the development of new formulations. Through extensive testing on a limited number of ingredients and formulations, an *art* (not a science) has been practiced in the design of new rocket motors and warheads using a well characterized, but limited set of ingredients. Thirty plus years ago when quite a number of current practitioners entered this business propellant development was referred to as a "black art". The bad news is that these methods are basically still used today to design "new" propellants and explosives.

To help shift focus from antiquated methods still in use to what will be required in the future, a detailed description/list of the various "things that matter", which was developed at the JANNAF meeting, is provided below as Table 2. These are all things, items, or issues that should frame any discussion of a new energetic material. Thus, it is important to recognize that experimental tools must focus on providing an understanding of reactivity over a wide range of conditions. The use of tools must also provide an understanding of this reactivity that can be used to design new compounds and materials.

Table 2: Things That Matter

Item	*Prop?*	*Exp?*	*Category*	*Reactive?*
Long-term stability	Y	Y	C	Y
Response in fires	Y	Y	S	Y
Response to impact – low rate mechanical energy input	Y	Y	S	Y
Response to shock -- high rate mechanical energy input	Y	Y	S	Y
Response to electrical stimuli	Y	Y	S, PF	Y
Coupling of mechanical/thermal in fire. Thermally induced changes alter response to mechanical energy.	Y	Y	S	Y
Toxicity & environmental compliance	Y	Y	S	N
Specific impulse	Y	N	PF	N
Pressure exponent	Y	N	PF	Y
Pressure oscillations	Y	N	PF	Y
Propellant or explosive integrity	Y	Y	PF, S	Y
Erosivity (guns)	Y	N	PF, C	Y
Tailor-able thrust	Y	N	PF	Y
Detonation velocity, detonation pressure	N	Y	PF	N
Processibility	Y	Y	M	Y
Dispersal of active compounds at target	Y	Y	D	Y
Response to Environmental Stressors (T, H, V, & S)	Y	Y	S, PF	Y

C - Compatibility; S - Safety; PF- Performance; M - Manufacturing; D - Disruptive technology Issues

Energetic Materials Research:

Modern experimental and computational methods have been brought to bear to understand reaction processes in energetic materials starting in the early 1980s. New research methods using laser-based optical diagnostics and mass spectrometers were developed to probe details of the reaction chemistry in propellants and explosives. Recent reviews of articles have shown how these instruments were used to probe the flame chemistry of propellants[3, 4] and reactions in shocks[5, 6]. The elementary reactions associated with processes that occur in flames have been probed experimentally and insight has been developed on the details of reactions at the atomic and molecular levels[7, 8]. Theoretical methods have also been used to calculate reaction pathways in both the gaseous[7] and condensed phases[10,11]. Much of this information has been used to construct mathematical representations of the combustion processes in solid propellants[13-15].

These review articles provide excellent summaries of the application of state-of-the-art methods of physical chemistry and chemical physics to understand these relatively complex gas-phase processes. The articles also point to the relative lack of understanding of reaction processes in the condensed phase. Much of the research has focused on developing a deep understanding of the reaction processes of a few energetic compounds commonly used in explosives and propellants. The application of these methods to a wide range of different types of energetic compounds has been limited to an extensive set of flame chemistry work[4].

While this research has provided a great deal of new understanding, there are two broad areas where our understanding remains quite limited. The first is how to connect the behaviors of *energetic materials* to their *molecular properties*. Brill has addressed this issue through extensive work examining the rapid thermolysis of many different types of energetic compounds. This work and those of others in this area has been summarized and general empirical correlations of behavior to different molecular properties developed[15]. As pointed out by Brill, "correlations between molecular properties and macroscopic bulk behavior are risky because of the myriad of processes taking place may defeat the simple fundamental connections with the parent molecule." This leads to the second area in which we lack understanding: the reaction of energetic materials in the condensed phase at low and moderate temperature. The response of energetic materials at low and moderate temperature to thermal, mechanical and electrical energy stimuli underlie their safety and aging characteristics. A myriad of reactions control their behavior.

The response of new energetic materials to thermal and mechanical stimuli at low and moderate temperatures is the leading cause of failure to introduce new energetic ingredients into propellants or explosives. As Brill indicates there are a myriad of process taking place in the response of a bulk sample. In other words, the reaction processes involve complex reaction mechanisms, which take place in systems that may be considered to have disordered kinetics. This concept of examining the means to determine complex reaction mechanisms has been examined quite extensively outside the field of energetic materials. Ross, Schreiber and Vlad have recently published a book summarizing the issues, terminology, ideas, and approaches associated with determining complex reaction mechanisms in chemical, biological and genetic systems[16]. While many of the concepts currently used to characterize complex reaction mechanisms in chemical and biological systems are applicable to investigations of reaction processes in the condensed phase of energetic materials, it must be recognized that most of the complex chemical and biological systems deal with reactions in dilute solutions, or low density gases, where the concepts of elementary reactions and the role of stochastic variations in disordered kinetics are fundamental features of these systems. In contrast, reactions of energetic materials in response to thermal or mechanical stimuli take place in concentrated solutions, or solids, that have localized reaction environments on a range of different spatial scales.

The successful development of new energetic materials will require using methods to identify, understand, and characterize the reaction process in the various reactive environments that may be formed within a bulk energetic material. The various types of reactive environments may be characterized by spatial scales that are intrinsic properties of a material, or develop during the course of reaction. The possible spatial scales that need to be considered and various means to address reaction environments on these spatial scales are illustrated by the magenta lines in Figure 1 (see following page).

Both experimental and modeling & simulation methods must be developed to investigate reaction processes of energetic materials at these various spatial scales. New instruments, experimental protocols, and modeling & simulation methods to probe complex reaction mechanisms and the associated reaction kinetics of energetic materials in response to thermal stimuli have been developed by Behrens and summarized in a recent review article[17]. This type of approach also needs to be developed to investigate the complex reaction mechanisms and associated reaction kinetic of energetic materials in response to other types of energetic stimuli.

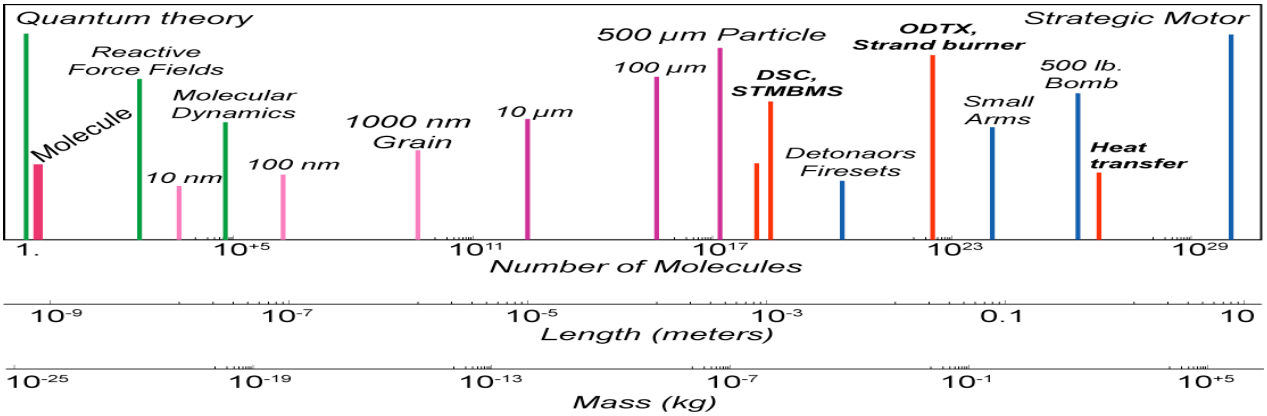

Figure 1. Illustration of spatial scales that may be characteristic of different reaction environments in energetic materials (magenta lines). Experimental methods (red), theory and modeling (green), energetic system articles (blue).

Figure 1: Scale of Issues

Ties between Research and Development:

The ties between research and development within the DoD in the area of propellant and explosive development have been limited. The development of new energetic materials for propulsion and warheads still relies on the empirical "Edisonian" approach of synthesizes, scale up, and test. No new experimental methods for research have been implemented in development venues. What is limiting the transfer of methods from the research community to the development community? First, most of the research has focused on the understanding elementary chemical reactions and the role that they play in combustion under propellant burning and explosive detonation conditions. While this provides valuable insight for connecting the properties of small energetic molecules to their behavior in combustion, to evaluate the burn rate or detonation velocity of new ingredients during the development process only requires a simple measurement. Thus, knowledge of the complex reaction processes that underlie combustion of a new propellant or detonation of a new explosive does not, in general, provide significant benefit in developing new ingredients by itself. In terms of performance, the development process requires the means to develop ingredients to tailor the burn rate of propellants as a function of pressure or make insensitive explosives. Research methods that can be transformed into development tools that will provide guidance for the development of new ingredients that meet these requirements would be beneficial.

It is also informative to consider the type of information that is required to develop new propellants and explosives. The developer needs to satisfactorily address the following issues: (1) Satisfactory burn rates and pressure exponents for propellants and detonation velocity and pressure for explosives, (2) Design materials to have the lowest impact and shock sensitivity, (3) Design materials to respond to slow and fast heating in a non-violent and relatively benign manner, (4) Design materials that are insensitive to electrostatic discharge, (5) Design materials that do not degrade with time, or degrade with time in a predictable and acceptable manner, (6) Provide a means to manufacture the material and not introduce any new features that may affect the material's performance, safety or aging behaviors, (7) Provide a means to assess the state of the munition in a relatively inexpensive, but thorough manner. (8) Not present health or environmental compliance issues, (9) Disposal in an inexpensive and environmentally benign manner, (10) Implement new design concepts that enable systems to meet new military requirements.

In examining this list, it is apparent that performance issues comprise only a small portion of the developer's tasks and associated issues. Research that will have the biggest impact on enhancing our ability to develop new energetic materials for propulsion and warheads will focus on addressing these

primary development issues. One current research area that can be tied into many of these development requirements are the methods that have been developed to investigate the reactions of energetic materials to thermal stimuli at low and moderate temperatures that are associated with burn rate modifiers, safety and long-term aging issues[17].

A New Paradigm vs. A Shift of the Current Paradigm:

The current paradigm of an empirical "Edisonian" approach to develop new propellants and explosives is perceived as being unsuccessful and is thus considered high risk and unworthy of significant investment by today's program managers. Given the large number of different requirements that must be satisfied to make a new propellant or explosive that meets very high performance goals while being as safe and as stable as possible, it is not surprising that the slow empirical "Edisonian" approach has not been successful.

The pharmaceutical industry often encounters similar problems of having to satisfy many different types of requirements, ranging from efficacy to safety[1] and cost. It has overcome these obstacles using and developing new scientific methods to probe the chemical, biological, and medical issues and requirements for new materials. It has developed new methods both to enhance screening methods and to develop a better understanding of diseases, in our terminology - requirements to guide the development of new drugs, vaccines and treatment therapies. When compared to the energetics product area, the pharmaceutical industry has somewhat clearer requirements statements such as the development of drugs for well-described diseases. However their quest for product improvement in efficacy, safety and cost can be seen as very similar to the need for the resolution of energetics products limitations that are well known and apparently acceptable status-quo. Table I depicts some areas of energetics performance for which successful focused R&D can result in significant product improvement.

Effective development of new energetic materials for munitions in the future will need to use a requirements-driven approach similar to that used by the pharmaceutical and biotechnology industries. This will require the development of a new paradigm that can develop new propellants and explosives much more rapidly, with orders of magnitude less material, and providing new data that can be used to guide the design of new compounds and composite materials.

Technical Opportunities:

Technical opportunities arise from addressing the technical challenges posed by future munition requirements. The technical challenges were uncovered by examining five areas at the workshop. These included: (a) Conventional methods for evaluating ingredients, (b) System requirements for new energetic materials, (c) Technical limits of implementation of new energetic ingredients in munitions, (d) New experimental concepts for evaluating performance and deleterious features of new ingredients, (e) New modeling/simulation methods for evaluating and predicting performance and deleterious features of new compounds and materials.

Material Design Parameters:

This section provides guidance to the developers of energetic material to enable them to focus on the attributes of the basic ingredients and formulations required for weapons of the future to have the desired effects on the target. However, it appears to represent a strategy very similar to the current state. Design goals are presented as incremental parameter performance improvements without regard to future weapons requirements. Goals and thresholds are represented without system performance rationale. Over 40% of the Material Design Parameters addressed indicate that the threshold parameter value, which is absolutely required for that particular parameter or application, is system or performance dependent. The objective of the Material Design Parameter Workshop Subgroup was to provide guidance to the developers of energetic molecules and materials to enable them to focus on the attributes of the basic ingredients and formulations required for weapons of the future to have the desired effects on the target.

This Subgroup would thus define the parameters of interest for ingredients for explosives, rocket and gun propellants and pyrotechnics used in DoD applications. These parameters include characteristics that contribute to energy content and release, safety, insensitive munitions (IM), service life, reliability, environmental compliance, health, processability, etc. Although difficult, due to varied Service requirements, there is a universal need to characterize energetics design characteristics and establish attainable values. Notwithstanding the differences between Services regarding energetics requirements and the difficulty in forecasting future weapons requirement, it is essential that energetics developers establish dialogue with war-planners to permit the early molding of weapons requirements based on reachable energetic material technology growth.

Experimental Methods and Diagnostics:

The primary objective is to provide the material scientist/engineer with the experimental tools needed to design new formulations required to meet system requirements of the future. The tools should provide the capabilities required to address new and different types of system requirements as the world geopolitical/military balance of power changes over long periods of time (many decades). For example, in the near term, the tools must provide the ability to design new materials to enable; (1) insensitive munitions, (2) low impact/shock sensitivity to enable earth penetrator design, and (3) tailor-able yields to enable design for asymmetric warfare scenarios. In the longer term, the tools must provide the capabilities to design weapons for (1) advanced naval conflicts and (2) space-based military encounters.

The tools must provide the nation with the capability to remain a leading world power and not be surprised by the military accomplishments of other societies on energetic technological fronts. It must be recognized that the challenge is to maintain military technologies with a smaller population compared to other emerging societies in the 21st century. This will require the ability to develop new energetic materials faster and in a smarter manner. It will also require increased efficiency in both the technical approach used to create and evaluate new materials and a more efficient and integrated use of manpower and resources, both at the national and international levels.

These capabilities must be maintained at a reasonable cost. This type of banal statement must be examined carefully and the underlying justification must be based on (1) a well-reasoned justification of what is a reasonable cost, and (2) what must be measured to determine if capabilities are indeed maintained. Some consideration should also be given to expandability, or elasticity, of the technical base.

By this, we mean what is the minimum level of effort or investment that will be required to provide a sustained basis for EM technology, but can be expanded rapidly to respond to potential military conflicts in the future. What is maintained as part of the nation's infrastructure? What is maintained by private industry? How can national infrastructure and private industry be efficiently integrated?
The experimental tool set must allow "out-of-the-box" munition concepts to be evaluated and developed if necessary. For example, the technical basis should provide the means to address issues such as: (1) diverse interactions with a target, (2) detect and interact with selected populations, (3) benign interaction with the target (i.e., temporary disablement), (4) intelligent countermeasures, (5) miniature and tailor-able propulsion and explosive systems, (6) the ability to disable systems remotely and when desired. While implementation of many of these concepts may be undesirable, having the technical basis to rapidly implement these concepts, if necessary, may enhance future security.

Technical Challenges:

To identify, define, and develop the experimental tools needed to design energetic materials for the future requires defining how energetic materials will behave over the various environments encountered by warheads and propulsion systems during their life cycle. Conversely, as these tools are developed and the most radical capabilities and possibilities become reachable, dialogue with war-planners can be initiated to permit the early molding of weapons requirements contributing to the rapid deployment of emerging weapons. The types of things that matter were identified during the JANNAF

August 2006 meeting and presented earlier as Table 2. The items were categorized by those related to: performance (PF), safety (S), long-term aging and compatibility (C), manufacturing (M) or disruptive technology (D). Most of the important features of a propellant or explosive are dependent on the chemical reactivity of the material. As such, the success or failure of a propellant or explosive depends on its ability to meet the various criteria associated with the items listed in Table 1: Things That Matter.

Testing:

If testing or analysis results in a value above (if < sign) or below (if > sign) that shown, it could indicate a potential performance, safety, health or environmental issue or hazard and further testing or analysis is required. Many factors are important in estimating adverse environmental or occupational outcomes. These environmental criteria shown are intended to be used in rough screening or ranking procedures. Evaluation of environmental criteria often requires a weight of evidence approach whereby experimental data are given more weight than modeled or estimated values. An understanding of the various processes involved in environmental fate and transport are also needed since these values are not mutually exclusive in their ability to predict environmental transport or persistence.

Thus, it is important to recognize that the experimental tools must focus on understanding reactivity over a wide range of conditions. It must also provide an understanding of this reactivity that can be used to design new compounds and materials. To assess the possibility of implementing a new paradigm for the development of new energetic materials for future munition requirements, the following questions must be addressed: (a) Identify what really matters, (b) What current methods are used to address the issue, (c) What are the issues underlying reaction processes in the materials, (d) What spatial scales will play a role, (e) What is the extent of disorder, (f) What are the variations in disorder, (g) How complex are the reactions likely to be, (h) What research methods, protocols, and results are currently available and can be used to address the issue, (i) What physical and chemical phenomena are still unknown and will require more directed basic research, (j) How much material will be required to conduct a series of tests to address the issue, (k) What can be done with current state-of-the-art R&D methods, (l) What may be the smallest amount of material that could be reasonably utilized, (m) Can current research methods be developed into laboratory-scale diagnostic equipment, (n) How likely are small-scale experiments to be good predictors of larger scale munition behavior, (o) How much information will be generated by the measurements, and (p) The amount of information that will be provided for the next design cycle.

In examining each of these areas, it is important to recognize that the focus is on understanding reactivity and using this understanding to design new materials. From a very general point of view, the issue is to assess how thermal, kinetic, mechanical, or electrical energy will lead to reaction of the material. This may range from a very slow response, which would be characteristic of processes associated with aging, up to a fast response, which may be associated with performance or the response in severe abnormal environments. In examining these issues, it is recognized that there are different classes of approaches that must be used for investigating reaction behaviors in energetic materials and munitions.

These may be divided into the following categories: (1) Functional – These are typically go/no-go tests. These types of tests are used to determine whether a material meets a specified criteria or whether a device works or not. (2) Global – These tests measure a behavior that is the sum of many underlying processes. Thermal analysis tests, such as DSC, TGA or ODTX, or performance tests, such as detonation velocity, cylinder expansion, or propellant burn rates, are examples of these types of tests. These tests are often used to determine whether a new ingredient meets a set of desired “target” properties. (3) Complex reaction determination -- These tests identify local reaction environments (LRE) and characterize the reaction manifolds that control the behavior in each LRE.

These tests provide information on the actual chemical reactions that occur in a material. They provide a scientific basis for predicting the behavior of energetic materials and provide insight into how to design better compounds and materials. These types of tests may be based on (1) post-mortem analysis of

samples exposed to various energetic stimuli, or (2) real-time measurements of a localized reaction environment. These types of measurements are currently used in research laboratories. However, they have not made their way into the formulation environment.

Summary:

There is a critical need to create a plan for national R&D investment strategies that would enable the rapid implementation of new energetic ingredients (e.g., high nitrogen compounds, energetic binders, ionic liquids, and future materials) while meeting insensitive munitions (IM), aging, quality assessment and cost requirements. There is a growing disparity between the availability of new energetic material technology and the need for increased functionality and preparedness in the future weapons arsenal.

The transition from the current Propellant and Explosive material design/development process "paradigm" requires an ability to leap ahead of war-planners and weaponeers to provide futuristic possibilities that can both elevate performance levels and provide new warfare tactics and strategies. That "leap ahead" can only be achieved with a new paradigm; one that embraces new sense, test, analyze, and design technology opportunities and developments and relies less and less on the "black art" or "Edisonian" approach of the past.

Conclusions:

We must develop near (2 year), mid (5 year) and long term (10+ year) strategies that seek to accomplish the following: (1) Establish dialogue with war-planners to permit the early molding of weapons requirements based on reachable energetic material technology growth contributing to the rapid deployment of emerging weapons, (2) Develop national initiatives to provide the material scientist/engineer with the experimental tools needed to design new formulations required to meet system requirements of the future, (3) Develop national strategies that result in a capability to design weapons for advanced land, air, and naval conflicts and space-based military encounters.

We should explore the concept of a national virtual laboratory enterprise or consortium to bring the scientific and engineering communities together to understand, measure, model, develop, and most importantly predict the actions and inter-relationships of complex energetic molecular formulations so that application developments can progress at a faster pace with greater assurances of safety, reliability, and performance.

Authors:

Richard Behrens Jr. Ph.D.; rbehren@sandia.gov
Sandia National Laboratories, Combustion Research Facility
P.O. Box 969, MS9052, Livermore, CA 94551-0969
Phone: (925) 294-2170, Fax: (925) 294-2276

Roger L. Swanson; Roger.Swanson@navy.mil
Naval Ordnance Safety and Security Activity, Farragut Hall (Bldg D-323)
3817 Strauss Avenue Suite 108, Indian Head MD 20640-5151
Phone: (301) 744-4447, Fax: (301) 744-6087

Acknowledgements:

The authors thank W. Anderson, B. Forch, R. Shaw for their efforts in organizing the JANNAF workshop and R. Blumenthal, S. Thynell and E. Kober for follow-up discussions of experimental and modeling issues. Sandia is a multiprogram laboratory operated by Sandia Corporation for the United States Department of Energy's National Nuclear Security Administration under Contract DE-AC04-94-AL85000.

References:

1. Lackman, T, Screening of Potentially Explosive Substances. *Proceedings of the 13th Jan Hansson Symposium on Chemical Problems Connected with the Stability of Explosives*, Backaskog, Sweden, 6-10 June 2004 p1
2. Swanson, R. L., Inter-Relationships between U.S. Navy Insensitive Munitions, Quality Evaluation (Aging), and Explosive Safety Programs. *Proceedings of the FINNEX 2002 Seminar*, 9-11 September 2002, Levi, Kittilä, Finland. p4
3. Korobeinichev, O. P., Study of Energetic Material Combustion Chemistry by Probing Mass Spectrometry and Modeling of Flames. In *Overview of Recent Research on Energetic Materials*, Shaw, R. W.; Brill, T. B.; Thompson, D. L., Eds. World Scientific Publishing Co.: Singapore, 2005; pp 75-102.
4. Parr, T.; Hanson-Parr, D., Optical Spectroscopic Measurements of Energetic Material Flame Structure. In *Overviews of Recent Research on Energetic Materials*, Shaw, R. W.; Brill, T. B.; Thompson, D. L., Eds. World Scientific Publishing Co.: Singapore, 2005; pp 103-127.
5. Greiner, N. R.; Fry, H. A.; Blais, N. C. In *Detonation Reaction Steps Frozen by Free Expansion and Analyzed by Mass Spectrometry*, 10th International Detonation Symposium, Boston, Massachusetts, 1993; Boston, Massachusetts, 1993.
6. Dlott, D. D., Multi-Photon Up-Pumping in Energetic Materials. In *Overview of Recent Research on Energetic Materials*, Shaw, R. W.; Brill, T. B.; Thompson, D. L., Eds. World Scientific Publishing Co.: Singapore, 2005; pp 303-333.
7. Dagdigian, P. J., Transient Gas-Phase Intermediates in the Decomposition of Energetic Materials. In *Overview of Recent Research on Energetic Materials*, Shaw, R. W.; Brill, T. B.; Thompson, D. L., Eds. World Scientific Publishing Co.: Singapore, 2005; pp 129-160.
8. Bernstein, E. R., Role of Electronic Excited States in the Decomposition of Energetic Materials. In *Overview of Recent Research on Energetic Materials*, Shaw, R. W.; Brill, T. B.; Thompson, D. L., Eds. World Scientific Publishing Co.: Singapore, 2005; pp 161-189.
9. Thompson, D. L., Gas-Phase Decomposition of Energetic Molecules. In *Overview of Recent Research on Energetic Materials*, Shaw, R. W.; Brill, T. B.; Thompson, D. L., Eds. World Scientific Publishing Co.: Singapore, 2005; pp 241-274.
10. Fried, L. E.; Manaa, M. R.; Lewis, J. P., Modeling the Reactions of Energetic Materials in the Condensed Phase. In *Overview of Recent Research on Energetic Materials*, Shaw, R. W.; Brill, T. B.; Thompson, D. L., Eds. World Scientific Publishing Co.: Singapore, 2005; pp 275-301.
11. Rice, B. M., Applications of Theoretical Chemistry in Assessing Energetic Materials for Performance or Sensitivity. In *Overview of Recent Research on Energetic Materials*, Shaw, R. W.; Brill, T. B.; Thompson, D. L., Eds. World Scientific Publishing Co.: Singapore, 2005; pp 335-367.
12. Anderson, W. R.; Fontijn, A., Gas-Phase Kinetics for Propellant Combustion Modeling: Requirements and Experiments. In *Overview of Recent Research on Energetic Materials*, Shaw, R. W.; Brill, T. B.; Thompson, D. L., Eds. World Scientific Publishing Co.: Singapore, 2005; pp 191-239.
13. Kim, E. S.; Yang, V., Combustion and Ignition of Nitramine Propellants: Aspects of Modeling, Simulation and Analysis. In *Overview of Recent Research on Energetic Materials*, Shaw, R. W.; Brill, T. B.; Thompson, D. L., Eds. World Scientific Publishing Co.: Singapore, 2005; pp 369-417.
14. Miller, M. S., Burning-Rate Models and Their Successors, A Personal Perspective. In *Overview of Recent Research on Energetic Materials*, Shaw, R. W.; Brill, T. B.; Thompson, D. L., Eds. World Scientific Publishing Co.: Singapore, 2005; pp 419-472.
15. Brill, T. B., Connecting Molecular Properties to Decomposition, Combustion, and Explosion Trends. In *Overview of Recent Research on Energetic Materials*, Shaw, R. W.; Brill, T. B.; Thompson, D. L., Eds. World Scientific Publishing Co.: Singapore, 2005; pp 1-27.
16. Ross, J.; Schreiber, I.; Vlad, M. O., *Determination of Complex Reaction Mechanisms - Analysis of Chemical, Biological, and Genetic Networks*. 1st ed.; Oxford University Press: New York City, 2006.
17. Behrens, R., Thermal Decomposition Processes of Energetic Materials in the Condensed Phase at Low and Moderate Temperatures. In *Overviews of Recent Research on Energetic Materials*, Shaw, R. W.; Brill, T. B.; Thompson, D. L., Eds. World Scientific Publishing Co.: Singapore, 2005; pp 29 - 74.